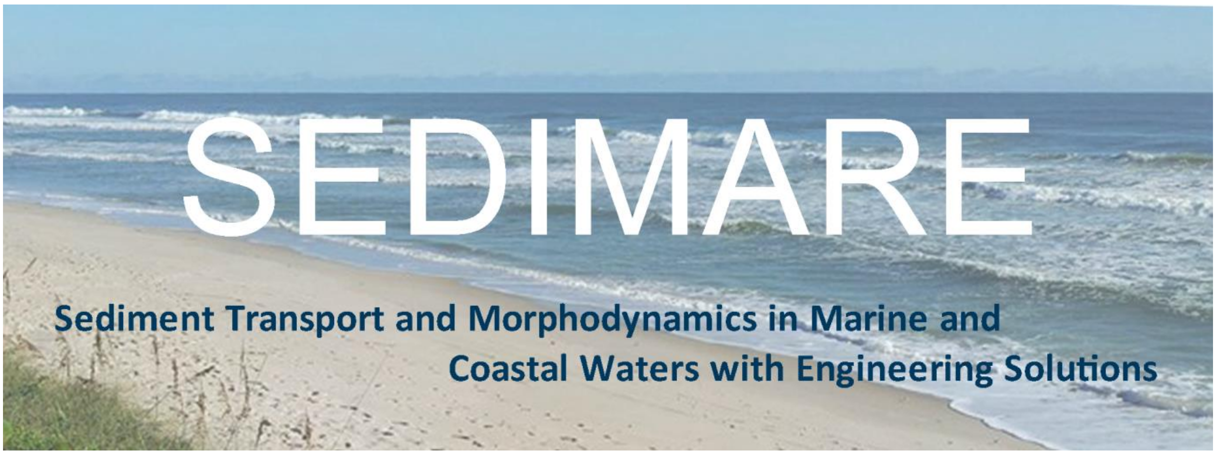

Project Number: 101072443

2nd NETWORK TRAINING SCHOOL

Deliverable 4.3

Dissemination level: PU - Public

Prepared by:

Athanassios Dimas, Coordinator, University of Patras

This project has received funding from the European Union's (EU) Horizon Europe Framework Programme (HORIZON) under Grant Agreement No. 101072443 as a MSCA Doctoral Network (HORIZON-MSCA-2021-DN-01).

Document Information

Project Title	Sediment Transport and Morphodynamics in Marine and Coastal Waters with Engineering Solutions
Project Acronym	SEDIMARE
Grant Agreement No.	101072443
Call	MSCA Doctoral Networks 2021 (HORIZON-MSCA-2021-DN-01)
Start Date of Project	01-02-2023
Duration of Project	48 months
Deliverable	D4.3: 2nd NETWORK TRAINING SCHOOL
No. of pages including cover	322

Version	Publication Date	Author(s)	Change
1.0	15.11.2024	Athanassios Dimas	Initial version

Date and Signature of Author(s): ATHANASIOS DIMAS
15/11/2024 15:46

Table of Contents

1. Program

The SEDIMARE "2nd Training School" was organized by the University of Twente and Deltares at Twente and Delft, respectively, in the Netherlands, on 5-8 November 2024. Local organizers were Prof. P. Roos and Prof. J. van der Werf. The event was attended in person by all DCs.

The SEDIMARE meeting consisted of two parts:

1. Training for the DCs at the University of Twente, Enschede on 5-6 November. The DCs followed a presentation skills training. They worked on the presentations to be given at Part 2 of the meeting. Draft presentations had to be ready before the start of the training.
2. Experimental & modeling workshop for all SEDIMARE members at Deltares, Delft on 7-8 November.

Tuesday 5 November (DCs only) - University of Twente, Horsttoren, room Z-203

08.45 – 09.00 walk-in

09.00 – 09.15 welcome by Kathelijne Wijnberg, UT professor Coastal Systems a& Nature-Based Engineering

09.15 – 12.30 training presentation skills

12.30 – 14.00 lunch

14.00 – 17.00 training presentation skills

Wednesday 6 November (DCs only) - University of Twente, Horsttoren, room Z-203

09.00 – 12.30 training presentation skills

12.30 – 13.00 lunch

~14.00 train to Delft

Thursday 7 November – Deltares, room Ganges Delta

Training School & Workshop "Experimental and Practical Modelling of Sediment Transport and Coastal Morphology"

09.00 – 09.30 walk-in

09.30 – 09.45 welcome by Dirk-Jan Walstra (managing director Deltares) & Jebbe van der Werf

09.45 – 10.00 Athanassios Dimas (PI) – introduction of SEDIMARE

10.00 – 10.40 Keynote 1: Bas van Maren (Deltares, TUDelft) – "Measurements and modeling of the erodibility of sand-mud beds" (30 min + 10 min discussion)

10.40-11.00 coffee/tea break

Morphodynamic modeling oriented DCs (10 min presentation, 10 min discussion)

11.00 – 11.20 Buckle Subbiah Elavazhagan (#5) - Morphodynamic analysis of the upper confined and unconfined beach profiles during episodic events

11.20 – 11.40 Jowi Miranda (#7) – Process-based modeling of sand mud morphodynamics

11.40 – 12.00 Nasim Soori (#4) - Mixing and transport in the coastal area

12.00 – 12.20 Nishchay Tiwari (#12) - Multi-models approach to scour in dynamics areas

12.20 – 13.30 lunch

13.30 – 14.10 Keynote 2: Sandra Soares-Frazão, UCL – "Breaching of earthen embankments: from small-scale laboratory experiments to field measurements using photogrammetry" (30 min + 10 min discussion)

Field/lab oriented DCs (10 min presentation, 10 min discussion)

14.10 – 14.30 Muhammed Said Parlak (#2) - Nearshore wave processes by remote sensing

14.30 – 14.50 Van Thi To Nguyen (#3) - Erosion and transport processes of sand-silt mixtures

14.50 – 15.10 coffee/tea break

15.10 – 15.30 Siyuan Wang (#8) - Morphodynamics of breach growth and bank erosion using laboratory experiments

15.30 – 15.50 Eloah Rosas (#9) - Characterization of stratification and near-bed dense layers in high-density sediment-laden flows

15.50 – 16.10 Saeed Osouli (#10) - Overtopping breakwater for energy conversion

16.10 – 17.00 discussion of DC secondments (lead by Athanassios Dimas)

19.00 "Meeting" dinner in the evening.

Friday 8 November – Deltares, room Ganges Delta

Training School & Workshop "Experimental and Practical Modelling of Sediment Transport and Coastal Morphology"

Detailed numerical modeling DCs (10 min presentation, 10 min discussion)

09.30 – 9.50 Ioannis Gerasimos Tsipas (#1) - Large-eddy simulations of turbulent oscillatory flow and sediment transport induced by waves

09.50 – 10.10 Quan Nguyen (#11) - Morphodynamic swash zone modelling

10.10 – 10.30 Evangelos Petridis (#6) - Mathematical modeling and numerical simulations of water-saturated granular materials

10.30 – 11.00 Keynote 3: Mark Klein Breteler – Deltares experimental facilities & measuring techniques (20 min + 10 min discussion)

11.00 – 11.15 coffee/tea break

11.15 – 12.30 guided tour of Deltares experimental facilities

12.30 – 13.30 lunch

2. Presentations

The theme of the 2nd Network Training School was "Experimental and Practical Modelling of Sediment Transport and Coastal Morphology". Therefore, the scope of the presentations by scientists was on the fundamentals and the applications of experimental and field methods, as well as on practical modelling to be used by the DCs in their research.

The corresponding presentations, as well as the presentations of all the DCs, are shown in the next pages.

“Measurements and modeling of the erodibility of sand-mud beds”

(Invited Speaker Bas van Maren, Deltares & TUDelft)

Deltares

Measurements and modeling of the erodibility of (sand)-mud beds

Recent insights into the role of density

Bas van Maren

(with most of the work done by others, especially Leo van Rijn, Roy van Weerdenburg, Marcio Boechat, Ana Colina, Irene Colosimo, Thijs van Kessel, Floris van Rees)

Wadden Sea fringing flats (near Koehool)

What is the mud content?

What is the dry density?

'Mud'
Density ~500 kg/m^3
Mud content ~50-60%

PhD work Irene Colosimo

Recent insights

- Role of density in erosion of sand-mud mixtures
  - MUSA experiments
  - Delft3D improvements
- Strength development during drying
  - Field experiments
  - Delft3D improvements

Erosion parameter

Critical bed shear stress for erosion

$$E = M\frac{(\tau_b - \tau_{cr})}{\tau_{cr}}$$

Role of density in erosion of sand-mud mixtures

- MUSA project (Improve understanding of erosion & sedimentation of sand-mud mixtures and implement it in engineering tools and numerical software)
- 2020 – 2023 (MUSA2 2024 – 2028)
- Consortium of Leo v. Rijn, WaterProof, Boskalis, DEME, Jan de Nul, RHDHV, Arcadis, DHI, HRW, Deltares (Svasek, Rijkswaterstaat, Waterbouwkundig Laboratorium Borgerhout)

Literature survey

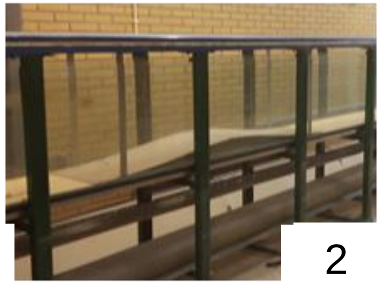

Lab experiments
- Erosion (flumes)
- Properties

Field surveys
- boat + frame
- Flocculation camera measurements

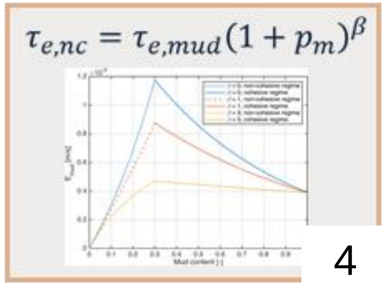

Analysis + Formulations

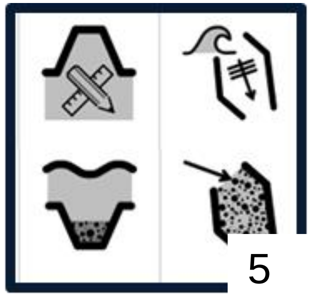

Toolbox
- Leo van Rijn tools
- CoDeS

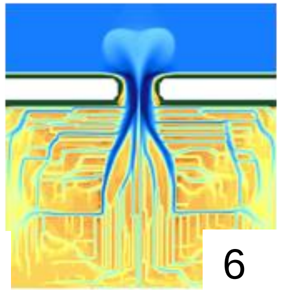

Upgrade numerical models: Delft3D + Mike

Deltares

Sample collection

- Bulk samples
- Undisturbed samples

Erosion tests

Small flume

Big flume

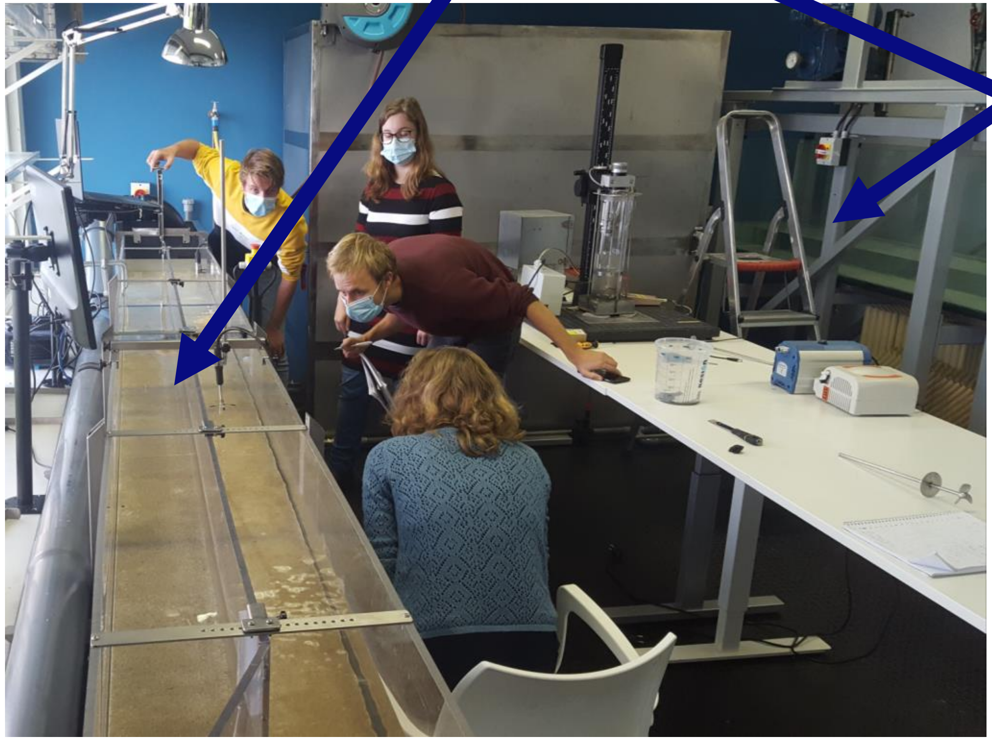

Deltares

Erosion tests

Erosion tests

Sediment beds:

- Placed beds (undisturbed samples)
- Remoulded beds
- Diluted, remoulded beds

verification

Observation method

- Visual determination of Critical Bed Shear Stress (τ_{cr}) (all samples)
- SSC conversion to erosion rate to determine τ_{cr} & erosion parameter (some samples)

Erosion tests – main findings

Critical Bed-Shear Stress of Mud–Sand Mixtures

L. C. van Rijn, Dr.Eng.[1]; M. Boechat Albernaz, Ph.D.[2]; L. Perk[3]; A. Colina Alonso, Dr.Eng.[4]; R. J. A. van Weerdenburg[5]; and D. S. van Maren, Ph.D.[6]

Muddy sediment consolidates slowly ➔ remains soft under Wadden Sea conditions

Sand erodes relatively easy

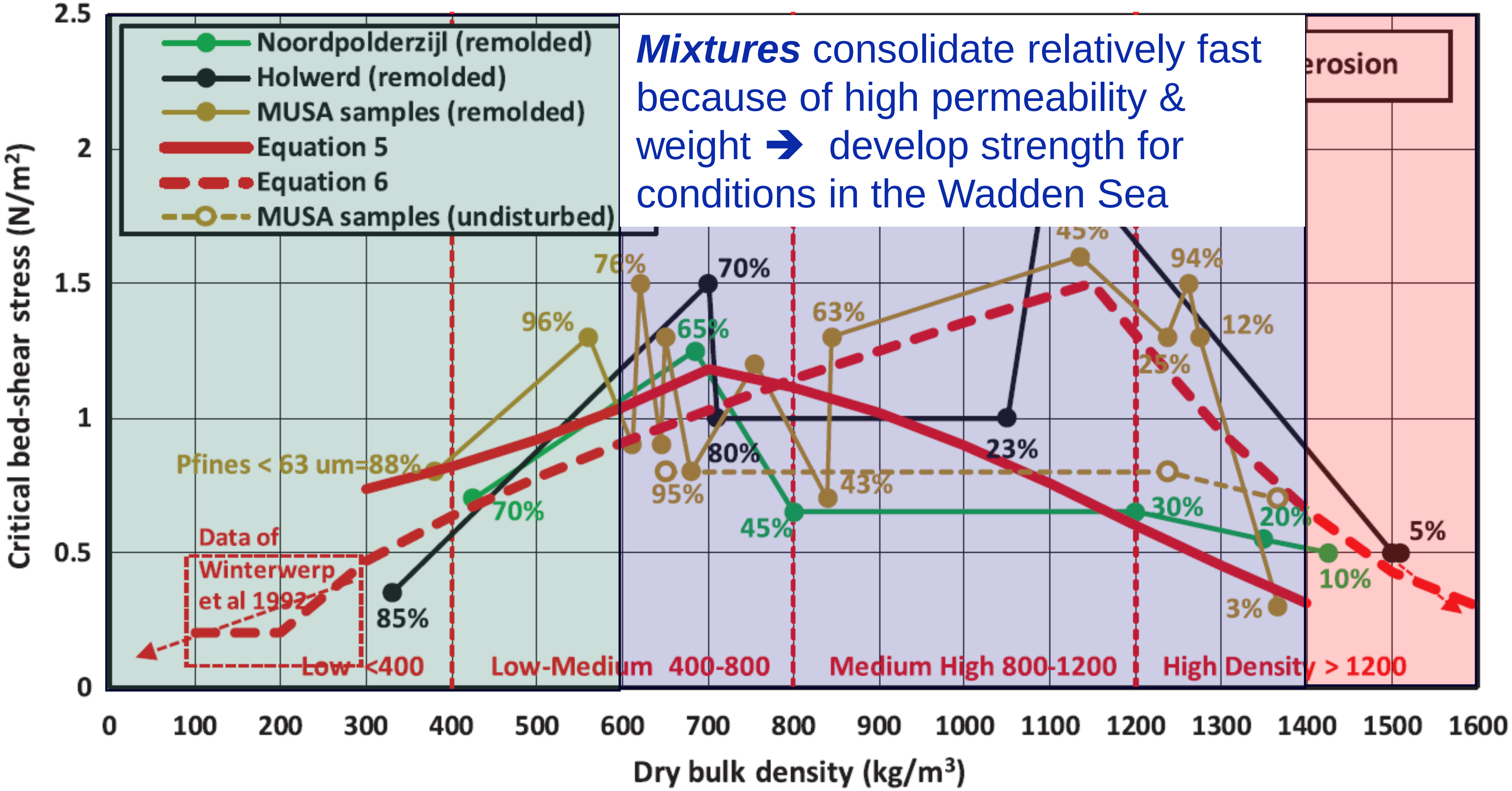

Mixtures consolidate relatively fast because of high permeability & weight ➔ develop strength for conditions in the Wadden Sea

- τ_{cr} is highest for intermediate density
- This corresponds to mixtures with a mud content of 30-70%
- High density: sandy mixtures with a low τ_{cr} (Shields curve erosion)
- Low density: muddy mixtures with a low τ_{cr}

Erosion tests – main findings

Critical Bed-Shear Stress of Mud–Sand Mixtures

L. C. van Rijn, Dr.Eng.[1]; M. Boechat Albernaz, Ph.D.[2]; L. Perk[3]; A. Colina Alonso, Dr.Eng.[4]; R. J. A. van Weerdenburg[5]; and D. S. van Maren, Ph.D.[6]

Muddy sediment consolidates slowly ➔ remains soft under Wadden Sea conditions

Mixtures consolidate relatively fast because of high permeability & weight ➔ develop strength for conditions in the Wadden Sea

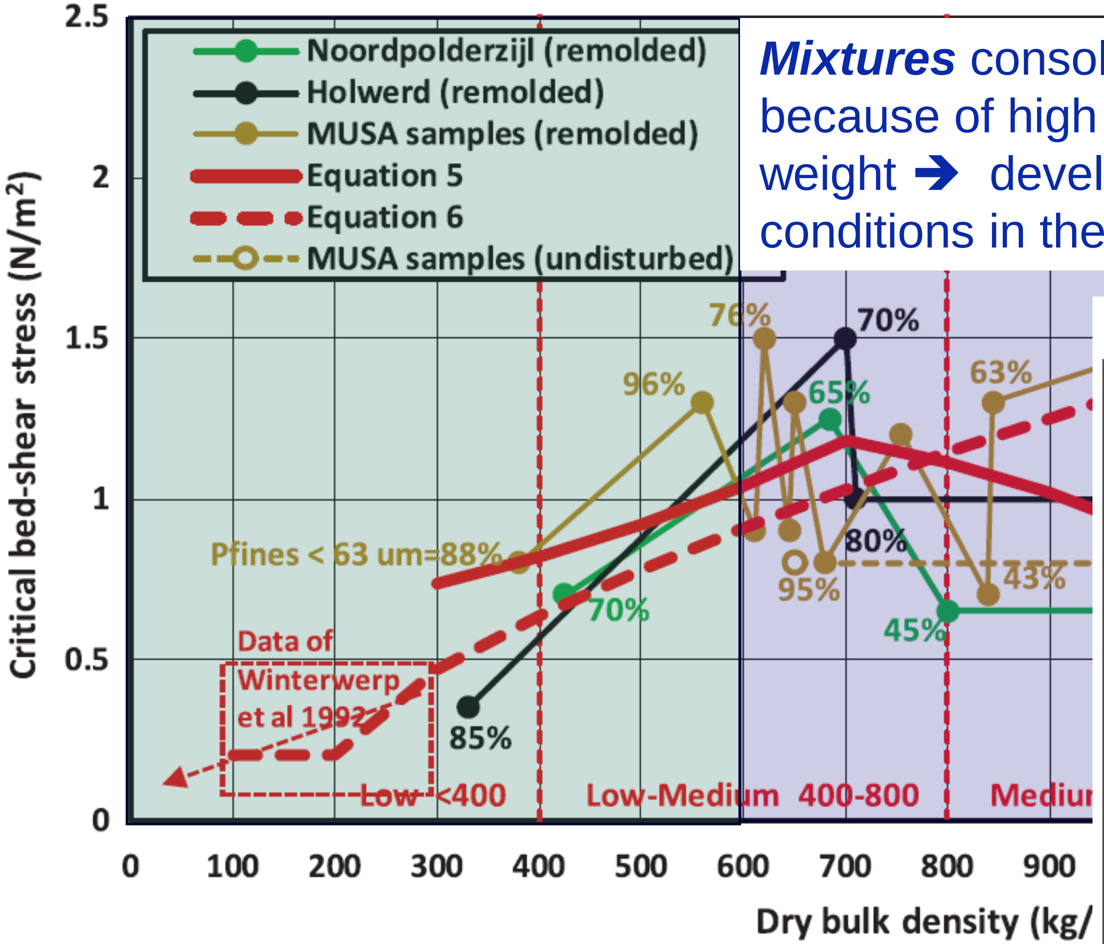

Pure muds do not exist in the exposed Wadden Sea (only depositing in sheltered areas)

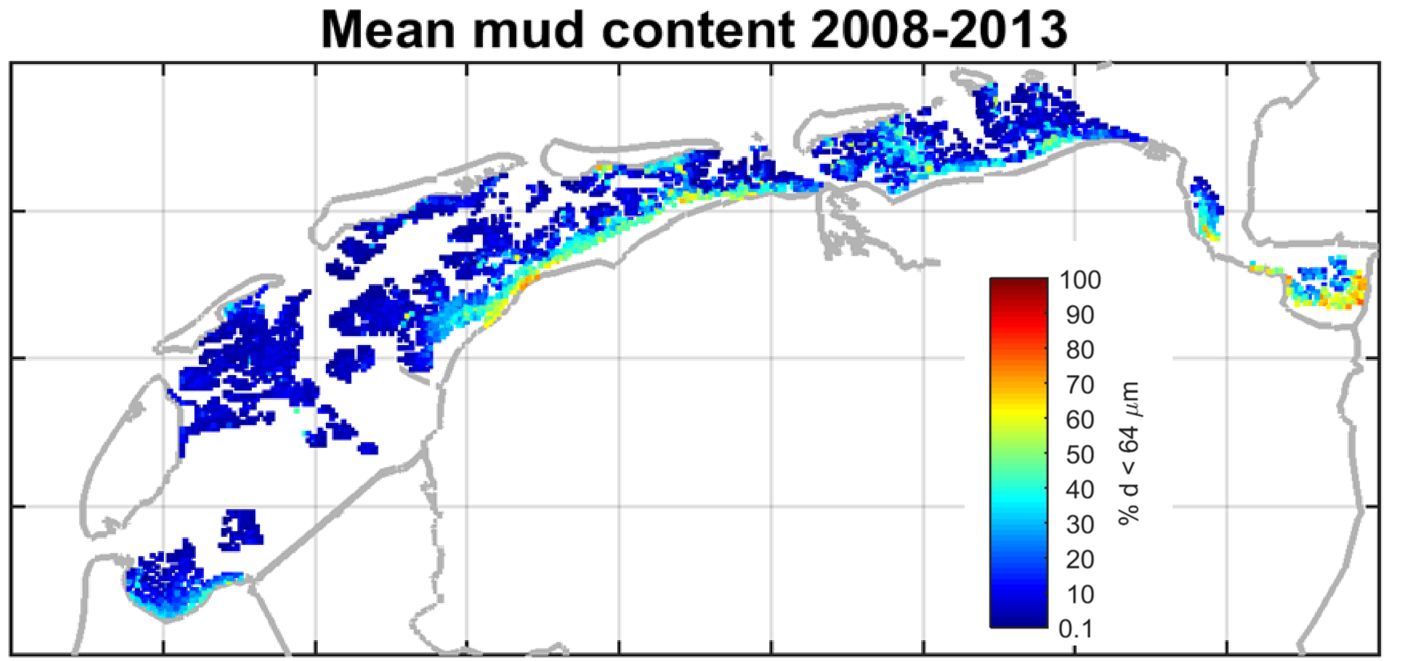

Erosion tests – main findings

- Why not relating directly to mud content? Correlation with density is stronger.

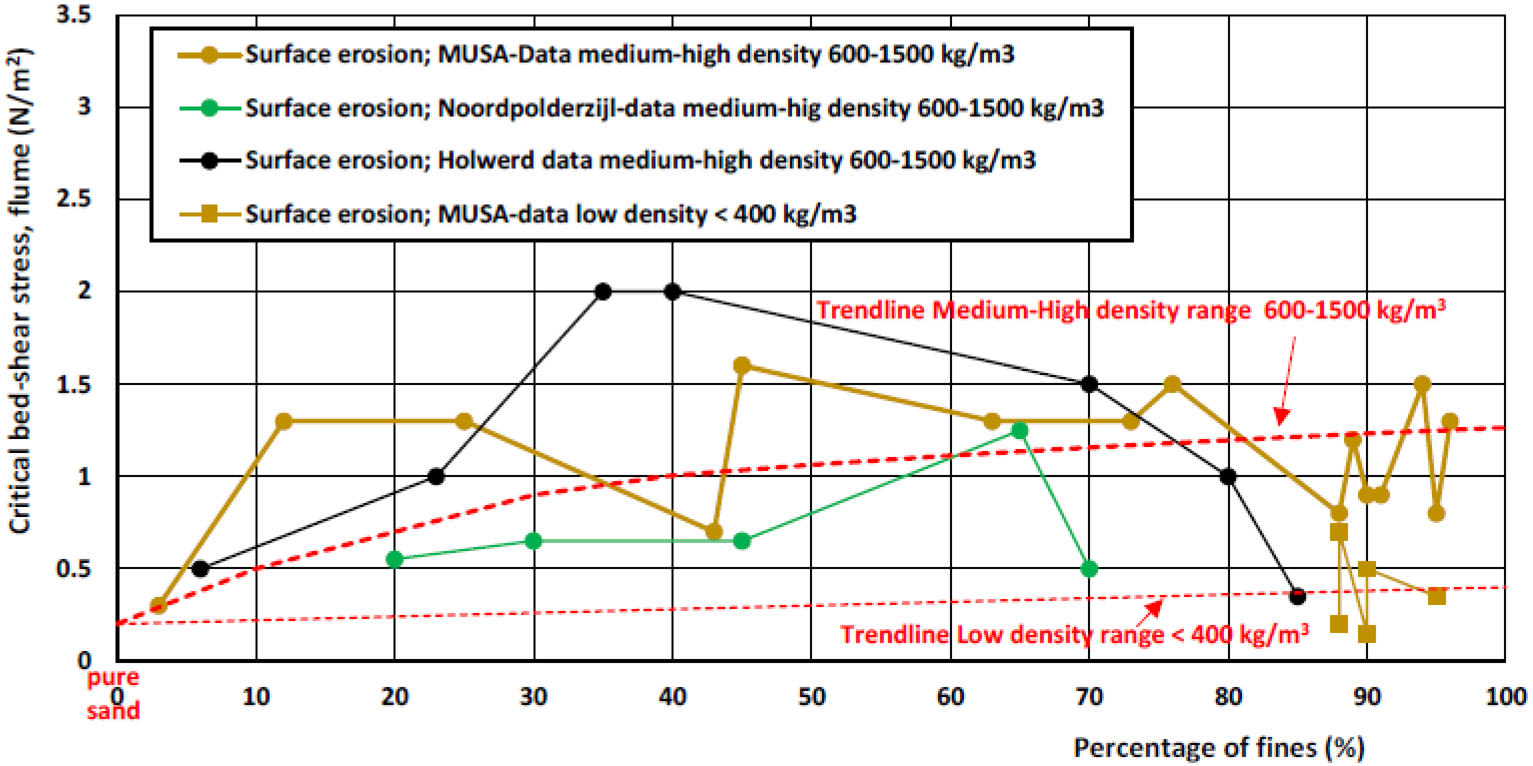

Deltares

Erosion tests – main findings

So what is new?

- Most earlier work focussed on ***maximum*** densities, not ***actual*** densities, of the sand-mud mixtures
- But in dynamic systems with regular resuspension and deposition as fluid mud, muddy mixtures do not have time to consolidate

Mitchener & Torfs, 1996

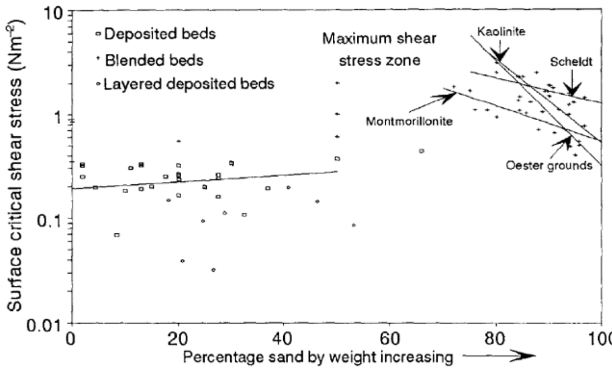

Panagiotopoulos et al., 1997

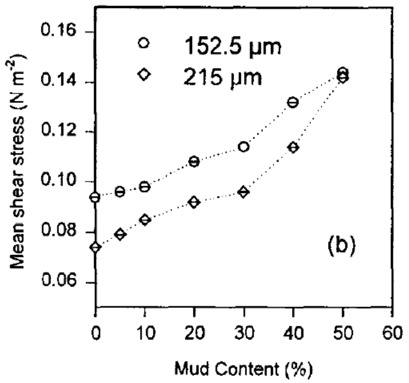

Ye et al., 2011

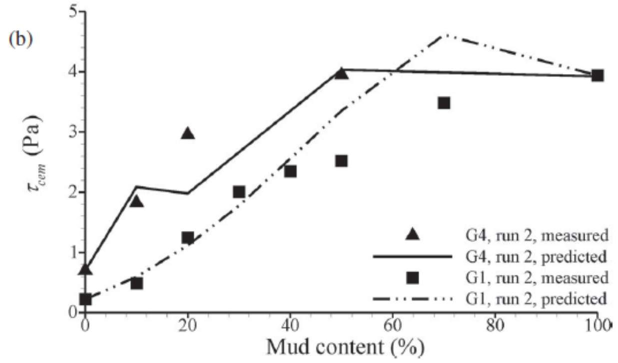

Smith et al., 2015

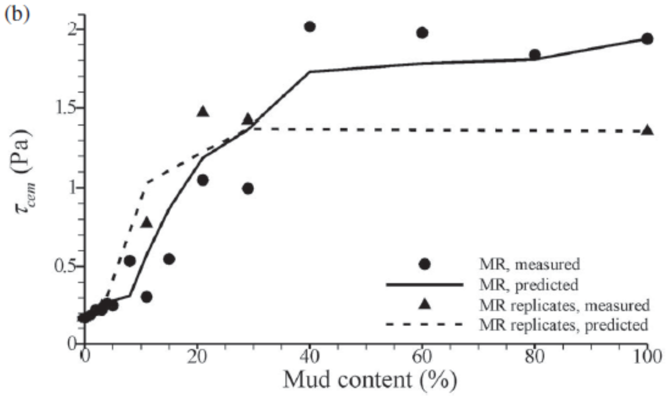

Implementation in Delft3D

- Equation 6 implemented in Delft3D
- Density related to mud content via empirical site-specific relation $\rho_{dry} = 500p_{fines} + 1600p_{sand}$.

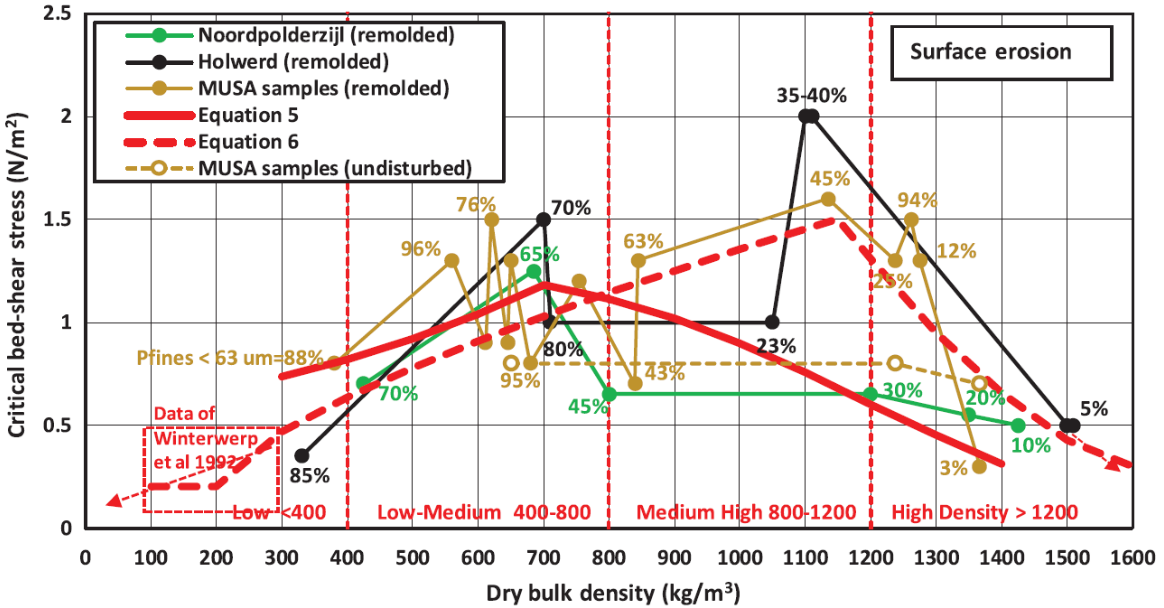

Van Rijn et al., 2024

$$\tau_{cr,\text{fines}} = \tau_{cr,\min 1} + [(\rho_{\text{dry}} - \rho_{dry,\min})/(\rho_{\text{dry},*} - \rho_{dry,\min})]^{\alpha 1}(\tau_{cr,\max} - \tau_{cr,\min 1}) \quad \text{for } \rho_{\text{dry}} < \rho_{\text{dry},*} \qquad (6a)$$

$$\tau_{cr,\text{fines}} = \tau_{cr,\min 2} + [(\rho_{dry,\max} - \rho_{\text{dry}})/(\rho_{dry,\max} - \rho_{\text{dry},*})]^{\alpha 2}(\tau_{cr,\max} - \tau_{cr,\min 2}) \quad \text{for } \rho_{\text{dry}} > \rho_{\text{dry},*} \qquad (6b)$$

Testing with Delft3D

- Schematized tidal basin with uniform initial bathymetry consisting of 95% sand and 5% mud
- Mud and sand prescribed at open boundary conditions
- Model is run for tidal conditions with mild waves for 45 years to generate a typical tidal basin morphology
- Followed by 5 years with more energetic wave conditions

Constant τ_{cr}

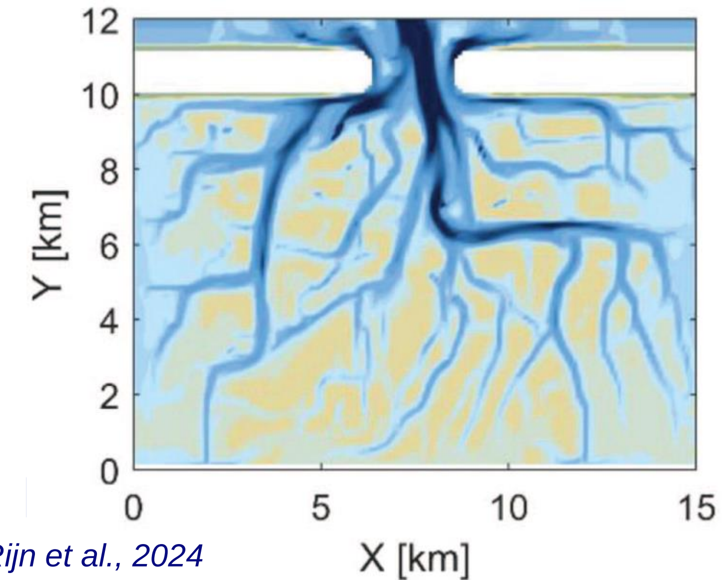

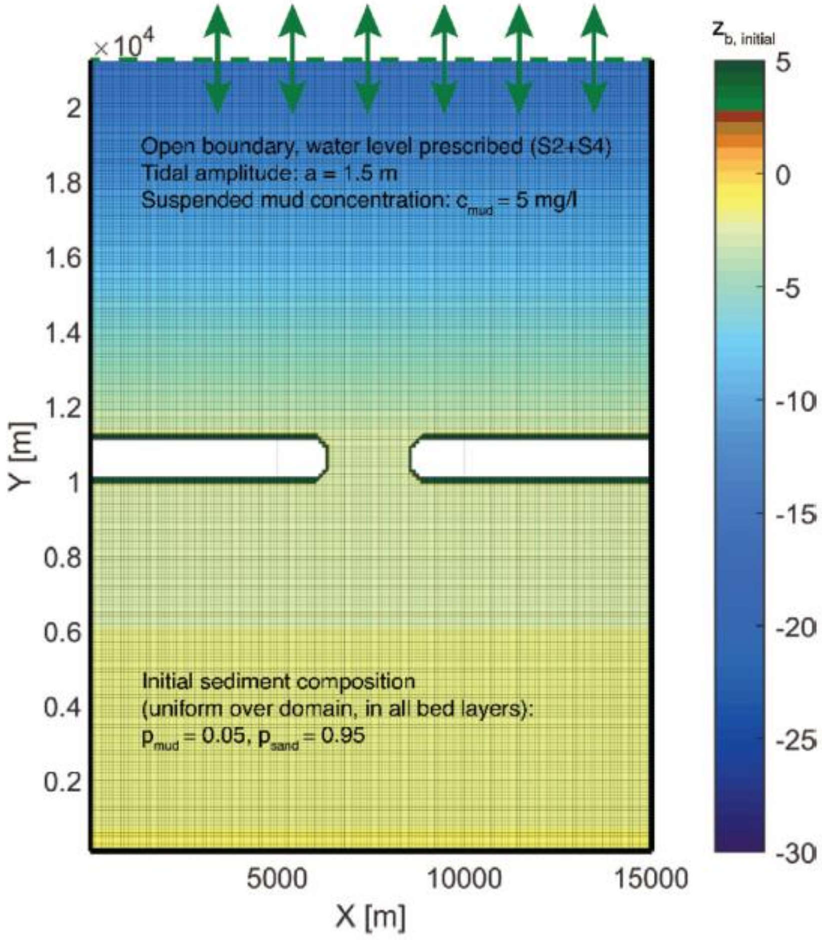

Van Rijn et al., 2024

Testing with Delft3D

- Calm conditions (45 years):
  - marginal effect of a density-depending τ_{cr}

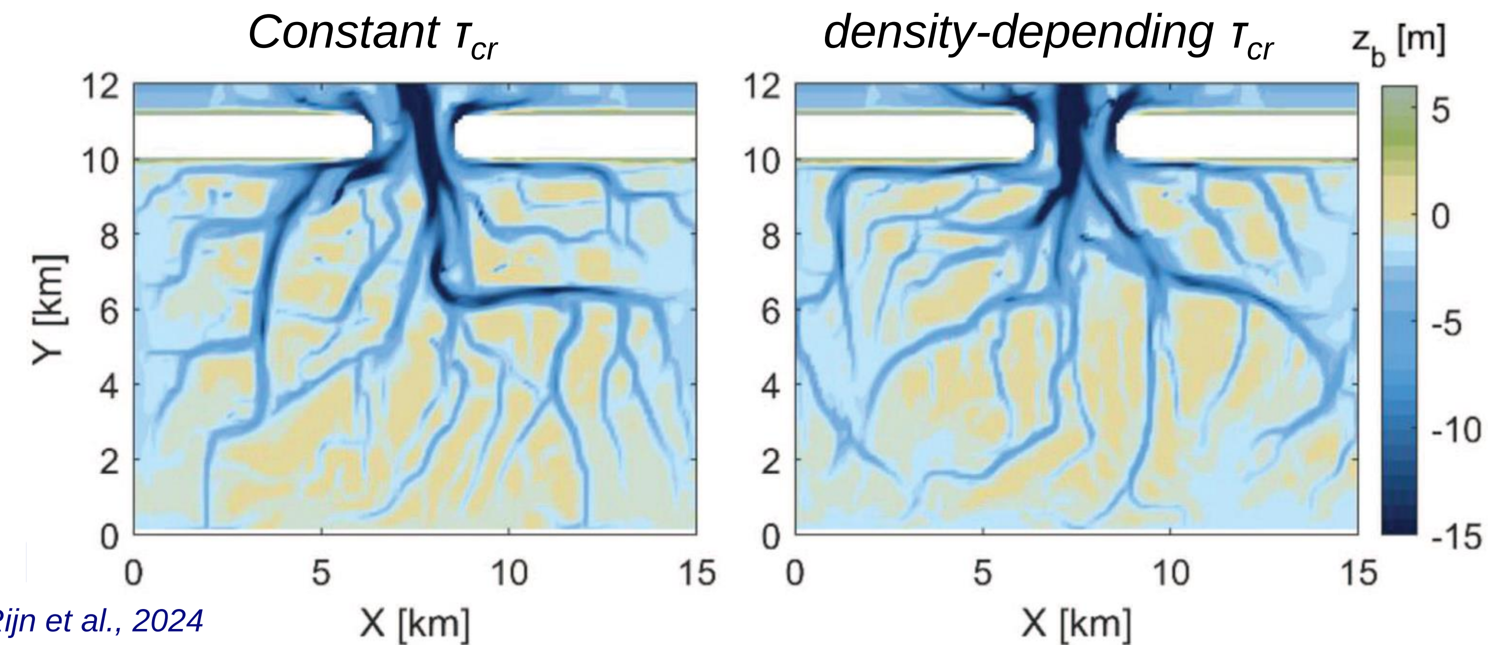

Van Rijn et al., 2024

Testing with Delft3D

- Calm conditions (45 years):
  - marginal effect of a density-depending τ_{cr}
  - Mud deposits on the higher flats

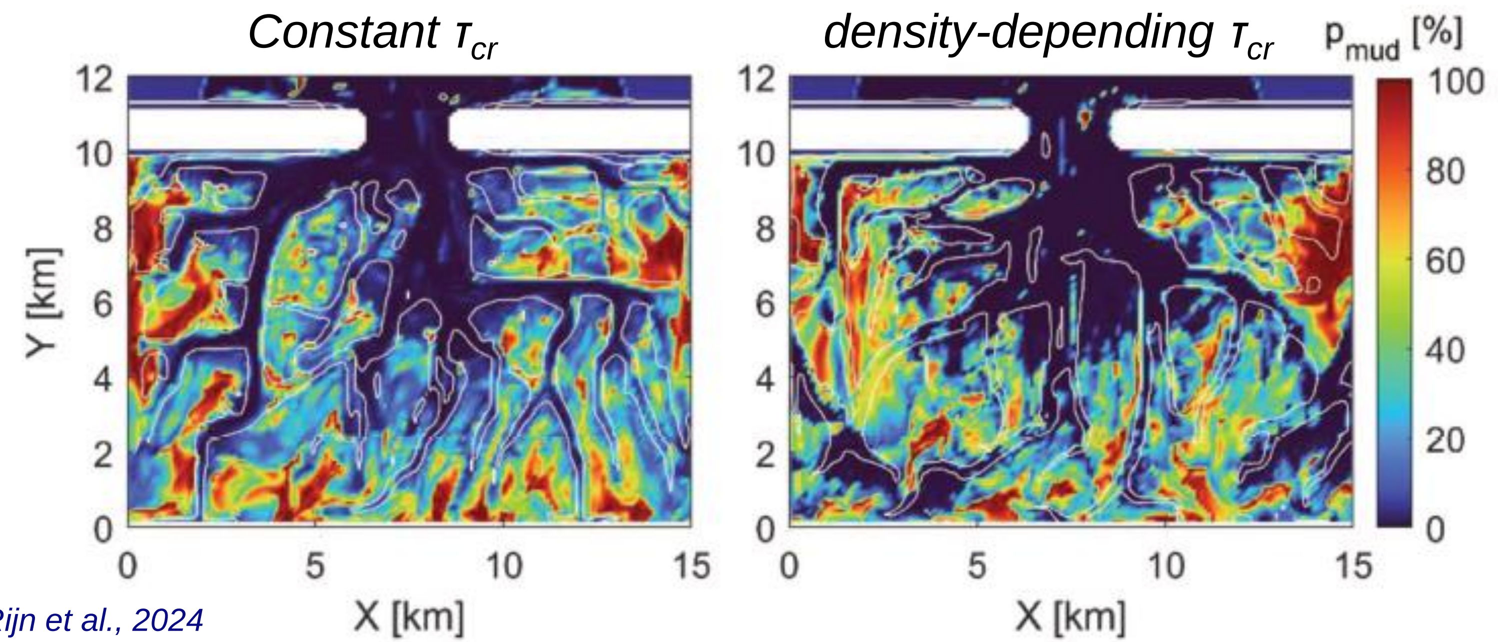

Van Rijn et al., 2024

Testing with Delft3D

A simple parameterization for a complex process:
- Tides bring sediment to the flats
- Muddy sediments consolidate and gain strength to withstand erosion
- But then… without a complex consolidation model
- And including sand-mud

- Calm conditions (45 years):
  - marginal effect of a density-depending τ_{cr}
  - Mud deposits on the higher flats
- Storm conditions (5 years)
  - For constant τ_{cr}, a large amount of mud deposited during calm conditions is eroded
  - For density-depending τ_{cr}, the mud largely remains on the flats

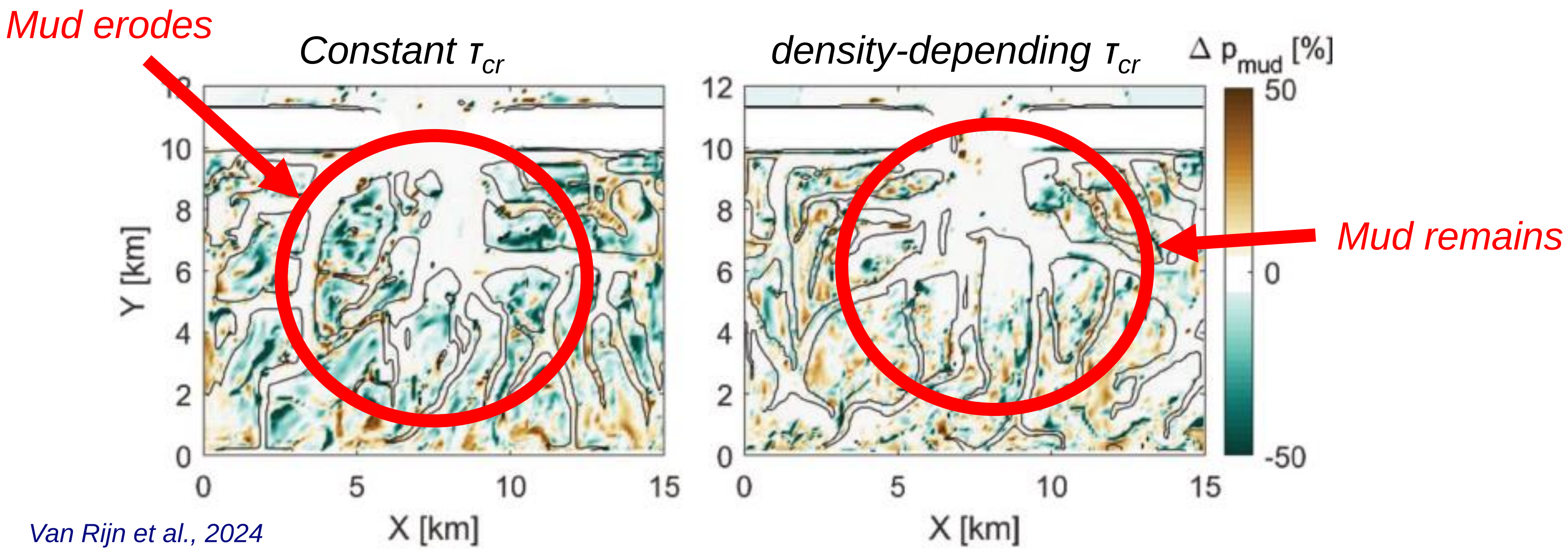

Van Rijn et al., 2024

Drying of intertidal flats

Colisomo et al., 2023

- Detailed observations of erosion during storm conditions on muddy, fringing flats along the Wadden Sea
- Four frames equiped with ADV (velocity & bed level), SSC, pressure. Converted to bed level change (BLC) & bed shear stress τ_b

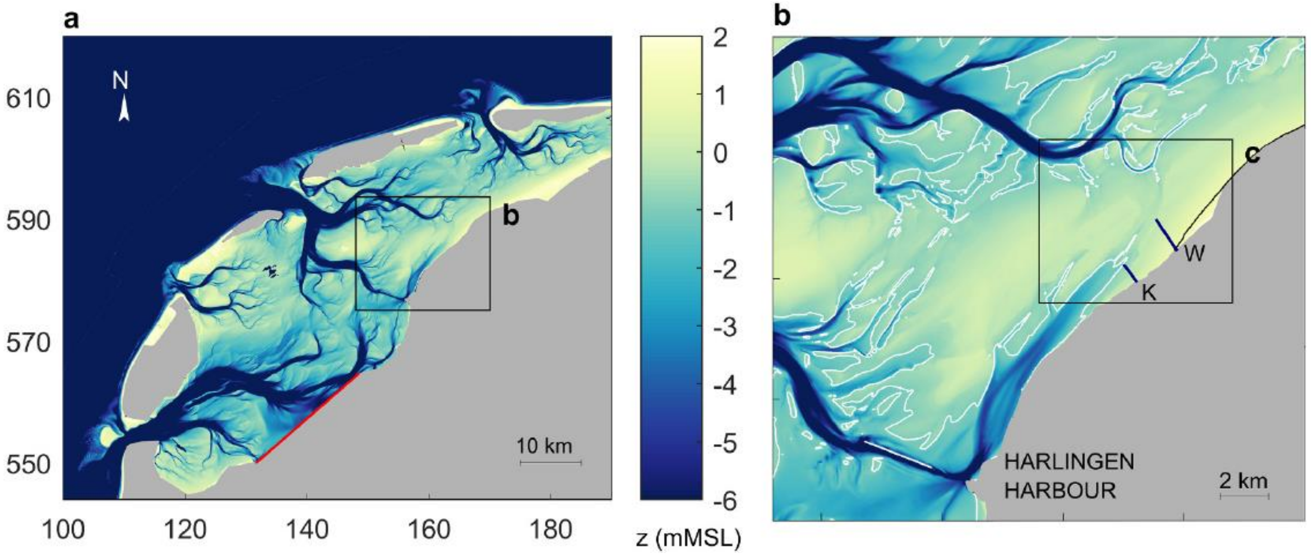

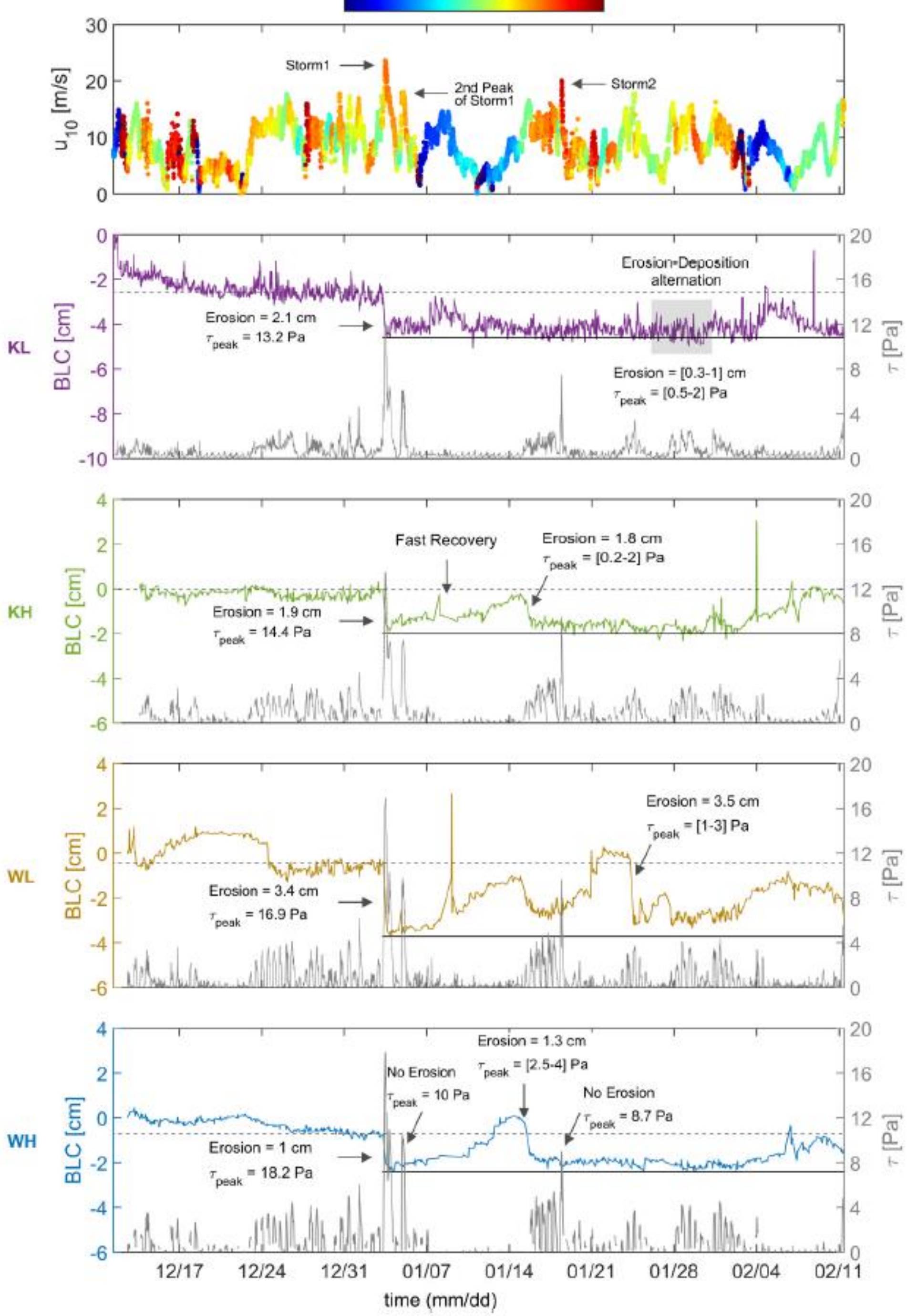

Colisomo et al., 2023

Drying of intertidal flats

- Detailed observations of erosion during storm conditions on muddy, fringing flats along the Wadden Sea
- Four frames equiped with ADV (velocity & bed level), SSC, pressure. Converted to bed level change (BLC) & bed shear stress τ_b

τ_b remains 4 Pa but no more erosion

Event 1: τ_b = 4 Pa; erosion of 1.5 cm

Event 2: τ_b = 17 Pa; erosion of 3 cm

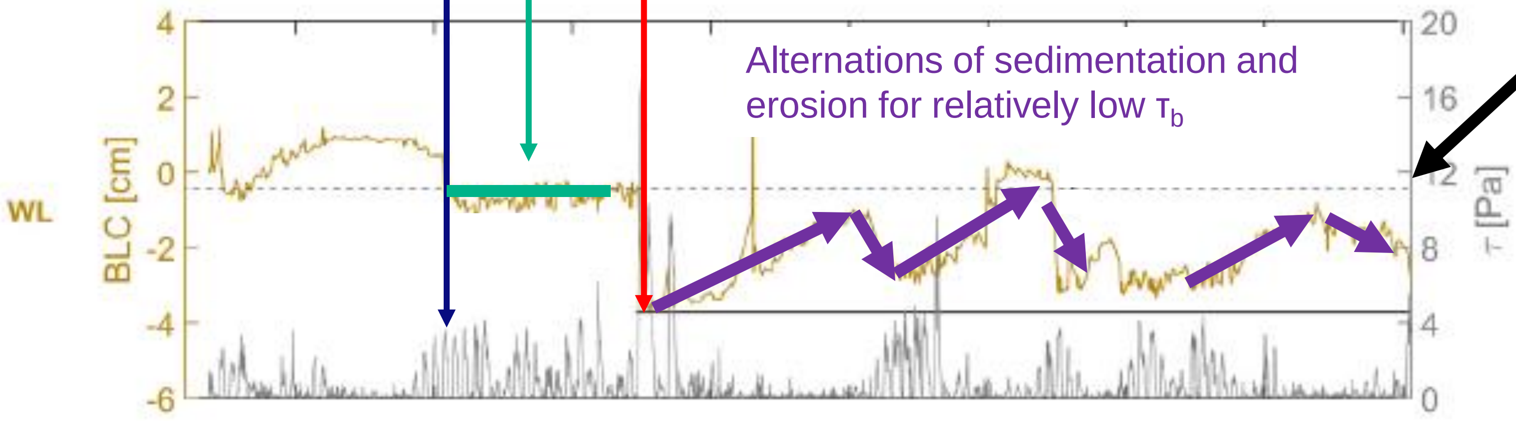

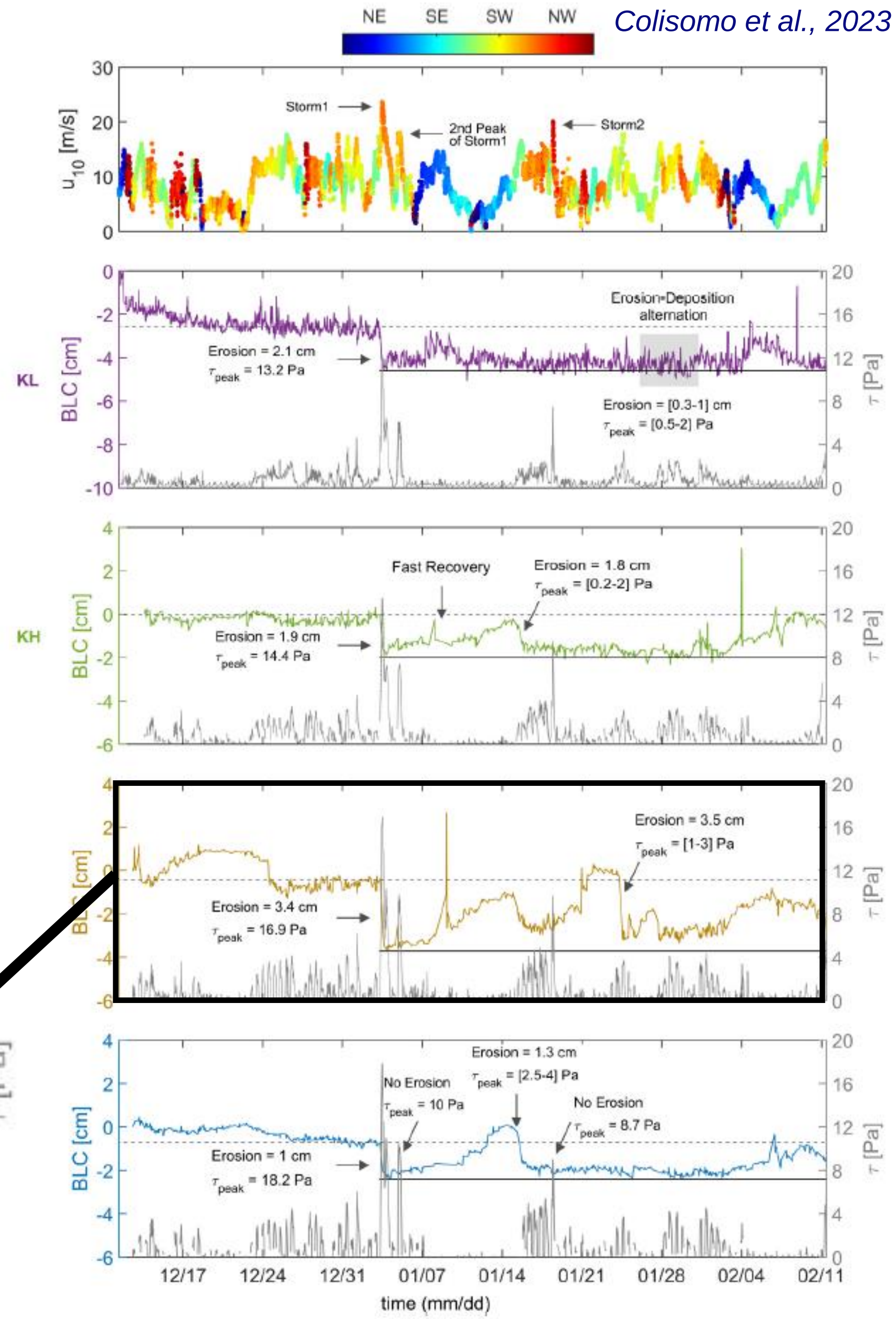

Drying of intertidal flats

Colisomo et al., 2023

- Critical bed shear stress increases with depth to values of several Pa.
- Eroded sediment is quickly replaced by new sediment
- But: this sediment has low resistance to erosion and is washed away at every new cycle with moderate wave energy (every 1-2 weeks in winter)
- ***What are conditions that the bed gains sufficient strength to withstand erosion? ➔ drying of intertidal flats***

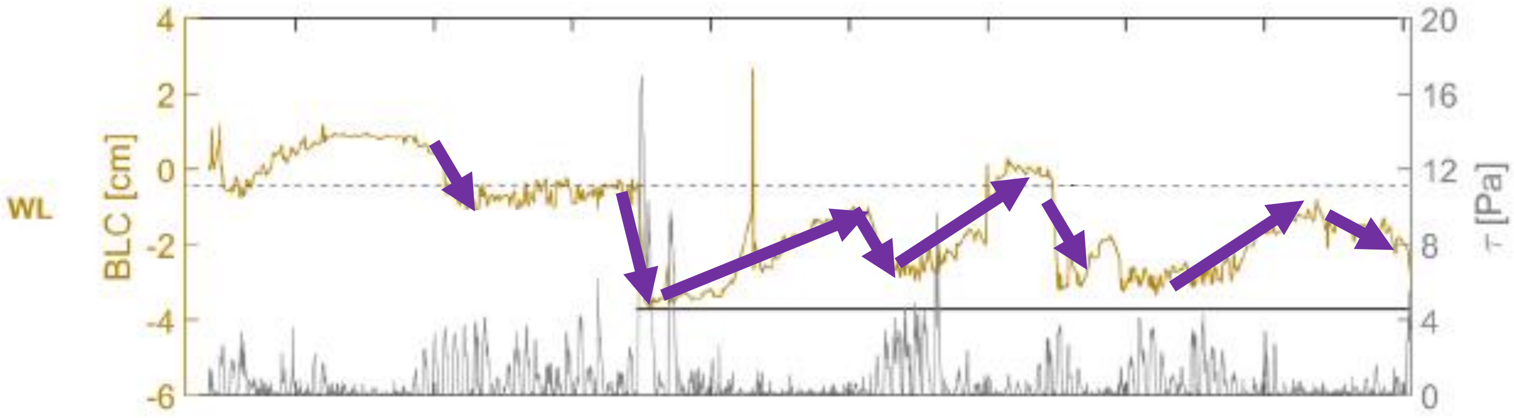

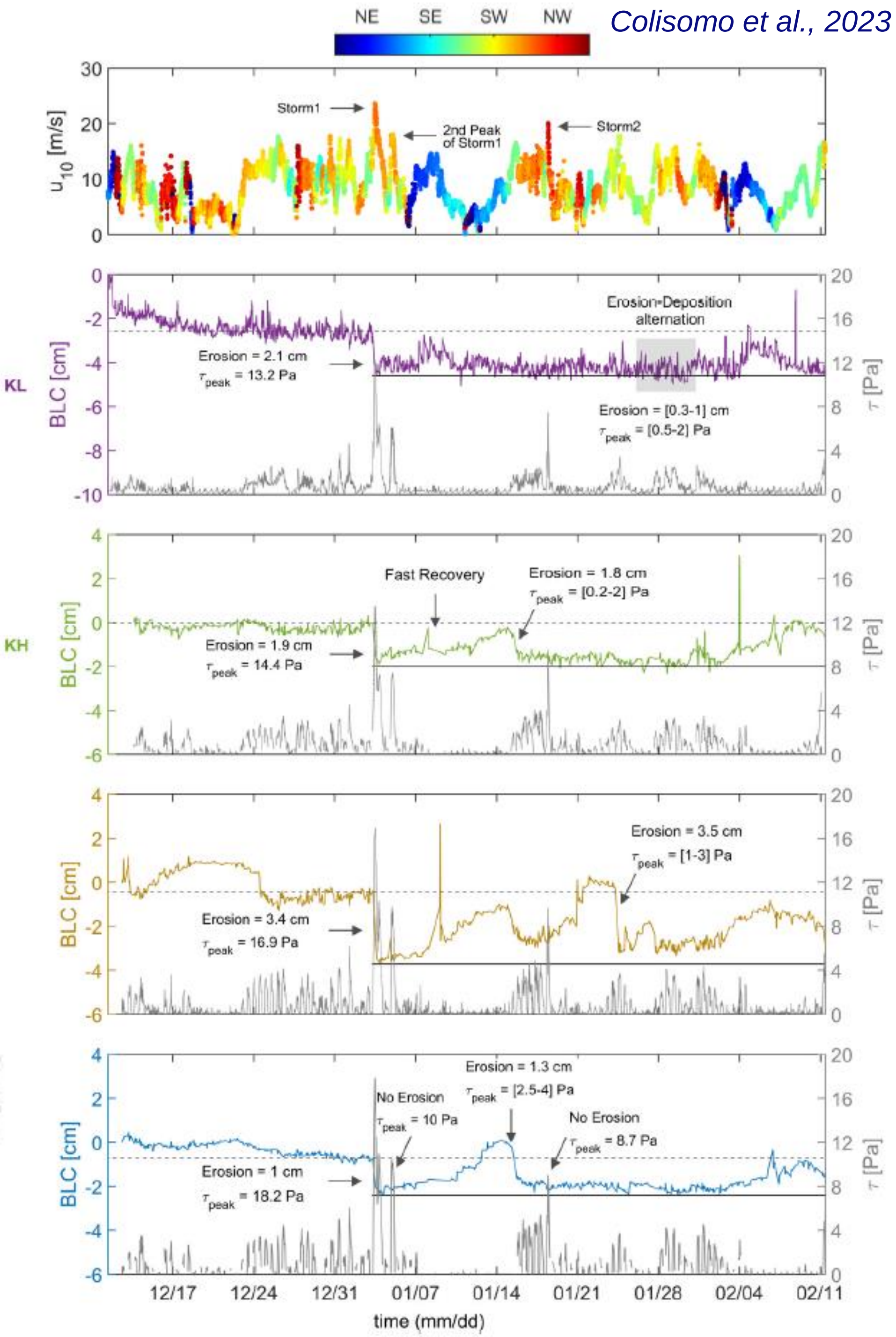

Drying of intertidal flats

- Key to gaining strength against energetic conditions is emergence of tidal flats
  - Negative pore pressures
  - Drying
- In the Wadden Sea, emergence is strongly regulated by wind effects
- The upper intertidal remains dry multiple tidal cycles during periods with wind-induced setdown

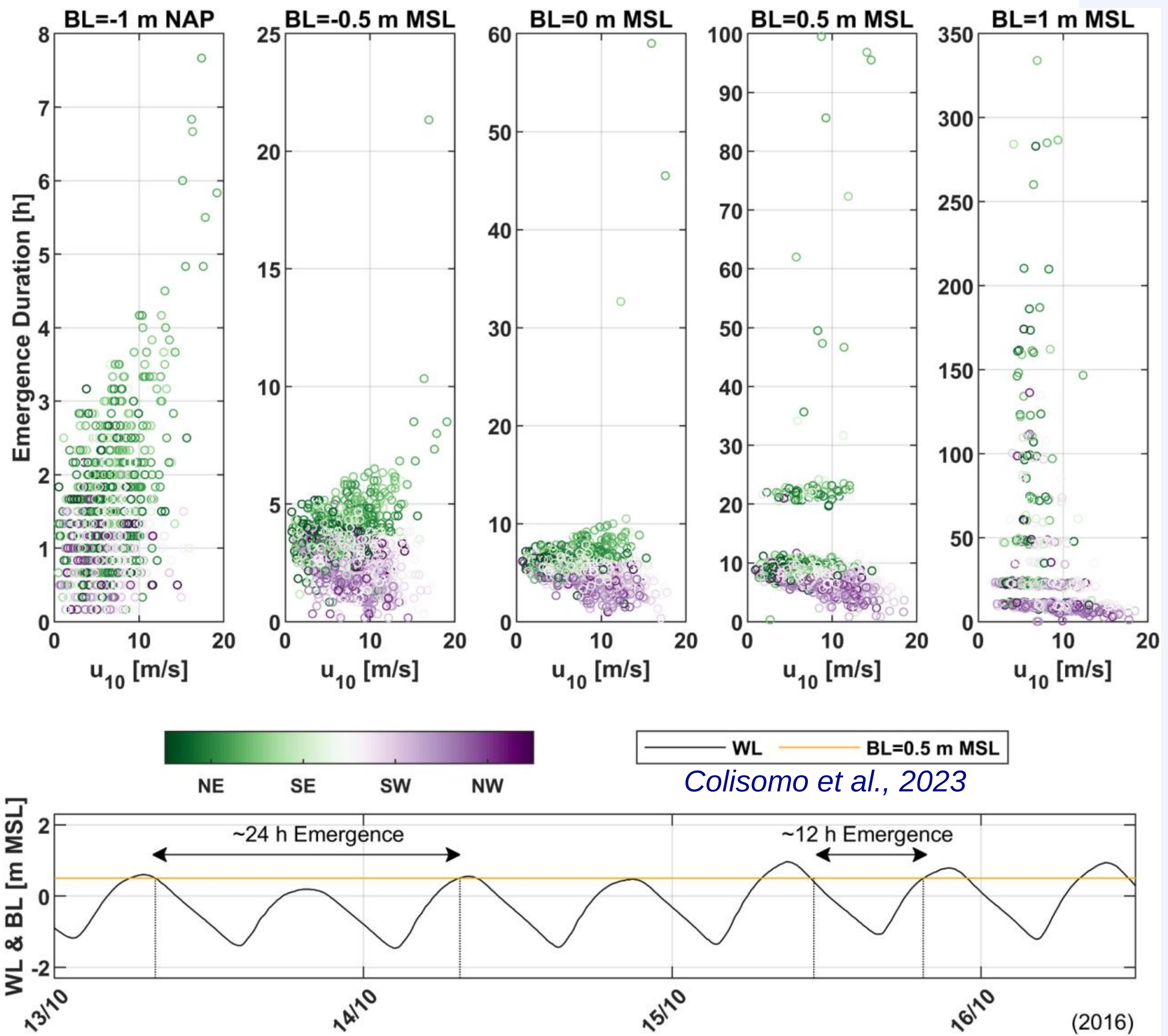

Colisomo et al., 2023

ELSEVIER

Contents lists available at ScienceDirect

Geomorphology

journal homepage: www.journals.elsevier.com/geomorphology

Winds of opportunity: The effects of wind on intertidal flat accretion

Irene Colosimo [a], Dirk Sebastiaan van Maren [a,b,c,*], Paul Lodewijk Maria de Vet [a,c], Johan Christiaan Winterwerp [a], Bram Christiaan van Prooijen [a]

Drying of intertidal flats

Continental Shelf Research 245 (2022) 104802

Contents lists available at ScienceDirect

Continental Shelf Research

journal homepage: www.elsevier.com/locate/csr

ELSEVIER

Modeling the effects of aerial temperature and exposure period on intertidal mudflat profiles

Hieu M. Nguyen[a,*], Karin R. Bryan[a,b], Zeng Zhou[c,**], Conrad A. Pilditch[a]

Modelling effect of drying on erodibility

1. Empirical model of Nguyen et al. (2022)

- τ_{cr} (and M) as a function of
  - Chlorofyll content
  - Exposure duration
  - Air temperature

- Implemented in the BMI environment of Delft3D-FM

$$E = M\frac{(\tau_b - \tau_{cr})}{\tau_{cr}}$$

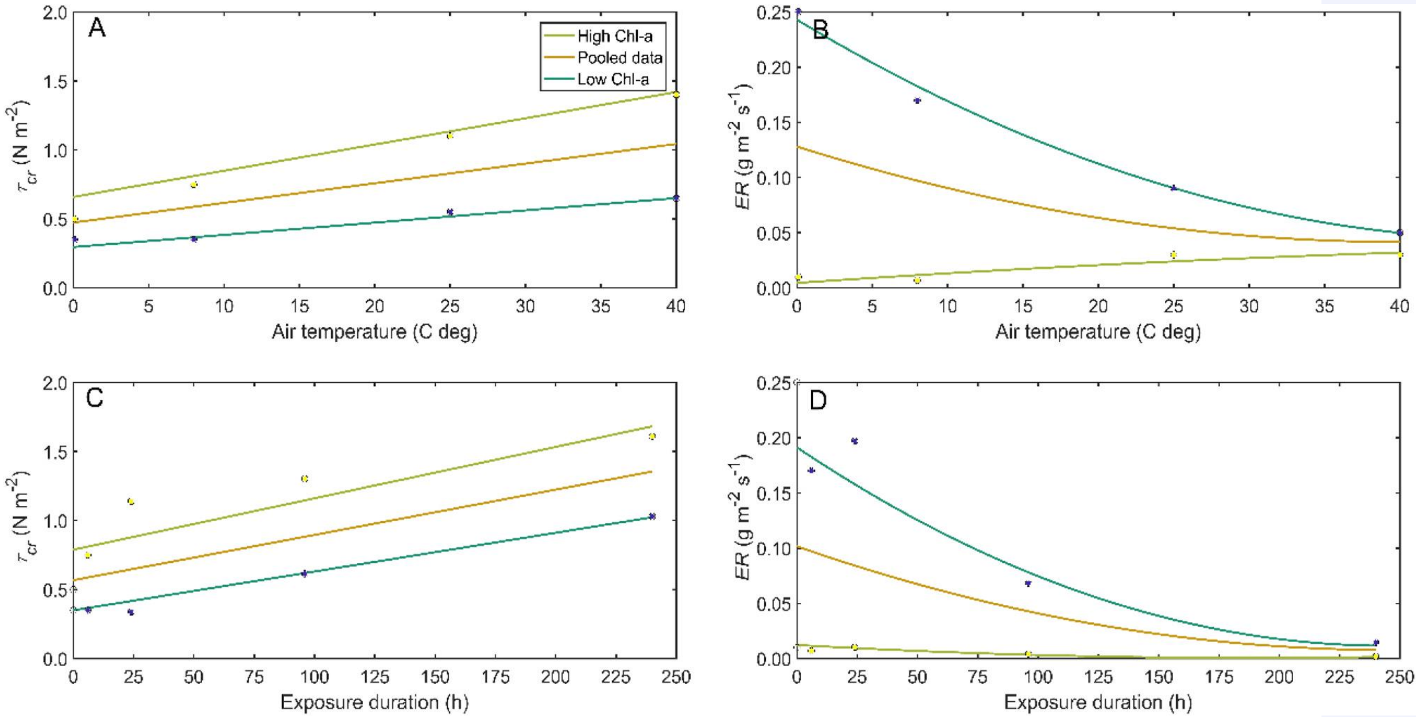

Drying of intertidal flats


Continental Shelf Research 245 (2022) 104802

Contents lists available at ScienceDirect

Continental Shelf Research

journal homepage: www.elsevier.com/locate/csr

ELSEVIER

Check for updates

Modeling the effects of aerial temperature and exposure period on intertidal mudflat profiles

Hieu M. Nguyen[a,*], Karin R. Bryan[a,b], Zeng Zhou[c,**], Conrad A. Pilditch[a]

Modelling effect of drying on erodibility

1. Empirical model of Nguyen et al. (2022)

- τ_{cr} (and M) as a function of
  - Chlorofyll content
  - Exposure duration
  - Air temperature

- Implemented in the BMI environment of Delft3D-FM
- First experiences… this method has some intrinsic instabilities

High elevation ➔ more evaporation➔ high τ_{cr} ➔ deposition

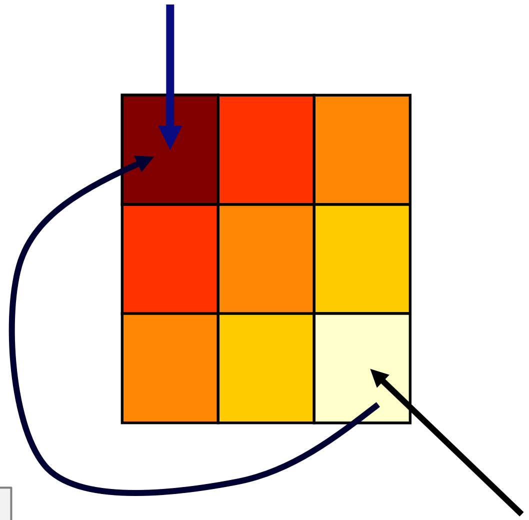

Low elevation ➔ less evaporation➔ low τ_{cr} ➔ easily eroded

Sediment settles on nearby high point with high τ_{cr} ➔ erosion

Relationships tends to enlarge existing topographic differences in the intertidal zone

Deltares

Drying of intertidal flats - modelling

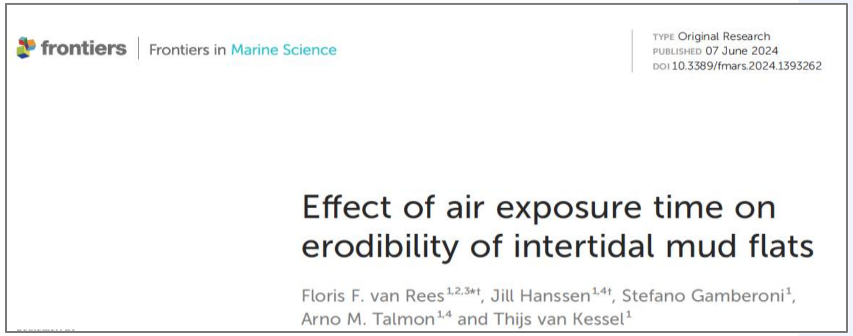
frontiers | Frontiers in Marine Science

TYPE Original Research
PUBLISHED 07 June 2024
DOI 10.3389/fmars.2024.1393262

Effect of air exposure time on erodibility of intertidal mud flats

Floris F. van Rees[1,2,3*†], Jill Hanssen[1,4†], Stefano Gamberoni[1], Arno M. Talmon[1,4] and Thijs van Kessel[1]

Modelling effect of drying on erodibility

1. Empirical model of Nguyen et al. (2022)
2. Darcy-based model of van Rees at al. (2024), for mixtures with mud content >30%

$$E = M\frac{(\tau_b - \tau_{cr})}{\tau_{cr}}$$

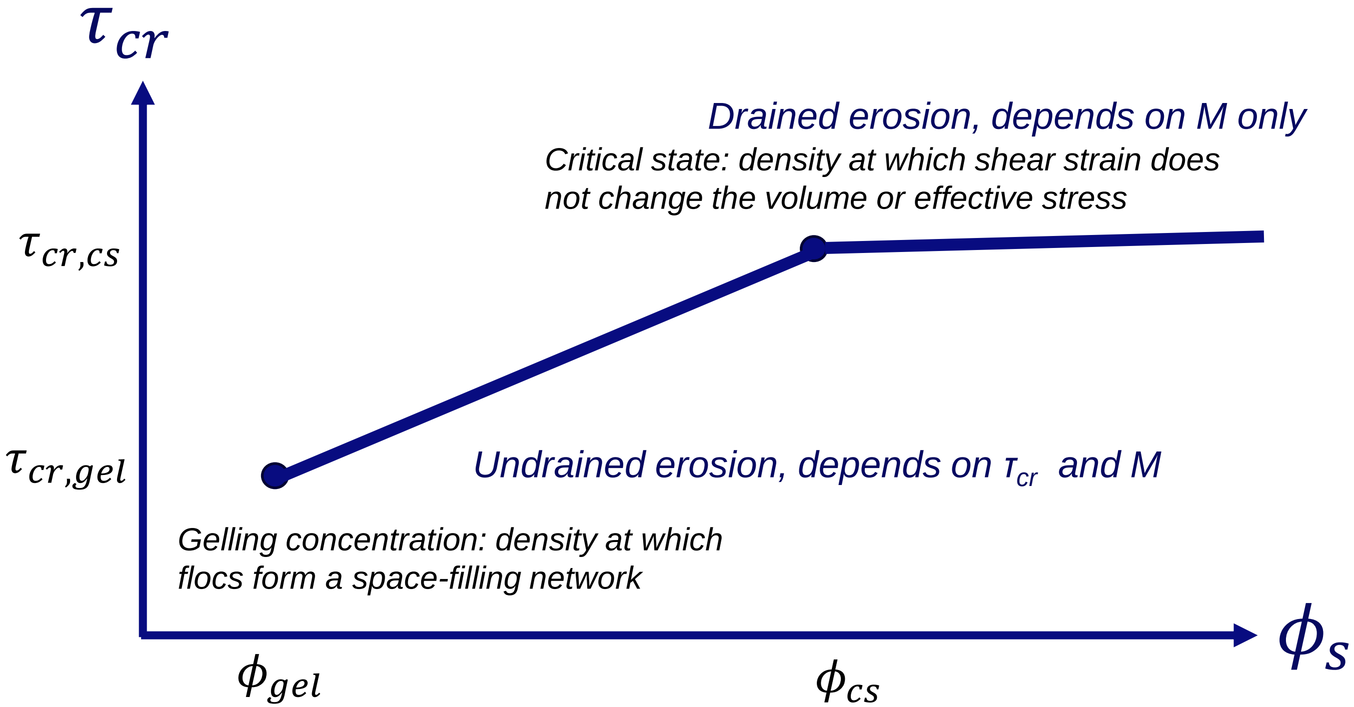

Deltares

Drying of intertidal flats - modelling

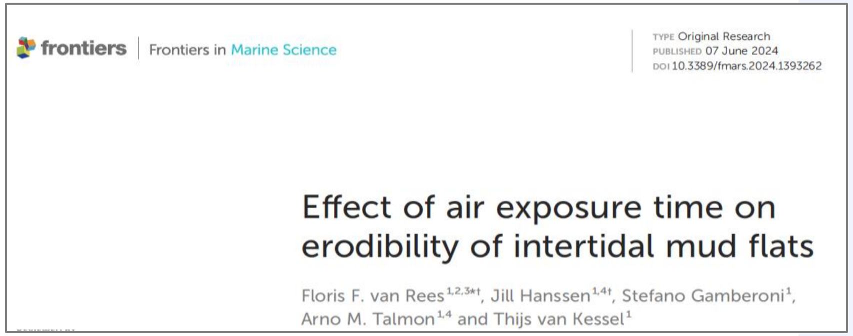
frontiers | Frontiers in Marine Science

TYPE Original Research
PUBLISHED 07 June 2024
DOI 10.3389/fmars.2024.1393262

Effect of air exposure time on erodibility of intertidal mud flats

Floris F. van Rees[1,2,3*†], Jill Hanssen[1,4†], Stefano Gamberoni[1], Arno M. Talmon[1,4] and Thijs van Kessel[1]

Modelling effect of drying on erodibility

1. Empirical model of Nguyen et al. (2022)
2. Darcy-based model of van Rees at al. (2024), for mixtures with mud content >30%

$$E = M\frac{(\tau_b - \tau_{cr})}{\tau_{cr}}$$

ϕ_{cs} computed with a Darcy model including evaporation

Input parameters for M and τ_{cr} derived from sediment properties (lab analyses)

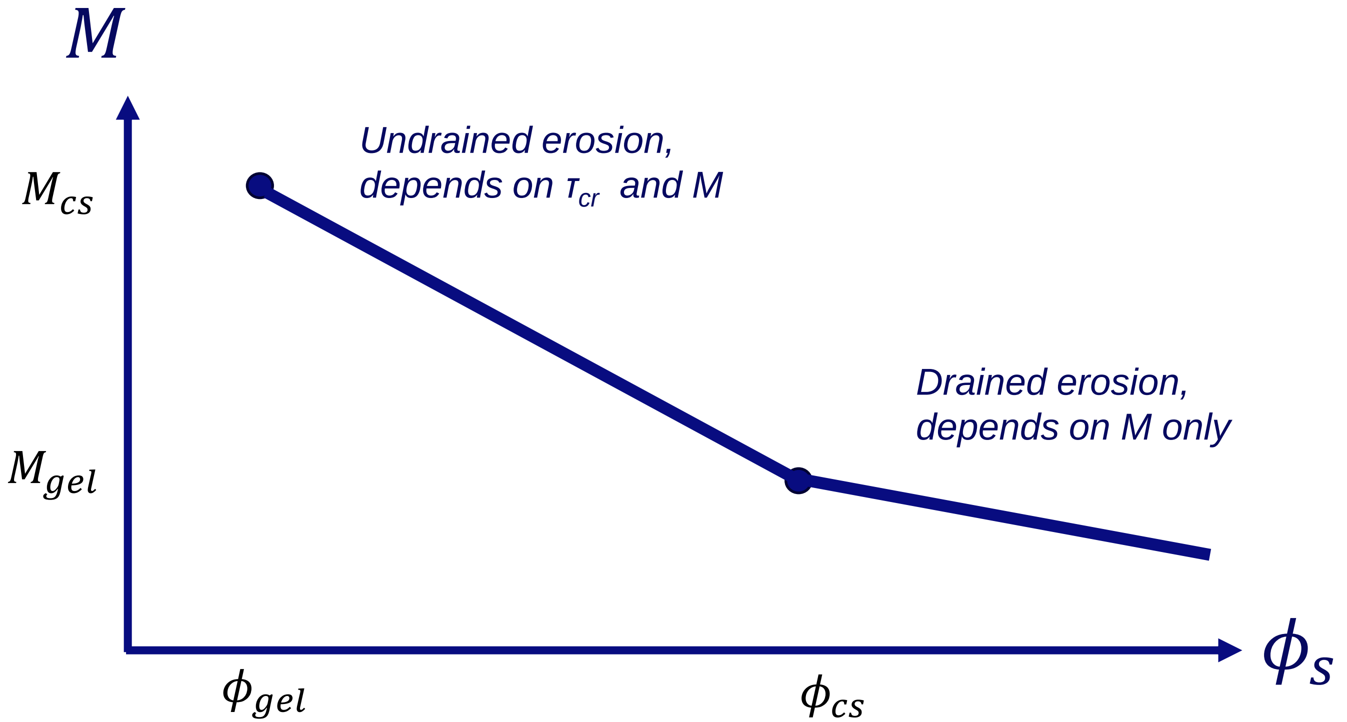

Drying of intertidal flats - modelling

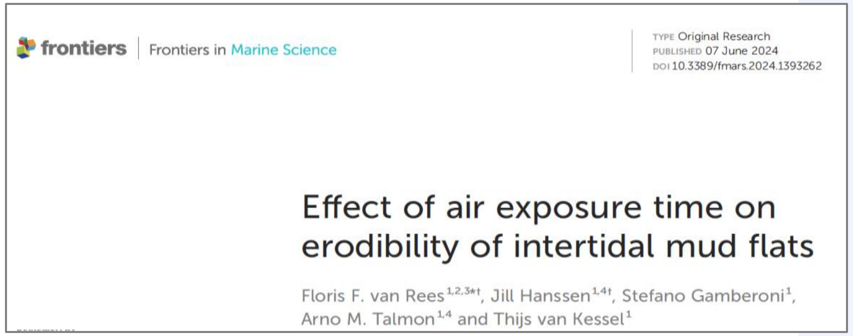

Modelling effect of drying on erodibility

1. Empirical model of Nguyen et al. (2022)
2. Darcy-based model of van Rees at al. (2024), for mixtures with mud content >30%

ϕ_{cs} computed with a Darcy model including evaporation

Input parameters for *M* and τ_{cr} derived from sediment properties (lab analyses)

1DV model & Delft3D-Delwaq implementation (ongoing work)

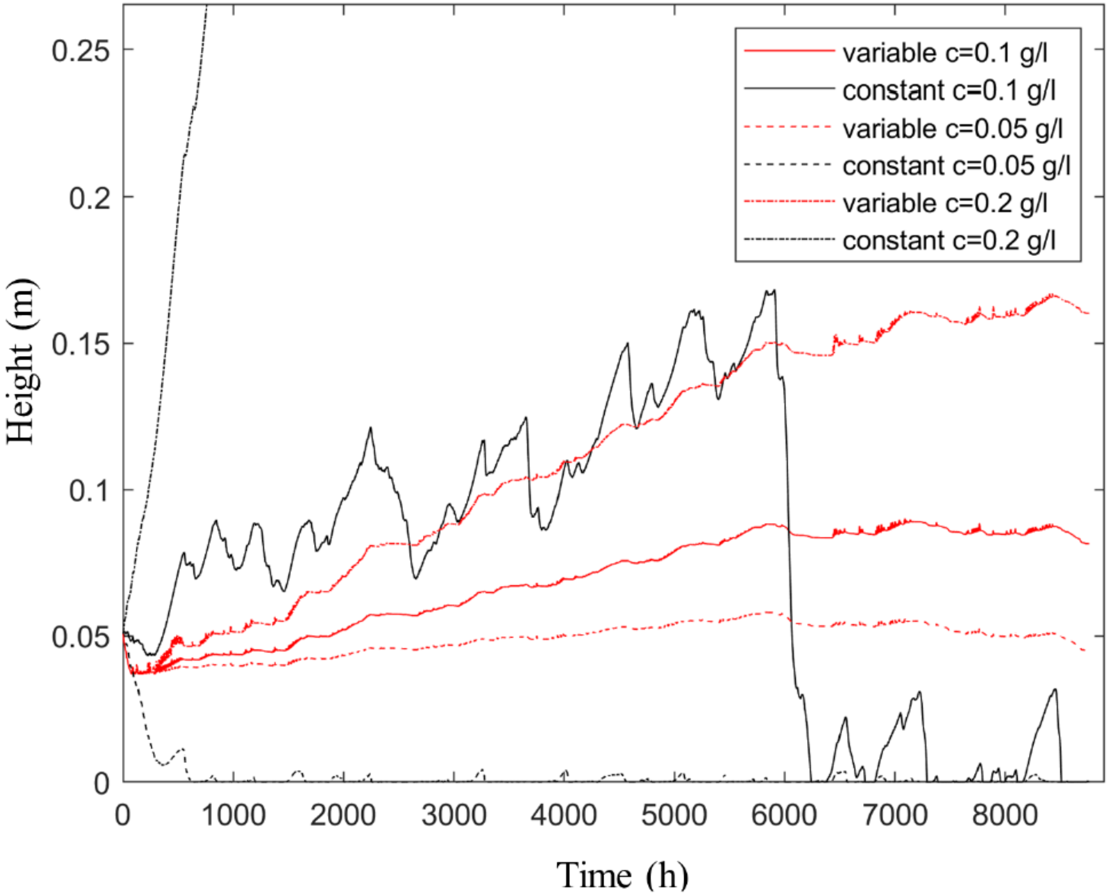

Deltares

Main takeaways

- Erosion of sand-mud mixtures depends more strongly on density than on mud content
- In wave-influenced environments very muddy mixtures are easily erodible because they consolidate slowly (and therefore do not exist in the Wadden Sea)
- Sand-mud mixtures especially gain resistance against erosion during dry periods

- We have some new modelling tools accounting for these effects….

Deltares

“Breaching of earthen embankments: from small-scale laboratory experiments to field measurements using photogrammetry”

(Sandra Soares-Frazão, UCLOUVAIN)

Breaching of earthen embankments
From small-scale laboratory experiments to field measurements using photogrammetry

Sandra Soares-Frazão
Masoumeh Ebrahimi, Nathan Delpierre, Jiangtao Yang

Outline

- Dikes, embankments, levees
- Failure modes
- What information do we need ?
- Laboratory experiments
- Field tests

Earth dams

Banasura Sagar Dam, India

Embankment dam at Diamond Valley Lake, an off-stream reservoir in Riverside County, California

River dikes

Paved bike path on top of earthen dike levee along Mississippi River in Louisiana

Sea dikes and dunes

Sea-dike in Westkapelle, the Netherlands

Dunes in Belgium

These structures can fail…

Teton dam, USA, 1976

These structures can fail…

Steinbach-dam
Germany
July 2021

These structures can fail…

Tous dam, Spain
1982

These structures can fail…

The 17th Street Canal, New Orleans, 2005

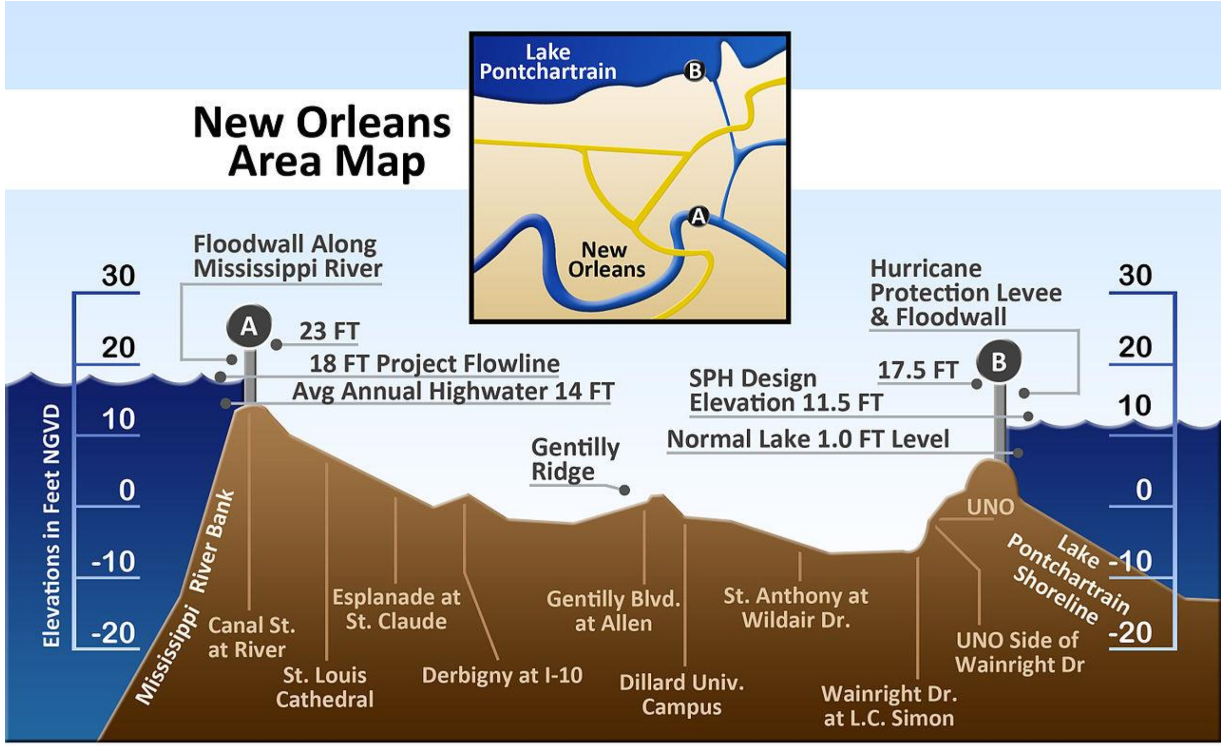

City of New Orleans Ground Elevations
From Canal St. at the Mississippi River to the Lakefront at U.N.O.

These structures can fail…

Baige landslide dam, Jinsha River, China, 2018

Failure modes

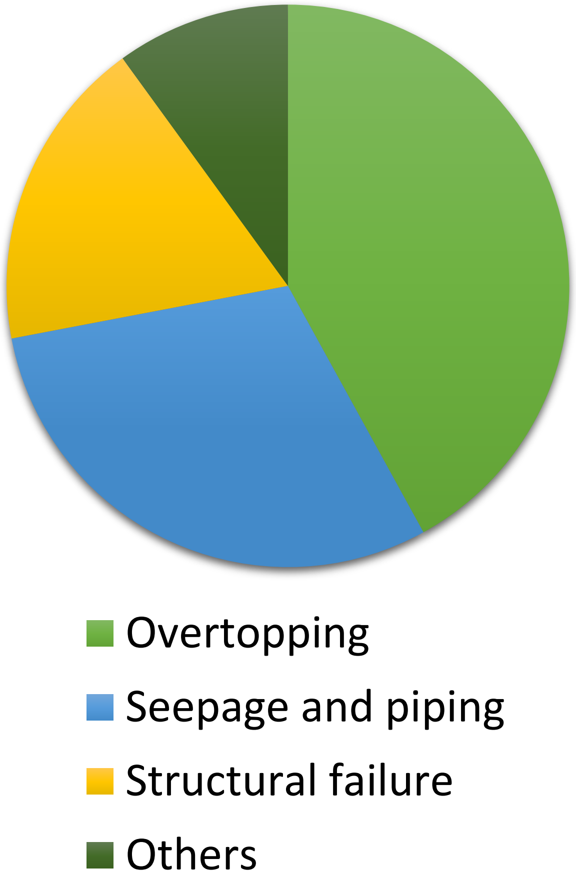

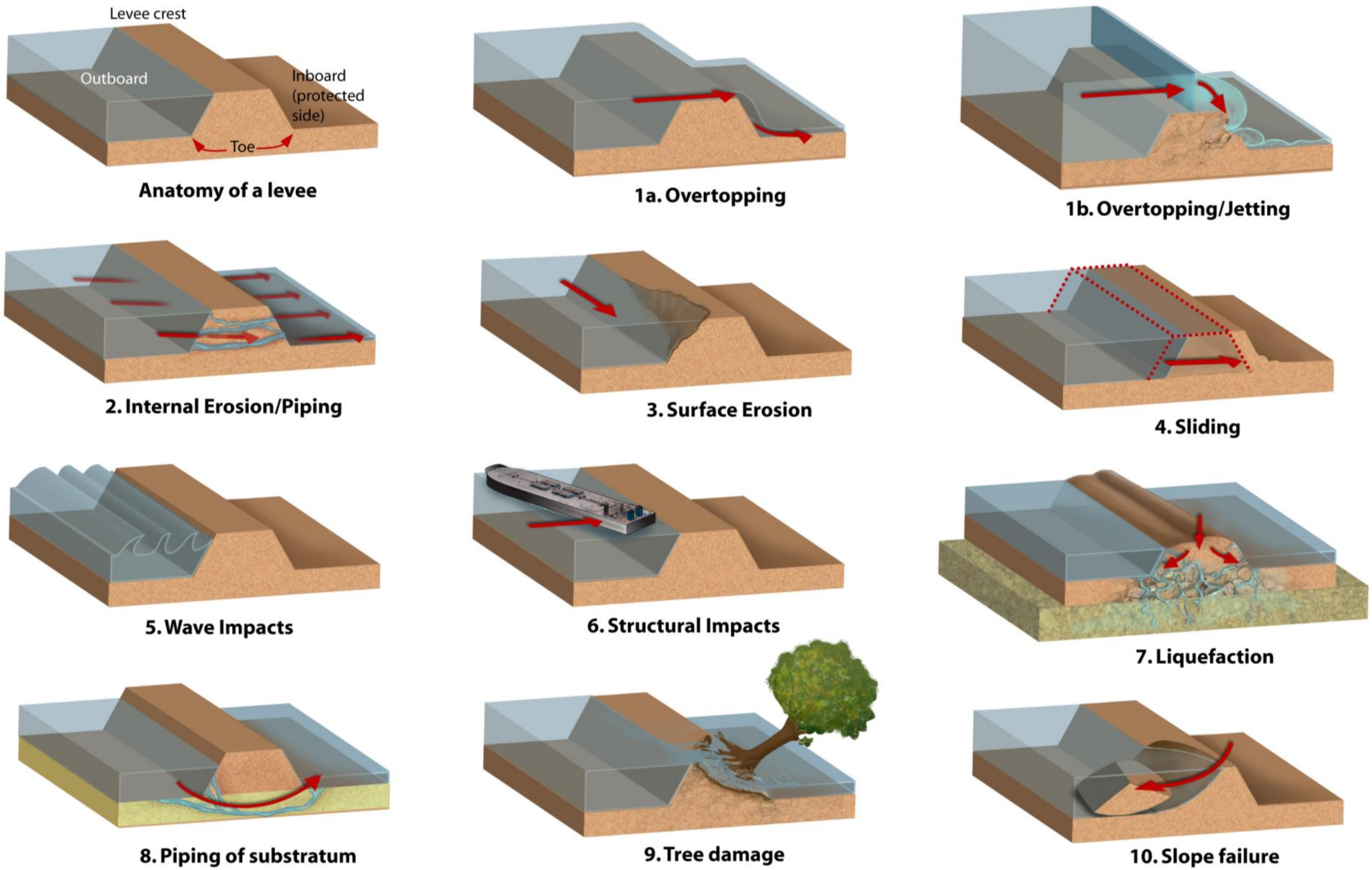

Overtopping

- Non-cohesive: progressive, surface erosion
- Cohesive: mass failure, steep bank slopes

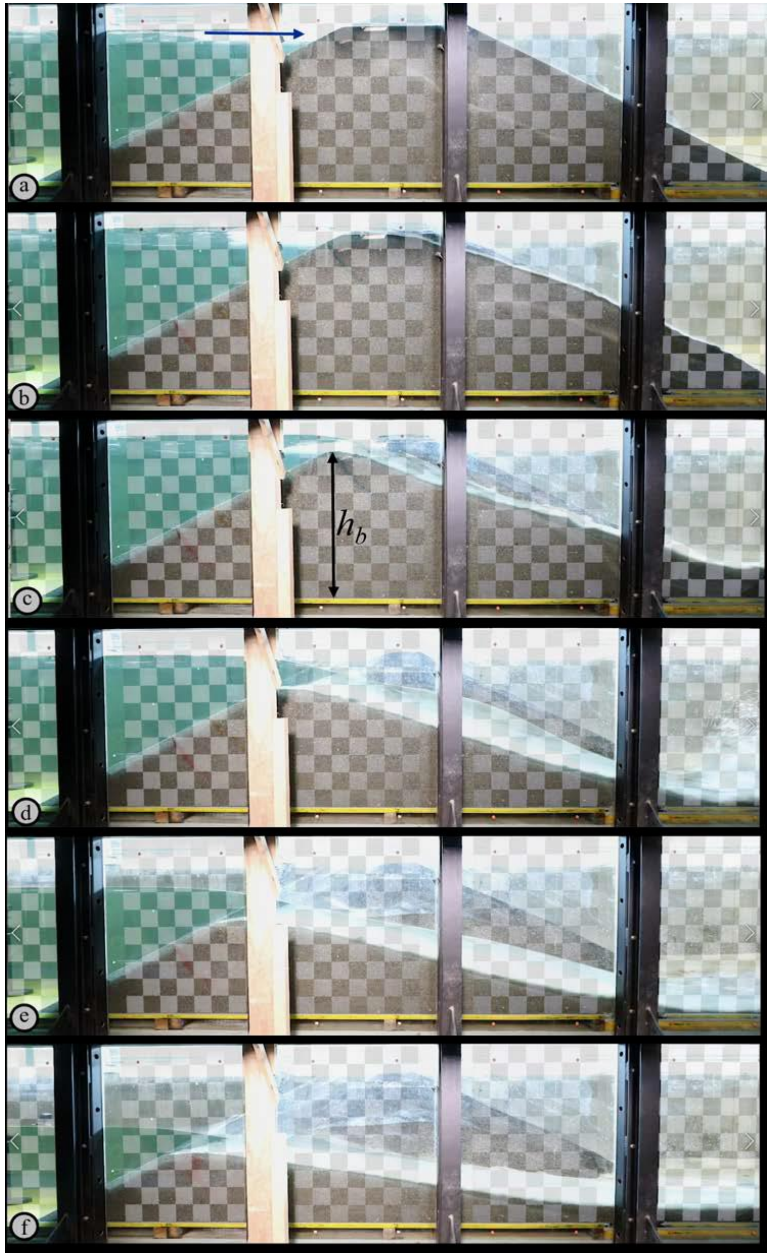

(a) Headcut erosion through a test levee [Photo: USDA-ARS-HERU Stillwater, OK. US]

Walder et al. 2015

Key variables to know

- Breach hydrograph
- Breach formation and widening
- Failure time

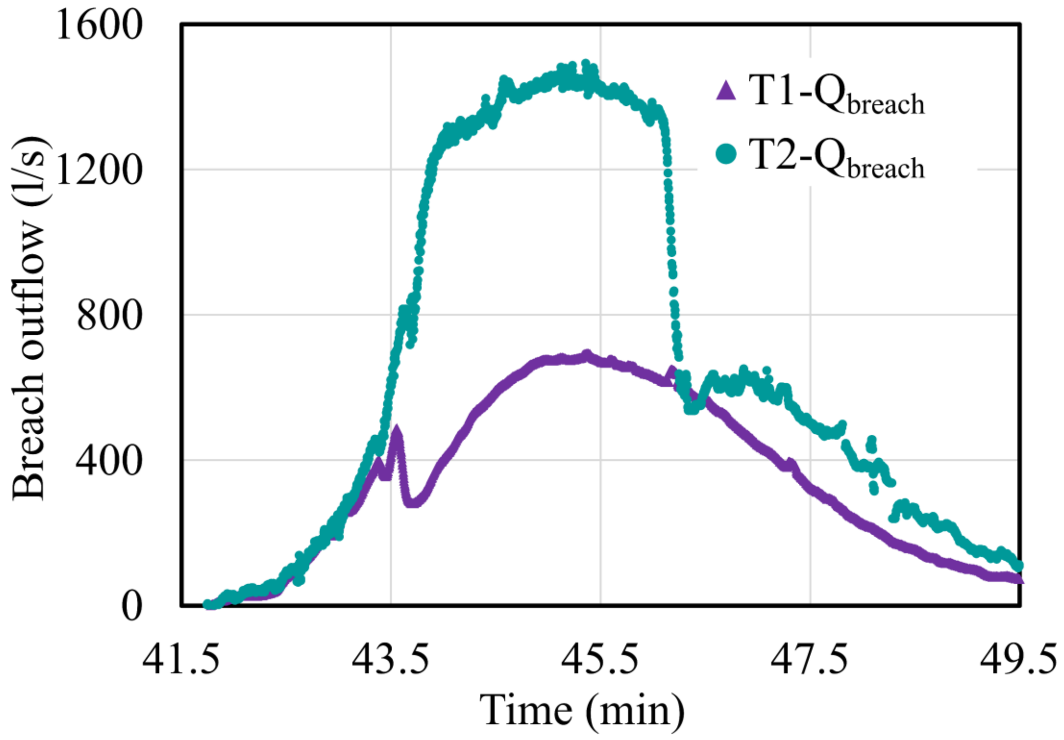

IMPACT, Mo i Rana, Norway, 2002

Laboratory experiments

- Scale effects: Froude

$$\lambda_v = \lambda_t = \lambda^{1/2}$$

$$\lambda_Q = \lambda^{5/2}$$

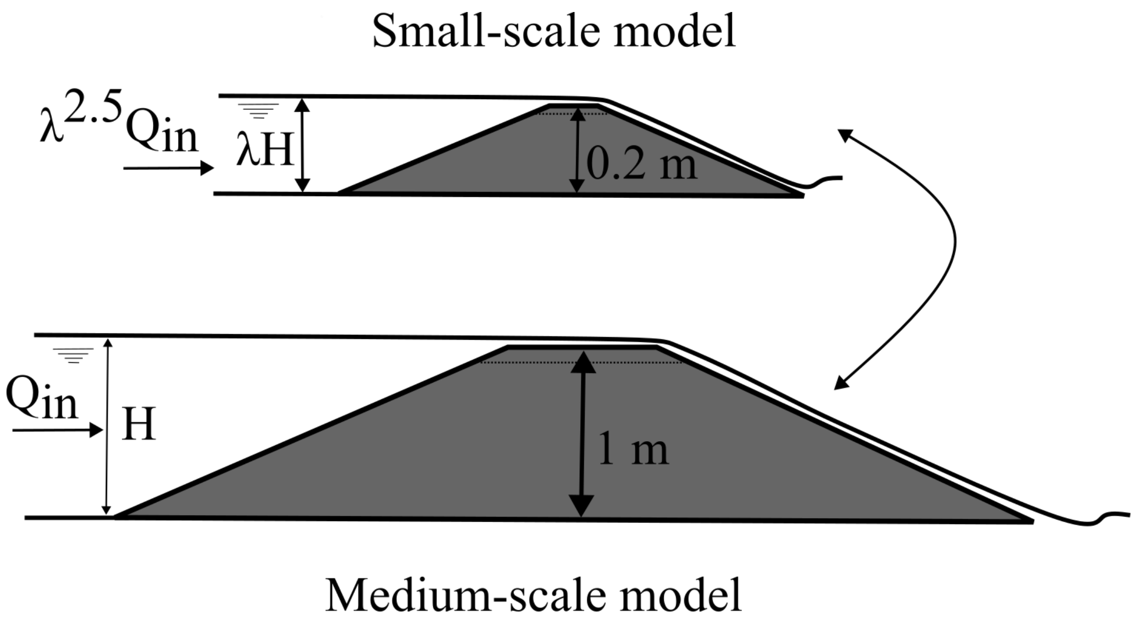

Embankment height: 0.2 m

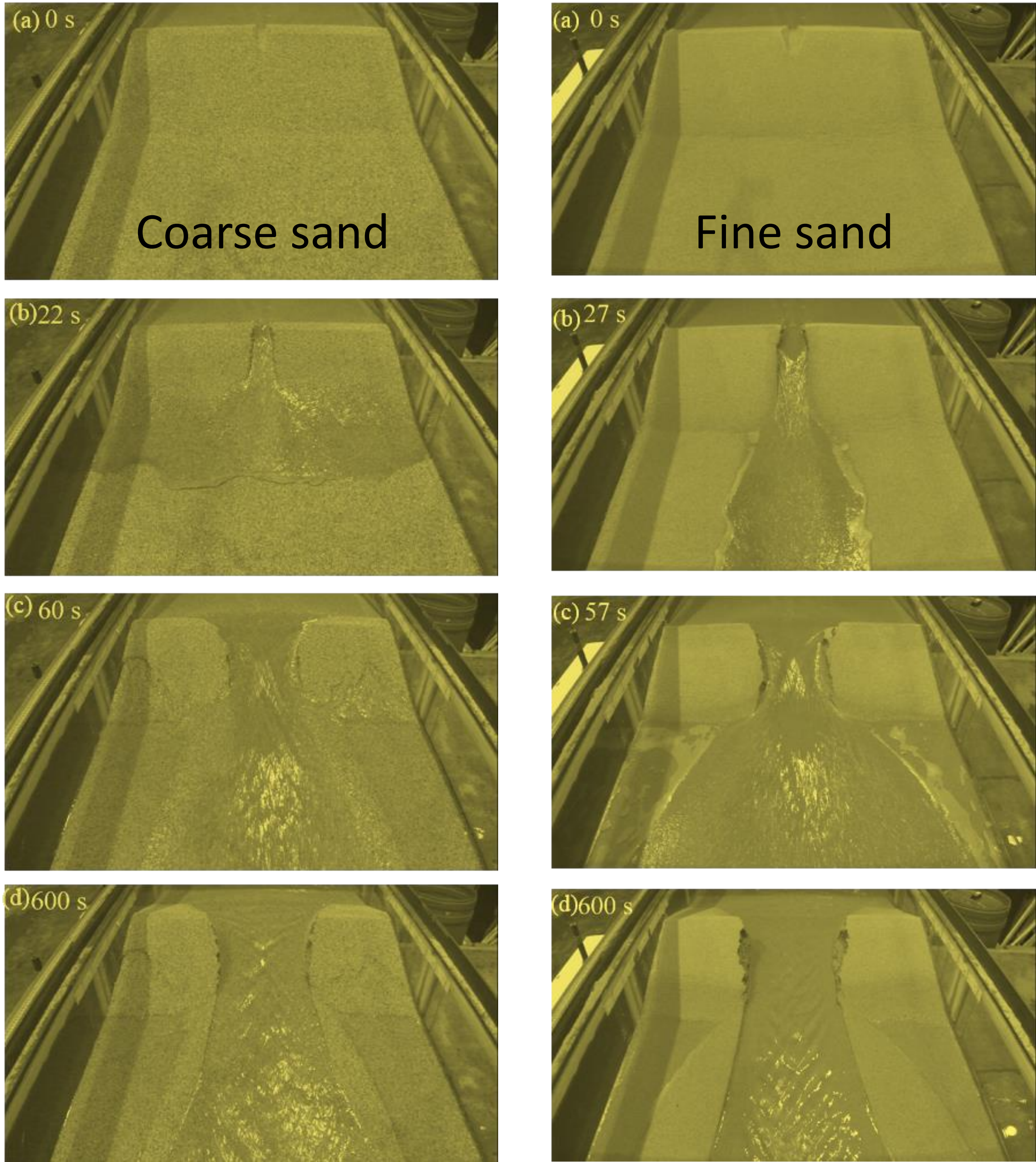

Laboratory experiments

- Dam layout
- Scale
- Dam material
- Inflow conditions
- Measurements

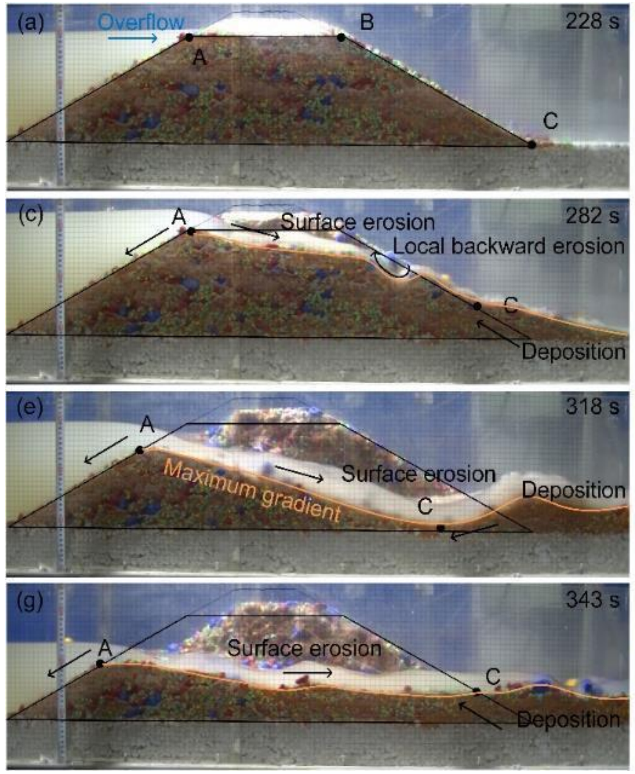

Bimodal grain distribution

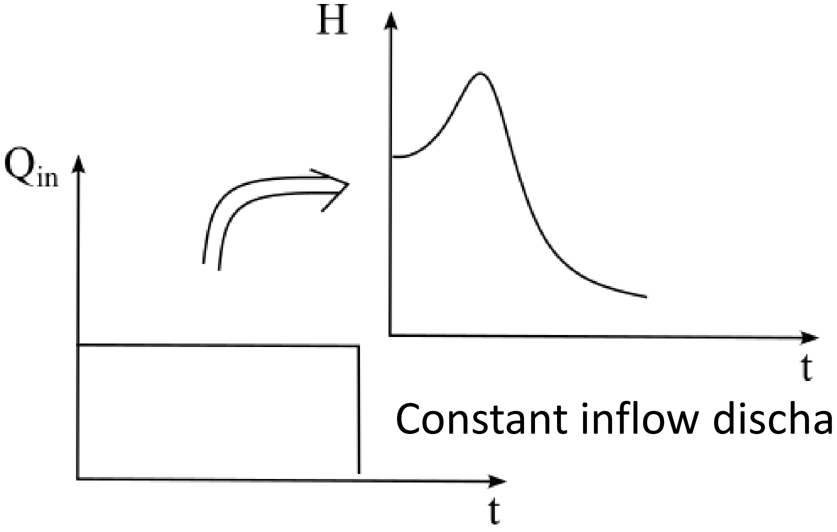

Constant inflow discharge

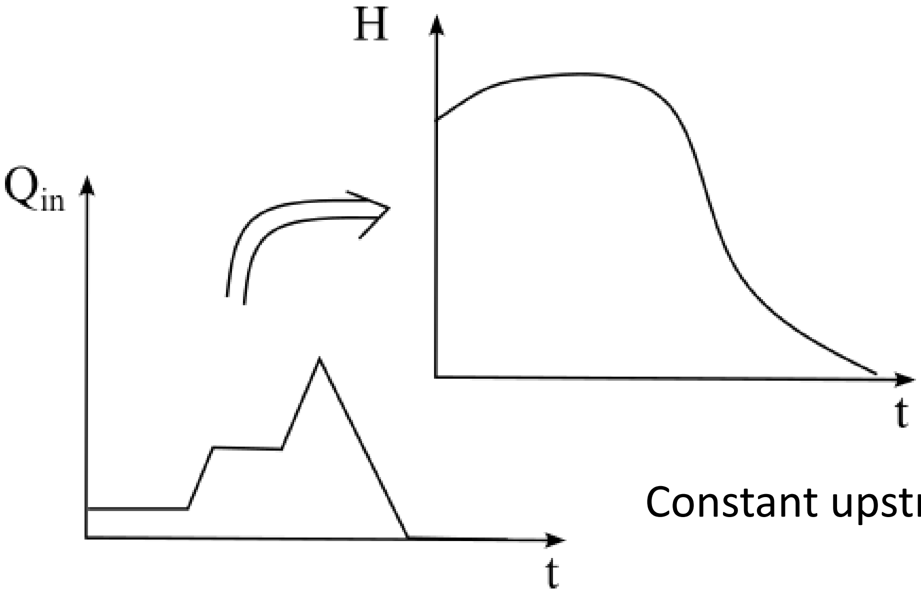

Constant upstream water level

Medium-scale experiments

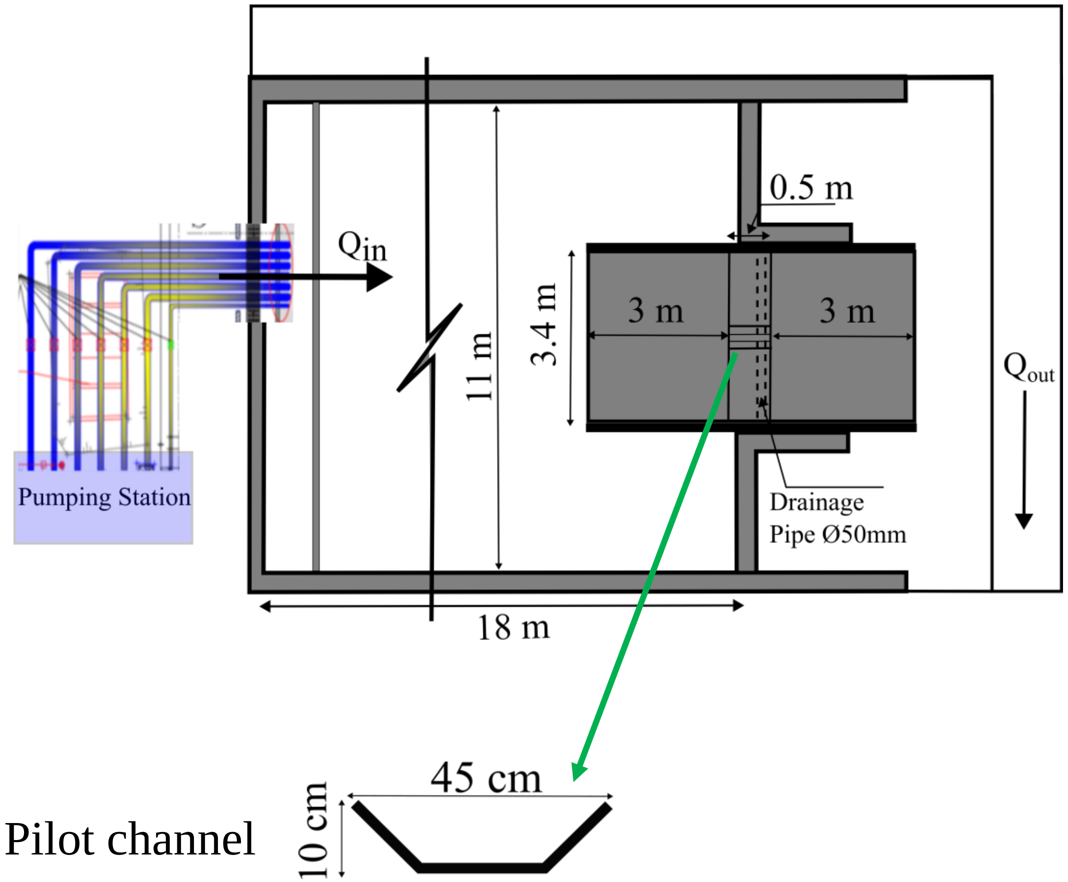

Pilot channel

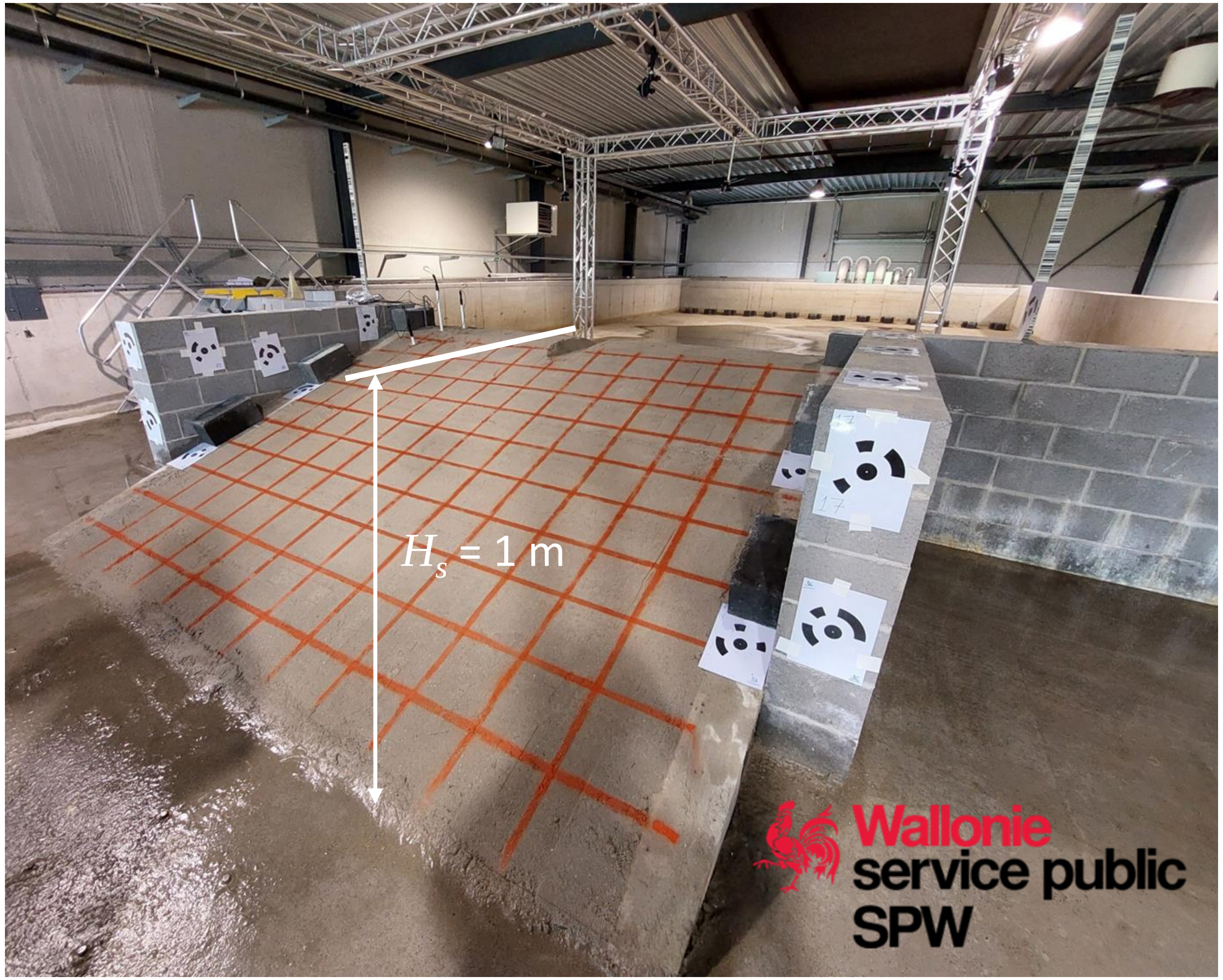

Medium-scale experiments

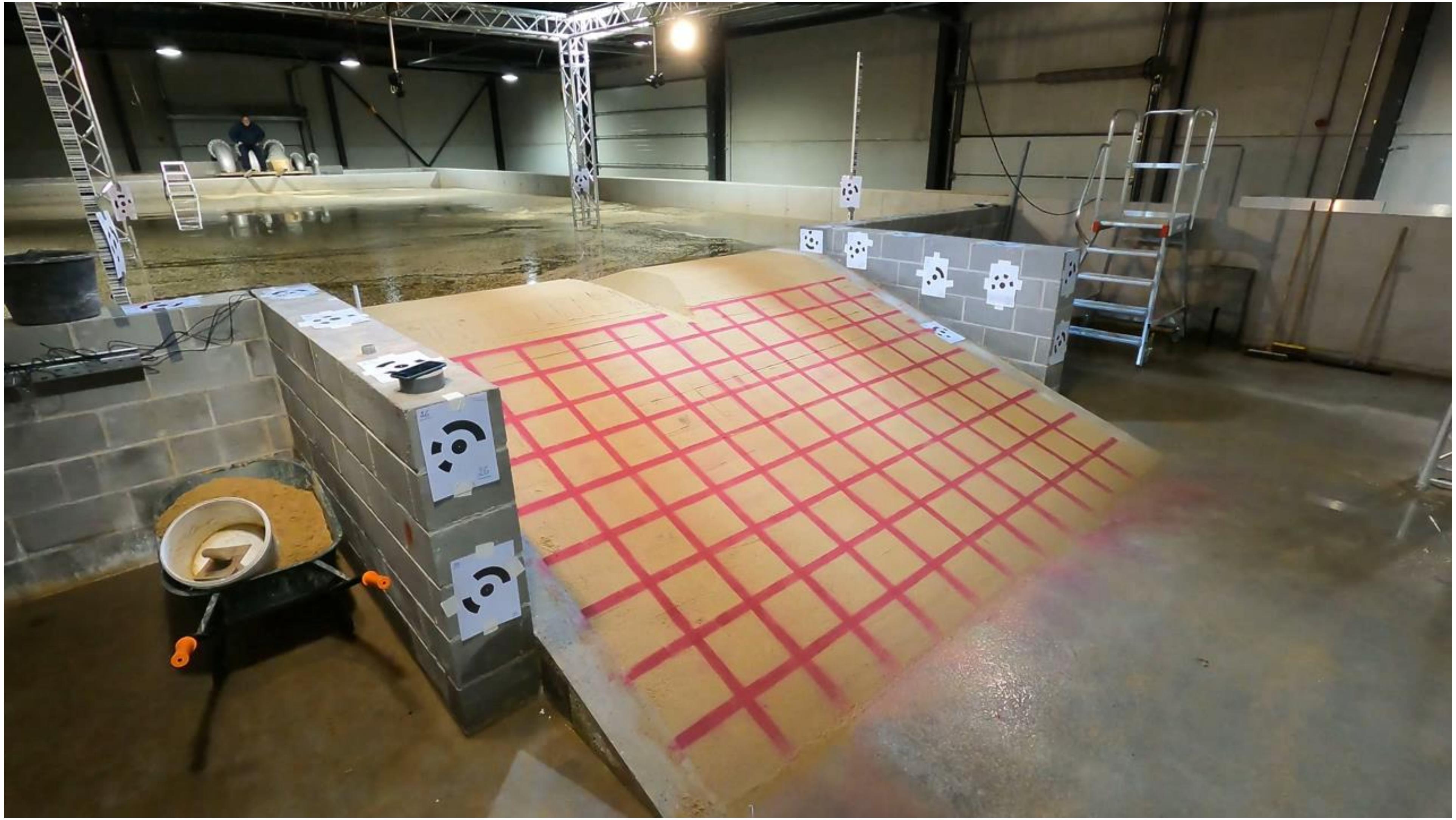

Photogrammetry measurements

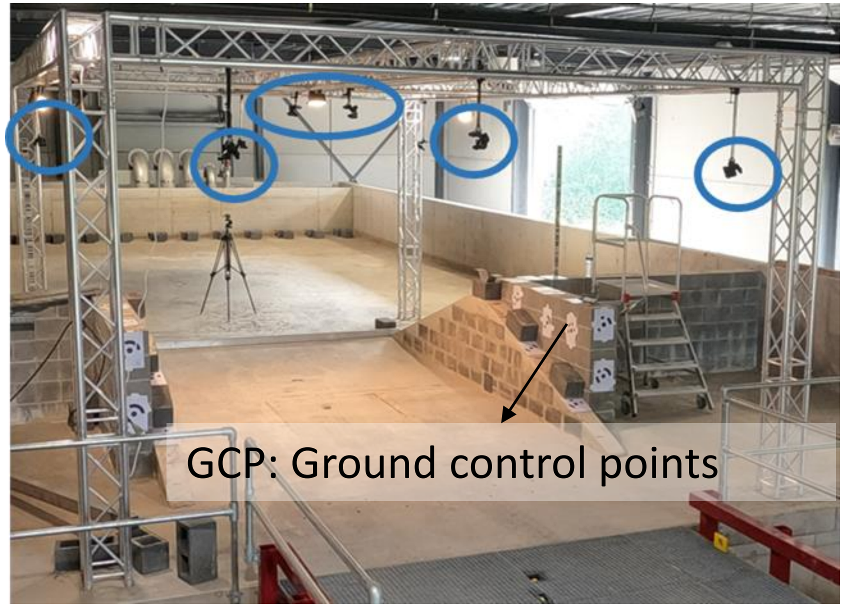

Multi-stationary synchronized cameras
10 Fixed cameras on time-lapse mode

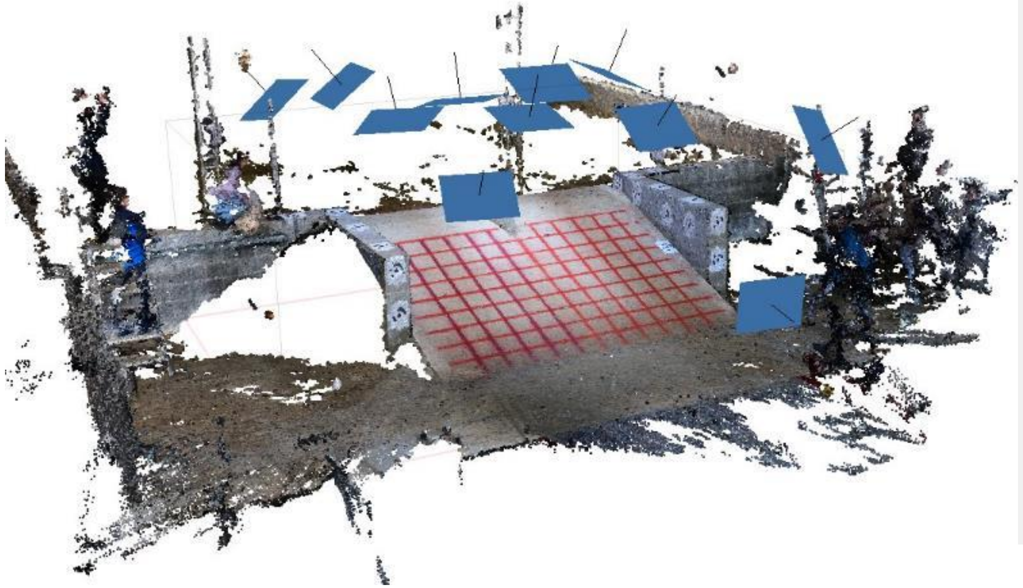

Dense Point Cloud
2,000,000 points

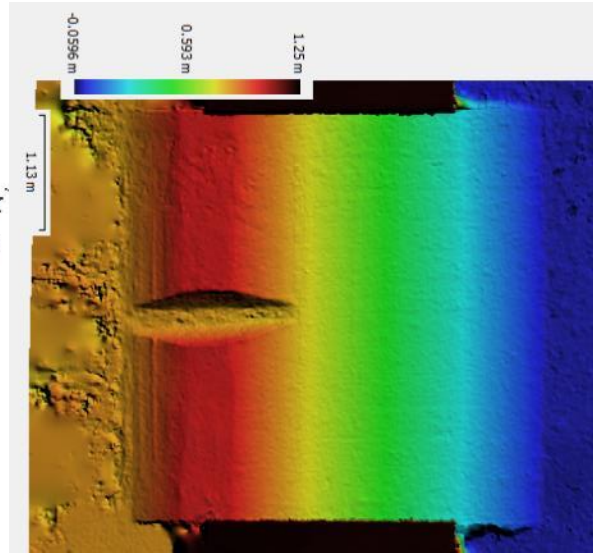

Elevation Map (DEM)
Pixel size: 0.006 (m)

Photogrammetry measurements

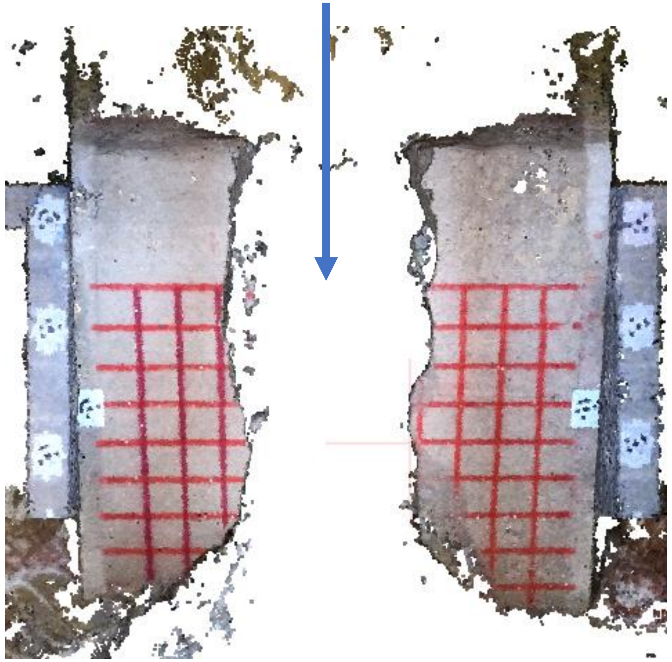

Dense Point Cloud
No point or few points inside the flow

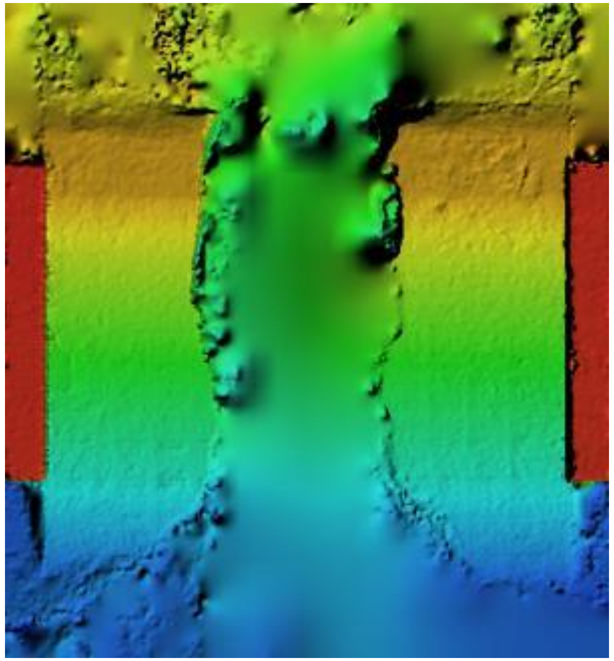

Elevation Map (DEM)
Interpolation

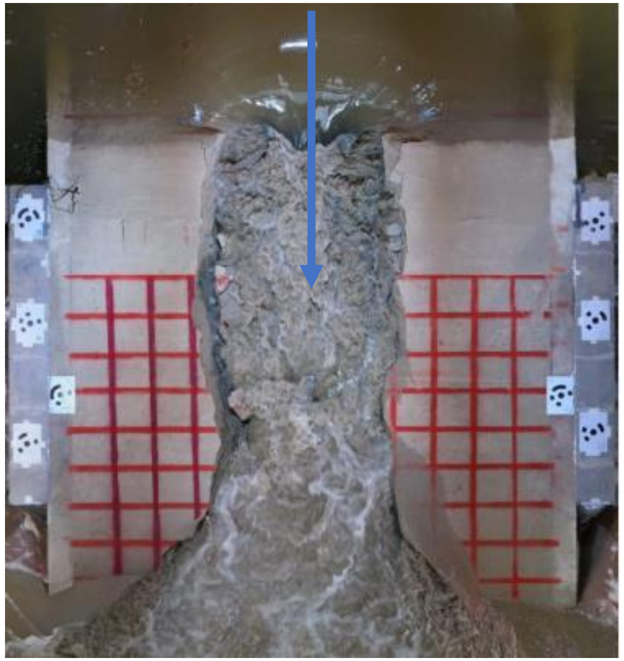

Orthophoto
Resolution: 1.39 mm/pix

Breach evolution

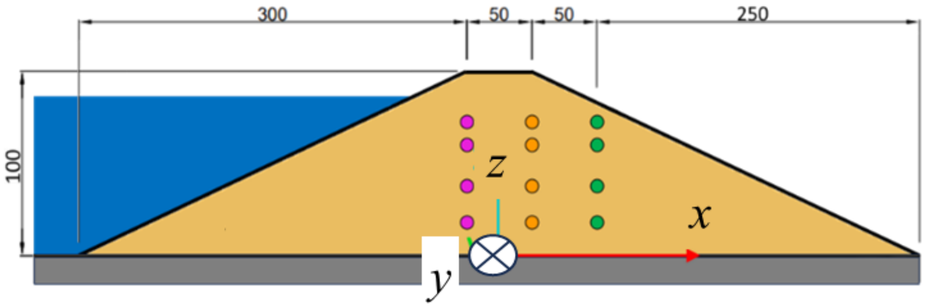

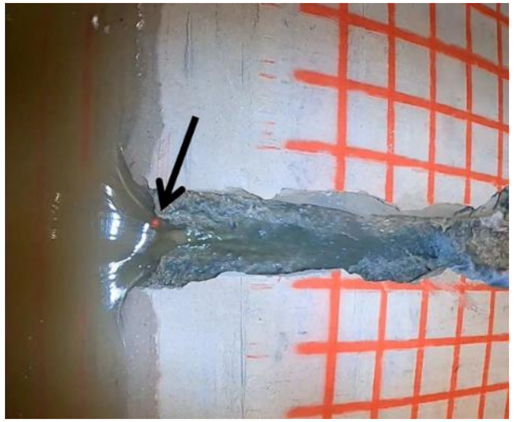

Continuous segment : above water
Dashed segment: interpolated area inside the flow

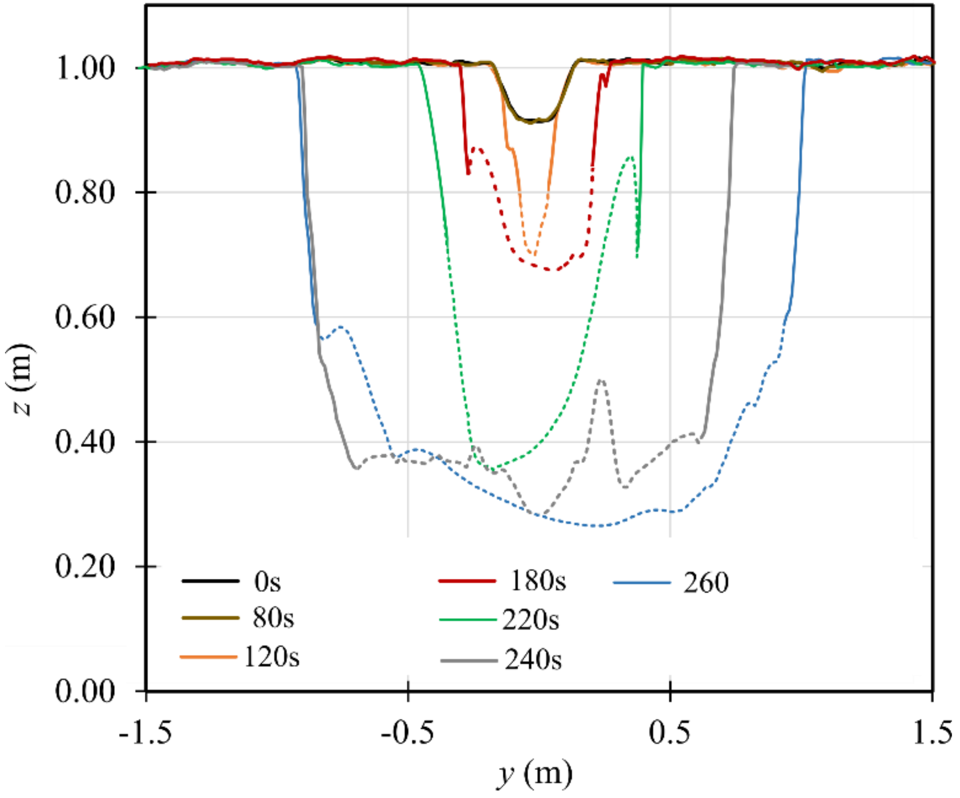

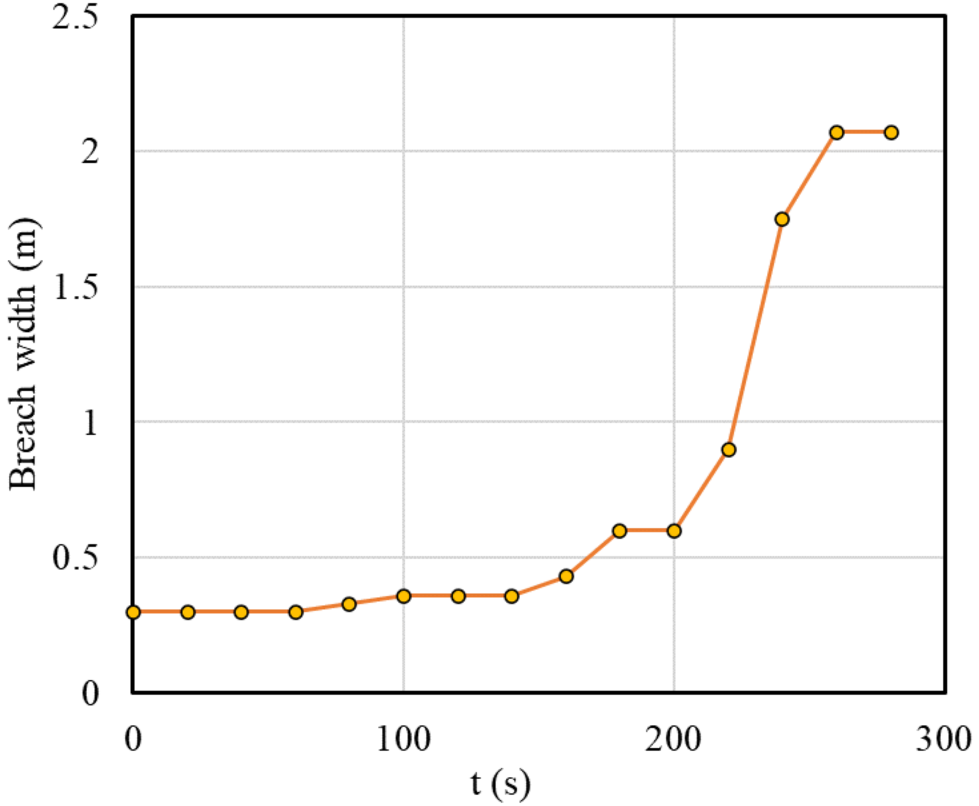

Breach hydrograph

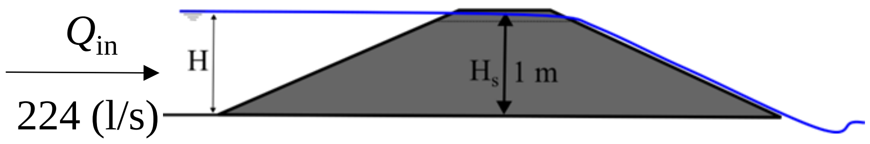

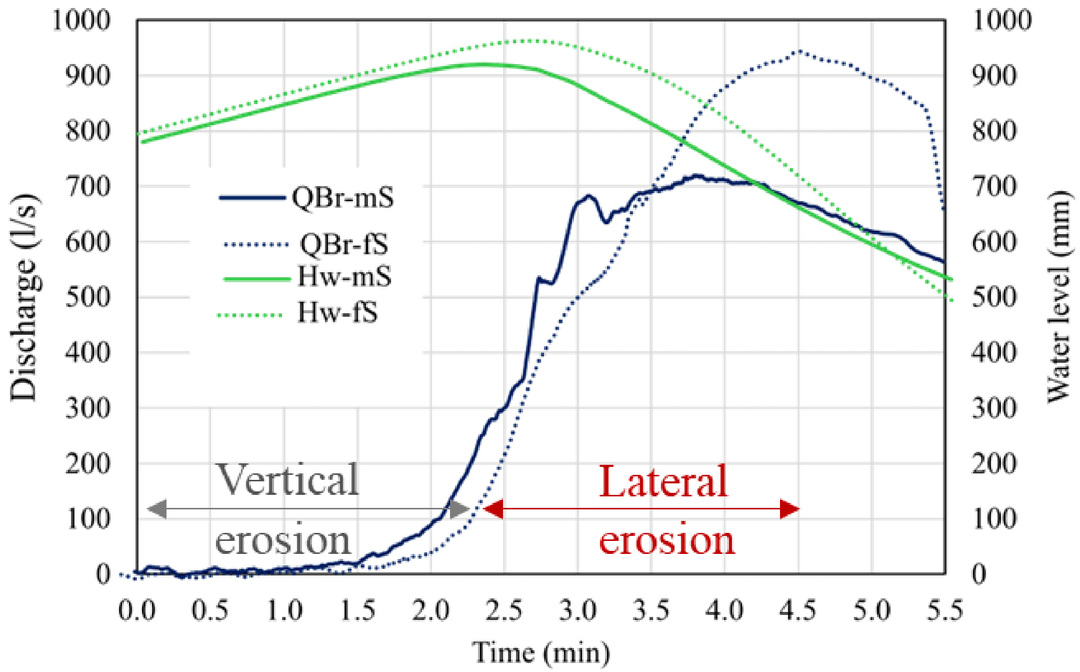

Fine Sand

Medium Sand

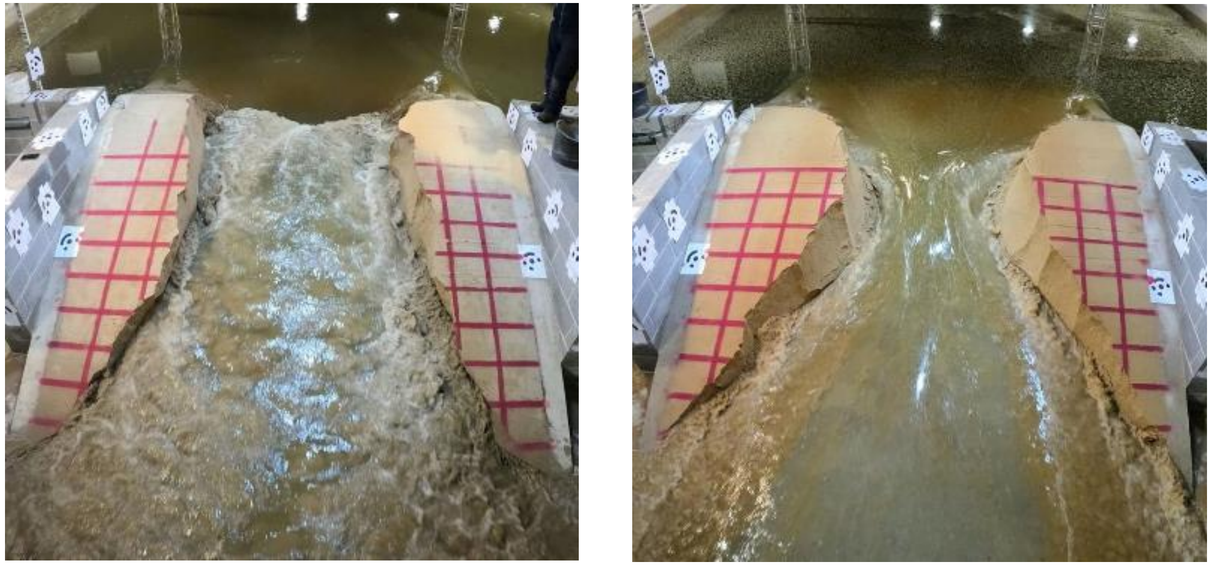

Time =3.1 min

Fine Sand (fS)
Medium Sand (mS)

$$Q_{breach} = Q_{in} - A\frac{dz_w}{dt}$$

Water content in the embankment

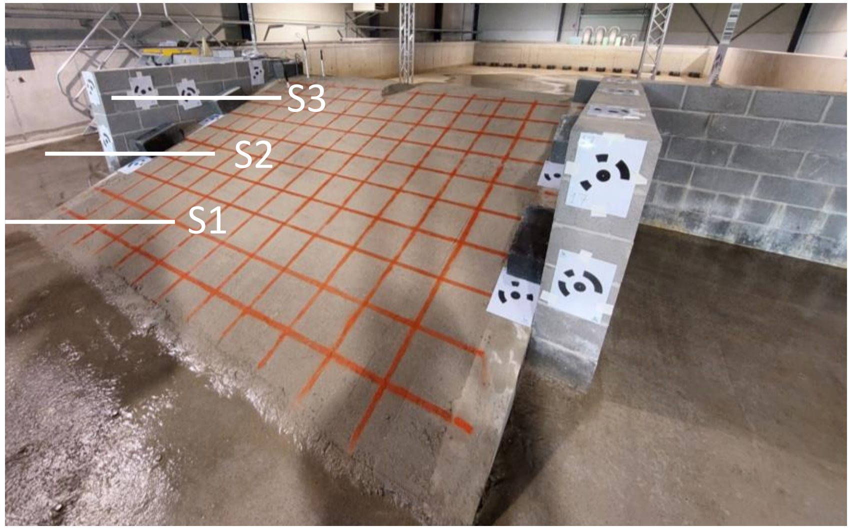

Sensors visible after dike failure

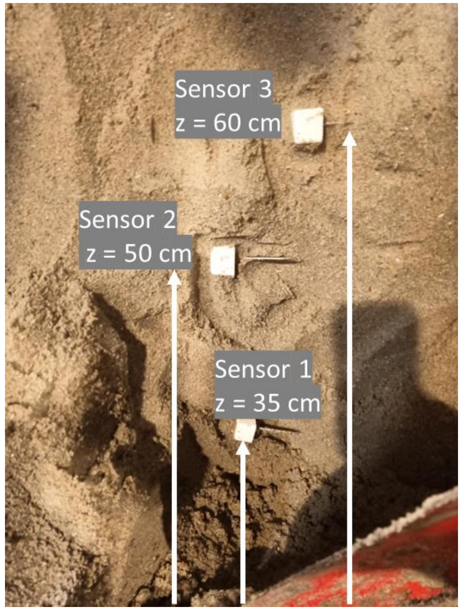

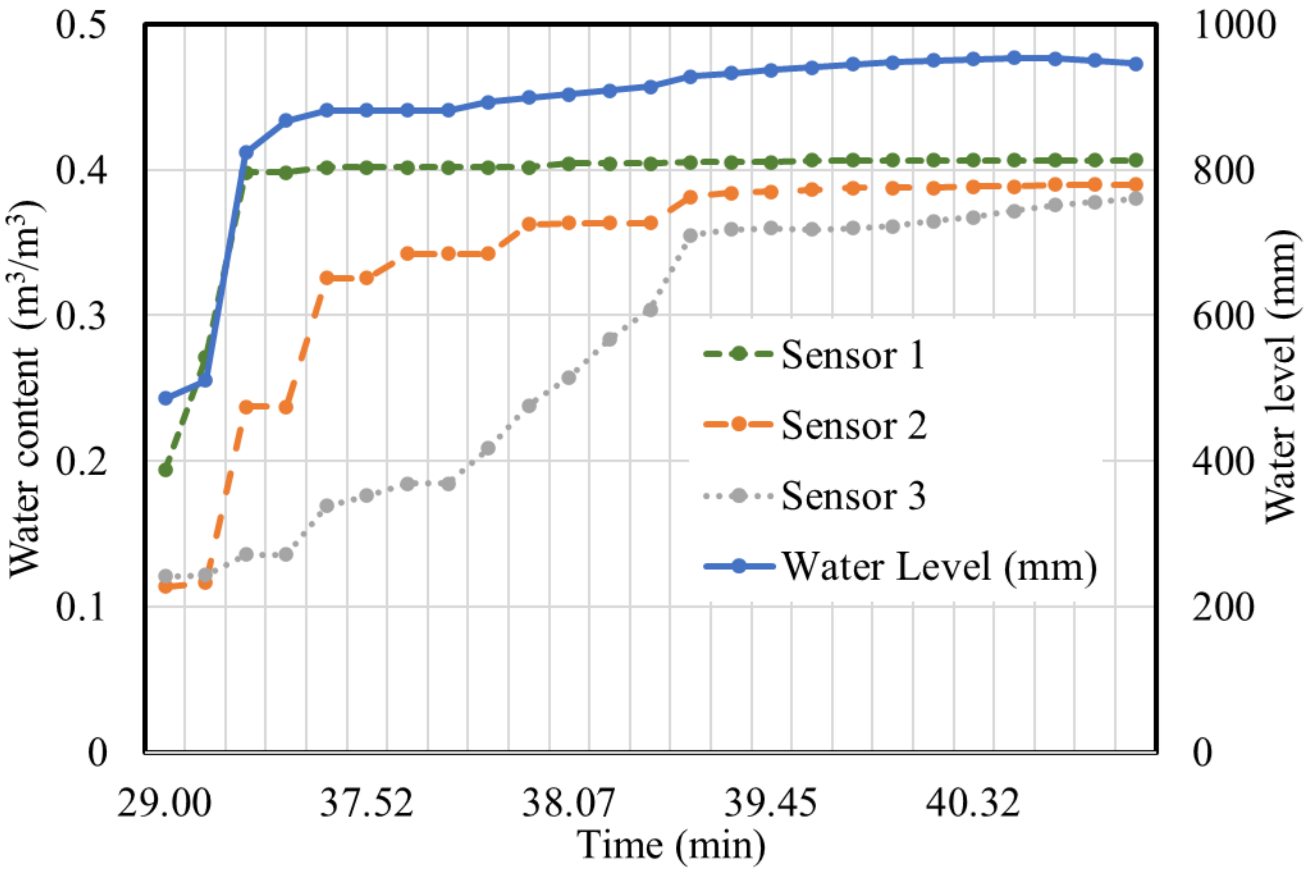

Field measurements - Polder2C's

Field measurements - Polder2C's

Interreg
2 Seas Mers Zeeën
Polder2C's

Wave overtopping tests

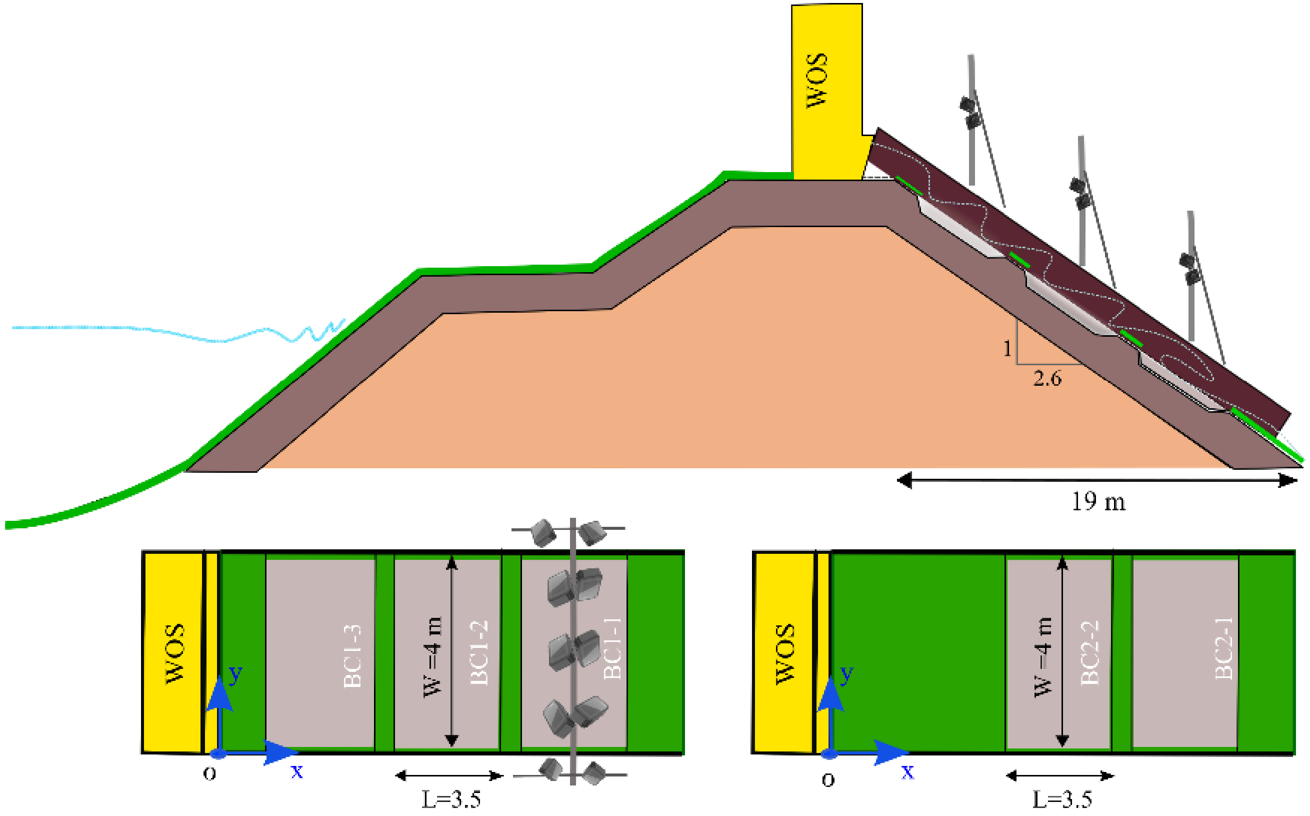

Field measurements

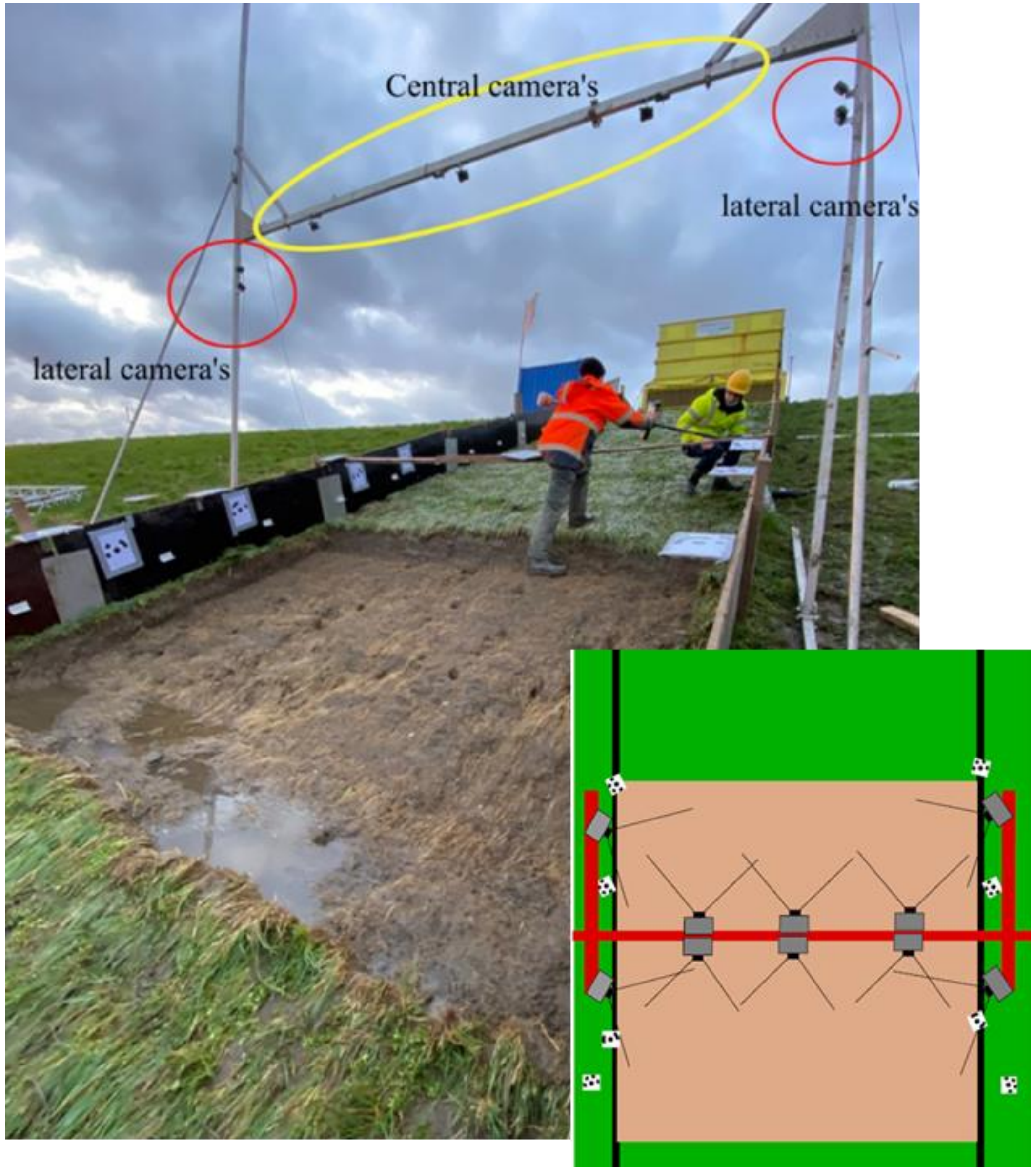

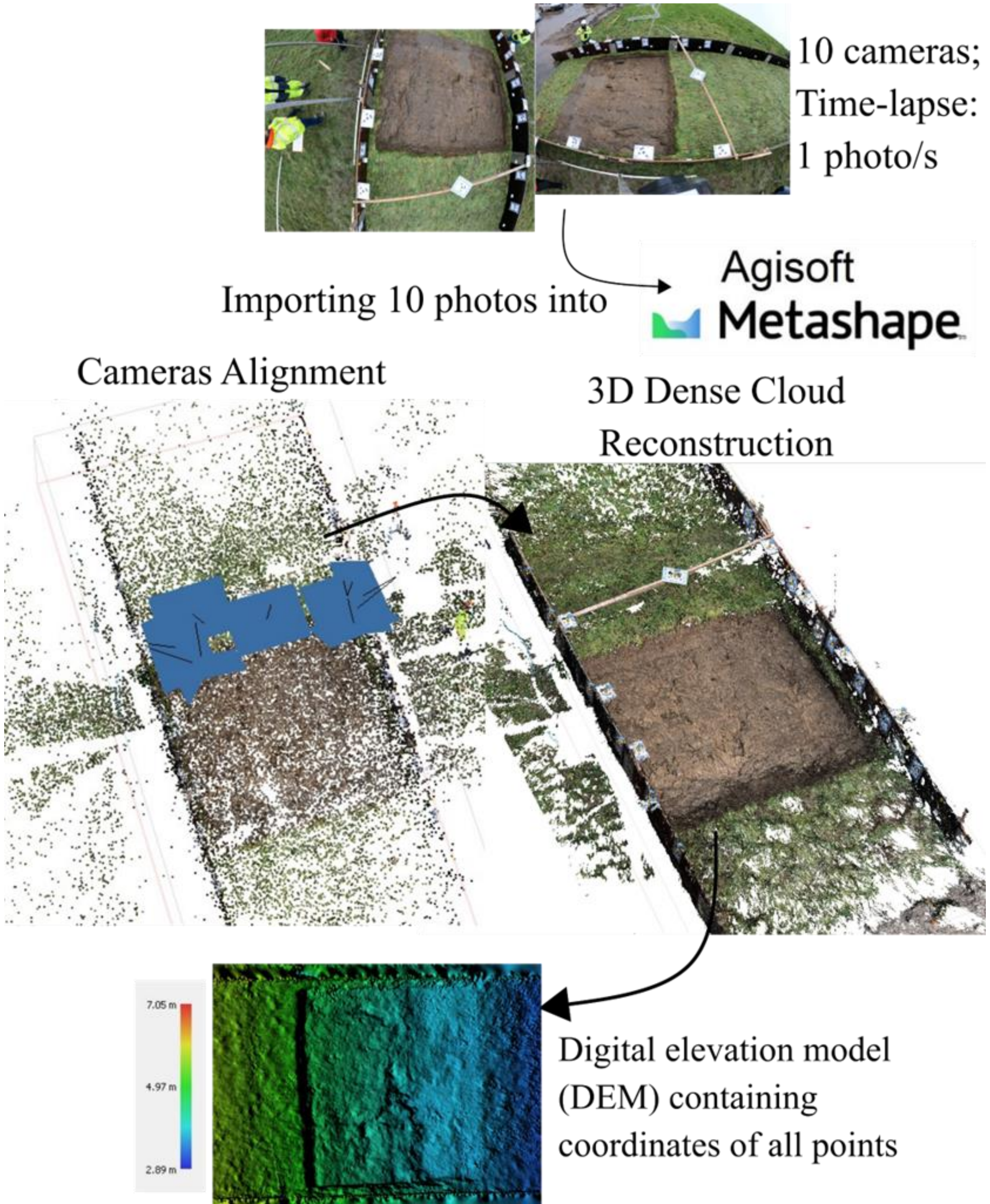

Field measurements - Polder2C’s

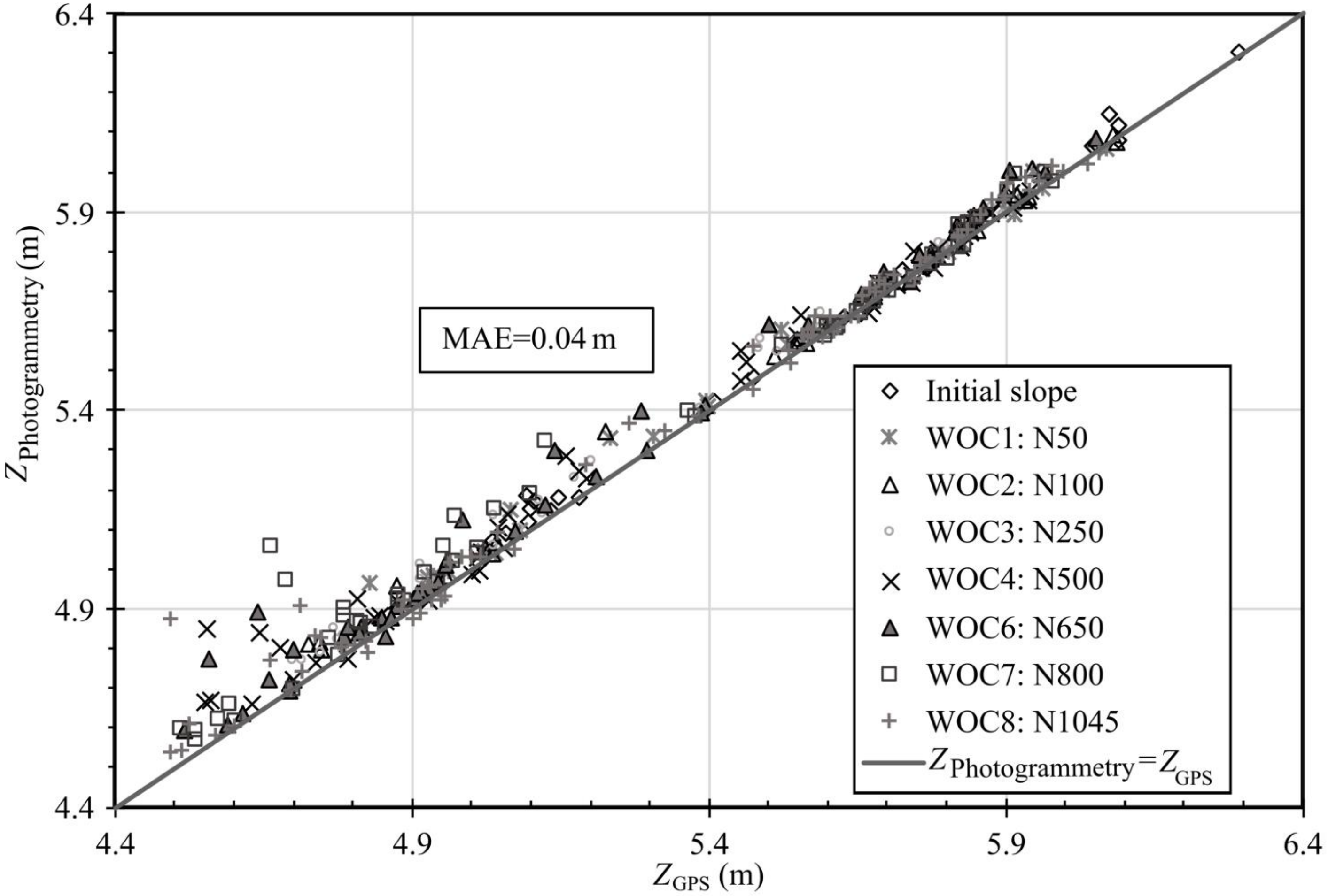

Field measurements - Polder2C's

Erosion measurements

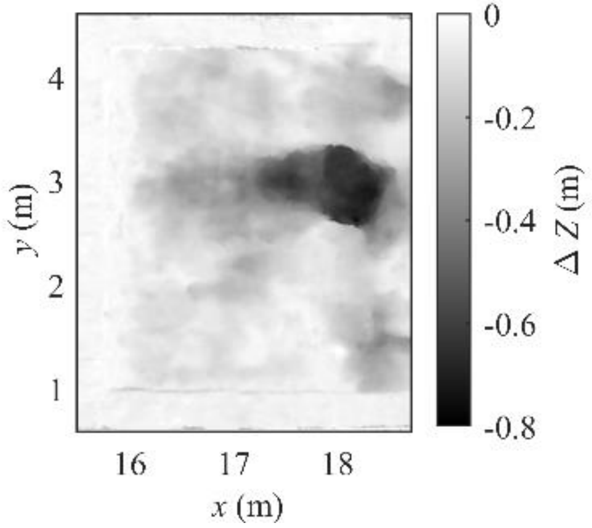

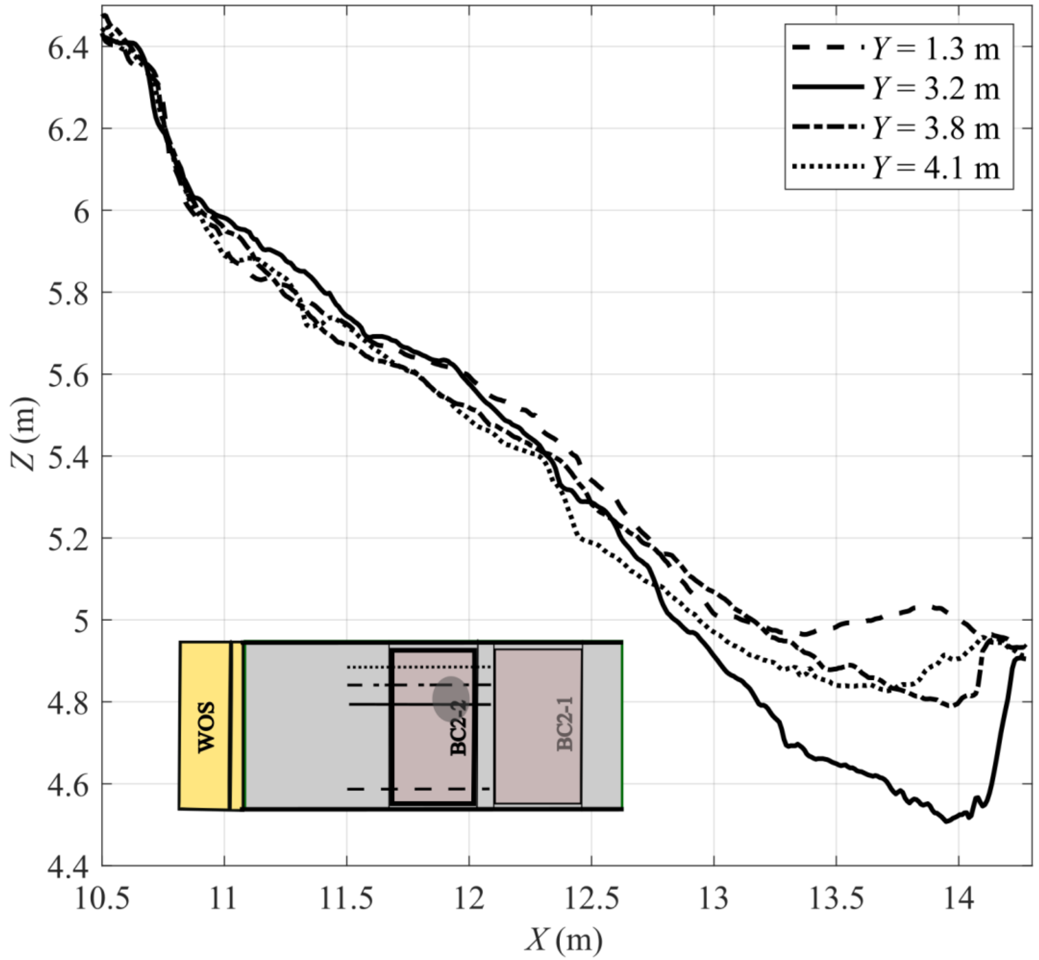

What’s next ?

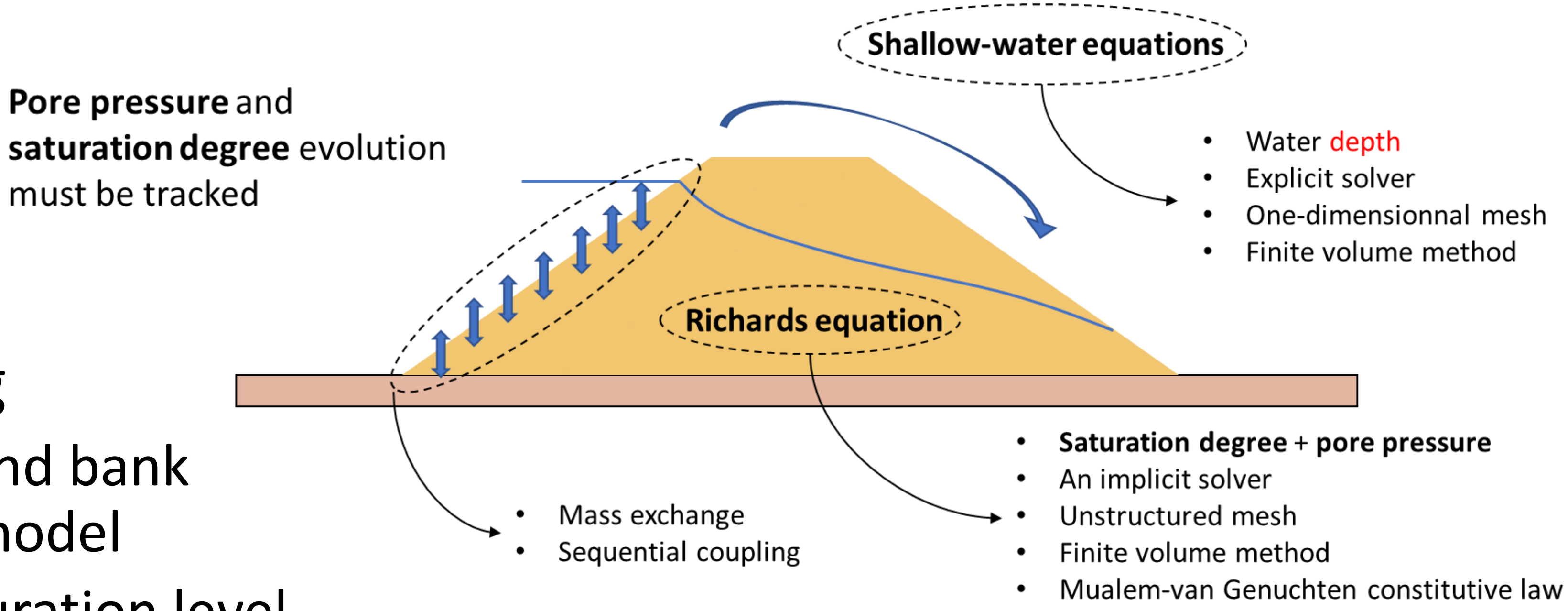

- Numerical modelling
  - Breaching process and bank erosion: improved model
  - Influence of soil saturation level
- Experiments
  - Small and medium scales, various materials
  - Flow though the dike
  - Velocity measurements
- Field work
  - Bonsai project

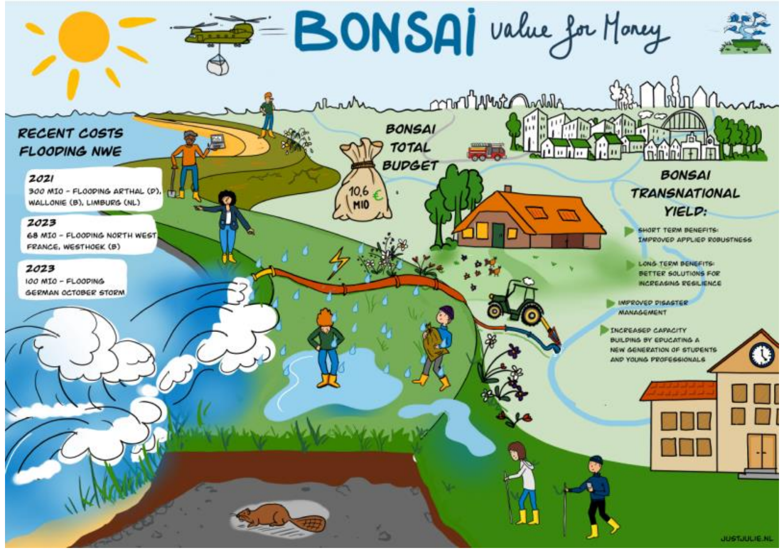

Numerical modelling

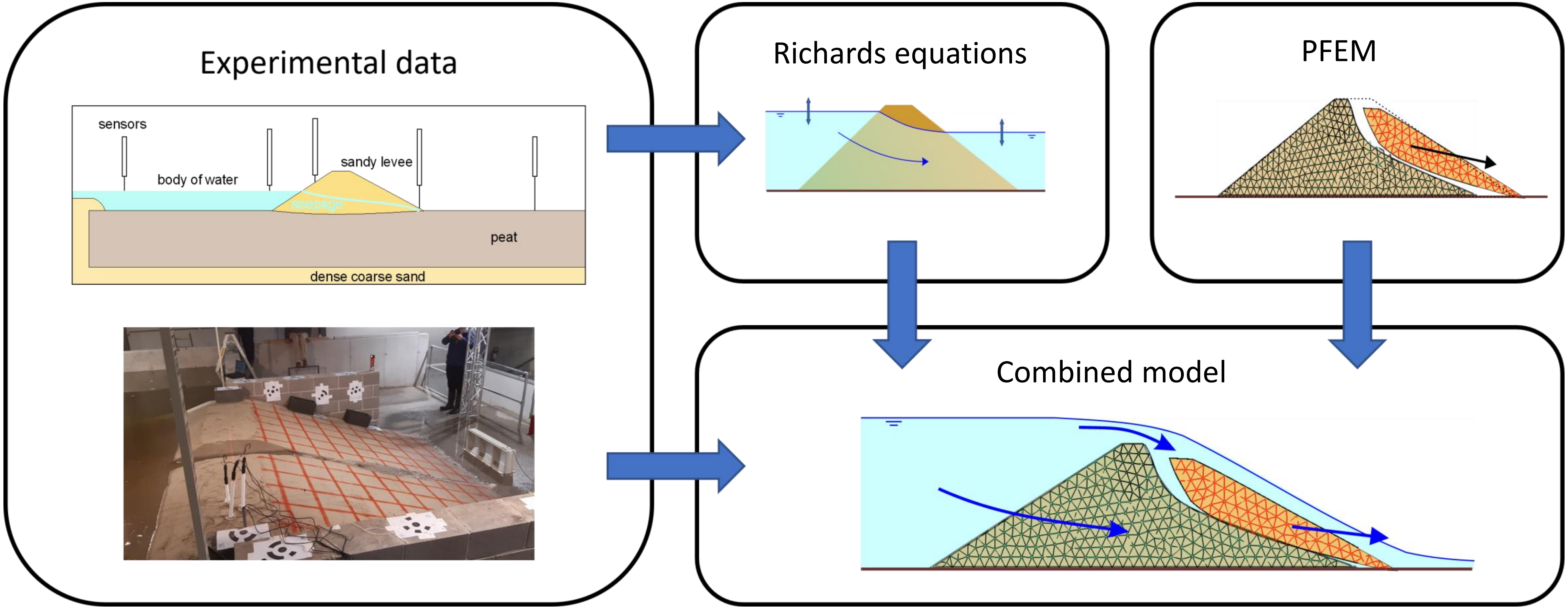

https://sites.uclouvain.be/hydraulics-group/watlab/index.html

Flow through the embankment

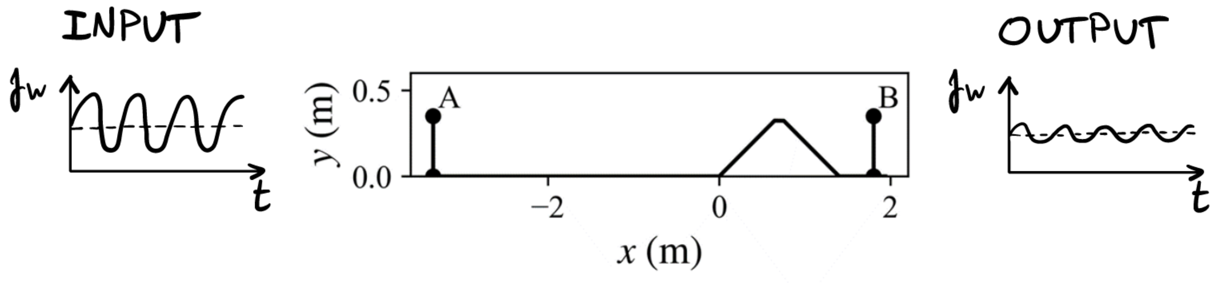

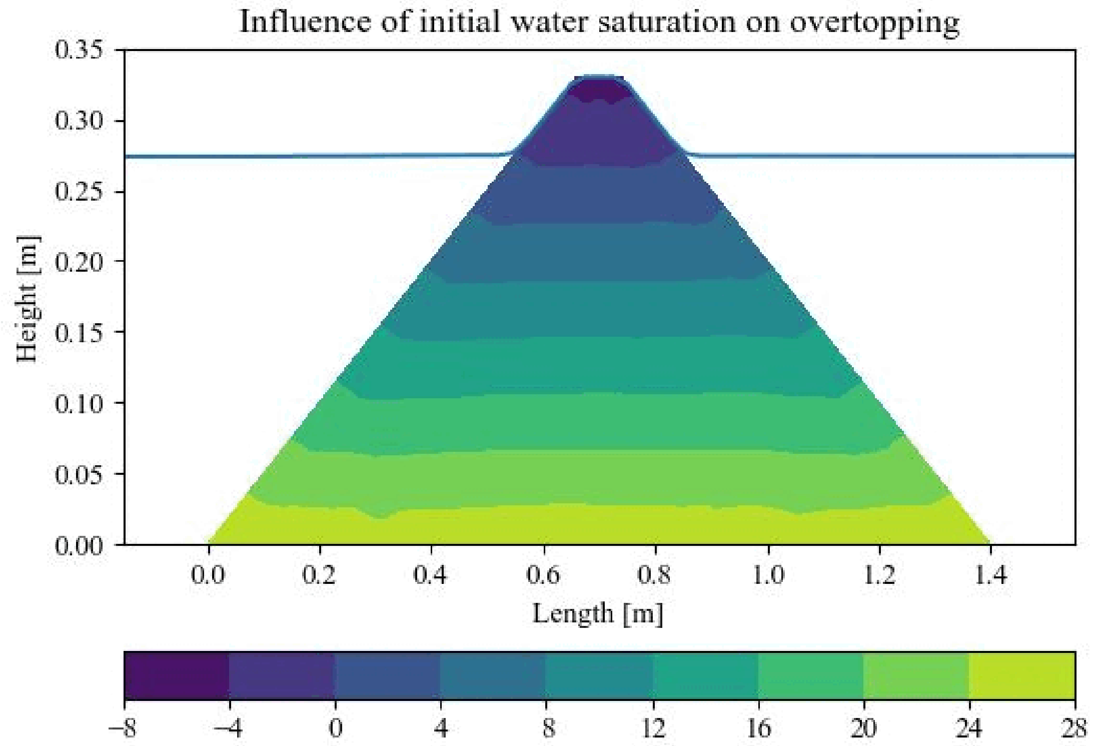

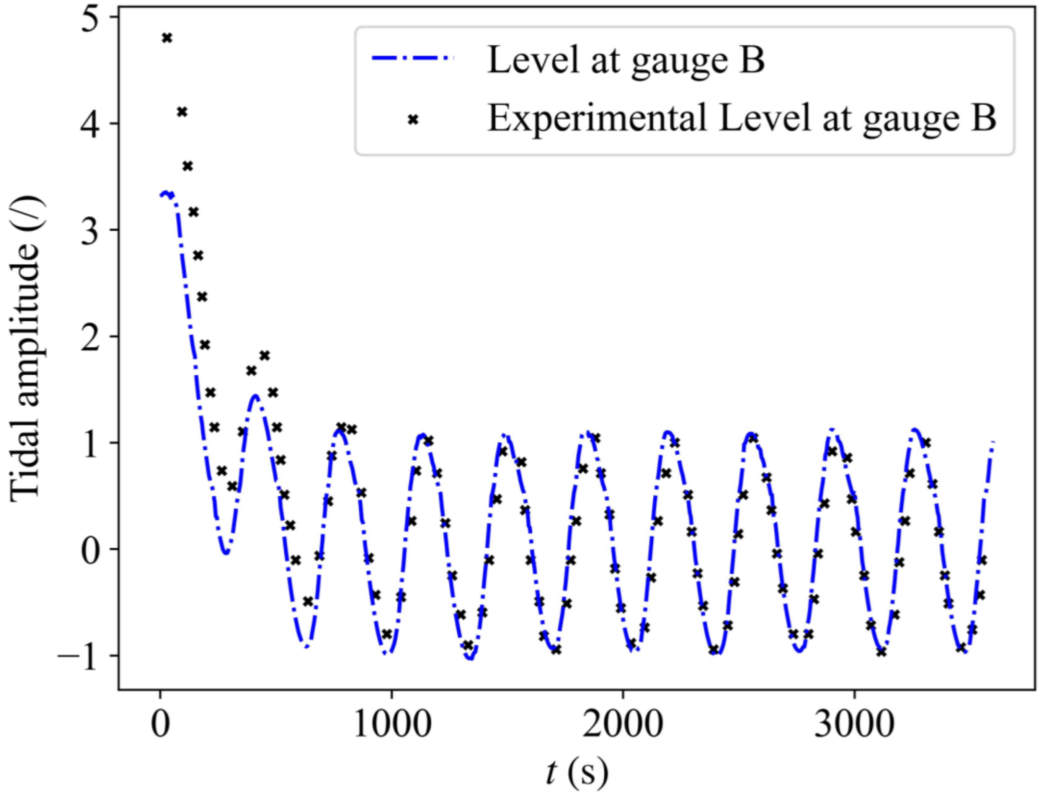

Surface erosion

2D shallow-water equations
Exner equation for sediment continuity
Multi-layered and non-uniform sediment transport

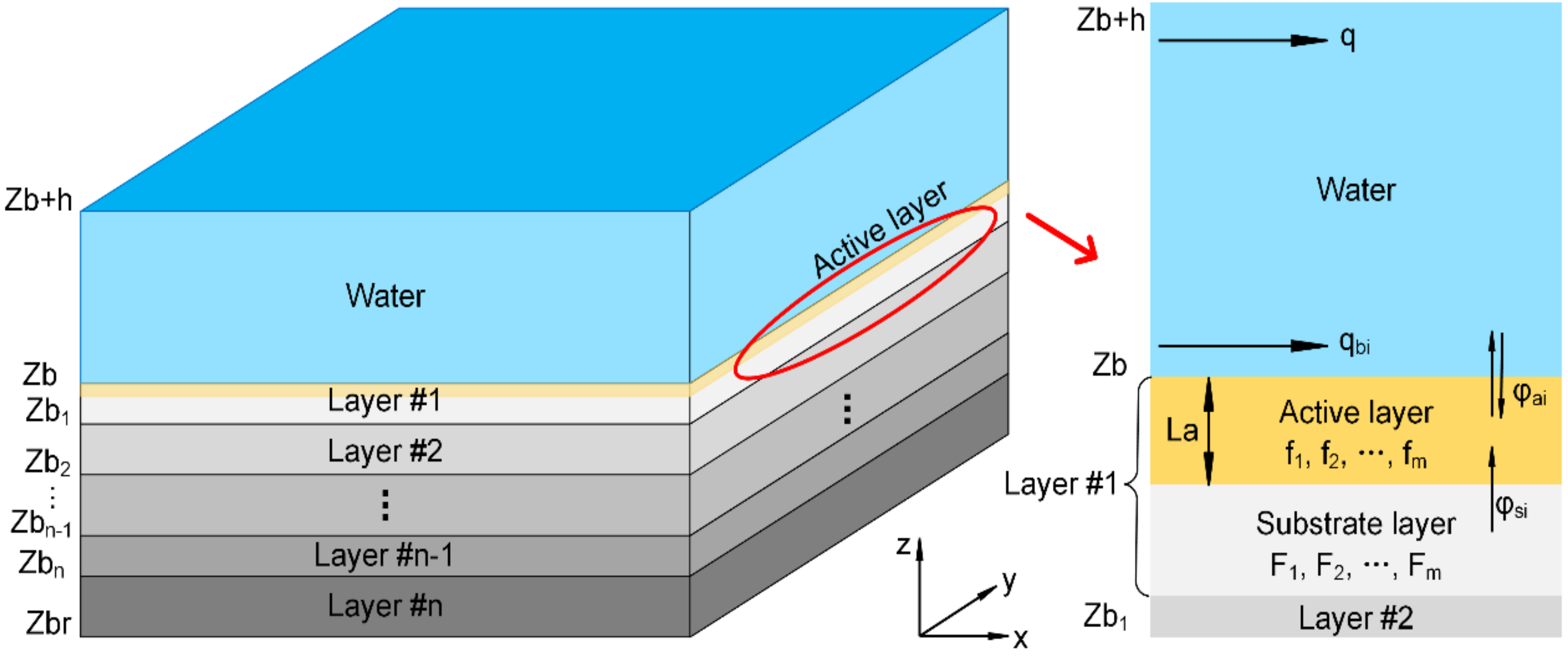

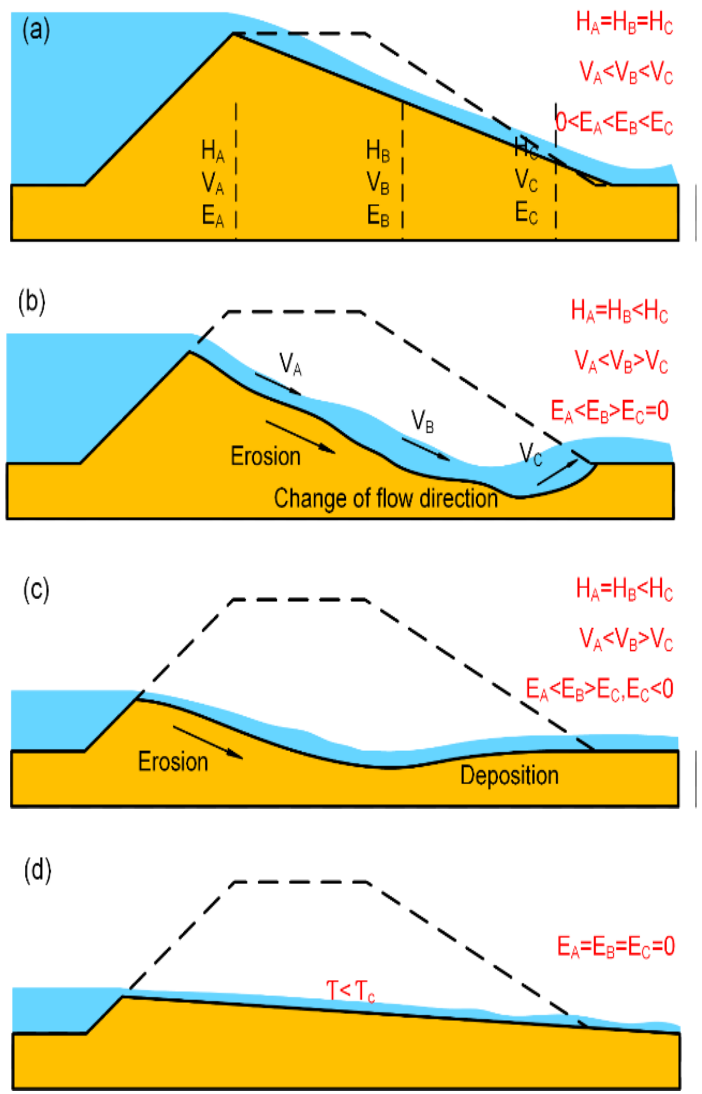

Dike erosion with different « fine » content

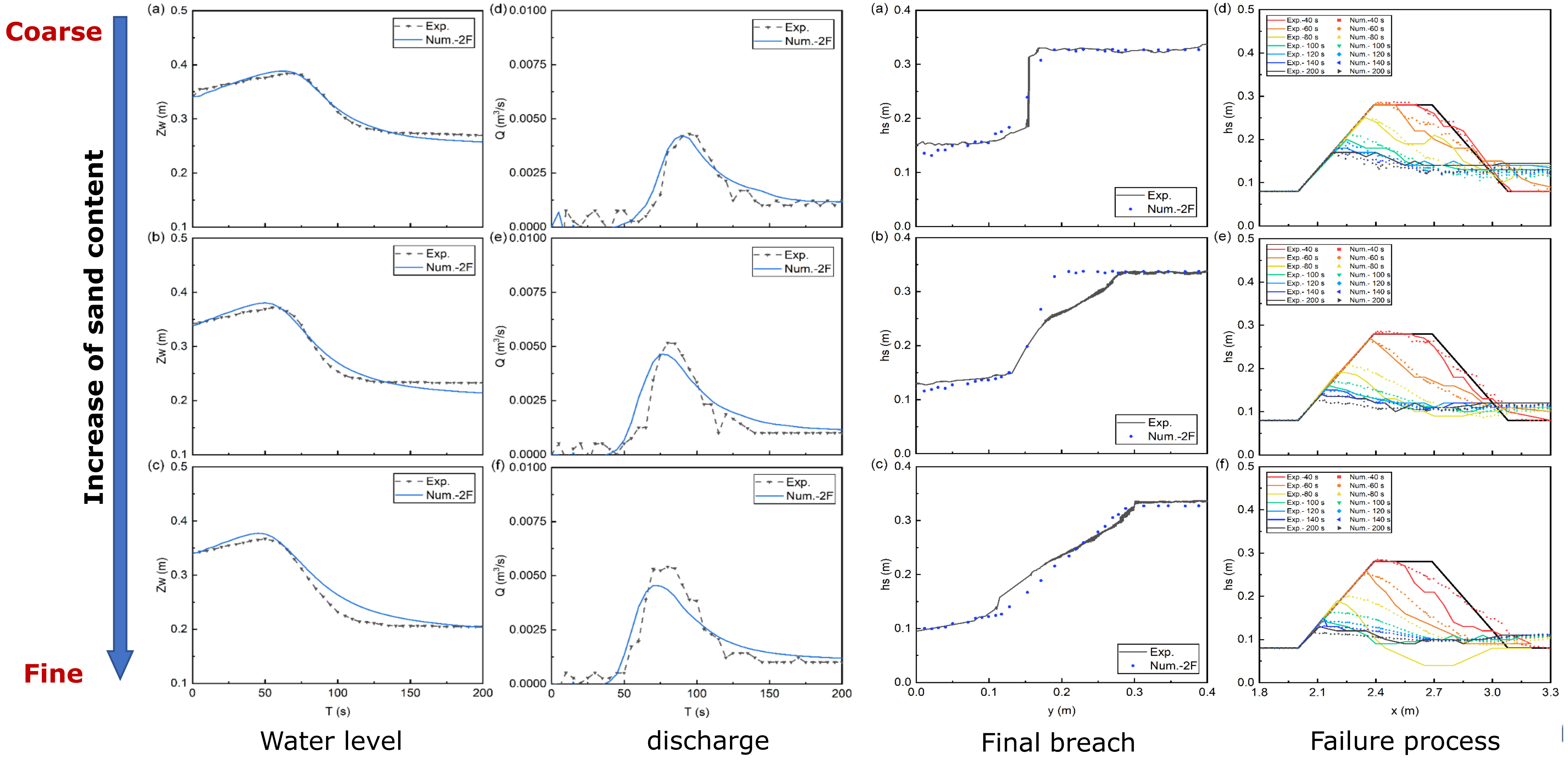

Mass movement using PFEM

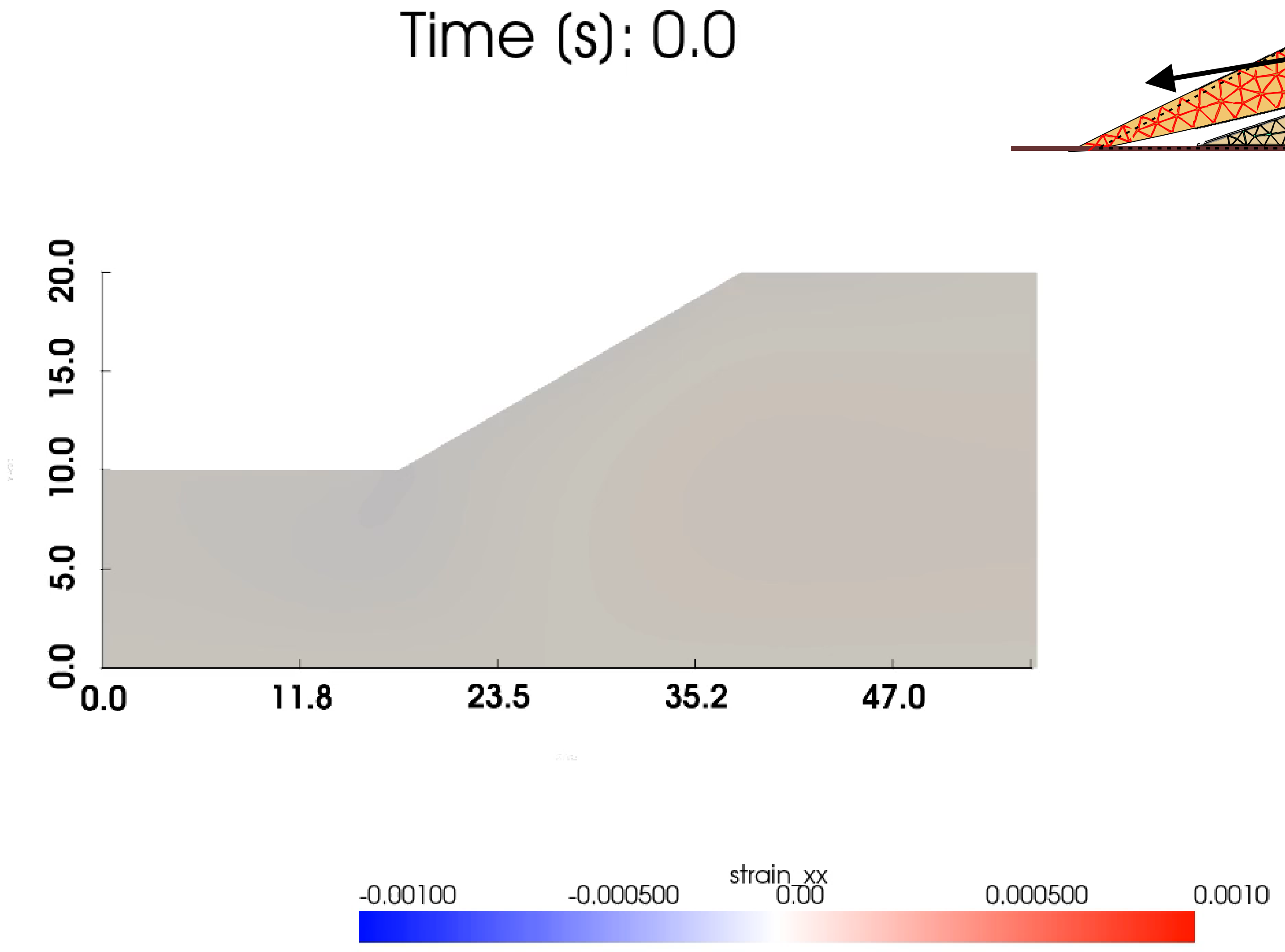

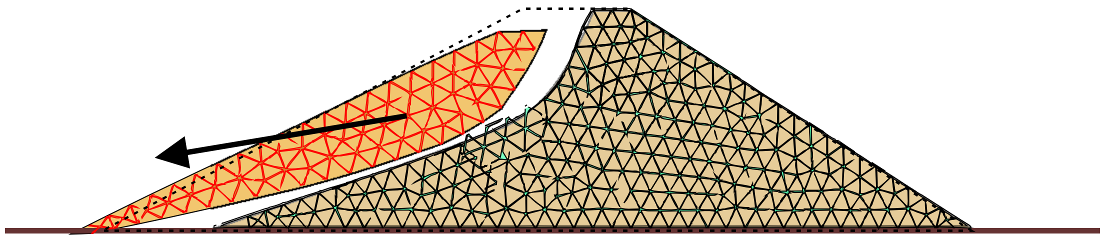

Thank you for your attention

"Deltares experimental facilities & measuring techniques"
(Invited Speaker Mark Klein Breteler, Deltares)

SEDIMARE

Experimental facilities & measurement techniques at Deltares

Mark Klein Breteler

Ivo van der Werf

Tijl Wijnants

Contents

- Introduction to Deltares (wave-related) facilities
  - Scheldt Flume
  - Delta Basin
  - Atlantic Basin
- Typical projects & measurements for small scale facilities
- A deeper dive into the Delta Flume

Physical modelling at Deltares

Wave flumes and wave basins:

		L (m)	W (m)	h (m)	H_s (m)
• 2D, small scale:	Scheldt Flume	110	1	1.2	0.28
• 2D & 3D, small scale:	Atlantic Basin	75	8.7	1.4	0.25
• 3D, small scale:	Delta Basin	50	50	1.4	0.25
• 2D, large scale:	Delta Flume	300	5	9.5	2.2

Projects in the Scheldt Flume

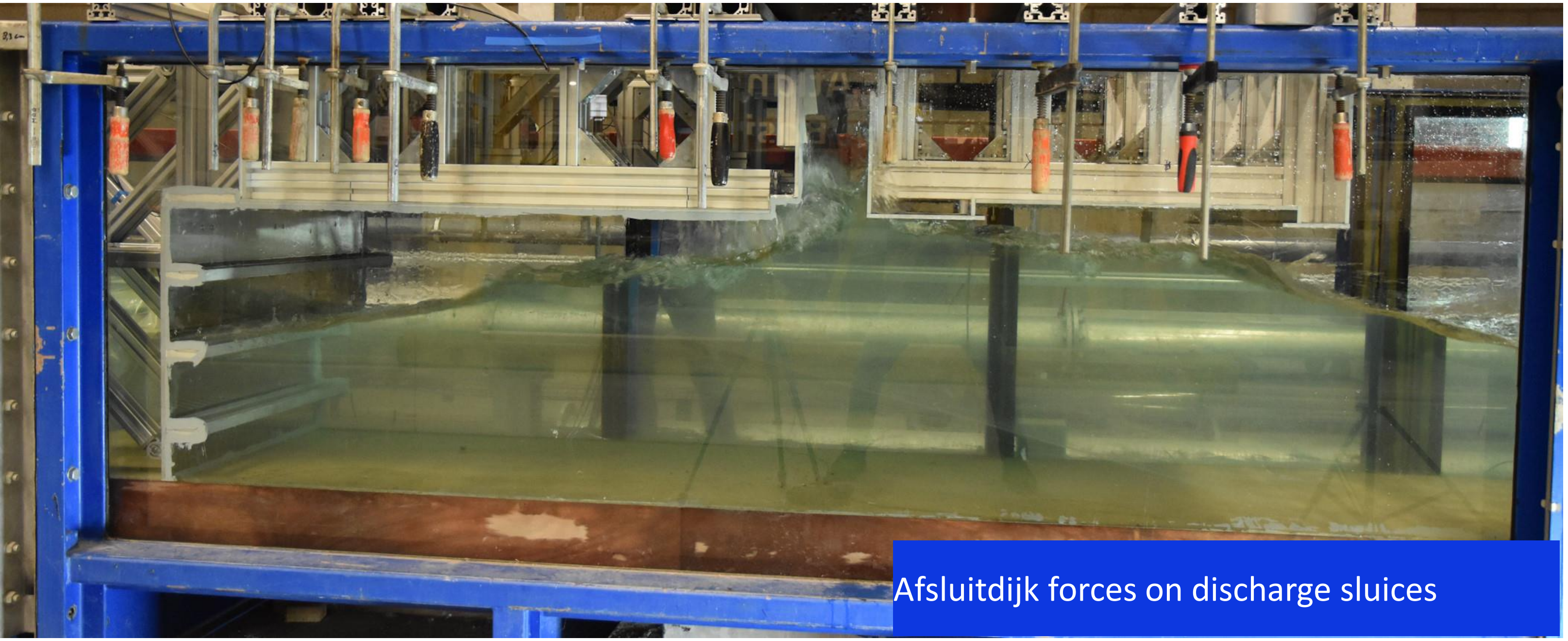

Afsluitdijk forces on discharge sluices

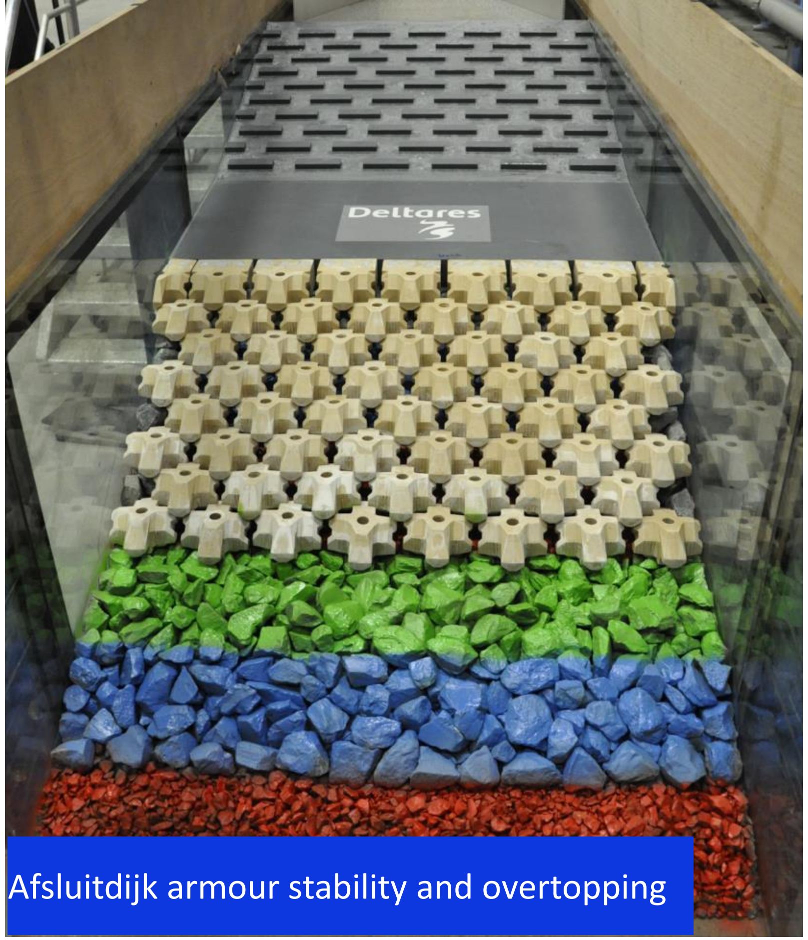

Afsluitdijk armour stability and overtopping

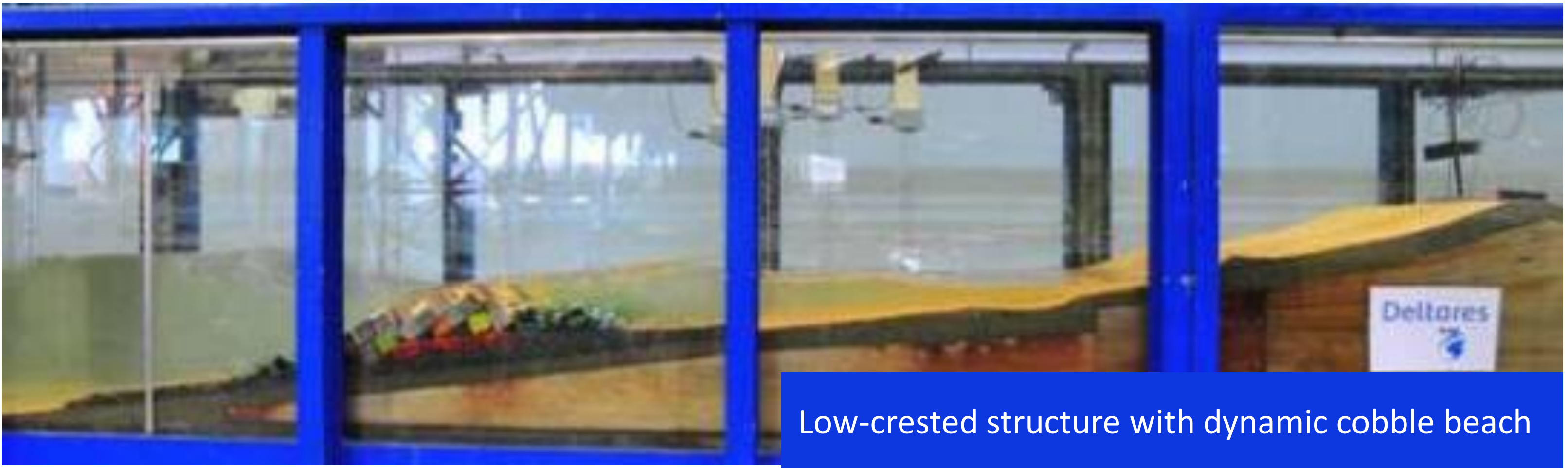

Low-crested structure with dynamic cobble beach

Toe stablity

Projects in the Scheldt Flume

Coastal structures

Low-crested structure with raised foreshore to lower wave overtopping

Projects in the Delta Basin

Forces on deck on piles

Modelling of stability of groynes

Forces and overtopping on quay wall

Projects in the Delta Basin

Ship motions

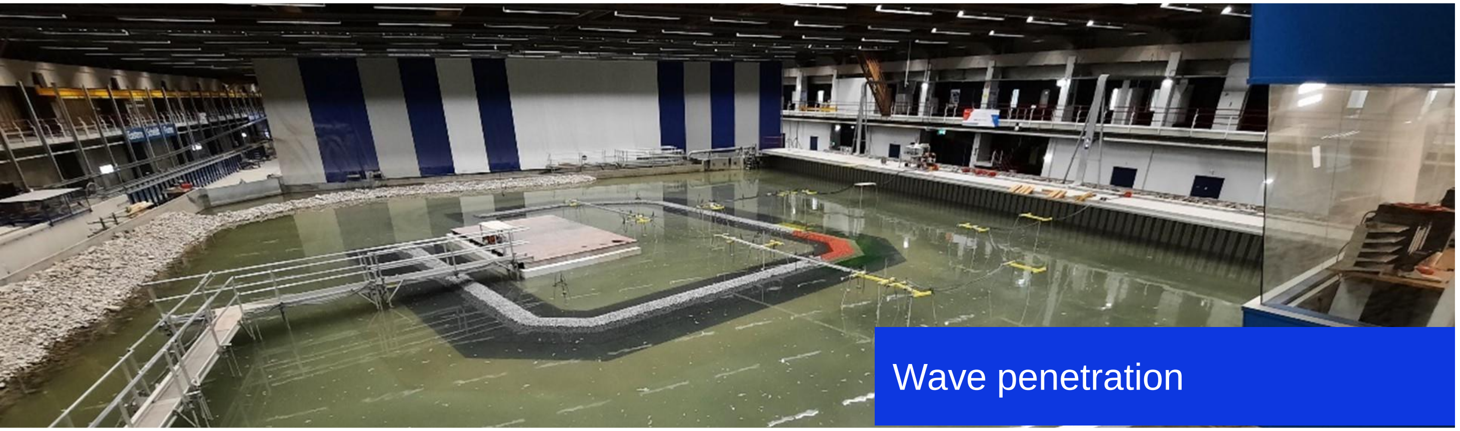

Wave penetration

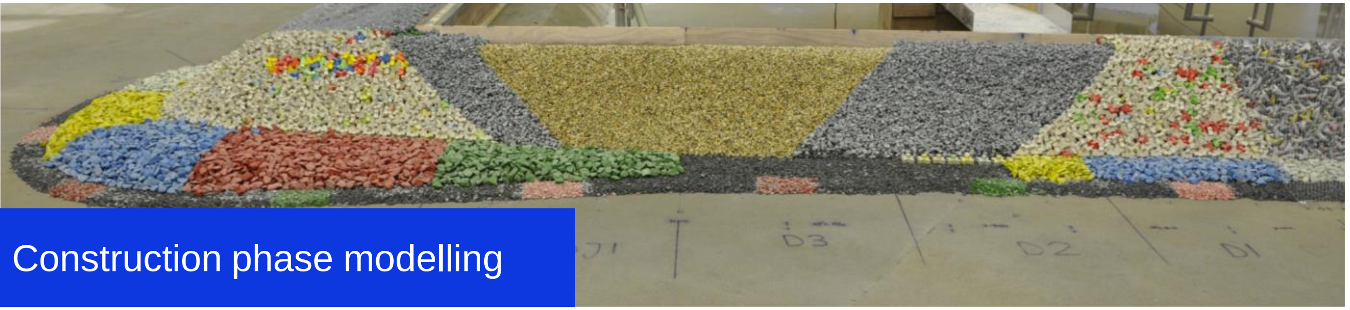

Construction phase modelling

Wave penetration

Deltares

Projects in the Atlantic Basin

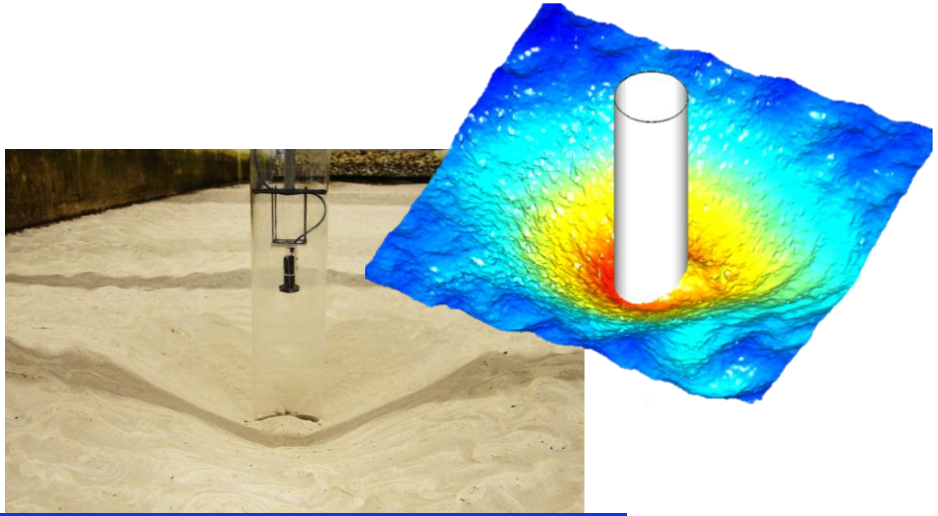

Scour around monopile foundations

Scour around jacket foundations

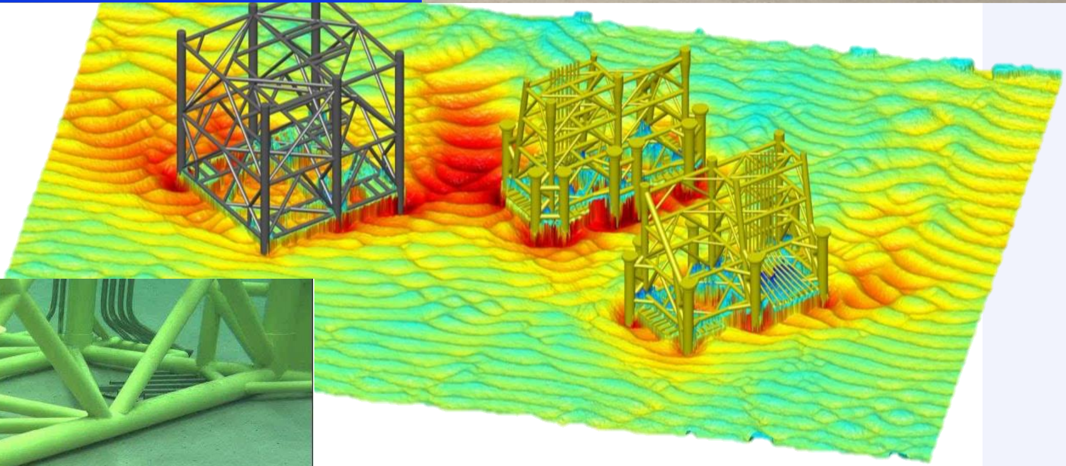

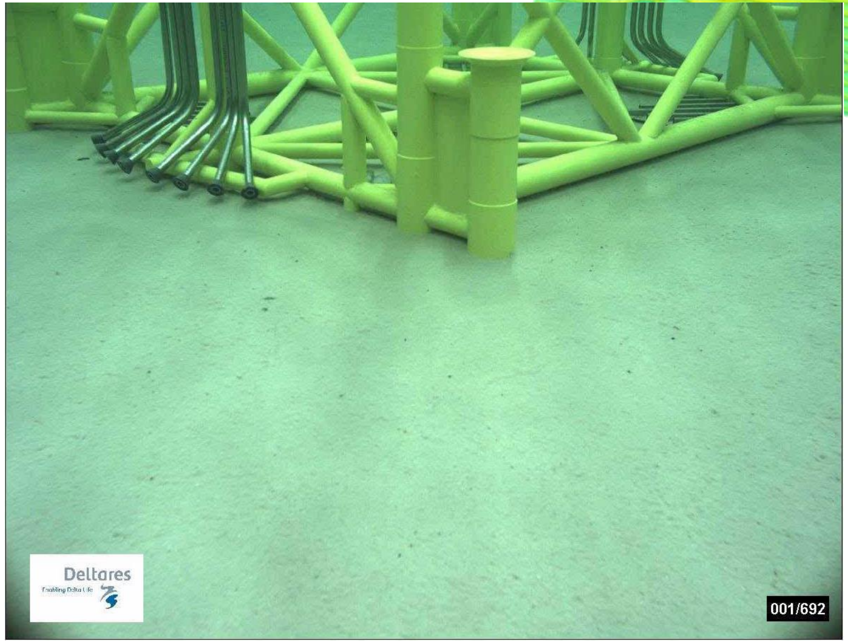

Deltares

Small-scale measurement techniques

- Hydrodynamic measurements
  - Wave gauges
  - Velocity meters
- Camera measurements
  - Underwater camera
  - Internal camera
  - PIV
- 3D stereophotography
- 3D Terrestrial laser scanner
- Additional project-specific measurements
  - e.g. force sensors, run-up markers etc.

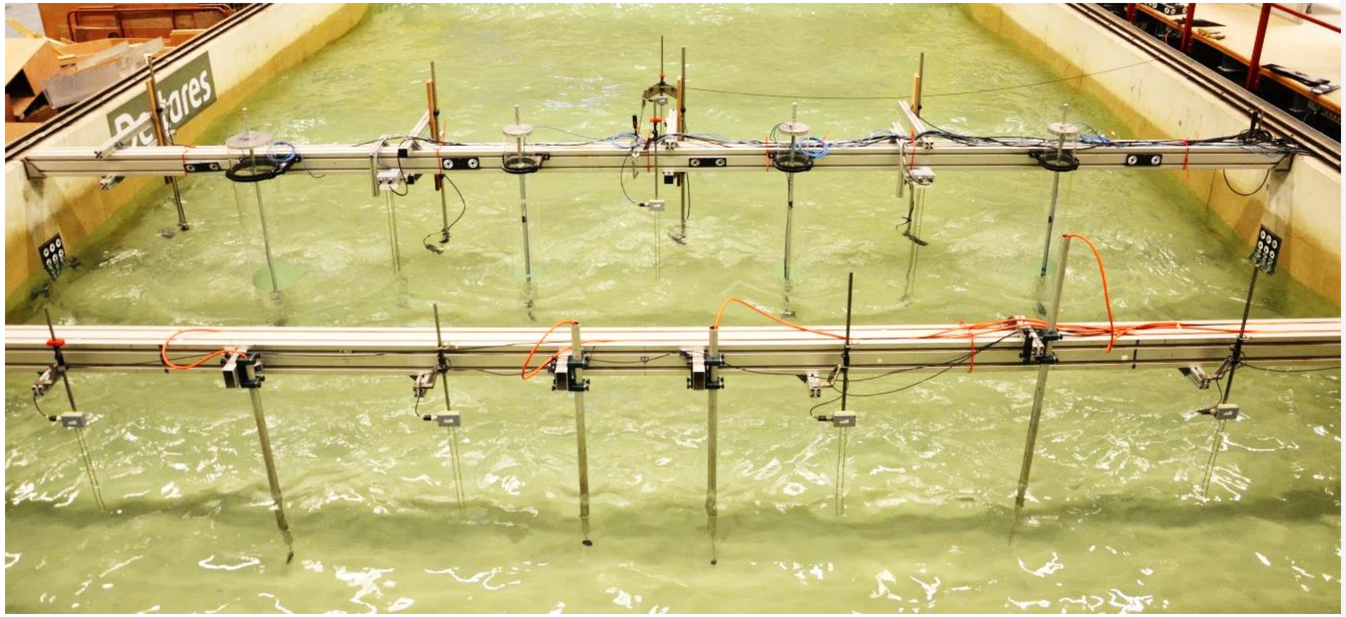

Small-scale measurement techniques

- Hydrodynamic measurements
  - Wave gauges
  - Velocity meters
- Camera measurements
  - Underwater camera
  - Internal camera
  - PIV
- 3D stereophotography
- 3D Terrestrial laser scanner
- Additional project-specific measurements
  - e.g. force sensors, run-up markers etc.

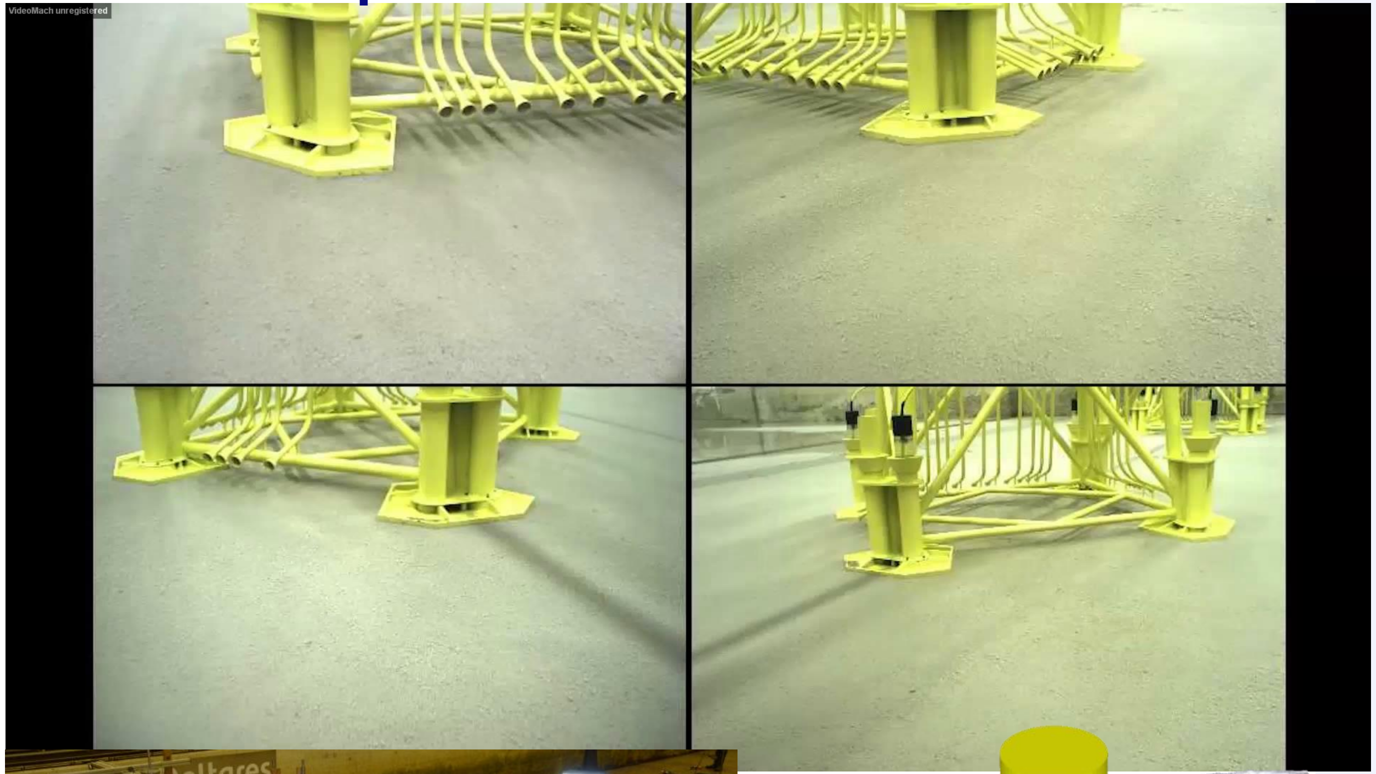

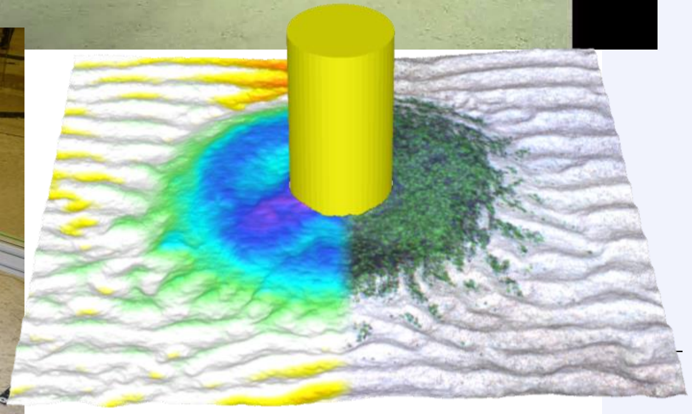

Delta Flume - Specifications

- Wave height: $H_{s,max}$ = 2.1 m, H_{max} = 4.7 m
- Regular waves H_{max} = 3.2 m
- Length: 300 m
- Width: 5 m
- Depth: 9.5 m
- Active reflection compensation
- Tidal water level variation during tests

Delta Flume - Examples of projects

- **Coastal structures:**
  - Wave impacts
  - Vegetation (building with nature)
- **Energy transition: offshore wind**
  - Wave attack on offshore wind turbine substructure
  - Scour protection
- **Soilmechanics:**
  - deformations
  - erosion

Deltares

Building with nature

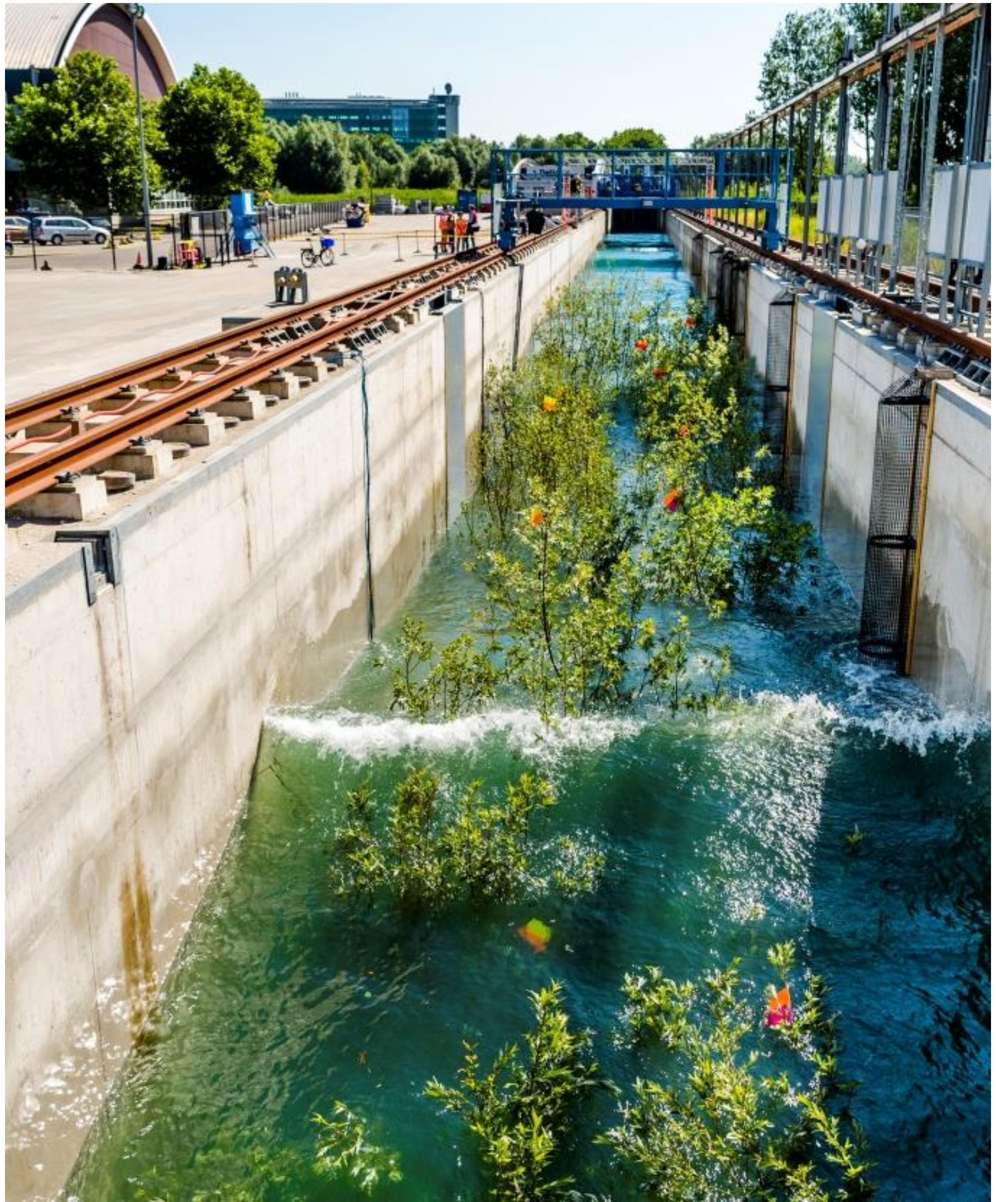

Delta Flume at Deltares

Energy transition: offshore wind

- Wave attack on offshore wind turbine substructure
- Scour protection

Delta Flume at Deltares

Delta Flume - Examples of instruments

- Wave gauges:
  - Resistant type
  - Radac (acoustic)
  - Lidar
  - Video AI
- Flow meters
  - Electromagnetic
  - ADV and ADCP
- Pressure cells
- Accelerometers
- Faro laser scanner
- Video

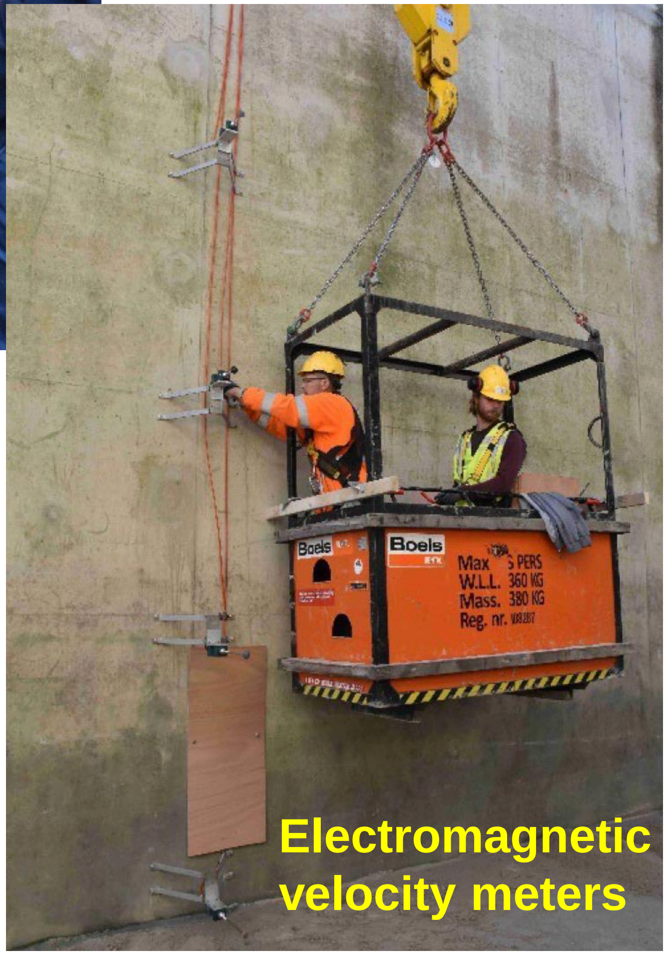

Delta Flume – Example project
Erosion of clay embankements by wave attack

Erosion of clay embankements by wave attack

Structures clay with mature grass from old embankement

Blocks of 2x2 m^2, 0.85 m thick

Erosion of clay embankements by wave attack

Construction of full scale embankment

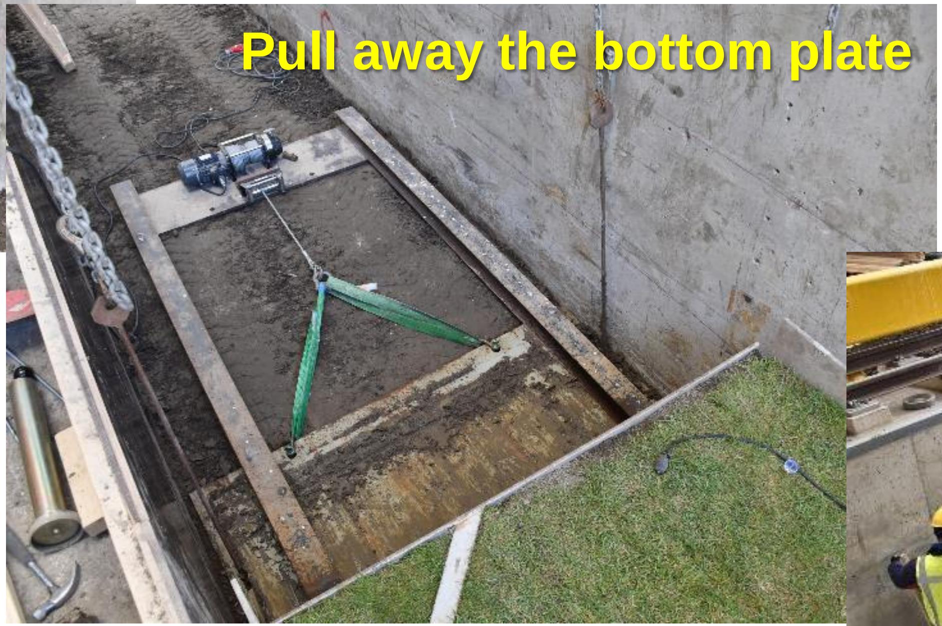

Erosion approach

Projects aimed at characterisation of erosion process


Observed erosion process:

Phase 1: erosion grows mainly in depth

Phase 2: terrace and cliff erosion
eroded volume increases faster

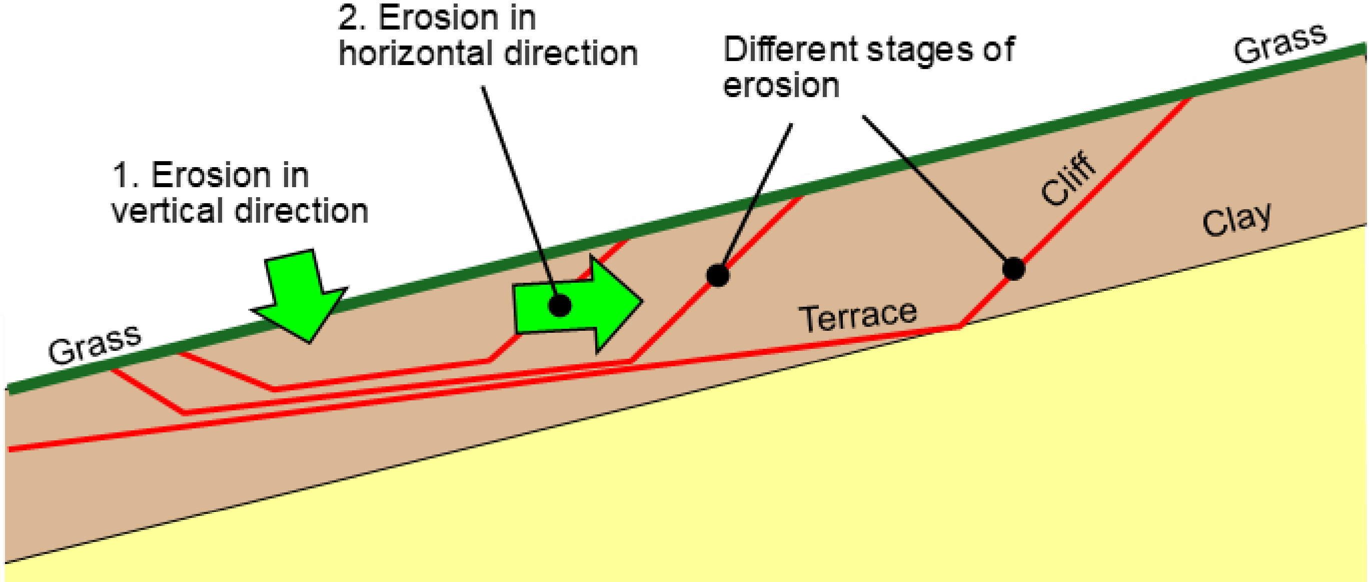

Erosion approach

Projects aimed at characterisation of erosion process

Physical modelling	• Erodibility of clay • Erosion process
Numerical modelling	• Extension of the Delta flume experiments • Detailled information on the hydraulic loads
Erosion formulas	• Emprical formulas to describe the erosion rate • Description of the erosion profile over time
Probabilistic calculations	• Expected return period of erosion depths • Minimum required thickness of the clay revetment

Delta Flume – Example project
Climate impact on atoll islands (ARISE)

- Modelling of climate impact on Atoll islands
  - Large scale because of scale effects
- Runup, overwash, erosion of island
- Validation of Xbeach numerical model

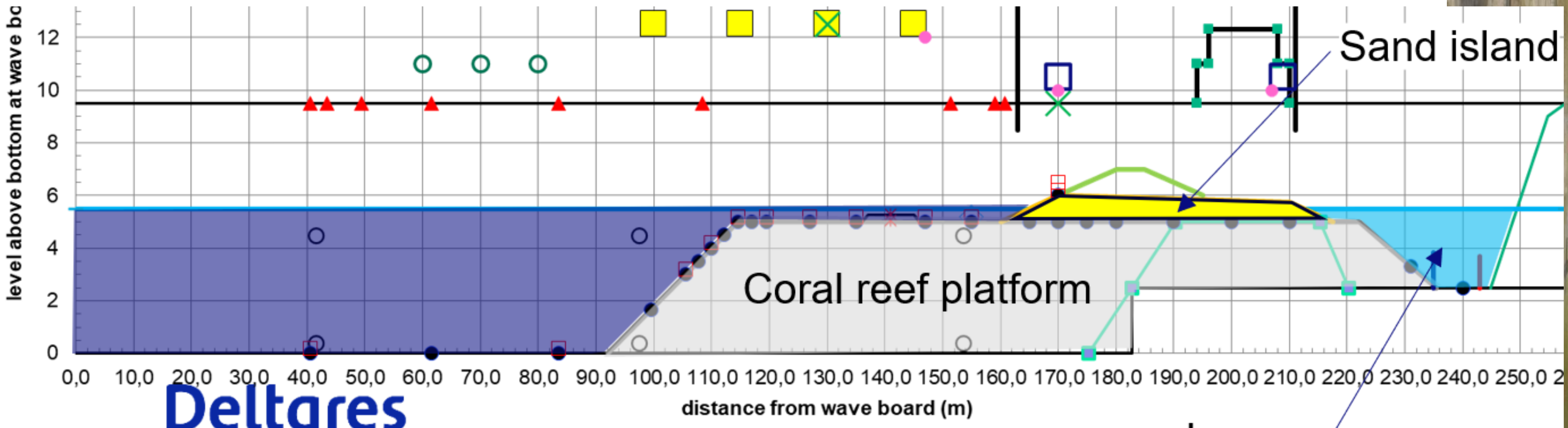

Deltares

Delta Flume – Example project
Climate impact on atoll islands (ARISE)

- Modelling of climate impact on Atoll islands
- Runup, overwash, erosion of island

Deltares

Delta Flume – Example project
Climate impact on atoll islands (ARISE)

- Modelling of climate impact on Atoll islands
- Runup, overwash, erosion of island

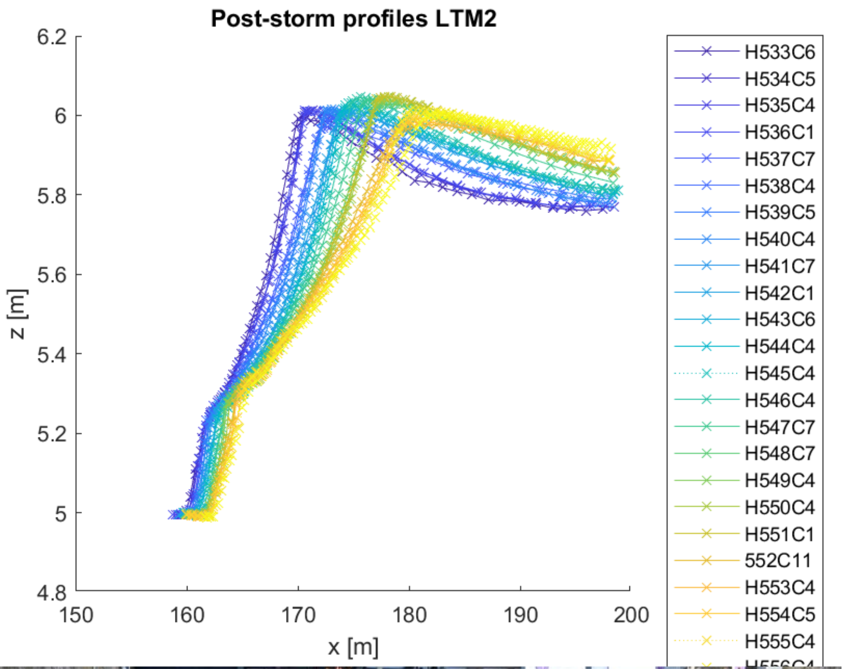

Deltares

Contact

www.deltares.nl | @deltares | linkedin.com/company/deltares

info@deltares.nl | @deltares | facebook.com/deltaresNL

DC Presentations

Morphodynamic Analysis of the upper confined and unconfined beach profiles during Episodic events

06/11/2024

SEDIMARE Workshop
Deltares

Buckle Subbiah Elavazhagan

SEDIMARE – DC 05
IH-Cantabria, Universidad de Cantabria

Javier L. Lara
Professor, Universidad de Cantabria

María Maza
Asoc. Professor, Universidad de Cantabria

Presentation on
Free long waves and its role in inaccurate numerical prediction of break bar formation

Currently in Month 9

SEDIMARE

Sediment Transport and Morphodynamics in Marine and Coastal Waters with Engineering Solutions

I INTRODUCTION

Applying IH2VOF –SED model to model different morphodynamic processes and the governing hydrodynamics on different beach configurations and sustainable protection measures

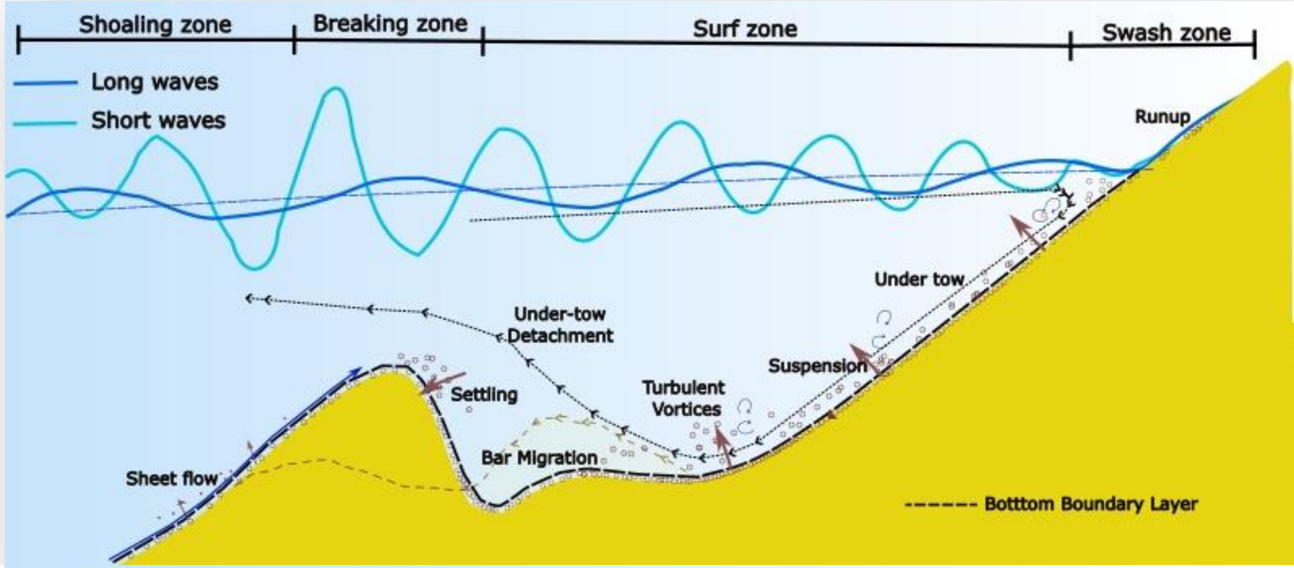

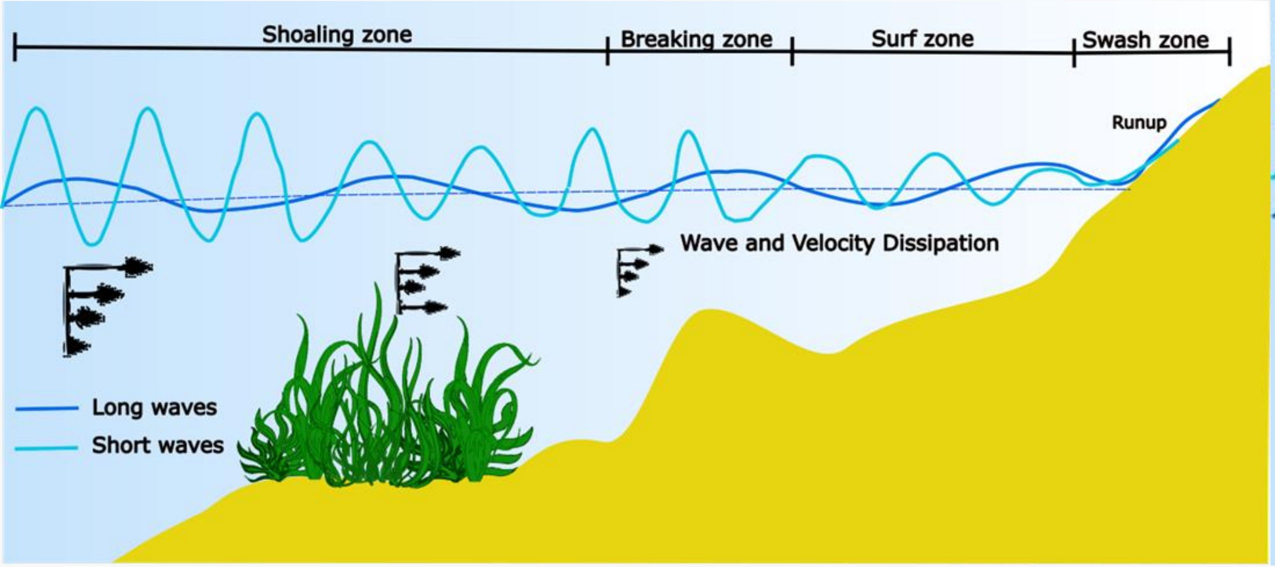

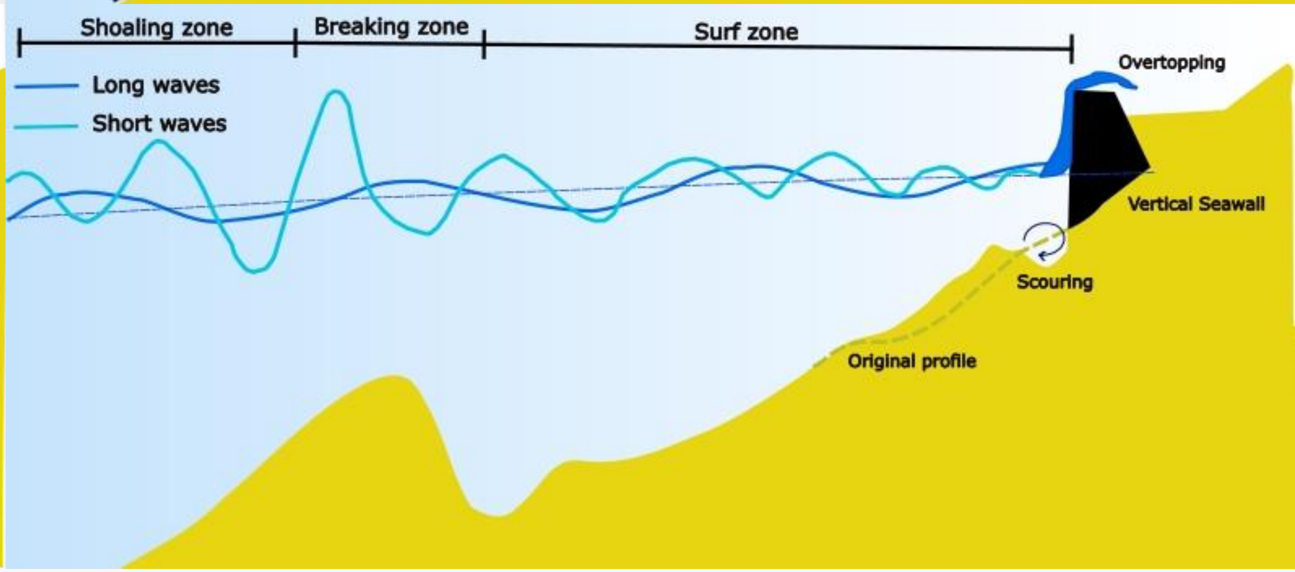

II NUMERICAL BACKGROUND

2DV RANS based solver

Turbulence is accounted using a k-ε closure model

Free surface reconstruction using Volume of Fluid technique

Roulond et.al 2006 Emprical formula for Bed load transport

Advective- Diffusive equation is solved for Suspended load transport

Cut-cell technique is used to model solid boundaries

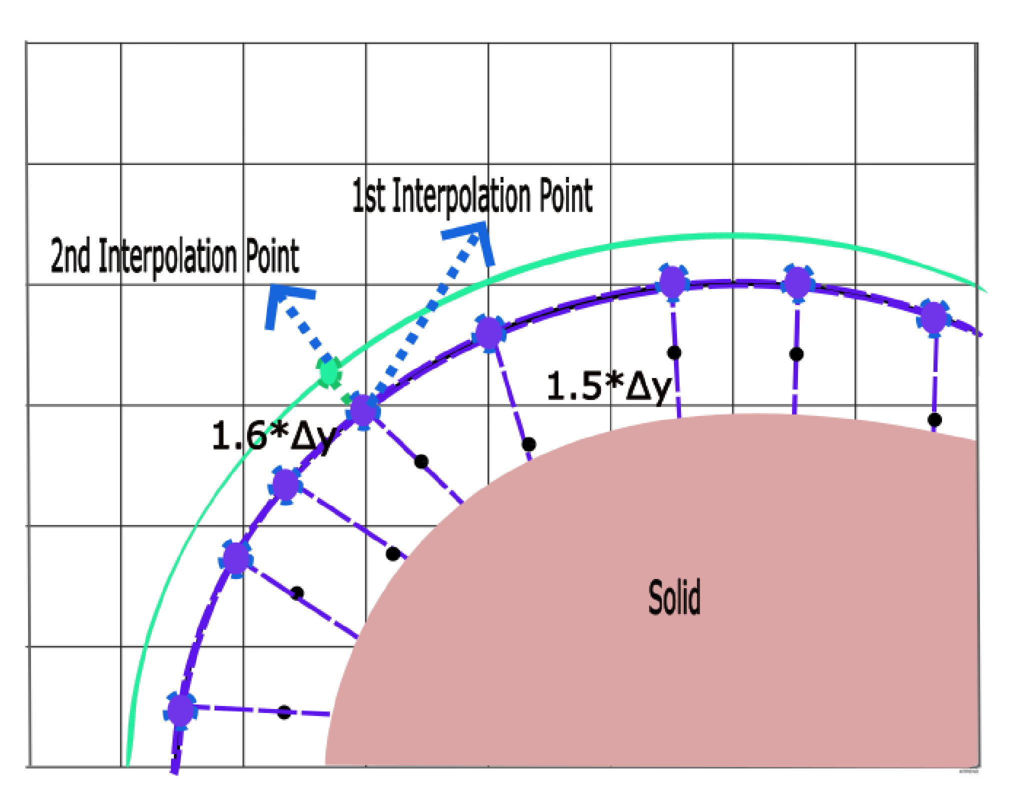

Made improvements to the existing code

Implemented Two point Friction velocity estimation method

This approach still use log-law for estimation

But removes assumption of Roughness Length

III Implementing Laboratory case

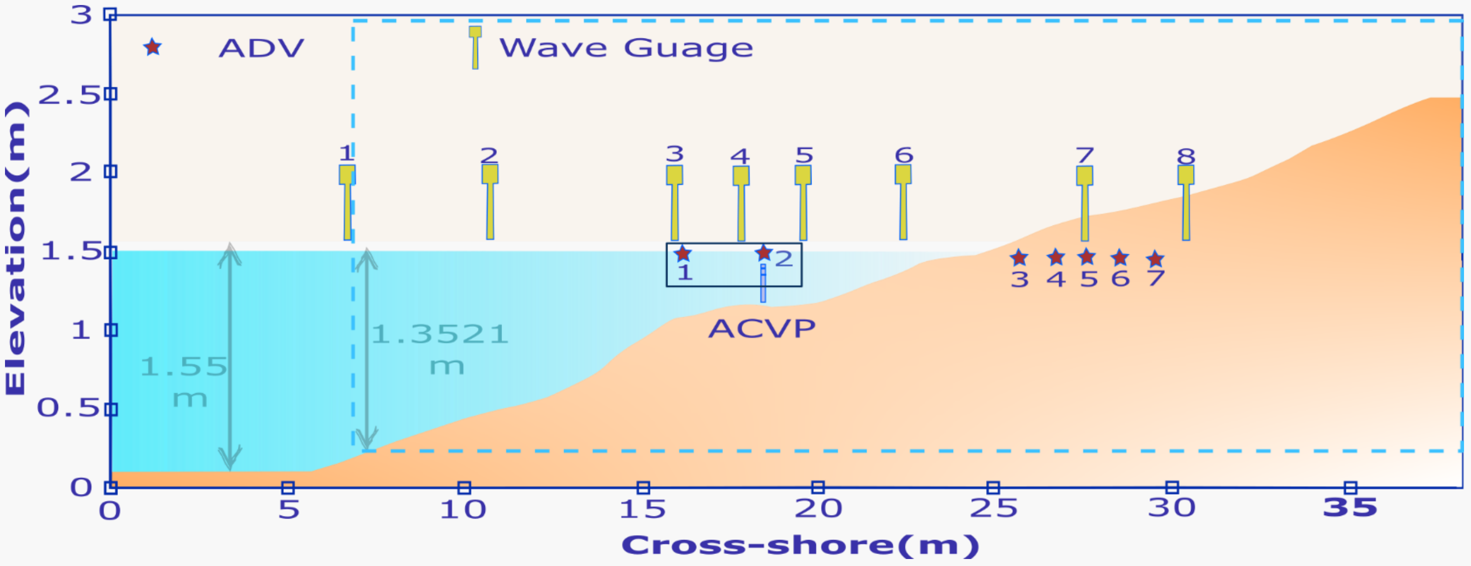

Near-Bed Sediment Transport during offshore bar migration in large-scale experiments . Florian Grossman et.al 2022

Erosive case using Bi-chromatic Waves

H1(m)	H2(m)	F1(Hz)	F2 (Hz)
0.245	0.245	0.3041	0.23657

3-different Initial beach states

Bar formation

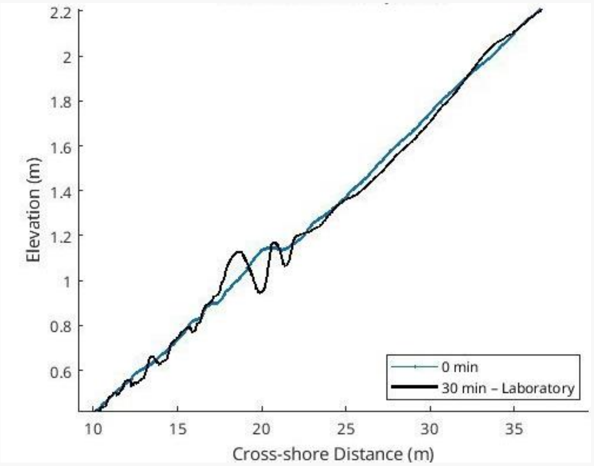

Bar movement

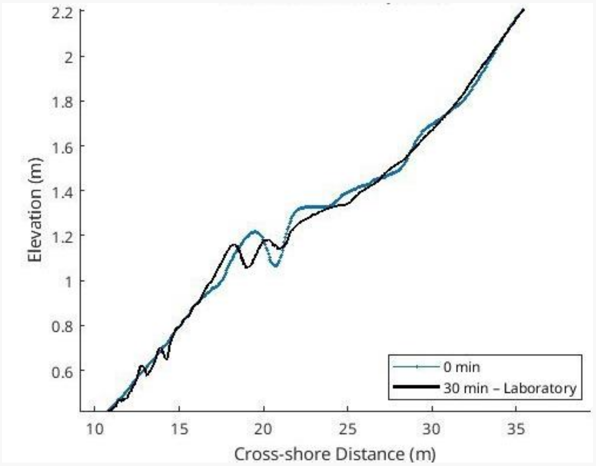

Berm Erosion

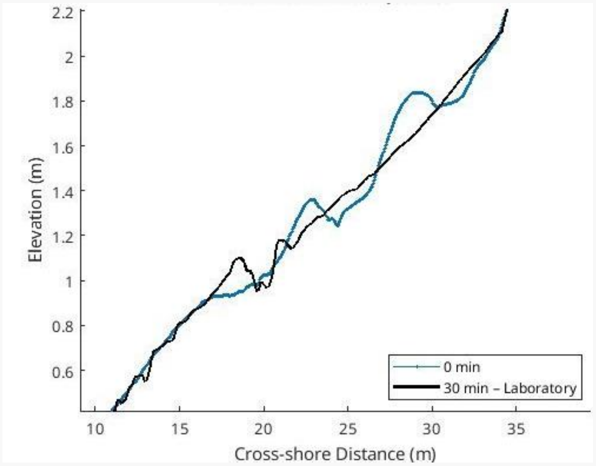

III Implementing Laboratory case

Experimental Limitation

1. First Order Wave generation
2. Significant Presence of Free long waves
3. No active wave absorption

Data Limitation

1. Didn't get wave paddle motion signals
2. Certain ADV and ADCP data are lacking due to unexpected sedimentation during the experiments

Numerical Capabilities

1. First and second order waves as boundary condition
2. Active wave absorption with possibility of disabling it

Numerical Limitation

1. 2D model
2. Difficulty in replicating entire length of the flume
3. High computational cost

1. Modelling entire length of the flume would be challenging for a Sediment transport model without coupling with a hydrodynamic model
2. No paddle signals means measured wave gauge data at a certain point would be used as a wave input

J.W.M. Kranenborg et.al, 2024

Effects of free surface modelling and wave-breaking turbulence on depth-resolved modelling of sediment transport in the swash zone, Coastal Engineering.

Joep van der Zanden et,al, 2019a
Sand transport processes and bed level changes induced by two alternating laboratory swash events, Coastal Engineering.

IV Free vs Bound Long waves

	Bound Long Waves	**Free Long Waves**
Source	Generated at the wave paddle bound to the primary wave group using 2nd order wave generation	Generated Freely in the lab through non linear interactions of primary wave group and wave reflections
Dependence	Tied to primary wave group, travels at wave group celerity	Independent, self-propagating
Trigger for Existence	After Wave breaking becomes free	Primary wave group interaction

V Free Wave Generation in the Lab

1st wave group vs 52nd wave group

H1(m)	H2(m)	f1(Hz)	f2 (Hz)
0.245	0.245	0.3041	0.23657

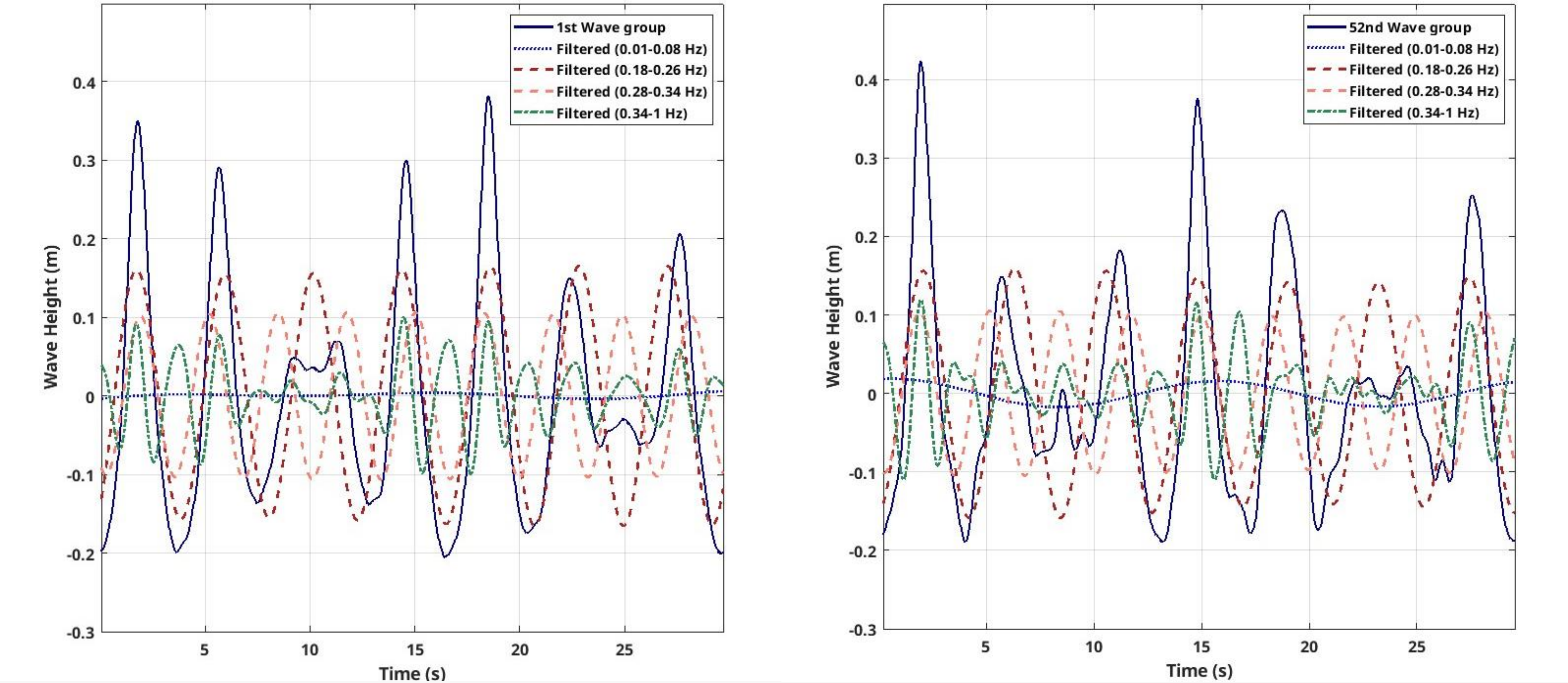

V Free Wave Generation in the Lab

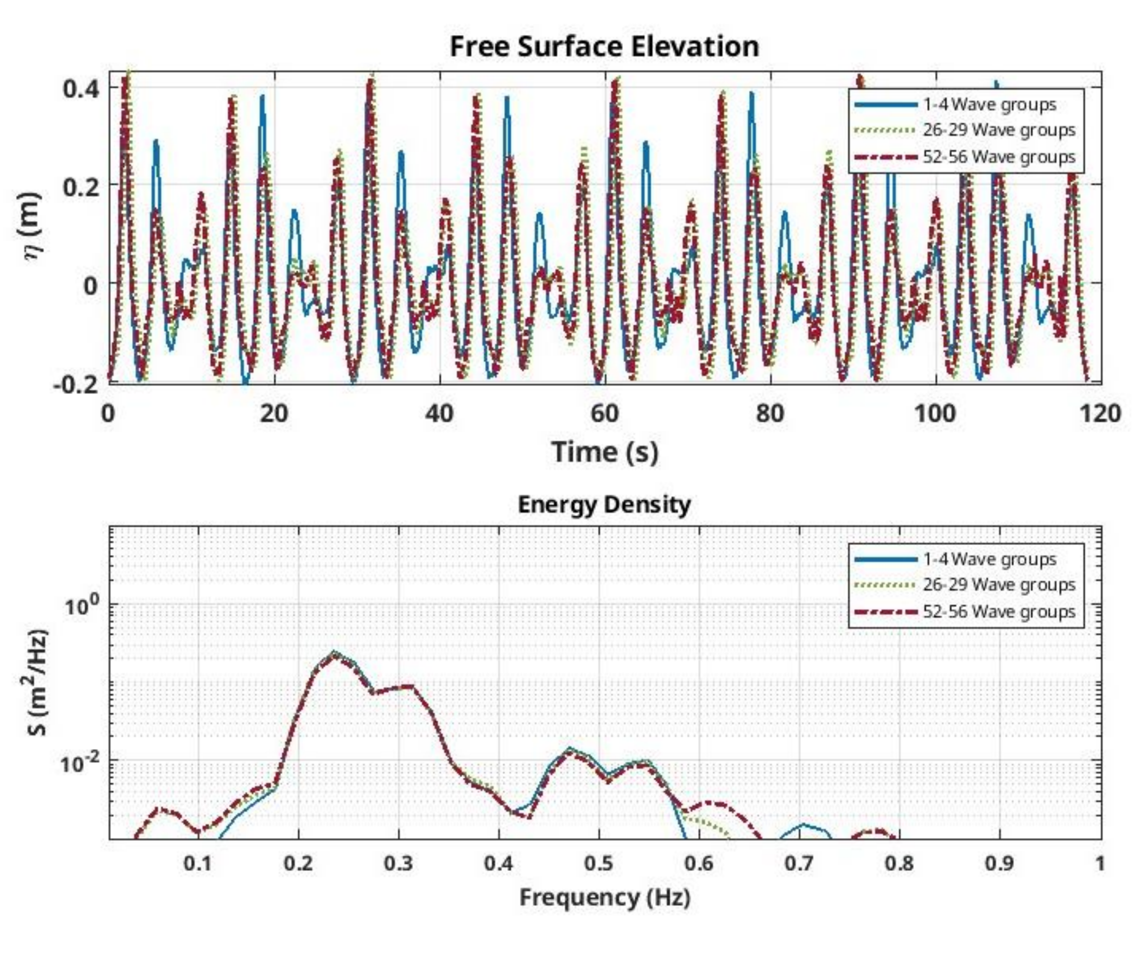

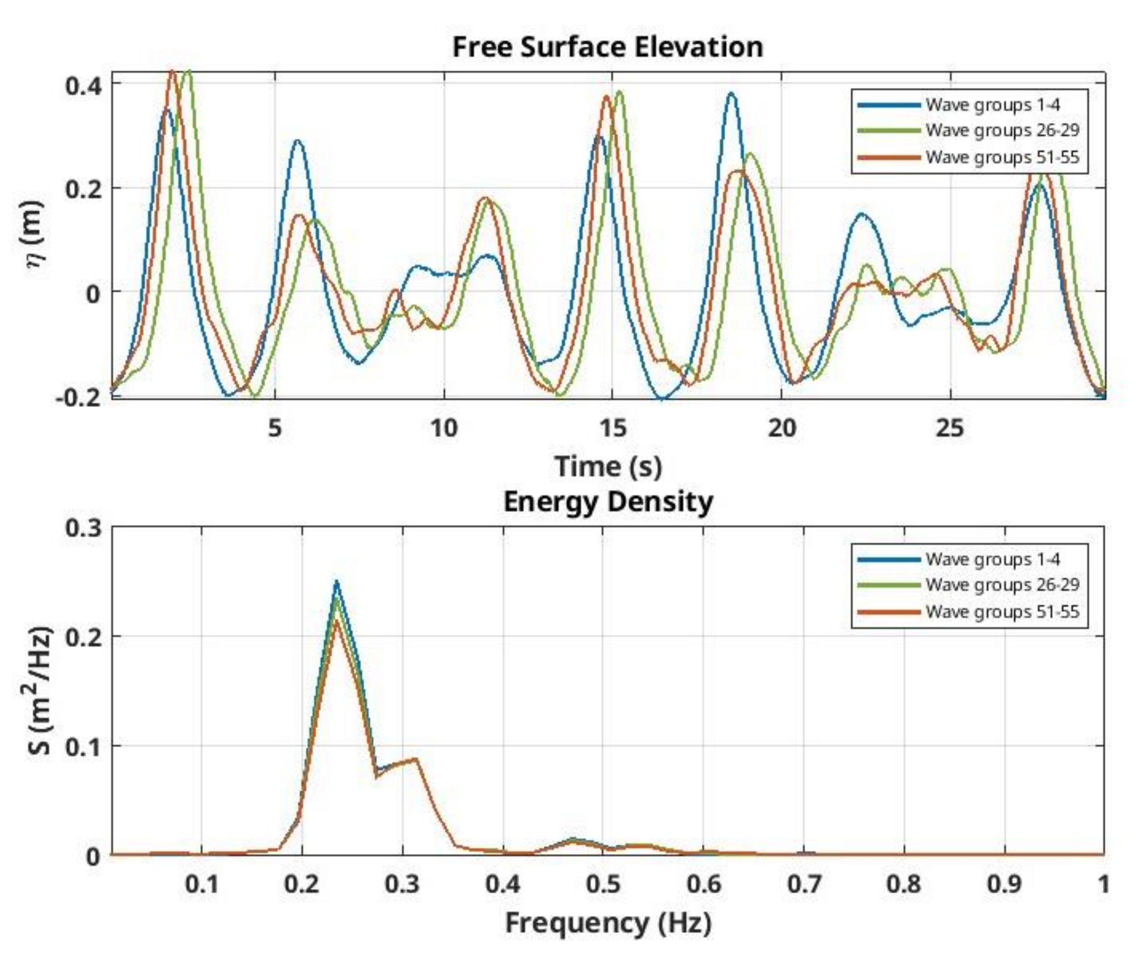

VI Results - Free Surface Elevation (Final 4 wave groups)

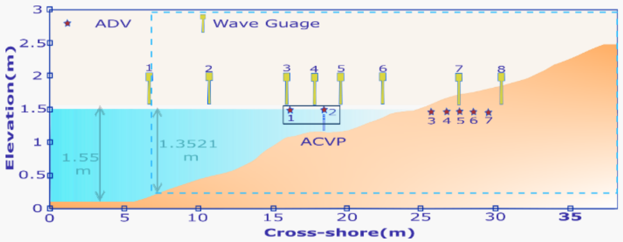

Original signal from wave guage

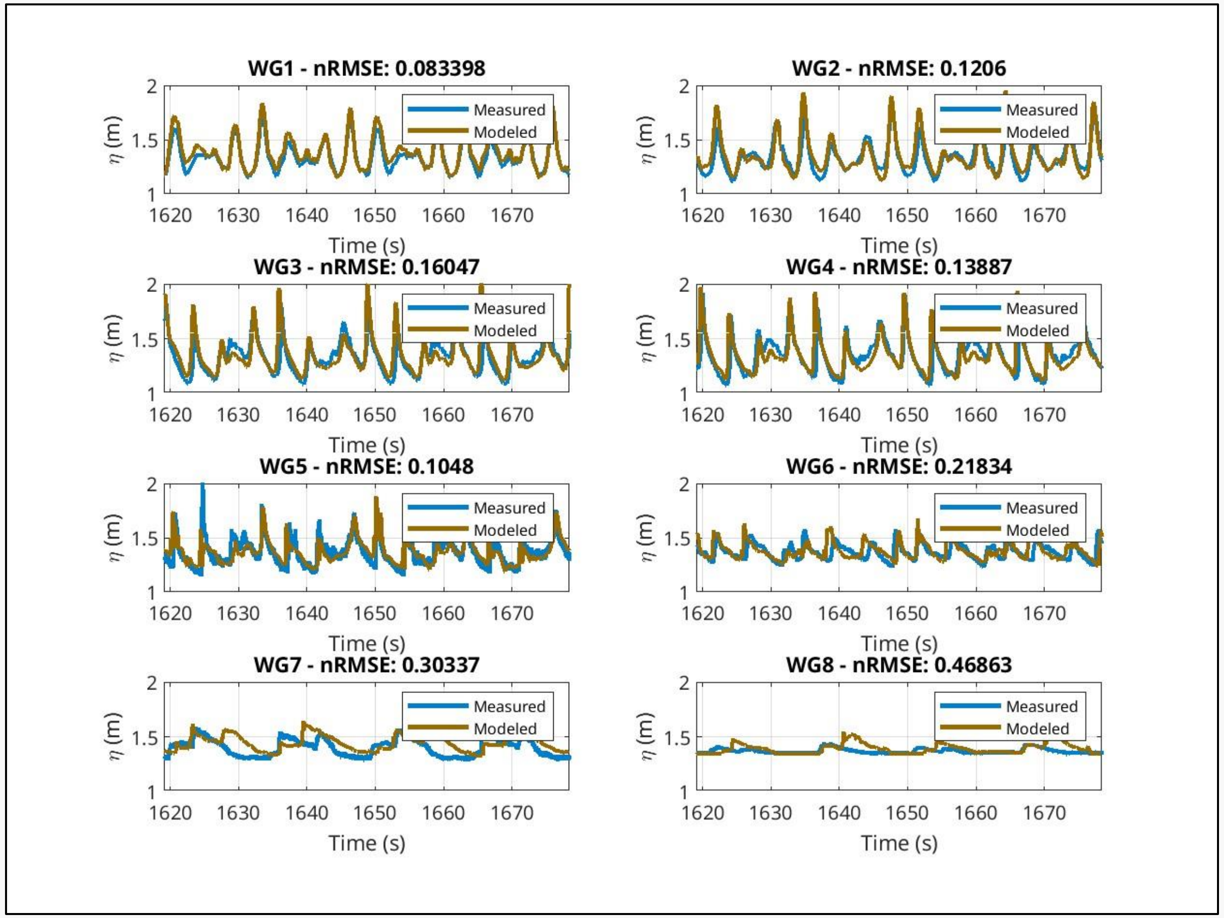

Filtered signal from wave gauge

Removed Free long wave and super-harmonics from the signal

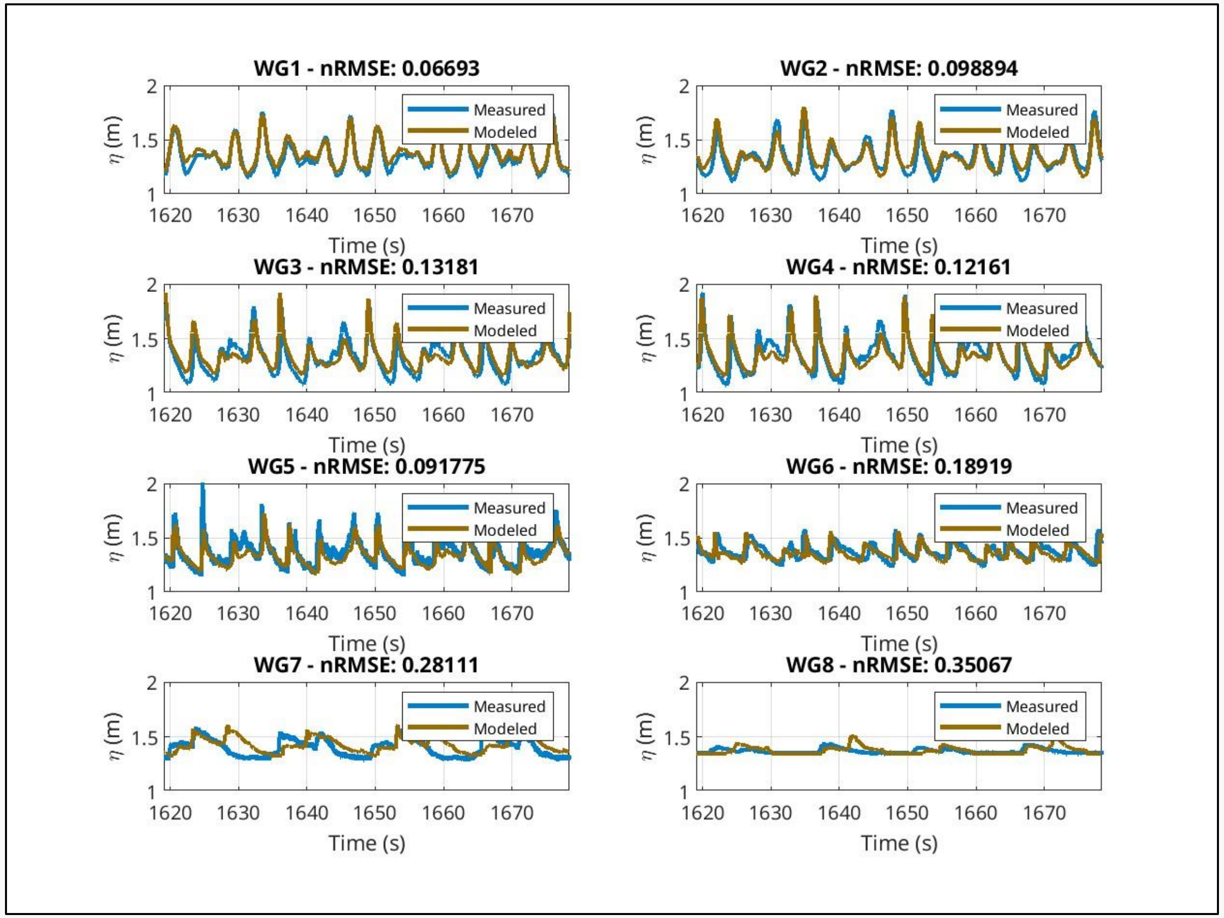

VI Results - Wave components(First 4 wave groups)

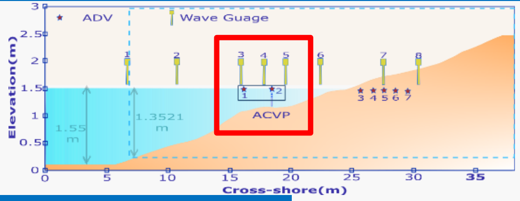

Original signal from wave gauge

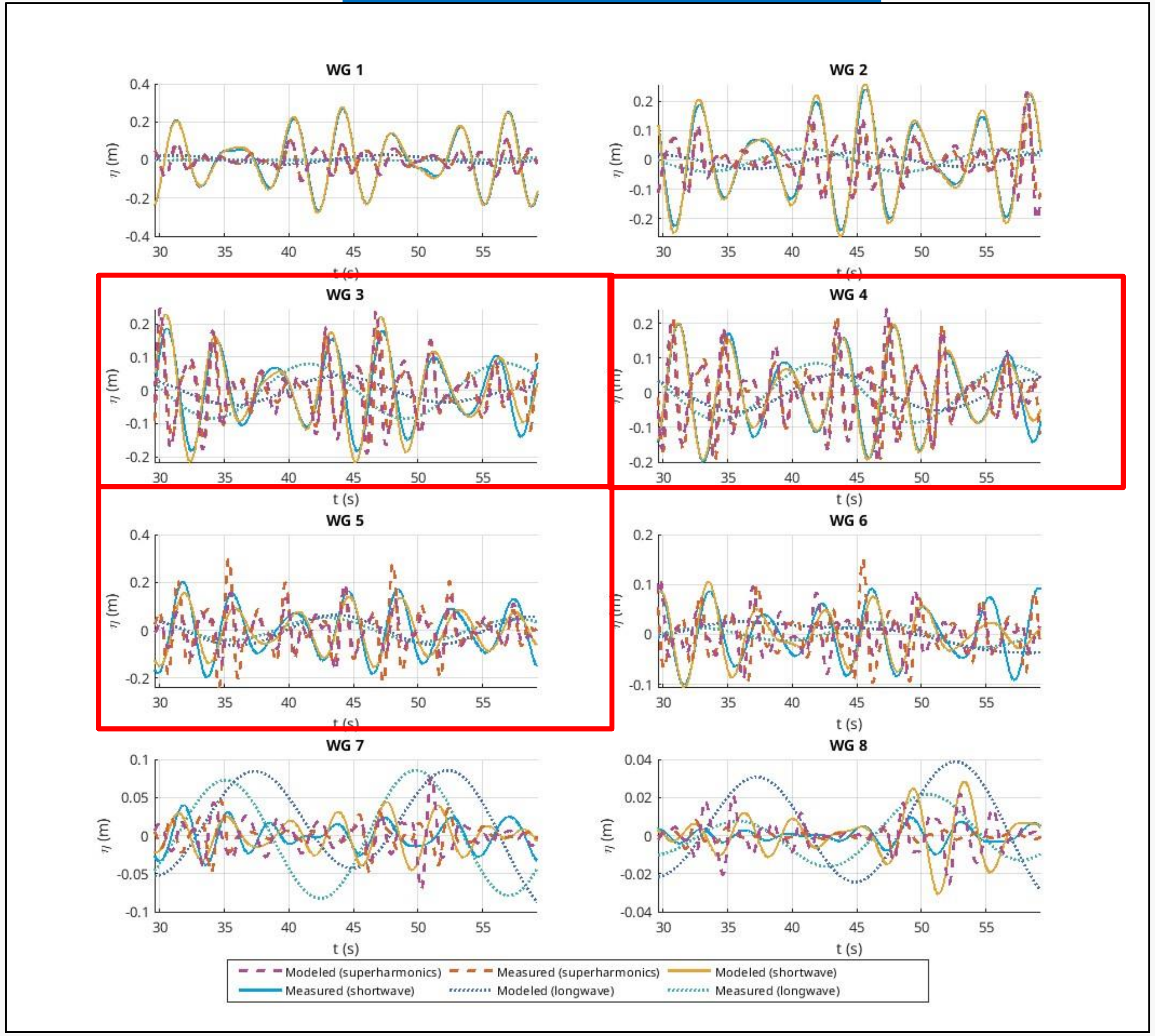

Filtered signal from wave gauge

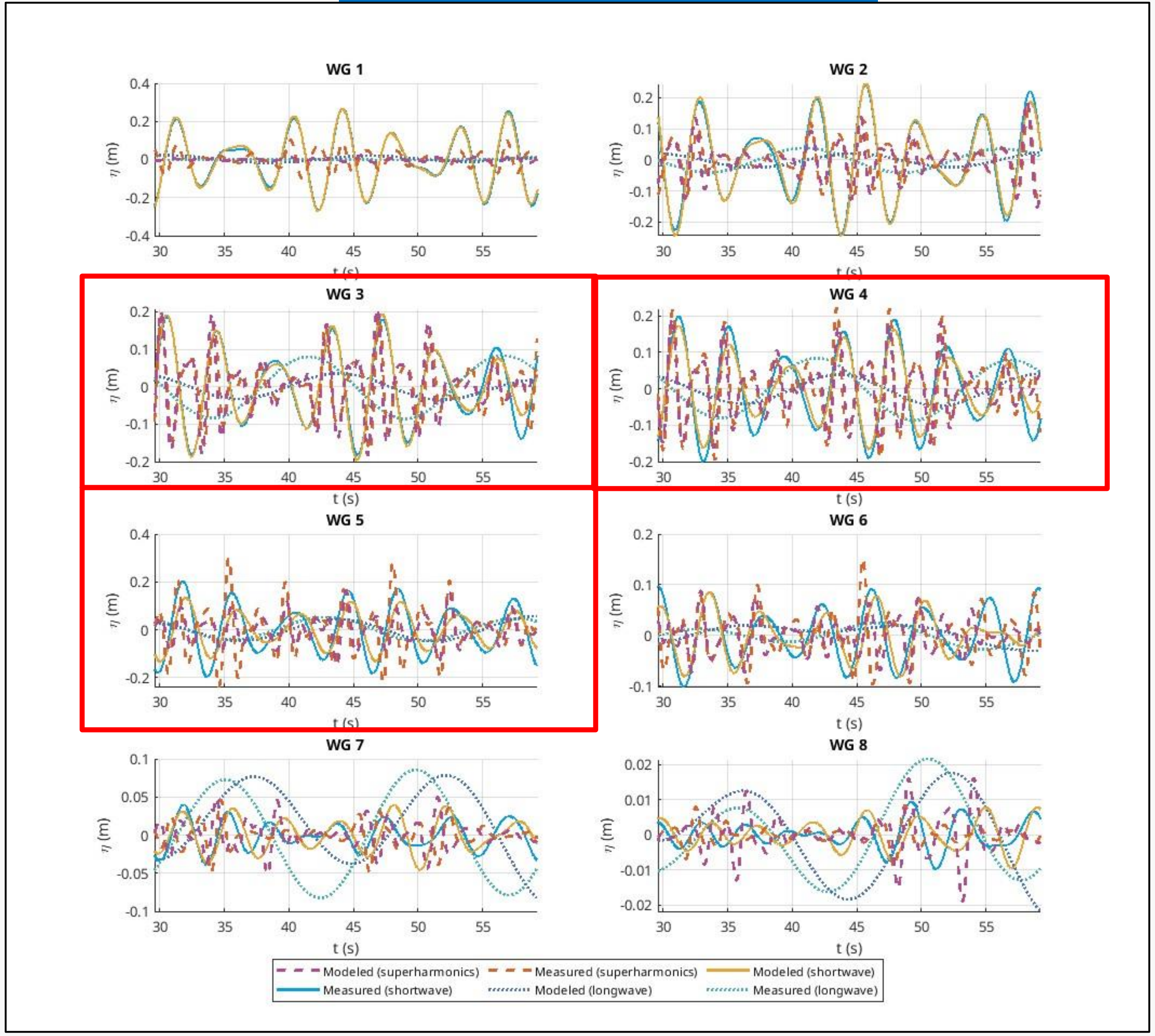

VI Results - Bed Level Evolution

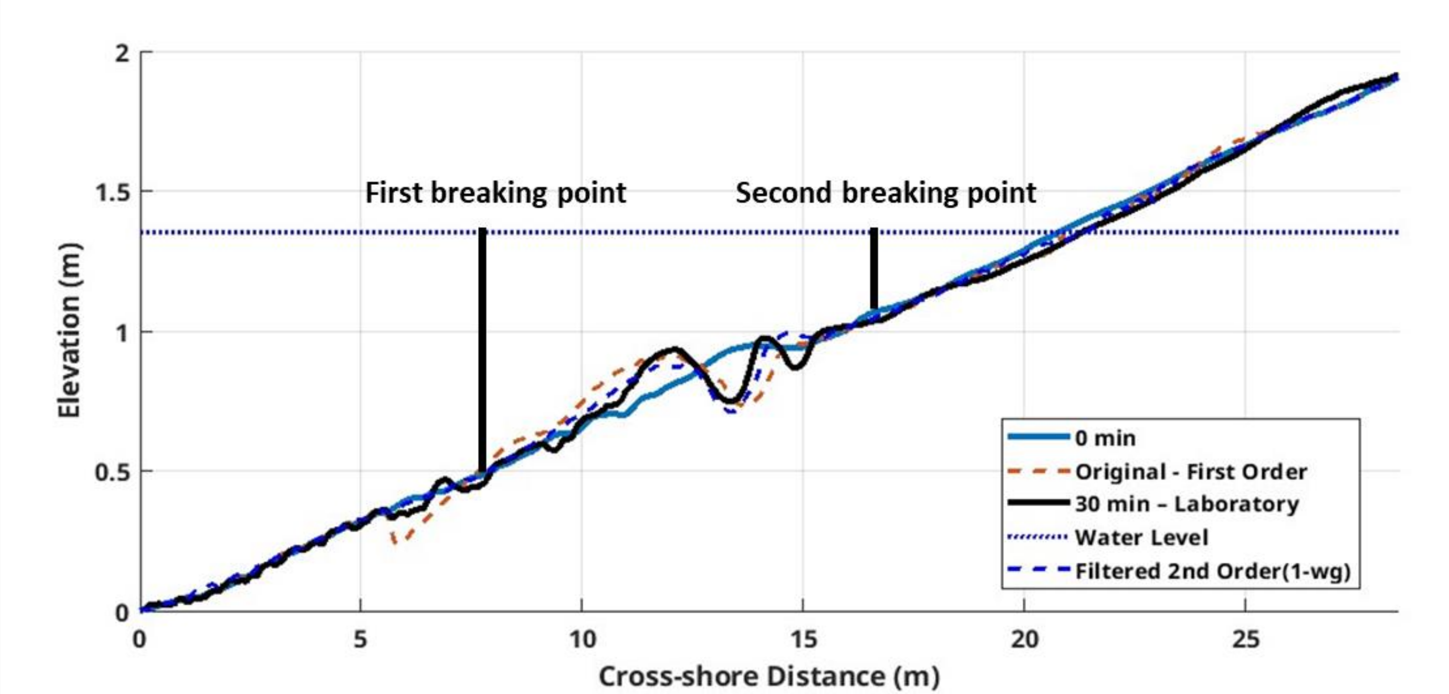

Desirable Primary breaking point

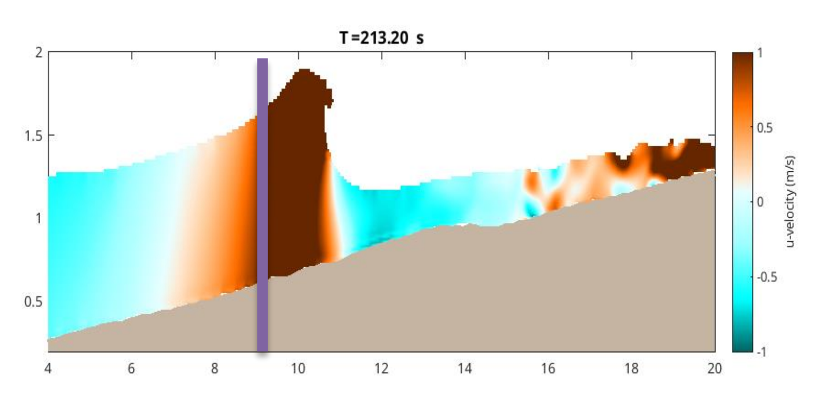

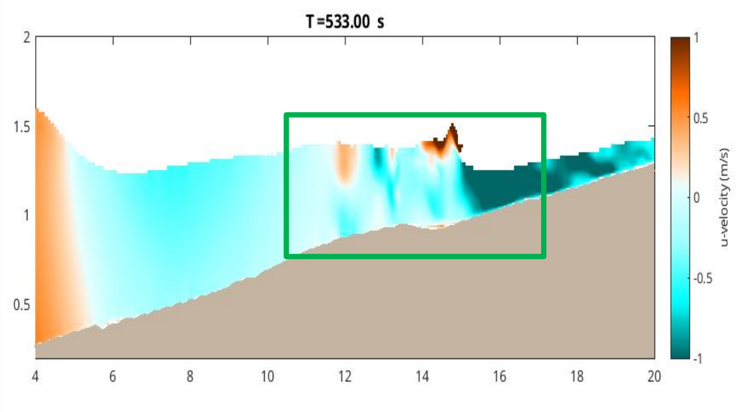

Twin velocity concentration points at the bed potentially leading to formation of two troughs

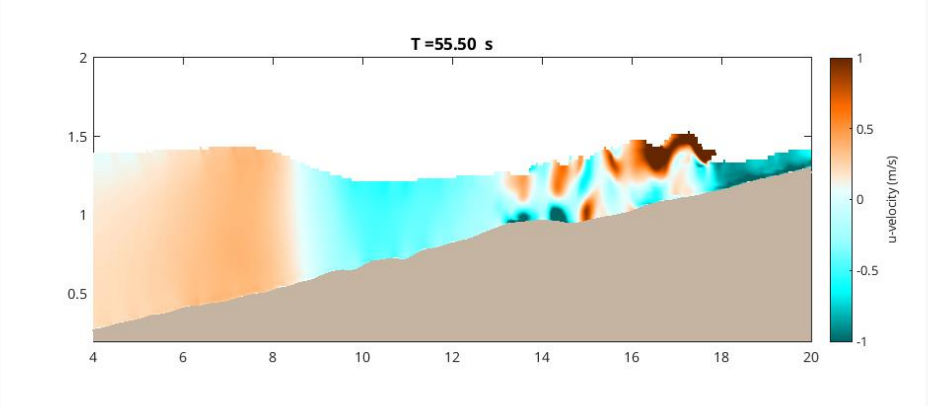

Single concentration point, potentially corresponding the larger of the two troughs

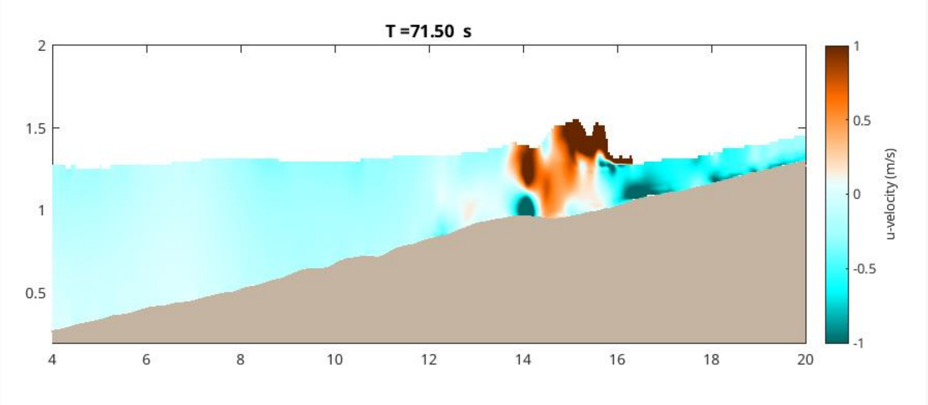

1. **First Breaking point is correctly modelled and thus formation of the primary bar**
2. **Second breaking influences the dynamics of swash zone and also the formation of the smaller bar**
3. **Strong off-shore directed current means, single concentration point on the bed or wave dissipates without significant impact to the bed**

VI Results - Sediment Transport

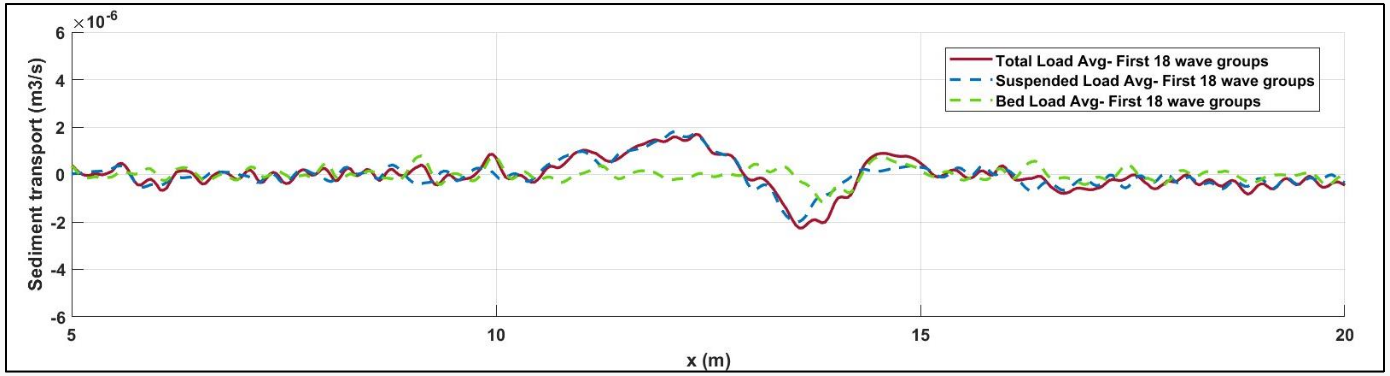

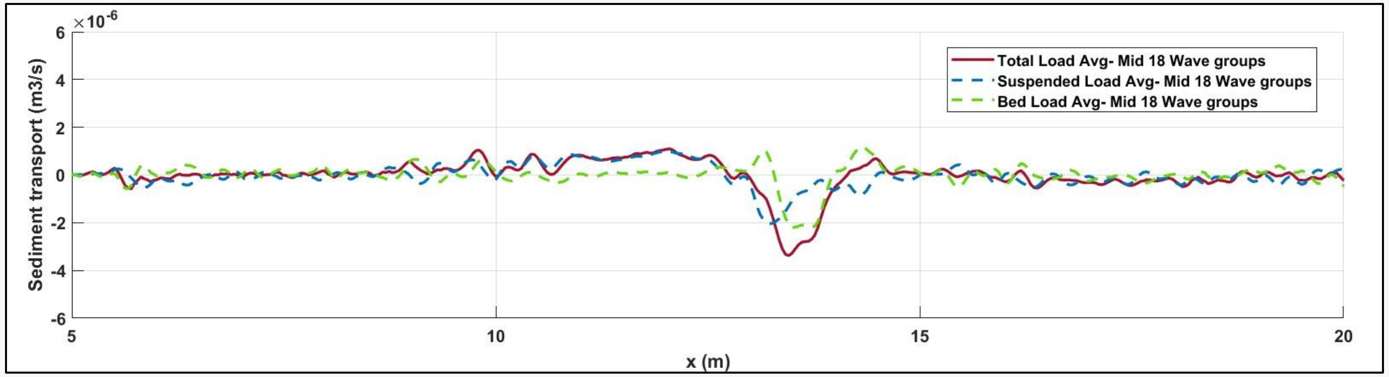

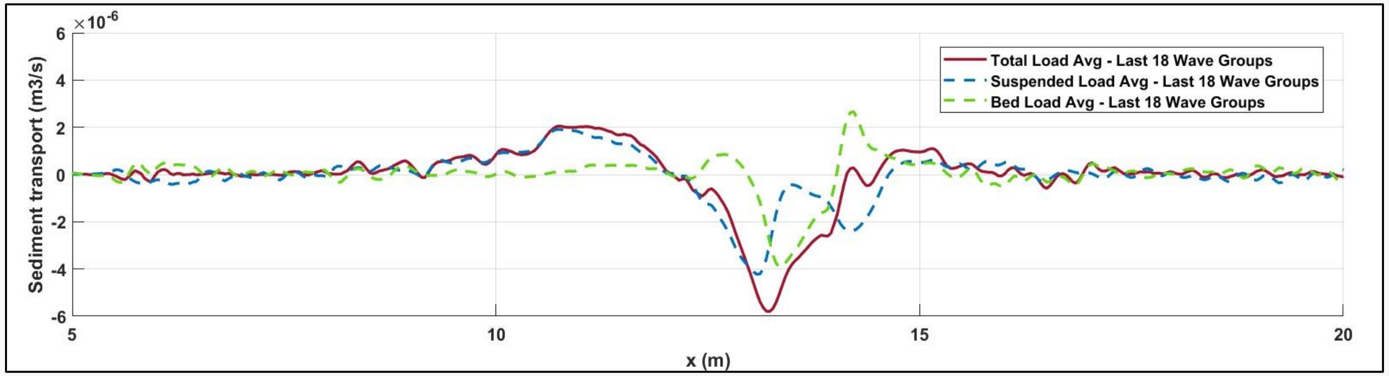

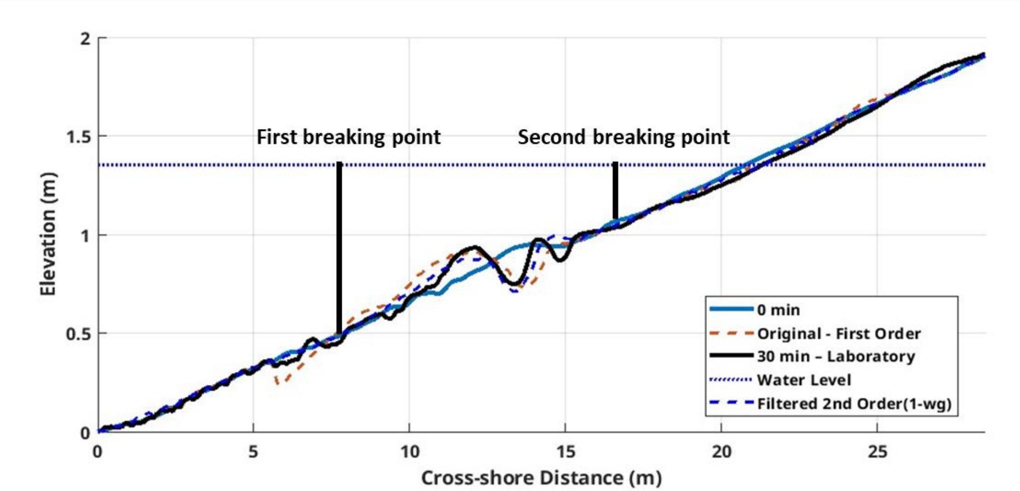

Representation of evolution of Sediment transport over 30minutes, in the Filtered + Second Order case

VI Results - Velocity and Sediment concentration during first 4 and final 4 wave groups

U- Velocity

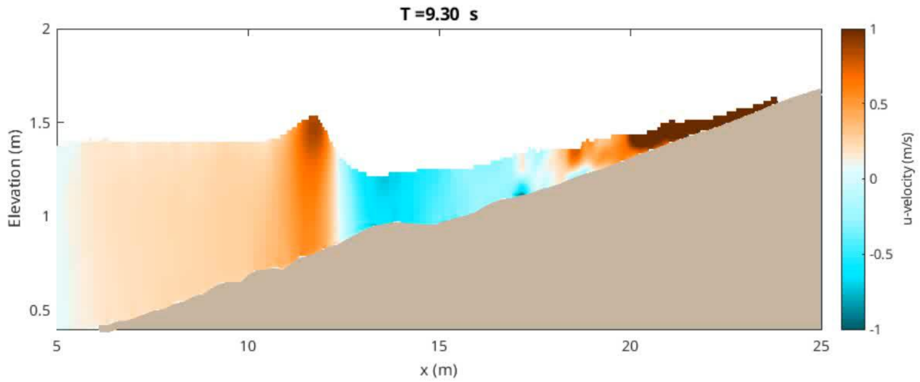

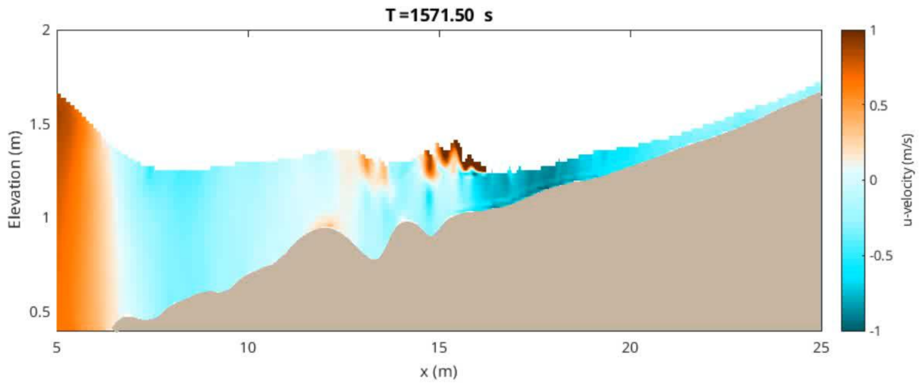

Sediment Concentration

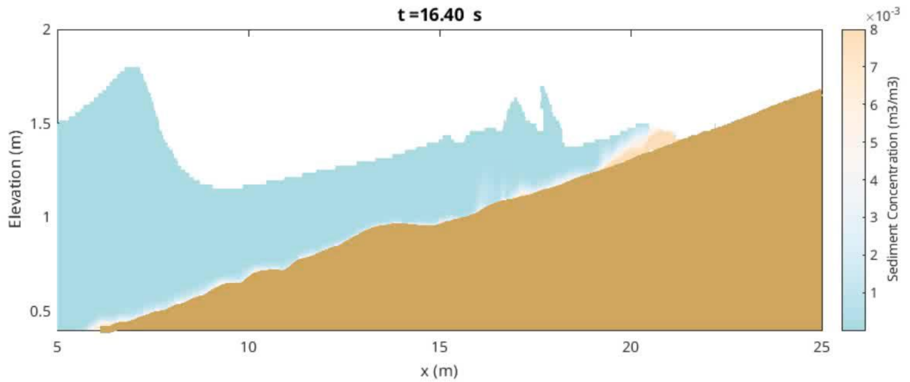

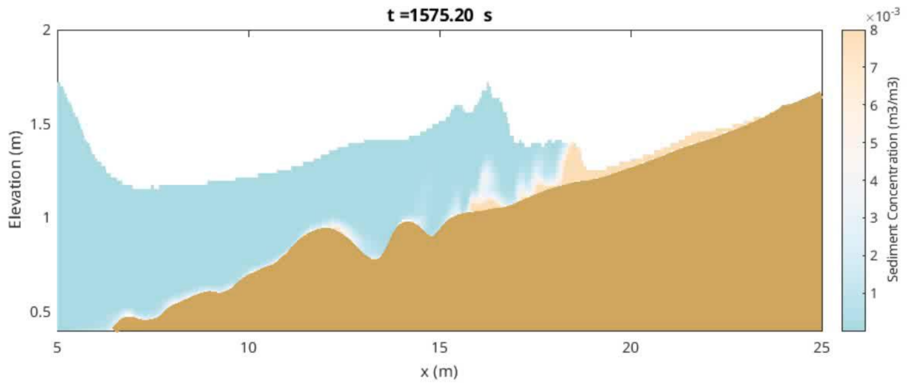

VII Conclusion

01 Accurate representation of phase of the long wave and free wave energy is needed for accurate representation of sediment transport

02 Using free wave contaminated waves from gauges changes the way the waves breaks in the model and thus bar formation

03 Free long waves generated in the model does not perfectly match the long waves generated in the Laboratory

04 In the breaking zone significant difference in free long wave presence alters the breaking and sediment dynamics

VIII What’s Next

01 The current work on free wave influence in numerical model will be developed and communicated

02 Next case will be validating the model with a bound wave component experiment

03 Validating the model for a case with submerged vegetation field

04 First Secondment in Deltares – September Next year (Planned – not confirmed)

05 Validating the model for seawall case (beach morphodynamics and wave overtopping)

06 Second Secondment in UNIVPM – in 2026

Morphodynamic Analysis of the upper confined and unconfined beach profiles during Episodic events

06/11/2024

SEDIMARE Workshop
Deltares

Buckle Subbiah Elavazhagan

SEDIMARE – DC 05
IH-Cantabria, Universidad de Cantabria

Javier L. Lara
Professor, Universidad de Cantabria

María Maza
Asoc. Professor, Universidad de Cantabria

Presentation on
Free long waves and its role in inaccurate numerical prediction of break bar formation

Currently in Month 9

Thank you!

References

1. Astudillo, C., Gracia, V., Cáceres, I., Sierra, J. P., & Sánchez-Arcilla, A. (2022). Beach profile changes induced by surrogate Posidonia Oceanica: Laboratory experiments. *Coastal Engineering*, *175*. https://doi.org/10.1016/j.coastaleng.2022.104144
2. Astudillo-Gutierrez, C., Gracia, V., Cáceres, I., Sierra, J. P., & Sánchez-Arcilla, A. (2024). Influence of seagrass meadow length on beach morphodynamics: An experimental study. *Science of the Total Environment*, *921*. https://doi.org/10.1016/j.scitotenv.2024.170888
3. García-Maribona, J., Lara, J. L., Maza, M., & Losada, I. J. (2021). An efficient RANS numerical model for cross-shore beach processes under erosive conditions. Coastal Engineering, 170. https://doi.org/10.1016/j.coastaleng.2021.103975
4. García-Maribona, J., Lara, J. L., Maza, M., & Losada, I. J. (2022). Analysis of the mechanics of breaker bar generation in cross-shore beach profiles based on numerical modelling. Coastal Engineering, 177. https://doi.org/10.1016/j.coastaleng.2022.104172
5. Grossmann, F., Hurther, D., Sánchez-Arcilla, A., & Alsina, J. M. (2023). Influence of the Initial Beach Profile on the Sediment Transport Processes During Post-Storm Onshore Bar Migration. Journal of Geophysical Research: Oceans, 128(4). https://doi.org/10.1029/2022JC019299
6. Lara, J. L., Losada, I. J., & Guanche, R. (2008). Wave interaction with low-mound breakwaters using a RANS model. Ocean Engineering, 35(13), 1388–1400. https://doi.org/10.1016/j.oceaneng.2008.05.006
7. Lara, J. L., Ruju, A., & Losada, I. J. (2011). Reynolds averaged Navier-Stokes modelling of long waves induced by a transient wave group on a beach. Proceedings of the Royal Society A: Mathematical, Physical and Engineering Sciences, 467(2129), 1215–1242. https://doi.org/10.1098/rspa.2010.0331
8. Maza, M., Lara, J. L., & Losada, I. J. (2013). A coupled model of submerged vegetation under oscillatory flow using Navier-Stokes equations. Coastal Engineering, 80, 16–34. https://doi.org/10.1016/j.coastaleng.2013.04.009
9. Roulund, A., Sumer, B. M., Fredsøe, J., & Michelsen, J. (2005). Numerical and experimental investigation of flow and scour around a circular pile. Journal of Fluid Mechanics, 534, 351–401. https://doi.org/10.1017/S0022112005004507
10. Streicher, M. ;, Kortenhaus, A. ;, Altomare, C. ;, Gruwez, V. ;, Hofland, B. ;, Chen, X. ;, Marinov, K. ;, Scheres, B. ;, Schüttrumpf, H. ;, Hirt, M., Cappietti, L., Esposito, A., Saponieri, A., Valentini, N., Tripepi, G., Pasqualini, D., Di Risio, M., Aristodemo, F., Damiani, L., & Kaste, . . (2017). (Wave Loads on Walls) Large-Scale Experiments in the Delta Flume.

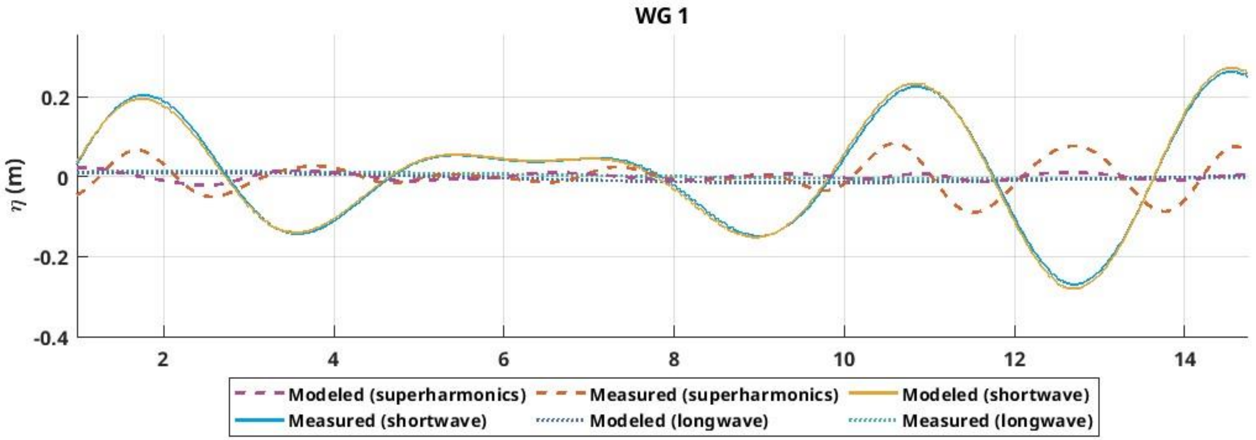

Free waves are filtered from the input wave, but
there also frequencies generated in the model.

VI Results - Velocity

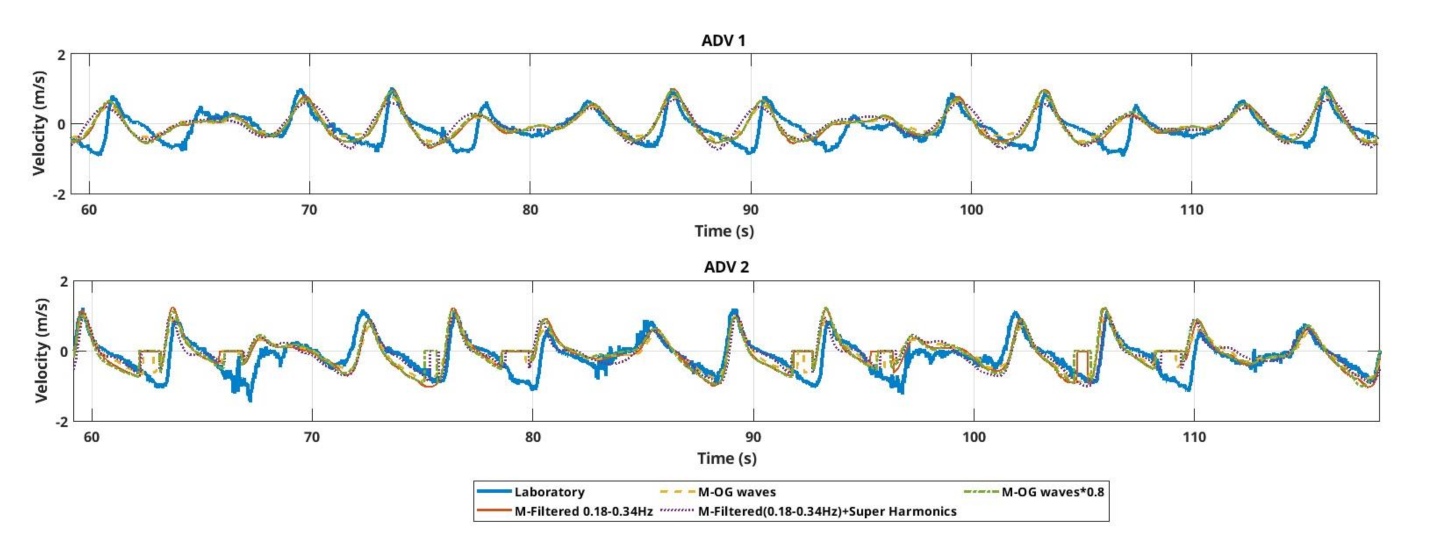

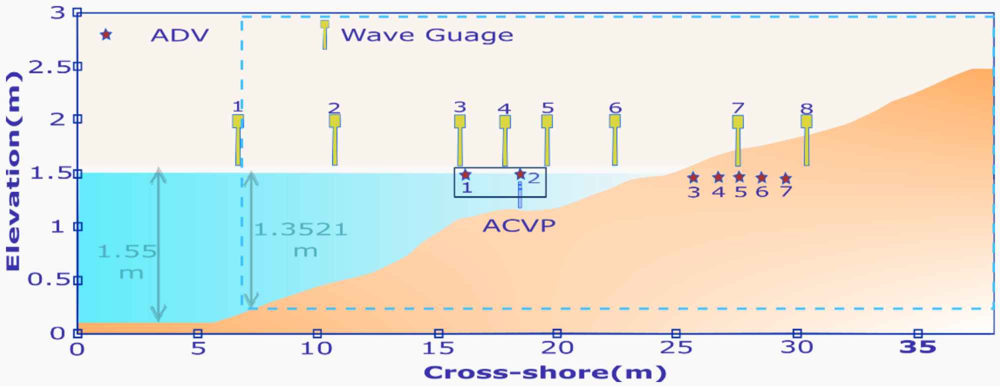

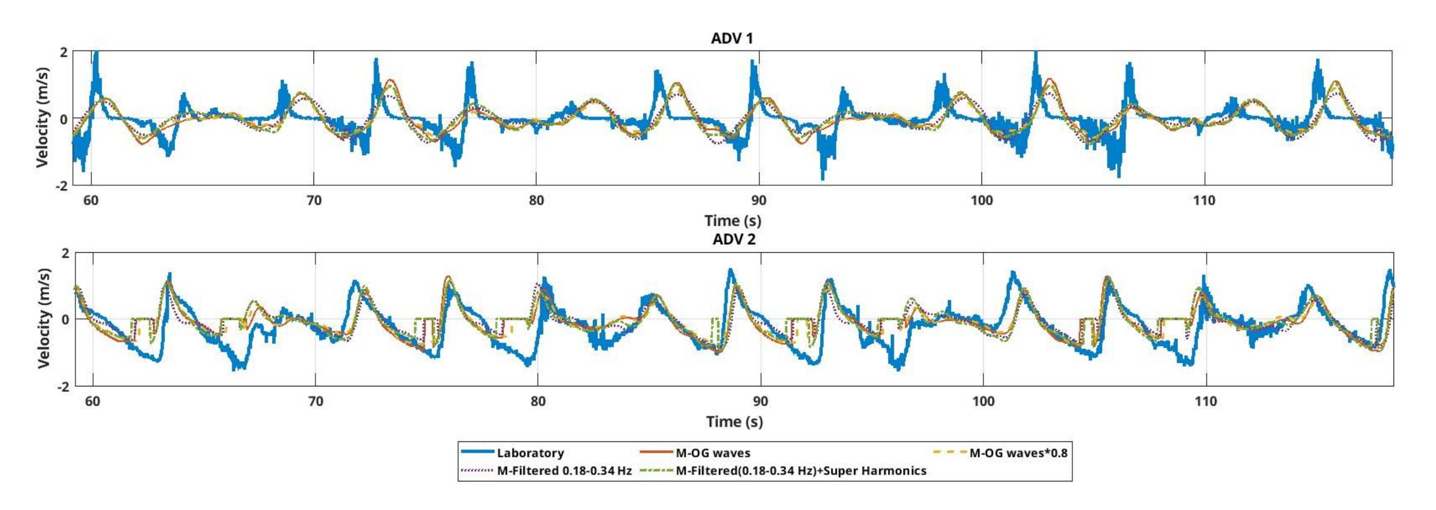

1. **No significant changes in the velocities for the change in wave conditions**
2. **Meaning wave breaking occurs quite similarly across the different cases.**
3. **RMSE values varies between 04 to 0.6 for the different cases**

VI Results - Free Surface Elevation (First 4 wave groups)

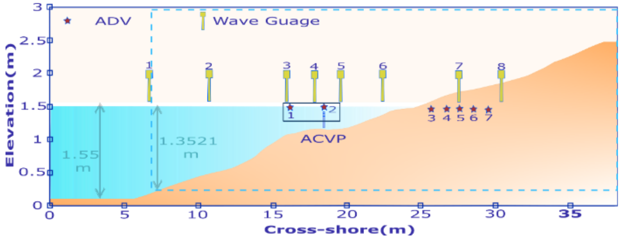

Original signal from wave gauge

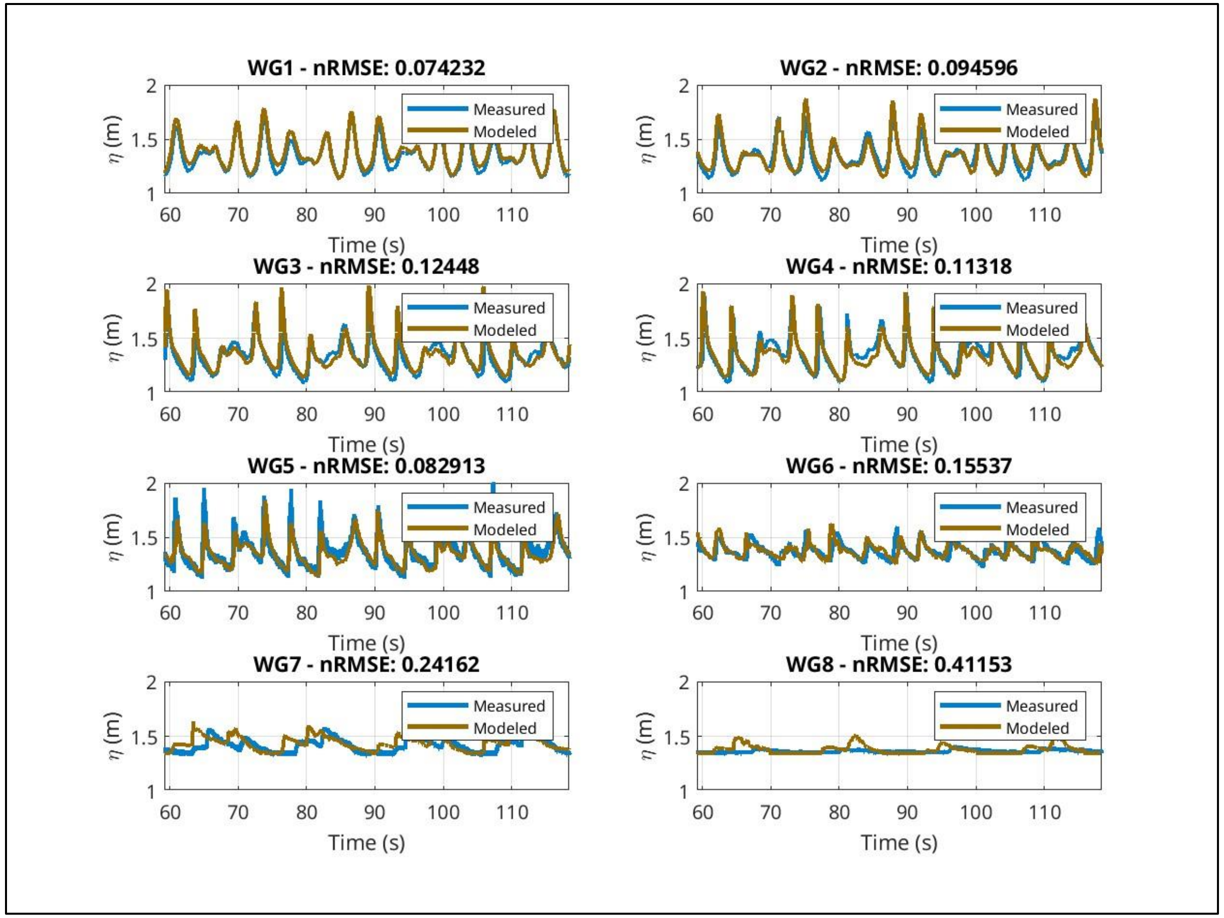

Filtered signal from wave gauge

Removed Free long wave and super-harmonics from the signal

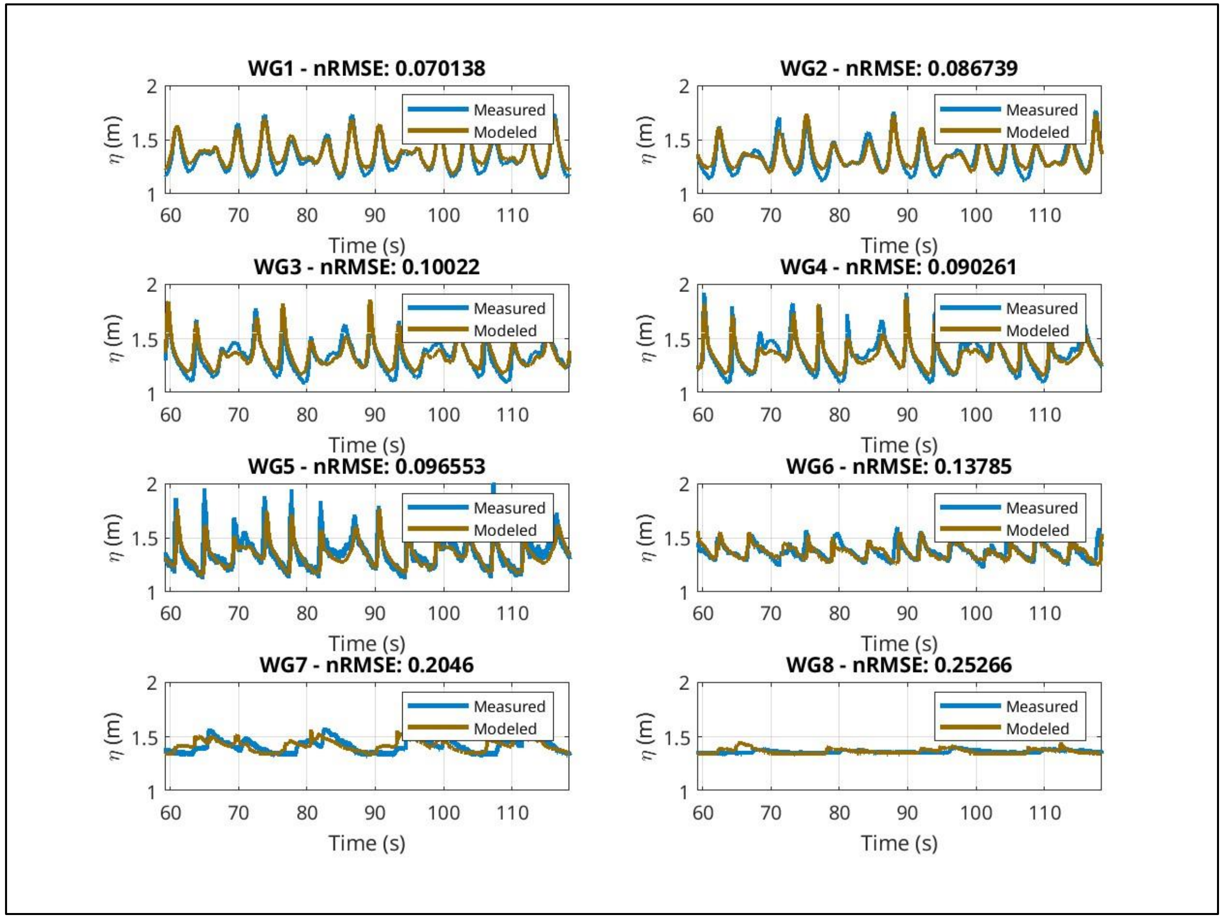

VI Results - Energy Density

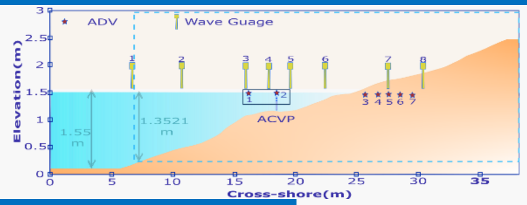

First Four Wave groups

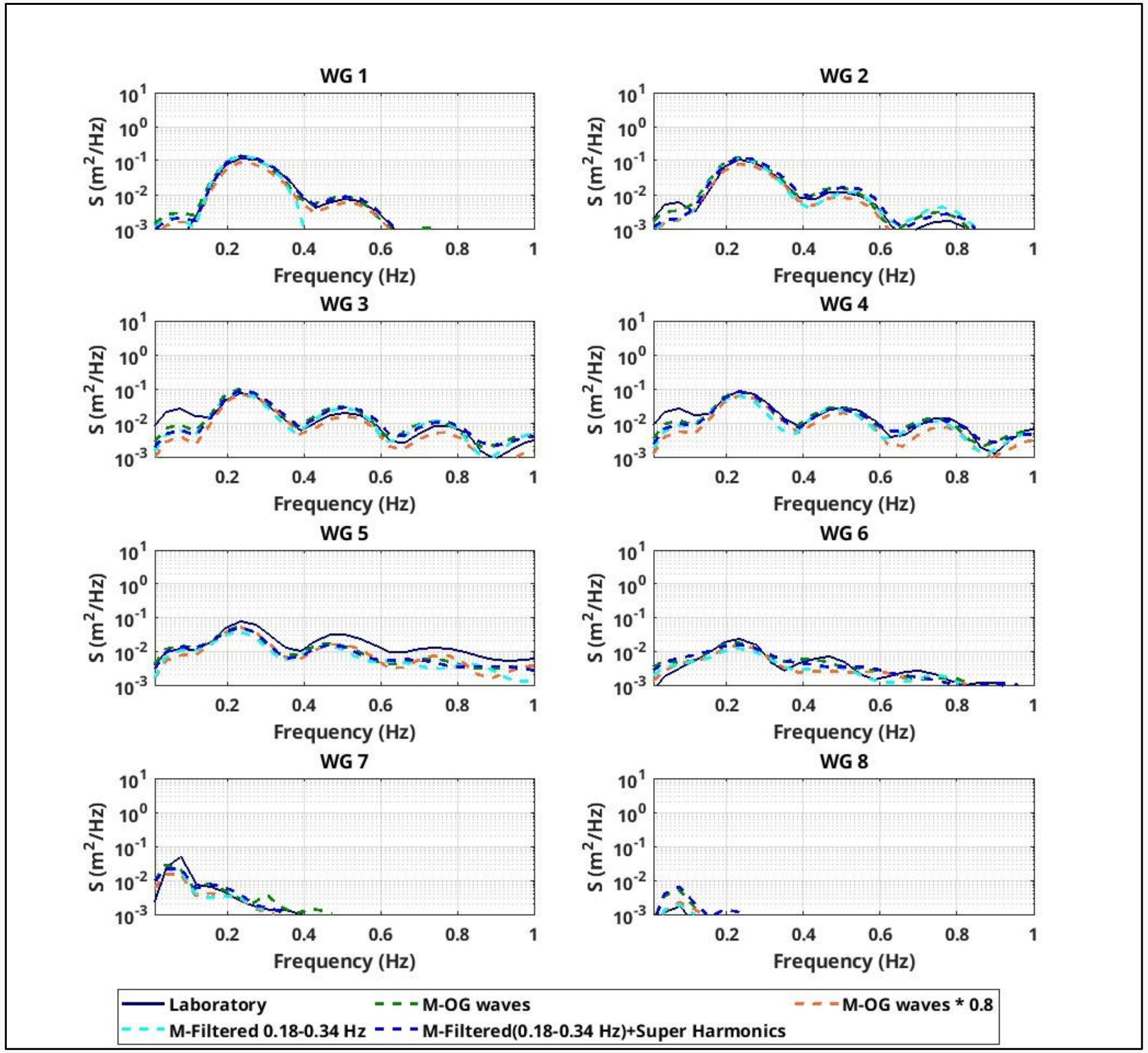

Final Four Wave groups

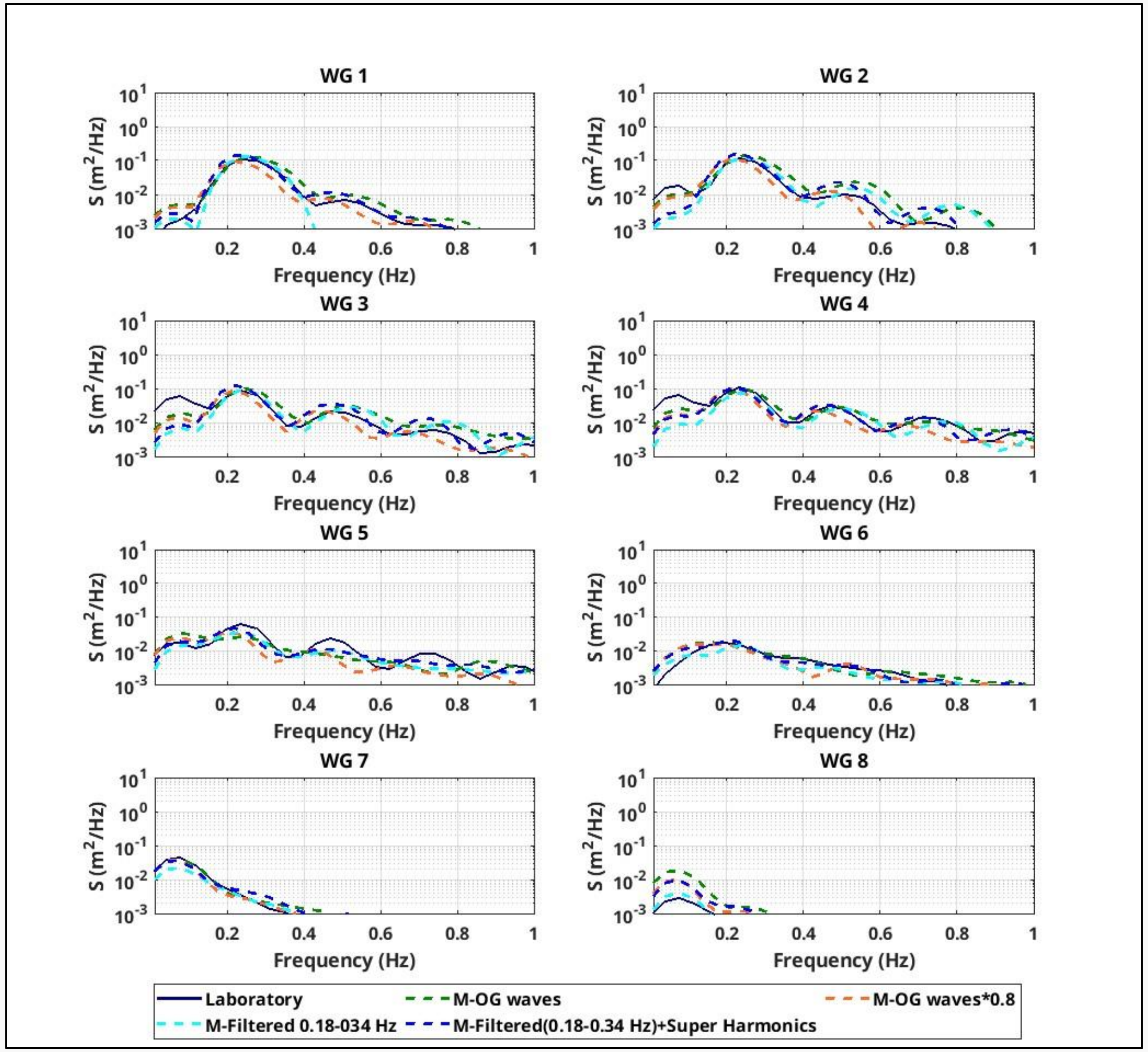

VI Results - Wave Components(Final 4 wave groups)

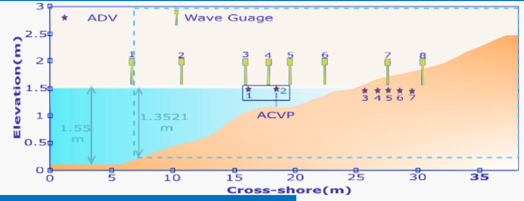

Original signal from wave gauge

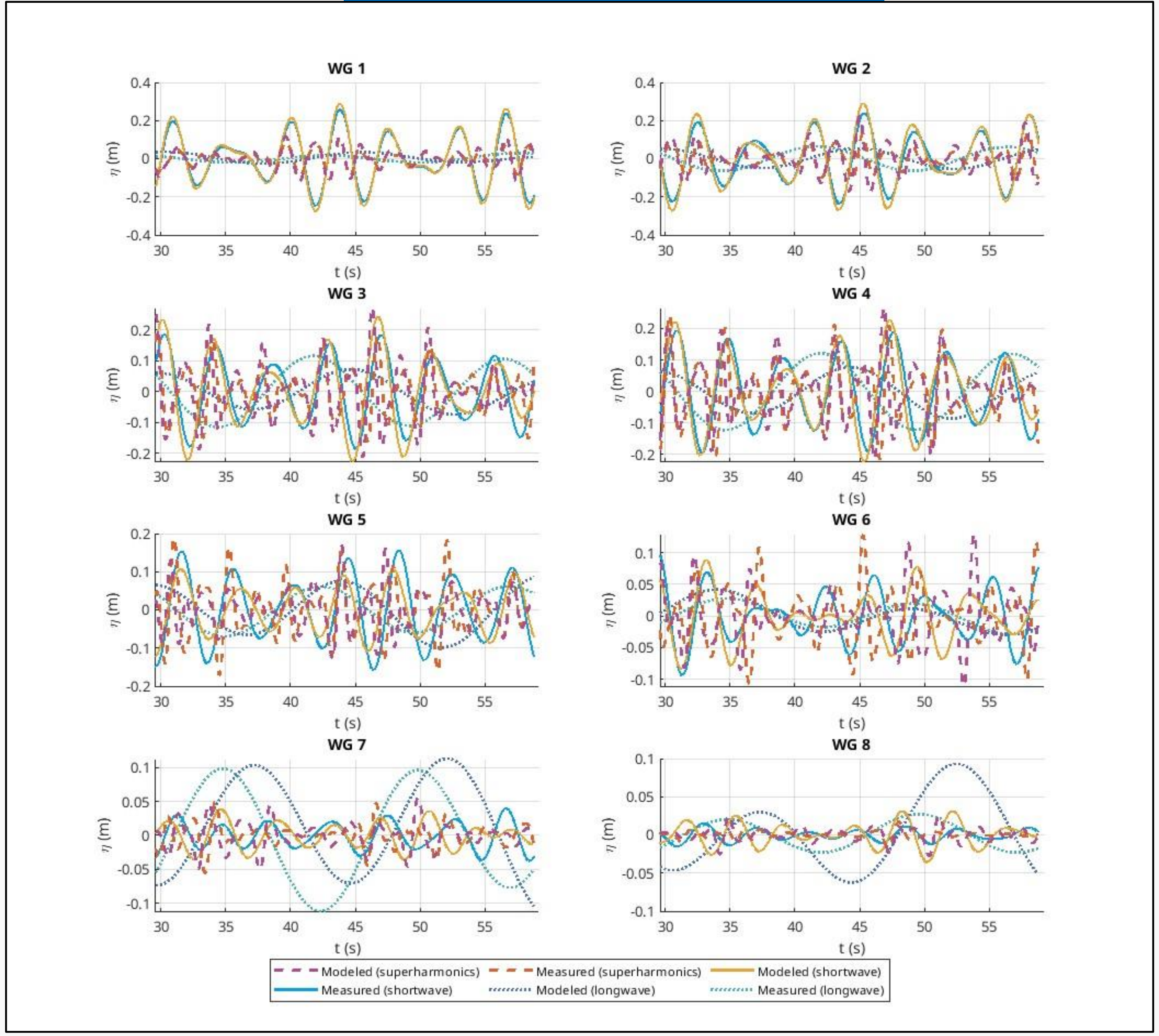

Filtered signal from wave gauge

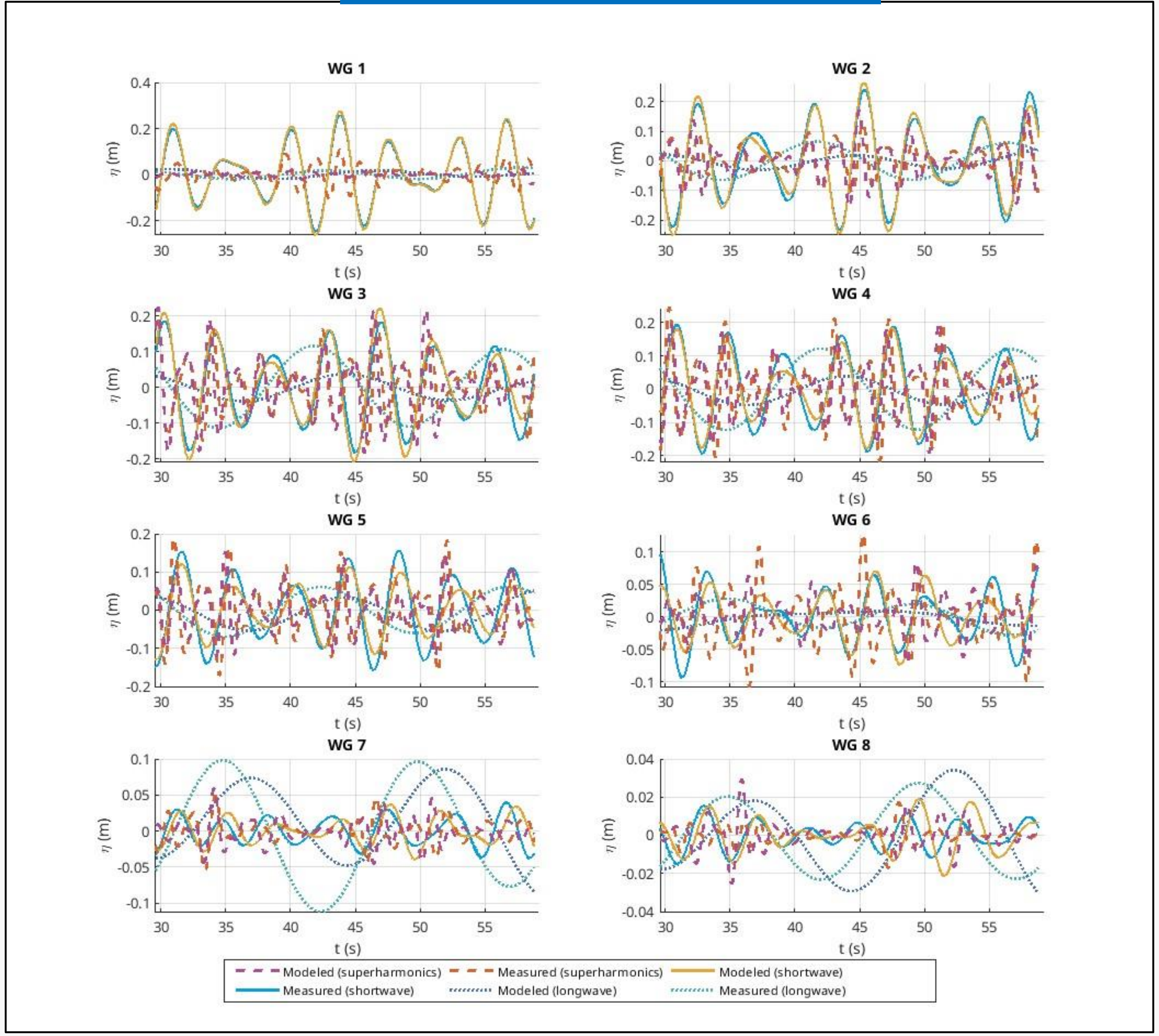

Initiation of motion of sand-mud beds

Paterno "Jowi" S. Miranda IV, MCE

Research update

p.s.miranda@utwente.nl
jowi.miranda@deltares.nl

patrno4

Deltares
UNIVERSITY OF TWENTE.
SEDIMARE
Sediment Transport and Morphodynamics in Marine and Coastal Waters with Engineering Solutions

Contents

- **Sand-mud erosion**
- **Initiation of motion of sediment classes (e.g. sand, silt, clay)**
- **Framework for initiation of motion of sand-mud**
- **Application of framework to collected data**
- **Next steps**

Sand-mud erosion

- Erosion of sediment bed containing both sand and mud
- Modes of erosion:
  - Particle / floc erosion
  - Surface erosion
  - Mass erosion
- Estimating erosion requires a definition for initiation of motion of both sand and mud
  - E [kg/(m^{2}s)] vs τ_b (Pa)
  - Definition of τ_{crit}

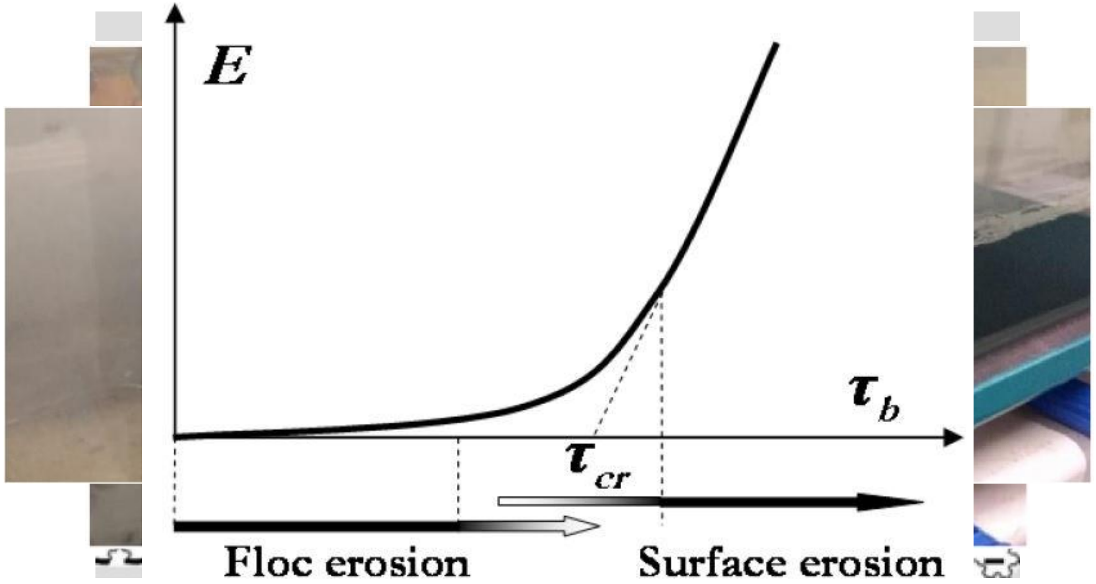

van Rijn, 2020
Jacobs, 2011

Deltares UNIVERSITY OF TWENTE. SEDIMARE
Sediment Transport and Morphodynamics in Marine and Coastal Waters with Engineering Solutions

Initiation of motion for each sediment class

Mud

Sand

- Silica material (quartz)
- Diameter: > 63 μm
- **Non-cohesive**

Suspended load

τ_{crit}

Shields parameter

Bedload

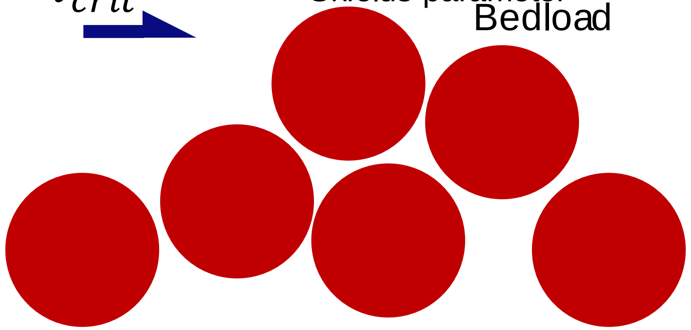

Silt

- Silica material (quartz)
- Diameter: 2 – 63 μm
- **Apparently cohesive:**
  - **Van der Waal forces of attraction**

Suspended load

τ_{crit}

Deformed to critical state of sediment
(Shear dilation)
→ Increased shear strength

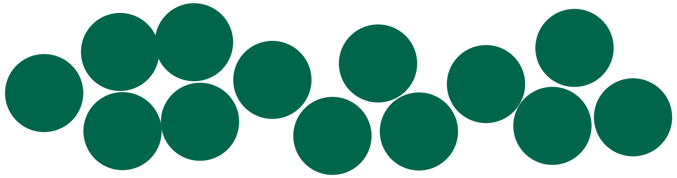

Clay

- Alumino-silica
- Diameter: < 2 μm
- **Cohesive:**
  - **Cationic nature of alumino-silica**
  - **Van der Waal forces of attraction**

Suspended load

τ_{crit}

Cohesive strength of clay
(True cohesion)
→ Increased shear strength

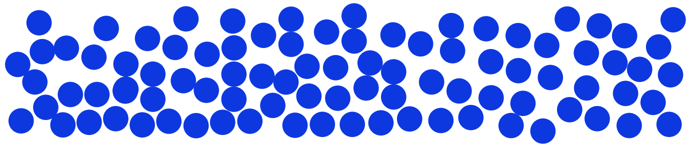

Initiation of motion

Sand-Mud (sand-silt-clay)

- What is the process for sand-mud beds?
  - Shields parameter?
  - Shear dilation?
  - True cohesion?

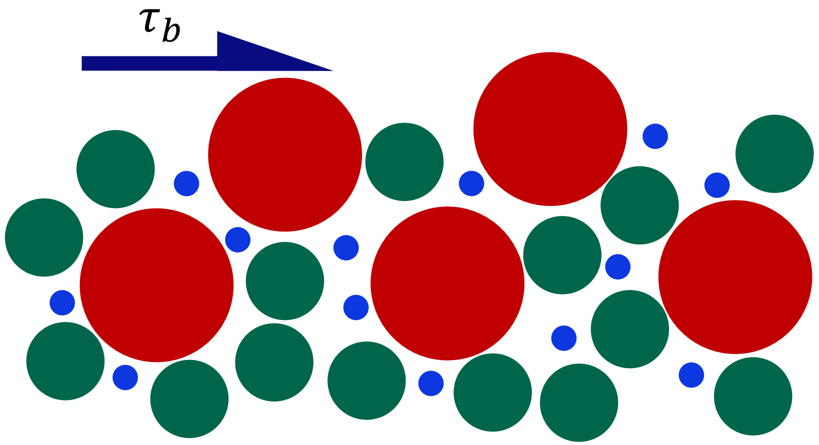

Framework for initiation of motion

- Current estimation methods for initiation of motion are a function of bulk geotechnical parameters:
  - Wet bulk density, ρ_{bulk}
  - Median grain size diameter, D_{50}
  - Dry volume percentage of mud, P_{mud}

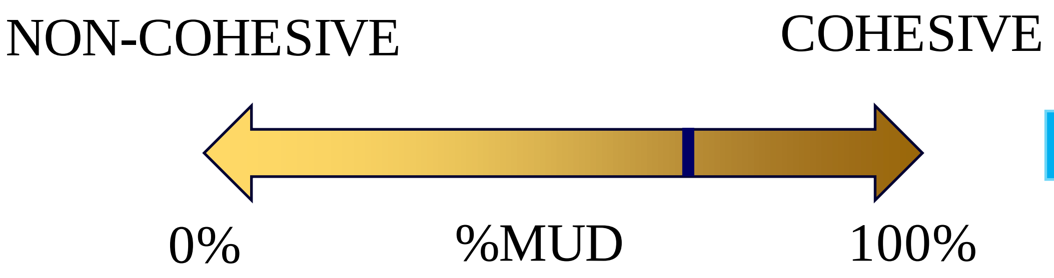

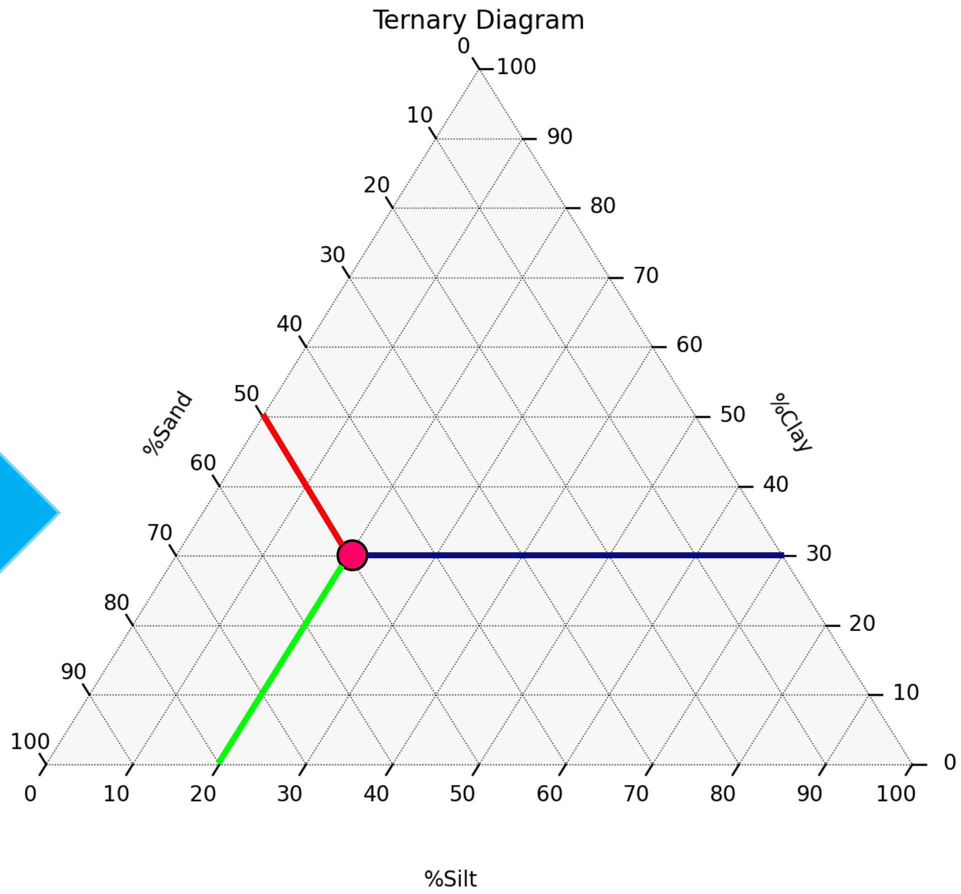

- Shift from a binary spectrum to a ternary analysis

Deltares
UNIVERSITY OF TWENTE.
SEDIMARE
Sediment Transport and Morphodynamics in Marine and Coastal Waters with Engineering Solutions

Framework for initiation of motion

- Van Ledden bed types
  - Based on information from ternary diagram and volume concentration of water
  - Framework characteristics:
    1. Cohesion
    2. Network structure

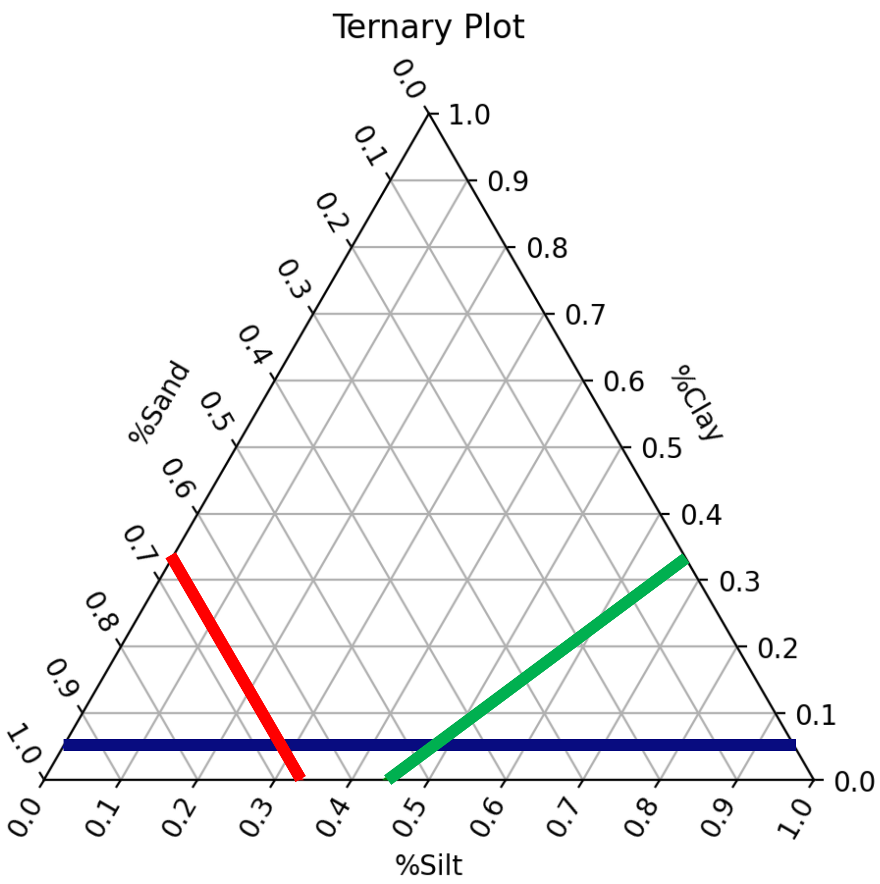

Framework for initiation of motion

- Cohesion
  - Based on dry volume percentage of clay
  - Literature provides a lower limit of 5-10%

$$P_{clay} = 5 - 10\%$$

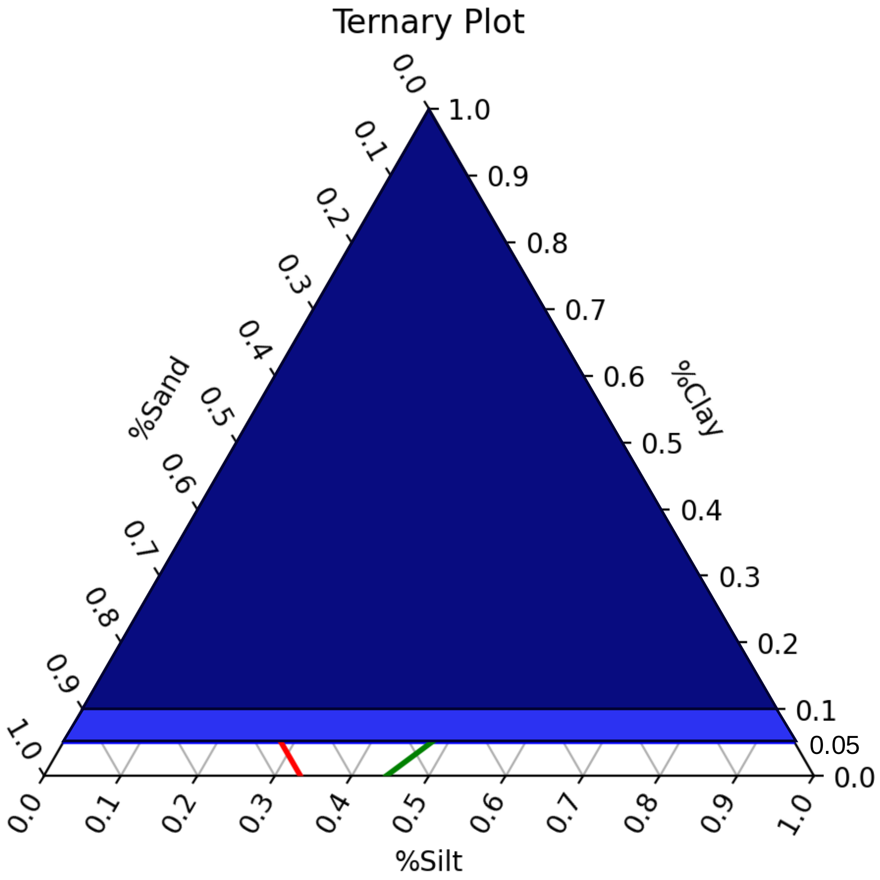

Framework for initiation of motion

- Network structure
  - Interaction of particles based on the volume content of water, ϕ_{water}
  - Illustration using pure sand:

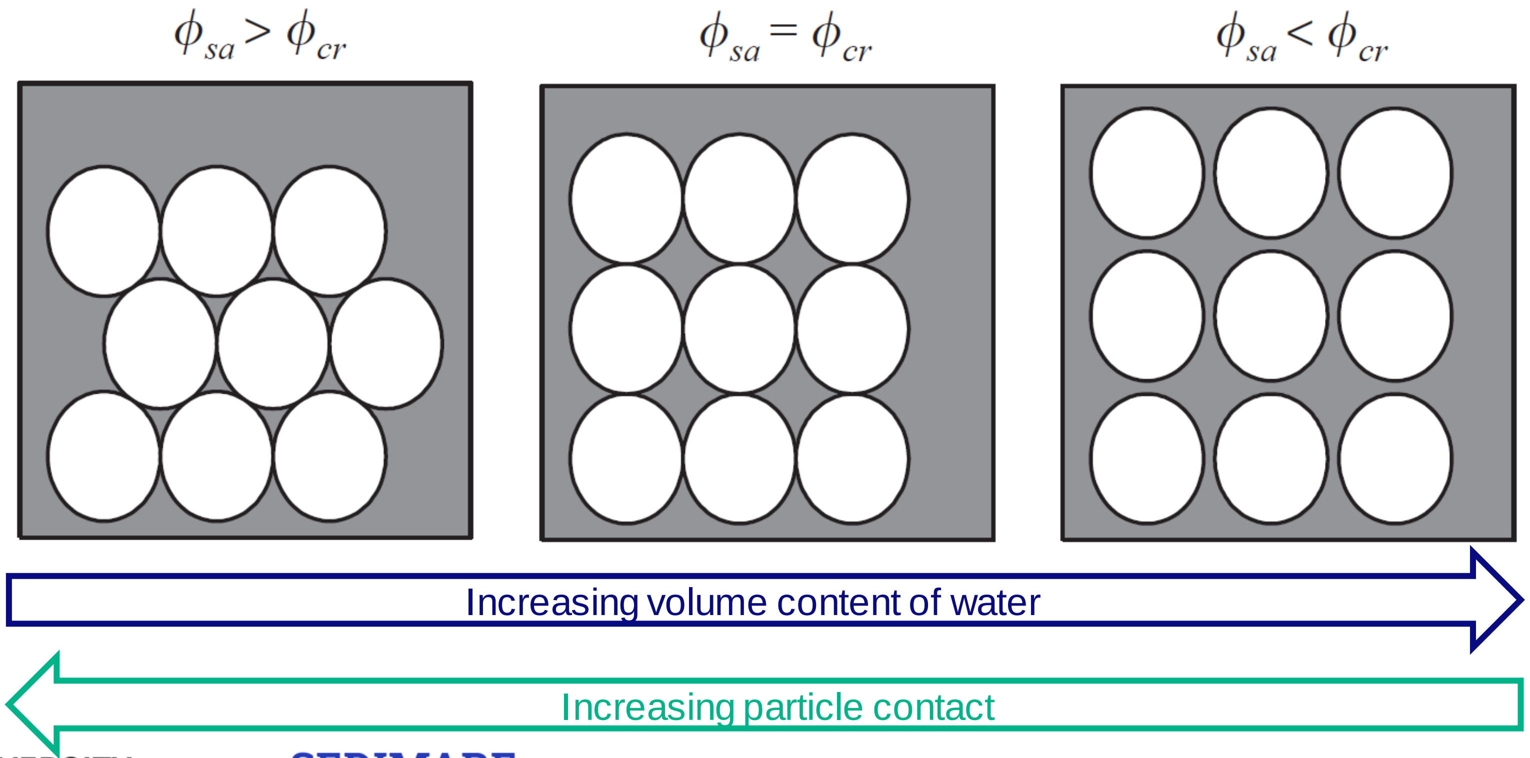

Van Ledden et al., 2003

Framework for initiation of motion

- Network structure
  - Van Ledden et al., 2003 suggests that for sand-mud, the dominant sediment can be based on wet volume percentage of sand , ϕ_{sand} , and silt, ϕ_{silt} .
  - Sand-dominated network structure:

$$\phi_{sand} \geq 40 - 50\%$$

  - Silt-dominated network structure:

$$\frac{\phi_{silt}}{(1 - \phi_{sand})} \geq 40 - 50\%$$

  - Other network structures:
    1. Clay-water matrix
    2. Mixed structures

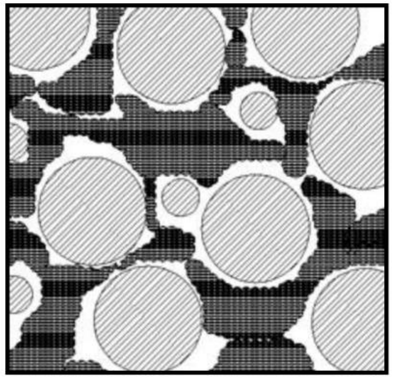

Jacobs, 2011

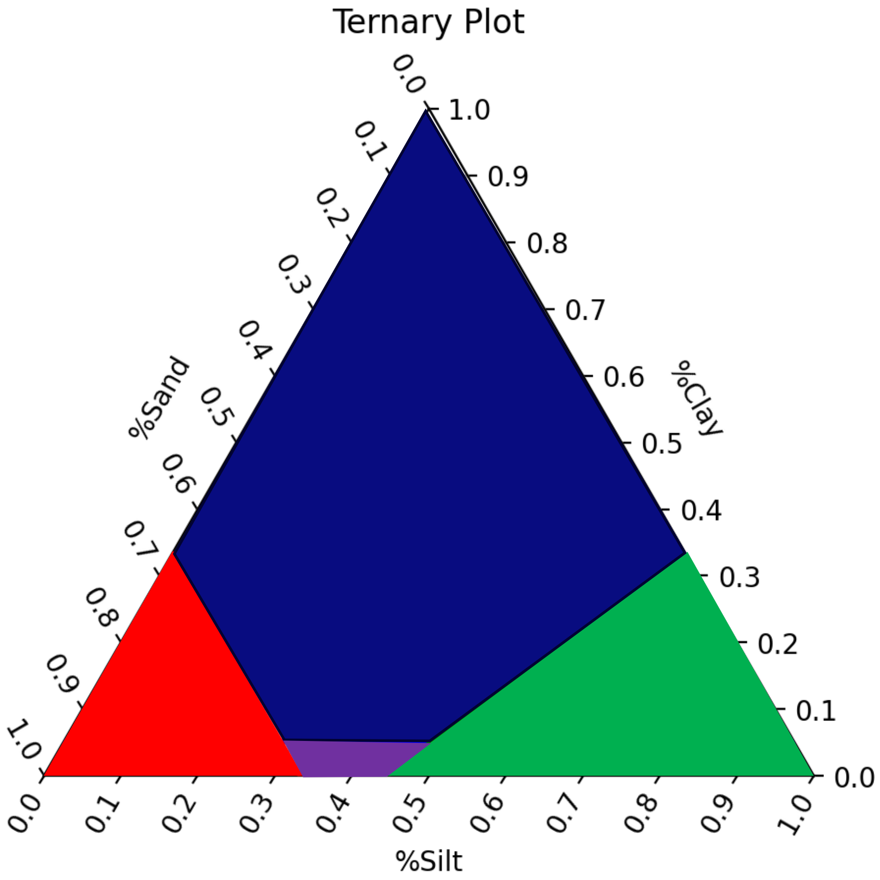

Framework for initiation of motion

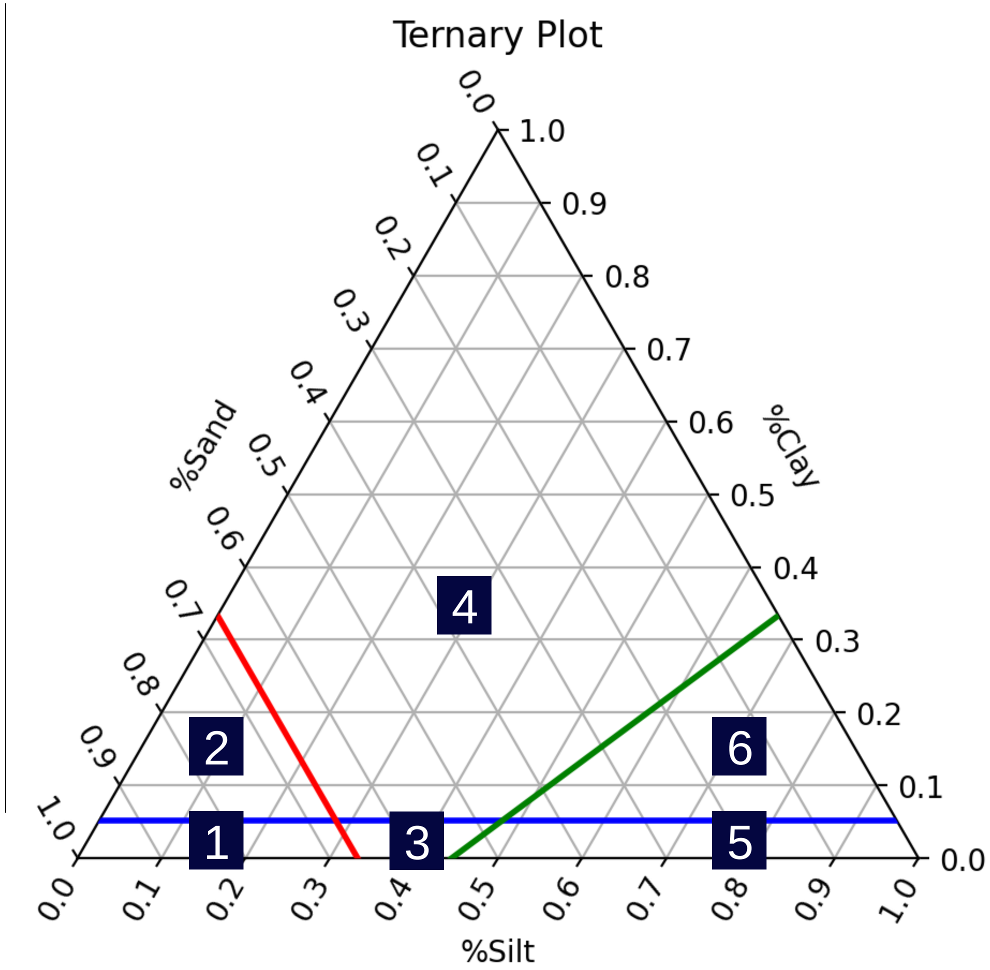

Cohesion	
on-cohesive $ay < 5 - 10\%)$	Cohesive $(P_{clay} \geq 5 - 10\%)$
minated, non- sediment bed	**Type 2:** Sand-dominated, cohesive sediment bed
nated, non- sediment bed	**Type 6:** Silt-dominated, cohesive sediment bed
diment, non- sediment bed	**Type 4:** Clay-water matrix, cohesive sediment bed

1. Sand-dominated non-cohesive
2. Sand-dominated cohesive
3. Mixed structure non-cohesive
4. Clay-dominated cohesive
5. Silt-dominated non-cohesive
6. Silt-dominated cohesive

Application of framework to collected data

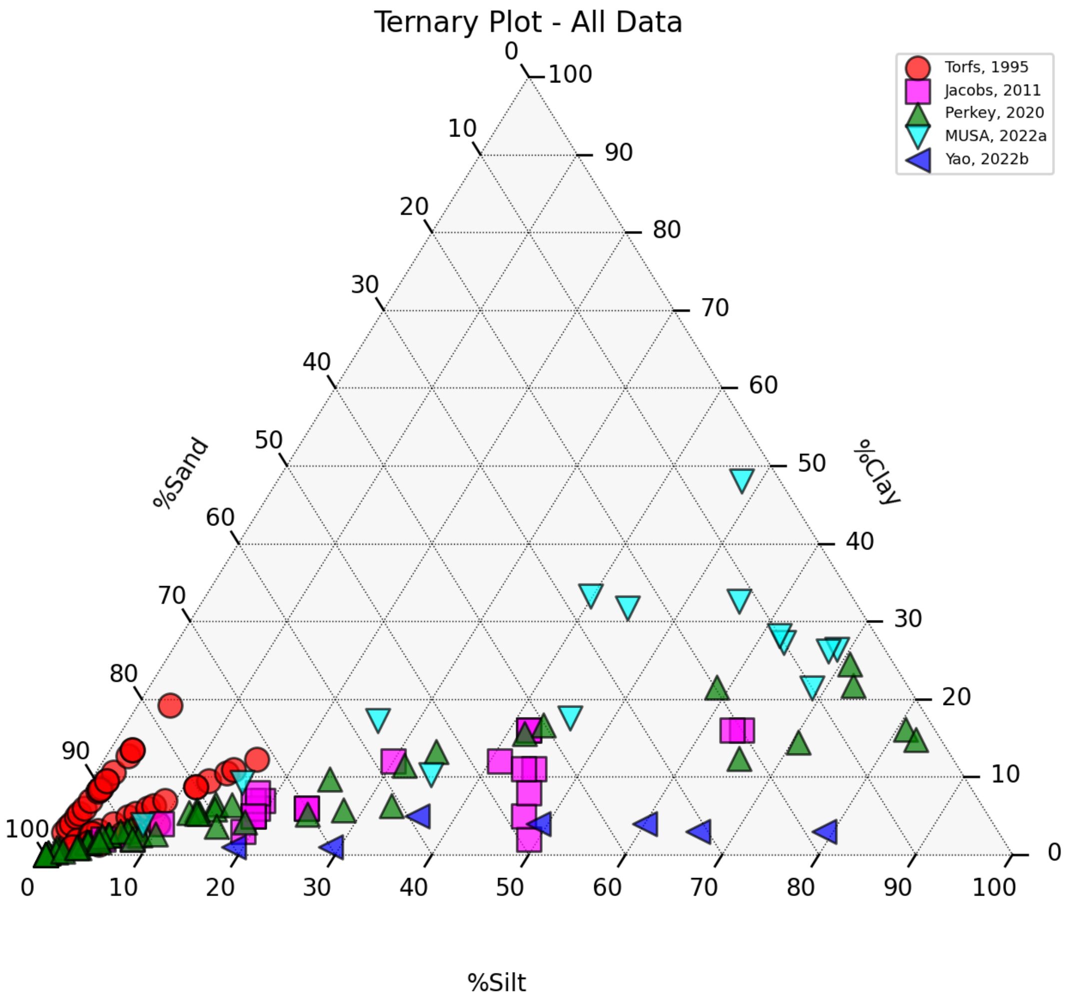

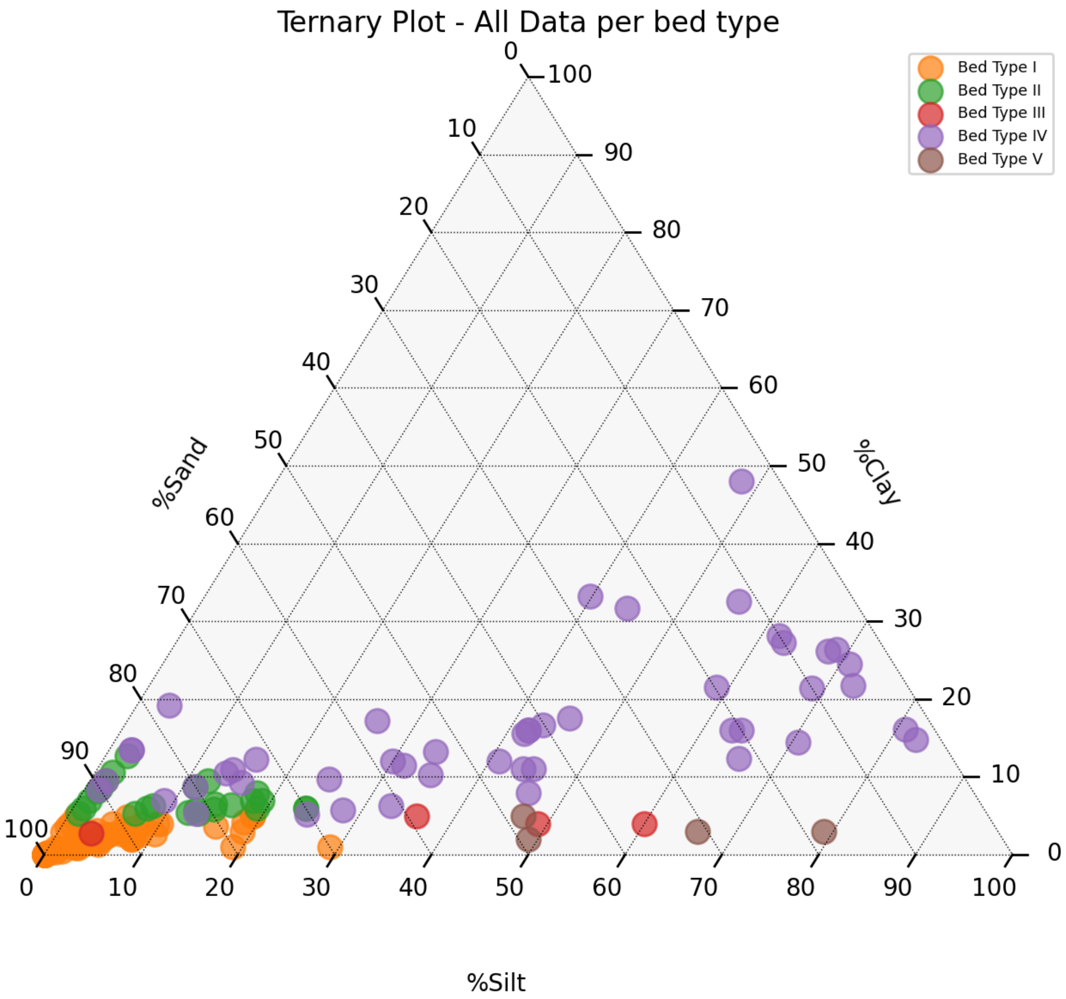

Deltares

UNIVERSITY OF TWENTE.

SEDIMARE

Sediment Transport and Morphodynamics in Marine and Coastal Waters with Engineering Solutions

Next steps

- Dominant initiation of motion process for each bed type
- Existing initiation of motion equations, τ_{crit}
  - Which equation best describes each Van Ledden bed type?
    1. Mehta, 1988
    2. Mitchener & Torfs, 1996
    3. Roberts et al., 1998
    4. Van Ledden et al., 2003
    5. Van Rijn, 2007
    6. Wu et al., 2018
    7. Yao et al., 2022

Initiation of motion of sand-mud beds

Paterno "Jowi" S. Miranda IV, MCE

Research update

p.s.miranda@utwente.nl
jowi.miranda@deltares.nl
patrno4

Deltares
UNIVERSITY OF TWENTE.
SEDIMARE
Sediment Transport and Morphodynamics in Marine and Coastal Waters with Engineering Solutions

UNIVERSITÀ POLITECNICA DELLE MARCHE

Nasim Soori

Supervisors:
Prof. Maurizio Brocchini – UNIVPM
Prof. Athanassios Dimas – UPATRAS
Prof. Matteo Postacchini – UNIVPM

DC 4: Mixing and transport in the coastal area

Netherland- 7 Nov., 2024

The nearshore area:
- dynamically evolving
- often densely populated
- under increasing threat

❑ **Estuarine environments** are dynamically complex, with hydrodynamics being triggered by many factors, e.g., nonlinear interactions between the bathymetry, the river current and many sea forcing actions.

➢ In our project, we are focusing on the **development of a 2D numerical solver** for the hydro-morphodynamics in the nearshore area **to extract the Lagrangian motion/flow field**.

✓ **To inspect the nearshore circulations**, three current values were tested, following the study of Olabarrieta et al. (2014).

- Olabarrieta et al. (2014): circulation of the New River inlet, North Carolina

Inrtoduction

Domain: 3 km long in both cross-shore and alongshore directions

- **Delft-3D- Flow,** to investigate the flow circulation

- **Computational mesh:** spacings Δx = 10 m, Δy = 20 m
- **The resolution of the grid:** 151 x 300 (M x N)
- **Boundary conditions:**

- **Inlet** Boundary, Estuarine Window: Current velocity

- **Right** Boundary: Riemann

- **Left** Boundary: Riemann

- **Top** Boundary: Total Discharge

- **Time Simulation:** 5 hrs

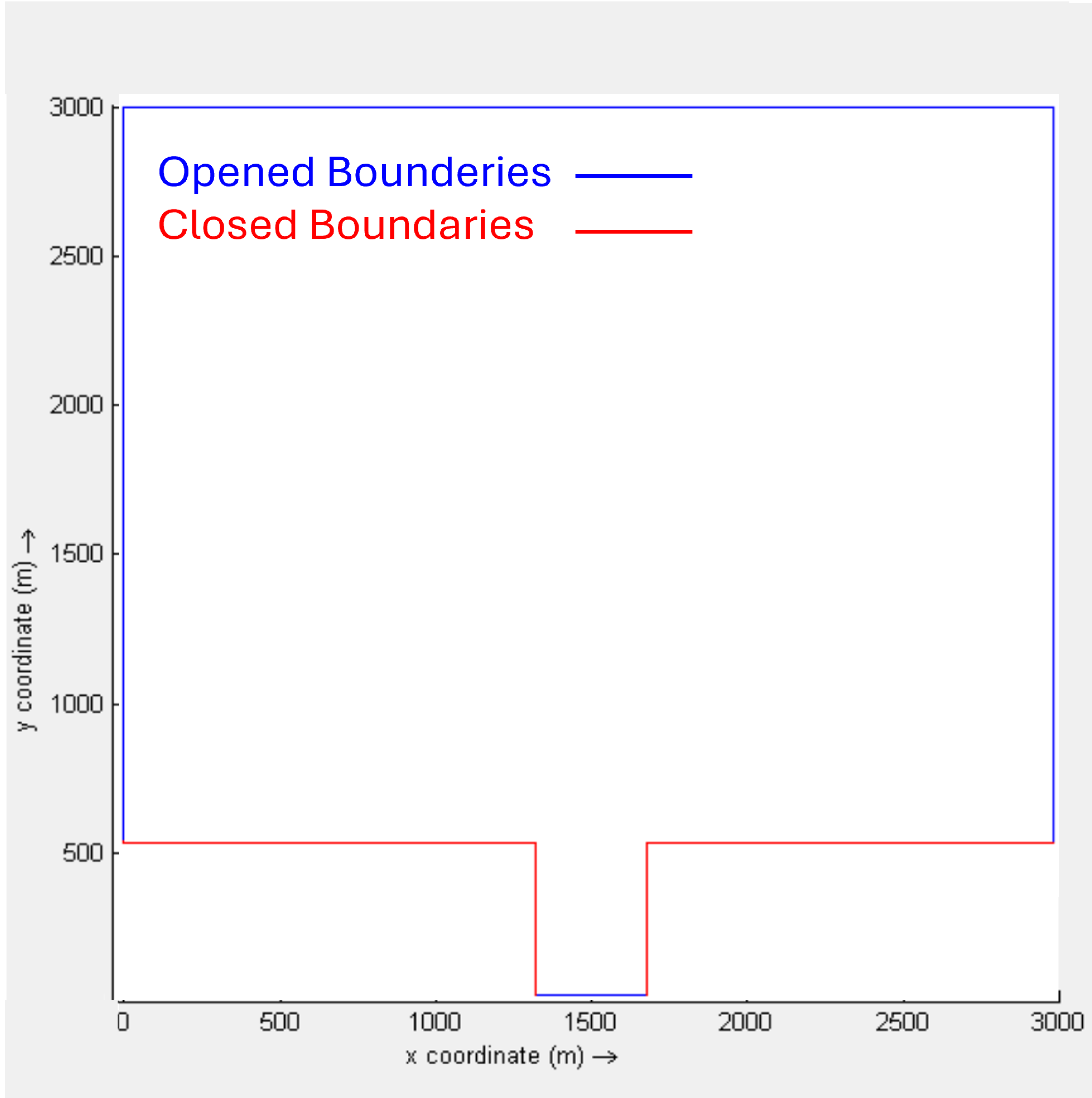

Numerical part

❑ Water Depth

Water Depth, our study(Delft3D)

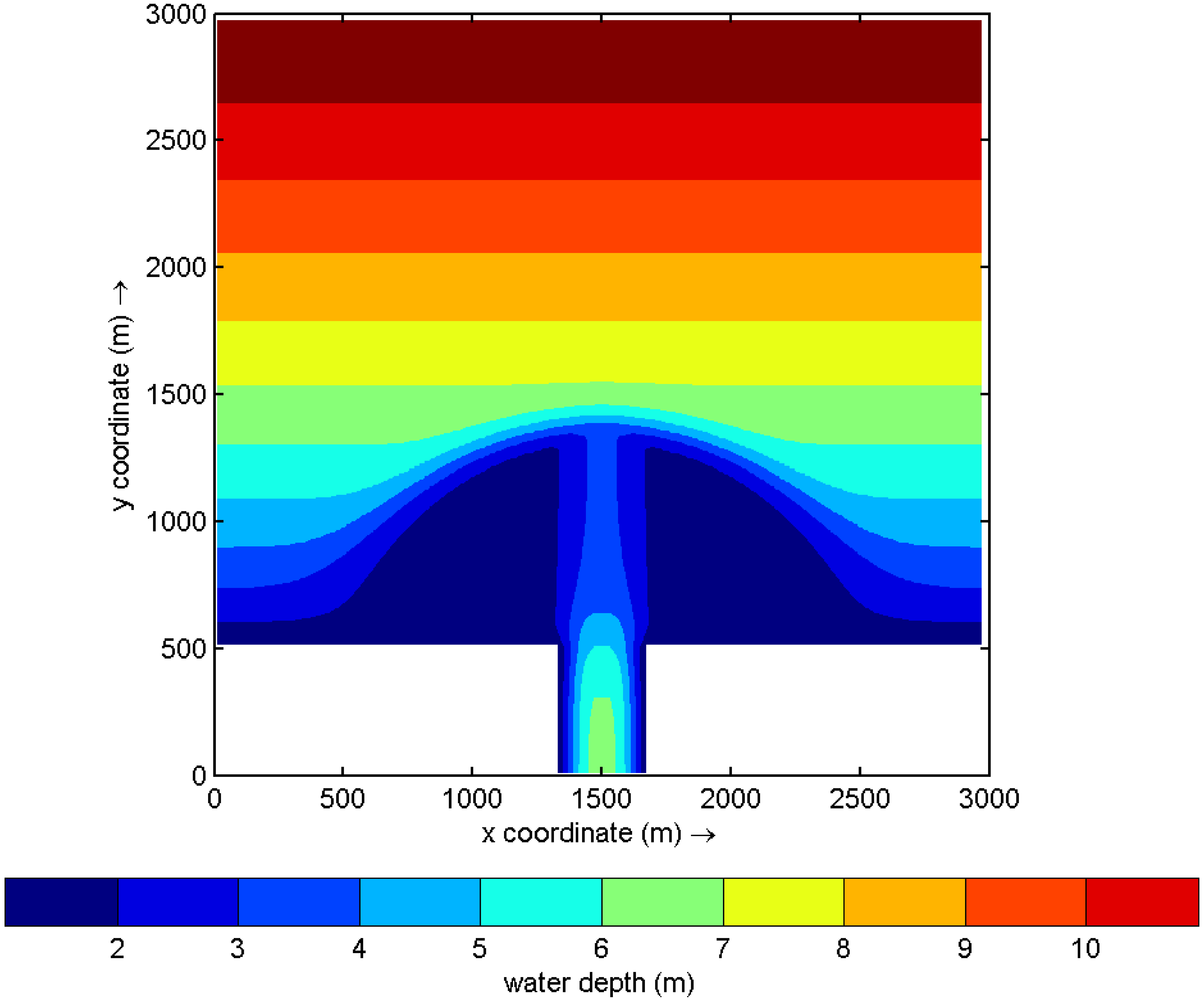

Water Depth, Olabarrieta et al. (2014)

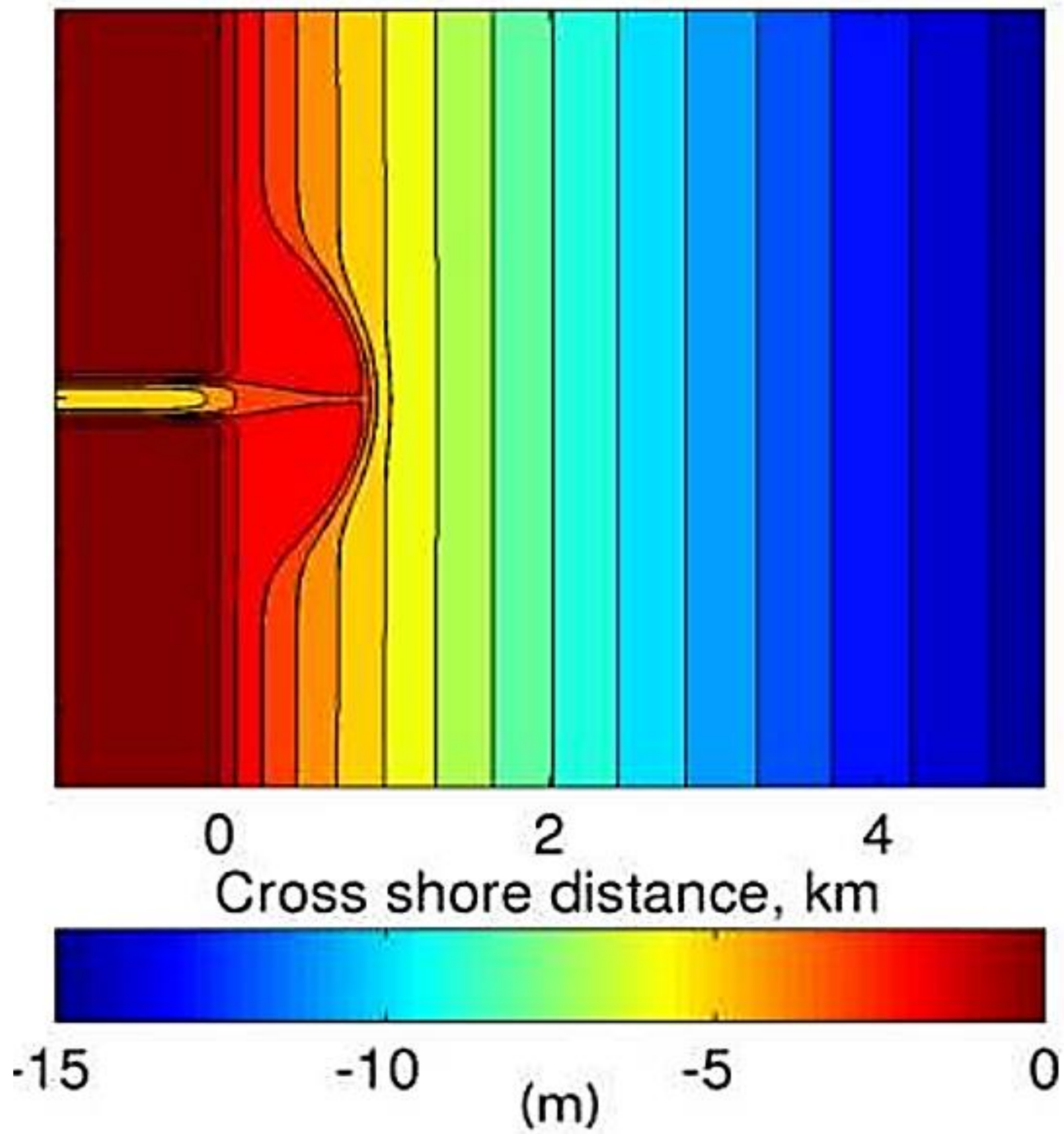

Numerical part

❑ Depth-averaged Velocity- Delft-3D: our study

U=0.6 m/s

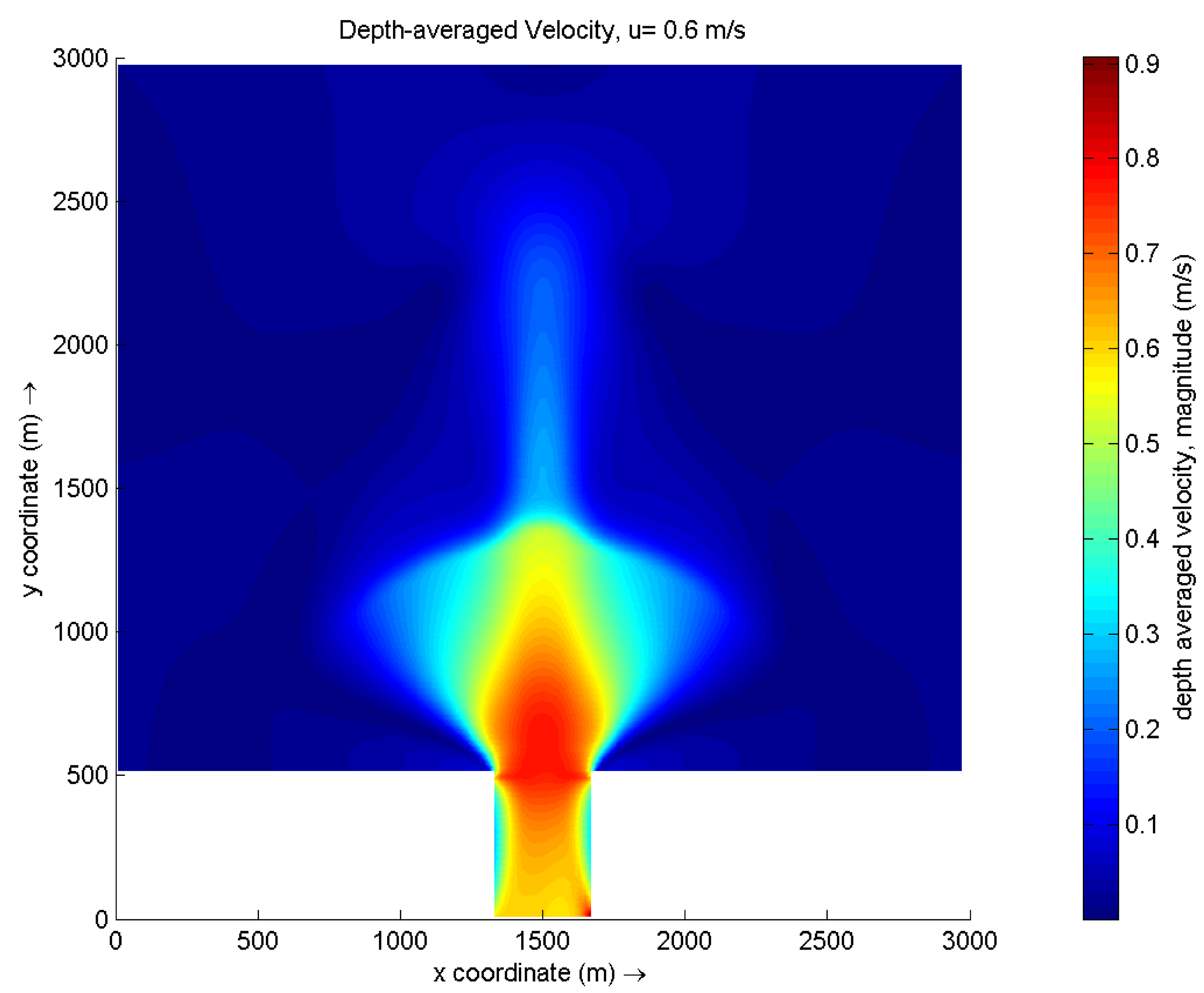

U=1.1 m/s

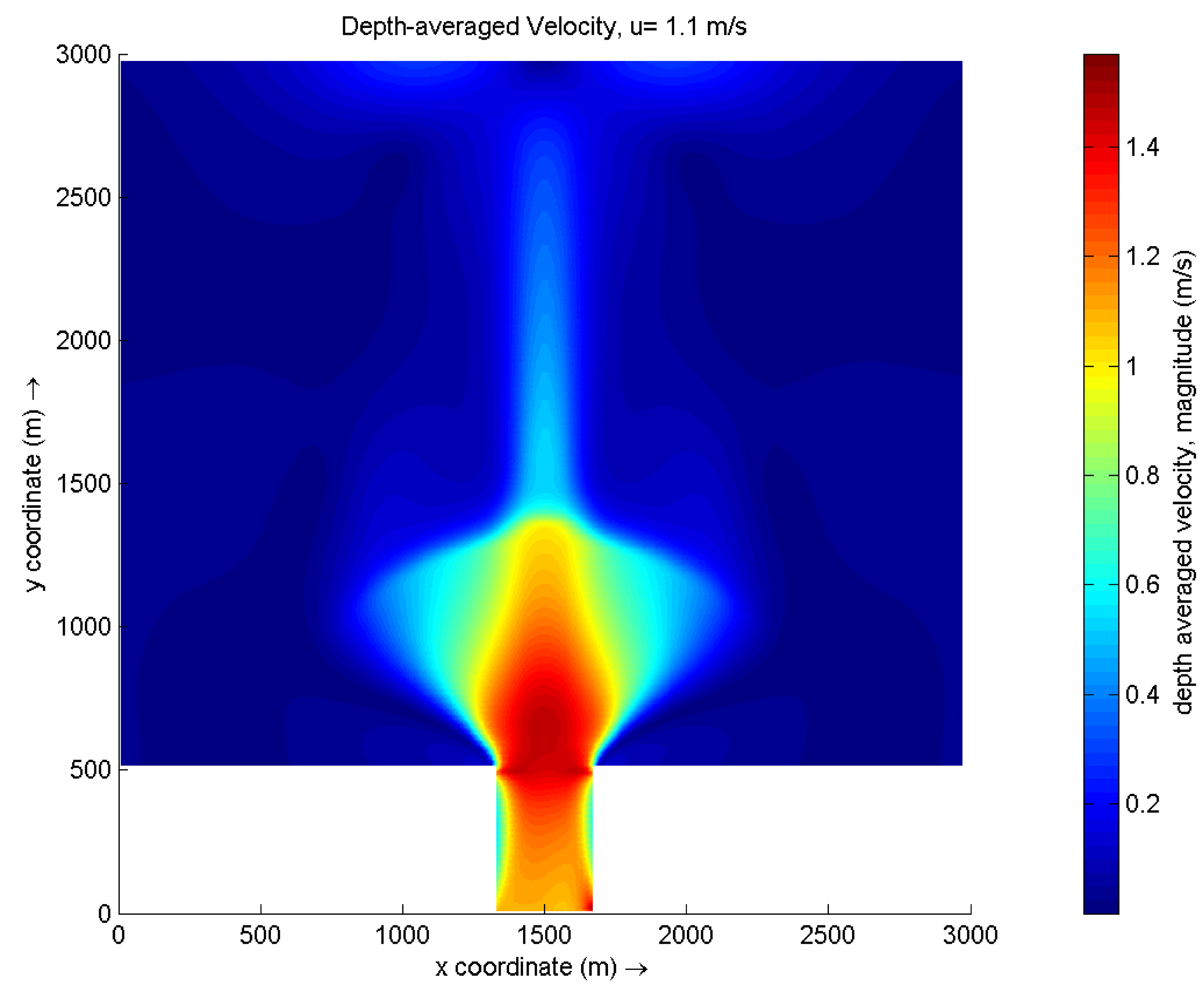

U=1.6 m/s

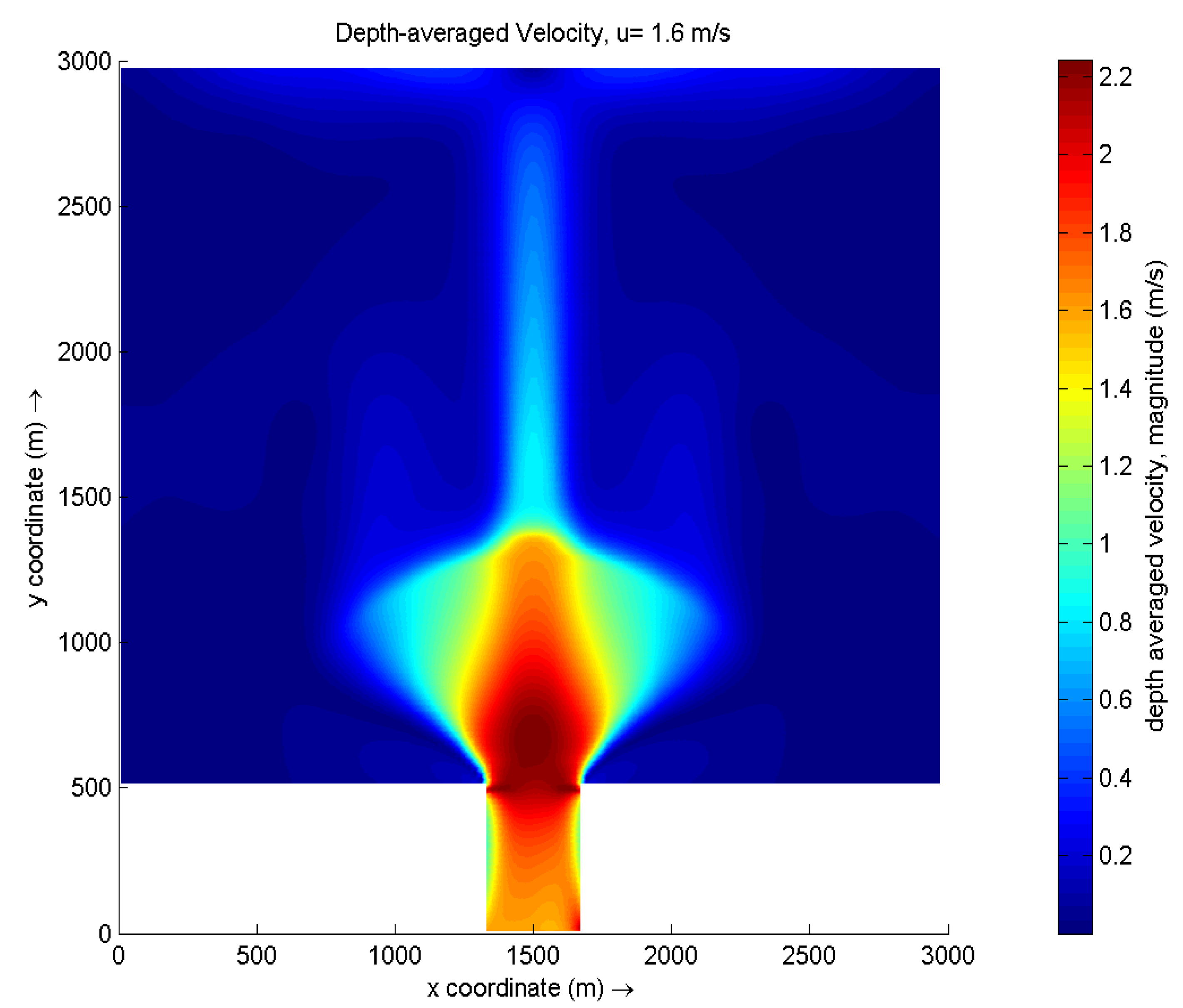

❑ Mean Velocity- NSWE Solver: Melito et al. (2019)

U=0.6 m/s

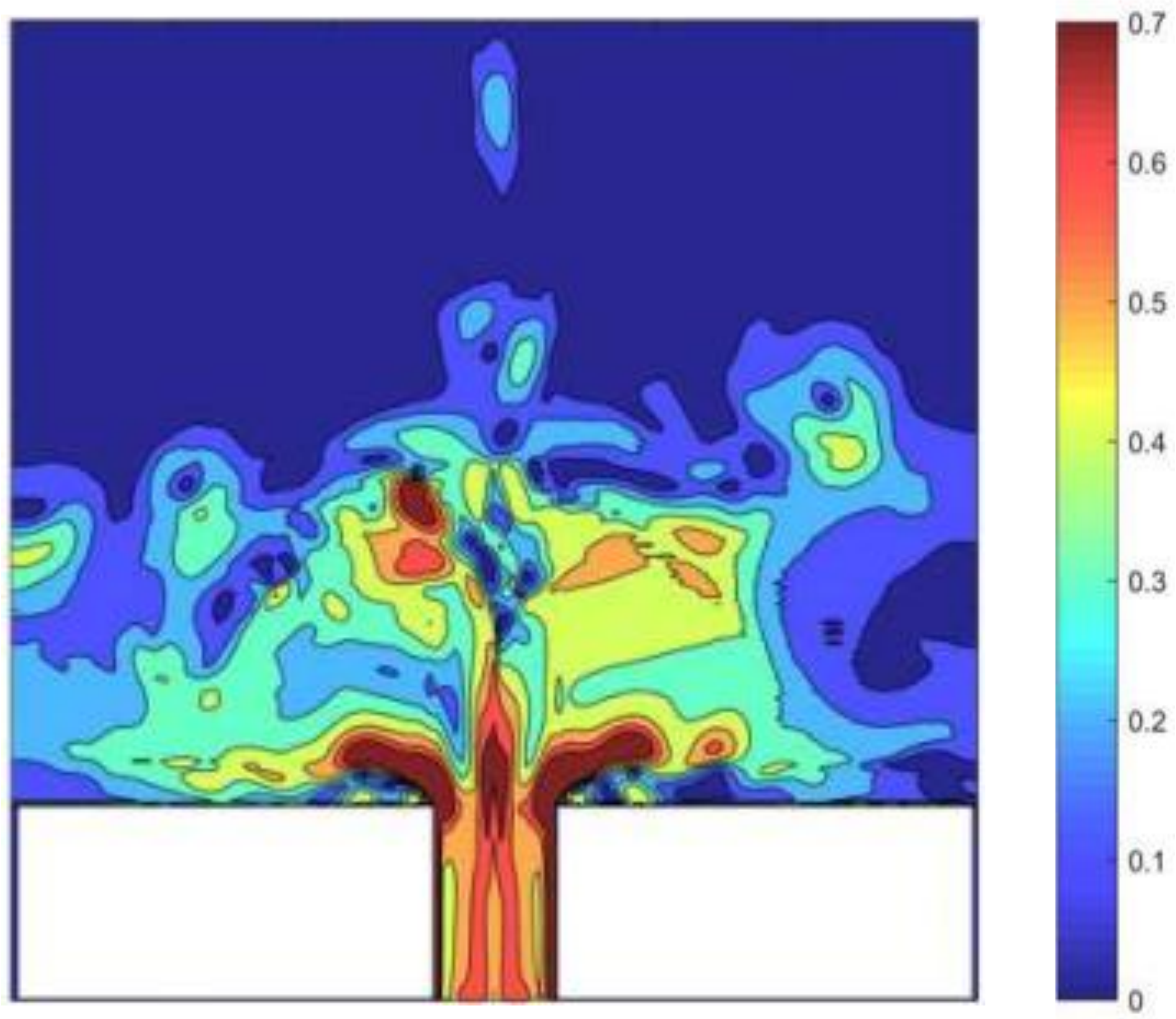

U=1.1 m/s

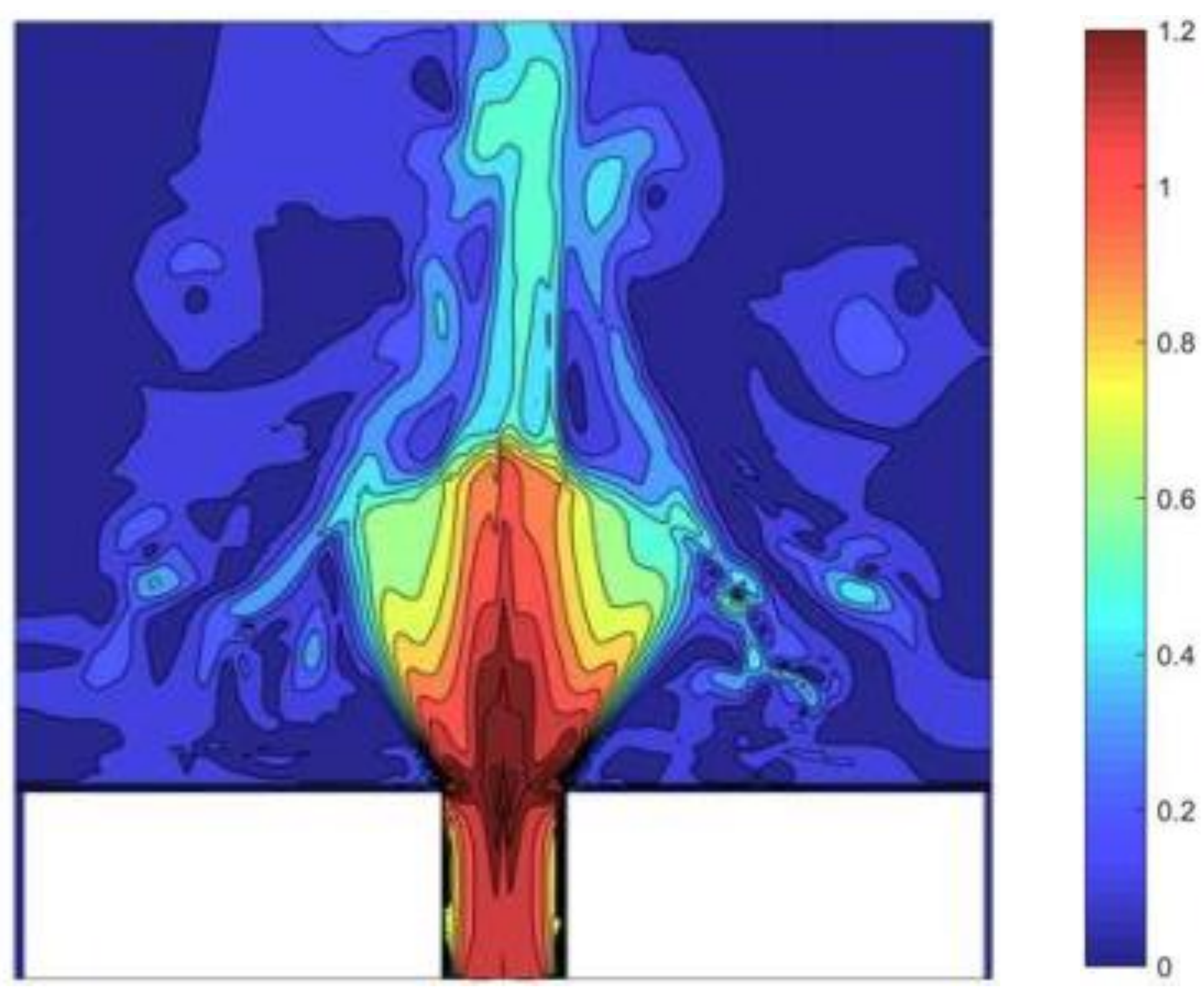

U=1.6 m/s

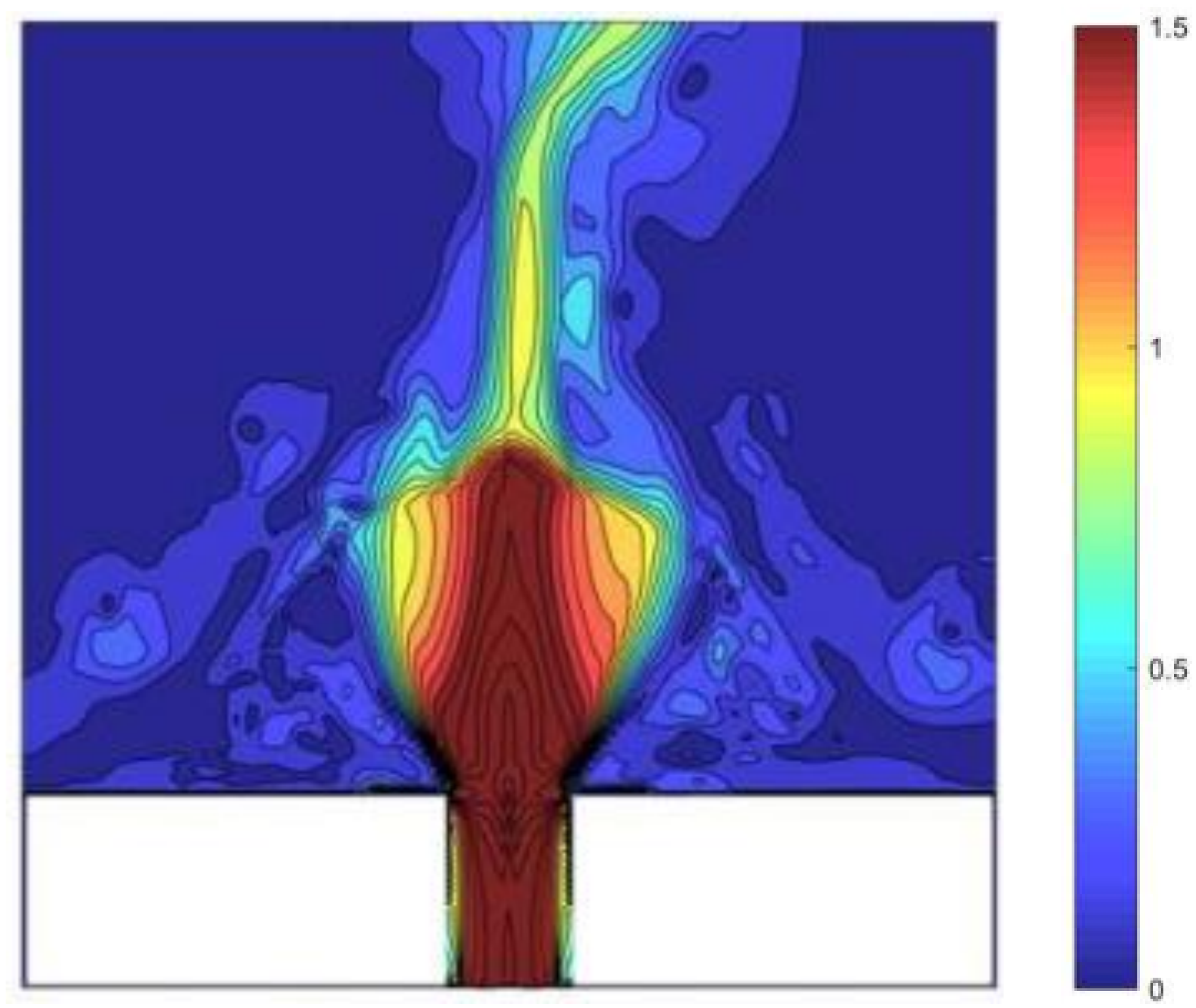

Numerical part: Delft-3D

❑ Particle Tracking:

✓ **Changes in sediment transport** ⟶ coastal erosion, adverse effects on habitats, infrastructure, and communities located along the coast.

✓ **Pollution transport** ⟶ detrimental effects on marine life and habitats.

➢ To effectively understand and model particle transport in coastal areas
- **hydrodynamic forces**
- **particle characteristics**
- **environmental conditions**

- D-WAQ PART is a random walk particle tracking model
- Horizontal dispersion due to turbulence.

Numerical part: Delft-3D

❑ Releasing particles from Estuarine part:

- The advection step due to the shear stresses from currents
- The random walk step is related to the horizontal dispersion.
- Horizontal dispersion due to turbulence., According to turbulence theory this dispersion increases in time.

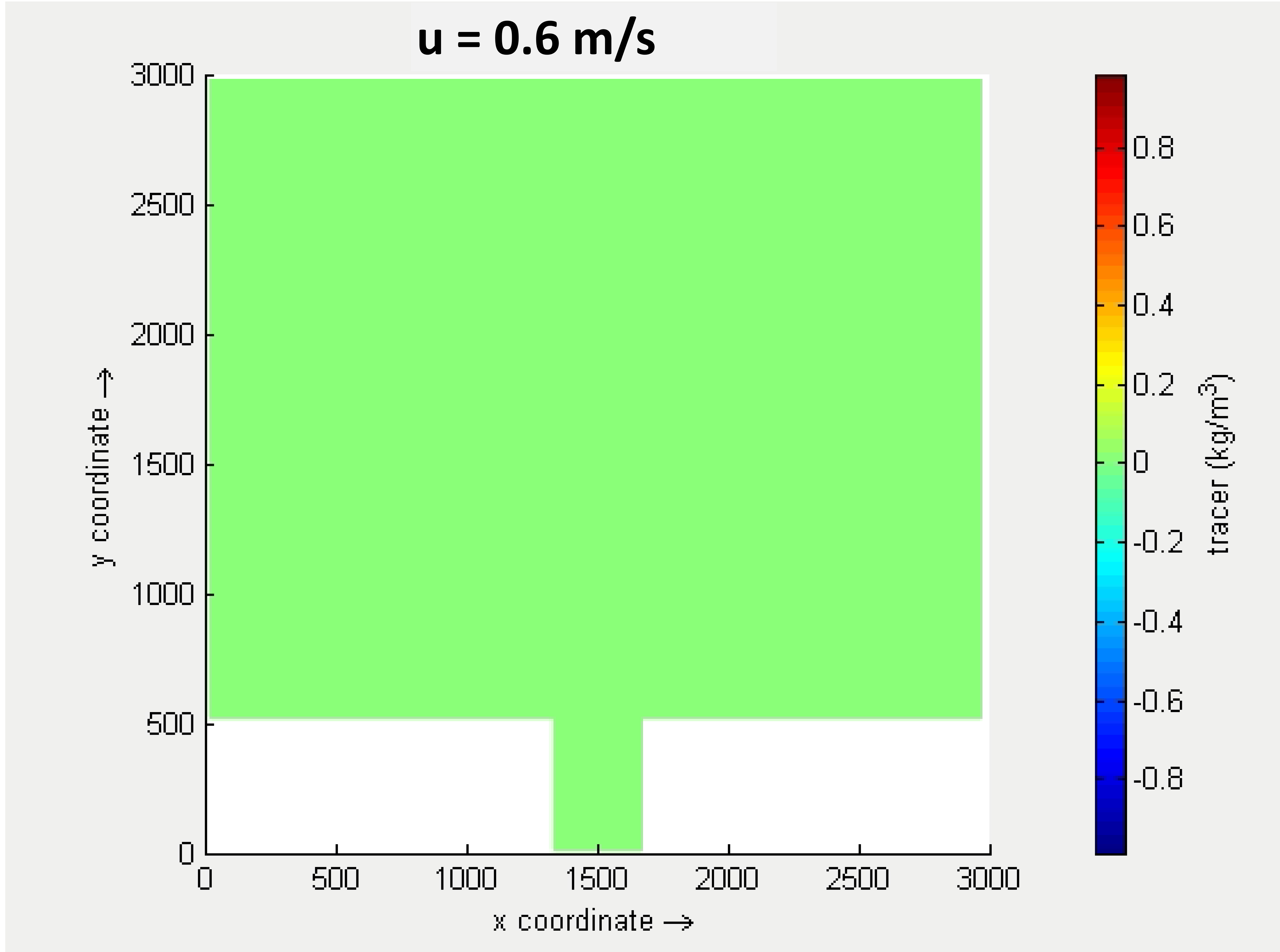

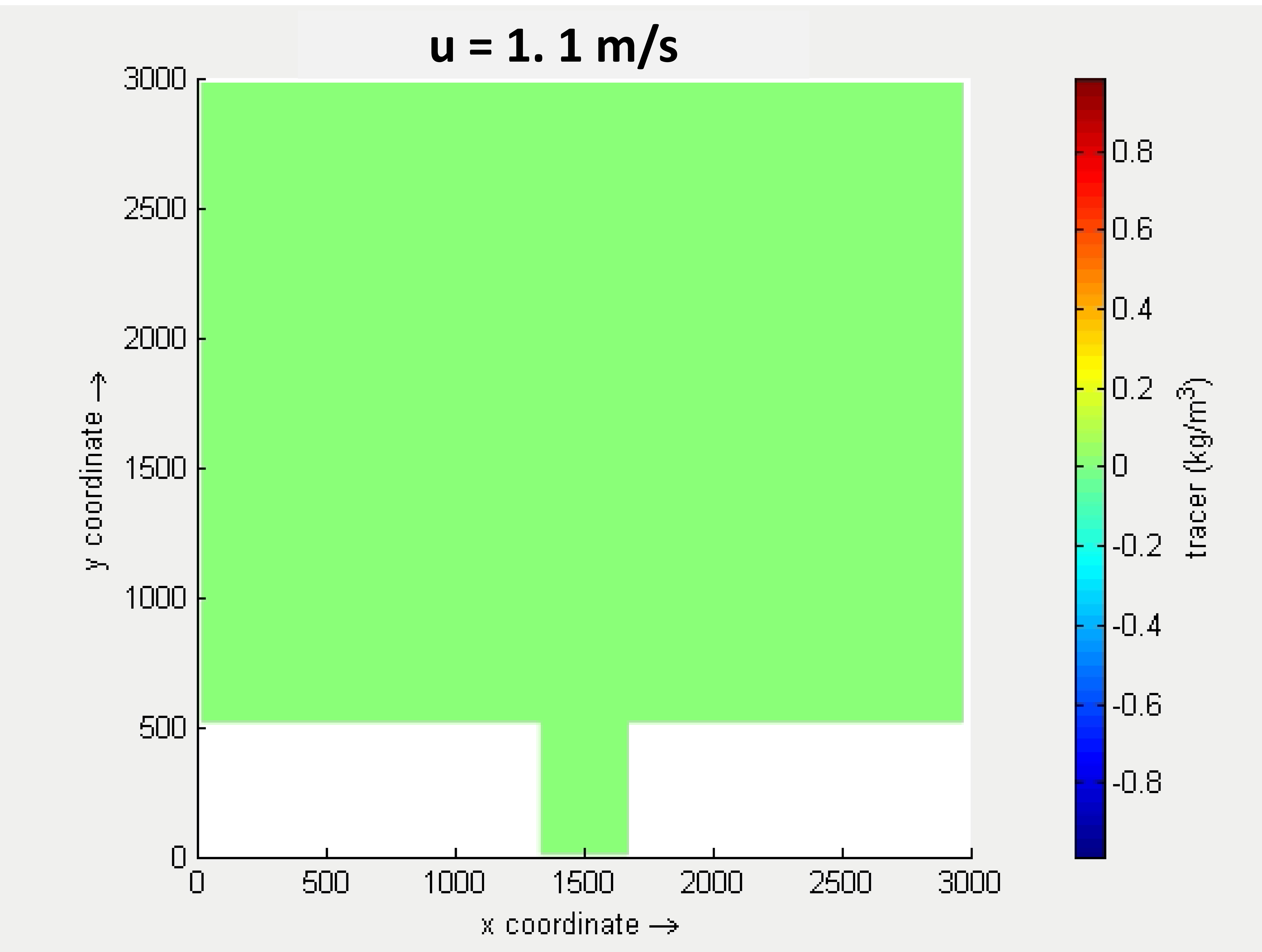

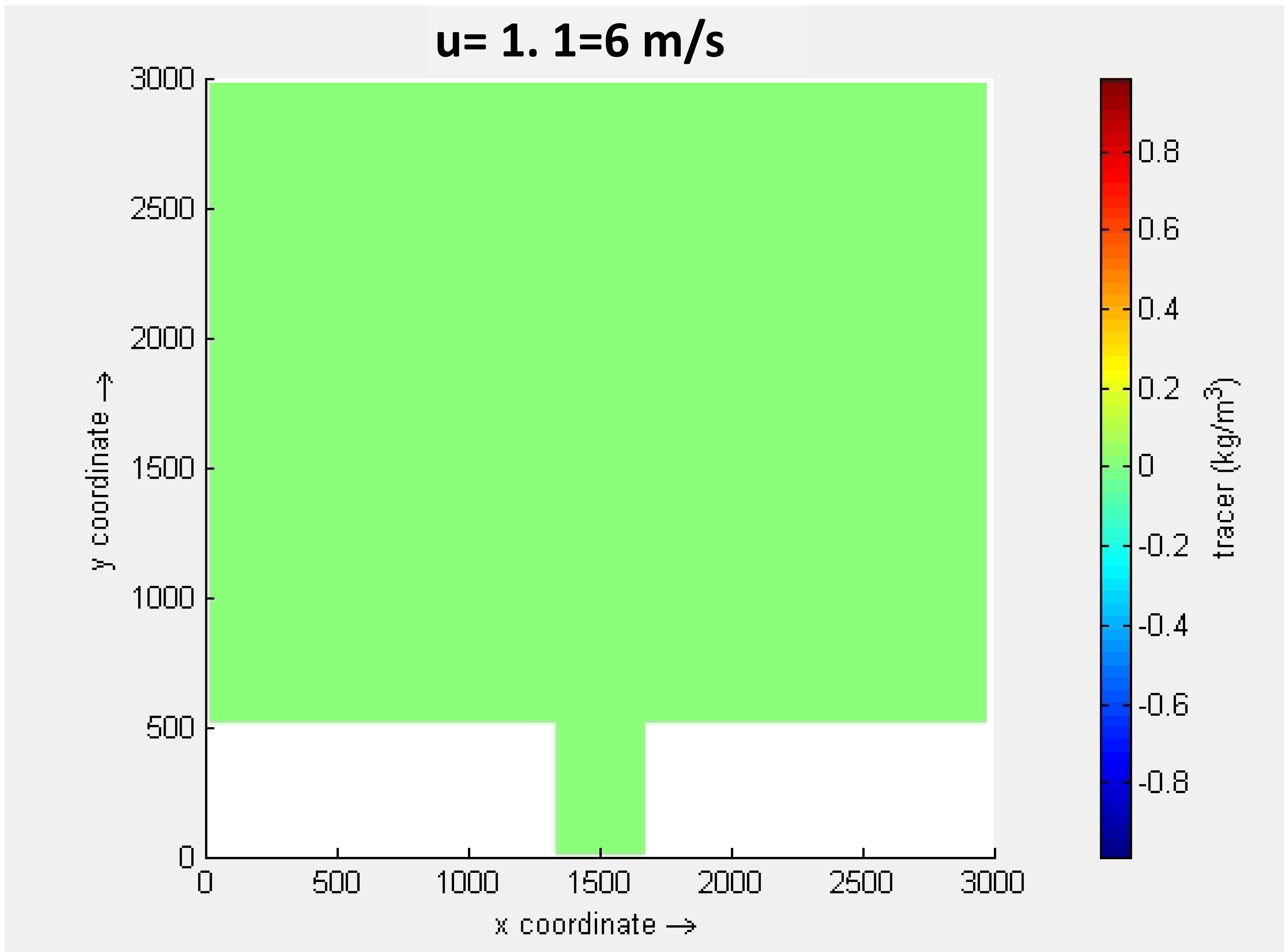

NSWE Solver

❑ **To investigate the dynamics of the nearshore zone:**
- Boussinesq-type Equations
- NSWEs

✓ Wave resolving 2DH methods, such as NSWEs, are among the most popular approximate models for investigation of the nearshore hydro-morphodynamics (Zyserman and Johnson (2002).

Water Depth, Our work

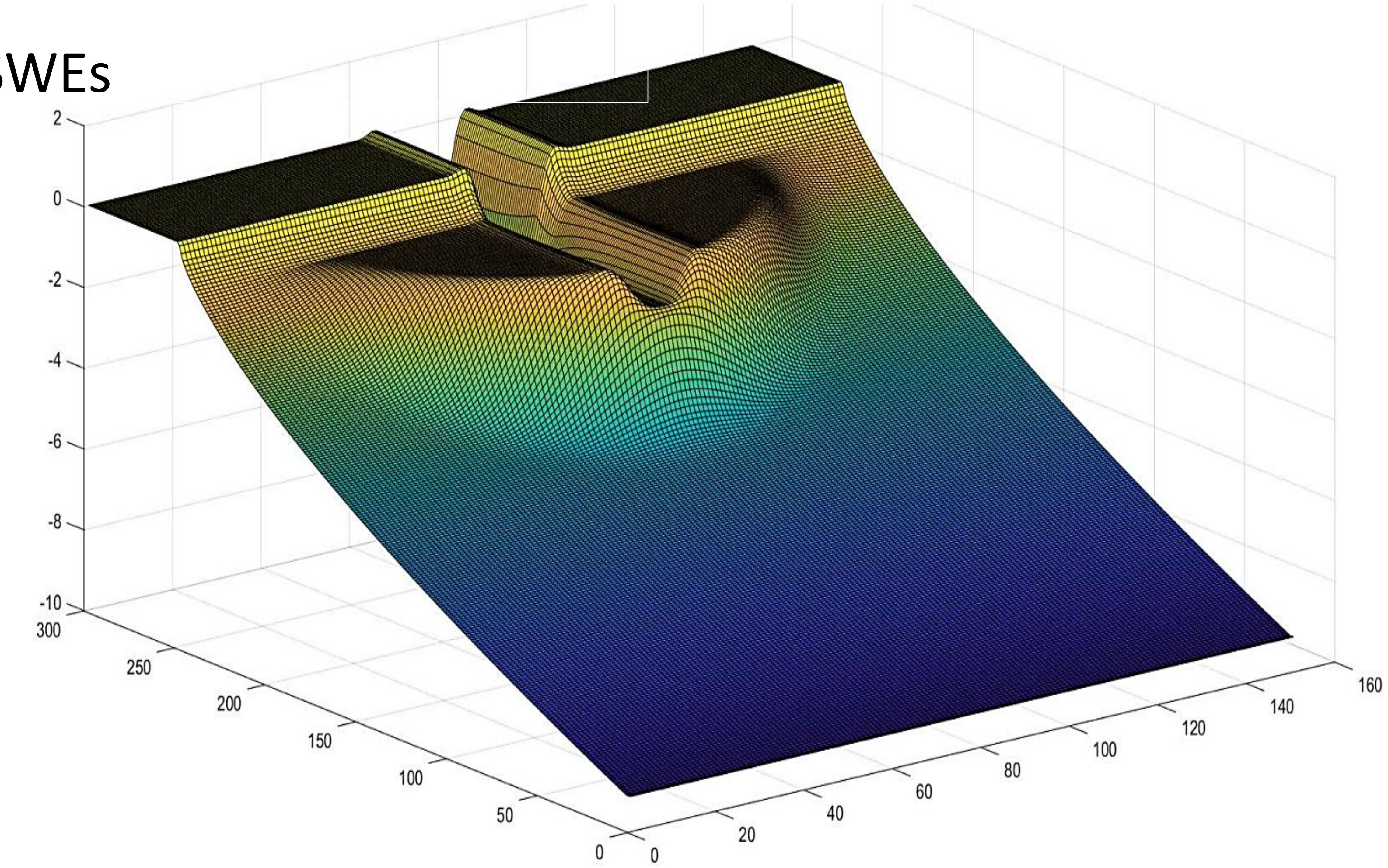

Water Depth, our work (by Delft3D)

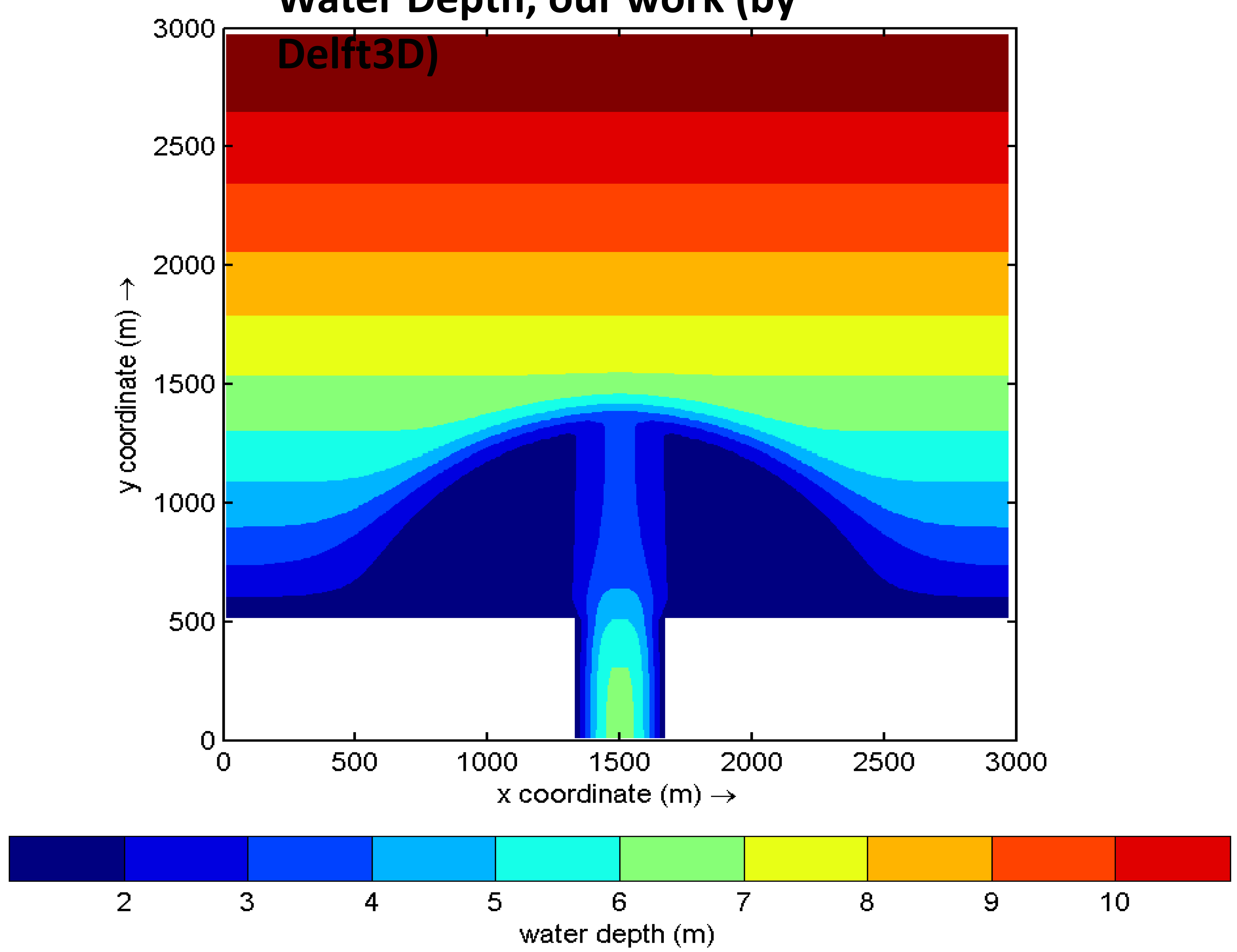

Water Depth, Olabarrieta et al. (2014)

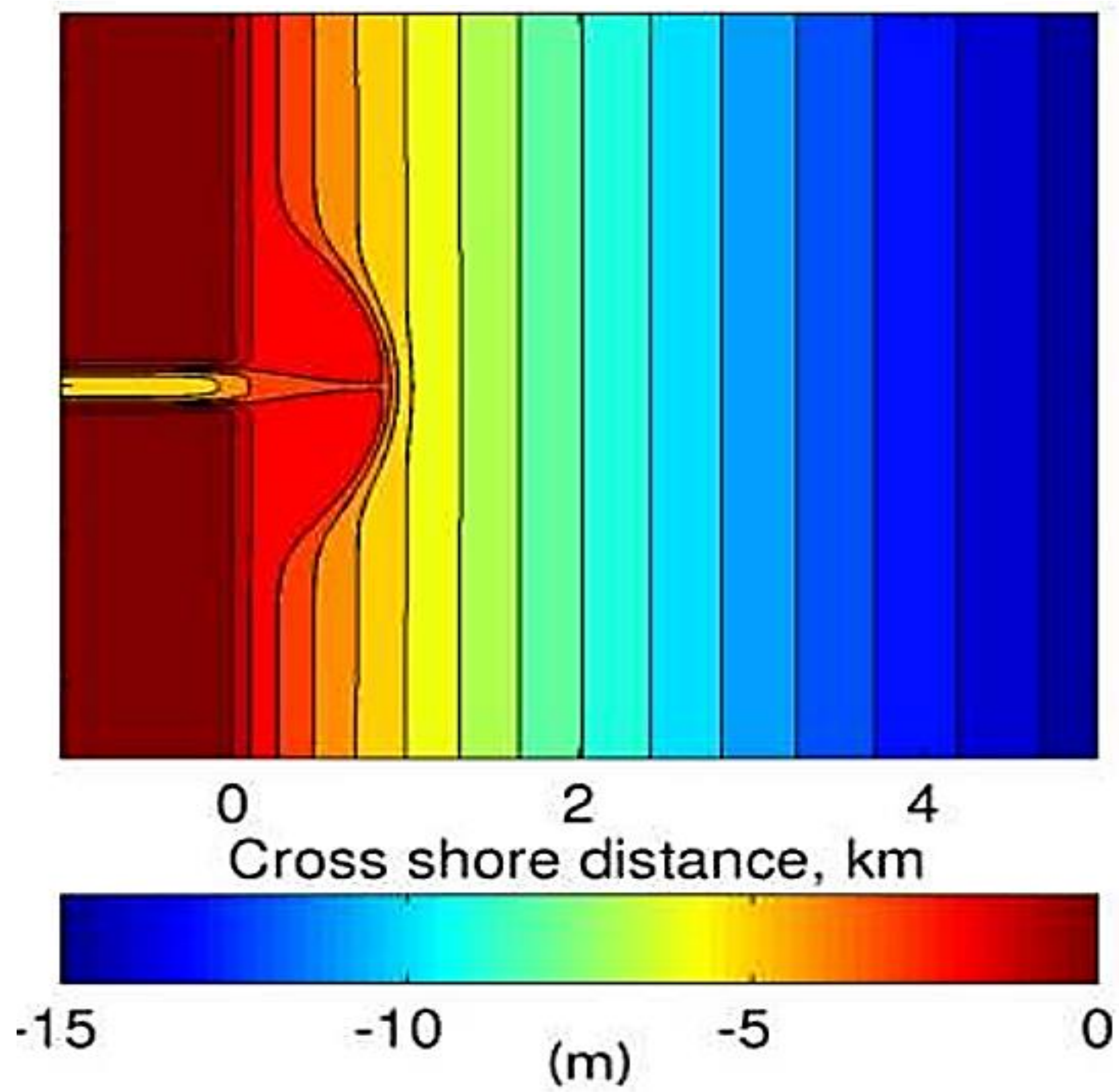

Numerical part: MATLAB Script for Particle tracking

- The code **solves** a system of equations for a **2D shallow water model** using finite differences and central differencing for spatial derivatives.

✓ How time stepping is applied:

1. Discretization of Equations:

- The **depth** d is updated using the continuity equation.

- The **velocities** u and v are updated based on momentum equations in the x and y directions, respectively.

2. Central Difference for Spatial Derivatives:

The code uses the central difference scheme to compute spatial derivatives:

3. Euler Time Stepping:

✓ The Euler method is used to advance the solution in time:

- The **depth** d and **velocities** u, v are updated *at each time step* by adding their time derivatives scaled by the time step dt.

$$d = d + \Delta t \cdot \frac{\partial d}{\partial t}$$

$$u = u + \Delta t \cdot \frac{\partial u}{\partial t}$$

$$v = v + \Delta t \cdot \frac{\partial v}{\partial t}$$

The new values of d, u, and v are then used in the next time step.

Numerical part: MATLAB Script

❑ Particle Tracking:

- ✓ Particles are tracked by interpolating the velocities (u_p and v_p) at the particle positions.
- ✓ The positions of the particles are updated based on the velocities using a forward Euler step.

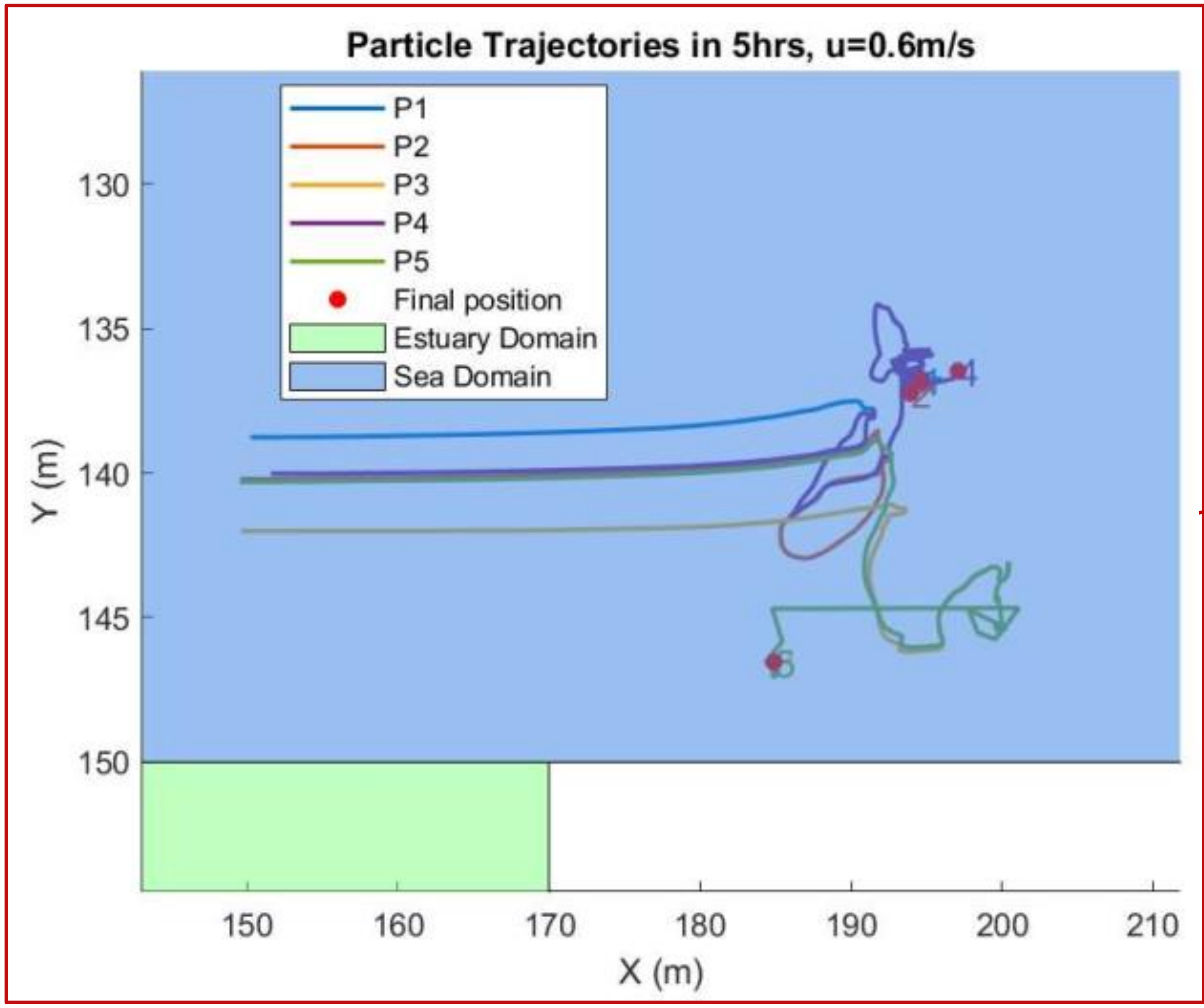

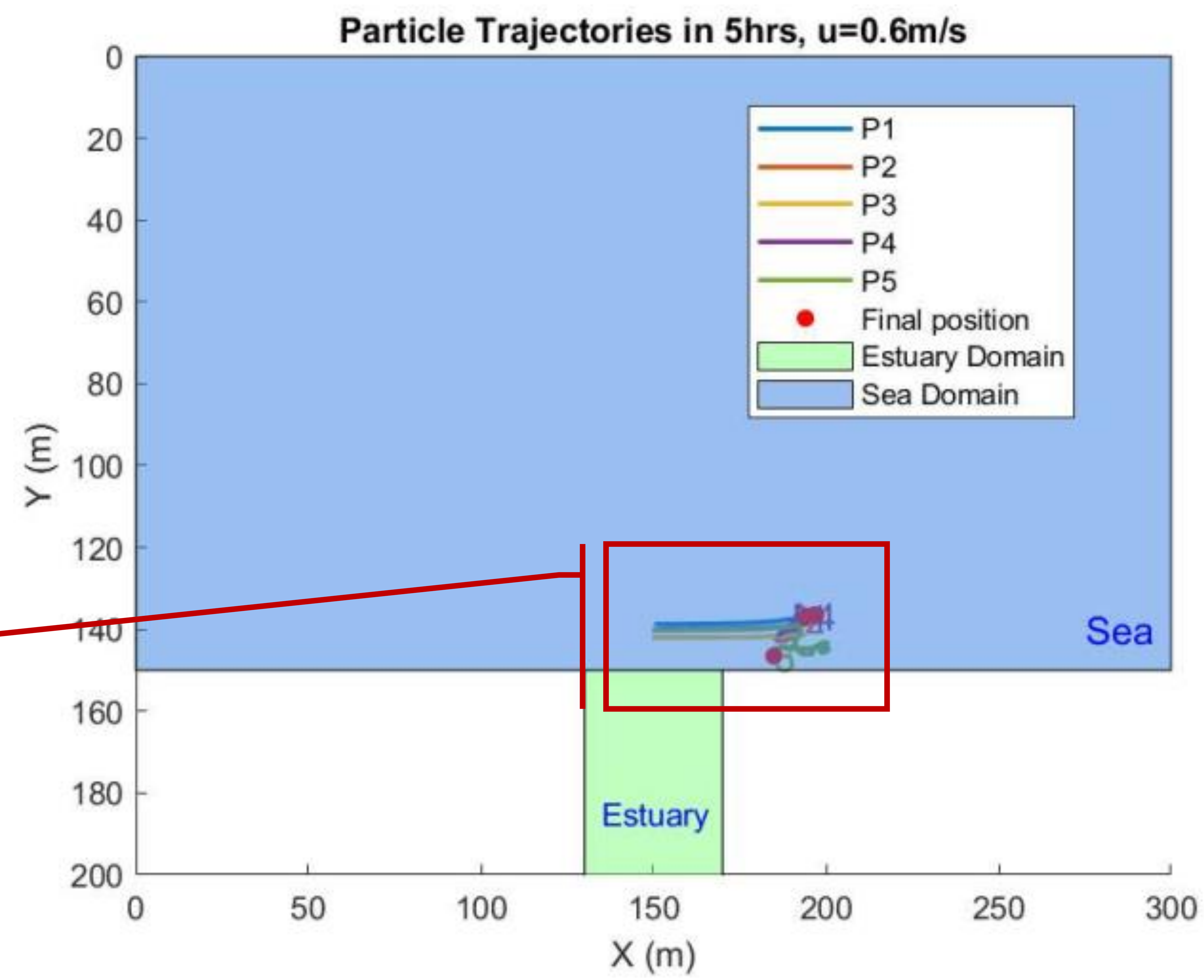

❑ Particle Tracking by MATLAB Script:

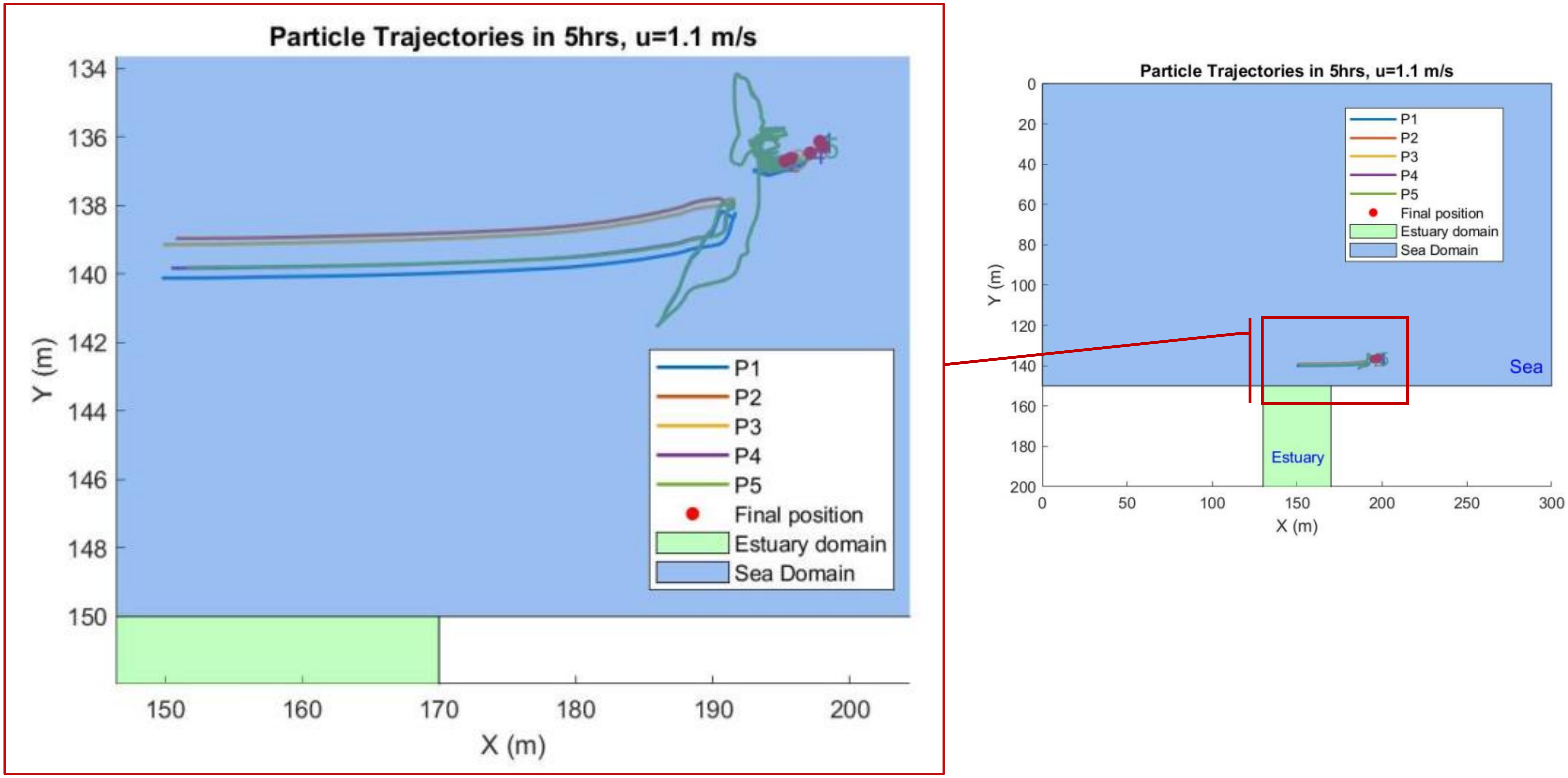

Numerical part: MATLAB Script

❑ Particle Tracking by MATLAB Script:

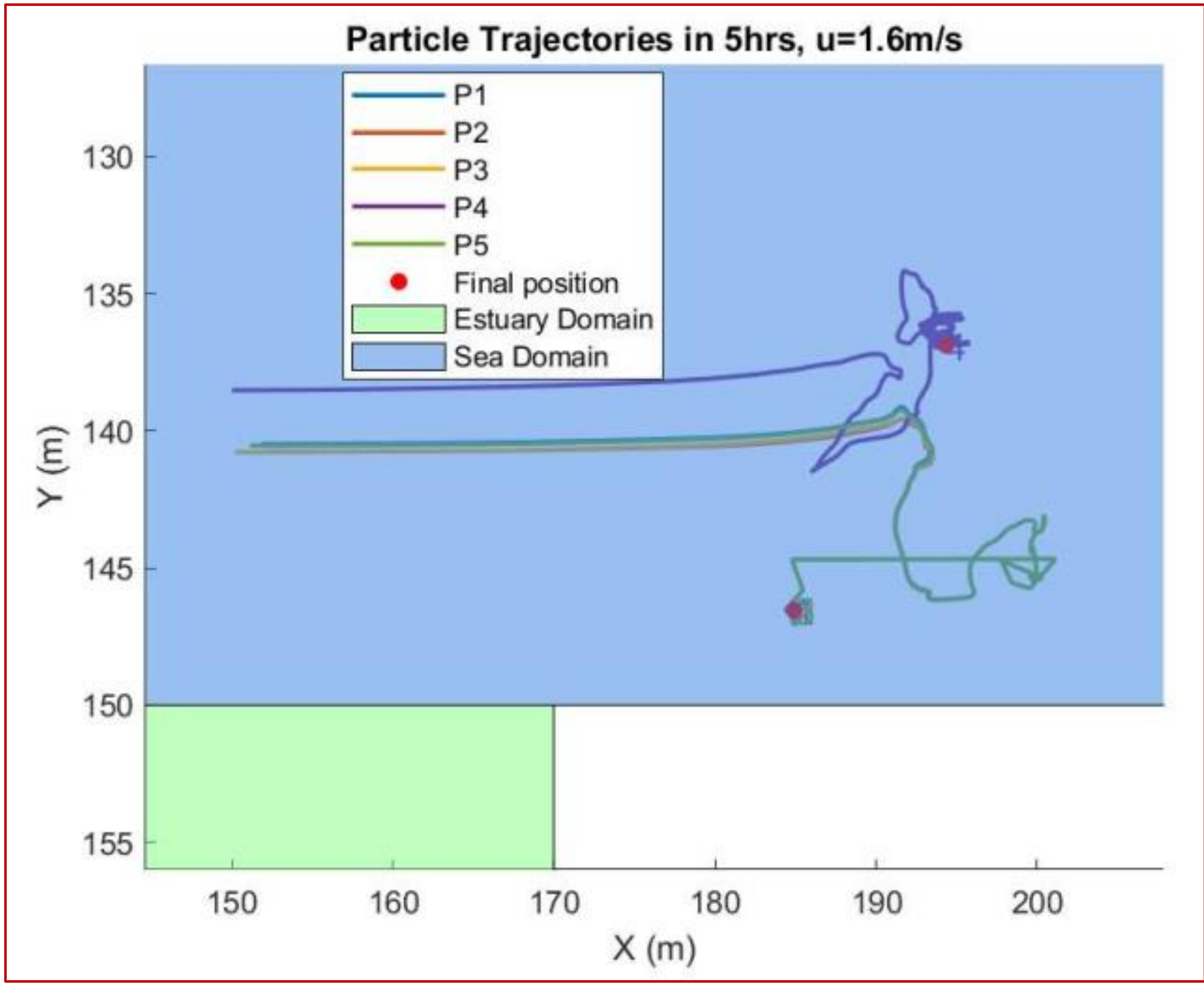

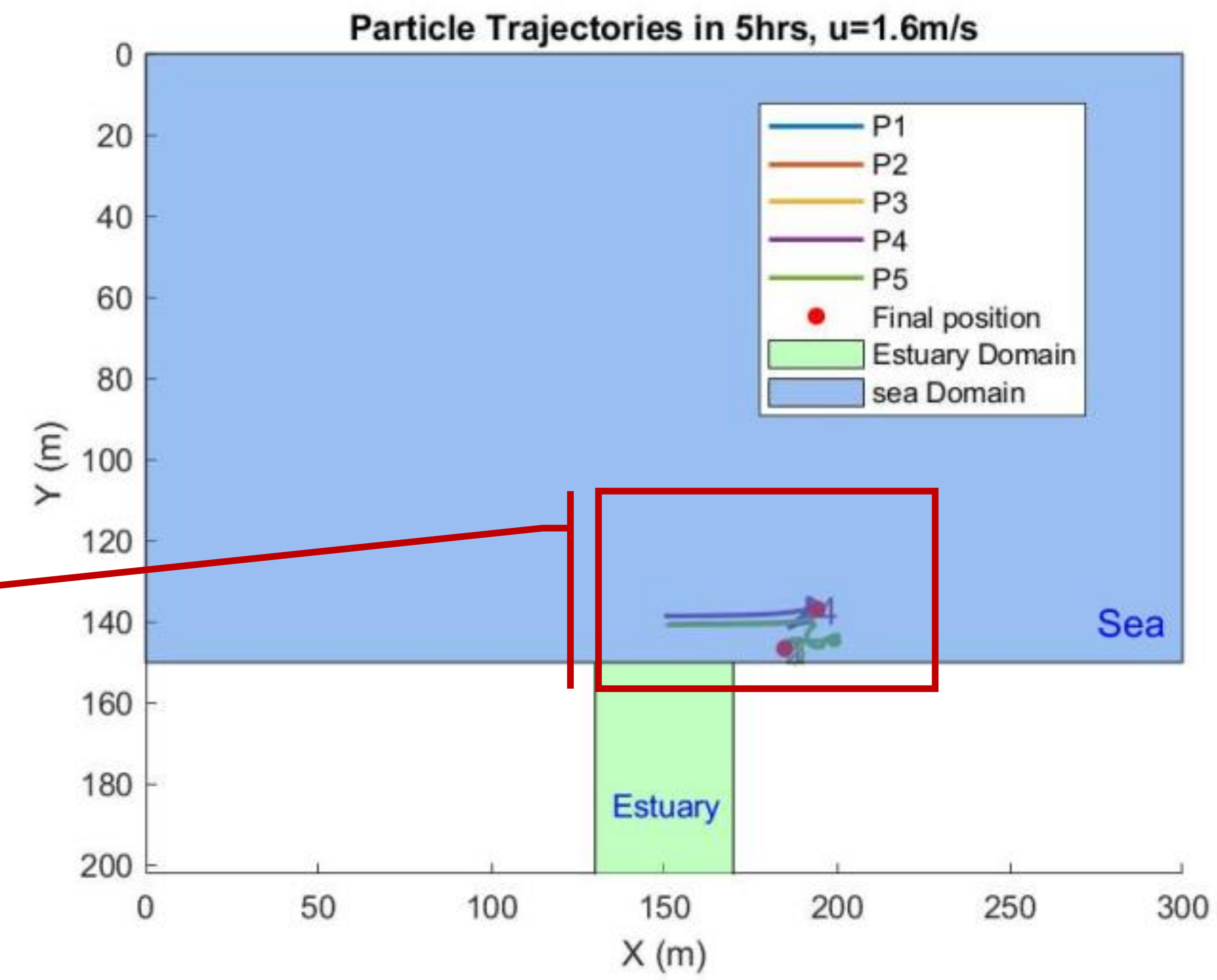

Compare: Partilce Tracking

- Delft3D Results

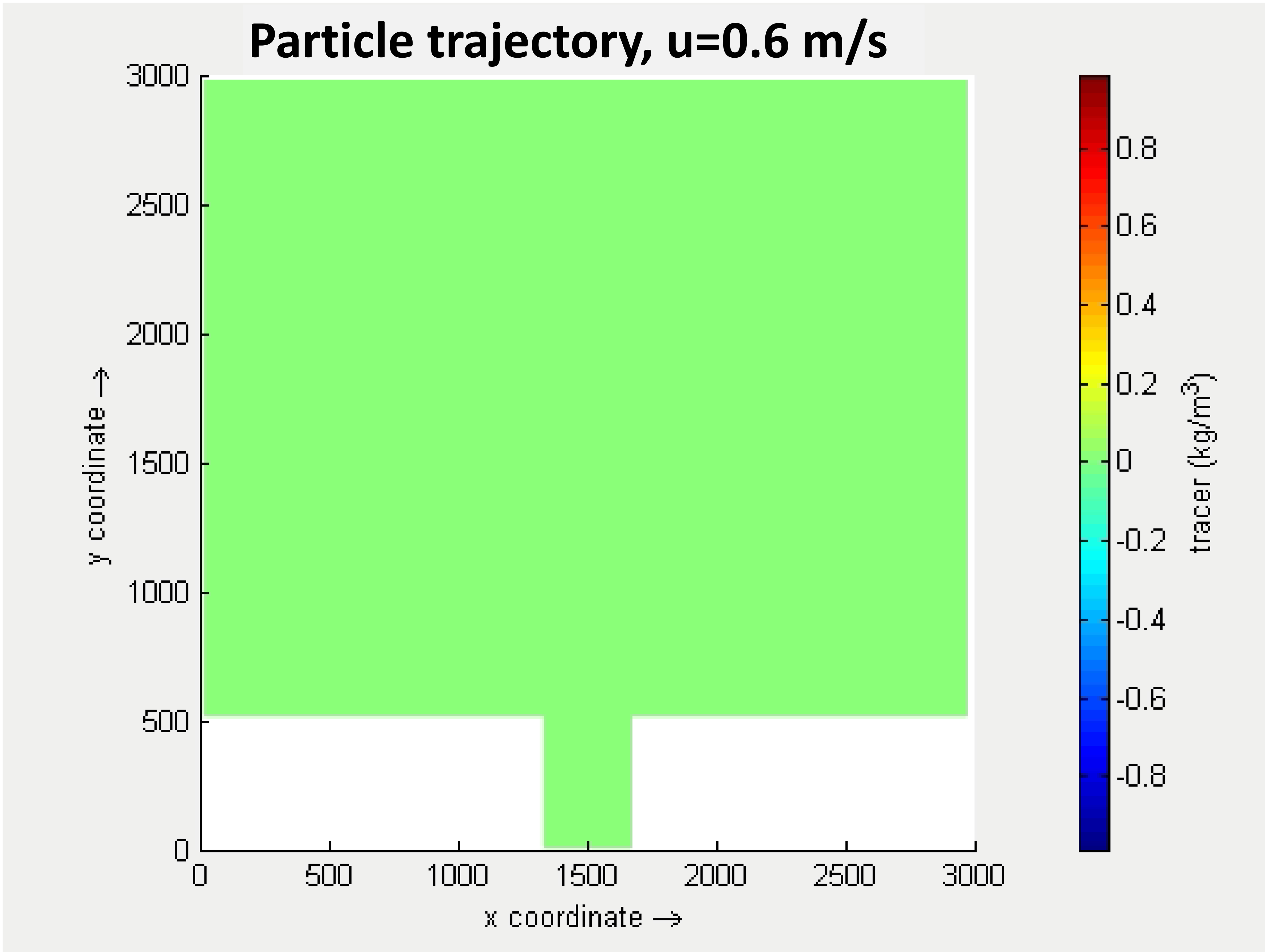

- MATLAB Script Results

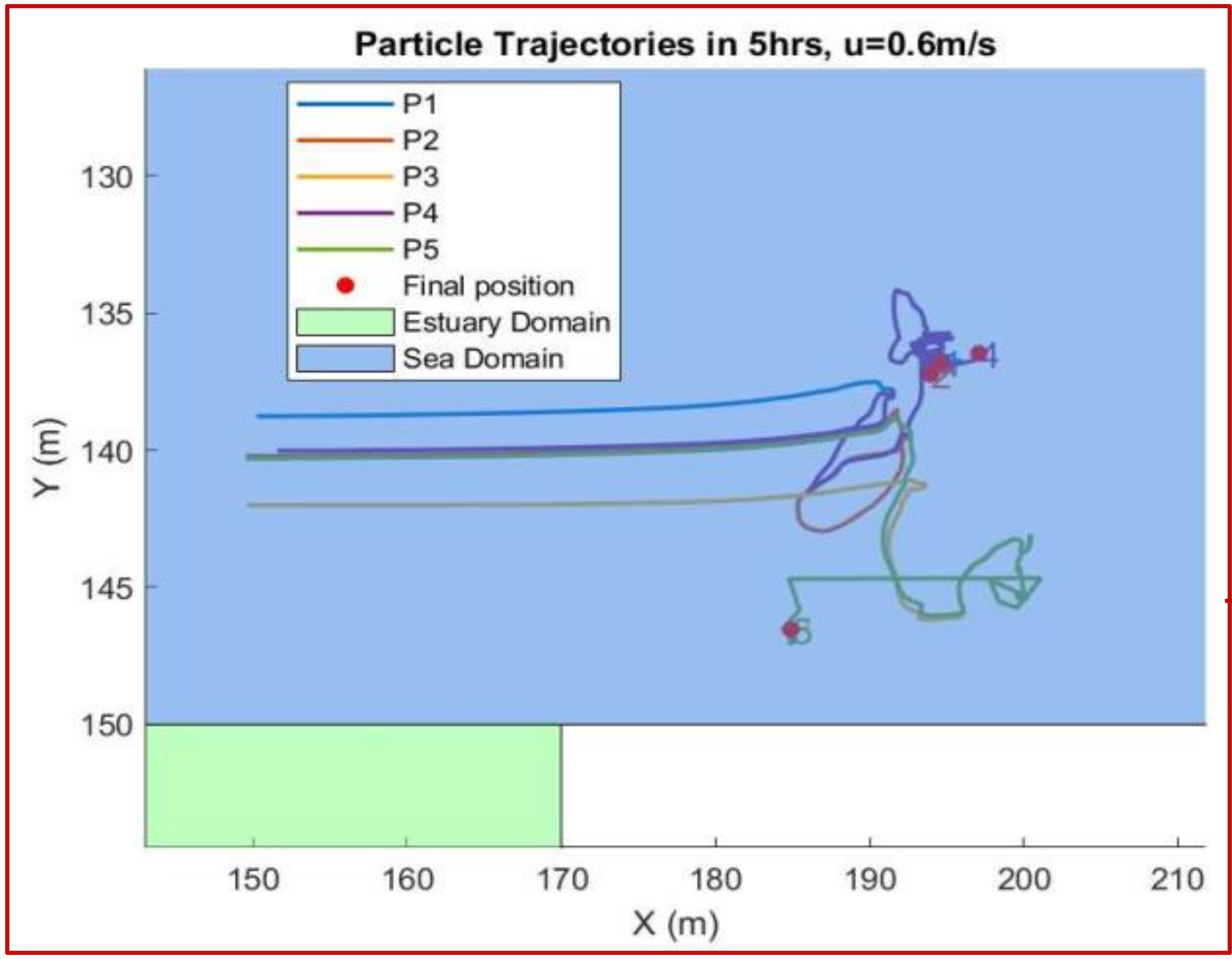

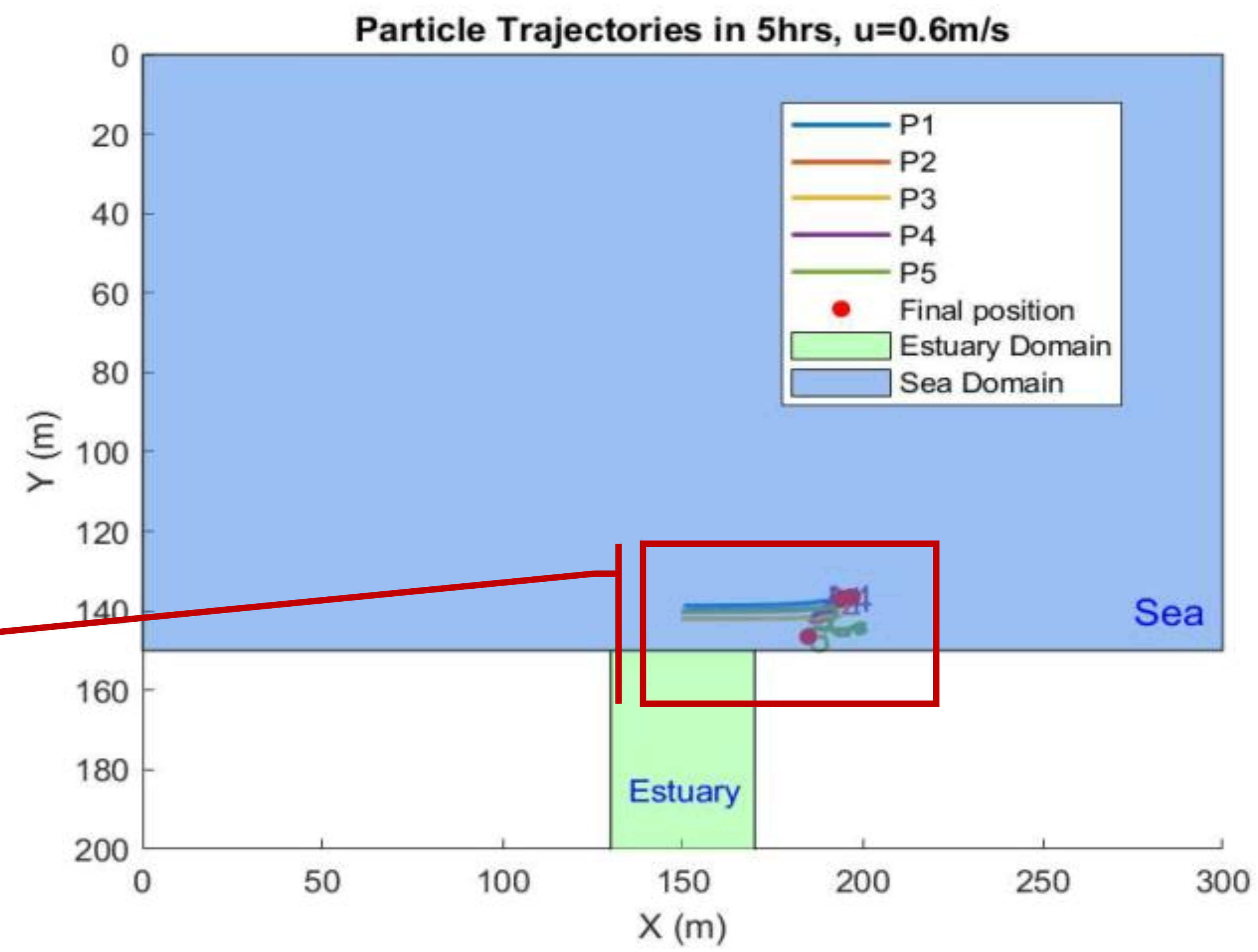

Thank you
for your attention!

Numerical part: Delft-3D

❑ Comparison of releasing particles from Estuarine part:

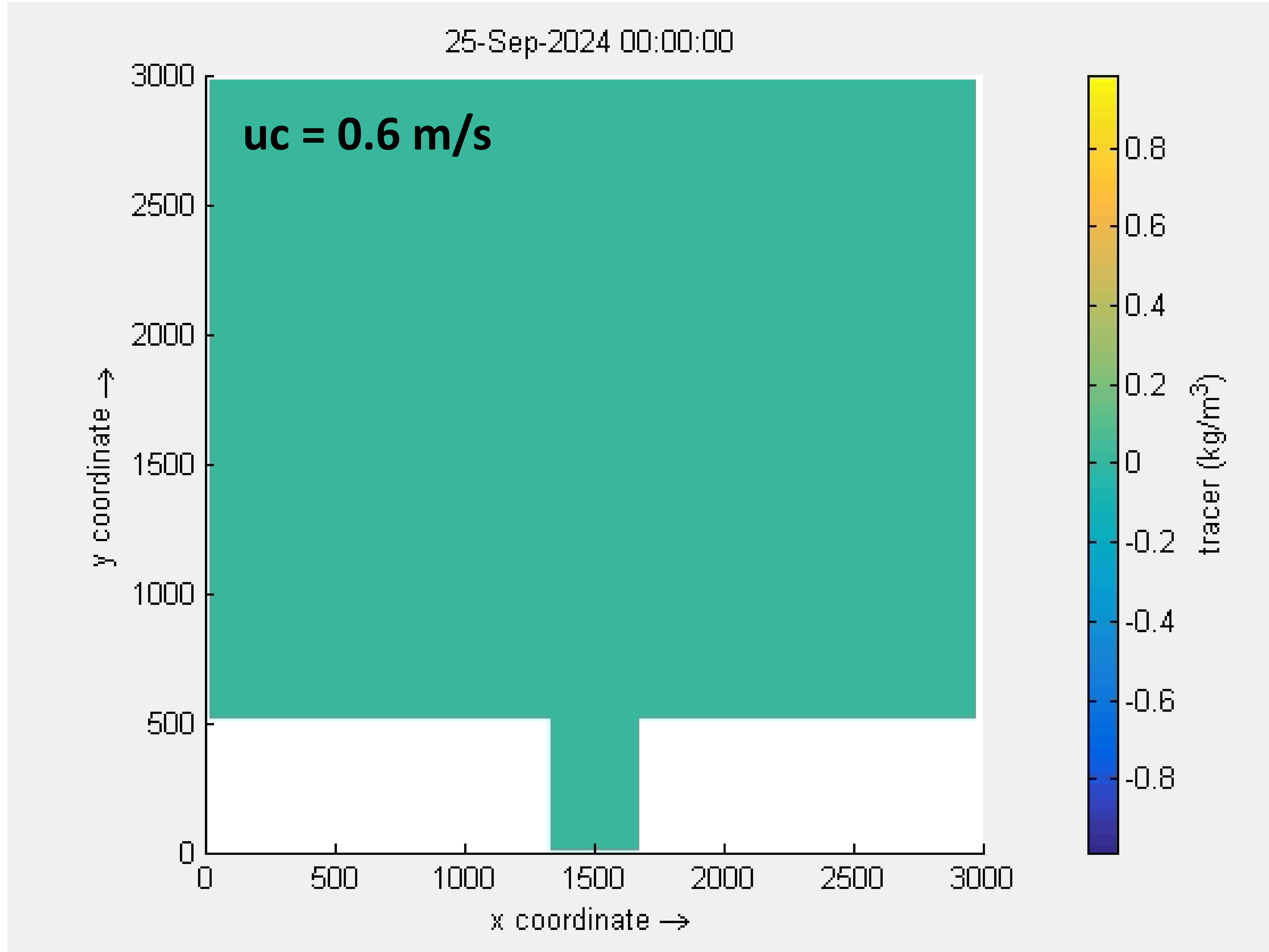

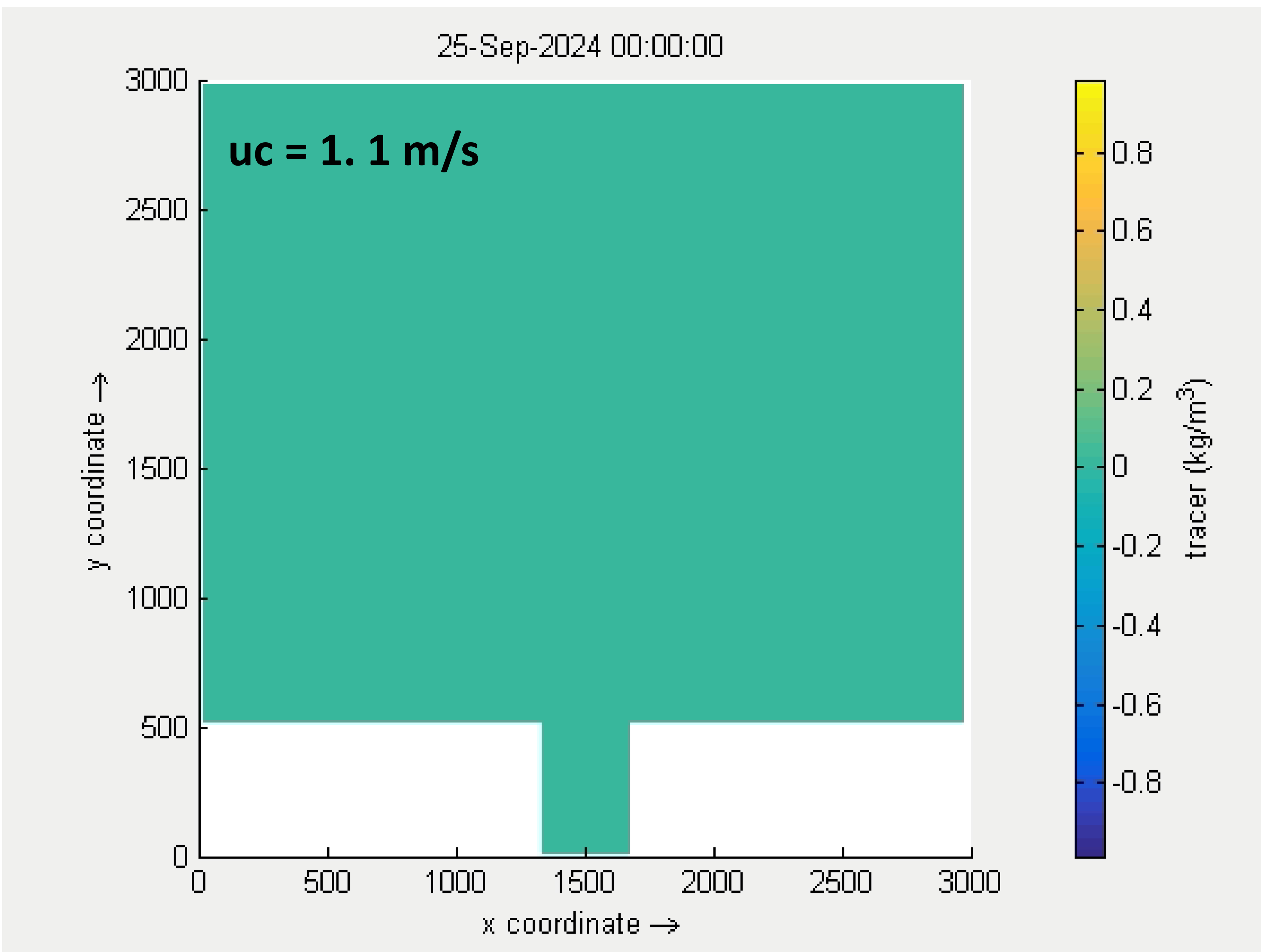

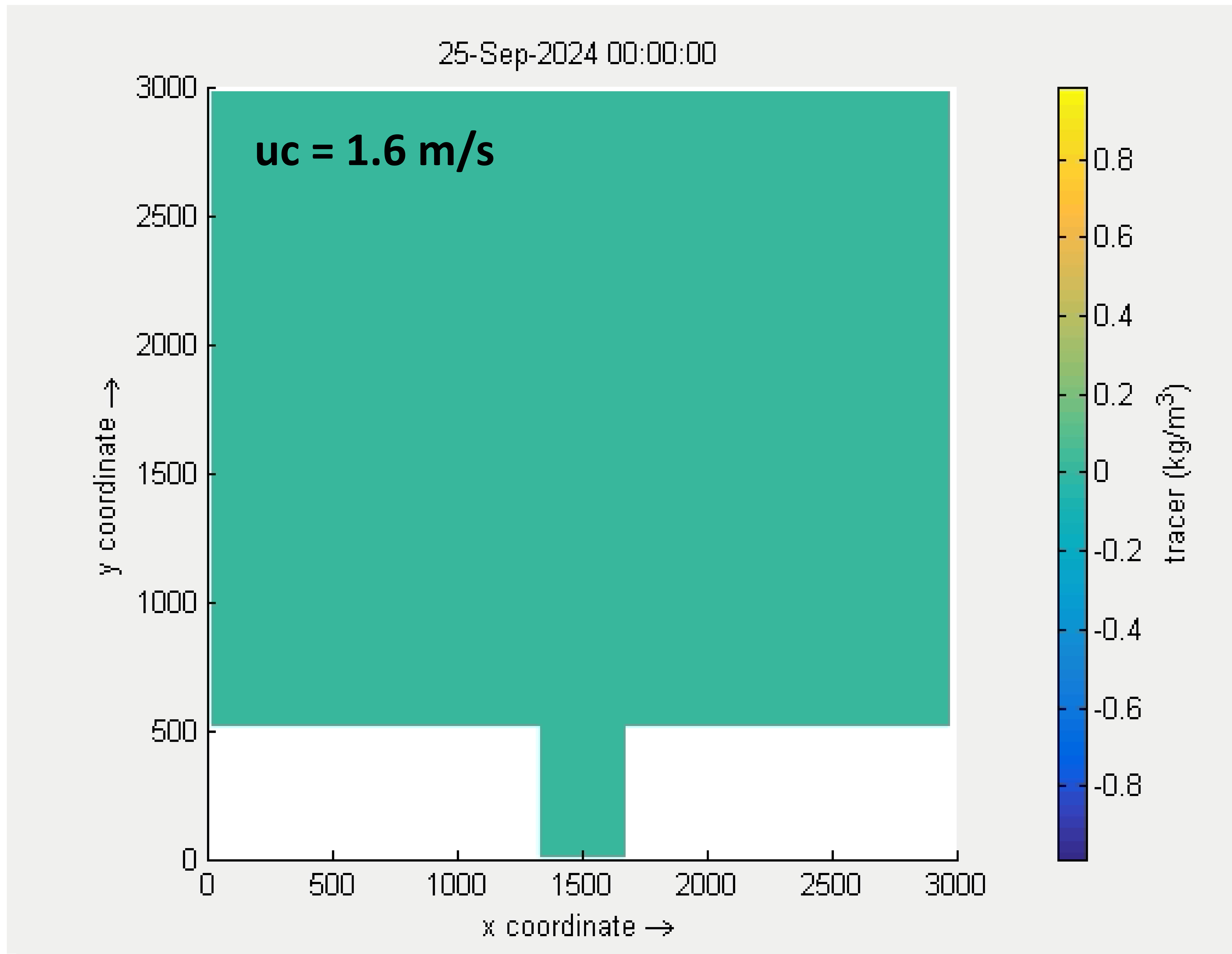

Numerical part: Delft-3D

Simulation for all regions:

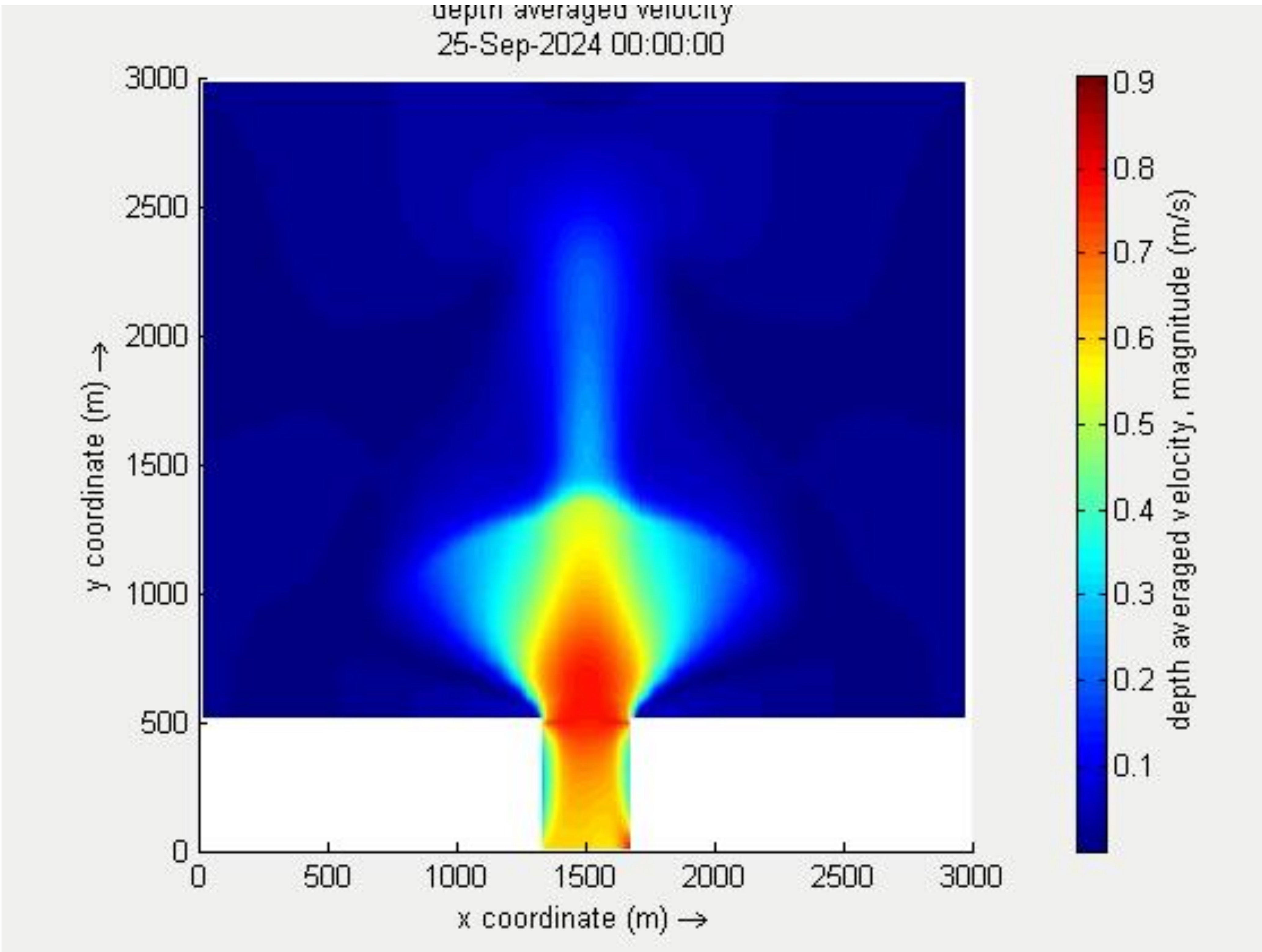

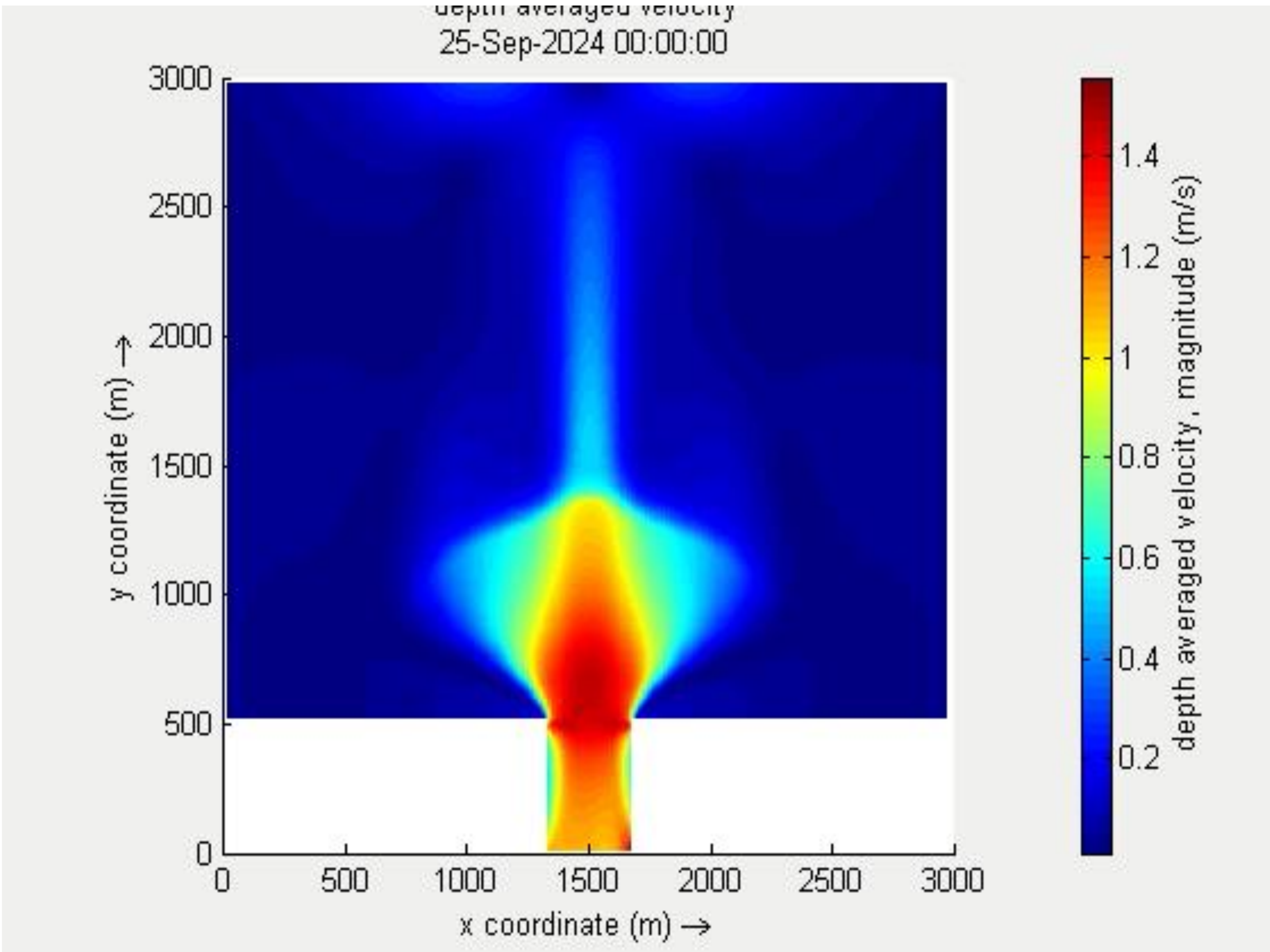

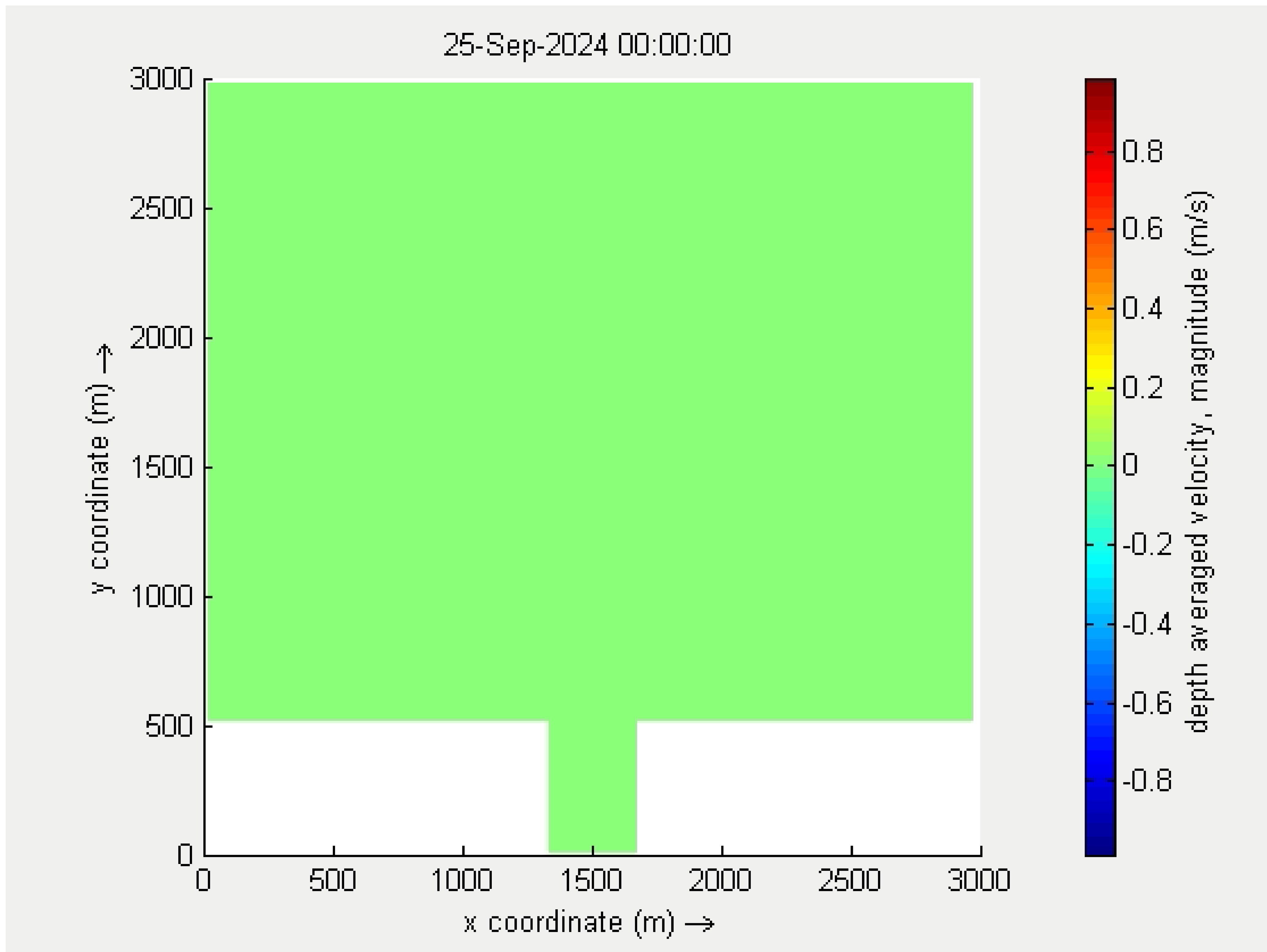

NSWE Solver

❑NSWE Solver: u=0.6 m/s

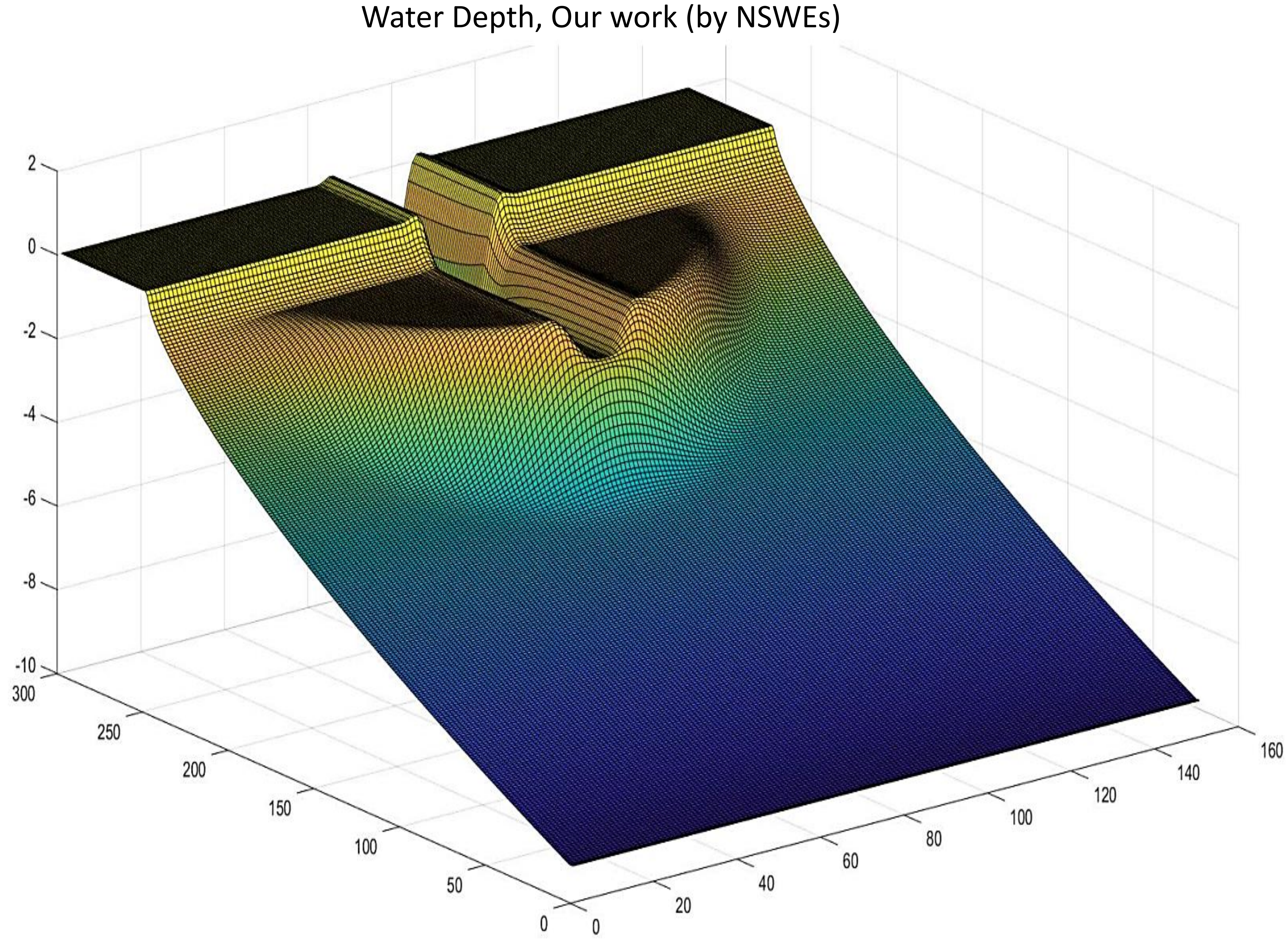

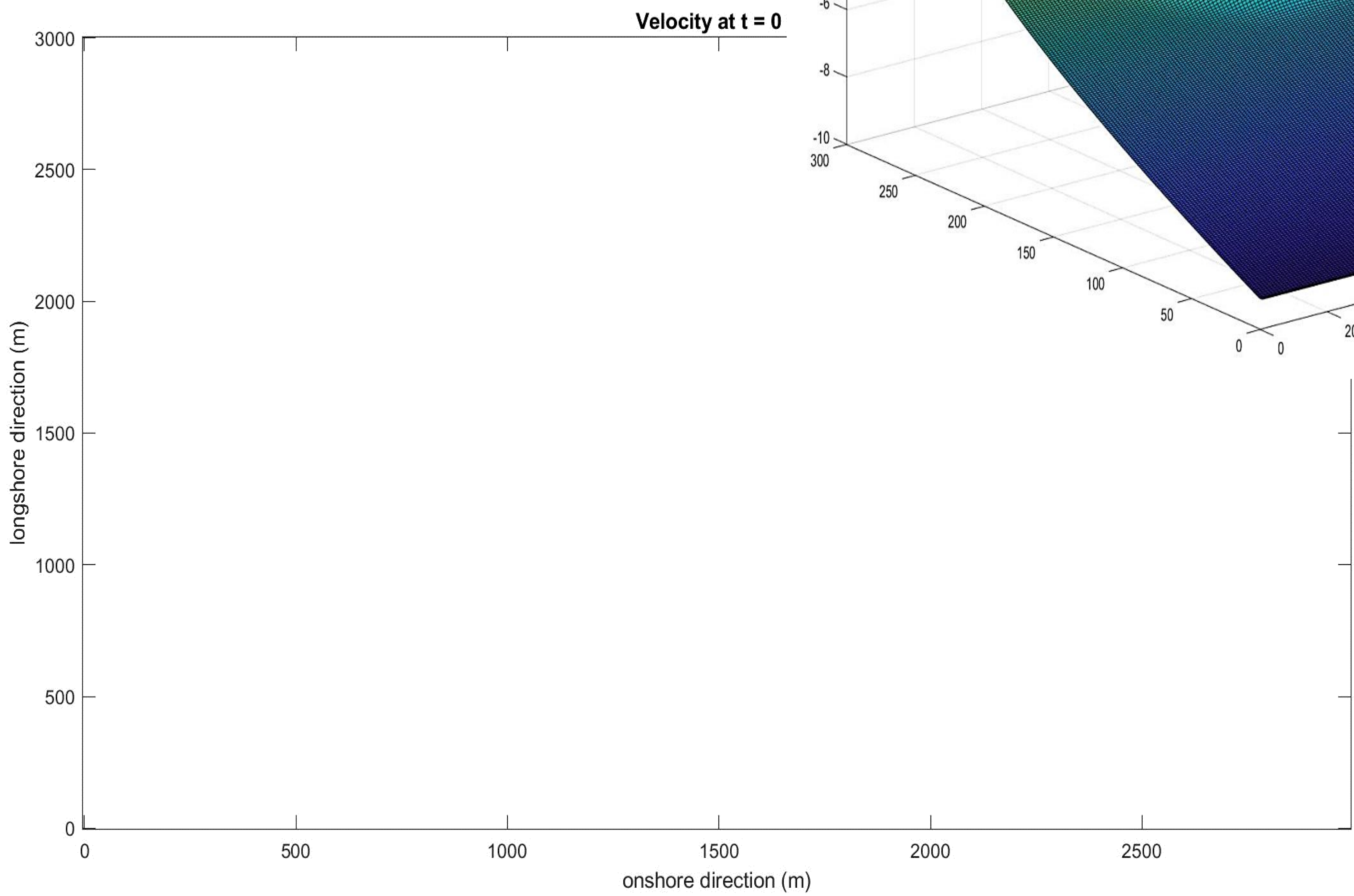

Multi-model approach to scour in dynamic areas

Nishchay Tiwari
HR Wallingford, UK

Supervisors and Advisors:
Michiel A.F. Knaapen
Sina Haeri
Richard Whitehouse

Marie Curie Grant Agreement Number: 101072443

Contents

Objective & State of the Art

- To investigate and develop methods for extracting/deriving information from the CFD model to improve the accuracy and resolution of the large-scale simulations.

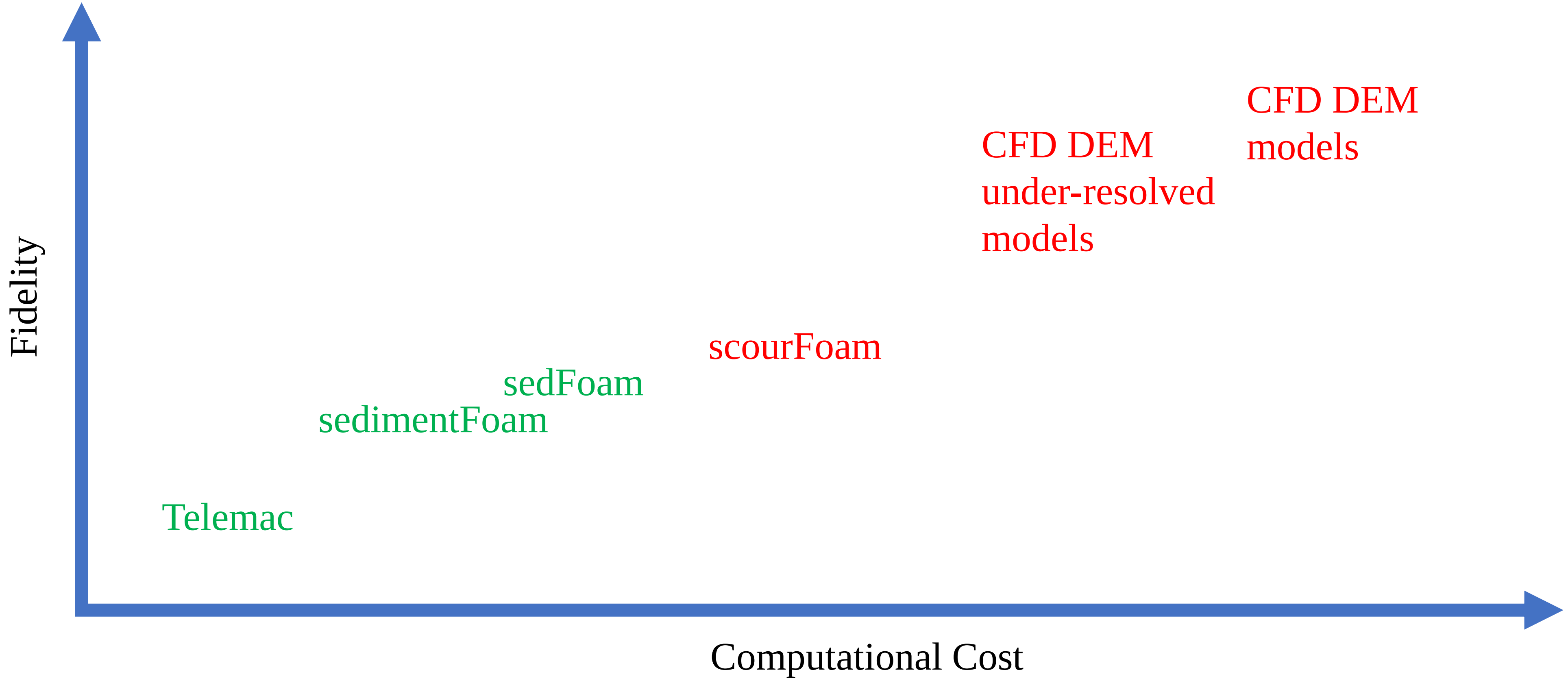

hrwallingford

OpenFOAM

- An open-source CFD toolbox that provides ready-to-use **solvers**, **utilities**, and **libraries**.
- Offers a versatile collection of efficient, **object-oriented C++ modules**.
- Utilizes the **Finite-Volume Method (FVM)** to solve systems of partial differential equations on any **3D unstructured** polyhedral cell mesh.
- Supports efficient **parallelization**.

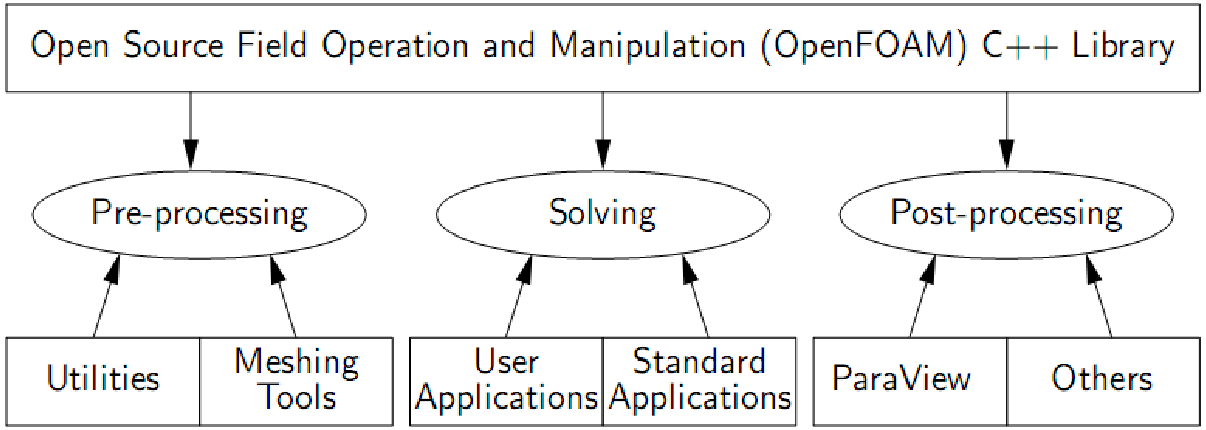

sedFoam: Numerical Modelling

Inputs

Experimental Data

- Obtaining the transport properties of sand and water phase used in Flumes experiment.
- Use the geometrical dimensions of cofferdam models.
- Using the input flow velocity

Solver

Two-phase Eulerian RANS OpenFOAM

- Creating 3D domain
- Using sedFoam :
  - Granular Rheology properties (muI)
  - Interfacial properties (drag model)
  - Transport properties
  - Modified Two-phase RAS equations

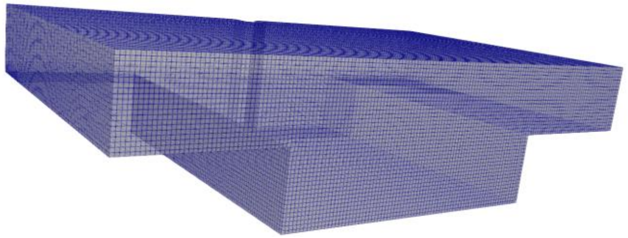

Outputs

Scour Depth

- Estimation of volume fraction of water and sand to predict the bed formation.
- Comparison with experiments

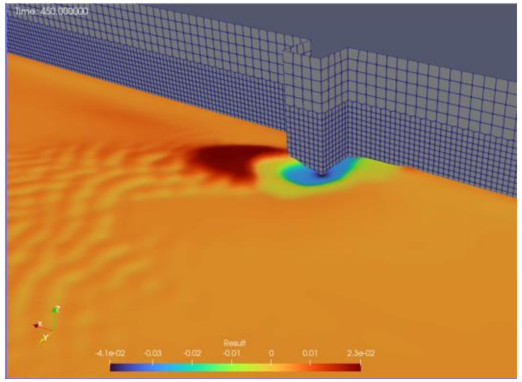

Experimental Data

- To develop a numerical model for the behaviours of scour using experiments performed on cofferdam models
- General Purpose Flume
  - Dimensions (25m long, 2.4m wide and 0.9m deep)
  - 0.5m deep bed with medium grained sand.
  - Flow discharge, Flow velocity and Water levels are recorded.
  - Duration of experiment: 50-75 hours

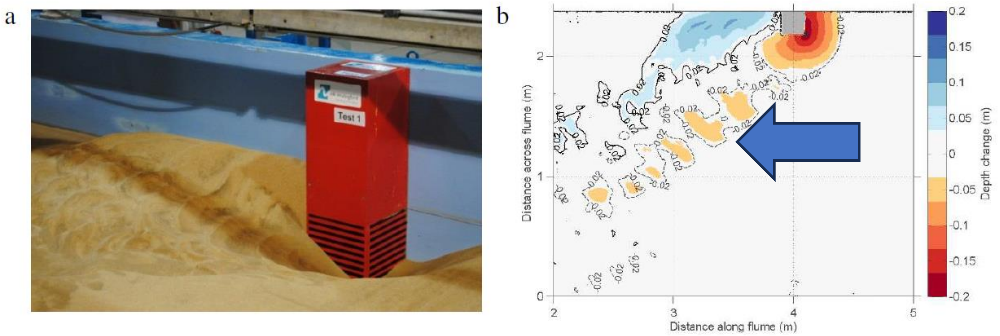

Figure 2: Test 1 result (flow from right to left); a. photograph of the post-test result (black and red graduations at 10 mm spacing) and b. difference in bed elevation between start and end of test.

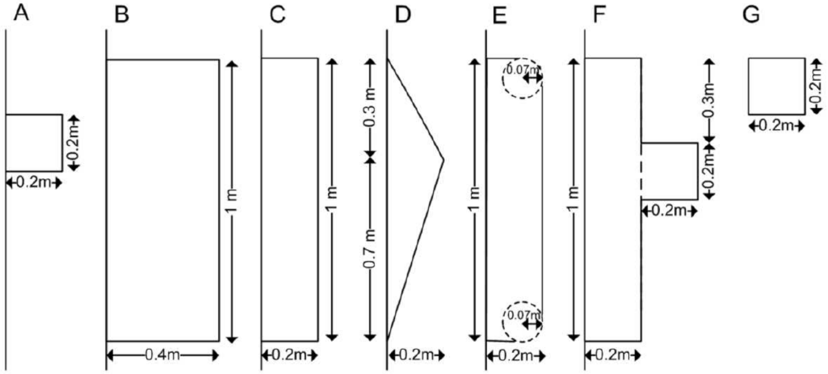

Figure 3: Cofferdam shapes used in the model experiments. The wall is on the left hand side of Structures A to F. The length of the structure is the distance along the wall and the width the distance the structure protrudes from the wall.

Richard J.S Whitehouse, 2021

hr wallingford

Experimental Data

- Inputs from Experiments
  - Grains (quartz sand):
    - d_{10}= 0.326mm
    - **d_{50}= 0.525mm**
    - d_{90}= 0.673mm
  - Flow speeds : **0.177m/s, 0.244m/s** (currents)
  - Water depths : **0.2m,0.1m**
- Geometries of cofferdams
- Dimensions of the Flume

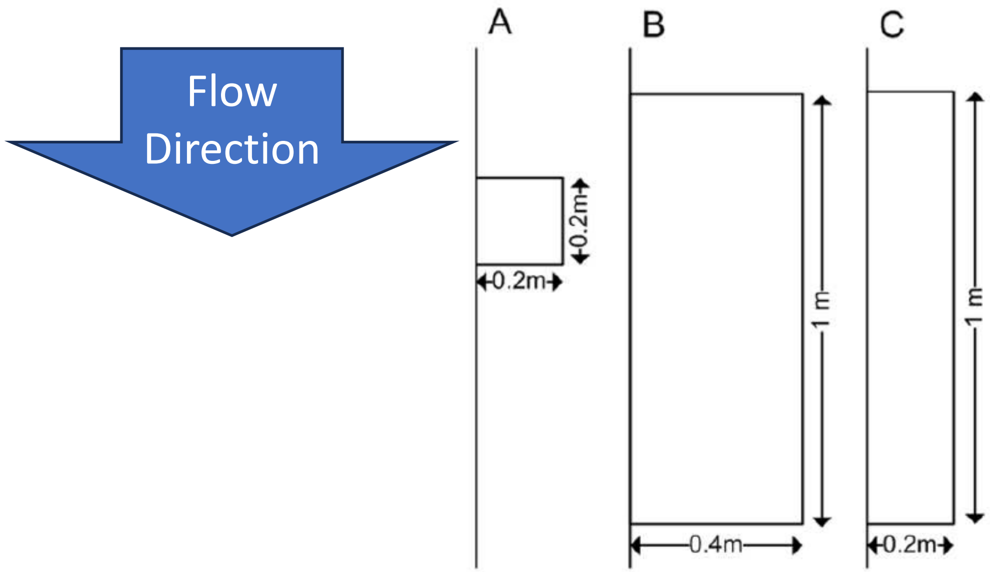

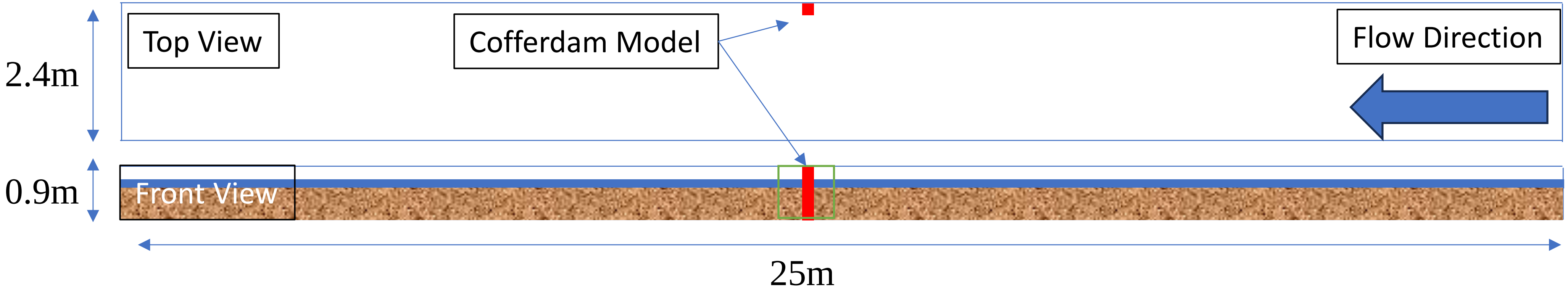

sedFoam

Closure Models for Stress Tensors

- Turbulence Models
  - SedFoam uses different turbulence closures for fluid flow, such as k-ϵ, **k-ω**, and a simple mixing length model, to capture the effects of turbulent eddies on sediment transport.

- Granular Stress Models
  - SedFoam implements granular stress models to simulate dense granular flows. The kinetic theory of granular flows and the **μ(I)-rheology** (derived from the Jop et al., 2006 model) are commonly used.
  - In dense flows, the granular stress is influenced by **particle-particle collisions** and **inter-particle friction**, represented by the effective viscosity, which is a function of the shear rate and pressure.
  - Unlike the kinetic theory of granular flows (which works well for dilute conditions), the μ(I) rheology is phenomenological and based on dimensional analysis, focusing on frictional contacts.

Domain and Boundary Conditions

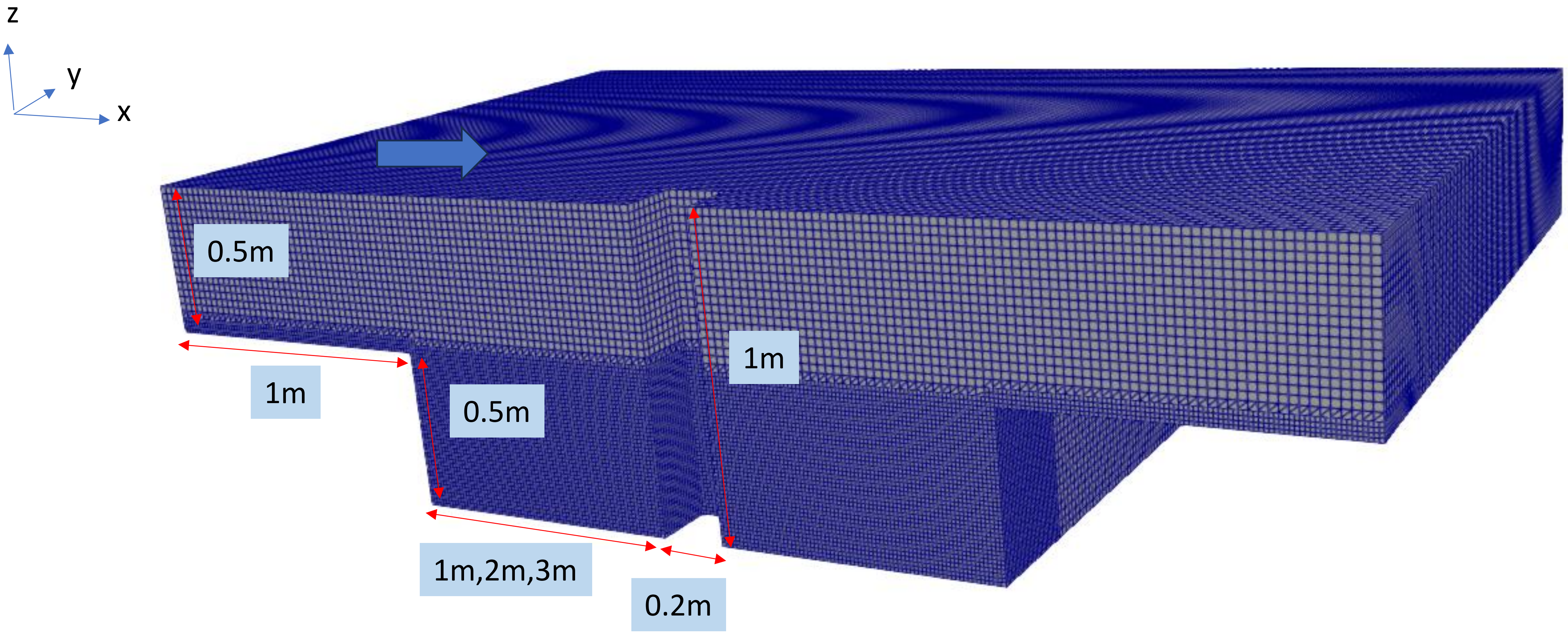

Total Cells = 596844

Domain and Boundary Conditions

Patch - zeroGradient

Inlet

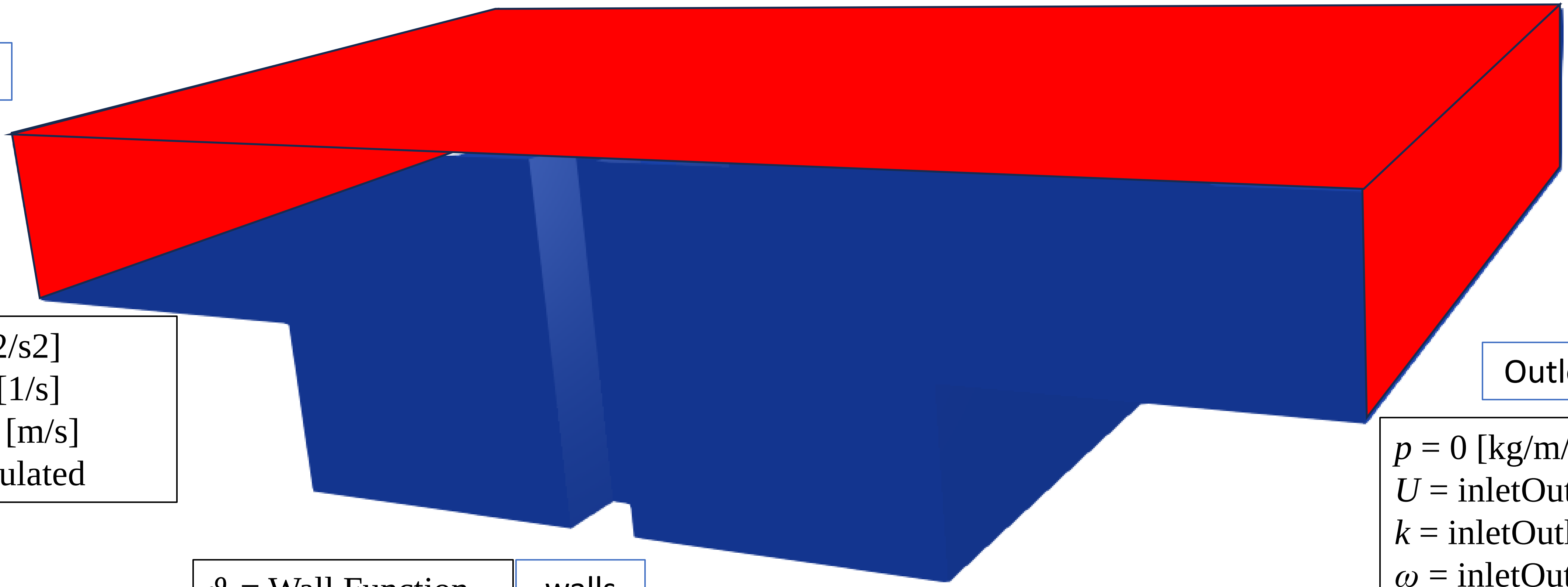

k = 1 [m2/s2]
ω = 125 [1/s]
U = 0.25 [m/s]
ϑ_t= calculated

Outlet

p = 0 [kg/m/s2]
U = inletOutlet
k = inletOutlet
ω = inletOutlet

walls

ϑ_t= Wall Function
k = Wall Function
ω = Wall Function
U = 0 [m/s]

Domain and Boundary Conditions

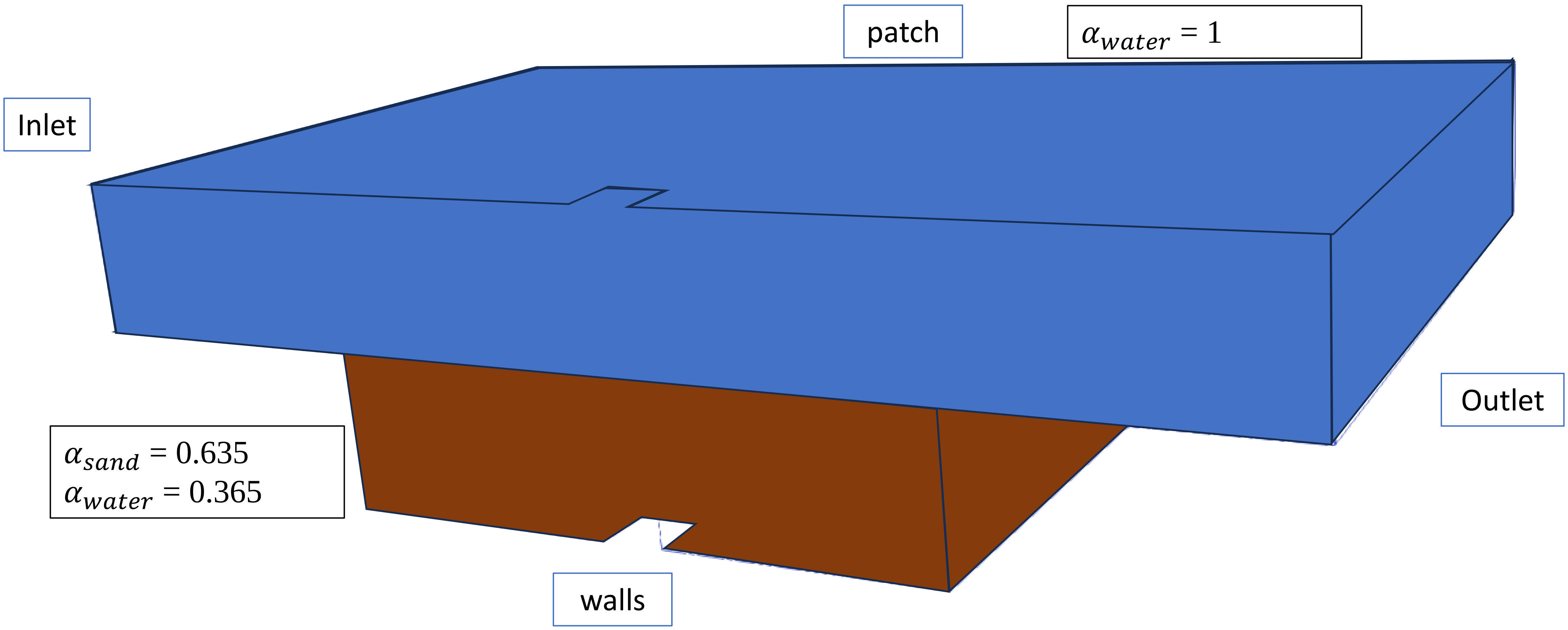

Results

Bedform comparison at 3hr (scour depth: surface elevation)

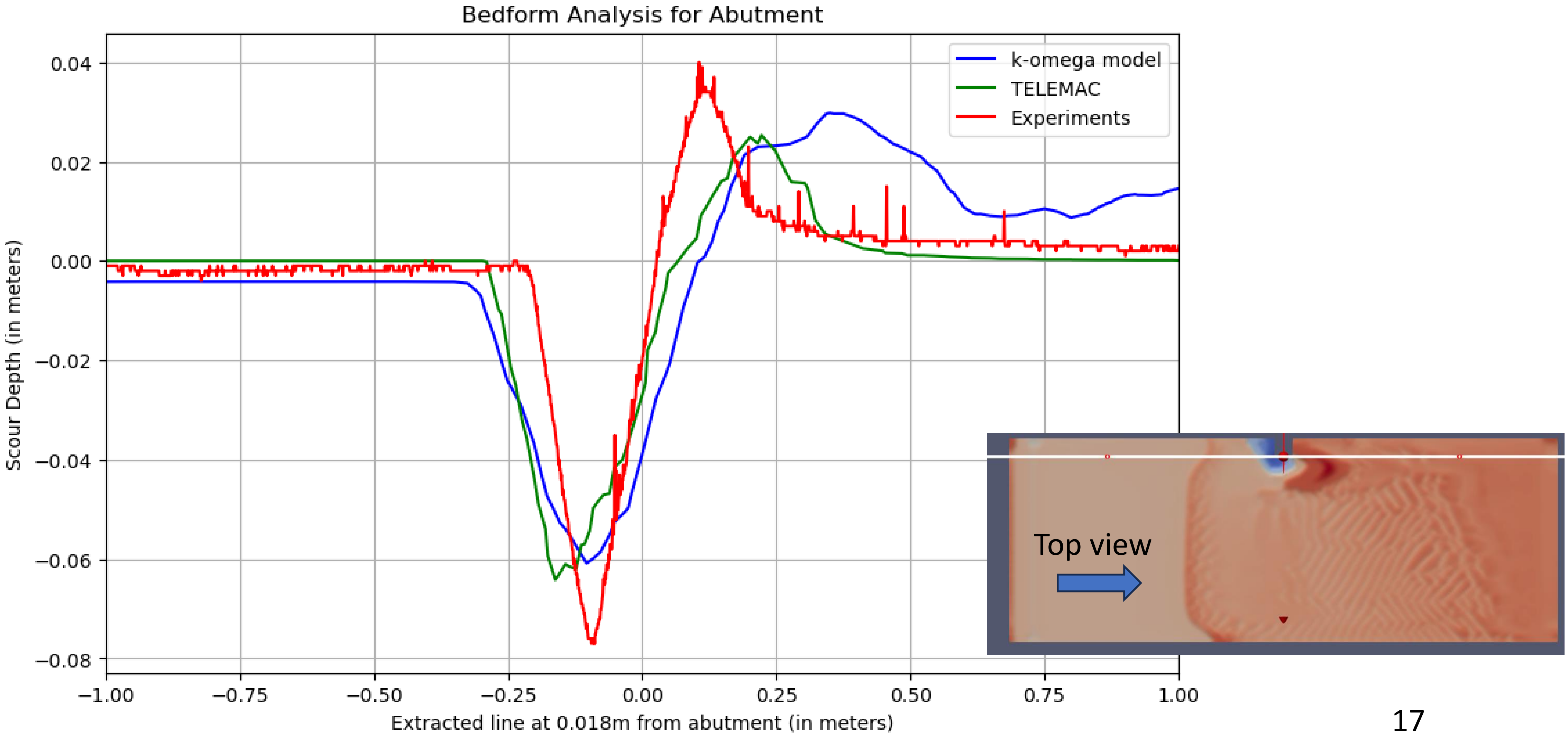

hr wallingford

Results

TKE profile at 3hr

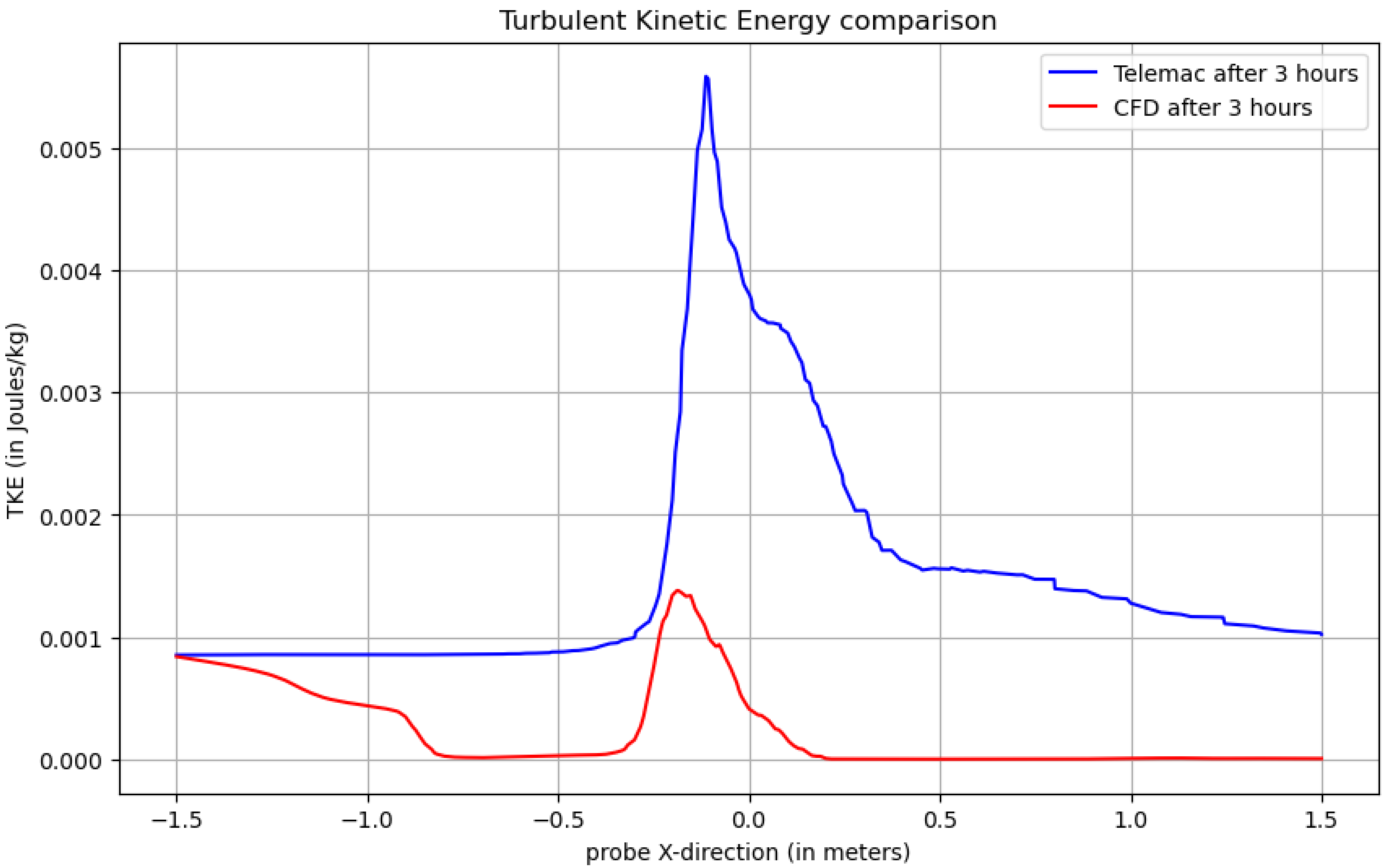

SEDIMARE

Results

Bedform evolution (Surface Elevation)

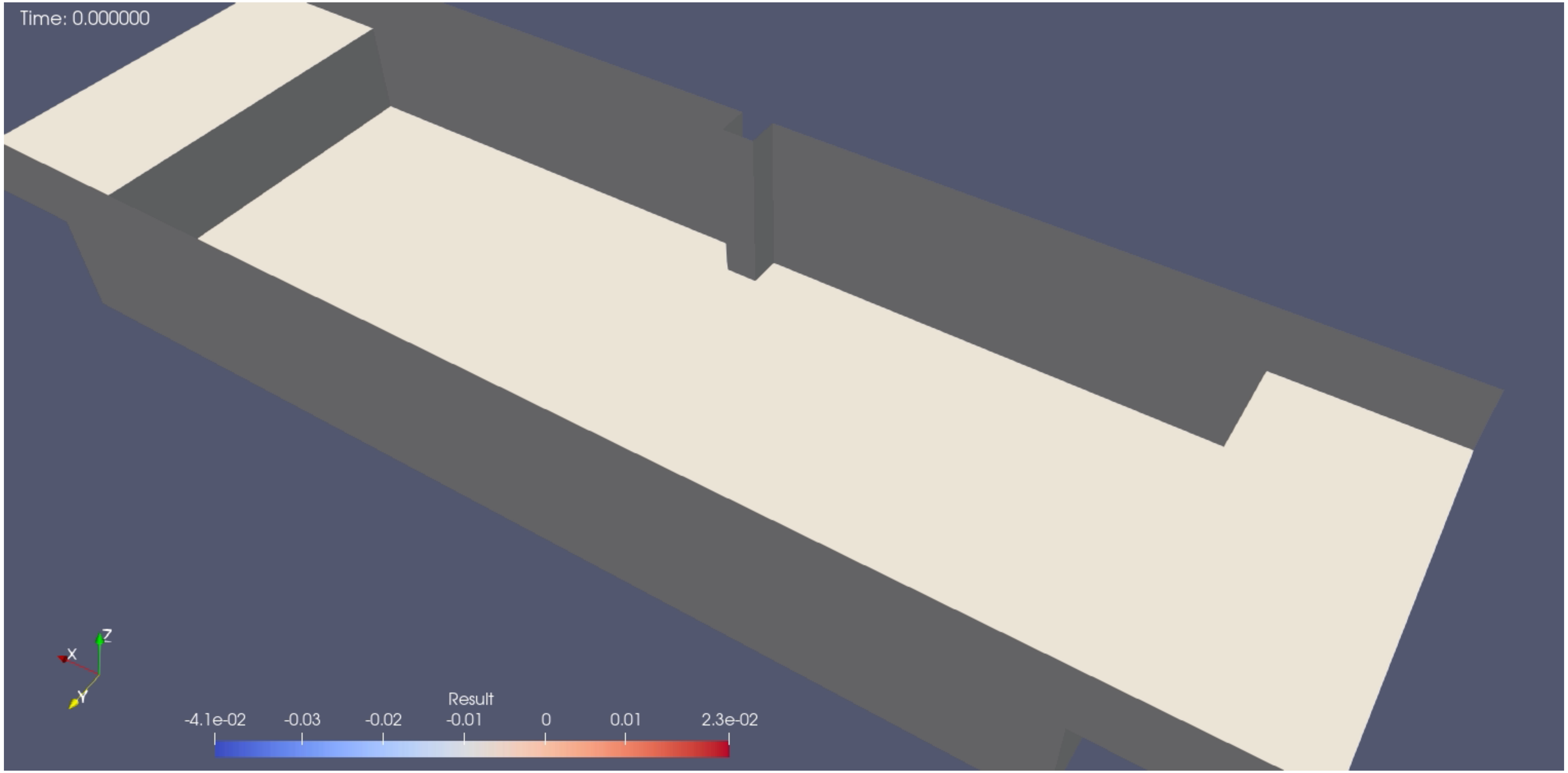

Results

Bedform evolution (Surface Elevation) after 3 hours

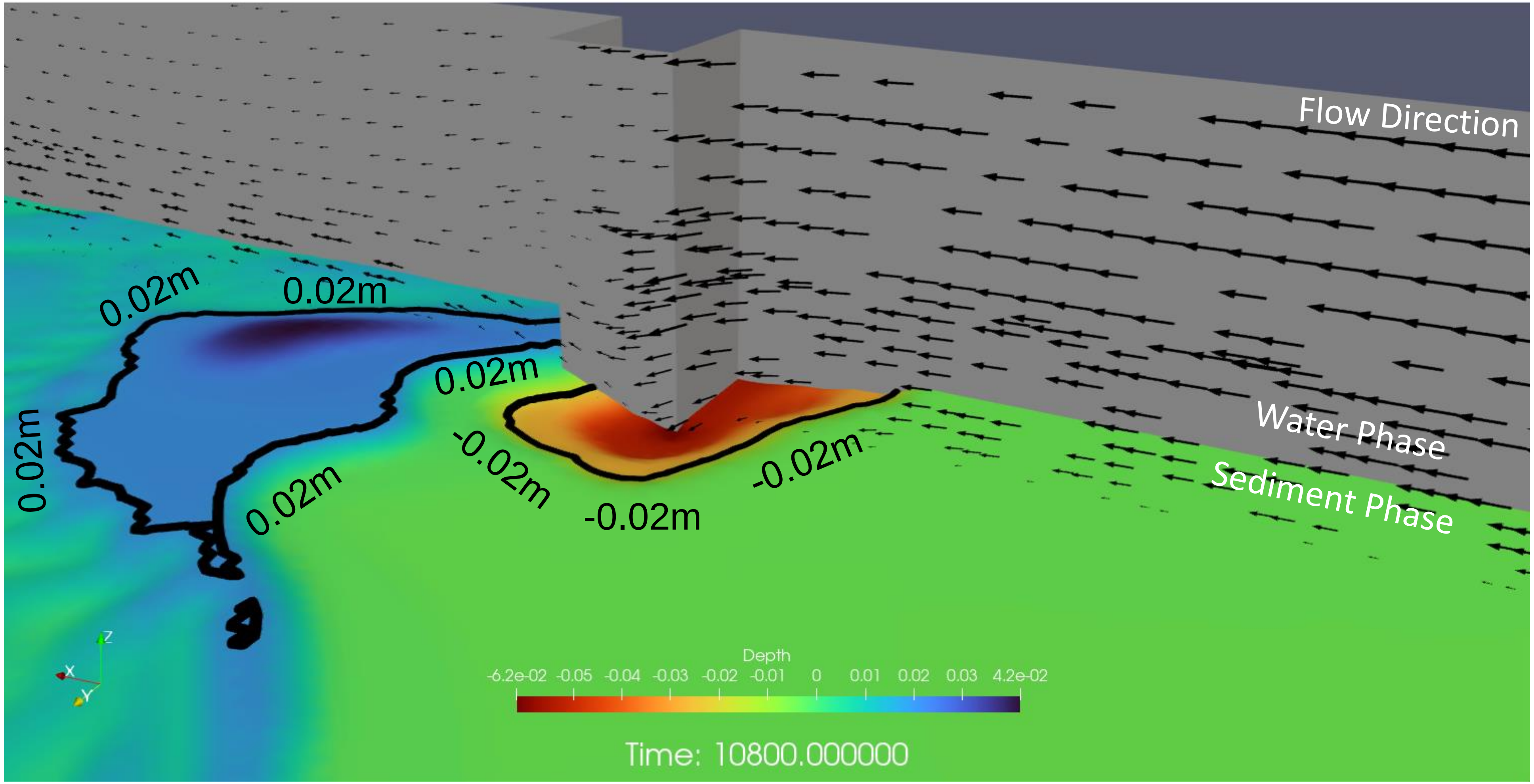

sedimentFoam: Numerical Modelling

Inputs

Reference from Experimental Setup

- Obtaining the transport properties of sand and water phase used in Flumes experiment.
- Use the geometrical dimensions of the monopile.
- Velocity profile available at the location of monopile

Solver

GFM-tetMotion RANS FOAM-extend

- Creating 3D domain
- Using sedimentFoam :
  - Sediment Transport properties
  - VOF Method
  - Finite Area Method
  - Mesh motion

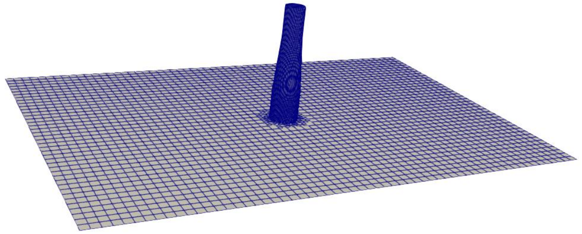

Outputs

Scour Depth

- Estimation of surface elevation of sand to predict bed formation.
- Comparison with experiments

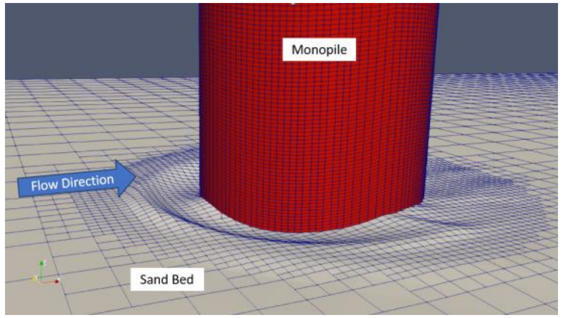

hr wallingford

FVM to FAM

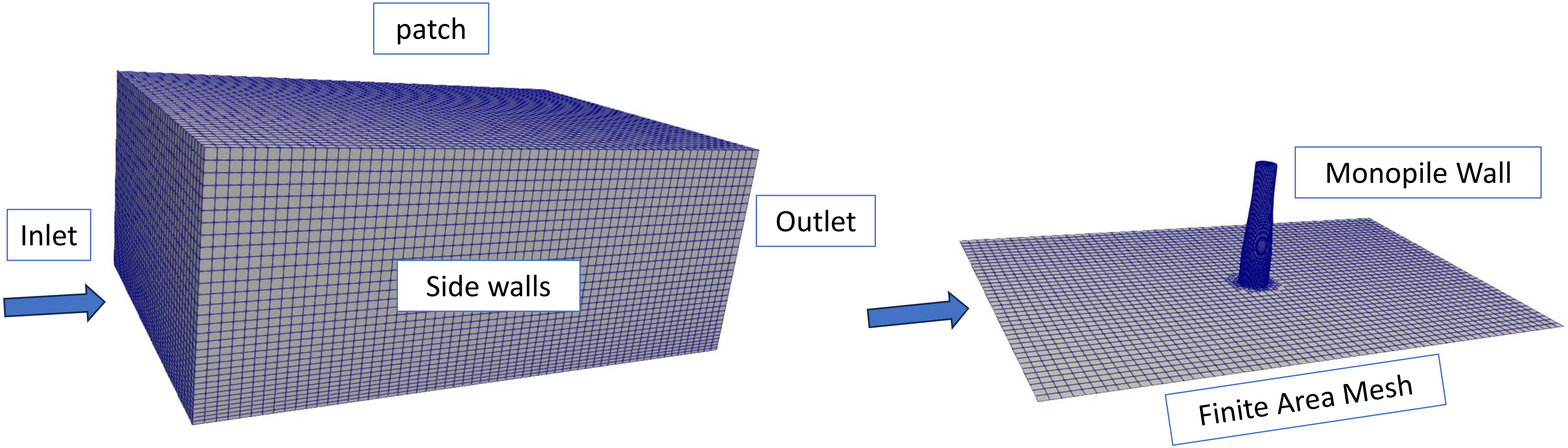

Solve Fluid Flow Equations → Calculate suspended sediment transport → Calculate surface bed-load transport flux and solve Exner Equation → Adjust mesh motion using tetMotionSolver

Preliminary Results

(80 seconds)

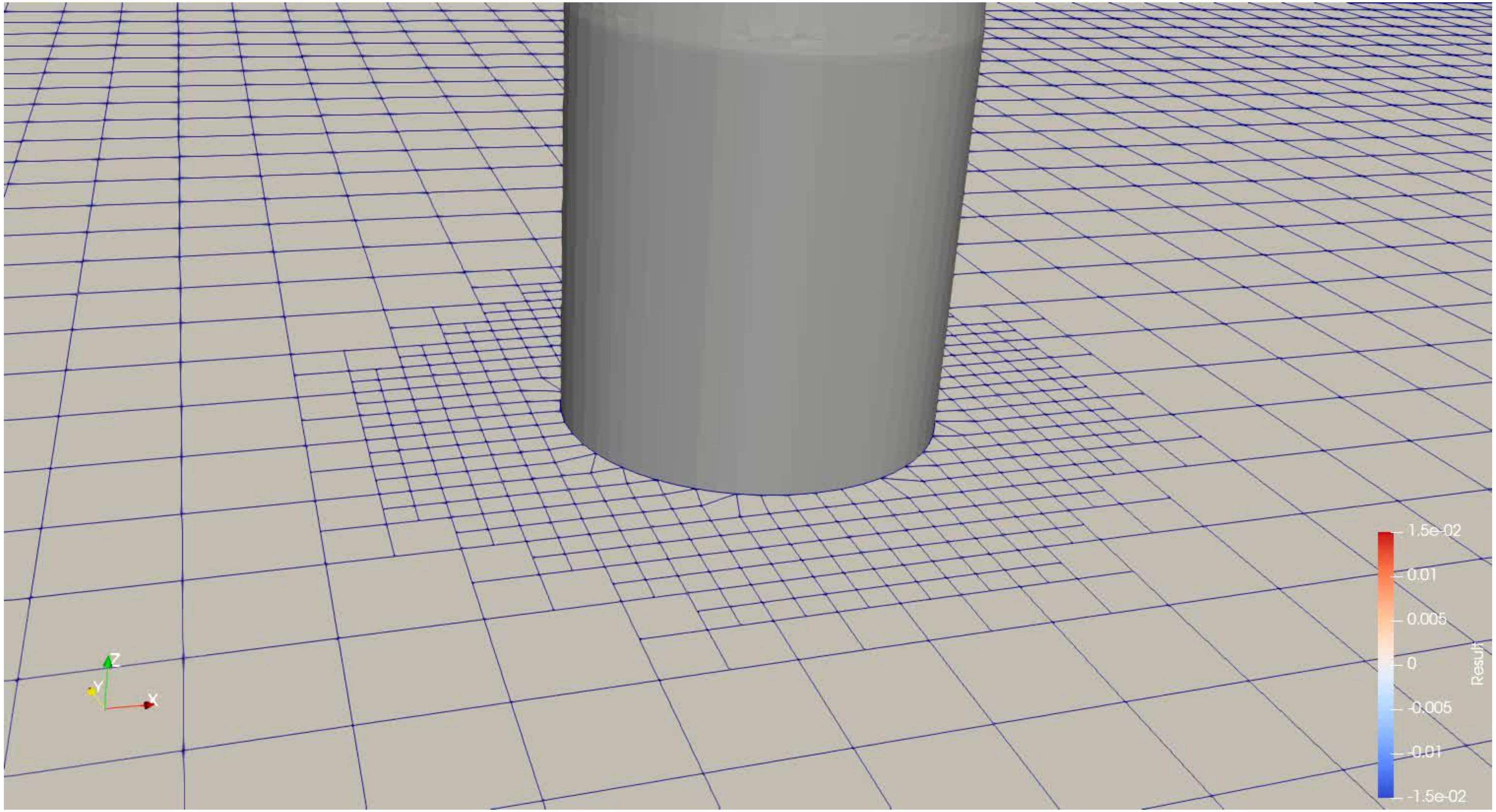

SEDIMARE

sedFoam vs sedimentFoam

(80 seconds)

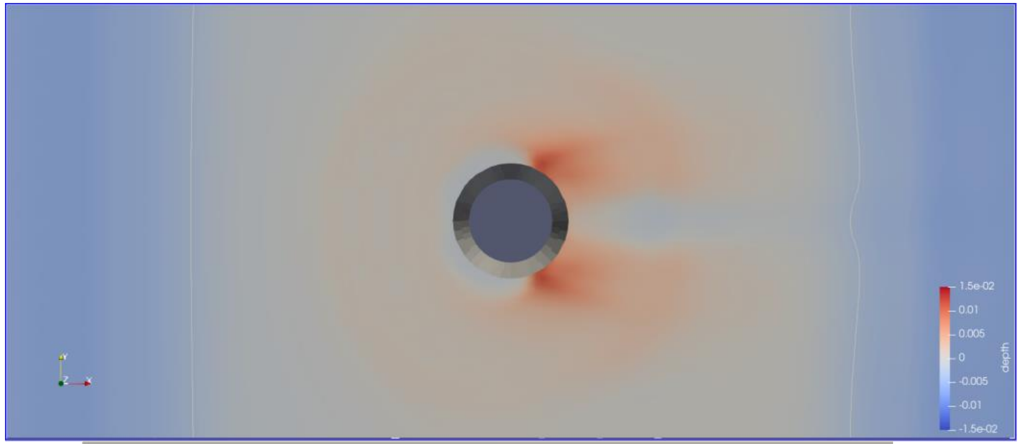

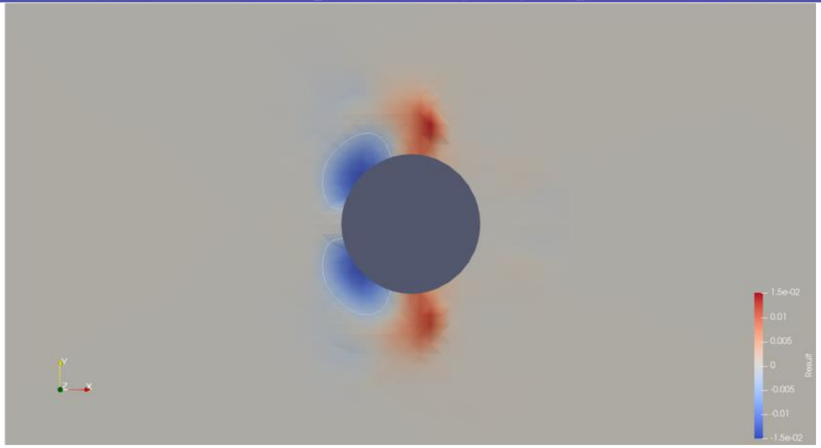

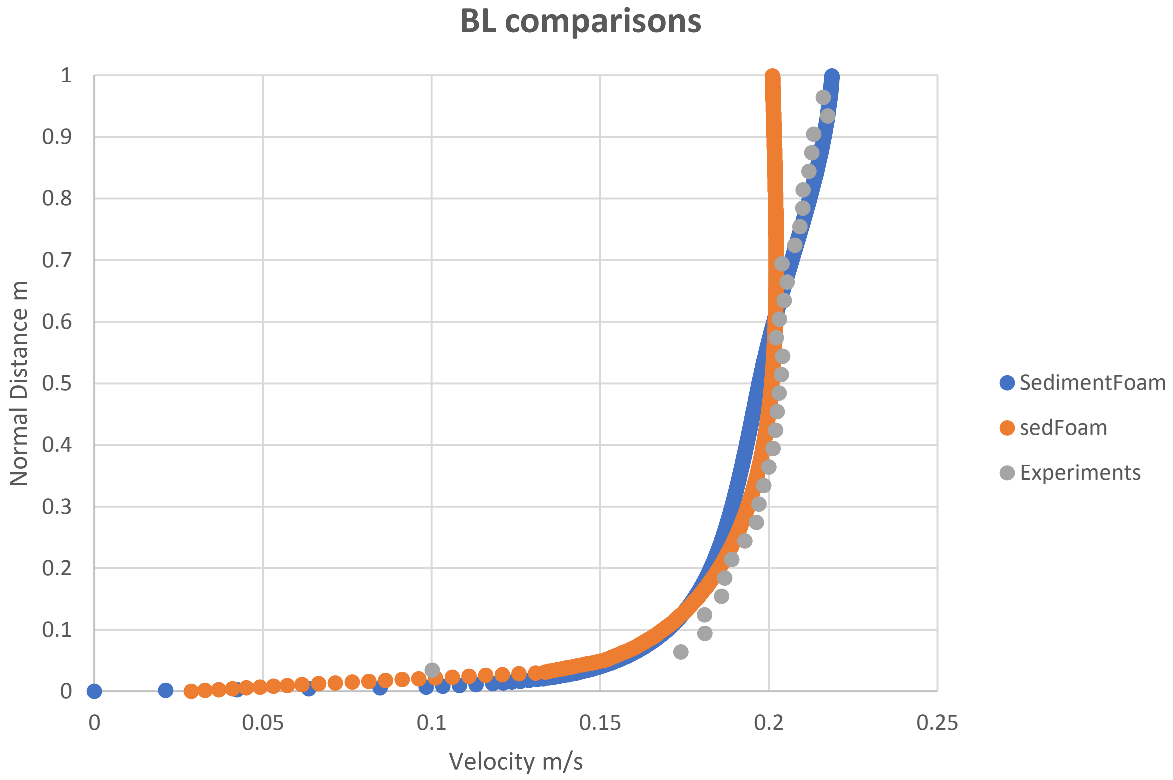

At 600 seconds

SEDIMARE

hr wallingford

Thank You

SEDIMARE DC MEETING

07.11.2024-08.11.2024

Delft, the Netherlands

Nearshore Wave Processes by Remote Sensing

Name	Muhammed Said Parlak
Supervisors	Maurizio Brocchini Nicholas Dodd Matteo Postacchini

Introduction

→ Nearshore dynamics are dominated with nonlinear mechanisms due to multiple interactions.

→ Wave propagation is one of the crucial driver of these interactions and nearshore sea state.

→ Observation of sea state is essential for human activities and marine environment.

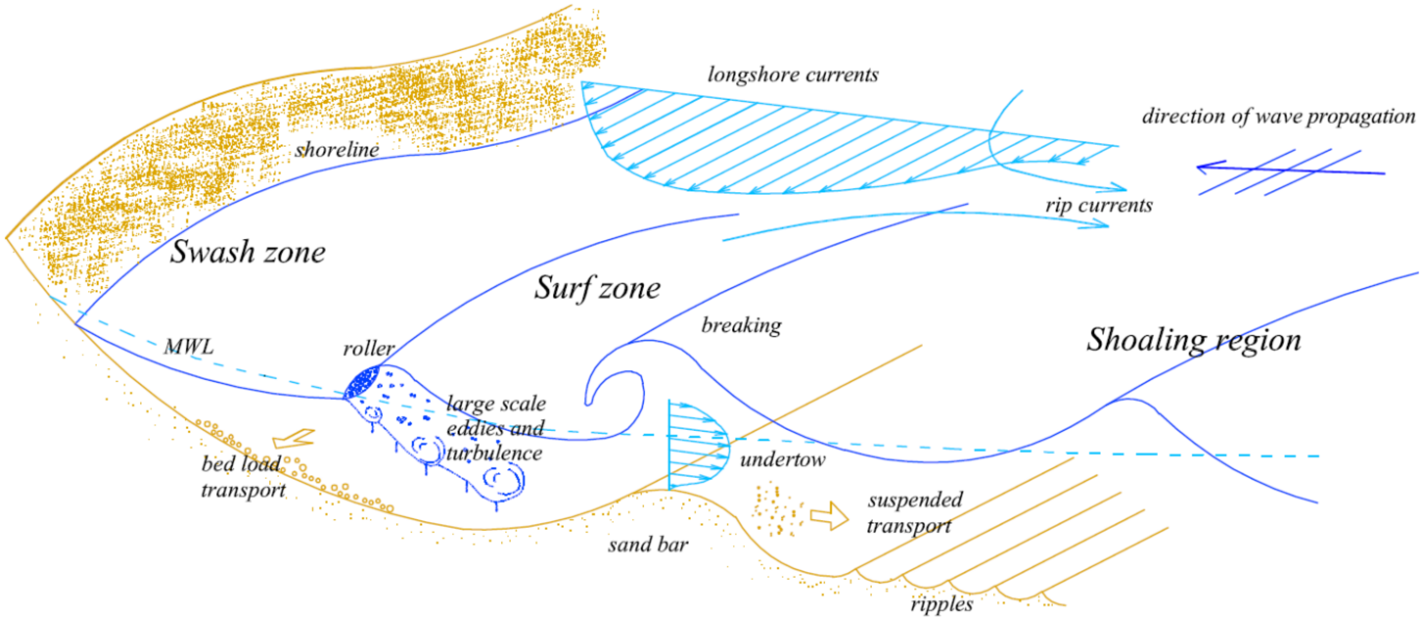

[Viviano et al., 2010]

Introduction

→ Nearshore measurement with in-situ tools is a tough task due to complex processes.

→ They have many components and need regular maintenance and calibration.

→ Remote sensing tools judicious alternatives since they have larger coverage area, and they are easier to maintain.

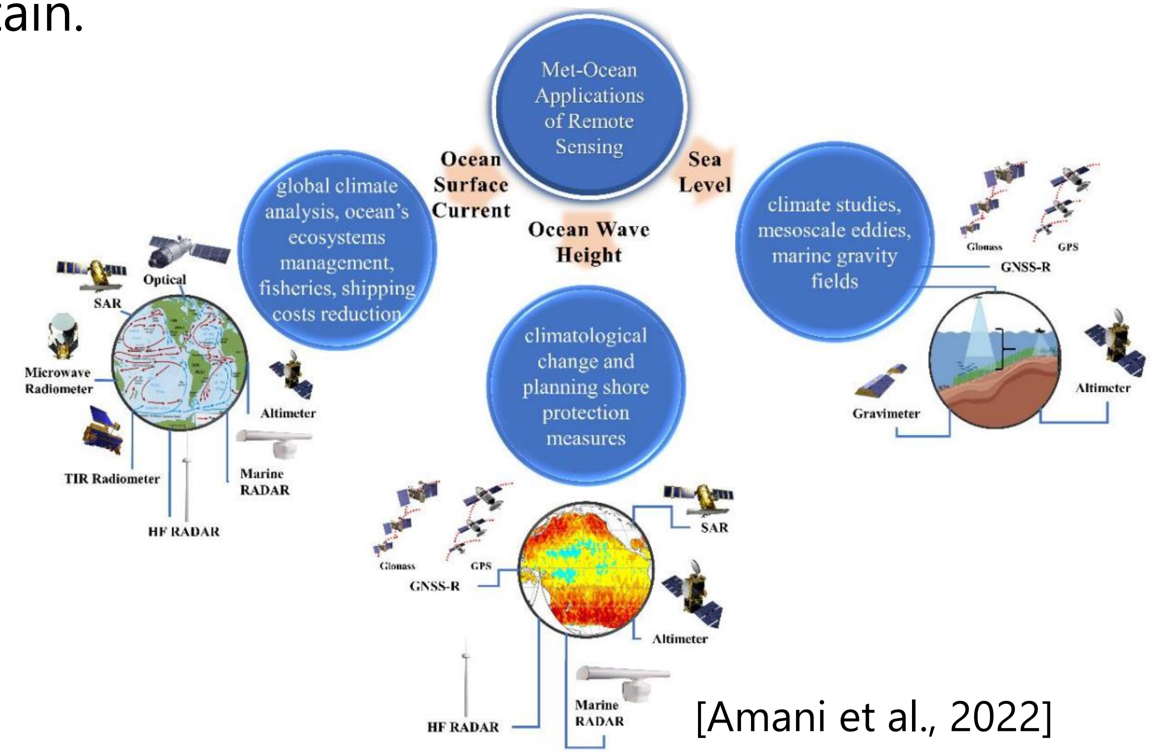

[Amani et al., 2022]

Study Site

→ Senigallia, Italy
- Senigallia Harbour, Misa River Estuary
- Strong interactions between sea and river

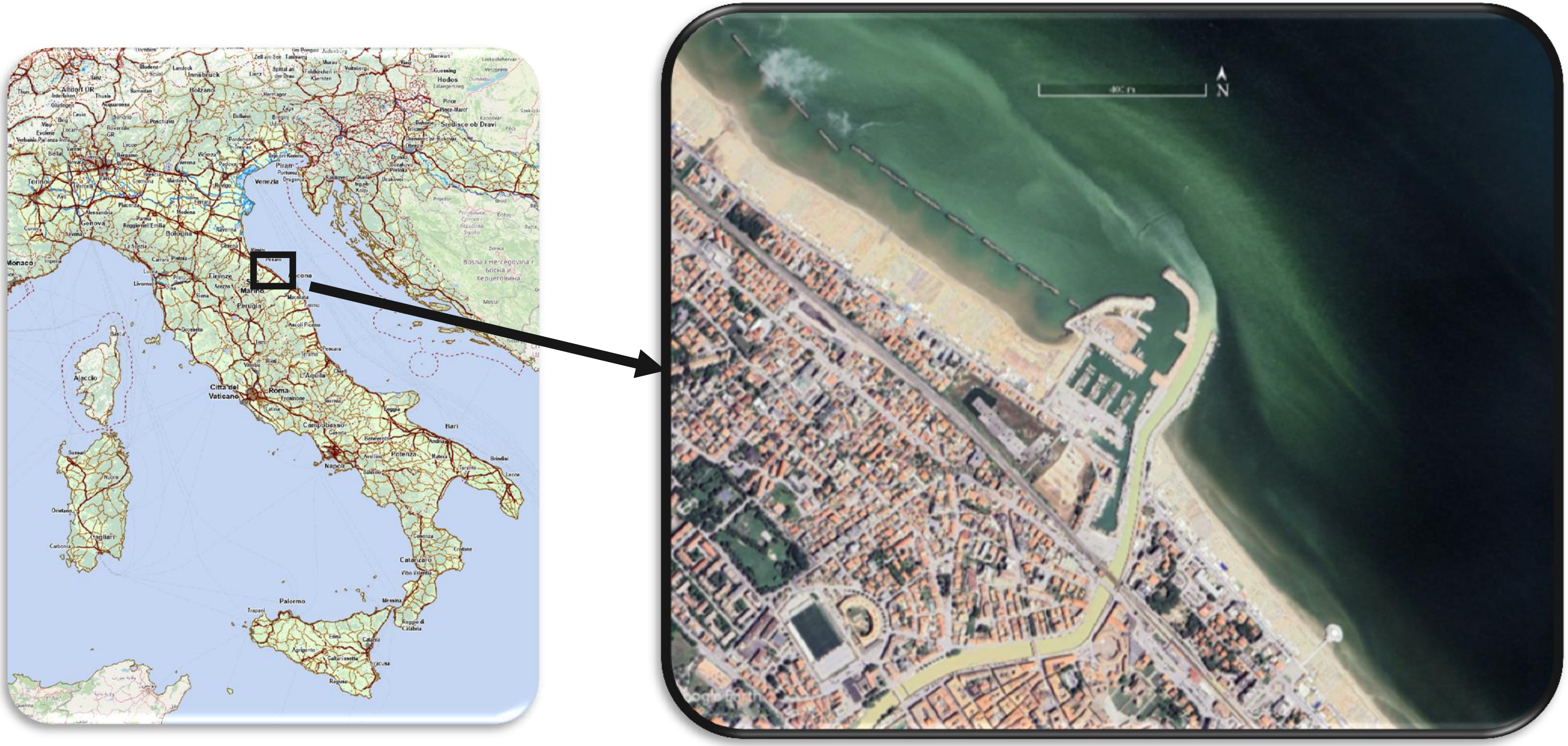

[Brocchini et al., 2017]

Study Site

→ Senigallia, Italy
- SGS: 5 cameras, 2 Hz sampling, 10 min-long
- XBR: X-Band RADAR, 0.5 Hz sampling, 63 scans

Locations of XBR and SGS

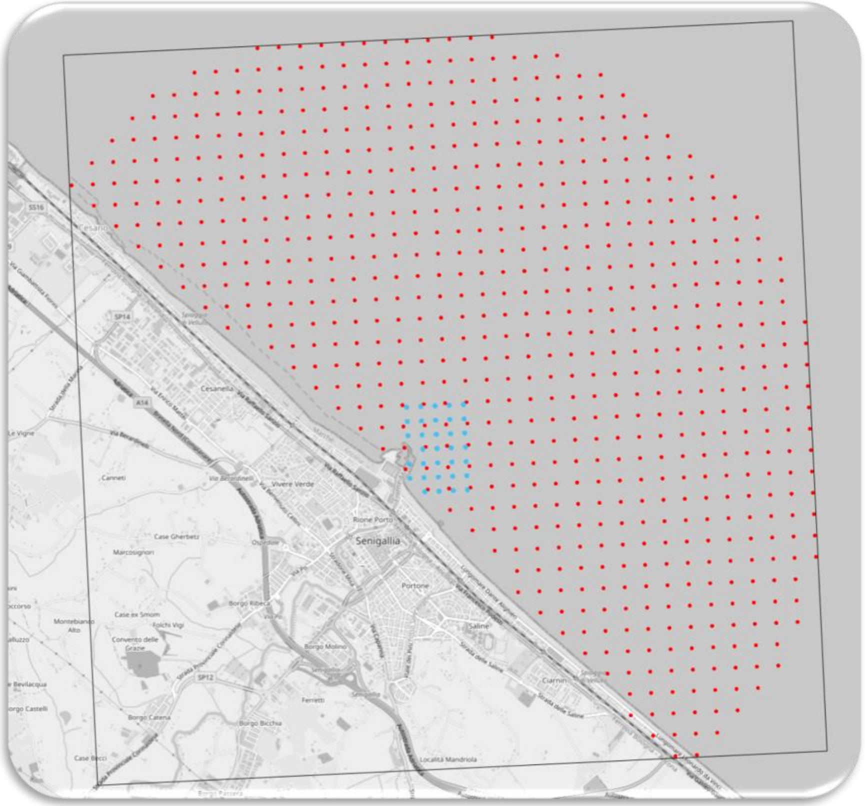

Coverage area

Methodology

→ Processing data obtained from remote sensing tools (cBathy).
- cBathy algorithm flowchart

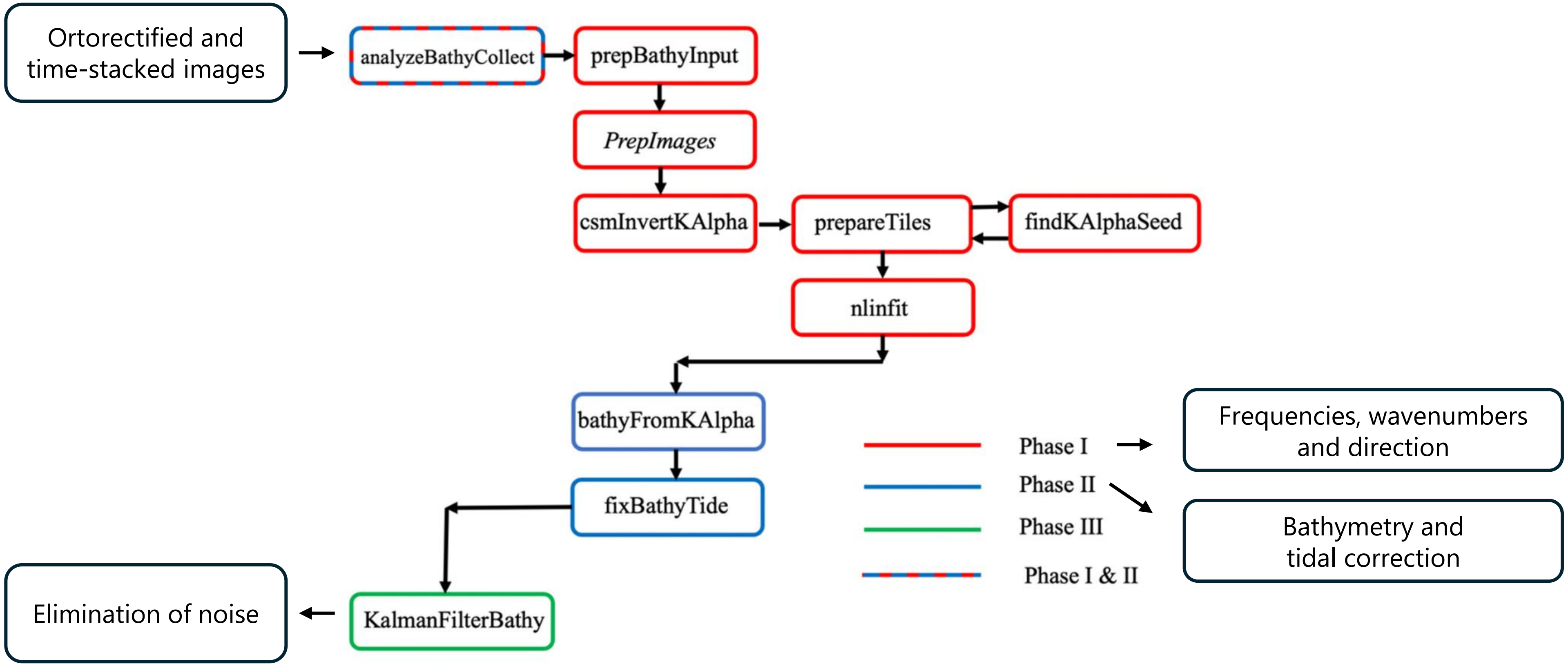

[Holman et al., 2013]

Methodology

→ Processing data obtained from remote sensing tools (cBathy).

- cBathy algorithm flowchart

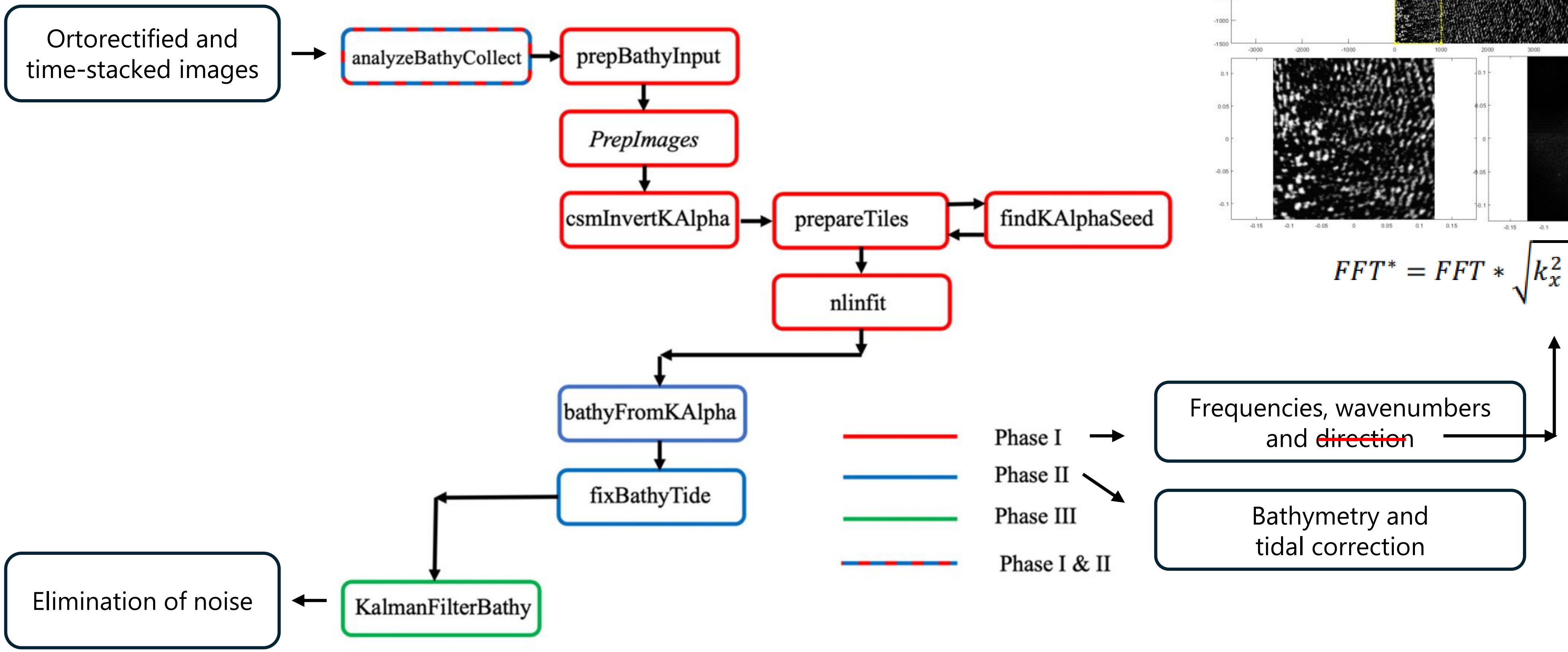

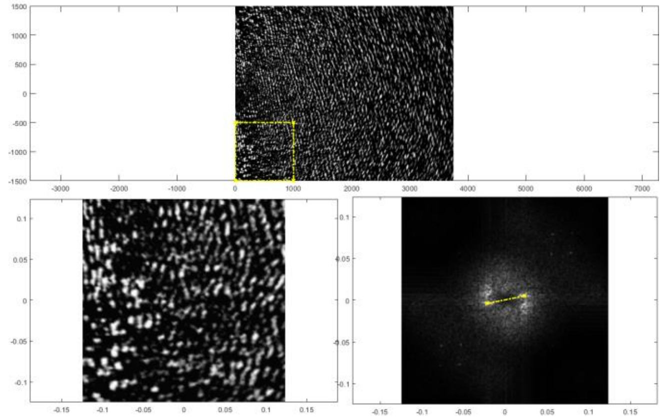

$$FFT^* = FFT * \sqrt{k_x^2 + k_y^2}$$

[Holman et al., 2013]

Methodology

→ Processing data obtained from remote sensing tools (cBathy).

- Assumed that the most coherent frequency is close to the peak frequency, f_p.
- Hence:

$$C_p = \frac{\omega_p}{k} = \frac{2\pi f_p}{k} \qquad \lambda_p = \frac{2\pi}{k}$$

- C_p is the peak celerity, ω_p is the peak angular frequency, k is the wavenumber, and λ_p is the peak wavelength.

Methodology

→ Processing data obtained from remote sensing tools (cBathy).

- Significant wave height, H_s, is approximated with an emprical approach based on water depth, d, and C_p.

$$H_s = \frac{C_p^2}{g\ A^*\ 1.8} \rightarrow A^* = \begin{cases} d^{\frac{1}{2}}, & d < d_{th} \\ d^{\frac{1}{3}} - d_{th}^{\frac{1}{3}} + d_{th}^{\frac{1}{2}}, & d \geq d_{th} \end{cases}$$

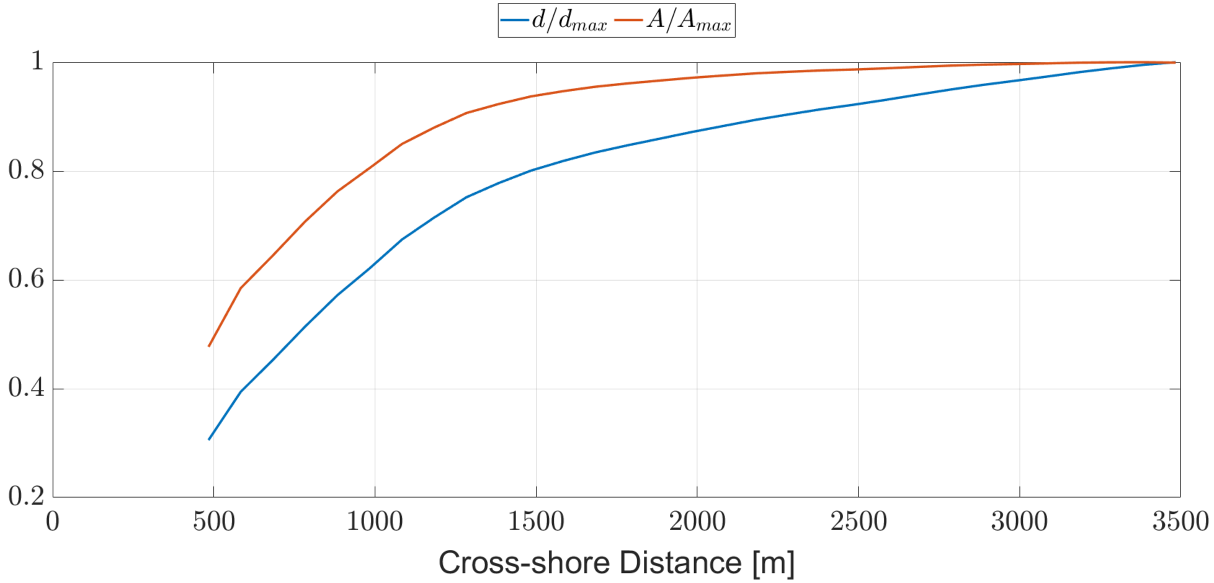

Methodology

→ Processing data obtained from remote sensing tools (cBathy).

- Significant wave height, H_s, is approximated with an emprical approach based on water depth, d, and C_p.

$$H_s = \frac{C_p^2}{g\ A^*\ 1.8} \rightarrow A^* = \begin{cases} d^{\frac{1}{2}}, & d < d_{th} \\ d^{\frac{1}{3}} - d_{th}^{\frac{1}{3}} + d_{th}^{\frac{1}{2}}, & d \geq d_{th} \end{cases}$$

- d_{th} depends on the bathymetric gradient e.g., 0,2 in this case

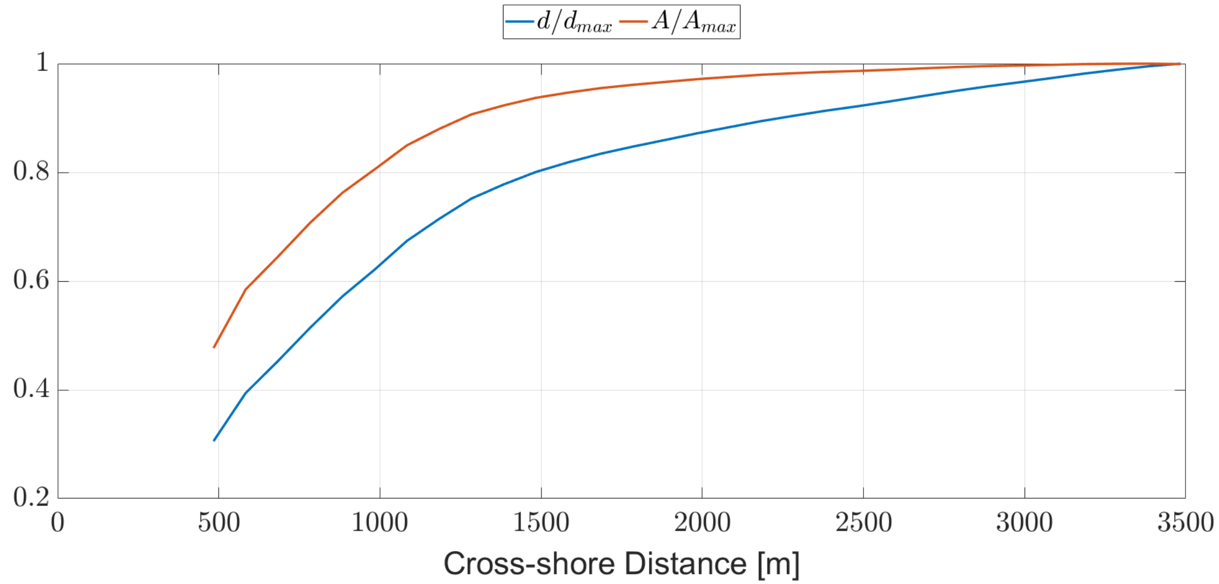

Methodology

→ Reconstruction of wave propagation (preliminary).

- The wave field is visible to XBR when the waves are relatively energetic.
- Radar return echo is maximized at the wave fronts.

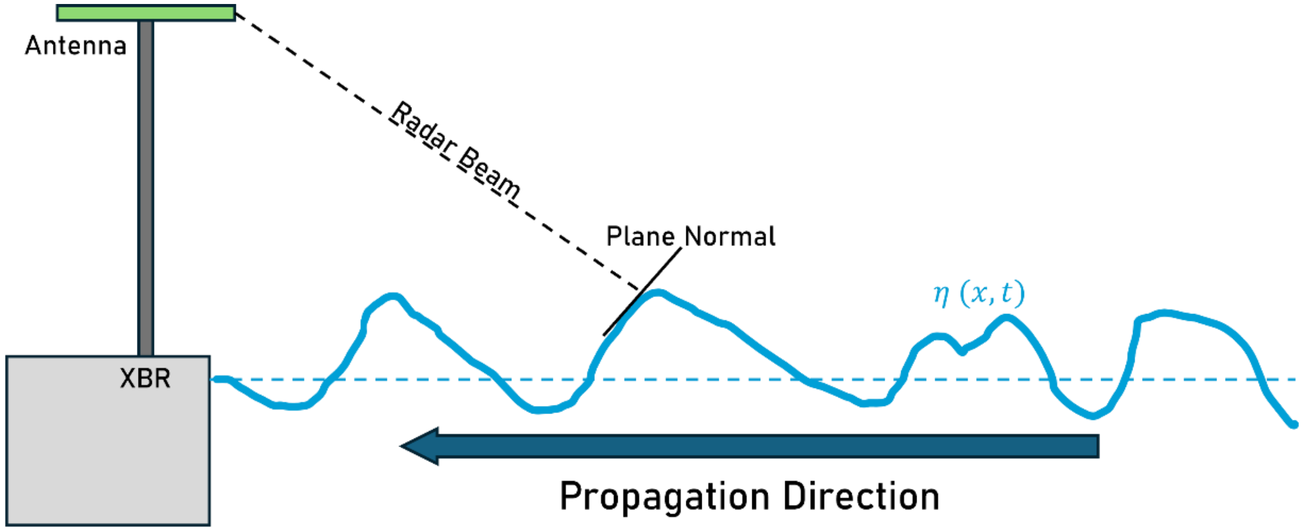

Methodology

→ Reconstruction of wave propagation (preliminary).

- Assumed that radar signals are correlated with wave slopes.

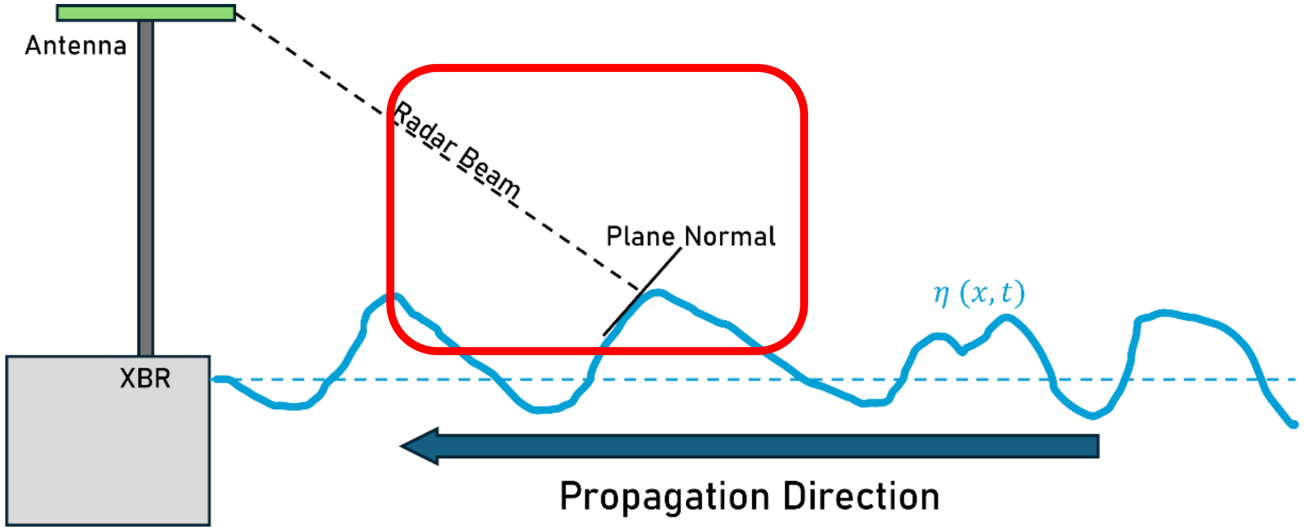

$$\sigma \propto \eta'$$

radar echo

First derivative of wave elevation

Methodology

→ Reconstruction of wave propagation (preliminary).

- Processing of radar signals:

$\hat{\sigma} = \sigma - \bar{\sigma}$ Mean extraction

$\sigma^* = \hat{\sigma} + |\min(\hat{\sigma})|$ Shifting signal above the zero axis

$\boldsymbol{P} = \max(\sigma^*)_{\mathrm{lc}}$ Local maxima △

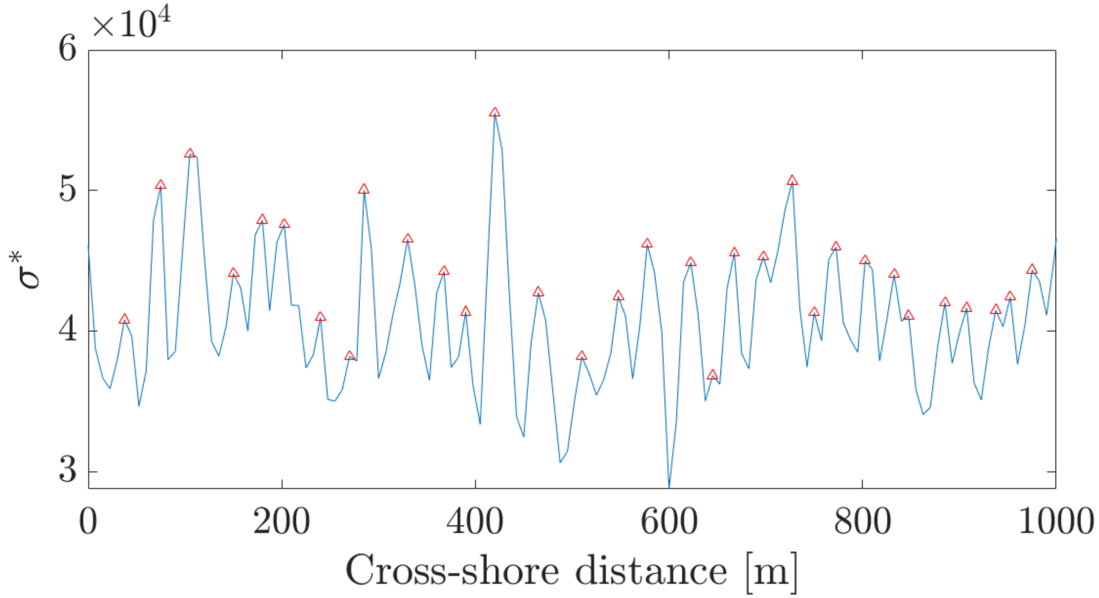

Methodology

→ Reconstruction of wave propagation (preliminary).

- Crest, trough slopes are arranged to resemble a sawtooth wave formation.
- Assumed that trough slopes are half of the average adjacent crest slopes.

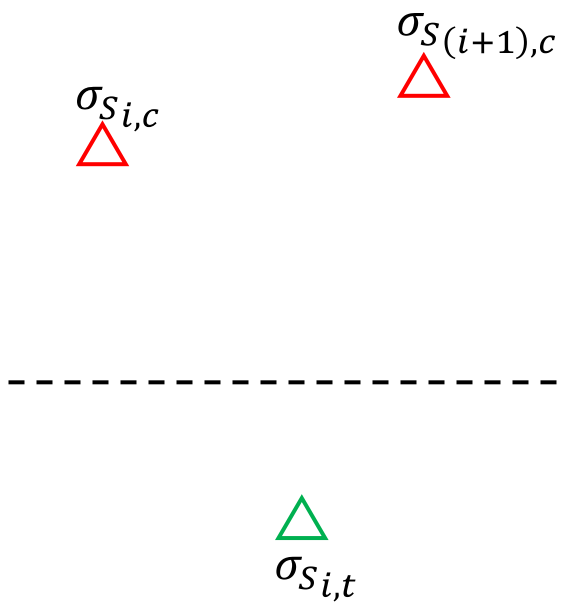

$$\sigma_{S\,i,t} = 0.5\,\frac{\left(\sigma_{S\,i,c} + \sigma_{S\,(i+1),c}\right)}{2}$$

Methodology

→ Reconstruction of wave propagation (preliminary).

- Crest, trough slopes are arranged to resemble a sawtooth wave formation.
- Assumed that trough slopes are half of the average adjacent crest slopes.
- The x location is determined to ensure zero-mean signal.

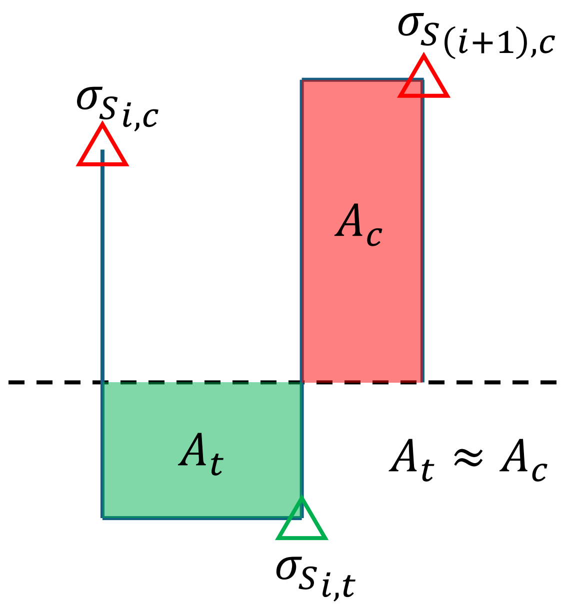

$$\sigma_{S\,i,t} = 0.5\,\frac{\left(\sigma_{S\,i,c} + \sigma_{S\,(i+1),c}\right)}{2}$$

Methodology

→ Reconstruction of wave propagation (preliminary).

- Crest, trough slopes are arranged to resemble a sawtooth wave formation.
- Assumed that trough slopes are half of the average adjacent crest slopes.
- The x location is determined to ensure zero-mean signal.

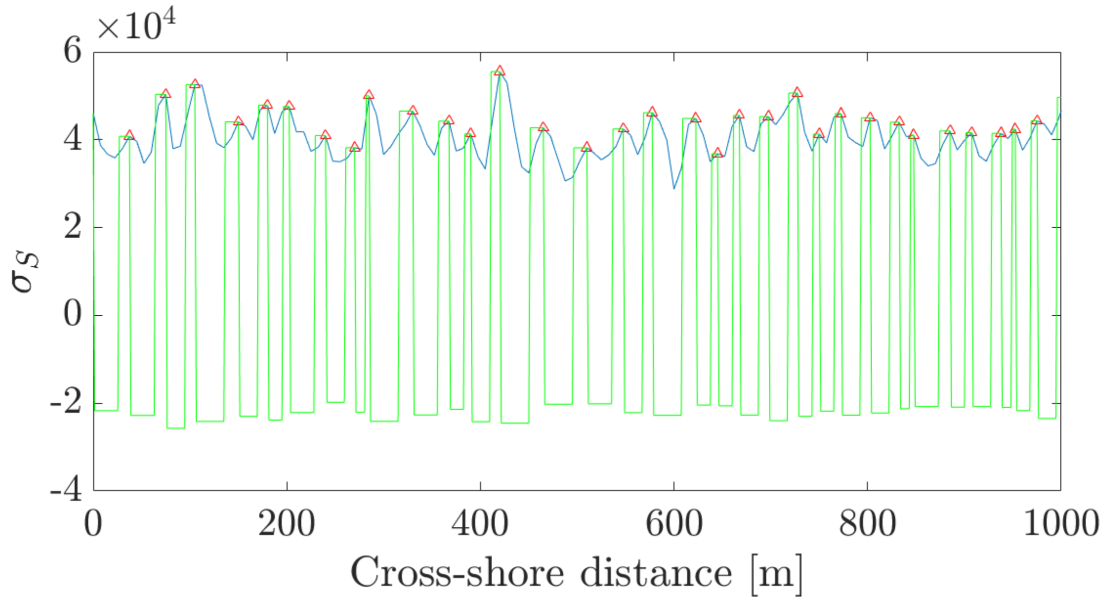

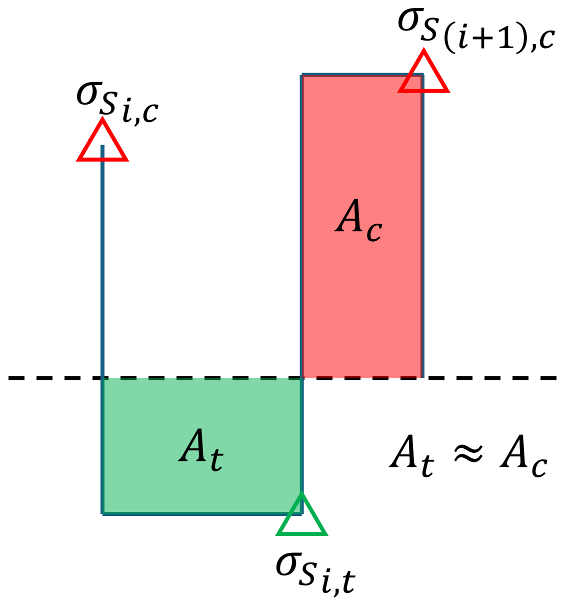

$$\sigma_{S\,i,t} = 0.5\,\frac{\left(\sigma_{S\,i,c} + \sigma_{S(i+1),c}\right)}{2}$$

Methodology

→ Reconstruction of wave propagation (preliminary).

- Crest, trough slopes are arranged to resemble a sawtooth wave formation.
- Assumed that trough slopes are half of the average adjacent crest slopes.
- The x location is determined to ensure zero-mean signal.
- Signal is integrated in spatial domain.

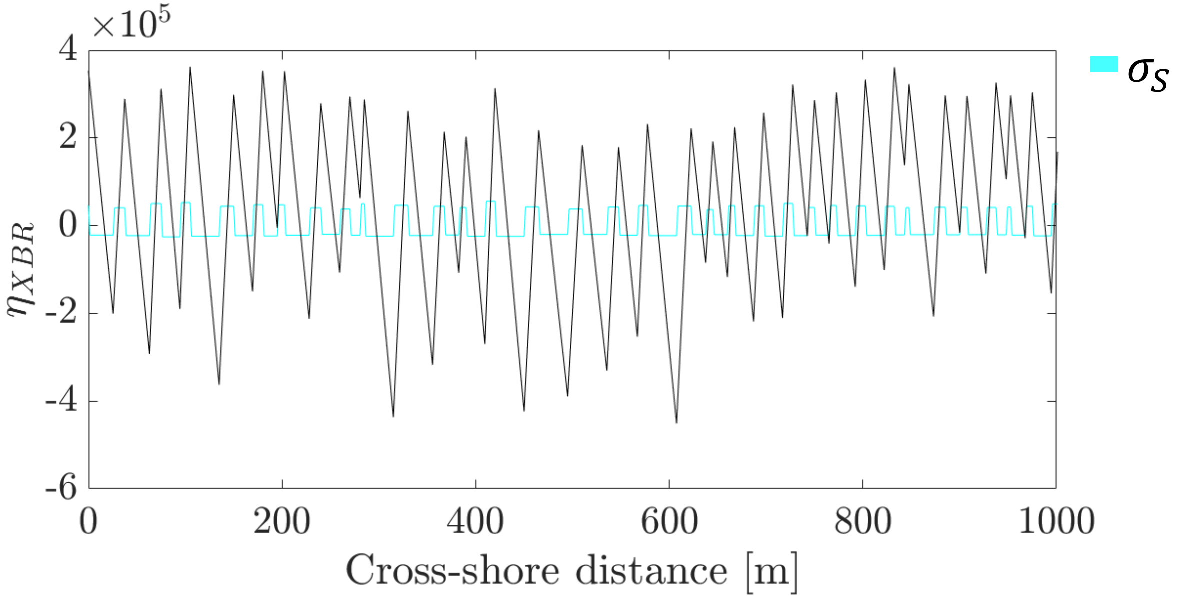

Methodology

→ Model Chain (SWAN).

- Spatial domain is determined by considering the available buoy locations.

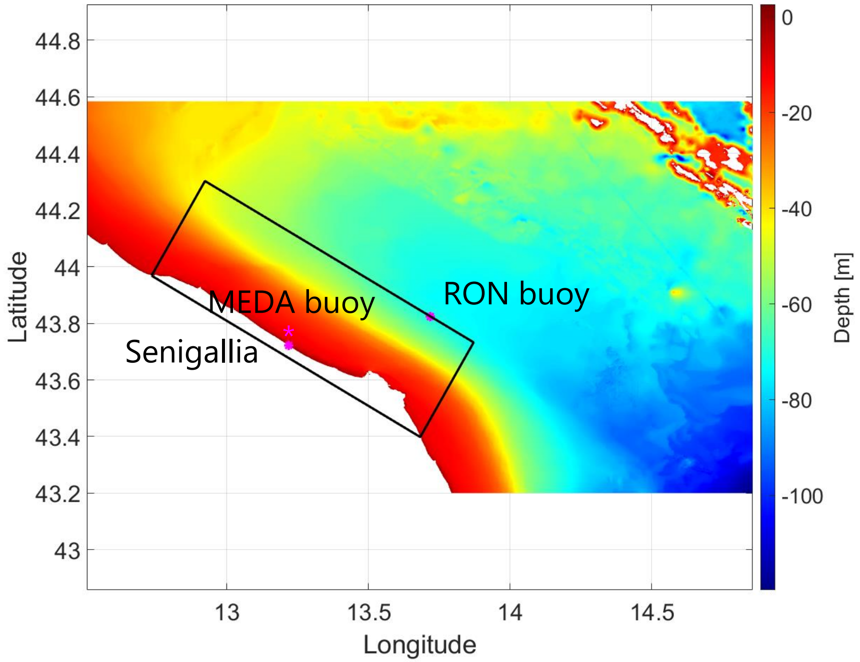

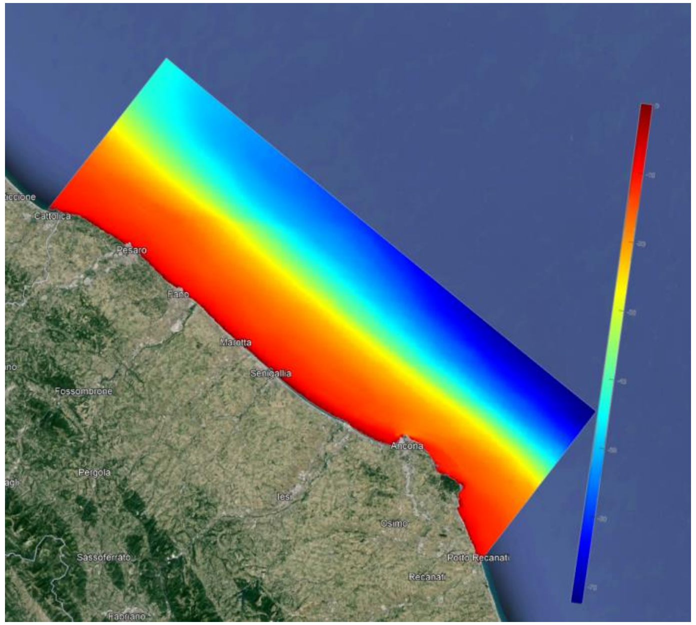

Methodology

→ Model Chain (SWAN).

- Spatial domain is determined by considering the available buoy locations.
- 3 open boundaries forced with wave characteristics obtained from RON.
- The grid is forced with winds from COPERNICUS database

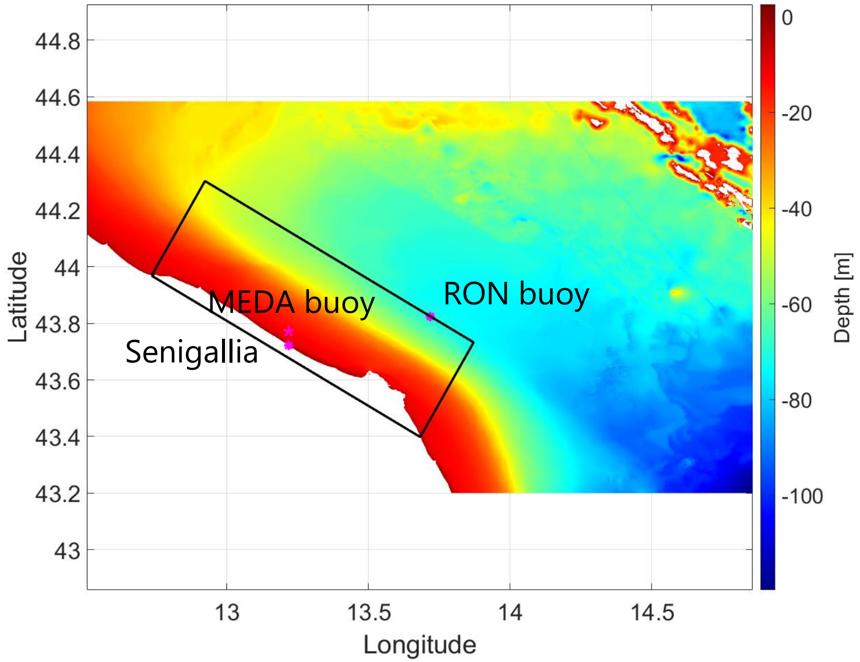

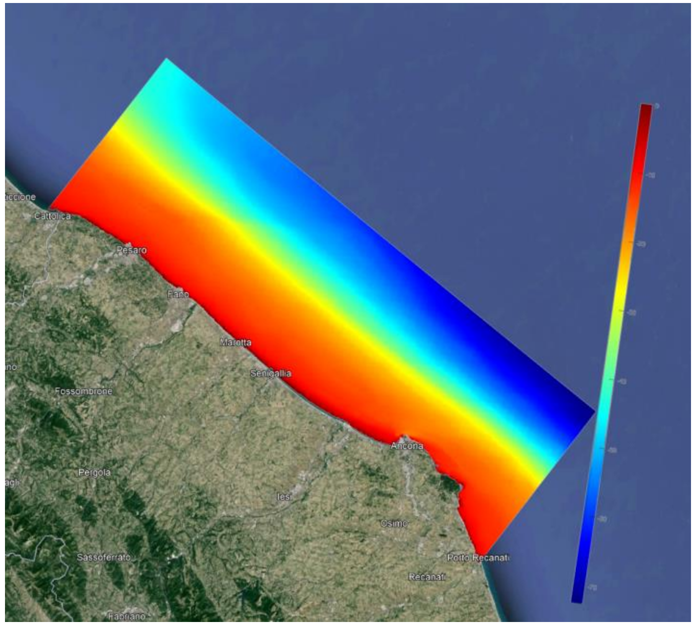

Methodology

→ Model Chain (FUNWAVE).

- Spatial domain is constructed around the harbour.

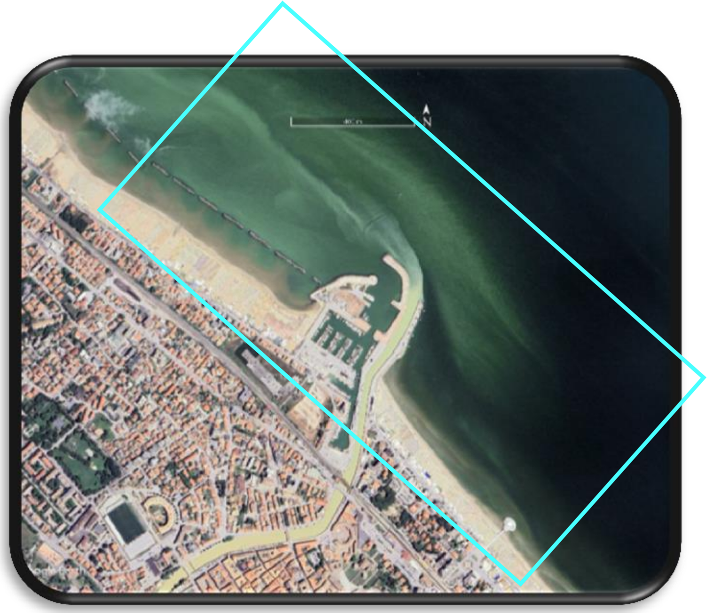

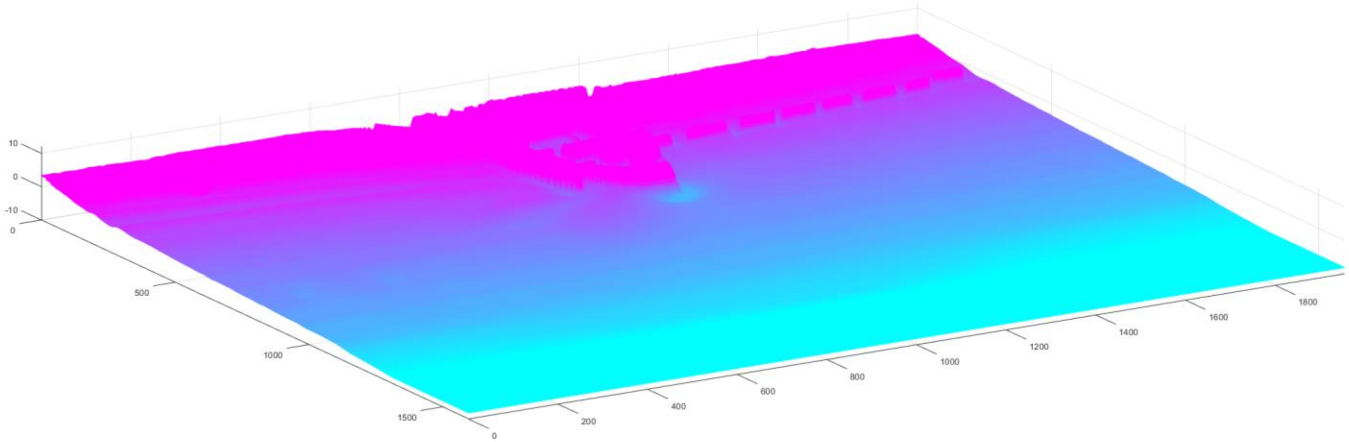

Methodology

→ Model Chain (FUNWAVE).

- Spatial domain is constructed around the harbour.
- WAVEMAKER input is obtained from SWAN results

Properties of WM_IRR WAVEMAKER

Parameter	$depth\ [m]$	$f_P\ [Hz]$	$H_{m0}\ [m]$	$\theta_P\ [deg]$	γ_{TMA}	f_{min} - f_{max}
Value	8.17	0.1337	1.27	-12.57	1.5	0.04 – 1.0

dx=dy=1 m
Grid Size= 1599x1957

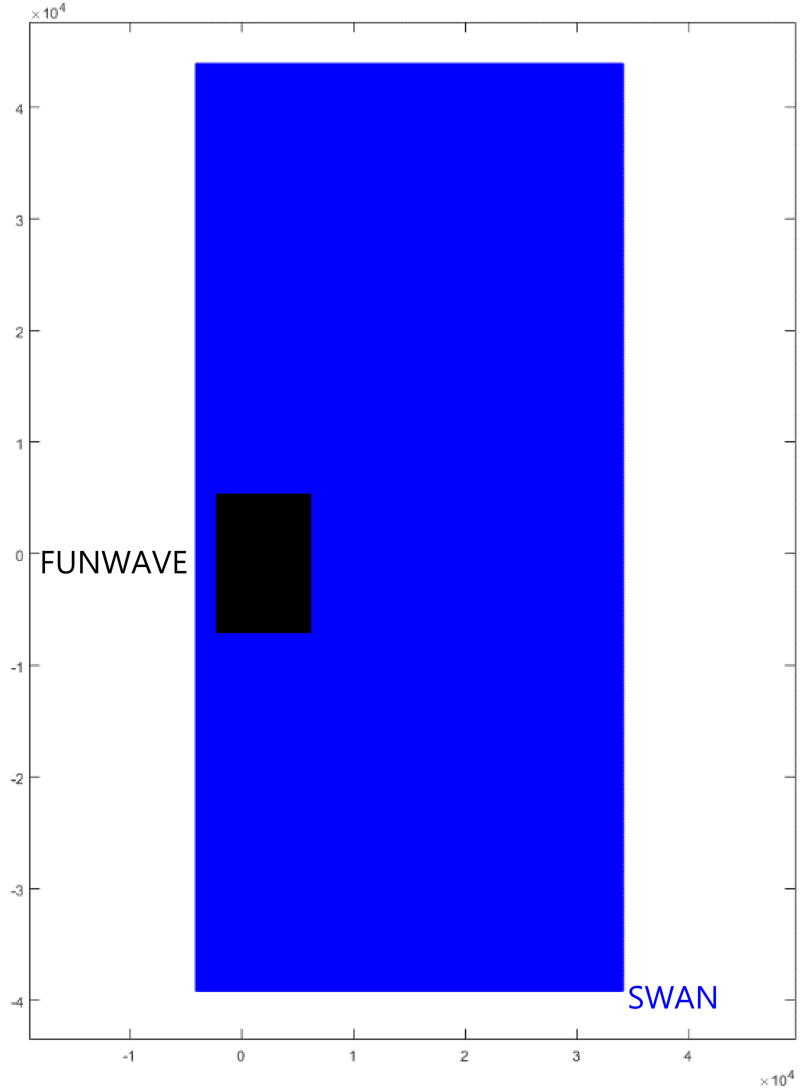

Preliminary Results

→ XBR sea state estimation performance.
- L_P, T_P and C_P are captured well

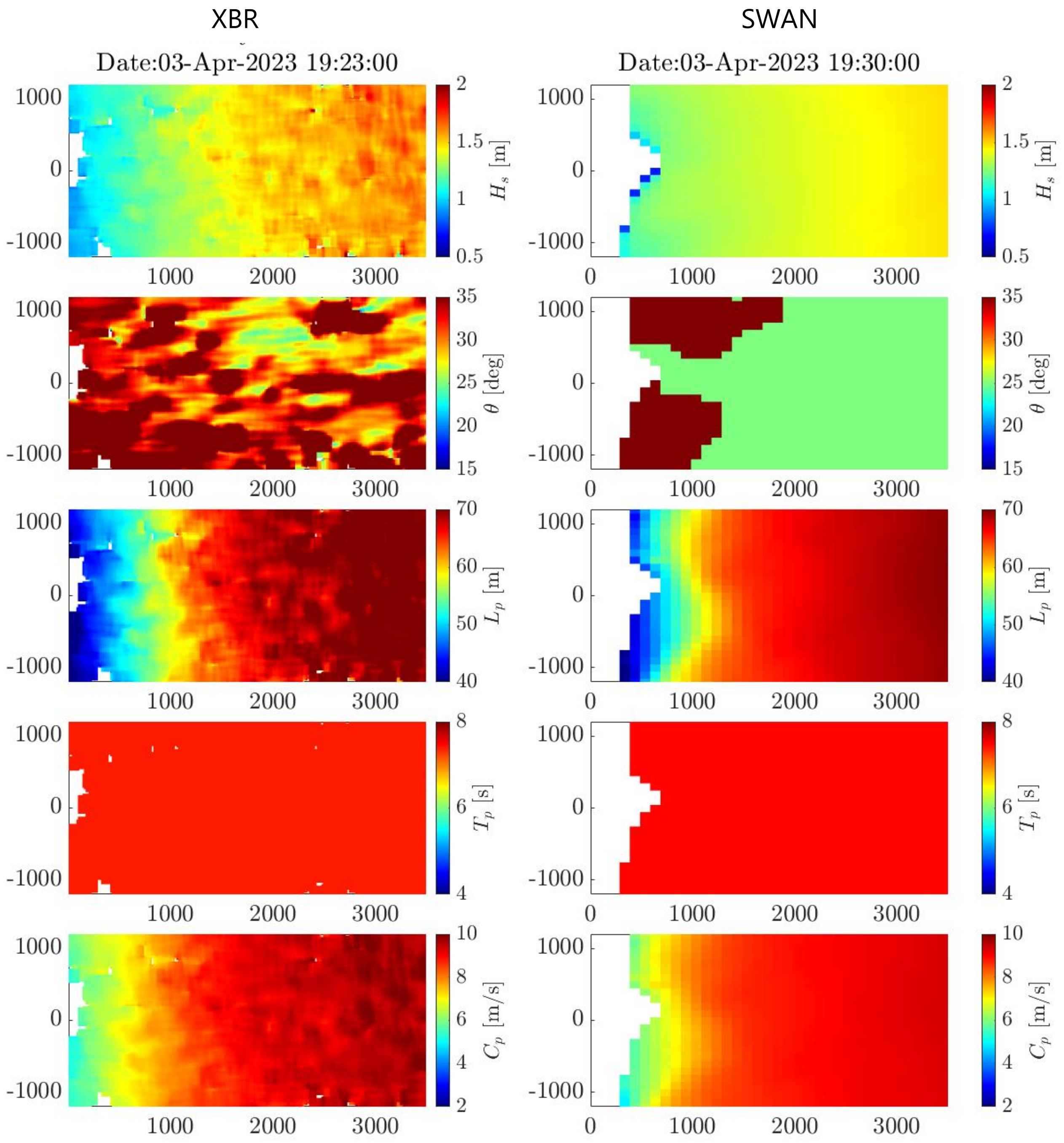

Preliminary Results

→ XBR sea state estimation performance.
- L_P, T_P and C_P are captured well
- θ_P estimation is better with new approach

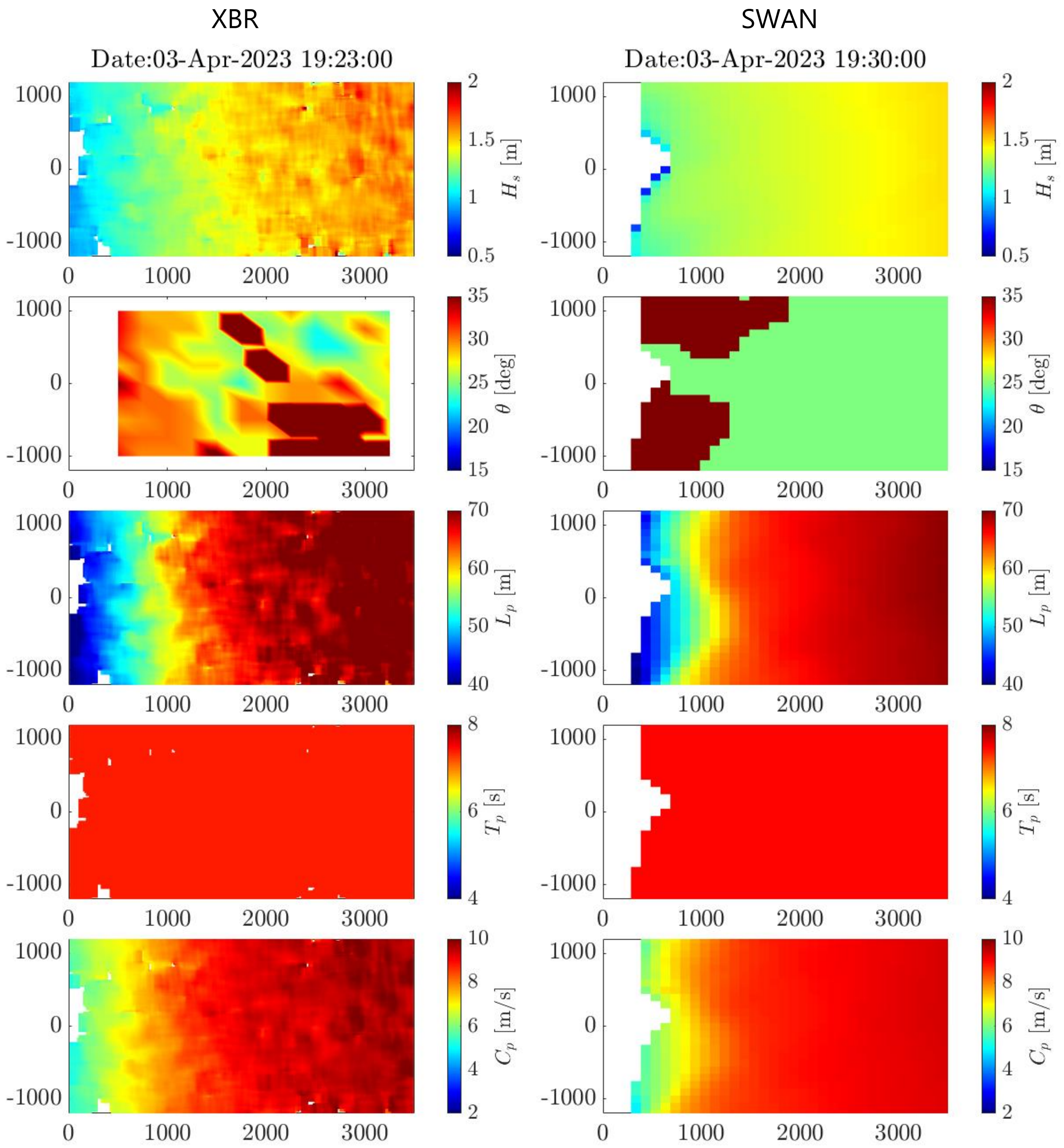

Preliminary Results

→ XBR sea state estimation performance.
- L_P, T_P and C_P are captured well
- θ_P estimation is better with new approach
- H_s needs more investigation

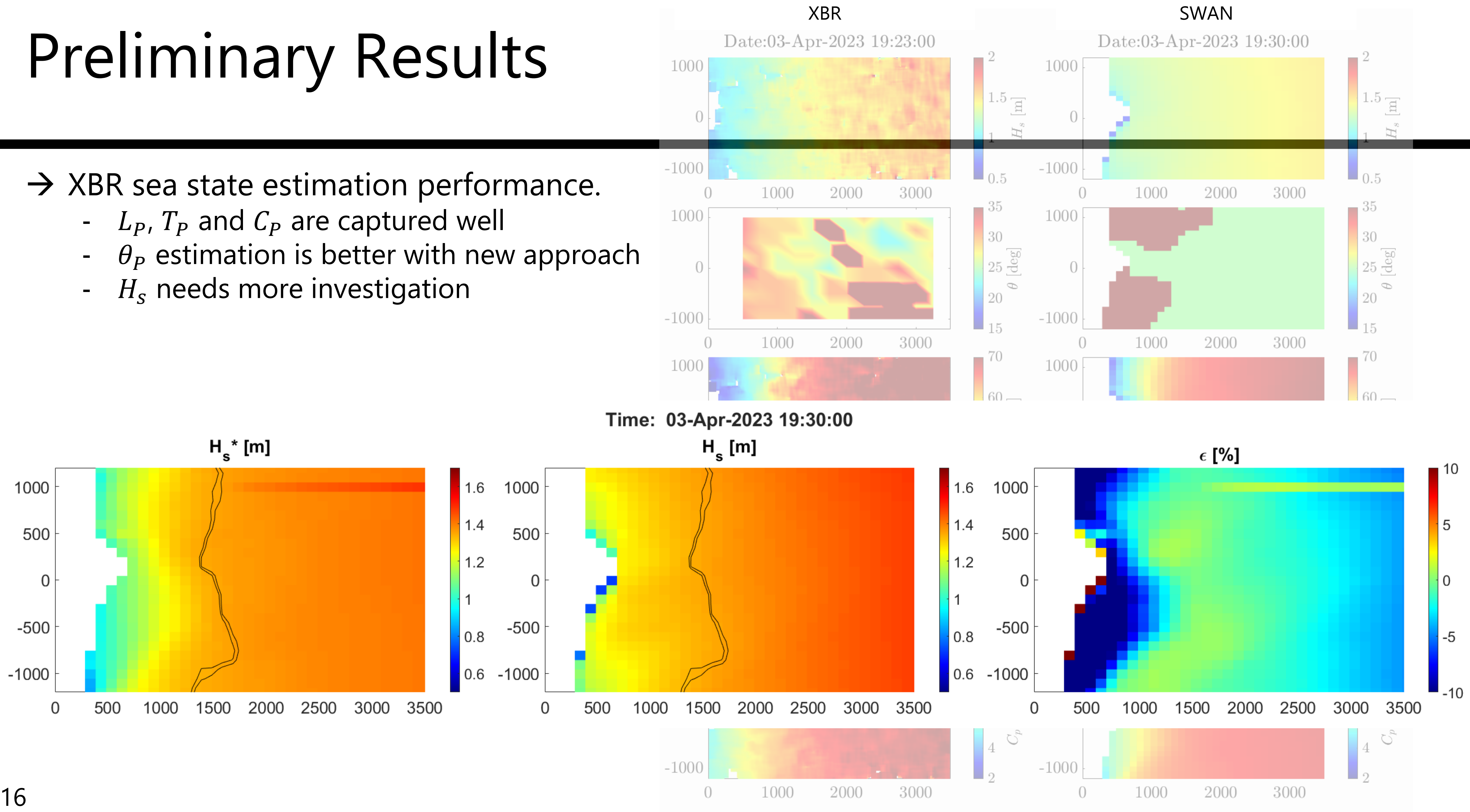

Preliminary Results

→ XBR wave propagation.
- Proposed approach is compared to FUNWAVE results

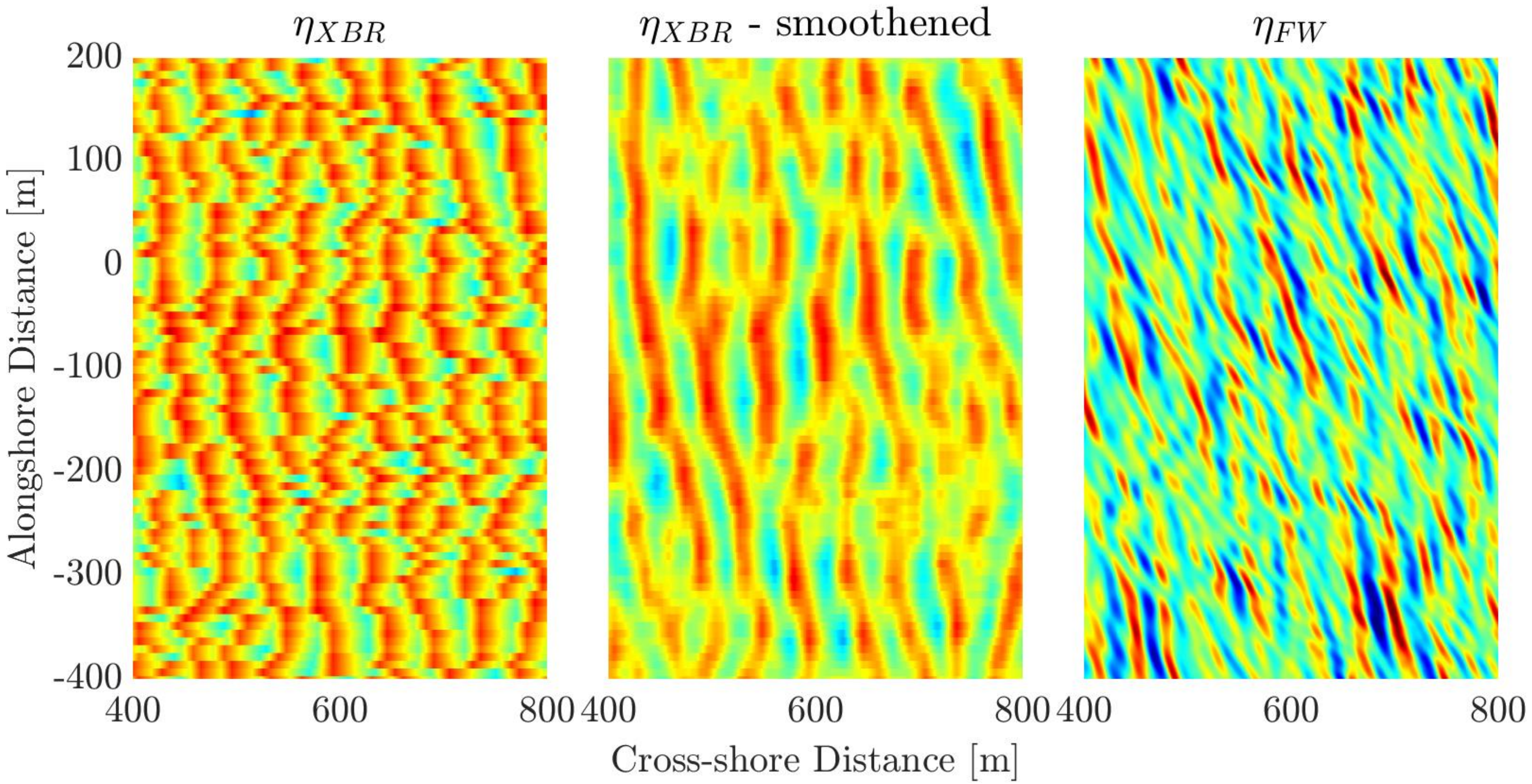

Preliminary Results

→ XBR wave propagation.
  - Scaler determined by $f - k$ spectra

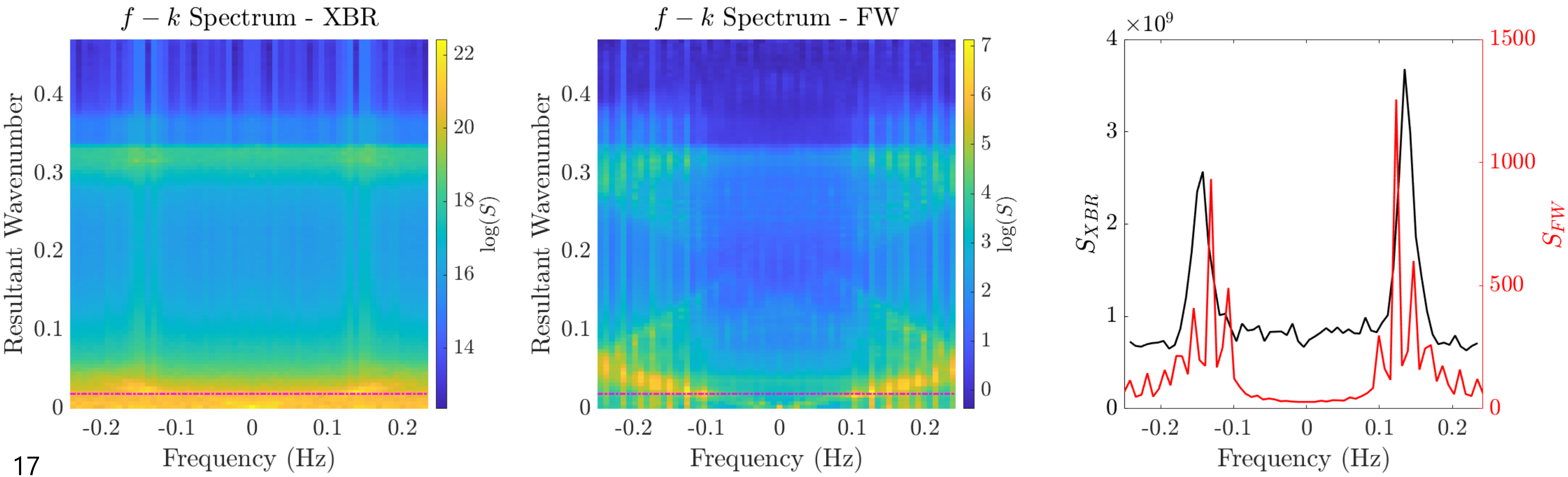

Preliminary Results

→ XBR wave propagation.

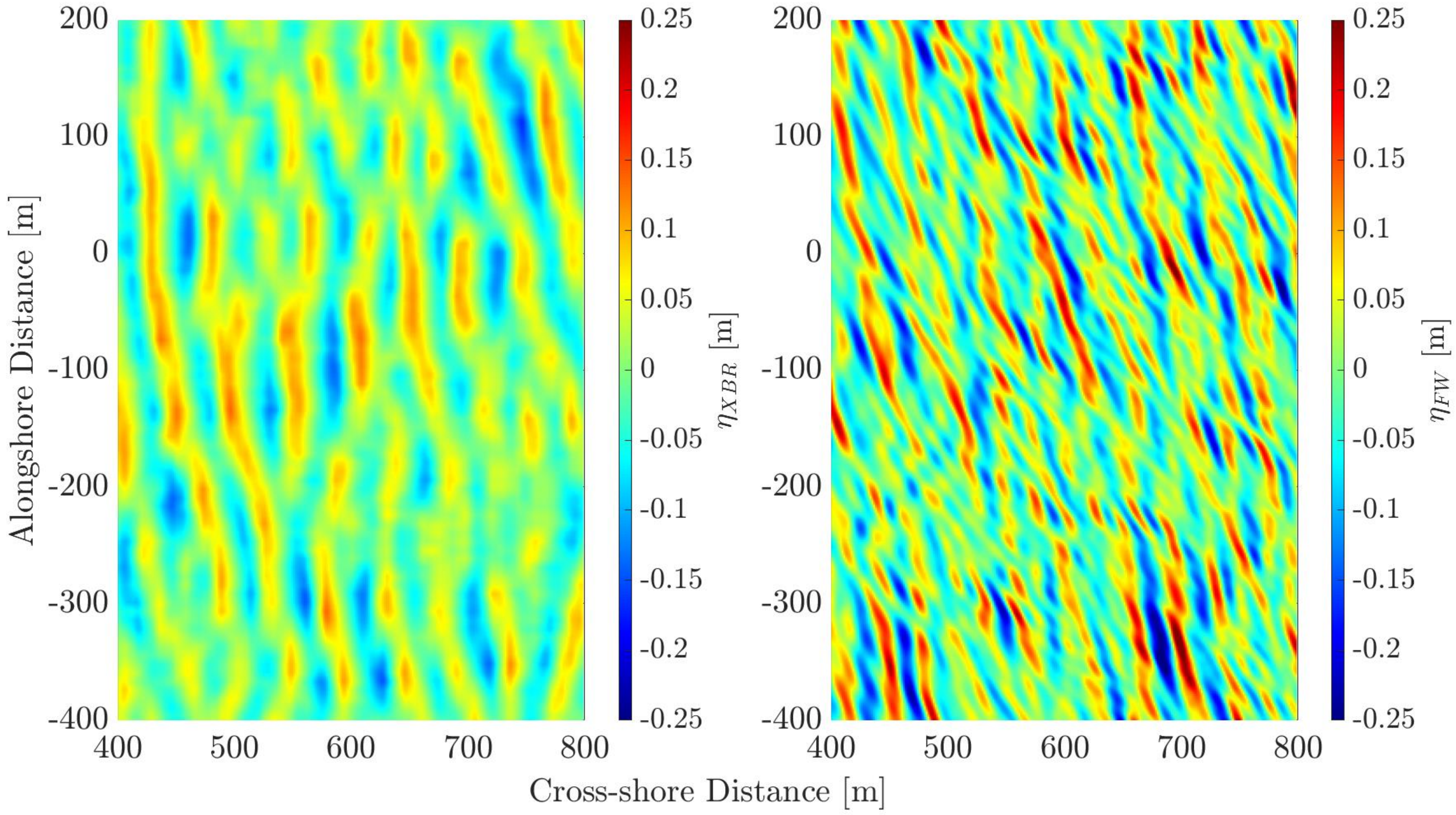

Preliminary Results

→ XBR wave propagation.

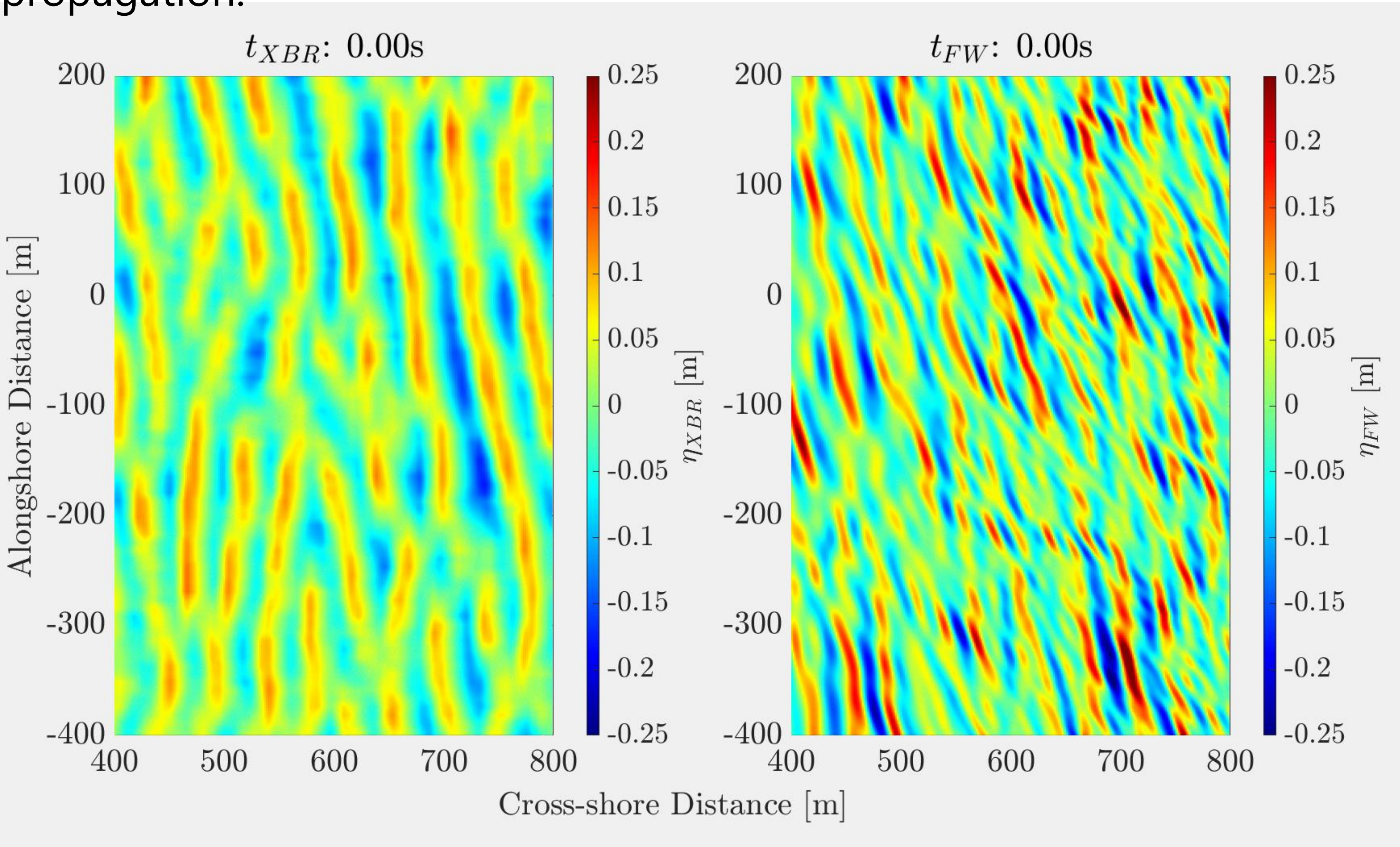

Ongoing Work

→ Processing of SGS.

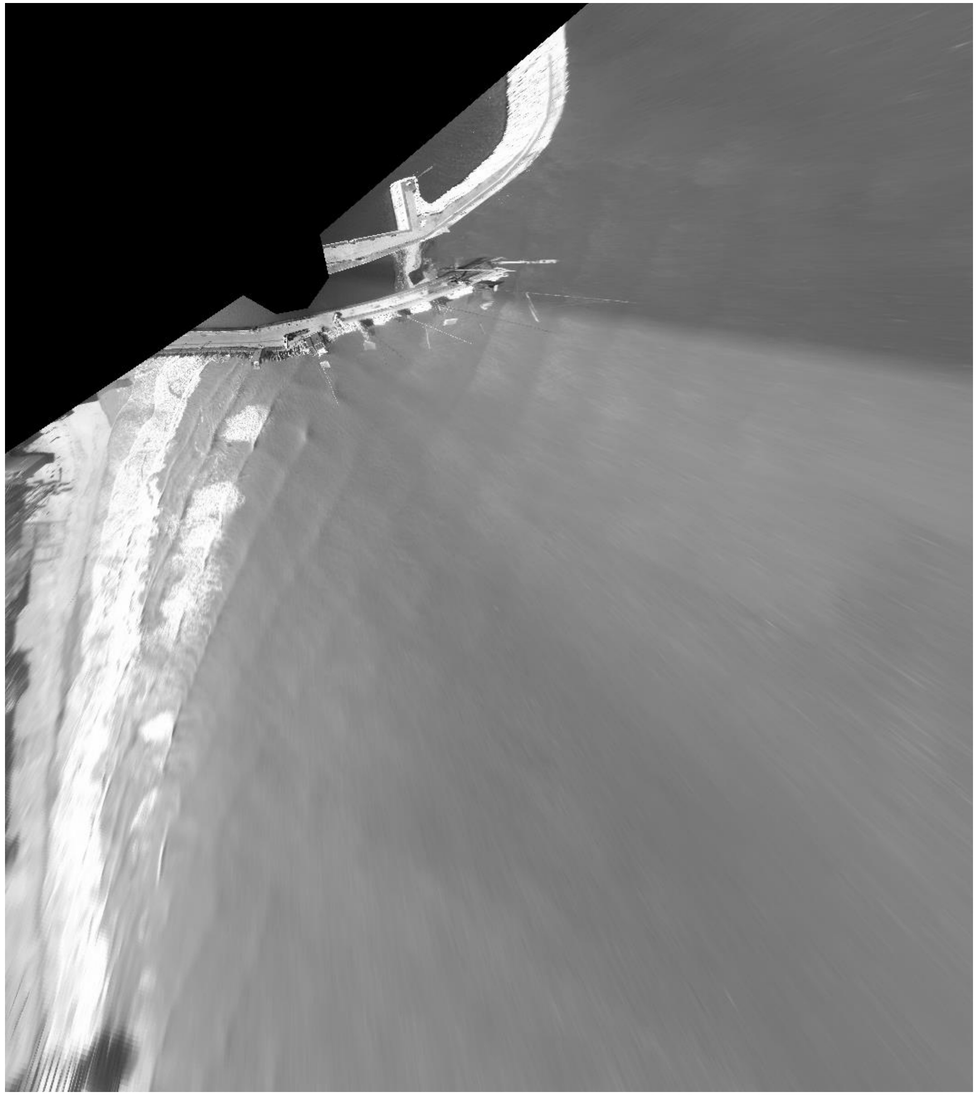

Ongoing Work

- → Processing of SGS.
- → Combining SGS, XBR and model chain

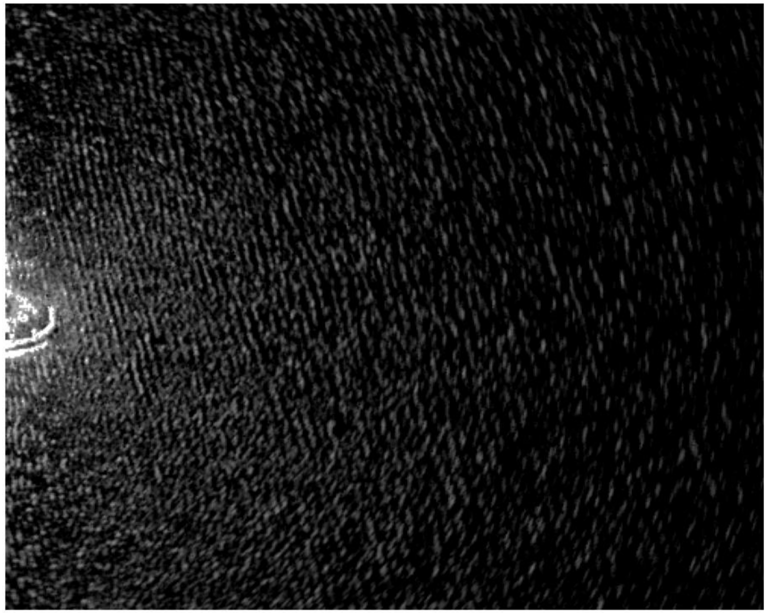

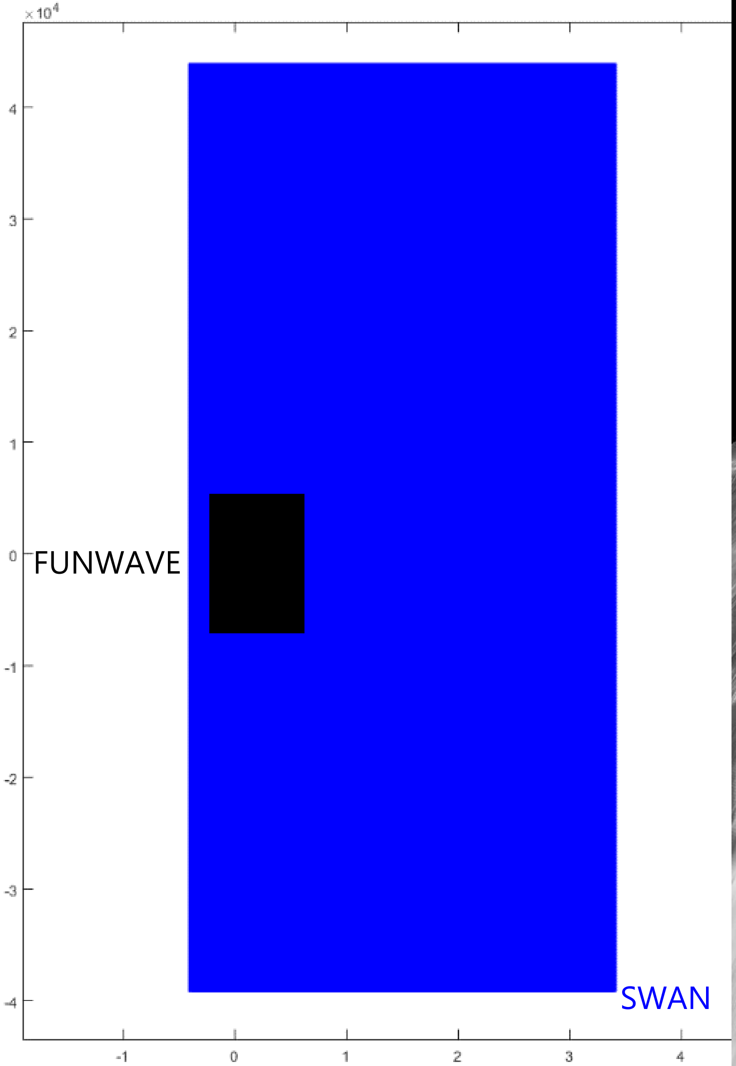

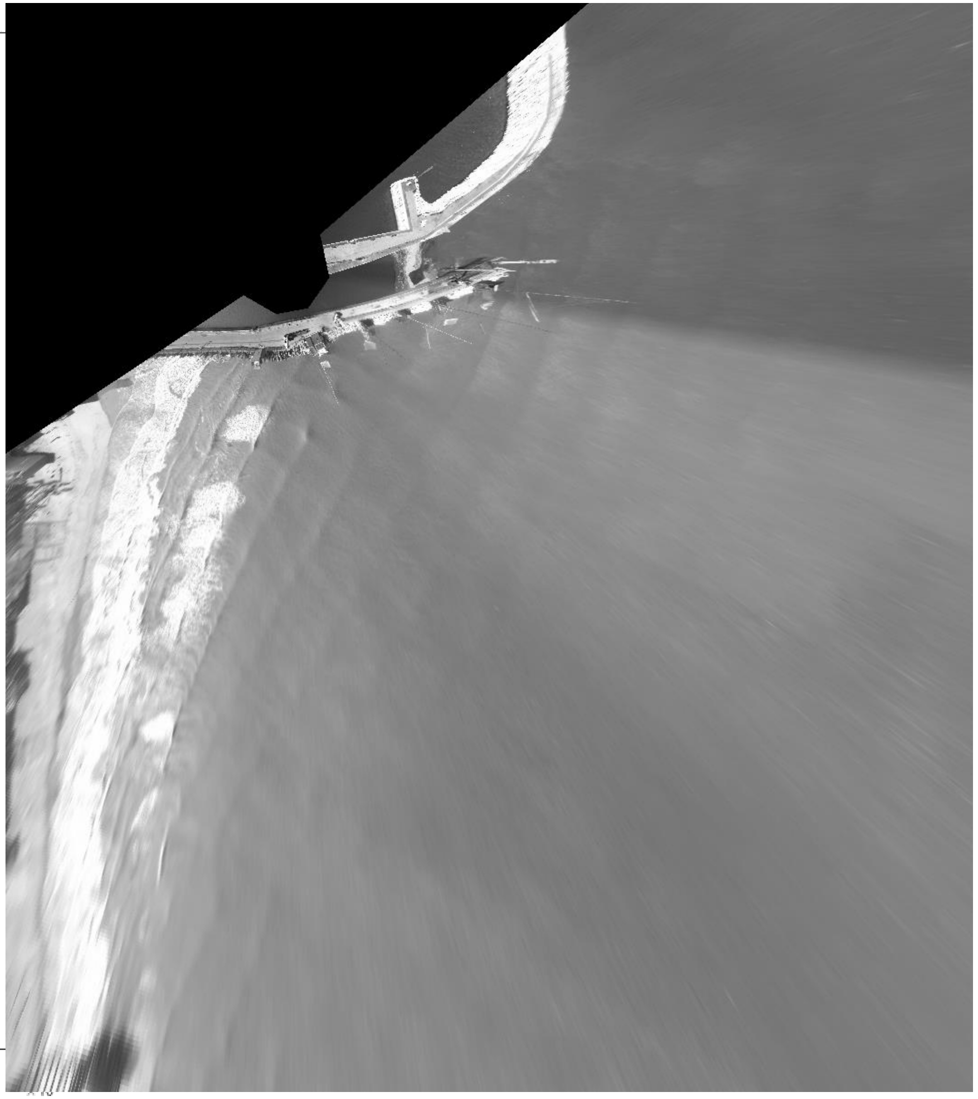

UNIVERSITÀ POLITECNICA DELLE MARCHE

DIPARTIMENTO INGEGNERIA CIVILE EDILE ARCHITETTURA

18|22 23|27 ECCELLENZA

European Commission

SEDIMARE DC MEETING

07.11.2024-08.11.2024

Delft, the Netherlands

Nearshore Wave Processes by Remote Sensing

Muhammed Said Parlak

m.s.parlak@univpm.it

https://sedimare.eu

Acknowledgement: This project has received funding from the European Union's (EU) Horizon Europe Framework Programme (HORIZON) under Grant Agreement No 101072443 as a MSCA Doctoral Network (HORIZON-MSCA-2021-DN-01) of

UNIVERSITY OF TWENTE.

SEDIMARE 2023 - 2027

Sediment Transport and Morphodynamics in Marine and Coastal Waters with Engineering Solutions

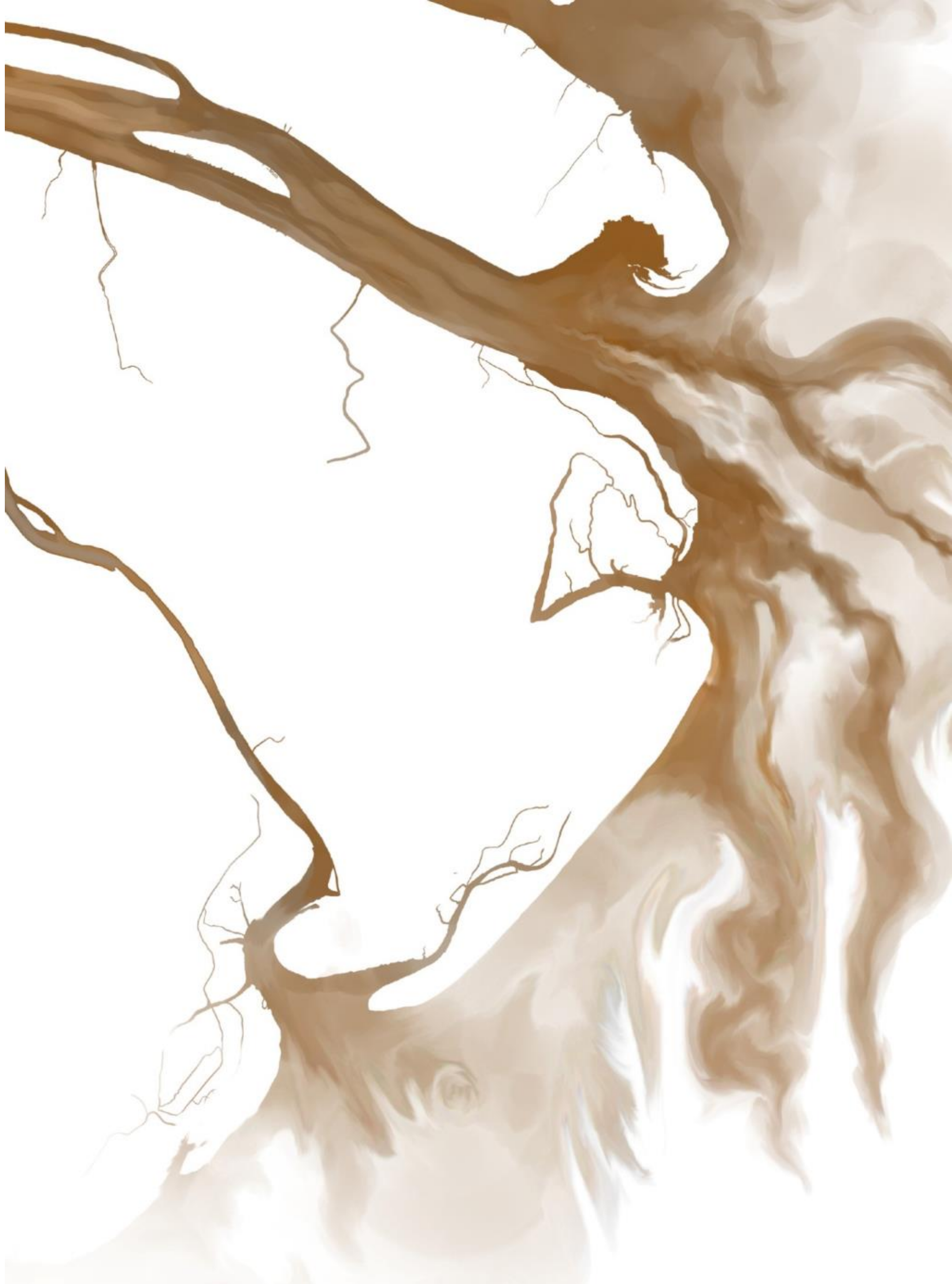

SEDIMARE PROJECT_DC #3

Netherlands Meeting

EROSION AND TRANSPORT OF SAND-SILT MIXTURES

PhD Candidate: Nguyen, Thi To Van (Van)
Promotor: P.C. Roos (Pieter)
Co-promotor: J.J. van der Werf (Jebbe)

Date: 2024 Nov 07th

Contents

1. Introduction

In nature, especially in coastal and fluvial systems, most of sediments are mixes of sand and fines (clay and silt).

Recently, there have been more studies focusing on the transport of sand-mud mixtures. However, most of these studies treated clay and silt collectively as mud (*Mitchener and Torfs, 1996; Van Ledden, 2003; Jacobs, 2011; Winterwerp et al., 2012; Colina Alonso et al., 2023*).

Silty sediments in Mekong Delta, Vietnam
[Photo by [MangLub project]]

Mudflat, Wadden Sea, Netherlands.

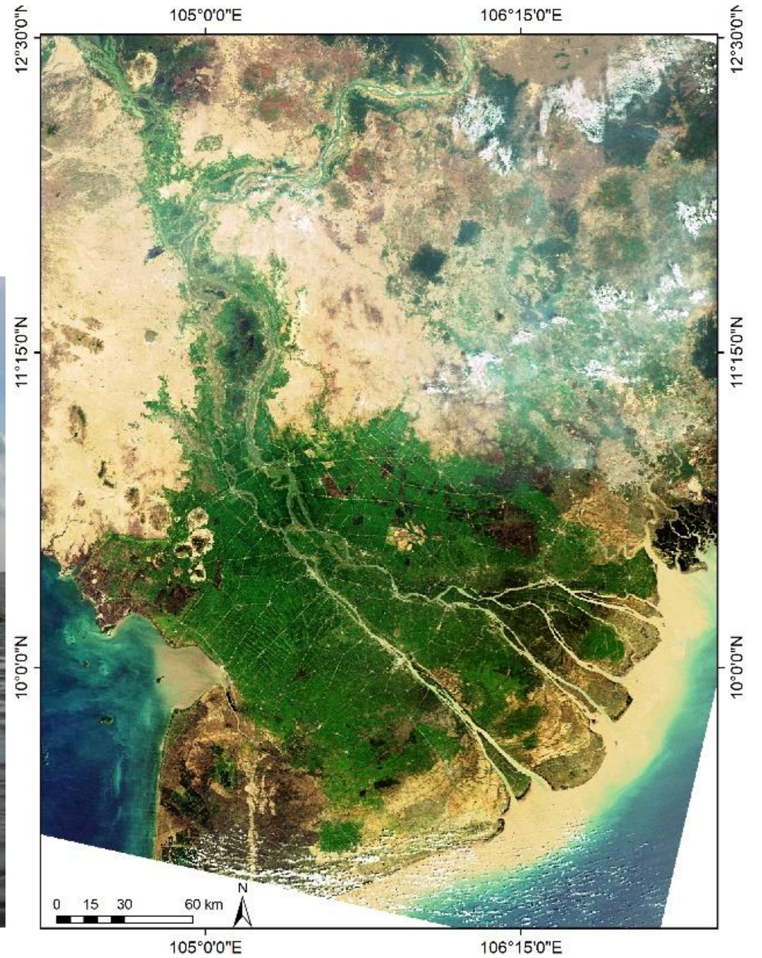

Satellite images of the Mekong Delta taken by Envisat

1. Introduction

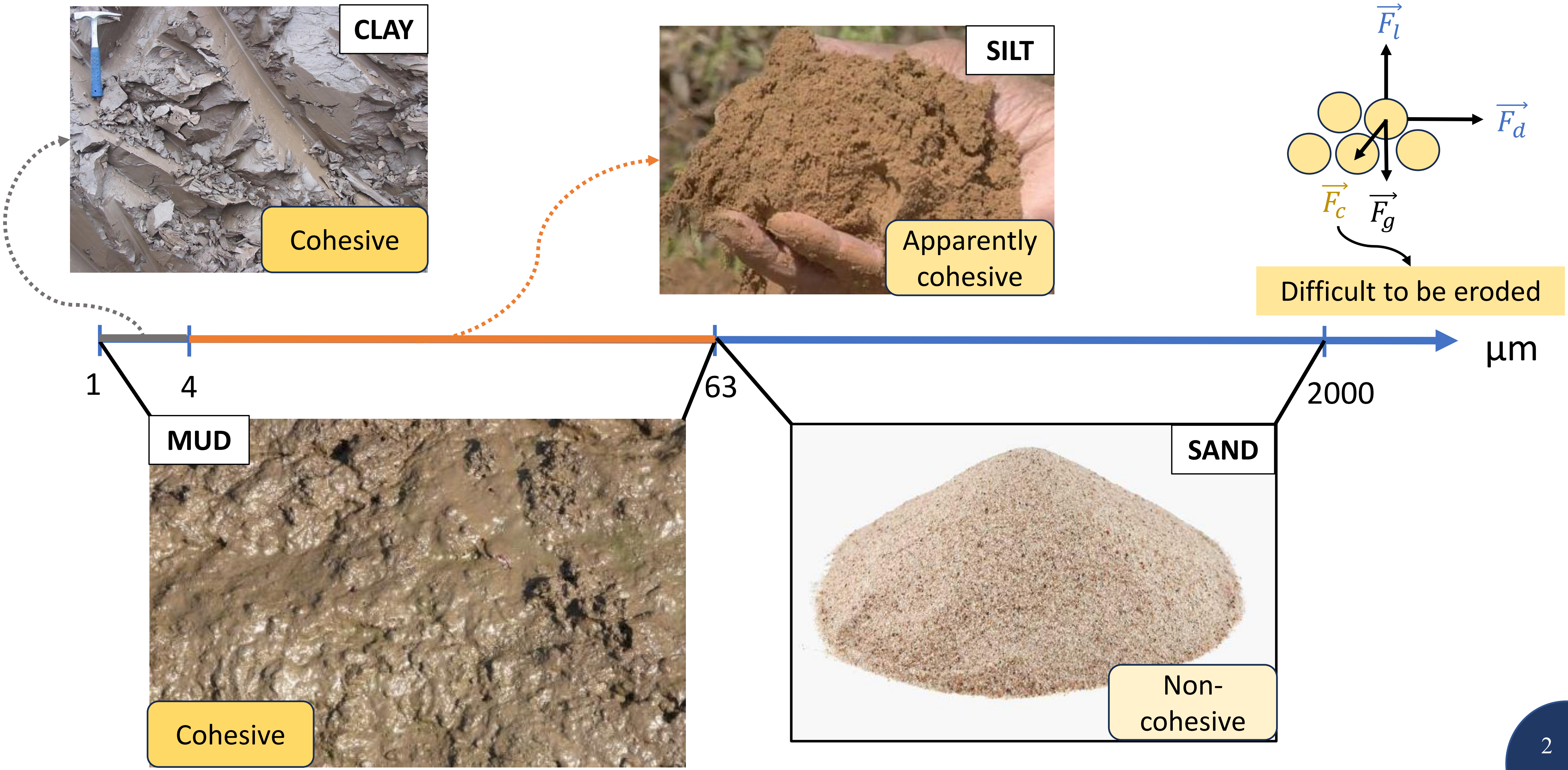

1. Introduction

SILT

Apparently cohesive

Small RD

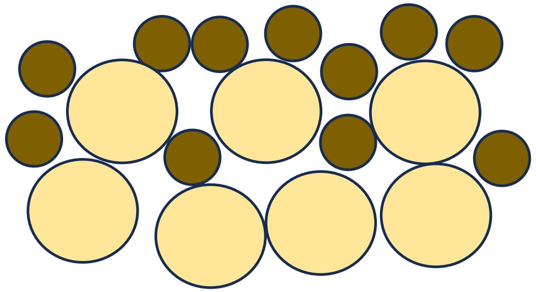

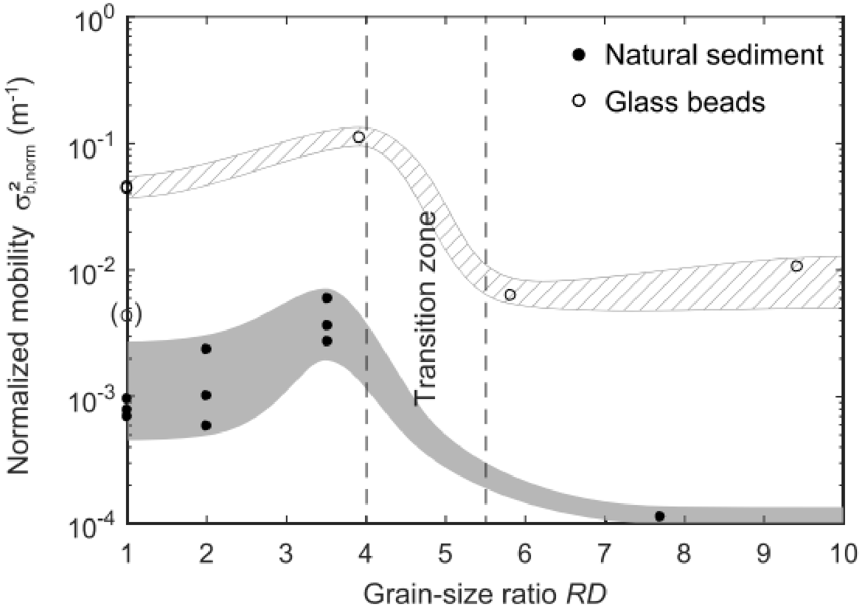

Normalized mobility (logarithmic scale), with varying grain-size ratio (Staudt et al., 2019)

4

63

Large RD (grain-size ratio)

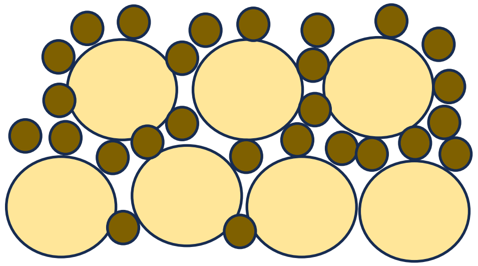

SAND

Non-cohesive

2. Research progress

The second preparatory experiment in the small-scale oscillatory tunnel, also known as the **Aberdeen Mini Tunnel** (AMT). For our experiment, we will use solid glass beads as the material. These beads are round and well-sorted.

Observations, results, and experiences obtained from the preparatory experiments will inform the conditions, bed configurations and procedures of the main AOFT experiments.

Sediment fractions	Mixtures	Silt content (%)	Velocity conditions (m/s)
Sand ($D_{50} \approx 150\ \mu m$)	Sa	0	0.2
			0.3
Sand ($D_{50} \approx 150\ \mu m$) and Coarse silt ($D_{50} \approx 50\ \mu m$)	SaCs20	20	0.2
			0.3
	SaCs40	40	0.2
			0.3
Sand ($D_{50} \approx 150\ \mu m$) and Medium silt ($D_{50} \approx 25\ \mu m$)	SaMs20	20	0.2
			0.3
	SaMs40	40	0.2
			0.3

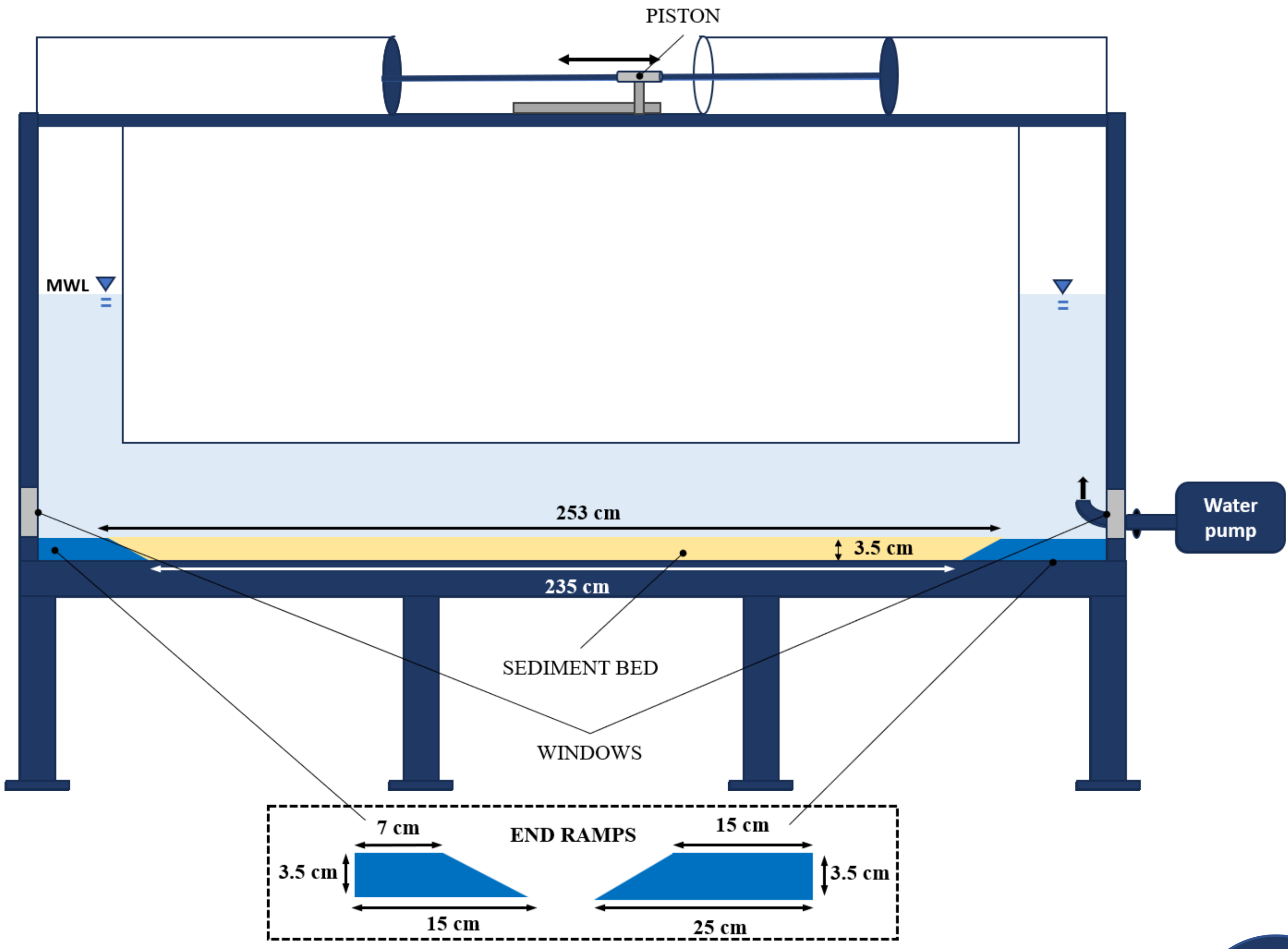

The Aberdeen Mini Tunnel (AMT) at the University of Aberdeen.

2. Research progress

Flow condition: T = 3s, U_{max} = 0.2 m/s

- Bedform development over approximately **450 flow cycles** (~23 mins) for different beds was observed.
- For the mixed bed containing **40% silt**: **Higher** suspended sediment concentration (**SSC**) and **ripples developed more slowly** compared to others.

Pure-sand

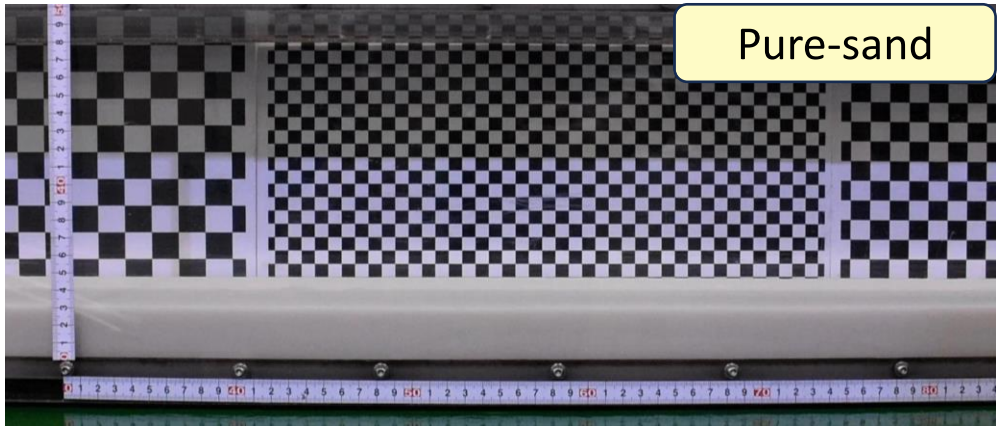

Mixtures of sand and coarse silt

SaCs20

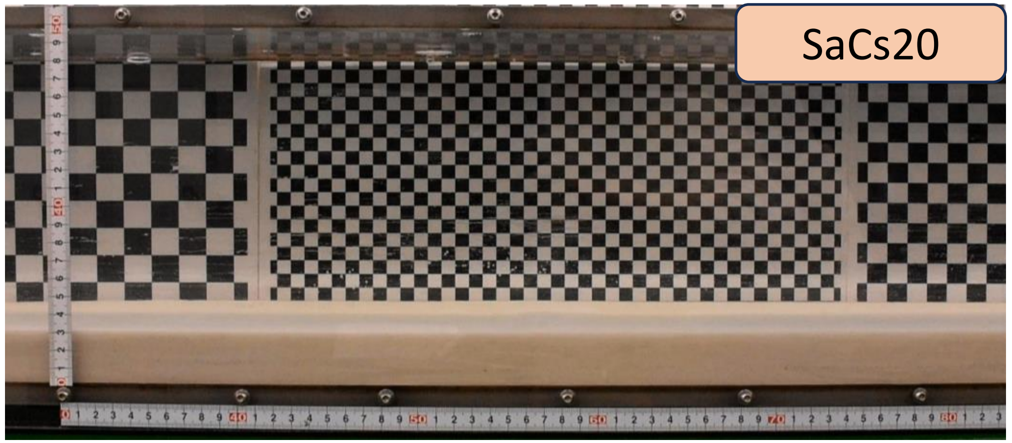

SaCs40

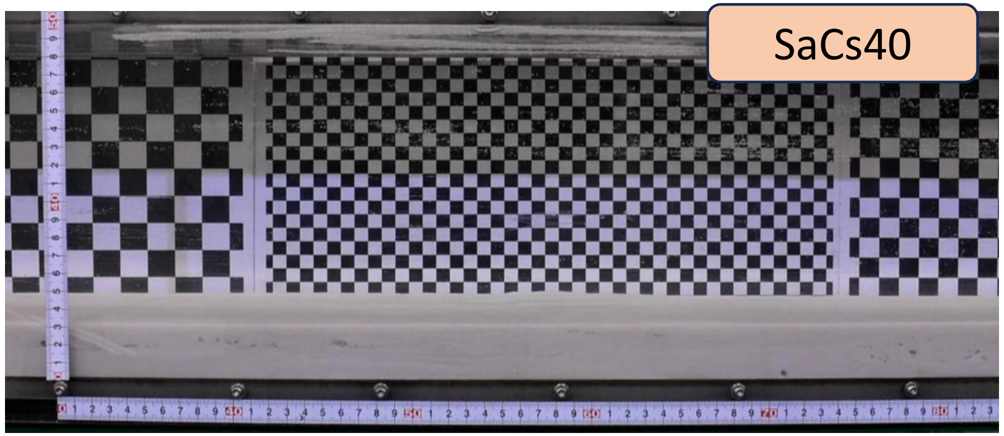

Mixtures of sand and medium silt

SaMs20

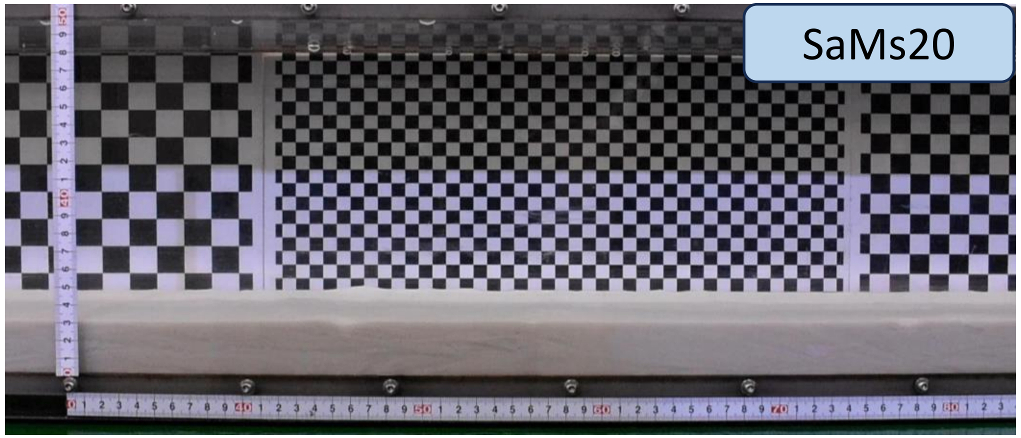

SaMs40

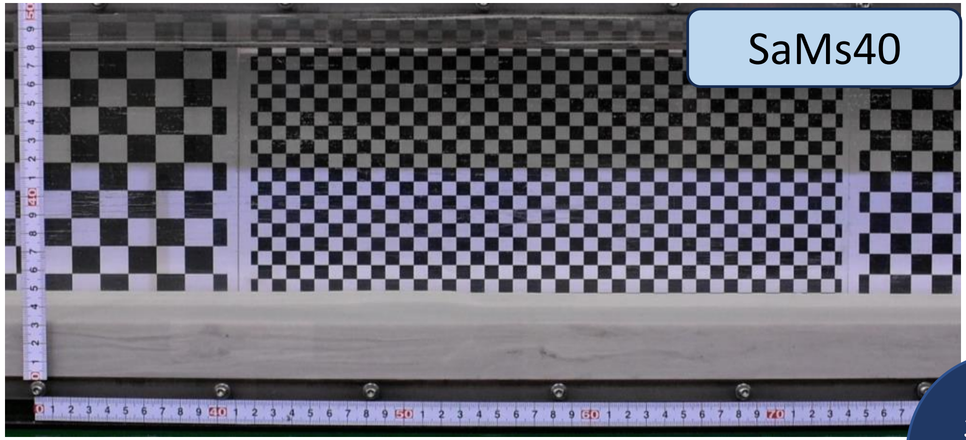

2. Research progress

Flow condition: T = 3s, U_{max} = 0.3 m/s

- Bedform development over approximately **450 flow cycles** (~23 minutes) was observed for different beds.
- Under **higher-velocity** conditions, a **high suspended concentration** was easily seen during the initial cycles.
- **Ripples were forming faster** compared to the 0.2 m/s condition.

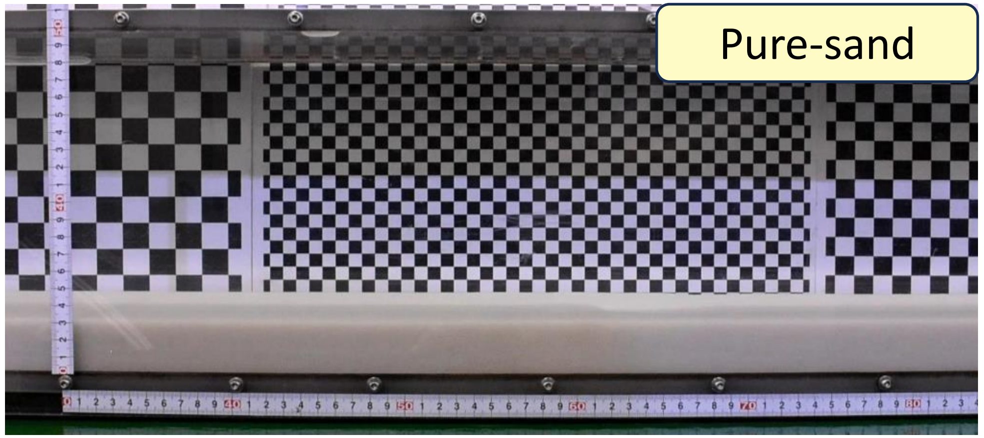

Pure-sand

Mixtures of sand and coarse silt

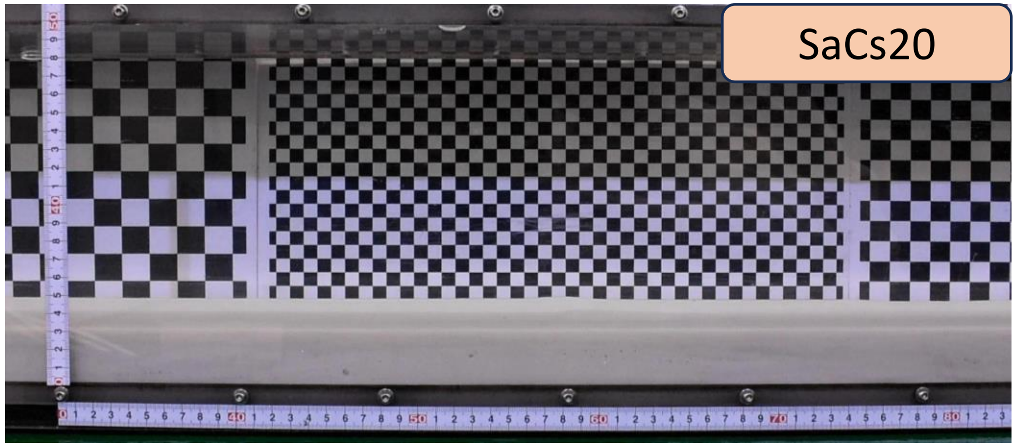

SaCs20

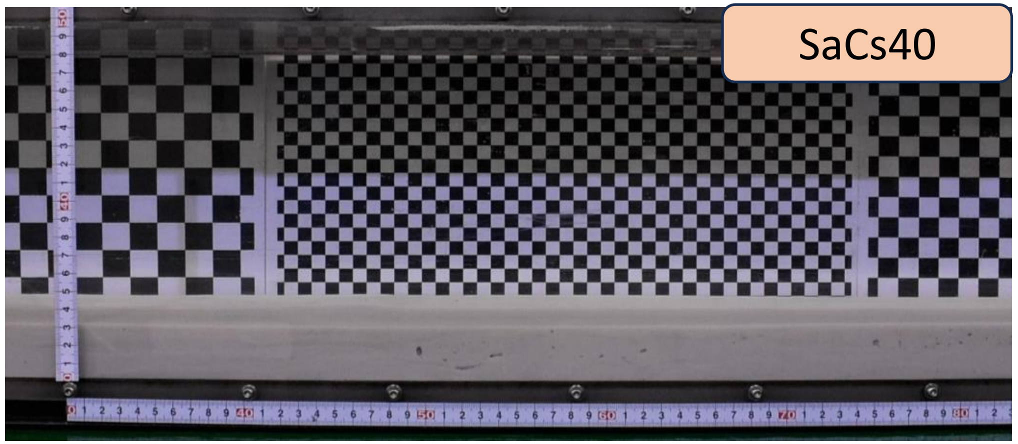

SaCs40

Mixtures of sand and medium silt

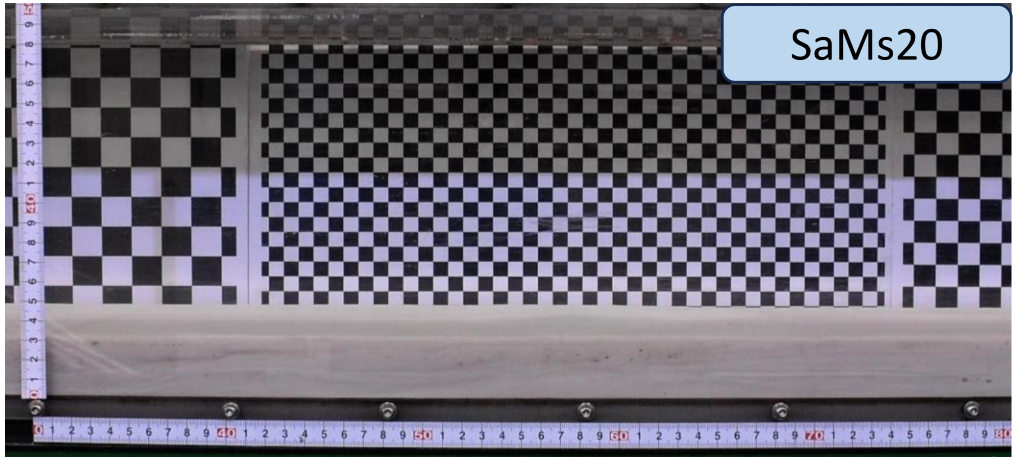

SaMs20

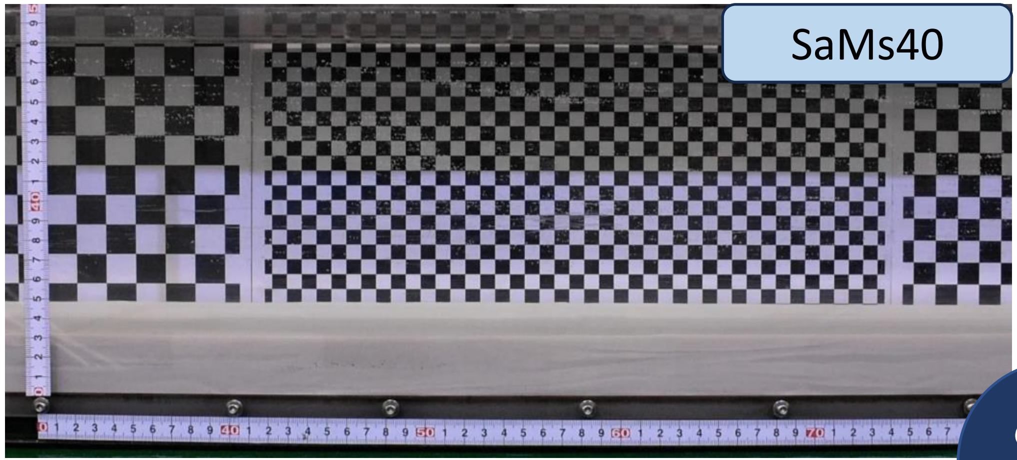

SaMs40

2. Research progress

Flow condition: T = 3 s, U_{max} = 0.2 m/s

- Bedform of different beds at **the end** of each experiment.
- 3D ripples were observed in mixed beds.
- Ripples of 40%-silt-content mixtures had smaller scales compared to 20% mixtures and pure-sand bed.

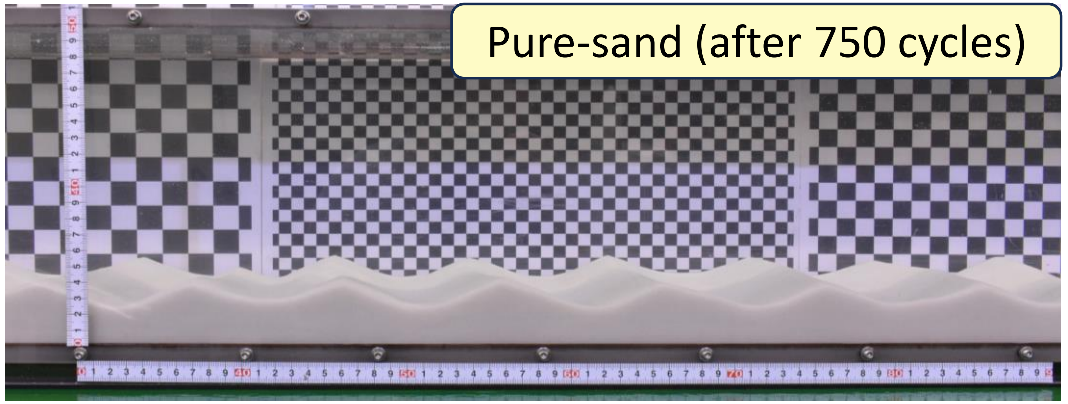
Pure-sand (after 750 cycles)

Mixtures of sand and coarse silt

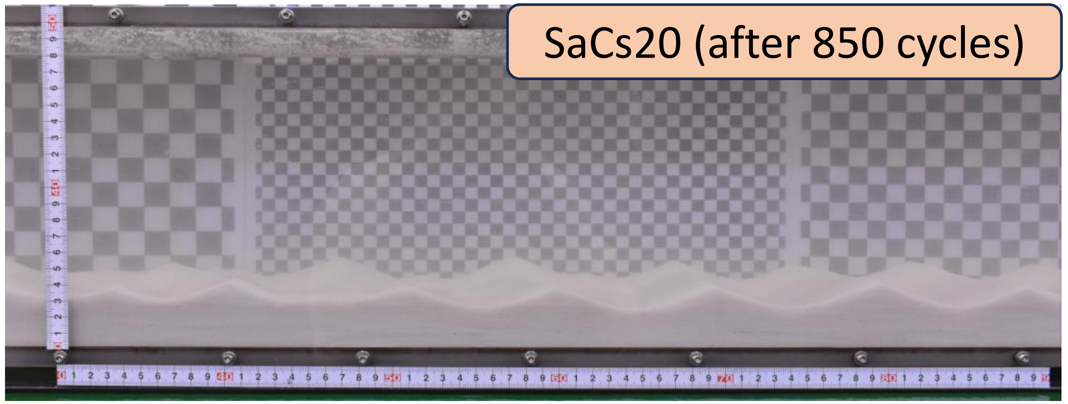
SaCs20 (after 850 cycles)

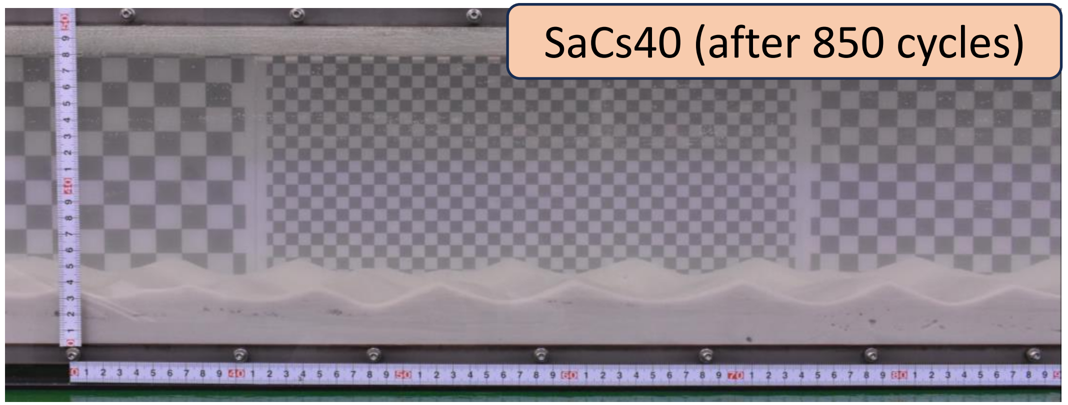
SaCs40 (after 850 cycles)

Mixtures of sand and medium silt

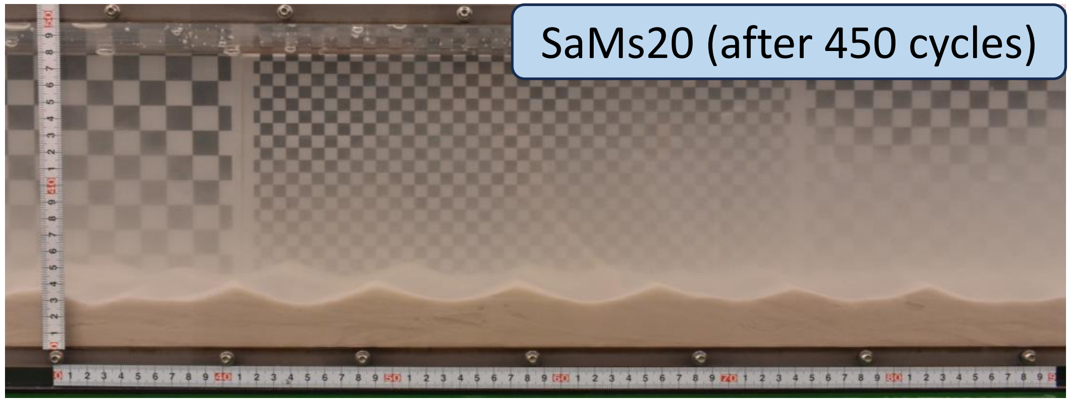
SaMs20 (after 450 cycles)

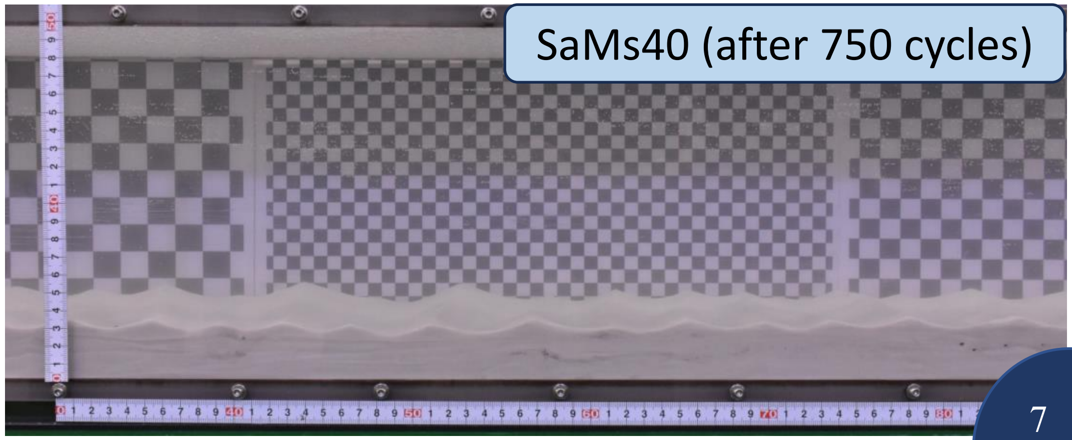
SaMs40 (after 750 cycles)

2. Research progress

Flow condition: T = 3 s, U_{max} = 0.3 m/s

Bedform of different beds at the end of each experiment. Compared to 0.2-m/s condition, 3D ripples developed faster with higher velocity. Suspended sediment concentrations were also higher (visual observations).

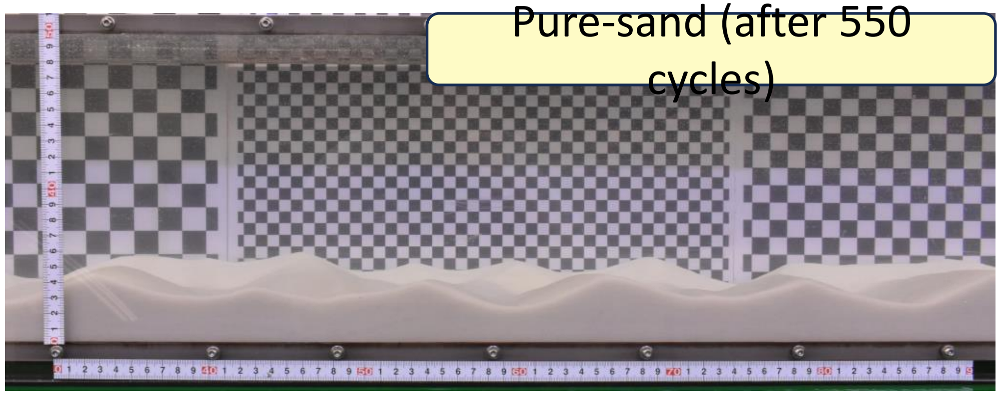

Mixtures of sand and coarse silt

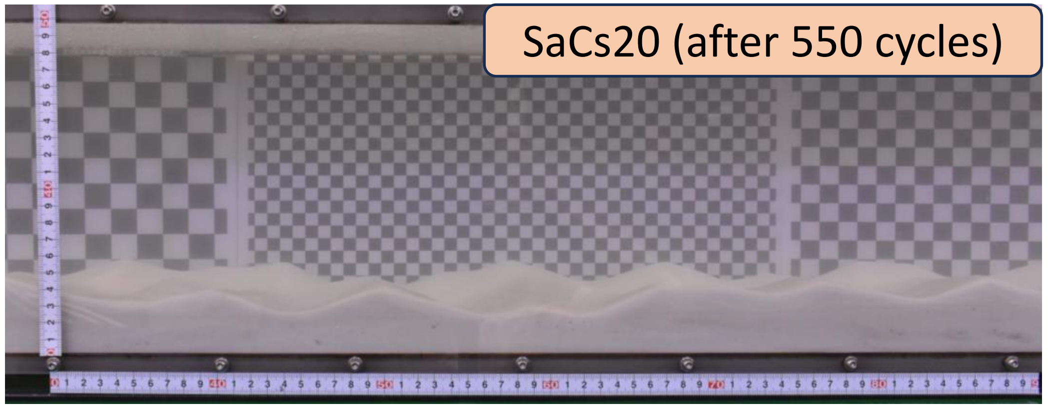

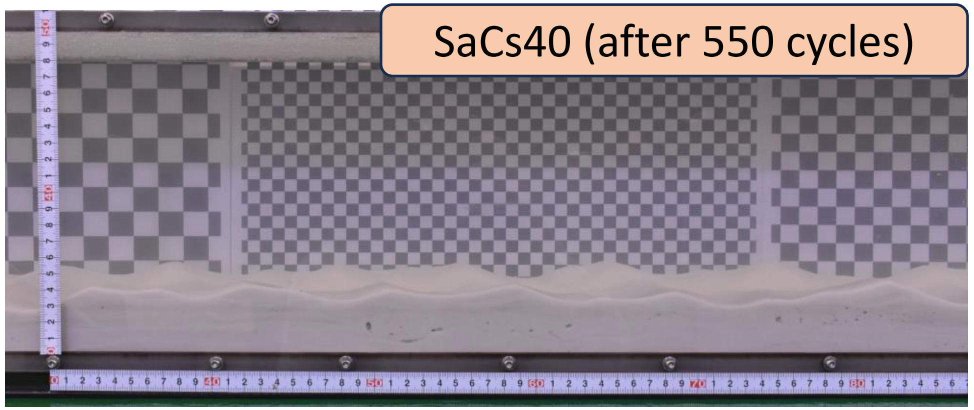

Mixtures of sand and medium silt

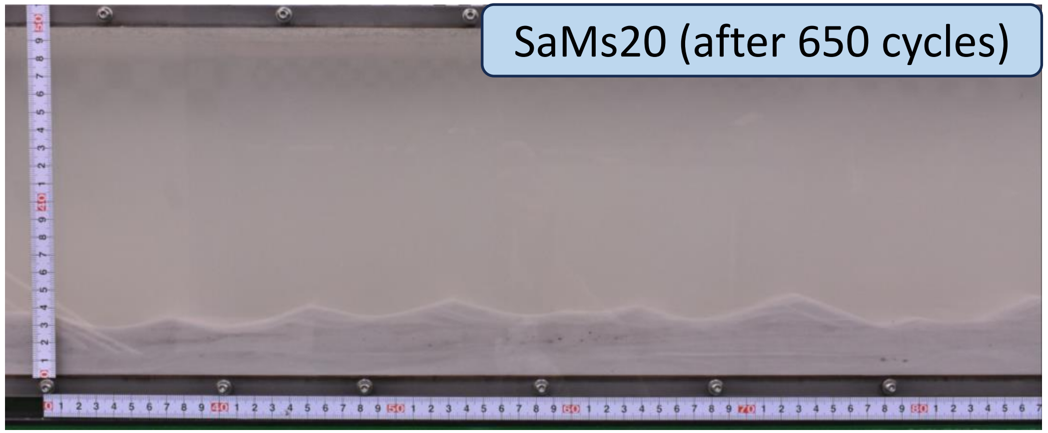

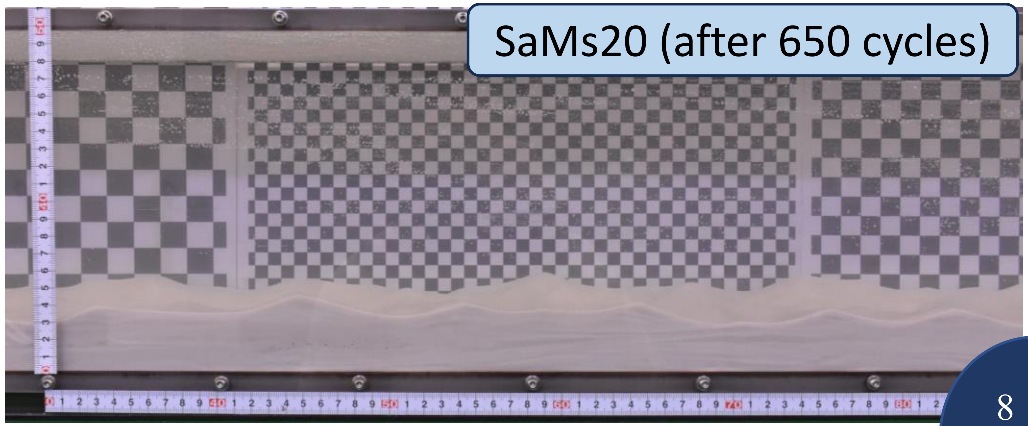

3. Upcoming plans

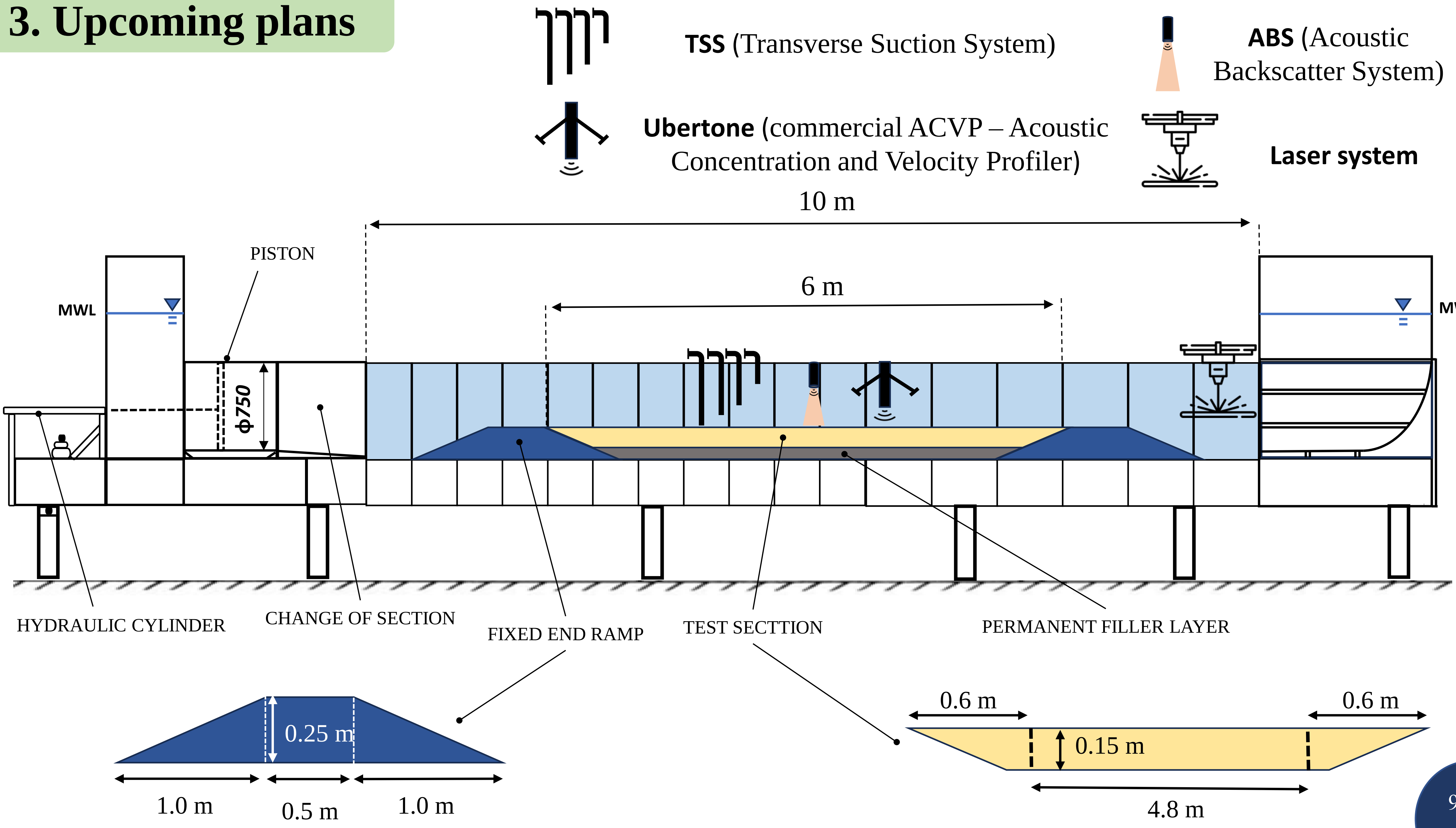

4. Conclusion

We have a nice preparatory experiment.

We are updating the experiment plan and preparing to have the main experiment conducted in Feb 2025.

THANK YOU FOR YOUR ATTENTION

Source: freepik

3. Upcoming plans

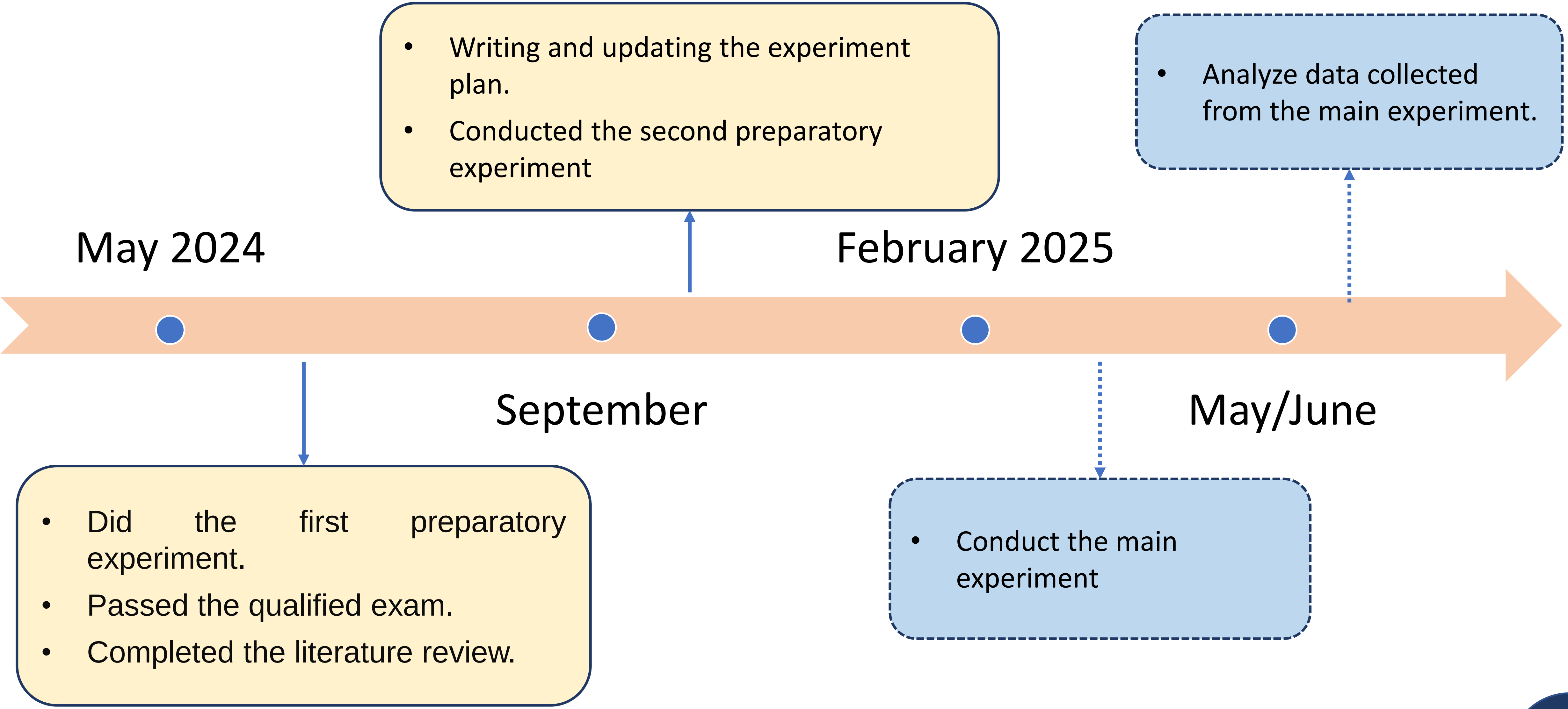

Ideas for SEDIMARE presentation:

Give introduction about sand-silt mixtures, effect of RD => filling-pores effect and hiding-exposure effect (coarser silt can enhance mobility of sand, and oppositely, fine enough silt can decrease mobility of the bed). Mention finding of Lange 2024 using the transport stage. Mention the difference between study of Lange and Staudt and Barzke

SEDIMARE DC8

Morphodynamics of Breach Growth and Bank Erosion using Laboratory Experiments

By Siyuan Wang

2024-11-06

Nelen & Schuurmans
UCLouvain
UNIVERSITY OF TWENTE.

CONTENT

- Introduction
- Bank Erosion and Dam Breaching
- Dam Breaching Experiment Design
- Previous Dam Breaching Experiments in UCLouvian

Introduction

Bank erosion refers to the process of **removing material** from a bank which is the land alongside **a body of water** in geography.

- Coastal and riverine environmen
- Two main modes
- Processes loop

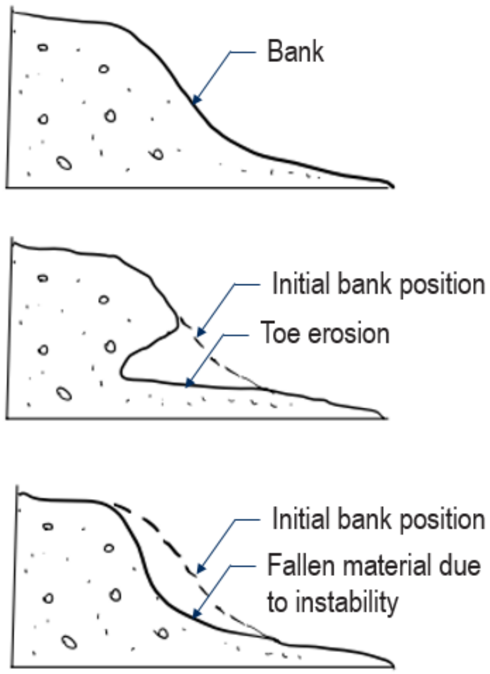

a) Initial bank position

b) Hydraulic erosion at the toe zone

c) Mechanical failure

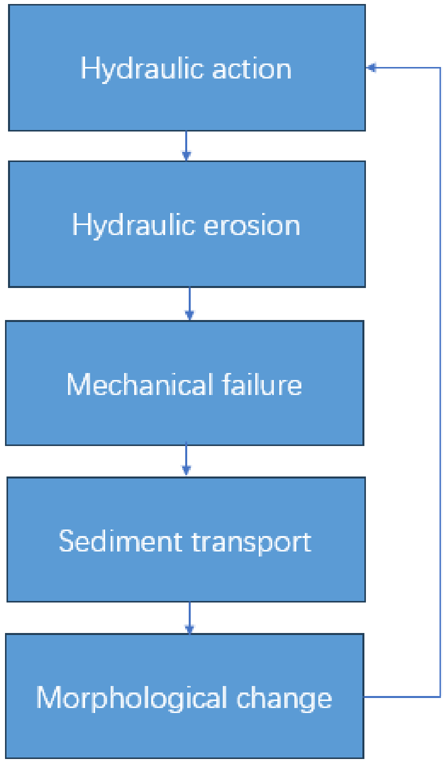

Bank Erosion and Dam Breaching

Similarities

- Environment conditions
- Hydraulic forces (in coastal setting)
- Processes

Differences

- Initiations
- Hydraulic forces (in riverine setting)
- Processes period

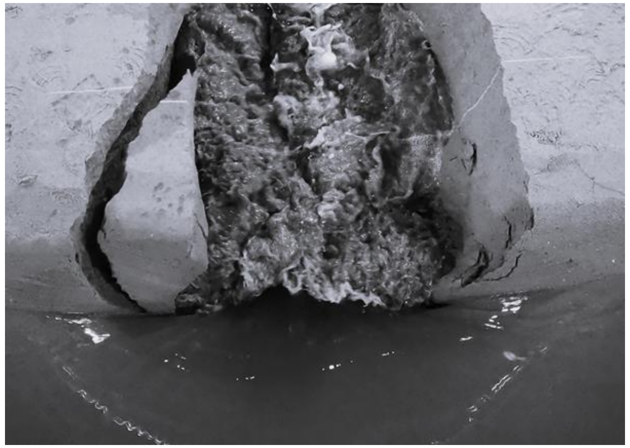

Ebrahimi, 2024

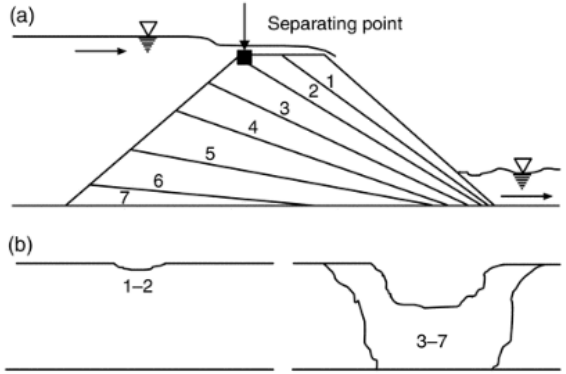

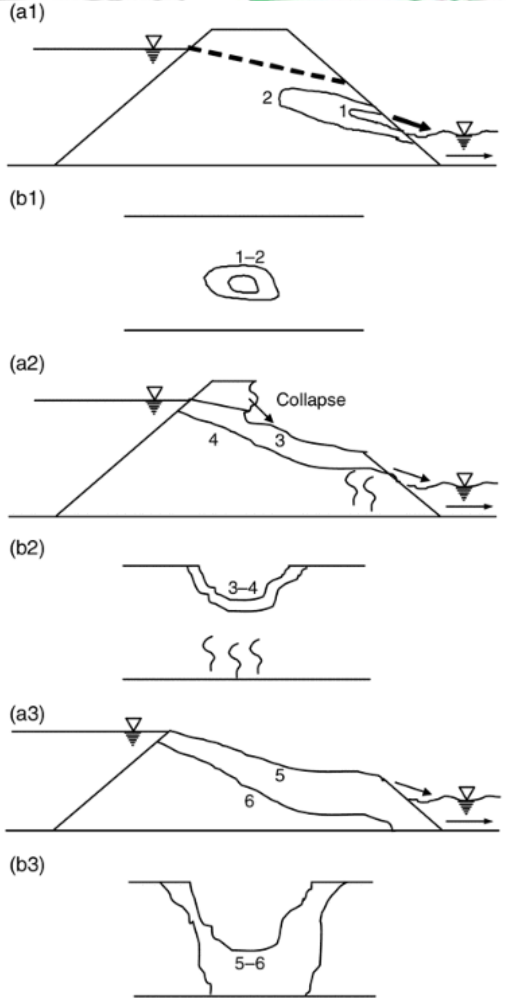

Zhang et al., 2016

Dam Breaching Experiment Design

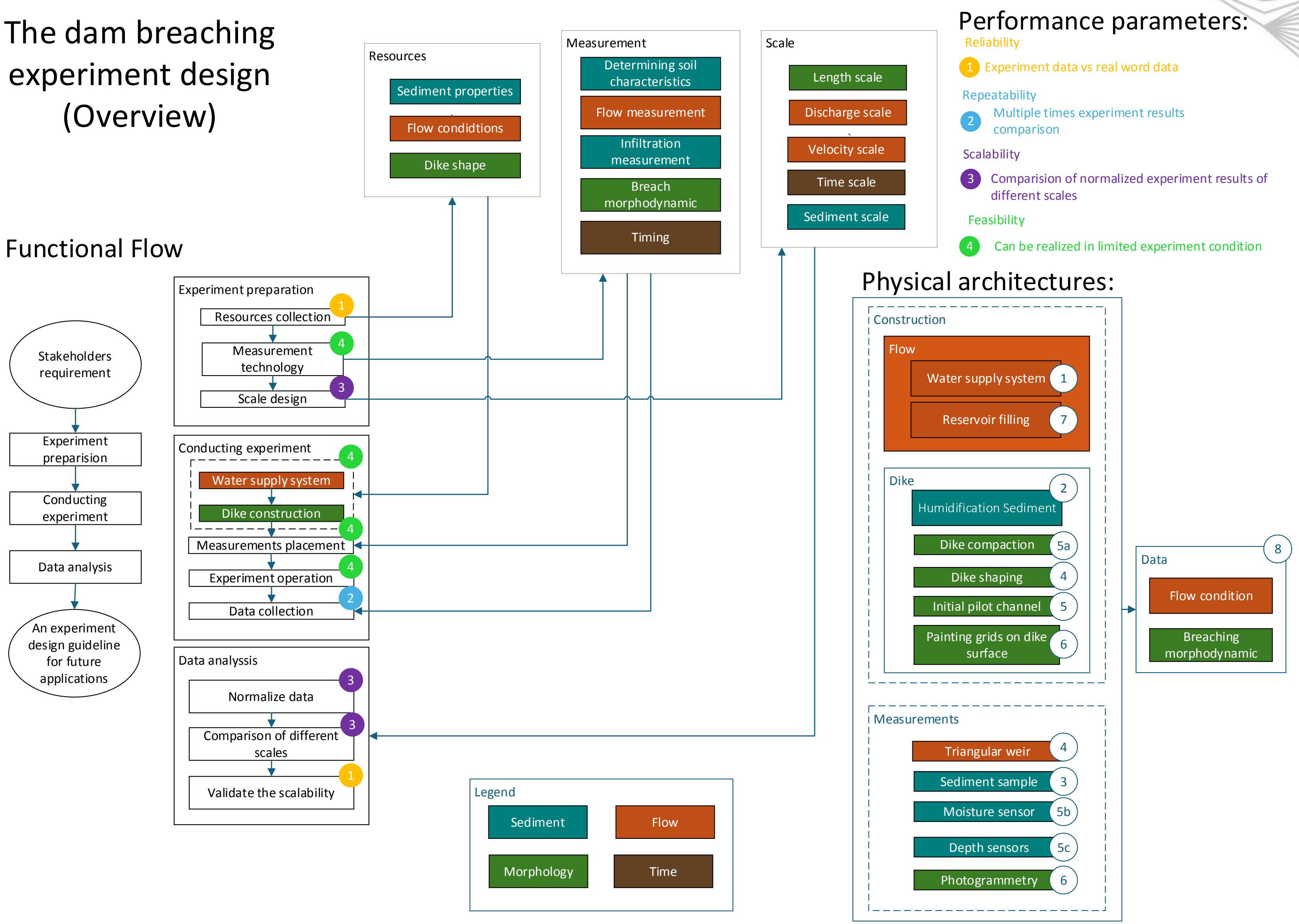

Dam Breaching Experiment Design

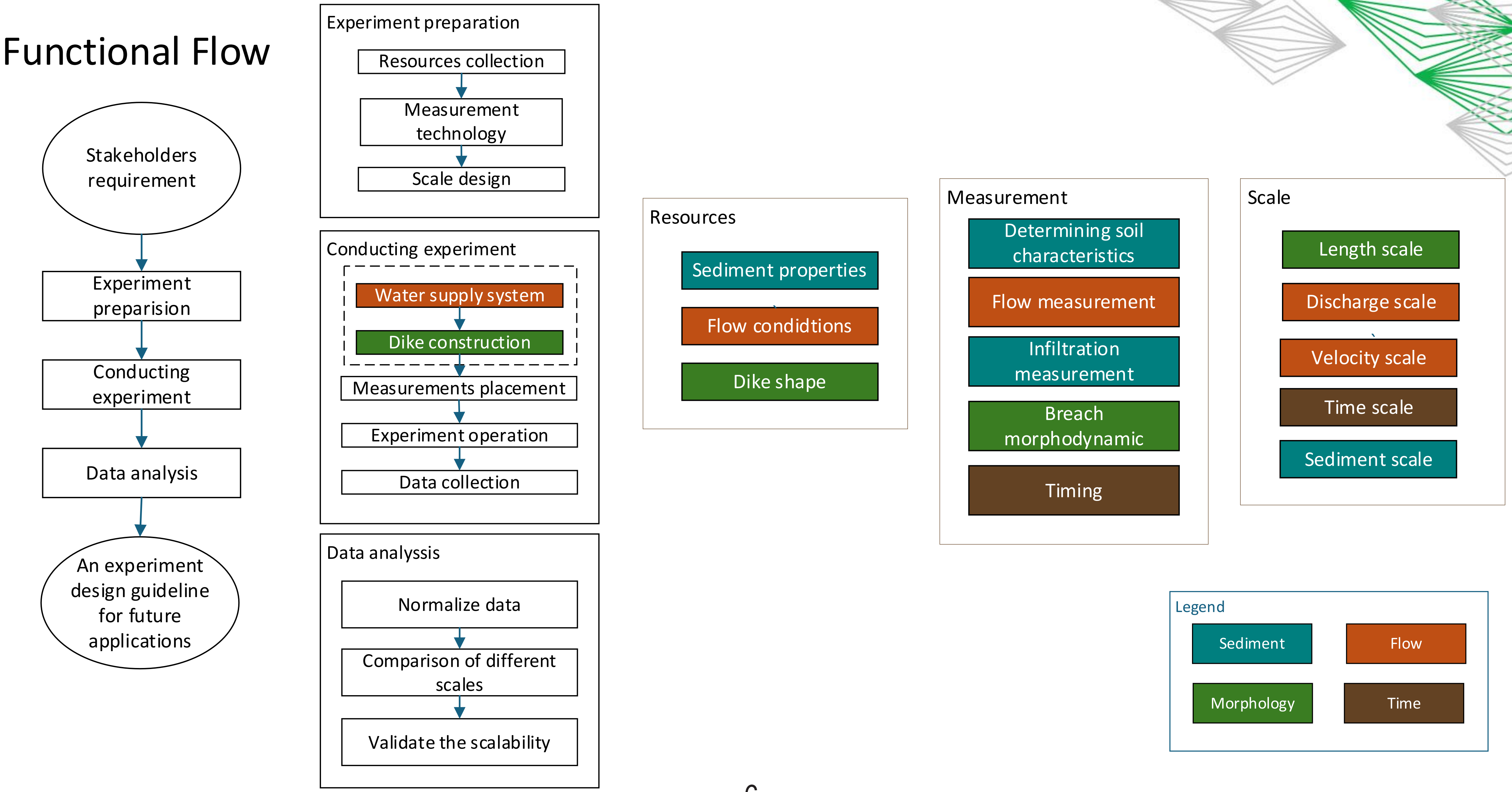

Dam Breaching Experiment Design

Functional Flow

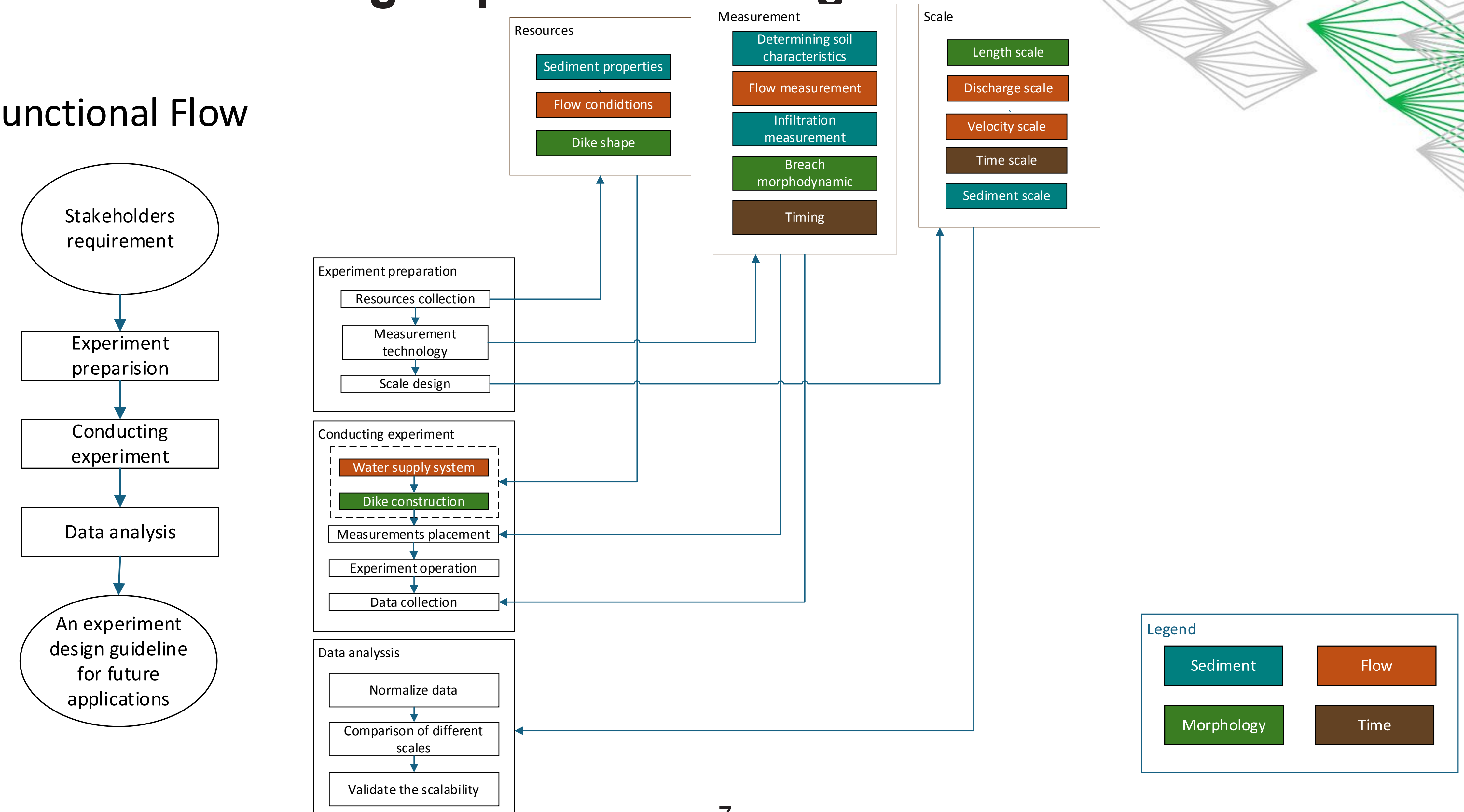

Dam Breaching Experiment Design

Functional Flow

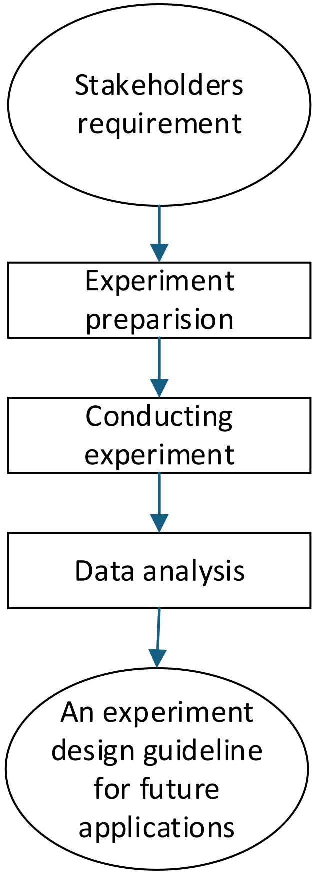

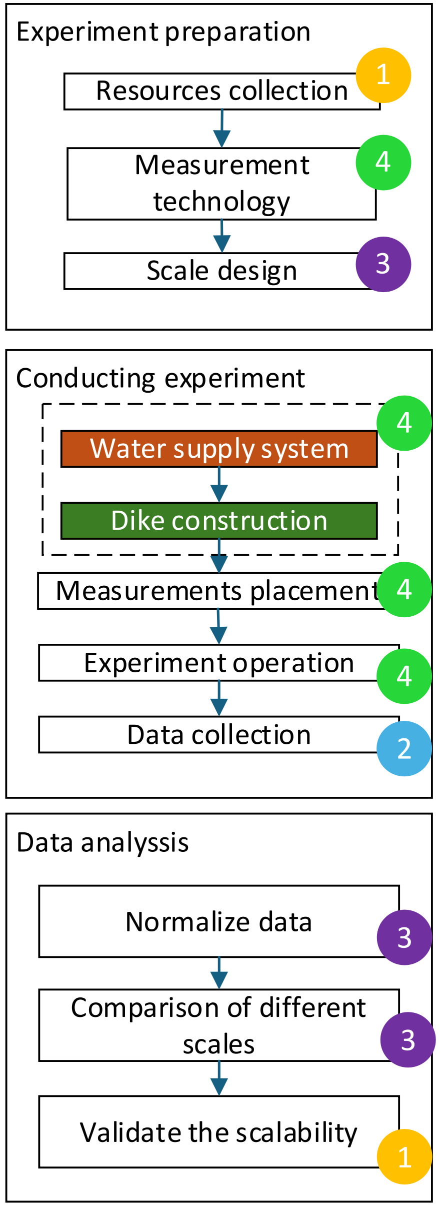

Performance parameters:

Reliability

1 Experiment data vs real word data

Repeatability

2 Multiple times experiment results comparison

Scalability

3 Comparision of normalized experiment results of different scales

Feasibility

4 Can be realized in limited experiment condition

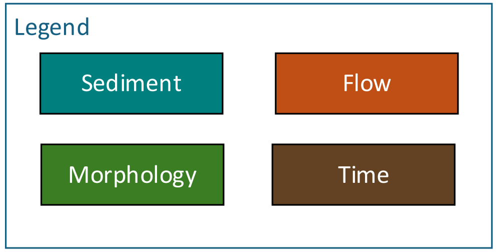

Dam Breaching Experiment Design

Physical architectures:

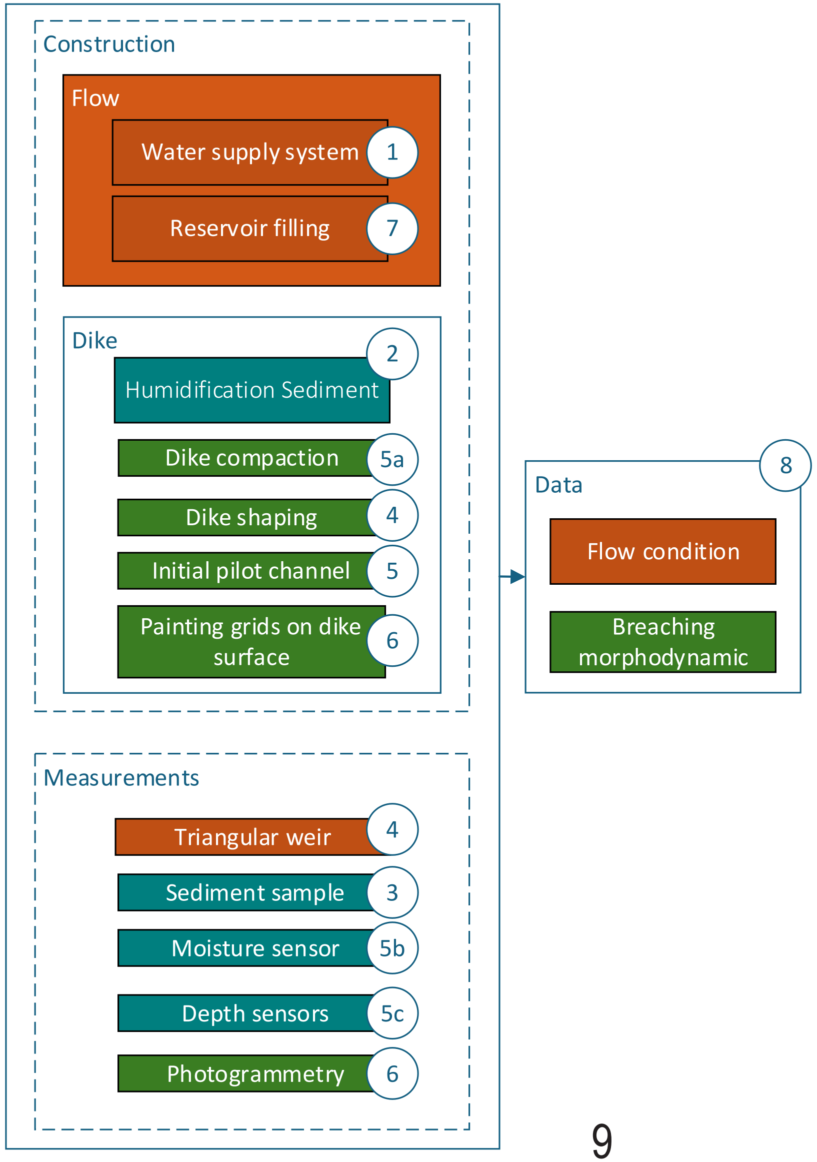

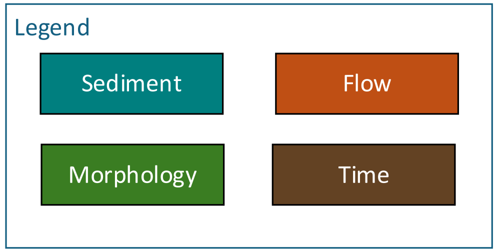

PREVIOUS DAM BREACHING EXPERIMENTS IN UCLOUVIAN

Experiment Scales

Delpierre, 2014

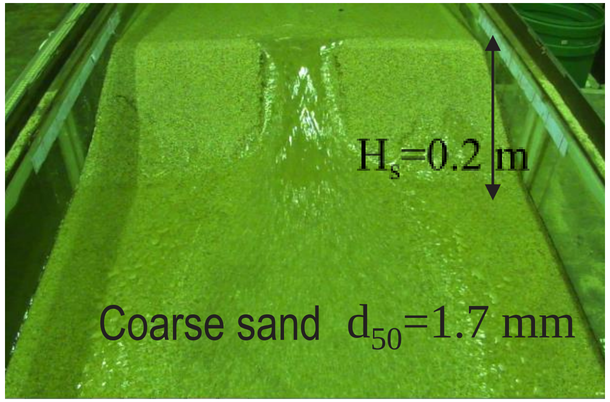

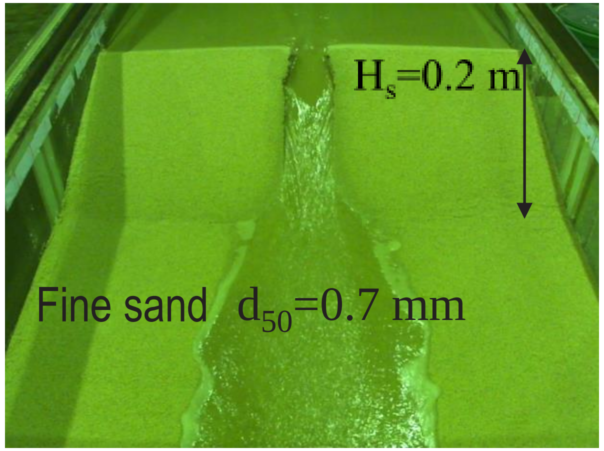

Small scale

Ebrahimi, 2024

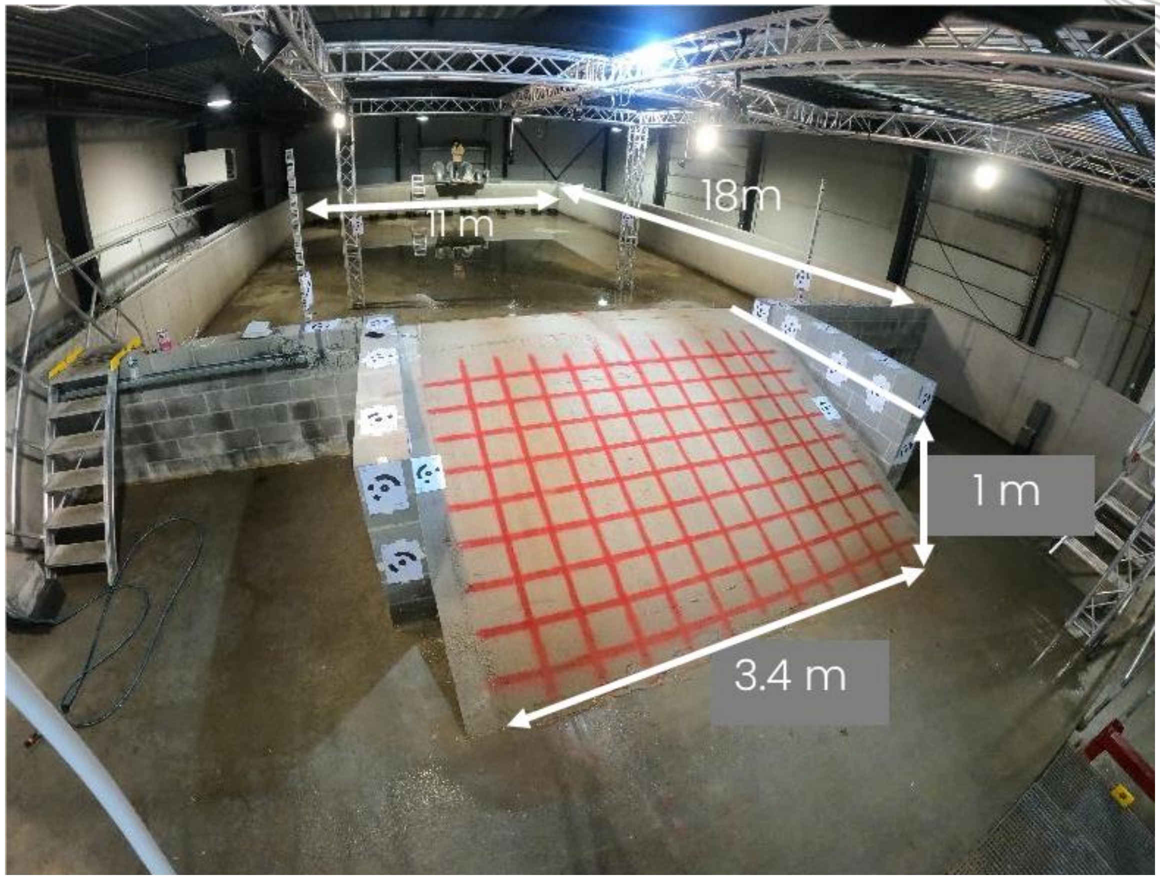

Medium scale

PREVIOUS DAM BREACHING EXPERIMENTS IN UCLOUVIAN

Water supply system

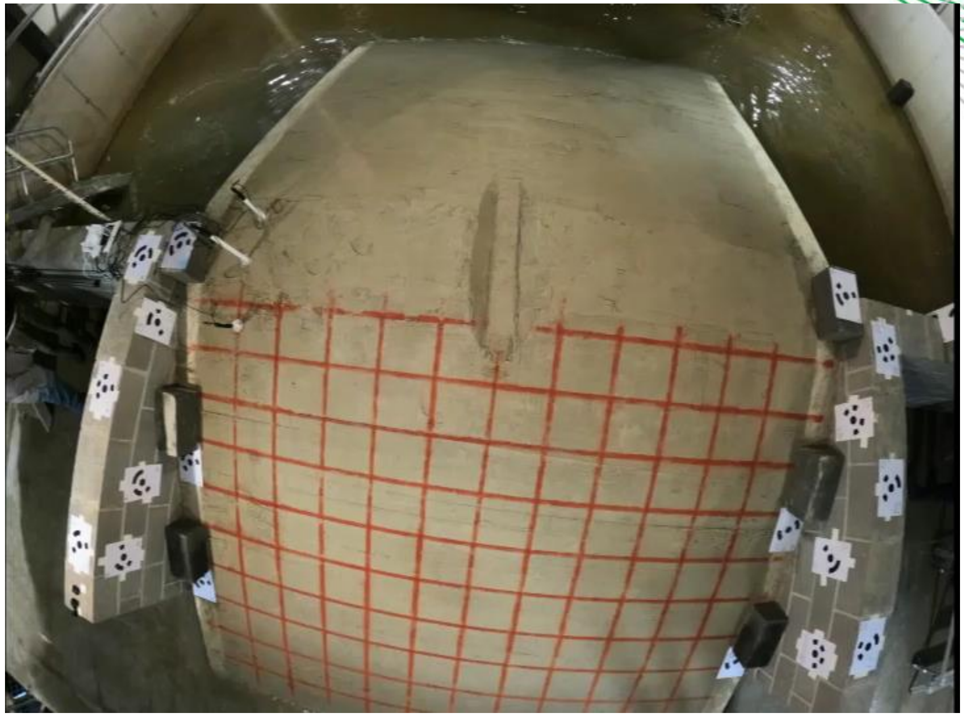

Constant inflow

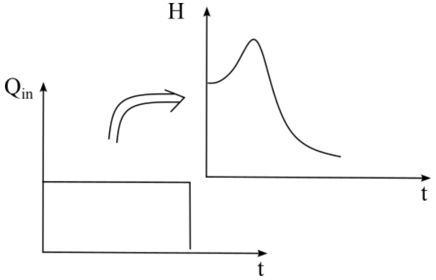

Constant water level

Or constant inflow

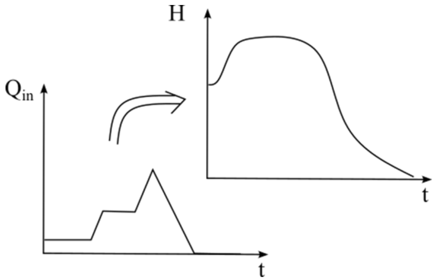

PREVIOUS DAM BREACHING EXPERIMENTS IN UCLOUVIAN

Measurement techniques

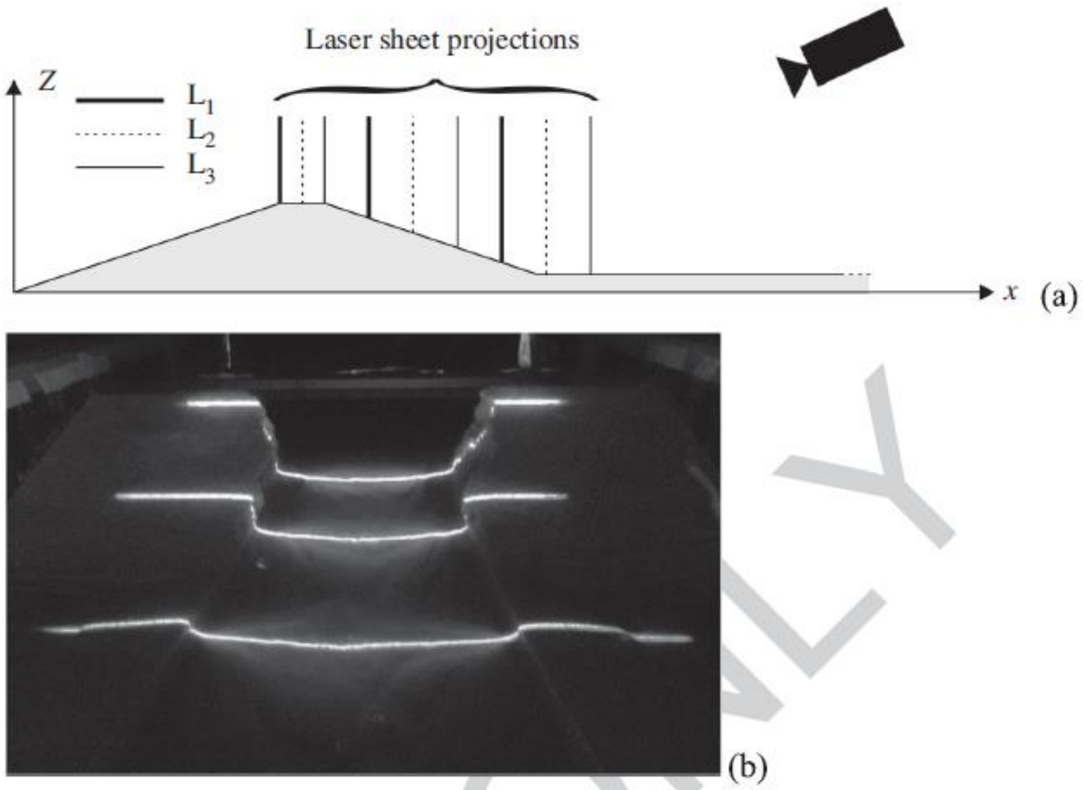

Laser-sheet and camera measurements

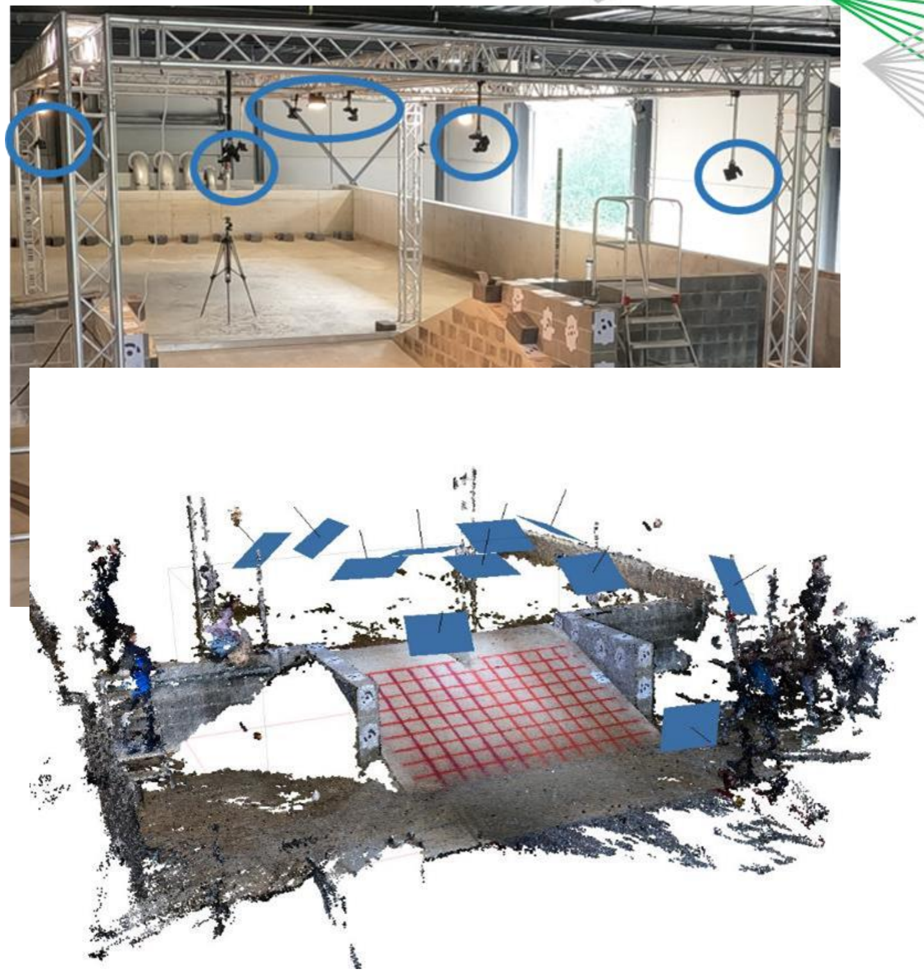

Photogrammetry


UNIVERSITY OF TWENTE
UNIVERSITY
OF TWENTE.

SEDIMARE

Sediment Transport and Morphodynamics in Marine and Coastal Waters with Engineering Solutions

UCLouvain

FUGRO

Characterization of stratification and near-bed dense layers in high-density sediment-laden flow

D.C 9- Eloah Rosas

Promoter

Benoit Spinewine

Sandra Soares

Background and motivation

Sediment-laden flow is characterized by unsteady, highly dense sediment concentrations and vertical stratification.

High-density sediment-laden flows is common in natural systems like rivers, deltas and coastal environments, and it can be initiated by natural or anthropogenic factors in the marine environment, such as:

Tsunamis, Earthquakes, Storms waves, Submarine Landslides, Dredging.

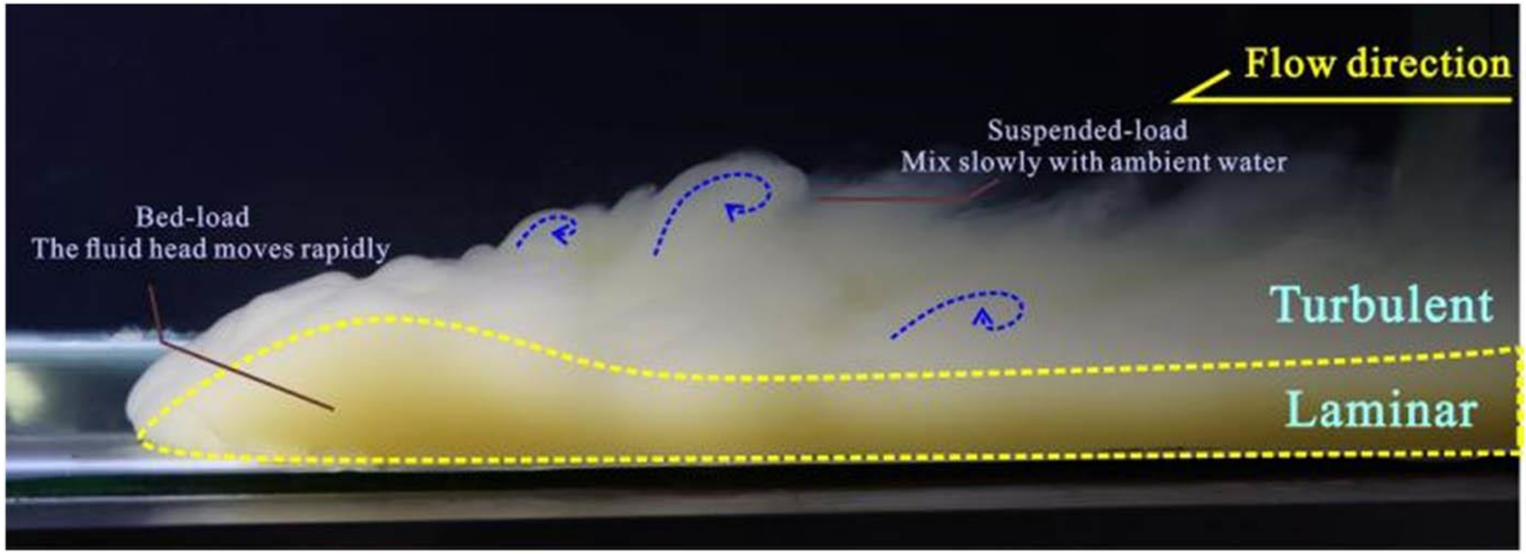

Background and Motivation

Studying the stratification and near-bed dense layers in high-density sediment-laden flows is crucial for several engineering applications, particularly in coastal and offshore infrastructure:

1. Wave-induced scour hole development around infrastructure such as wind turbines;

2. Storm-induced sheet flows on beaches causing dune instabilities and coastline retreat;

3. Turbidity currents, debris flows or submarine landslides posing a significant threat to pipelines or large submarine power cables

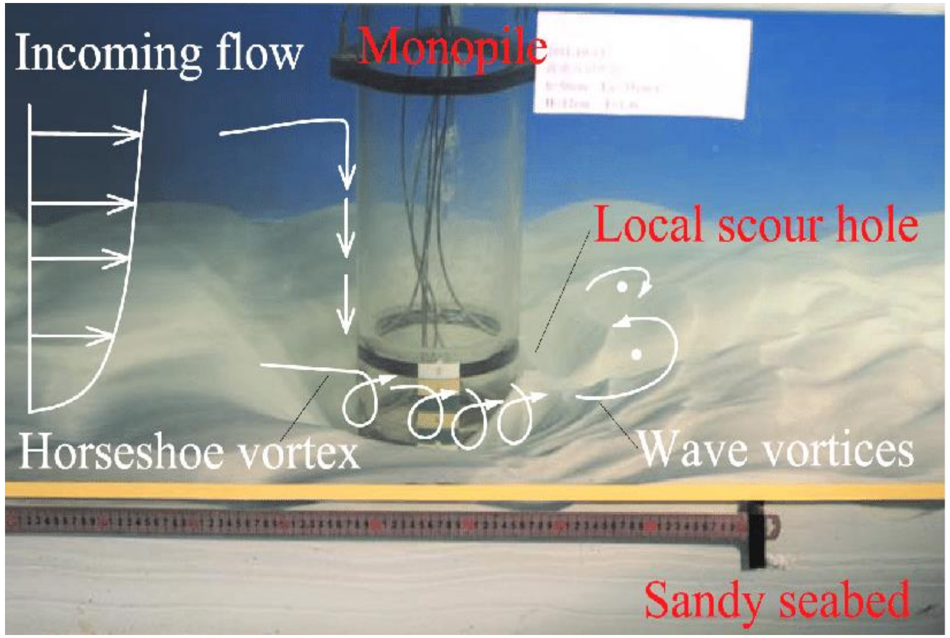

Flow pattern involving scour around monopile. Gao, F., & Qi, W. (2022).

Background and Motivation

Studying the stratification and near-bed dense layers in high-density sediment-laden flows is crucial for several engineering applications, particularly in coastal and offshore infrastructure:

1. Wave-induced scour hole development around infrastructure such as wind turbines;
2. Storm-induced sheet flows on beaches causing dune instabilities and coastline retreat;
3. Turbidity currents, debris flows or submarine landslides posing a significant threat to pipelines or large submarine power cables

Broken cables due to the turbidity currents and submarine landslides in Kaoping Canyon subsquently two earthquakes. Hsu et al. (2008).

Background and Motivation

Studying these flows involves a combination of **field observations,** laboratory experiments, and numerical simulations

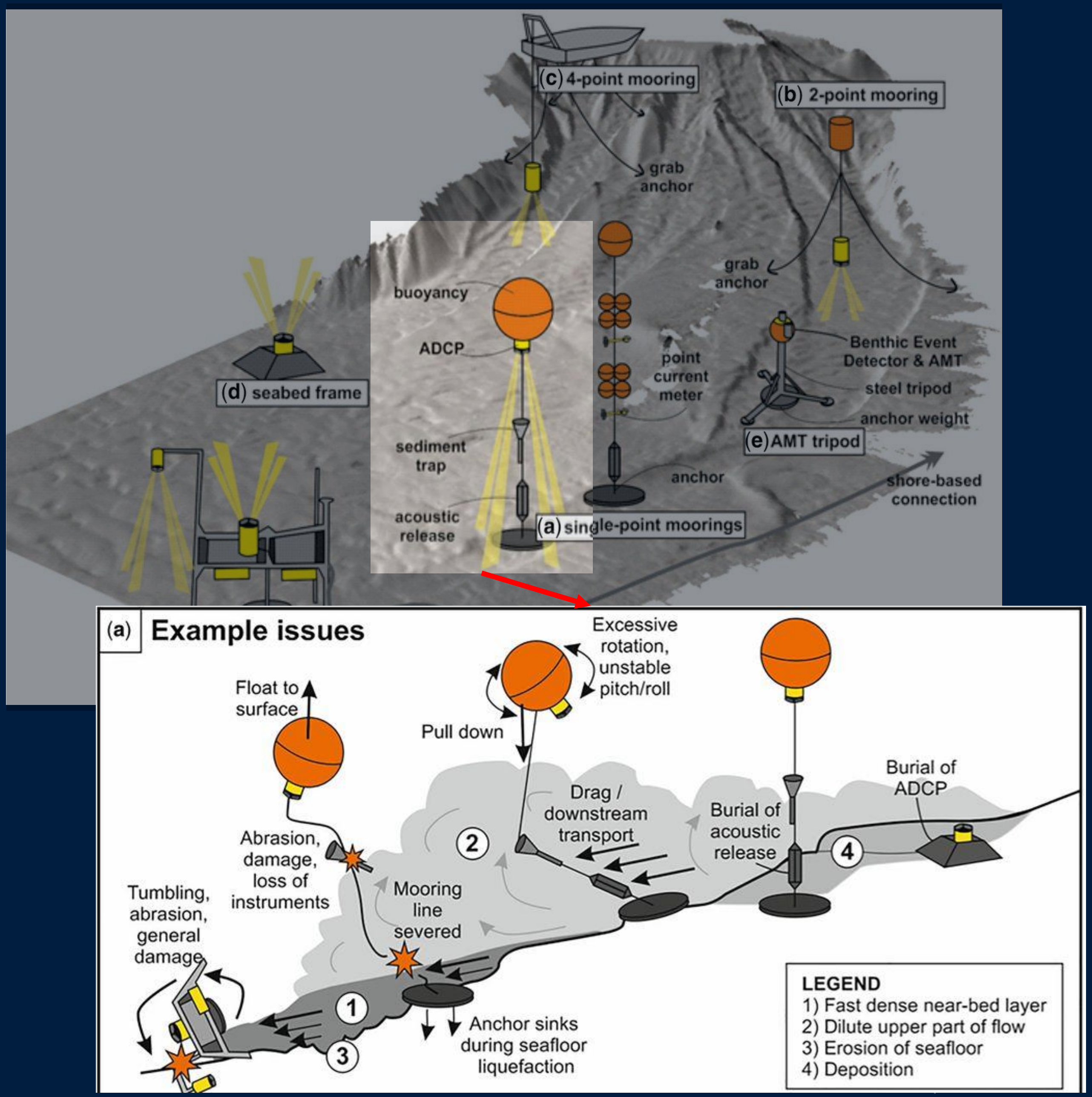

Background and Motivation

Studying these flows involves a combination of field observations**,** **laboratory experiments**, and **numerical simulations**

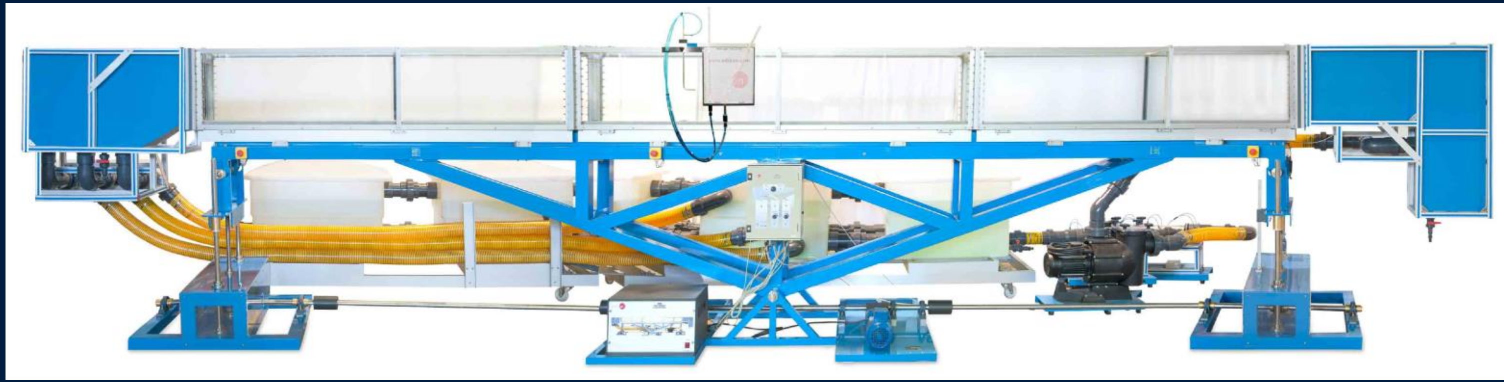

Background and Motivation

Bagnold **Sumer**	**Capart** **Spinewine**	**Armanini** **Francarollo**	**Matousek**
Close Duct Flume	Recirculating tilting Flume (6 m x 0.25 m x 0.70 m) Vertical gate at the middle section	Recirculating tilting Flume Conveyor belt recirculating sediment Dams	Recirculating Tilting Flume (8 m x 0.2 m x 0.27m)
Pressure sensors CCM Prandtl tube	High Speed CCD Camera Laser light sheet	High Speed CCD Camera	High Speed camera Laser UVP (4 MHz); Prandl tube Ultrasonic water level
Coefficient Friction Bedload power law velocity in the sheet flow	• Comprehensive characterization of flow regimes • Detailed profiles of velocity and granular concentration at different depths • Enhanced shallow water equations with vertical details	• Stratified flow with sub-layers • Transitions between sub-layer-based Stokes number • Richardson number constant in collisional.	• New linear equation • Measured local velocity and granular temperature in bedload. • layered structure in sediment with three sublayers based on the dominant transport method • Transport model with position of the interfaces of sublayers.

Background and Motivation

Bagnold

Sumer

Close

Duct Flume

Pressure sensors

CCM

Prandtl tube

Coefficient Friction Bedload

power law velocity in the sheet flow

Capart

Spinewine

Recirculating tilting Flume
(6 m x 0.25 m x 0.70 m)

Vertical gate at the middle section

High Speed CCD Camera

Laser light sheet

- Comprehensive characterization of flow regimes
- Detailed profiles of velocity and granular concentration at different depths
- Enhanced shallow water equations with vertical details

Armanini

Francarollo

Recirculating tilting Flume
Conveyor belt recirculating sediment
Dams

High Speed CCD Camera

- Stratified flow with sub-layers
- Transitions between sub-layer-based Stokes number
- Richardson number constant in collisional.

Matousek

Recirculating Tilting Flume
(8 m x 0.2 m x 0.27m)

High Speed camera

Laser

UVP (4 MHz);

Prandl tube

Ultrasonic water level

- New linear equation
- Measured local velocity and granular temperature in bedload.
- layered structure in sediment with three sublayers based on the dominant transport method
- Transport model with position of the interfaces of sublayers.

Background and Motivation

Bagnold
Sumer

Close

Duct Flume

Pressure sensors

CCM

Prandtl tube

Coefficient Friction Bedload

power law velocity in the sheet flow

Capart
Spinewine

Recirculating tilting Flume (6 m x 0.25 m x 0.70 m)

Vertical gate at the middle section

High Speed CCD Camera

Laser light sheet

- Comprehensive characterization of flow regimes
- Detailed profiles of velocity and granular concentration at different depths
- Enhanced shallow water equations with vertical details

Armanini
Francarollo

Recirculating tilting Flume
Conveyor belt recirculating sediment

High Speed Camera

- Stratified flow with sub-layers
- Transitions between sub-layer-based Stokes number
- Richardson number constant in collisional.

Matousek

Recirculating Tilting Flume (8 m x 0.2 m x 0.27m)

High Speed camera

Laser

UVP (4 MHz);

Prandl tube

Ultrasonic water level

- New linear equation
- Measured local velocity and granular temperature in bedload.
- layered structure in sediment with three sublayers based on the dominant transport method
- Transport model with position of the interfaces of sublayers.

Background and Motivation

Bagnold Sumer	Capart Spinewine	Armanini Francarollo	Matousek
Close Duct Flume	Recirculating tilting Flume (6 m x 0.25 m x 0.70 m) Vertical gate at the middle section	Recirculating tilting Flume Conveyor belt recirculating sediment Dams	Recirculating Tilting Flume (8 m x 0.2 m x 0.27m)
Pressure sensors CCM Prandtl tube	High Speed CCD Camera Laser light sheet	High Speed CCD Camera	High Speed camera Laser UVP (4 MHz); Prandl tube Ultrasonic water level
Coefficient Friction Bedload power law velocity in the sheet flow	• Comprehensive characterization of flow regimes • Detailed profiles of velocity and granular concentration at different depths • Enhanced shallow water equations with vertical details	• Stratified flow with sub-layers • Transitions between sub-layer-based Stokes number • Richardson number constant in collisional.	• New linear equation • Measured local velocity and granular temperature in bedload. • layered structure in sediment with three sublayers based on the dominant transport method • Transport model with position of the interfaces of sublayers.

Background and Motivation

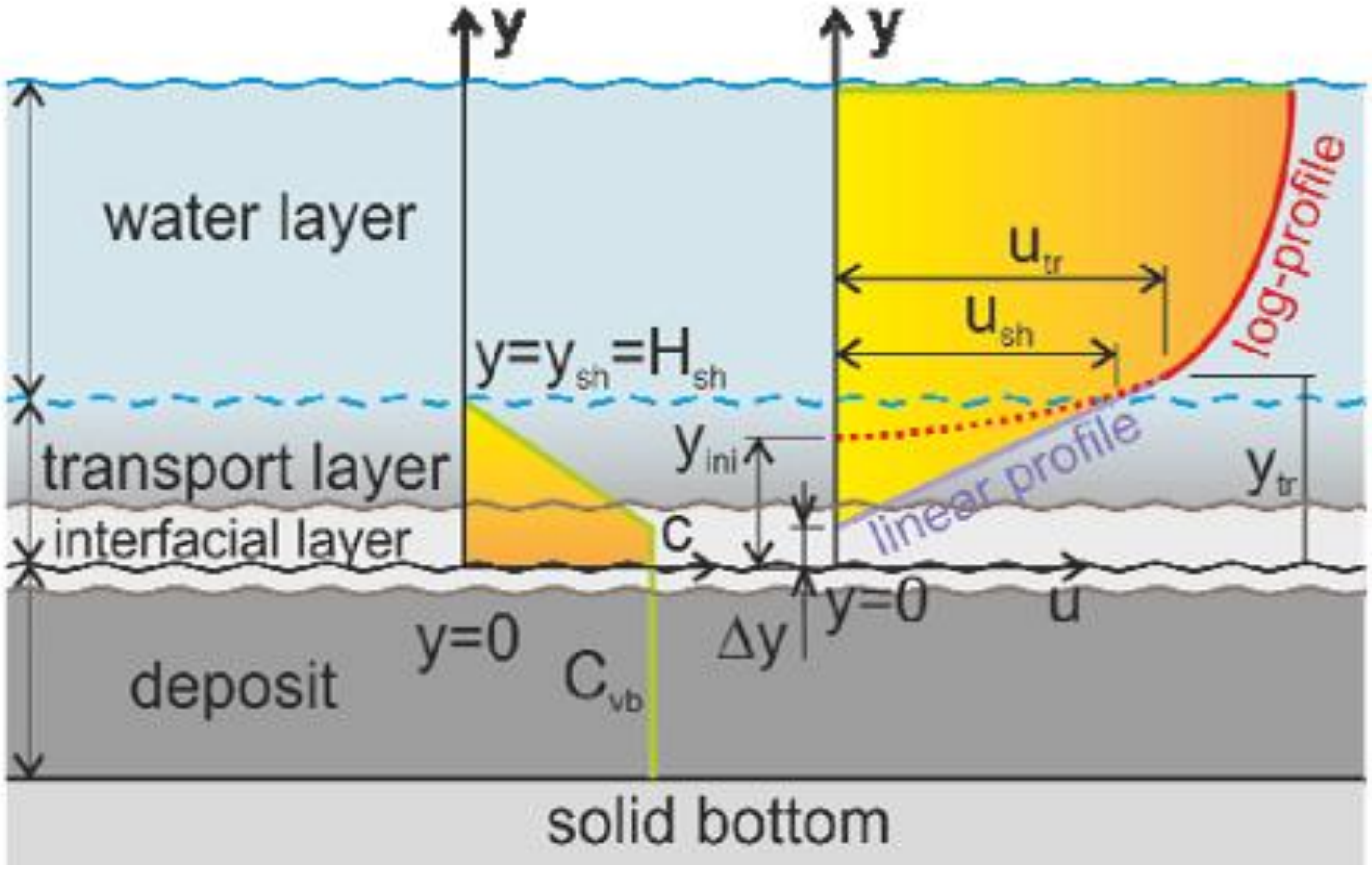

Matousek

Recirculating Tilting Flume
(8 m x 0.2 m x 0.27m)

High Speed camera

Laser

UVP (4 MHz);

Prandl tube

Ultrasonic water level

- New linear equation
- Measured local velocity and granular temperature in bedload.
- layered structure in sediment with three sublayers based on the dominant transport method
- Transport model with position of the interfaces of sublayers.

Objectives

1. Propose a **multi-layer shallow-water modelling** framework, and propose **practical parametrizations of inter-layer exchange processes** that may capture the behaviour of dense near-bed layers;

2. **Calibrate** these relations with well-controlled **small-scale laboratory experiments**

3. **Confront** the results with **documented case studies** or direct **field-scale observations**

Three-tier approach

1. Experimental results comparison
2. Validity of experimental setup assessment
3. Statistical interpretation

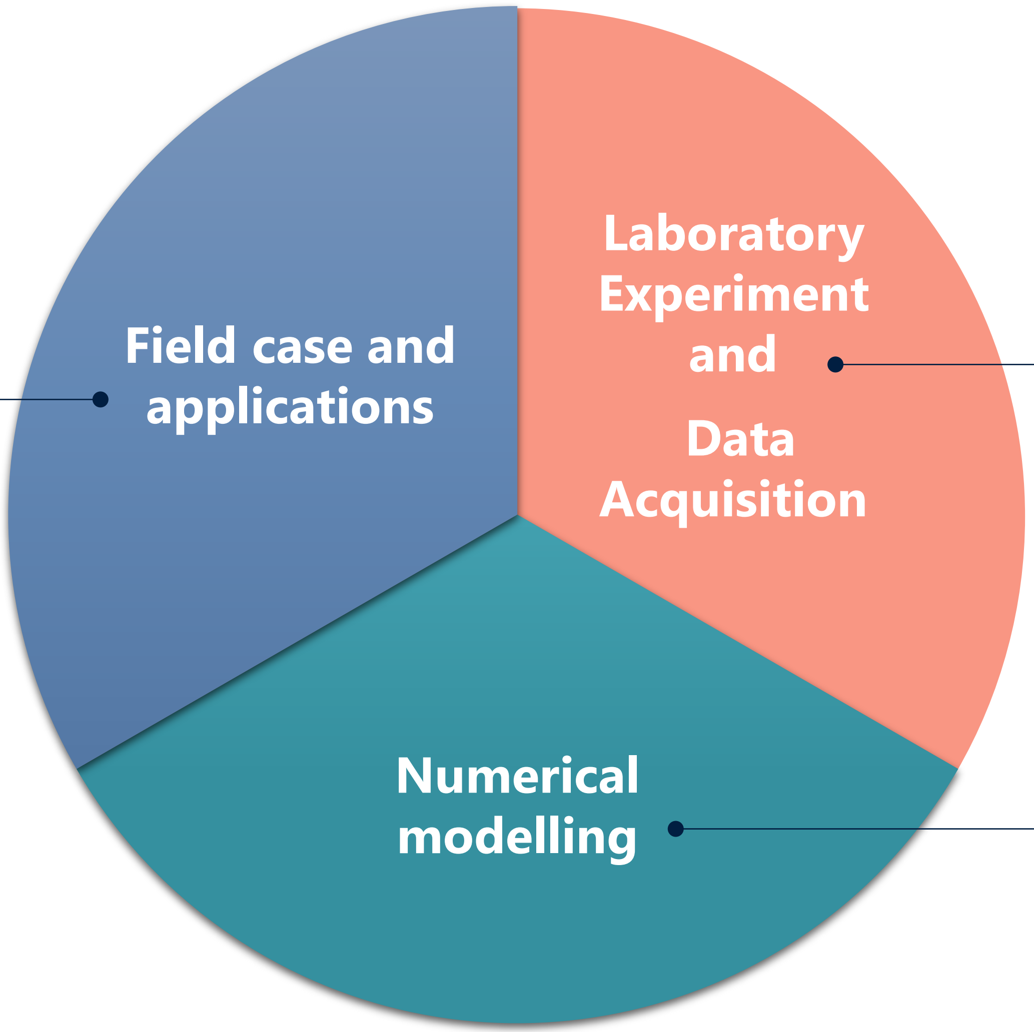

1. Flume experiments setup
2. Appropriate instrument installation

1. Implementation of acquired inputs
2. Process and modelling
3. Advanced interpretive

Three-tier approach

Setup 1: "Submerged Granular Column Collapse" experiments at UCL

- Experimental setup readily available
- Detailed measurements of sediment velocities in transport layer

Setup 2: "modular tilting / adverse slope flume " at Fugro or UCLouvain

- Configuration 1: rapid tilting of flume with a sediment layer initially at rest:
- Configuration 2: steady liquid-granular flow on adverse slope (water goes up, sediment goes down)

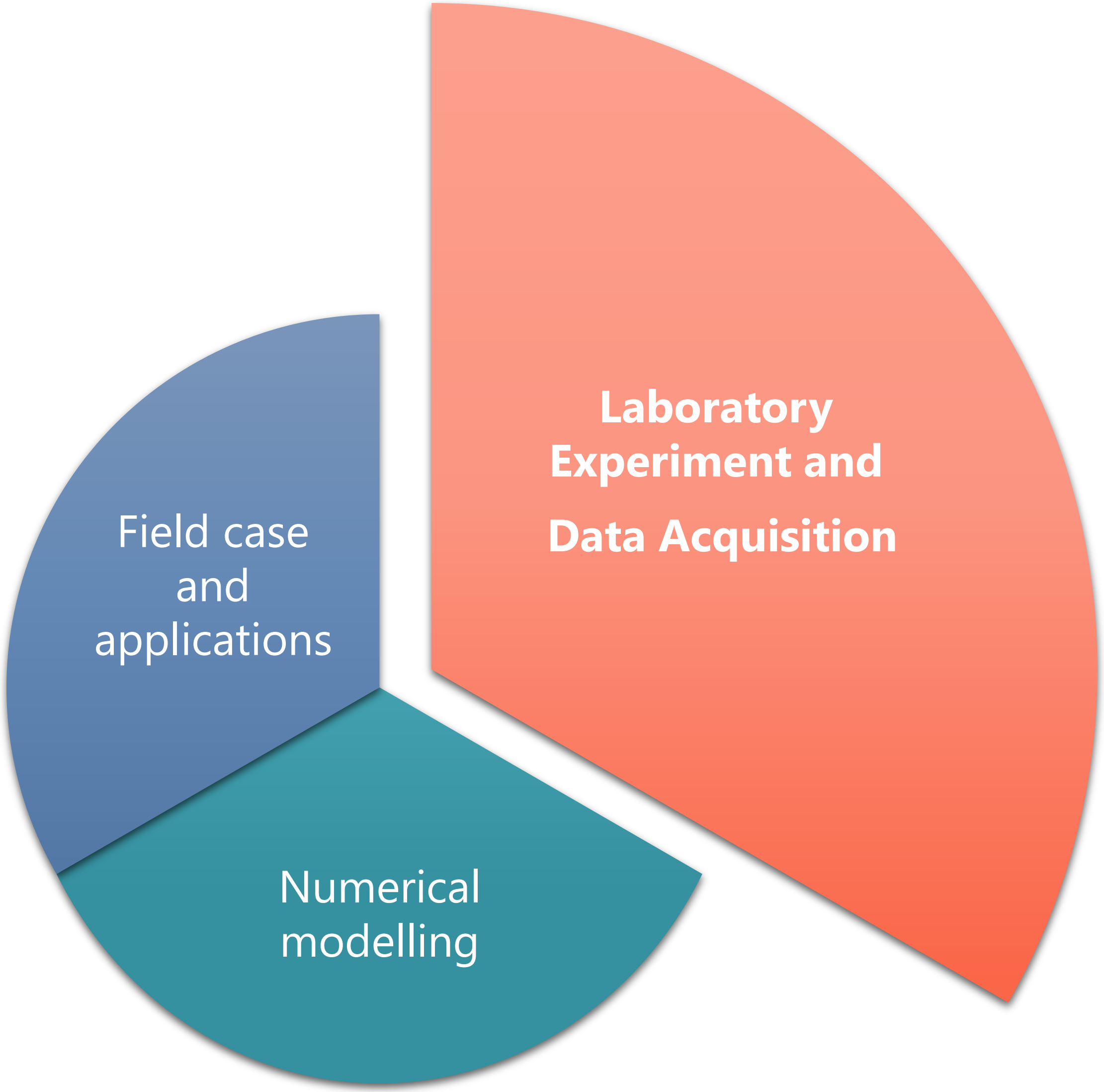

Thorpe Flume

Channel

- Length - 1830 mm
- Width – 100 mm
- Height – 30 mm
- Glass walls

Flume

- Tilting using Eletric Jack
- Tilting angle – 4.13 in 0.45 s

Duponcheel et al. 2017

Modifications Thorpe flume

New Channel

- Length - 3000 mm
- Width – 100 mm
- Height – 300 mm
- Transparent Plexiglas sidewalls

Tilting

- Tilting using Electric Jack
- \+ 20 °

Sediments Type

- Natural sediment (fine sediment – silt/ clay)
- Plastic grains (3 – 4 mm)

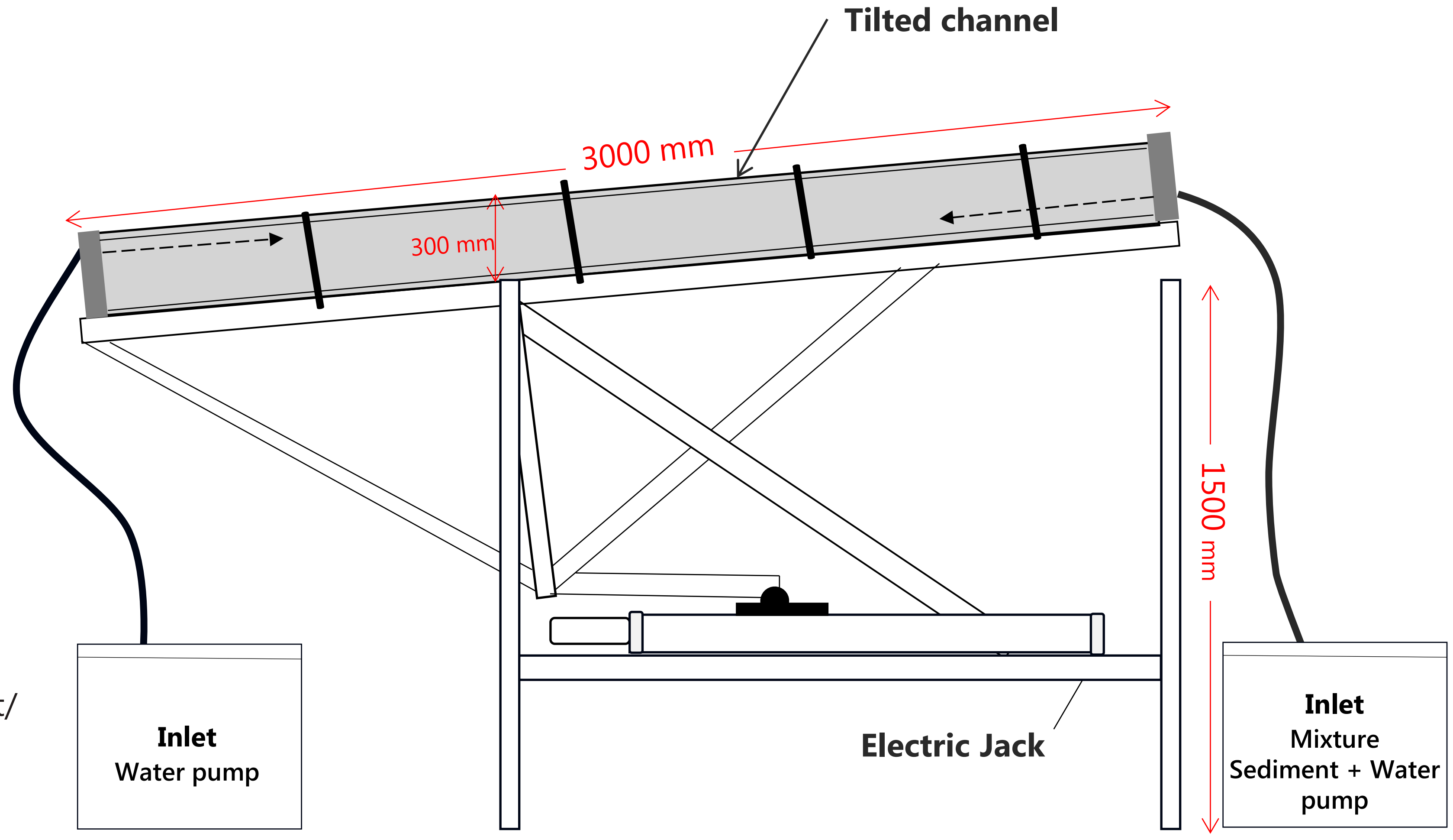

Measuring Procedures

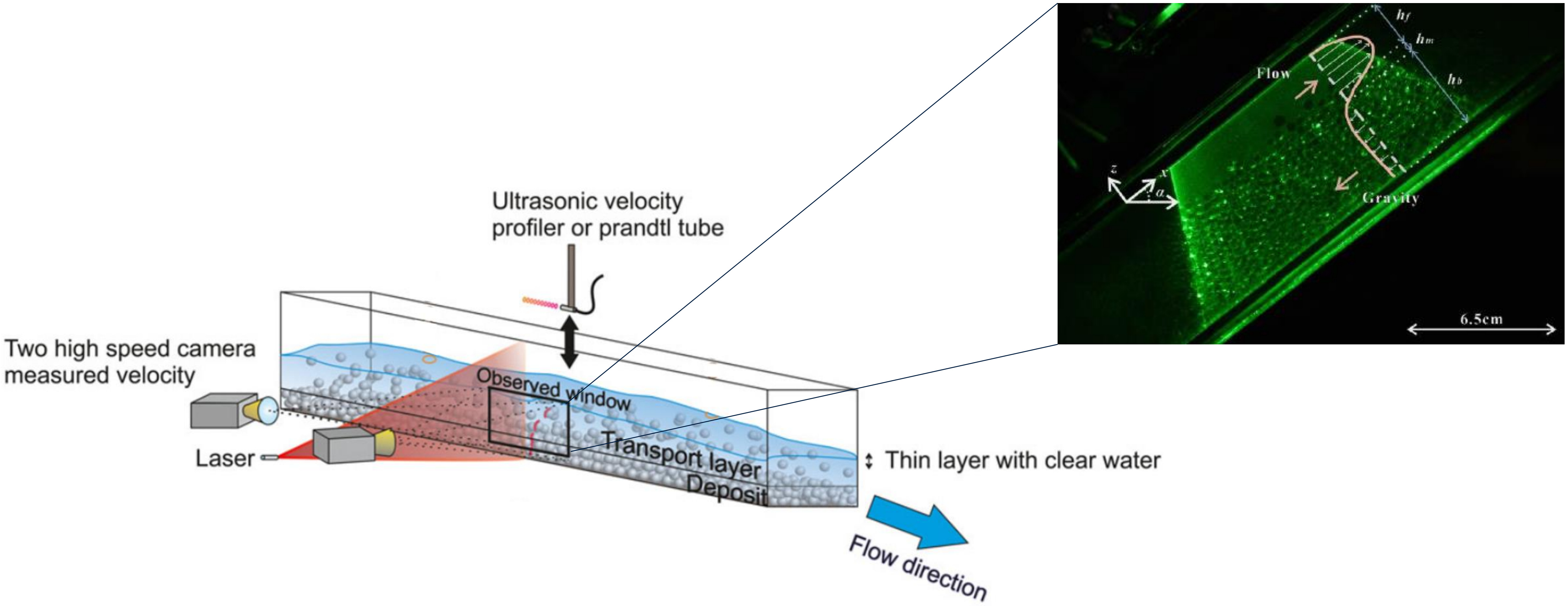

SEDIMARE

Sediment Transport and Morphodynamics in Marine and Coastal Waters with Engineering Solutions

UCLouvain

FUGRO

Characterization of stratification and near-bed dense layers in high-density sediment-laden flow

Eloah Rosas

e.rosas@fugro.com

Overtopping Breakwater For Energy Conversion (OBREC)

Saeed Osouli

Supervisors:

Prof. Matteo Postacchini – UNIVPM

DR. Ivan Sabbioni – MAC

Prof. Maurizio Brocchini – UNIVPM

SEDIMARE

2nd Network Training School: Experimental and Practical Modelling of Sediment Transport and Coastal Morphology

University of Twente/Deltares

5-8 November 2024

Outline

1. Introduction
2. Comparing and Selecting Data
3. Shallow water Solver
4. CFD Module
5. Conclusion

Motivations

- Advantages that characterize Wave energy:

❑ The high energy density.

❑ The easy prediction of the wave characteristics.

❑ The reduced energy loss

- Drawbacks:

❑ The high variability of the wave characteristic.

❑ WECs are exposed to large environmental forces.

❑ High production costs compared.

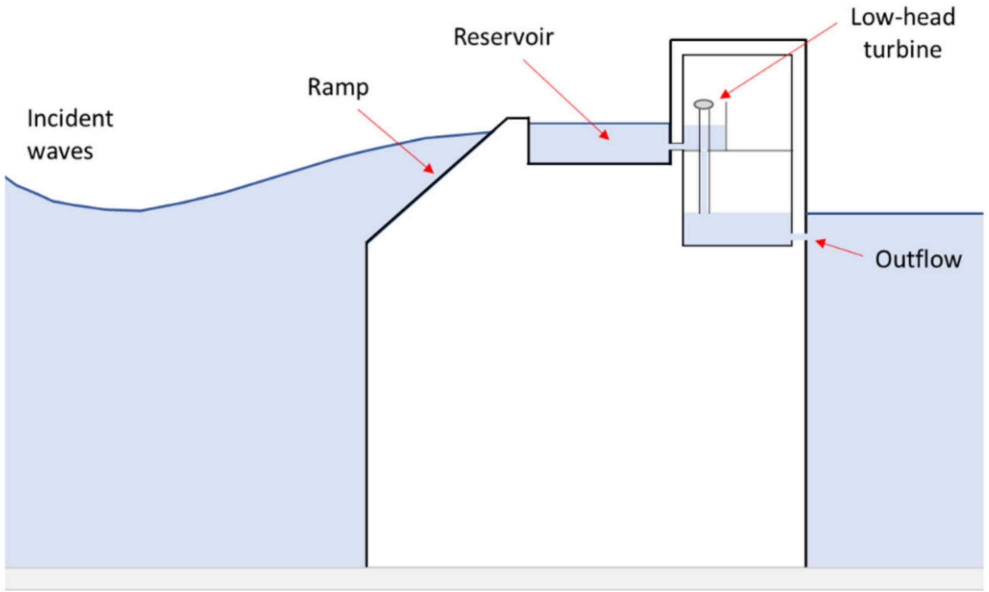

Scheme of the OTD integrated into a vertical caisson breakwater

Literature review

- OBREC

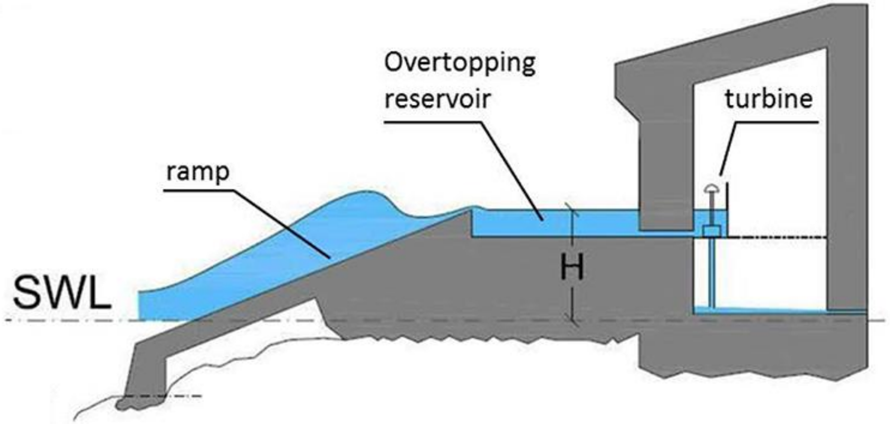

C. Iuppa, et al. Coastal Engineering 152 (2019) 103524

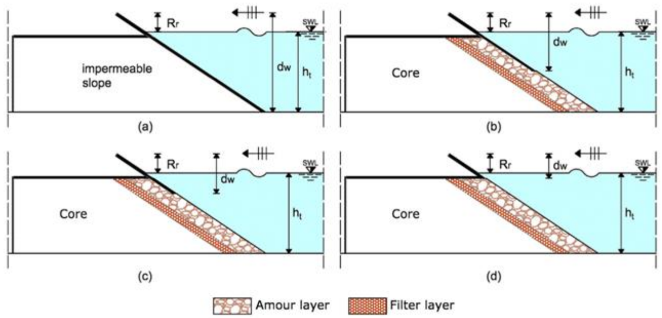

Fig. 3. OBREC configurations analyzed in the present experimental campaign: a) $d_w = 0.274$ m ($d_w^* = 1.0$); b) d_w 0.166 m ($d_w^* = 0.6$); c) $d_w = 0.113$ m ($d_w^* = 0.4$); d) $d_w = 0.064$ m ($d_w^* = 0.2$). R_r indicates the crest free-board and h_t indicates the water depth at the model toe.

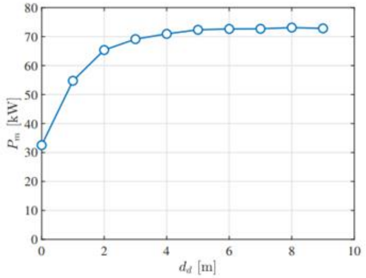

Figure 9. Yearly average output power versus the variation of d_d ($N = 50$, $R_r = 2.5$ m and $h_s = 2$ m).

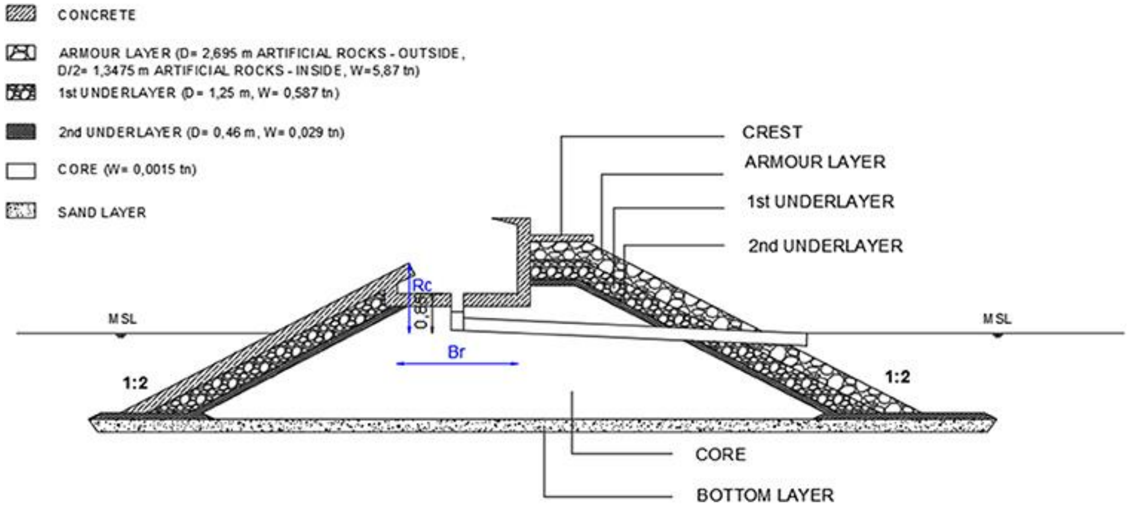

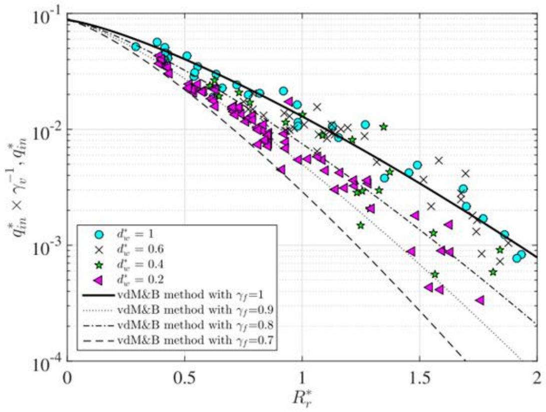

Fig. 8. Comparison of the average wave overtopping rates measured for all configurations tested in the present tests and those estimated by the prediction method of van der Meer and Bruce (2013) adopting four different values of γ_f. The experimental data were corrected using the coefficient γ_V.

Observed and Model data

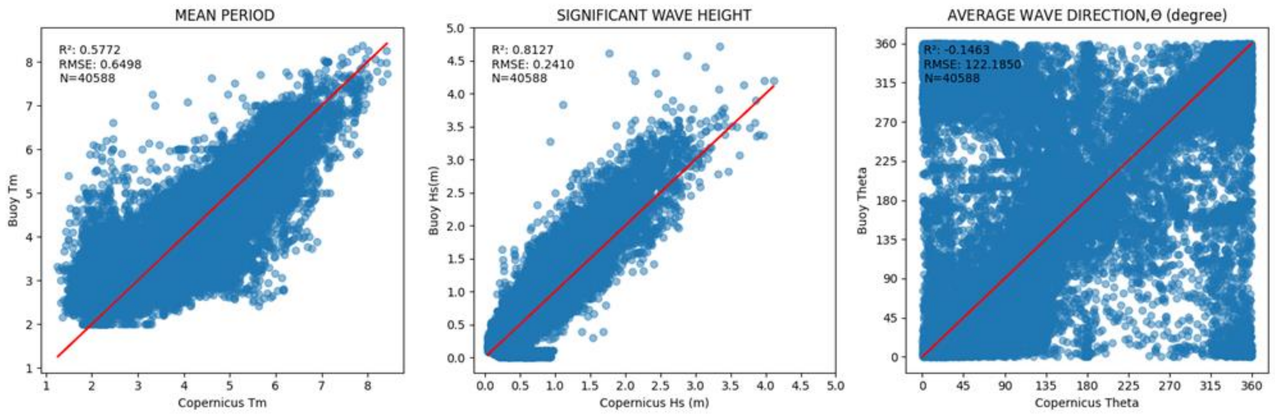

Comparison of wave parameters from buoy and Copernicus.

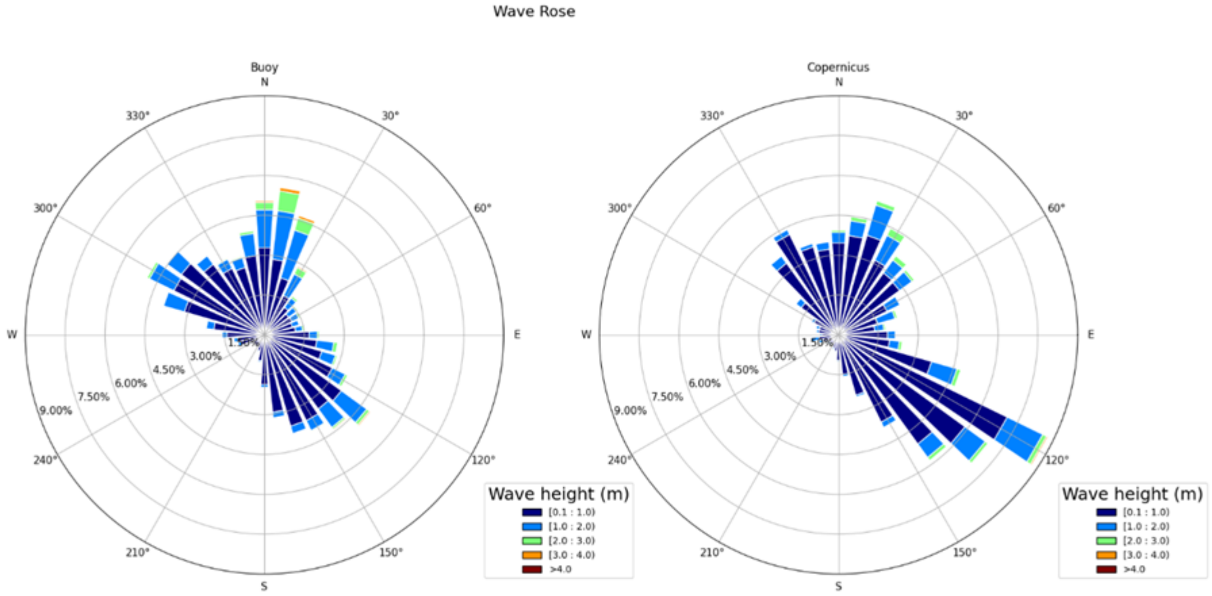

Wave Roses.

Wave selection

- min, max and average wave Heights based on 10-year average.
- Extreme Wave Conditions (EWC), with a 100-year return period, and Average Wave Conditions (AWC).
- Joint density functions.

Bivariate density contour lines of Tm and Hs corresponding to $p = 5 \cdot 10{-}3$

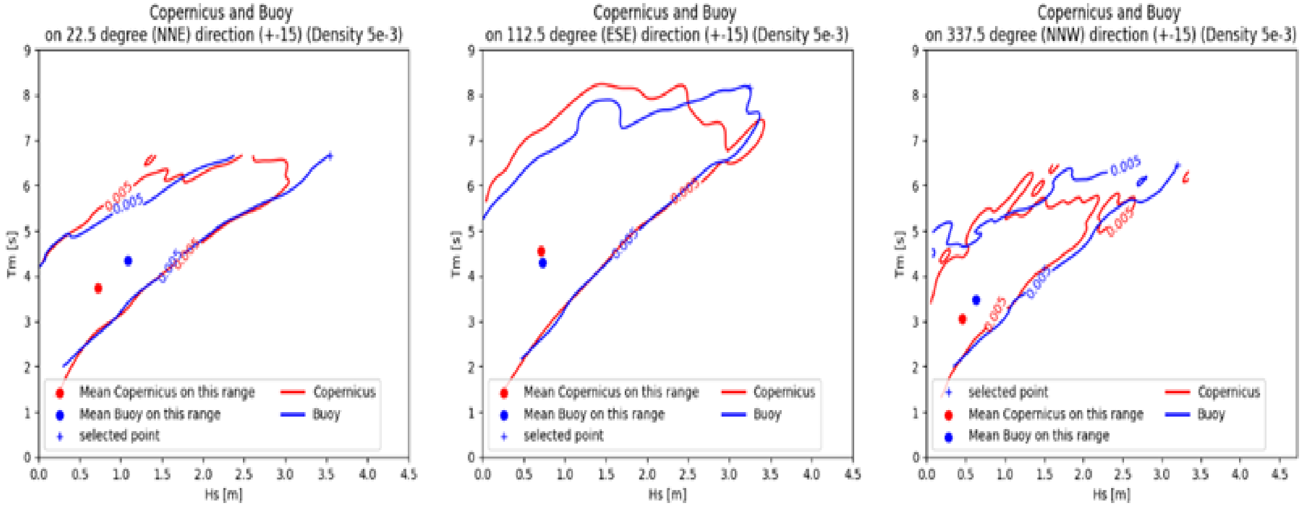

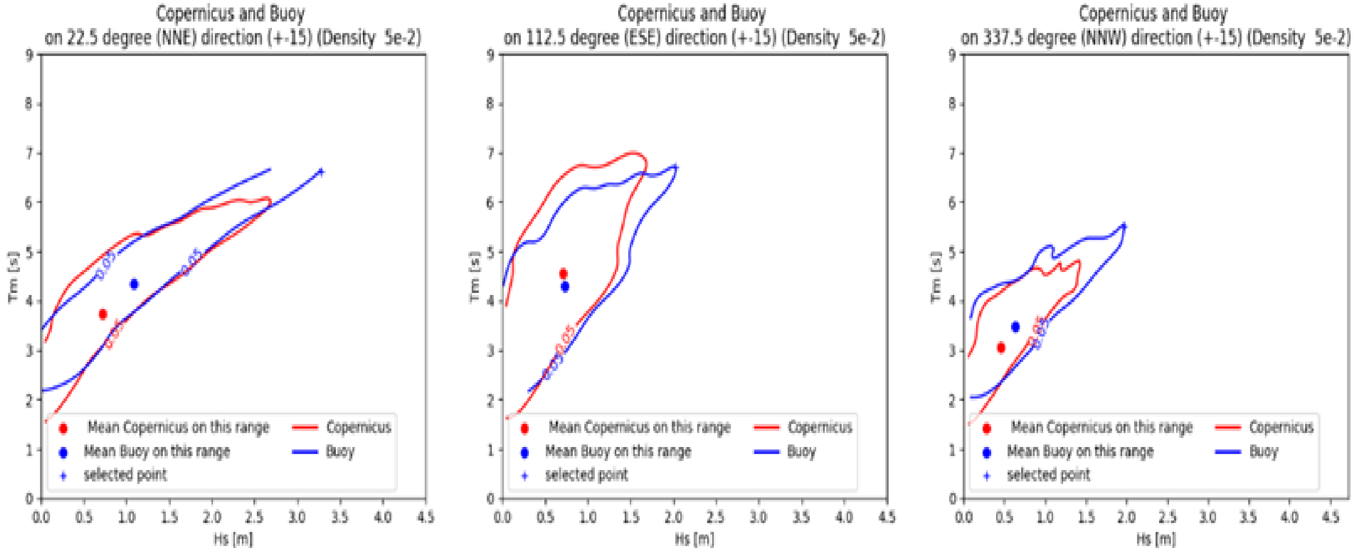

Bivariate density contour lines of Tm and Hs corresponding to $p = 5 \cdot 10{-}2$

Wave characteristics at the Buoy Location and numerical domain

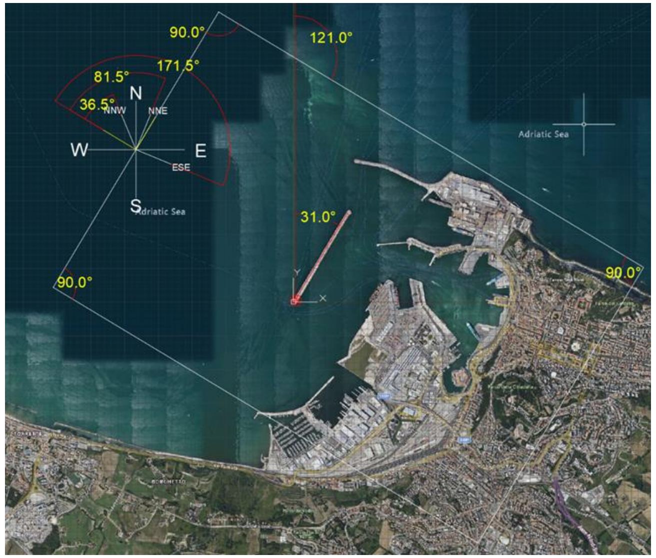

Inclination due to the boundary.

- ❑ Phase-averaged (ROMS-SWAN)
- ❑ Analytical model (Goda 201

		NNE	ESE	NNW
Mean	Hs (m)	1.09		0.63
	Tm (s)	4.35		3.49
	α (Respect to the North) [°]	22.5		337.5
	αp0(Respect to orthogonal line to boundary of the numerical domain) [°]	81.50		36.50
Density 0.05	Hs (m)	3.28		1.97
	Tm (s)	6.62		5.52
	α (Respect to the North) [°]	22.5		337.5
	αp0(Respect to orthogonal line to boundary of the numerical domain) [°]	81.50		36.50
Density 0.005	Hs (m)	3.54		3.2
	Tm (s)	6.67		6.46
	α (Respect to the North) [°]	22.5		337.5
	αp0(Respect to orthogonal line to boundary of the numerical domain) [°]	81.50		36.50

Wave characteristics at the Buoy Location.

		NNE	ESE	NNW
Mean	Hs (m)	0.90		0.59
	Tp (s)	5.13		4.12
	ap,h1 [°]	56.00		35.00
Density 0.05	Hs (m)	2.53		1.67
	Tp (s)	7.81		6.51
	ap,h1 [°]	35.00		27.00
	Hs			

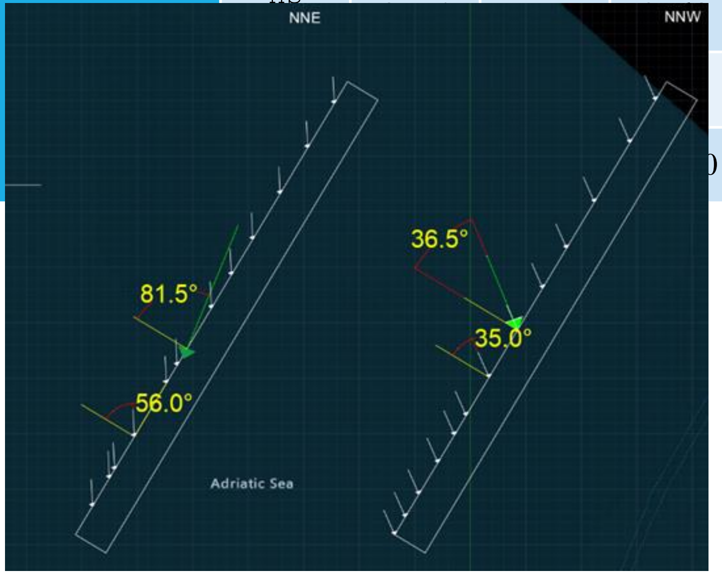

Transformation and Deformation of Sea Waves.

Monochromatic wave with similar characteristics of transforı

(Tp = 7.81 s and Hs = 2.53 m, theta = 35 degree)

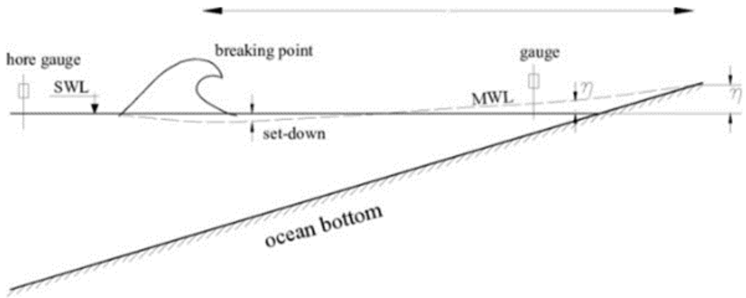

a set down and set up in coastal regions

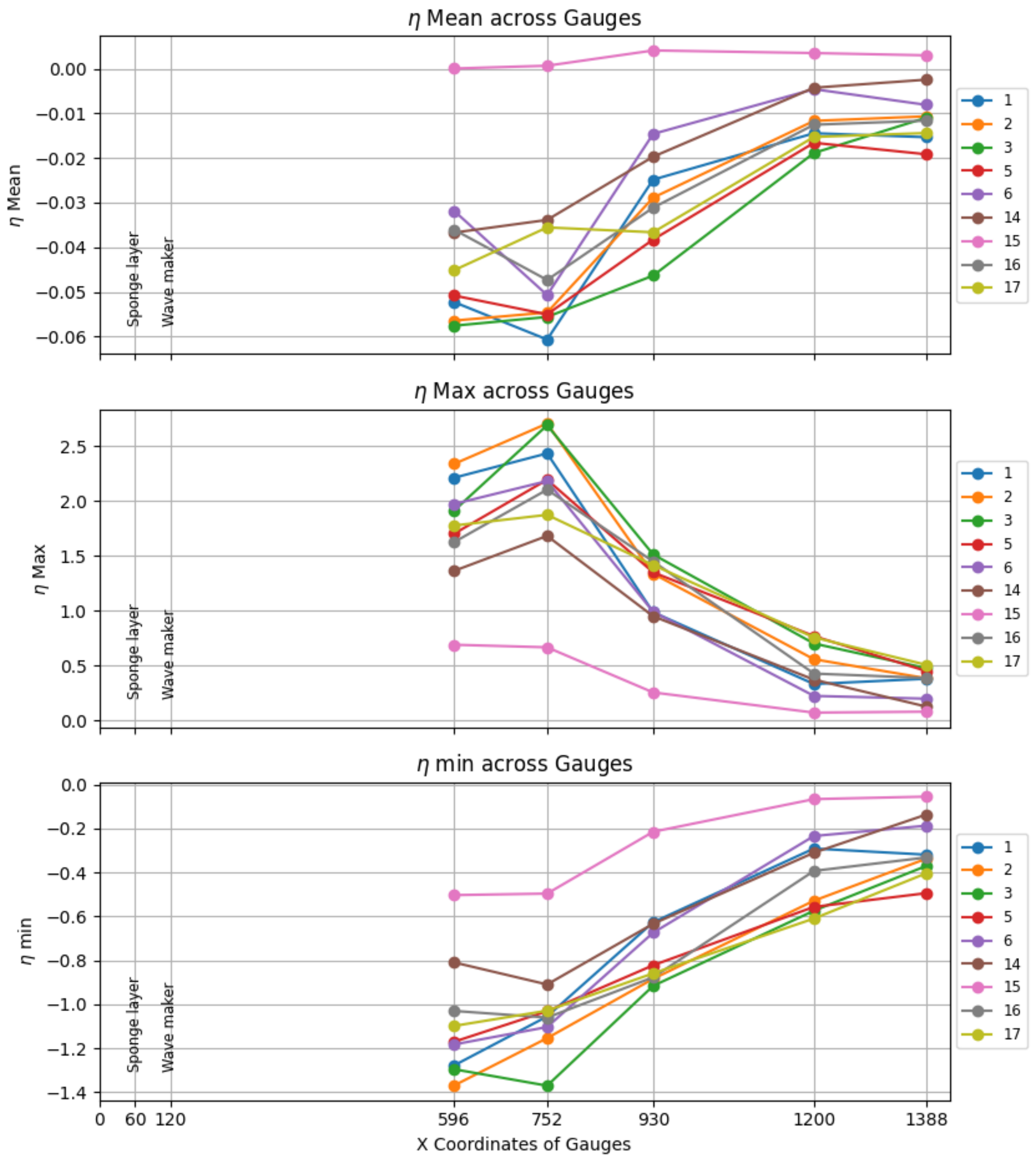

✓ Some simulations such as 6,14 and 15 are off.

(larger grid size and small domain)

✓ Simulations in which the depth of wavemaker was set to higher value provides much more energy. (3 and 17)

Configuration 3 was selected for next simulations.

Simulation time : 500 waves for each scenarios.

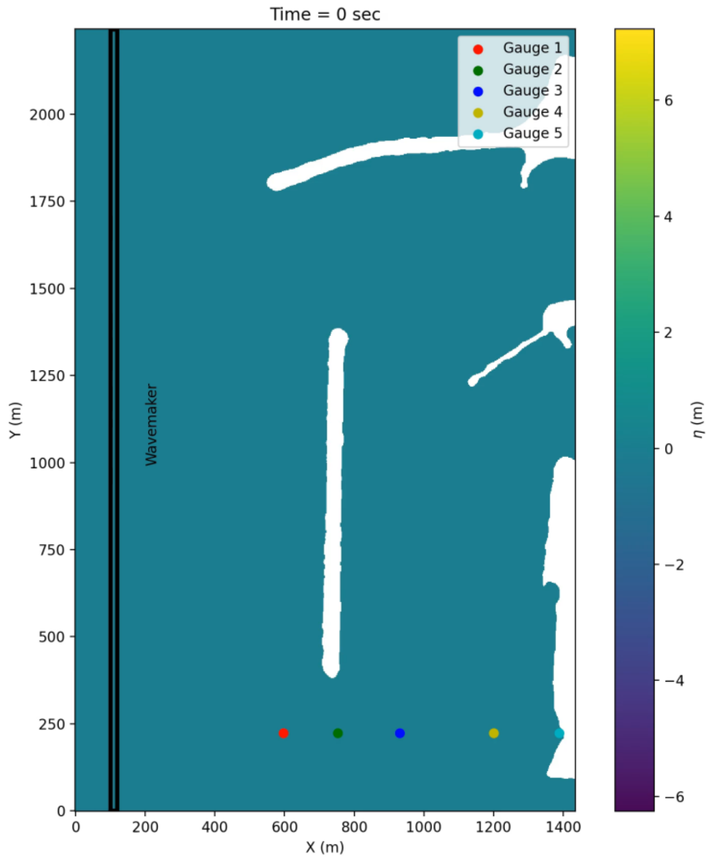

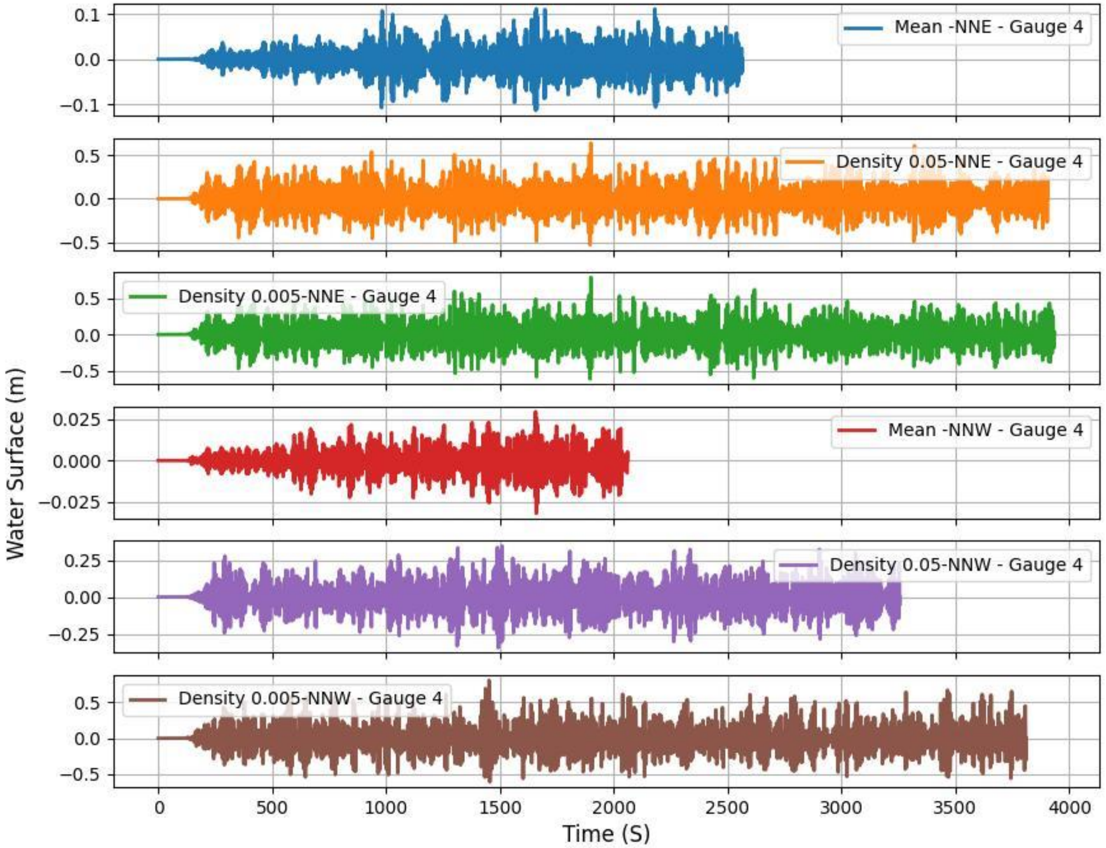

NNE Waves with 0.05 Density

FUNWAVE-TVD

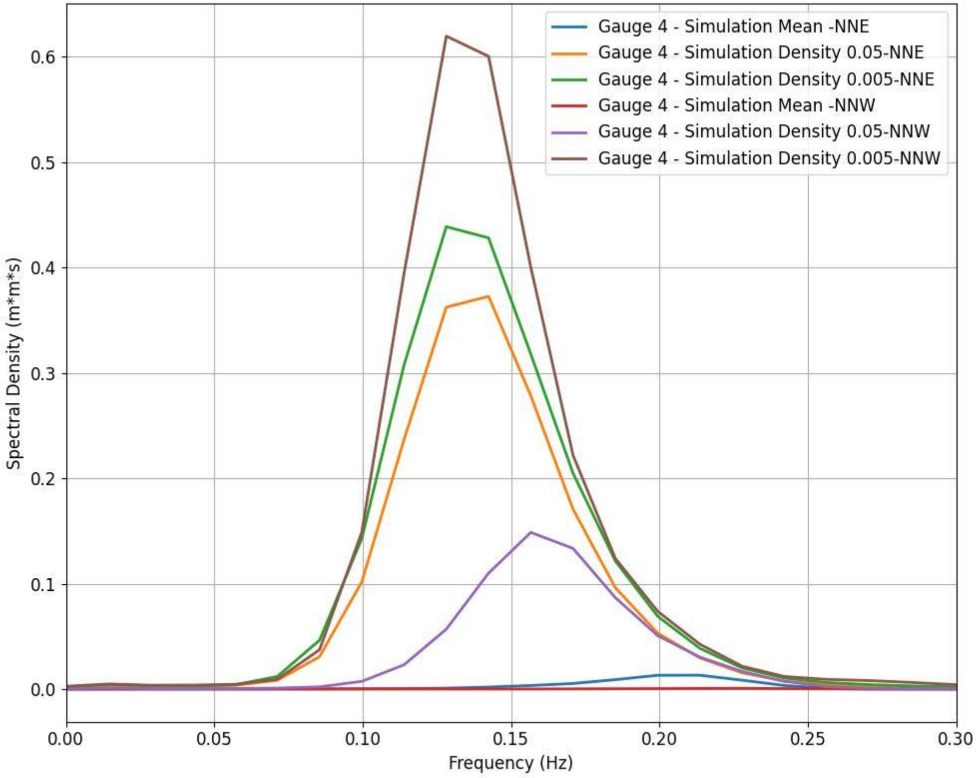

Gauge 4 - Simulation Mean -NNE
Gauge 4 - Simulation Density 0.05-NNE
Gauge 4 - Simulation Density 0.005-NNE
Gauge 4 - Simulation Mean -NNW
Gauge 4 - Simulation Density 0.05-NNW
Gauge 4 - Simulation Density 0.005-NNW
Spectral Density (m*m*s)
Frequency (Hz)

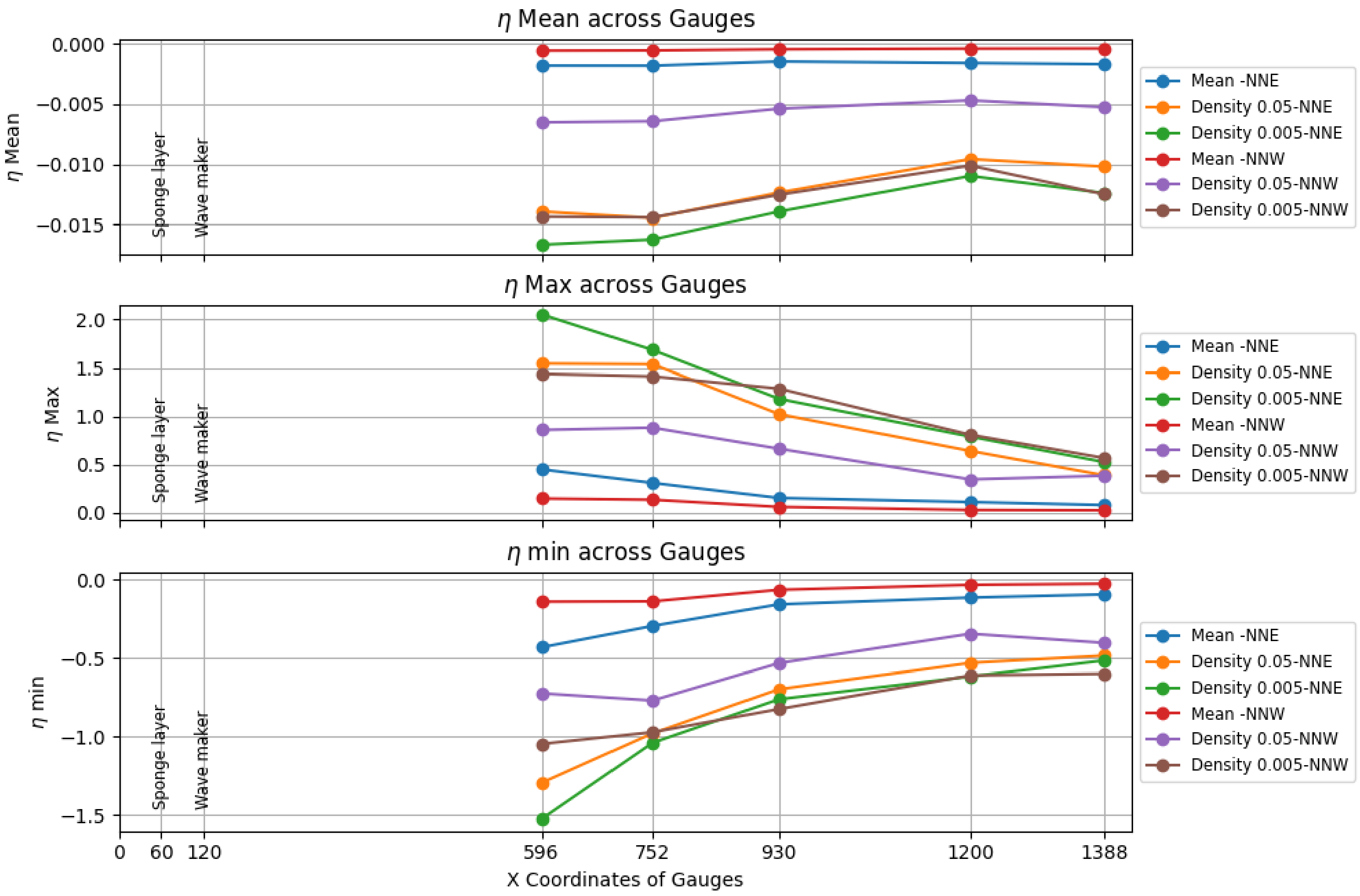

η Mean across Gauges
η Max across Gauges
η min across Gauges
η Mean
η Max
η min
Sponge layer
Wave maker
Mean -NNE
Density 0.05-NNE
Density 0.005-NNE
Mean -NNW
Density 0.05-NNW
Density 0.005-NNW
X Coordinates of Gauges

FLOW-3D

- Free surfaces are modeled with the Volume of Fluid (VOF) technique.
- Utilizing Navier-Stokes-based numerical simulation.
- Structured mesh can only be used.
- NNE waves with 0.05 density was used as Wave maker.
- Numerical domain was 227 m length, 4.4 m width and 7 m height.
- Water depth was set to 3 m. Simulation Time were 200 seconds.
- AutoCAD was used to create STL files as structures.

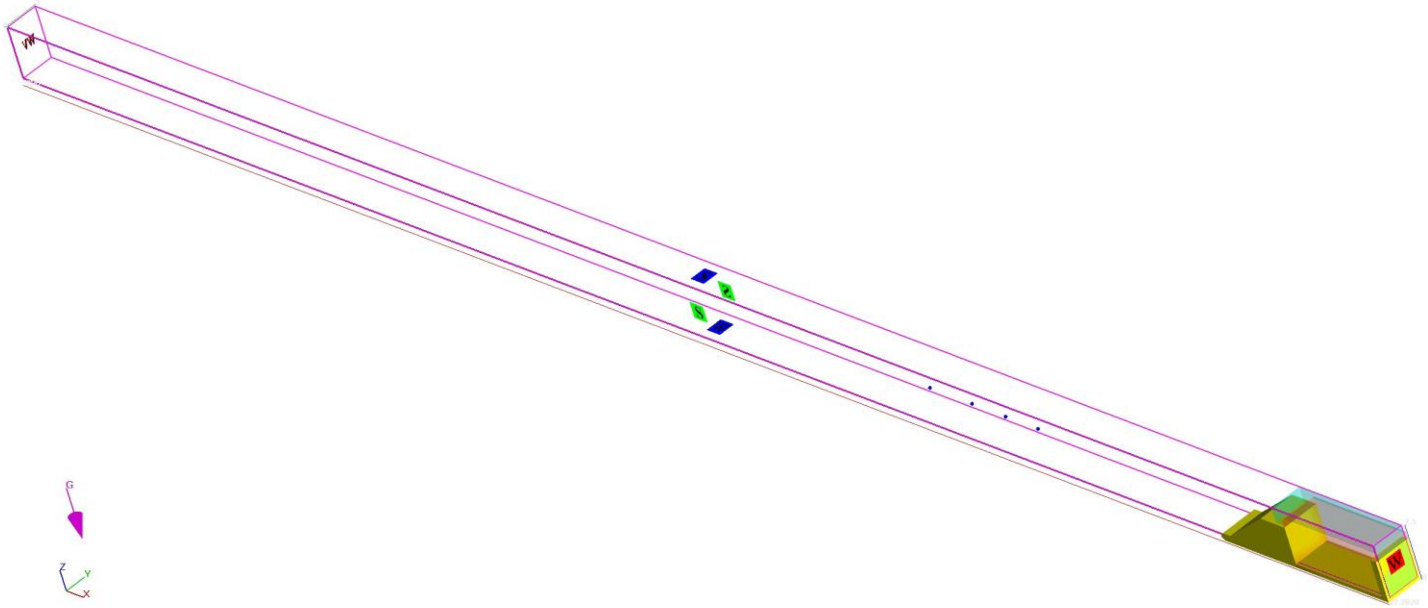

Boundary Conditions for numerical domain in Flow-3D

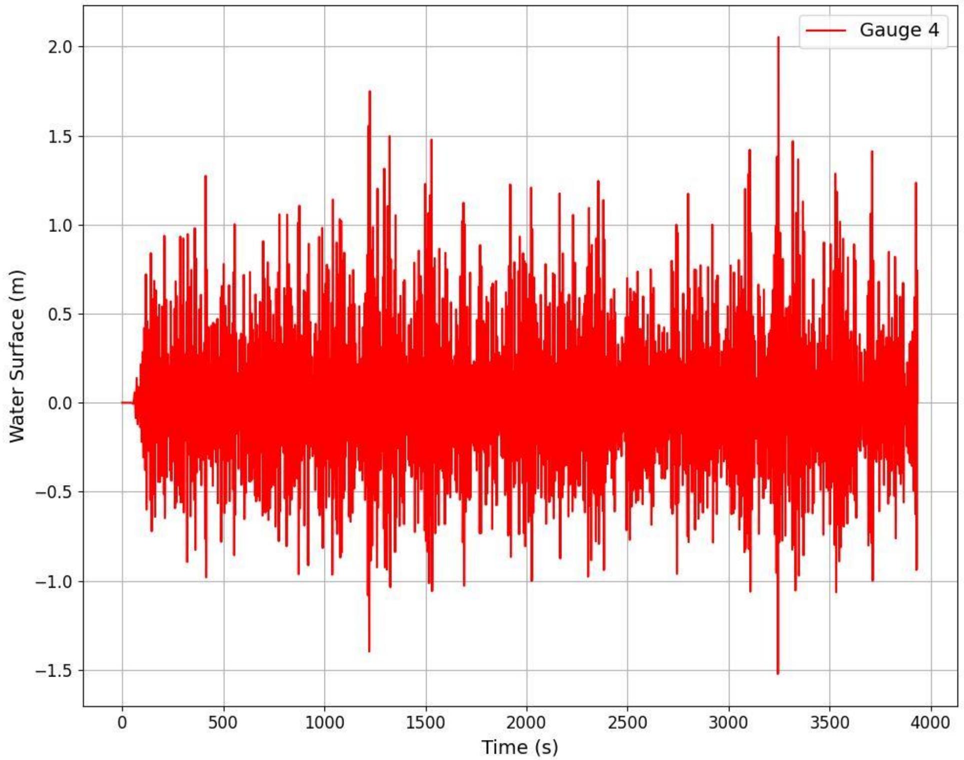

Time series of water surface for NNE waves with 0.05 Density at G4.

Results

OBREC Simulation under waves in NNE direction with Density = 0.05

34 degree slope with uniform Cell size: 0.2 m

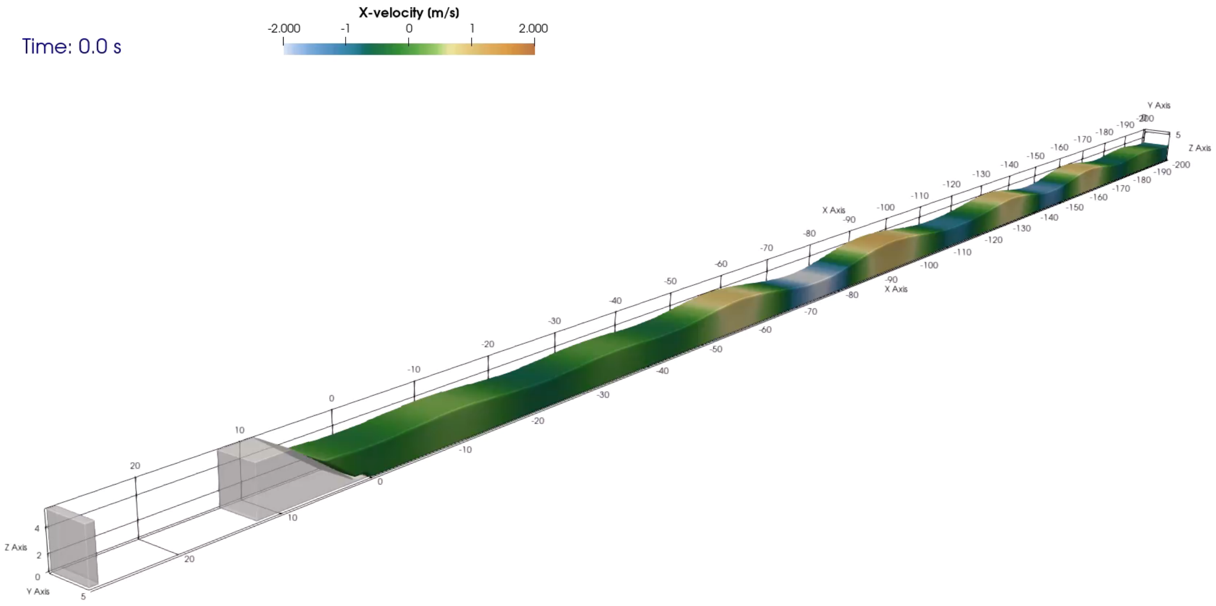

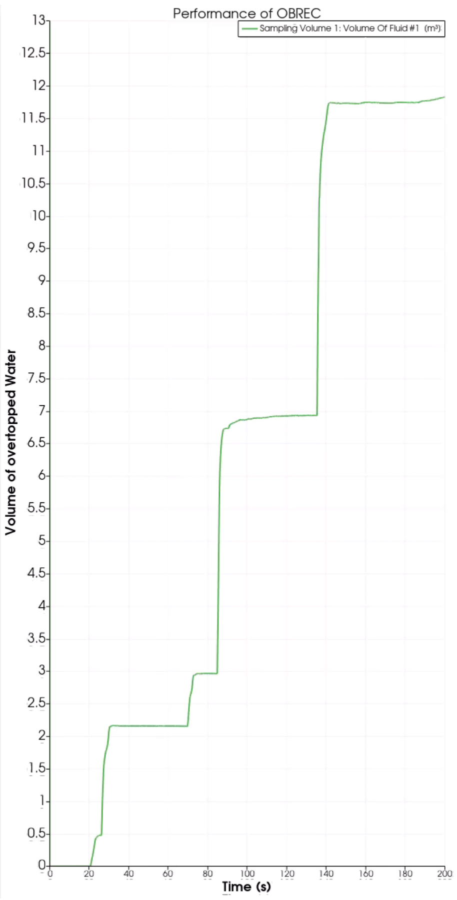

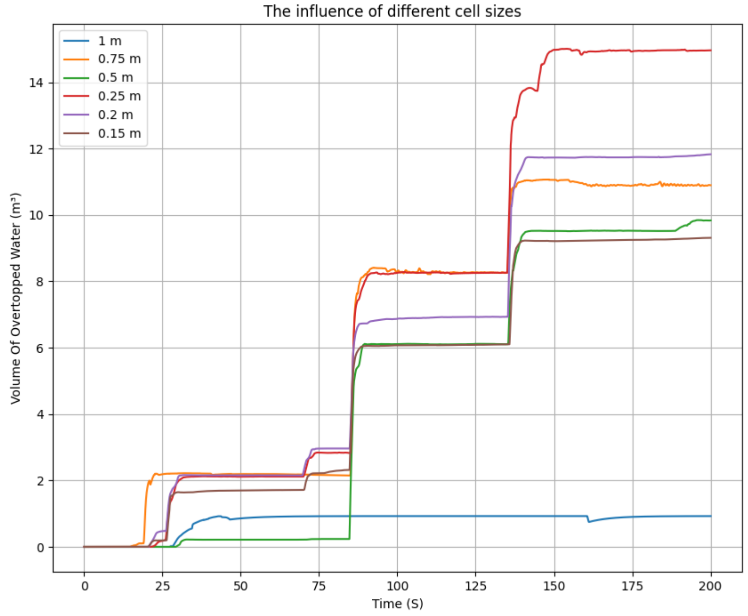

FLOW-3D HYDRO

FLOW-3D- Effect of 2D approach and Ramp slopes

MENTUCCIAldo impresa di costruzioni

Results

All simulations have cell sizes in X and Z direction with 0.2 m and different cell number in Y direction.

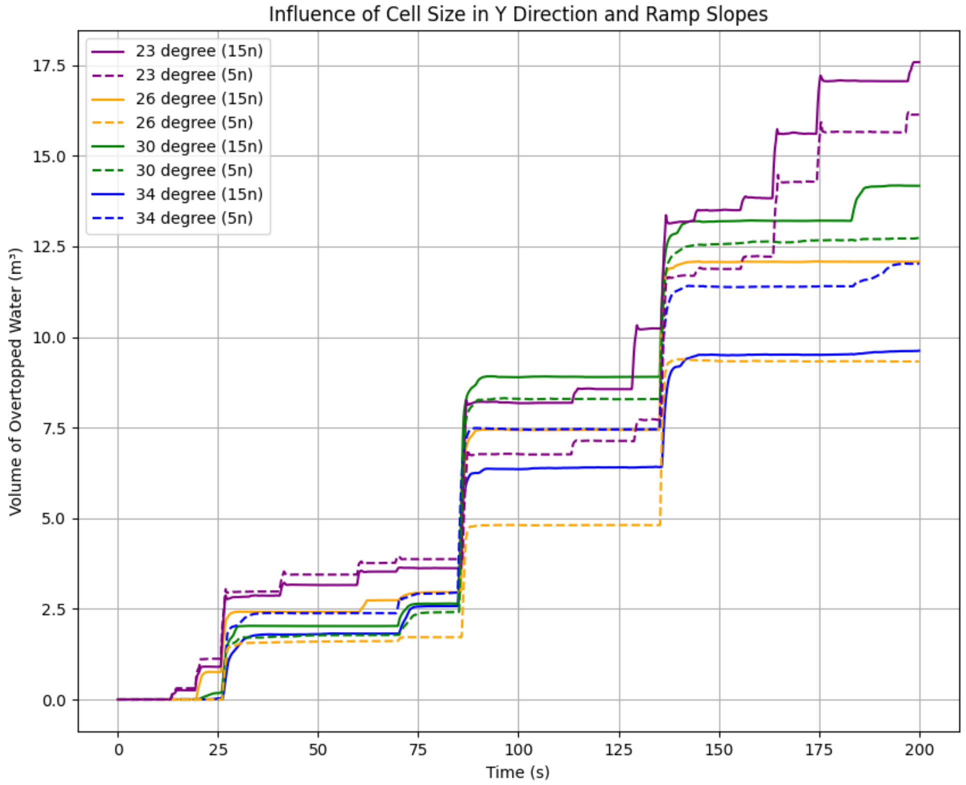

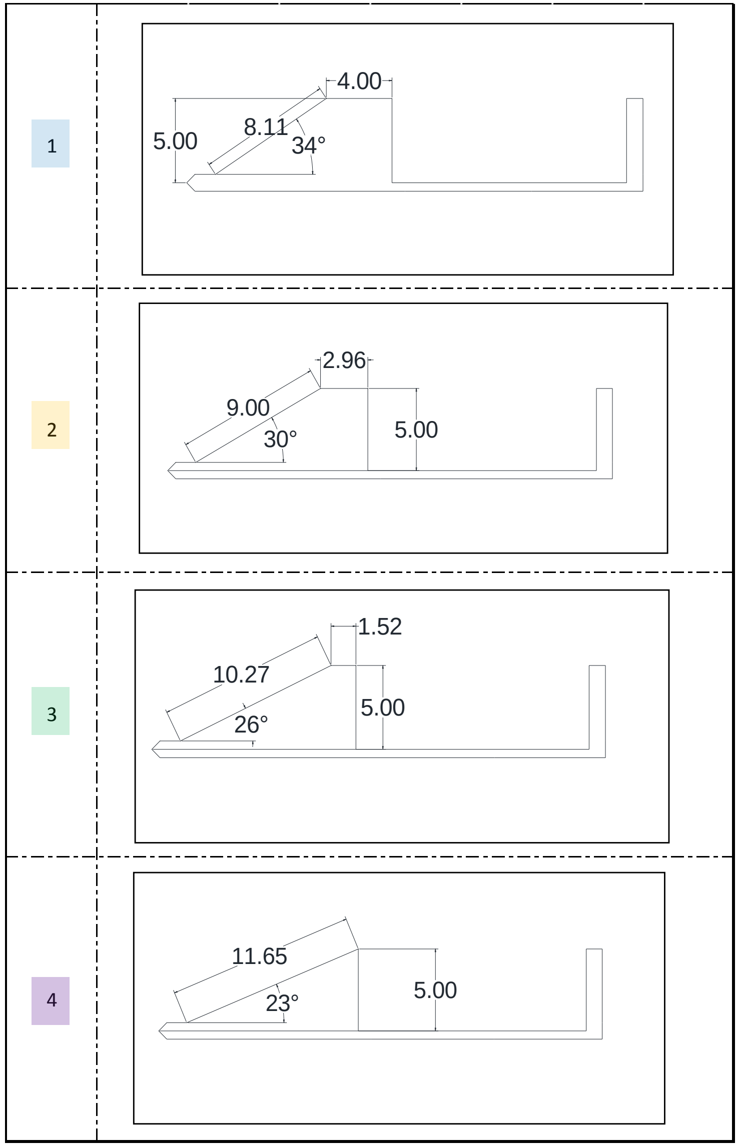

Conclusion and Discussion

- Copernicus data for the given period is not constant with buoy data.
- PDF diagrams was used to wave selection.
- Analytical model (Goda 2010) was used to transfer waves.
- FUNWAVE-TVD could represent set-down which is a non liner behavior of waves.
- FLOW-3D hydro was used to determine suitable grid size for evaluating various ramp shapes.
- More simulation on ramp shapes, including validation.
- Designing reservoir and convey system.
- Running simulations for other scenarios.

FUNWAVE-TVD

(Wave-resolving model) has been used as a shallow water solver.

It is based on Boussinesq-type equations in which Reynolds equations are integrated over the water depth, so the vertical structure is not directly resolved but only modelled. (2DH models)

Bathymetry of the Port of Ancona for FUNWAVE: Combination of port bathymetry from port Authorities (CAD) and EMODnet data.

Volume conservation:

$$\eta_t + \nabla \cdot M = 0$$

M is the horizontal volume flux.

The depth-averaged horizontal momentum:

$$u_{\alpha,t} + (u_\alpha \cdot \nabla)u_\alpha + g\nabla_\eta + V_1 + V_2 + V_3 + R = 0$$

R: diffusive and dissipative terms (e.g. bottom friction, sub-grid lateral turbulent mixing)

$V_1$and V_2 are terms representing the dispersive Boussinesq terms (function of z_α).

V_3 contribution of the order O(μ^2) (function of z_α). $\mu = \frac{h}{l}$

$z_\alpha = \zeta h + \beta\eta$ that $\zeta and\, \beta$ are constants.

u_α denotes the velocity at a reference elevation z = z_α.

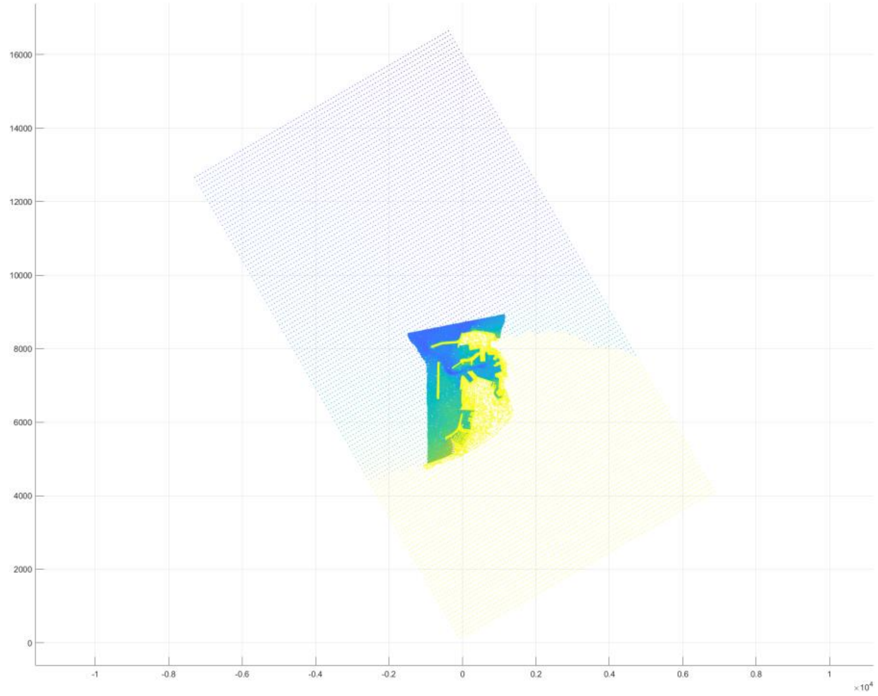

	dx (m)	dy (m)	simulation time (s)	Total number of Grids	Stability Condition	Condition								
						Smoothing (n)	Smoothing (Command)	obstacle height (m)	depth of WK and Spectrum	offshore platform	FroudeCap	CFL and min depth	Wall or Periodic boundary	VISCOSITY_BREAKING
1	2	2	1000	806,314	stable	7	smoothdata2/sgolay/movmean	7	8 - monochromatic	no	1	0.5/0.01	P.B	no
2	2	2	1,000	806,314	stable	7	smoothdata2/sgolay/movmean	7	12 - monochromatic	no	1	0.5/0.01	P.B	no
3	2	2	1,000	806,314	stable	7	smoothdata2/sgolay/movmean	7	16 - monochromatic	no	1	0.5/0.01	P.B	no
4	2	2	1000	806,314	stabe but a instability sign could be seen in the domain around 810 s	7	smoothdata2/sgolay/movmean	7	12 - monochromatic	no	1	0.5/0.1	P.B	no
5	2	2	4292	806,314	stable	7	smoothdata2/sgolay/movmean	7	12 - monochromatic	no	1	0.5/0.01	P.B	yes/ Cbrk1 = 0.45 Cbrk2 = 0.35
6	2	2	7870	374,468	stable	7	smoothdata2/sgolay/movmean	7	12 - monochromatic	no	1	0.5/0.01	P.B	no-small domain
7	2	2	467	806,314	instable (it happens around 330 s)	5	smoothdata/sgolay/sgolay	5	12 - monochromatic	no	1	0.5/0.01	P.B	no
8	2	2	734	806,314	instable (it happens around 180 s)	5	smoothdata/sgolay/sgolay	7	12 - monochromatic	no	1	0.5/0.01	P.B	no

	dx (m)	dy (m)	simulation time (s)	Total number of Grids	Stability Condition	Condition								
						Smoothing (n)	Smoothing (Command)	obstacle height (m)	depth of WK and Spectrum	offshore platform	FroudeCap	CFL and min depth	Wall or Periodic boundary	VISCOSITY_BREAKING
9	2	2	936	806,314	instable (it happens around 480 s)	7	smoothdata/sgolay/sgolay	5	12 - monochromatic	no	1	0.5/0.01	P.B	no
10	1.5	1.5	399	1,432,629	instable (it happens around 150 s)	7	smoothdata2/sgolay/movmean	7	12 - monochromatic	no	1	0.5/0.01	P.B	no
11	1.5	1.5	185	1,432,629	instable (it happens around 122 s)	7	smoothdata2/sgolay/movmean	7	16 - monochromatic	no	1	0.5/0.01	P.B	no
12	1.5	1.5	151	1,432,629	instable (it happens around 120 s)	7	smoothdata2/sgolay/movmean	7	16 - monochromatic	no	3	0.5/0.01	P.B	no
13	2	2	7870	806,314	instable (it happens around 930 s)	7	smoothdata2/sgolay/movmean	7	12 - monochromatic	no	1	0.5/0.01	Wall boundary	no
14	3	3	7870	358,771	stable	7	smoothdata2/sgolay/movmean	7	12 - monochromatic	no	1	0.5/0.01	P.B	no
15	5	5	7870	129,312	stable	7	smoothdata2/sgolay/movmean	7	12 - monochromatic	no	1	0.5/0.01	P.B	no
16	2	2	7870	806,314	stable	7	smoothdata2/sgolay/movmean	7	12	yes	1	0.5/0.01	P.B	no
17	2	2	7870	806,314	stable	7	smoothdata2/sgolay/movmean	7	16	Yes	1	0.5/0.01	P.B	no

Near the breakwater (G5), simulation 5 (VISCOSITY BREAKING)
provides much more energy.

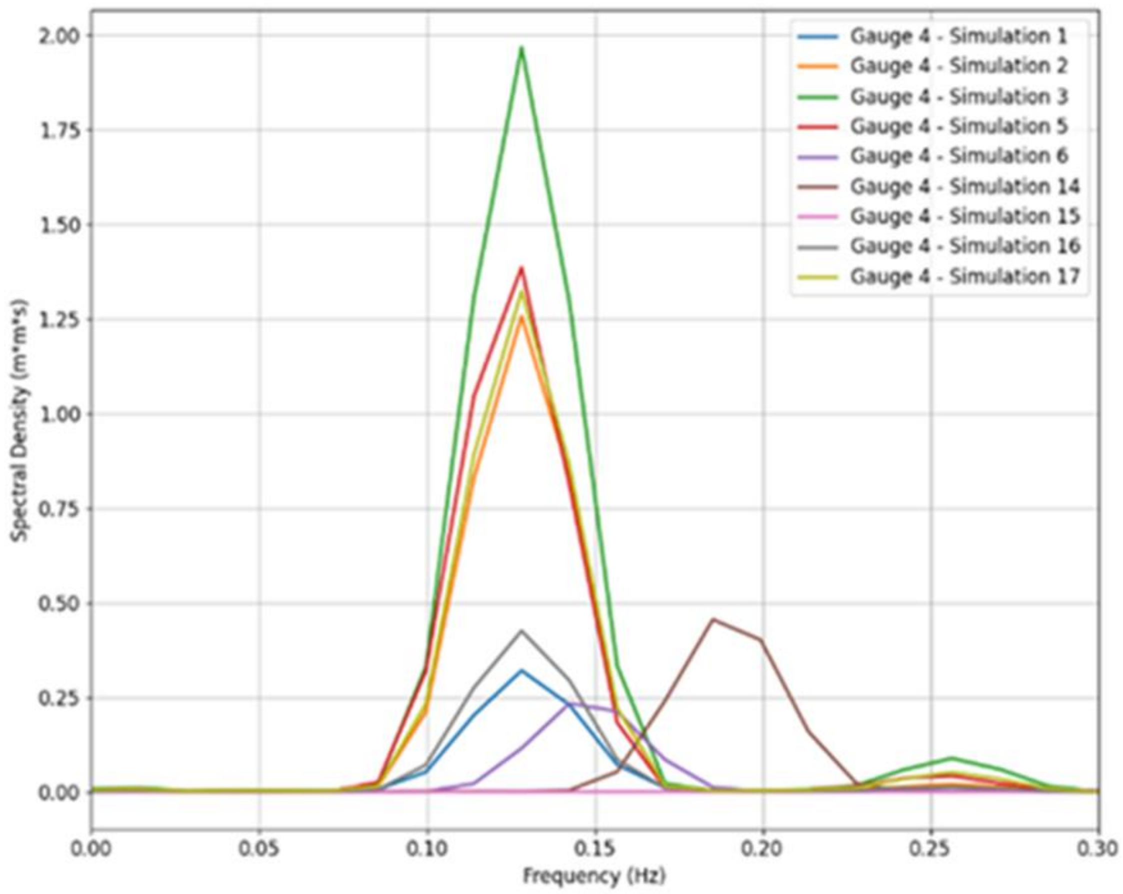

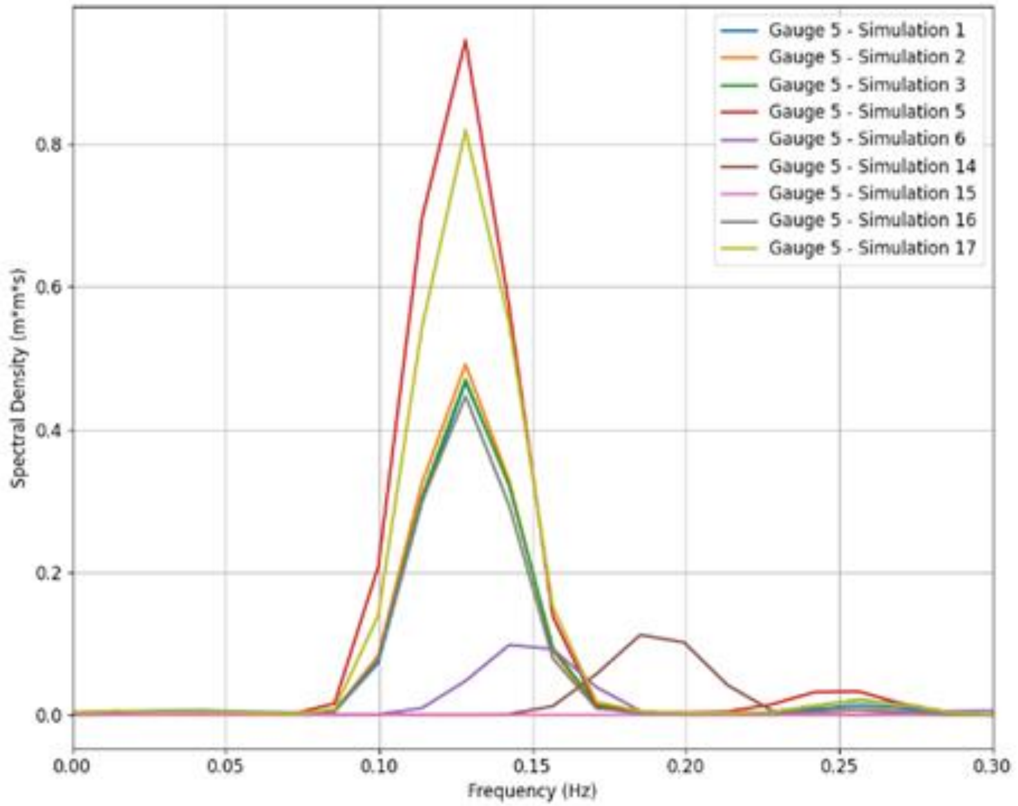

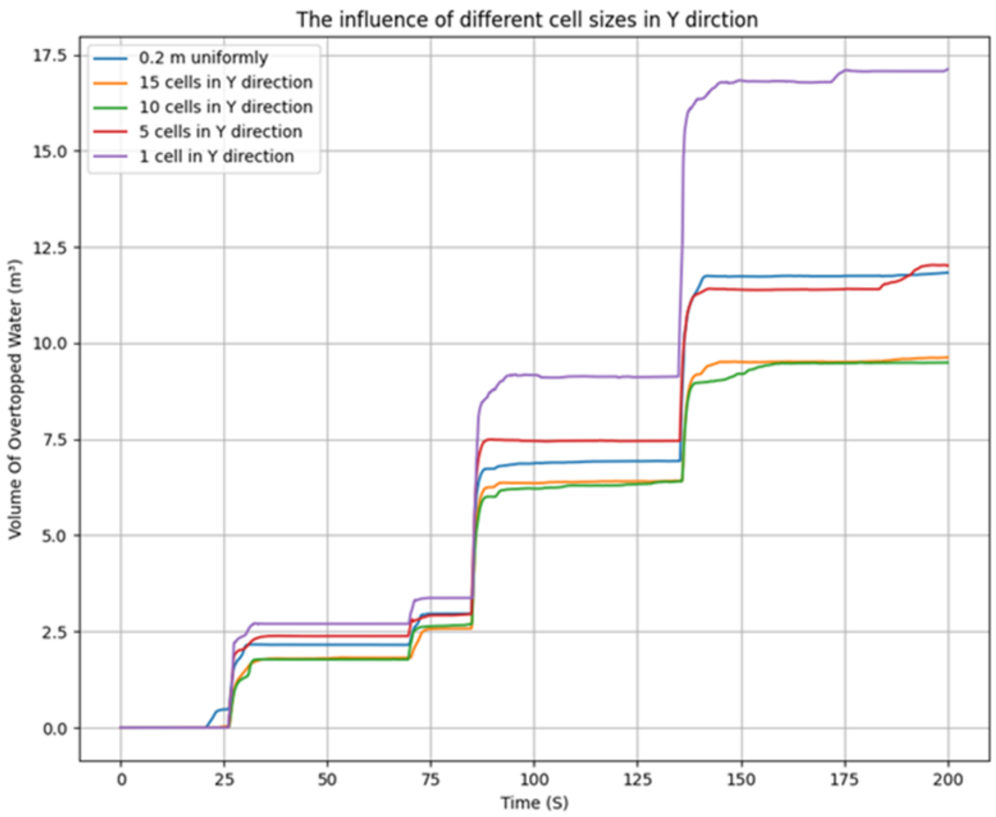

The influence of different cell sizes in Y dirction
0.2 m uniformly
15 cells in Y direction
10 cells in Y direction
5 cells in Y direction
1 cell in Y direction
Volume Of Overtopped Water (m³)
Time (S)
0.0
2.5
5.0
7.5
10.0
12.5
15.0
17.5
0
25
50
75
100
125
150
175
200

References

Vicinanza, D., Contestabile, P., Quvang Harck Nørgaard, J., & Lykke Andersen, T. (2014). Innovative rubble mound breakwaters for overtopping wave energy conversion. Coastal Engineering, 88, 154–170. https://doi.org/10.1016/j.coastaleng.2014.02.004

Iuppa, C., Contestabile, P., Cavallaro, L., Foti, E., & Vicinanza, D. (2016). Hydraulic performance of an innovative breakwater for overtopping wave energy conversion. Sustainability (Switzerland), 8(12). https://doi.org/10.3390/su8121226

Iuppa, C., Cavallaro, L., Musumeci, R. E., Vicinanza, D., & Foti, E. (2019). Empirical overtopping volume statistics at an OBREC. *Coastal Engineering*, *152*. https://doi.org/10.1016/j.coastaleng.2019.103524

Kralli, V. E., Theodossiou, N., & Karambas, T. (2019). Optimal Design of Overtopping Breakwater for Energy Conversion (OBREC) Systems Using the Harmony Search Algorithm. Frontiers in Energy Research, 7. https://doi.org/10.3389/fenrg.2019.00080

Cavallaro, L., Iuppa, C., Castiglione, F., Musumeci, R. E., & Foti, E. (2020). A simple model to assess the performance of an overtopping wave energy converter embedded in a port breakwater. *Journal of Marine Science and Engineering*, *8*(11), 1–20. https://doi.org/10.3390/jmse8110858

P. Contestabile, E. Di Lauro, M. Buccino, and D. Vicinanza, “Economic assessment of Overtopping BReakwater for Energy Conversion (OBREC): A case study in Western Australia,” Sustainability (Switzerland), vol. 9, no. 1, 2017, doi: 10.3390/su9010051.

P. Contestabile, G. Crispino, E. Di Lauro, V. Ferrante, C. Gisonni, and D. Vicinanza, “Overtopping breakwater for wave Energy Conversion: Review of state of art, recent advancements and what lies ahead,” Renew Energy, vol. 147, pp. 705–718, Mar. 2020, doi: 10.1016/j.renene.2019.08.115.

Serinaldi, F., Briganti, R., Kilsby, C. G., & Dodd, N. (2022). Sailing synthetic seas: Stochastic simulation of benchmark sea state time series. Coastal Engineering, 176. https://doi.org/10.1016/j.coastaleng.2022.104164

M. Postacchini et al., “A model chain approach for coastal inundation: Application to the bay of Alghero,”

Laboratory of Hydraulic Engineering
Department of Civil Engineering
University of Patras

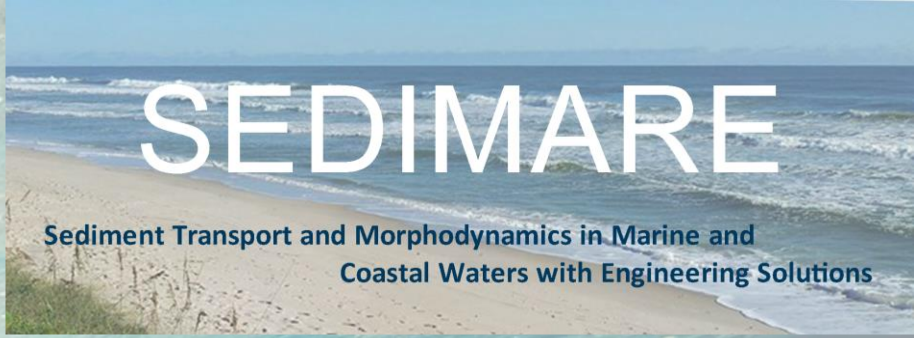

Large-eddy simulations of turbulent oscillatory flow and sediment transport induced by waves

Ioannis Gerasimos Tsipas

Supervisor: Athanassios A. Dimas, Professor

Funded by the European Union

This project has received funding from the European Union's Horizon Europe research and innovation programme under the Marie Skłodowska-Curie grant agreement No 101072443.

European Commission

Outline

- Introduction
- Objectives
- Methodology
- Simulation Set-up
- Results
- Conclusions/Future Work

- Surface waves induce oscillatory flow at seabed
- Generation of bed forms (ripples, dunes, bars)
- Significant impact on wave propagation and sediment transport by increasing bed roughness and promoting sediment suspension due to vortex shedding

The dynamics of turbulent oscillatory flow and sediment transport over sandy beds is critical for understanding various environmental and engineering processes, such as coastal erosion, sedimentation patterns, and habitat formation.

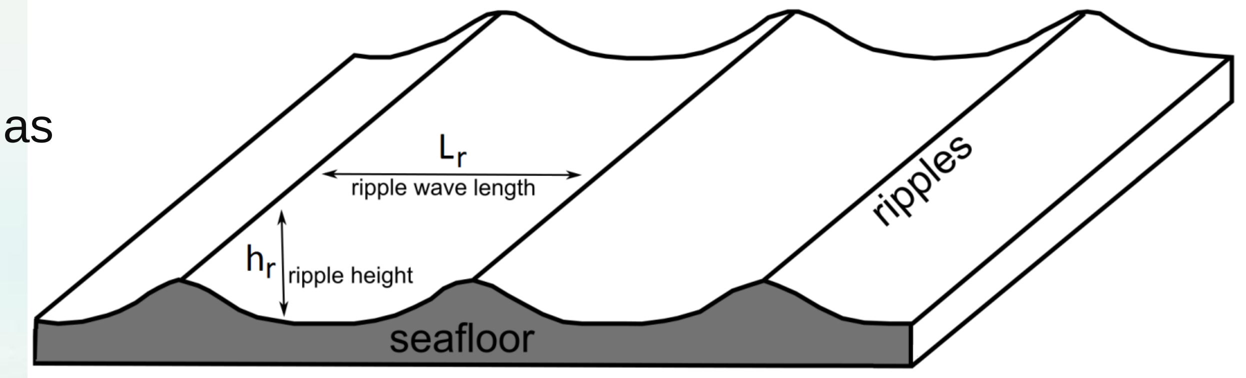

https://www.vhv.rs/viewpic/hbJbwRw_transparent-water-ripples-png-ripple-of-water-diagram/

Objectives

- Development of large-eddy simulation (LES) software to model turbulent oscillatory flow and mixed-grain sediment transport induced by waves.

- Methodology

Flow Equations (non-dimensional)

Continuity *equation*: $\frac{\partial u_i}{\partial x_i} = 0$

Navier-Stokes equations $\frac{\partial u_i}{\partial t} + \frac{\partial}{\partial x_j}\left(u_i u_j\right) = -\frac{\partial p}{\partial x_i} - \frac{\partial \tau_{ij}}{\partial x_j} + \frac{1}{\mathrm{Re}}\frac{\partial^2 u_i}{\partial x_j \partial x_j} + f_i$

$$Re = \frac{U_0 a_0}{\nu}$$

u_i is the resolved velocity field according to LES .

Dynamic pressure $p = P_o + P$ where P_o is the externally imposed pressure field.

$$u_o\left(t\right) = U_o\left(\cos\left(\omega t\right) + B\cos\left(2\omega t\right)\right)$$

$$\tau_{ij} = -2D_{wall}\nu_{sgs}S_{ij} = -2D_{wall}\left(C_s\Delta\right)^2\left|S\right|S_{ij} \qquad \Delta = \left(\Delta x_1 \Delta x_2 \Delta x_3\right)^{1/3} \qquad \left|S\right| = \left(2S_{ij}S_{ij}\right)^{1/2}$$

Subgrid-scale (SGS) stresses

$$S_{i,j} = \frac{1}{2}\left(\frac{\partial u_i}{\partial x_j} + \frac{\partial u_j}{\partial x_i}\right)$$

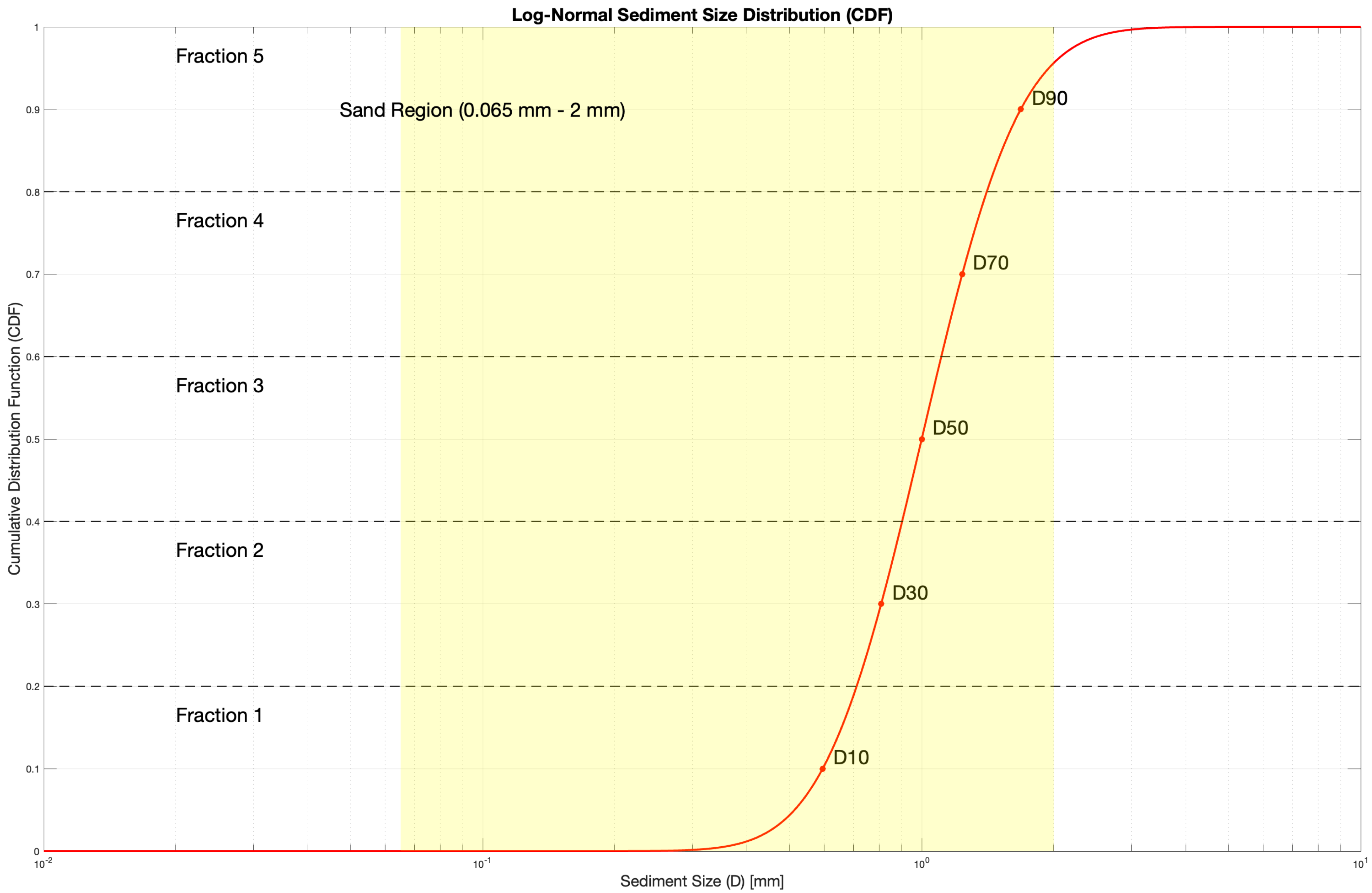

Log-Normal Sediment Size Distribution (CDF)
Fraction 5
Sand Region (0.065 mm - 2 mm)
D90
Fraction 4
D70
Fraction 3
D50
Fraction 2
D30
Fraction 1
D10
Cumulative Distribution Function (CDF)
Sediment Size (D) [mm]
0
0.1
0.2
0.3
0.4
0.5
0.6
0.7
0.8
0.9
1
10^{-2}
10^{-1}
10^{0}
10^{1}

Sediment Transport Equations

Bed load transport rate (Engelund and Fredsøe, 1976):

$$\frac{q_{b(nd)}}{\sqrt{(S-1)gDg_{(nd)}^3}} = \begin{cases} \operatorname{sgn}(\theta)\dfrac{5\pi}{3}\left[1+\left(\dfrac{\pi}{6}\dfrac{\mu_d}{\left|\theta_{(nd)}\right|-\theta_{c(nd)}}\right)^4\right]^{-\frac{1}{4}}\left(\sqrt{\left|\theta_{(nd)}\right|}-0.7\sqrt{\left|\theta c_{(nd)}\right|}\right), & \left(\theta_{(nd)} > \theta c_{(nd)}\right) \\ 0, & \left(\theta_{(nd)} < \theta c_{(nd)}\right) \end{cases}$$

Shields number : $\theta = \frac{\tau_b}{\rho_w(S-1)gDg_{(nd)}^3}$

Critical Shields number: $\theta_c\left(D_{g(nd)}, S\right)$

Grain diameters: $Dg_{(nd)}$

Sediment specific gravity: S

Dynamic friction coefficient: $\mu_d \approx 0.5\mu_s$

Advection-diffusion equation for the suspended sediment concentration:

$$\frac{\partial c_{(nd)}}{\partial t} + u_j \frac{\partial c_{(nd)}}{\partial x_j} - w_{s(nd)} \frac{\partial c_{(nd)}}{\partial x_3} = \frac{1}{\sigma Re} \frac{\partial^2 c_{(nd)}}{\partial x_j \partial x_j} - \frac{\partial \chi_j}{\partial x_i} + f_c$$

where $w_{s(nd)}$ is the sediment fall velocity (Hallermeier 1981) for each

$$\frac{w_{s(nd)} Dg_{(nd)}}{\nu} = \begin{cases} \mathrm{D}^3_{*(nd)}/18 & \mathrm{D}^3_{*(nd)} < 39 \\ \mathrm{D}^{2.1}_{*(nd)}/6 \quad for & 39 < \mathrm{D}^3_{*(nd)} < 10^4 \\ 1.05\mathrm{D}^{1.5}_{*(nd)} & 10^4 < \mathrm{D}^3_{*(nd)} \leq 3 \cdot 10^6 \end{cases} \quad .where. \quad D_{*(nd)} = Dg_{(nd)} \left(\frac{(S-1)g}{\nu^2} \right)^{1/3}$$

$$\chi_j = \frac{v_{sgs}}{\sigma_\iota} \frac{\partial c_{(nd)}}{\partial x_j}$$

σ is the Schmidt number, χ_j is the SGS turbulent term (Zedler and Street 2001):

and σ_t is the turbulent Schmidt number.

Suspended load transport rate: $q_{s1,2(nd)} = \int_{x_{3bed}}^{x_{3top}} u_{1,2} c_{(nd)} dx_3$

Simulation Set-up

Van Der Werf et al.(2007) , experiment Mr5b63

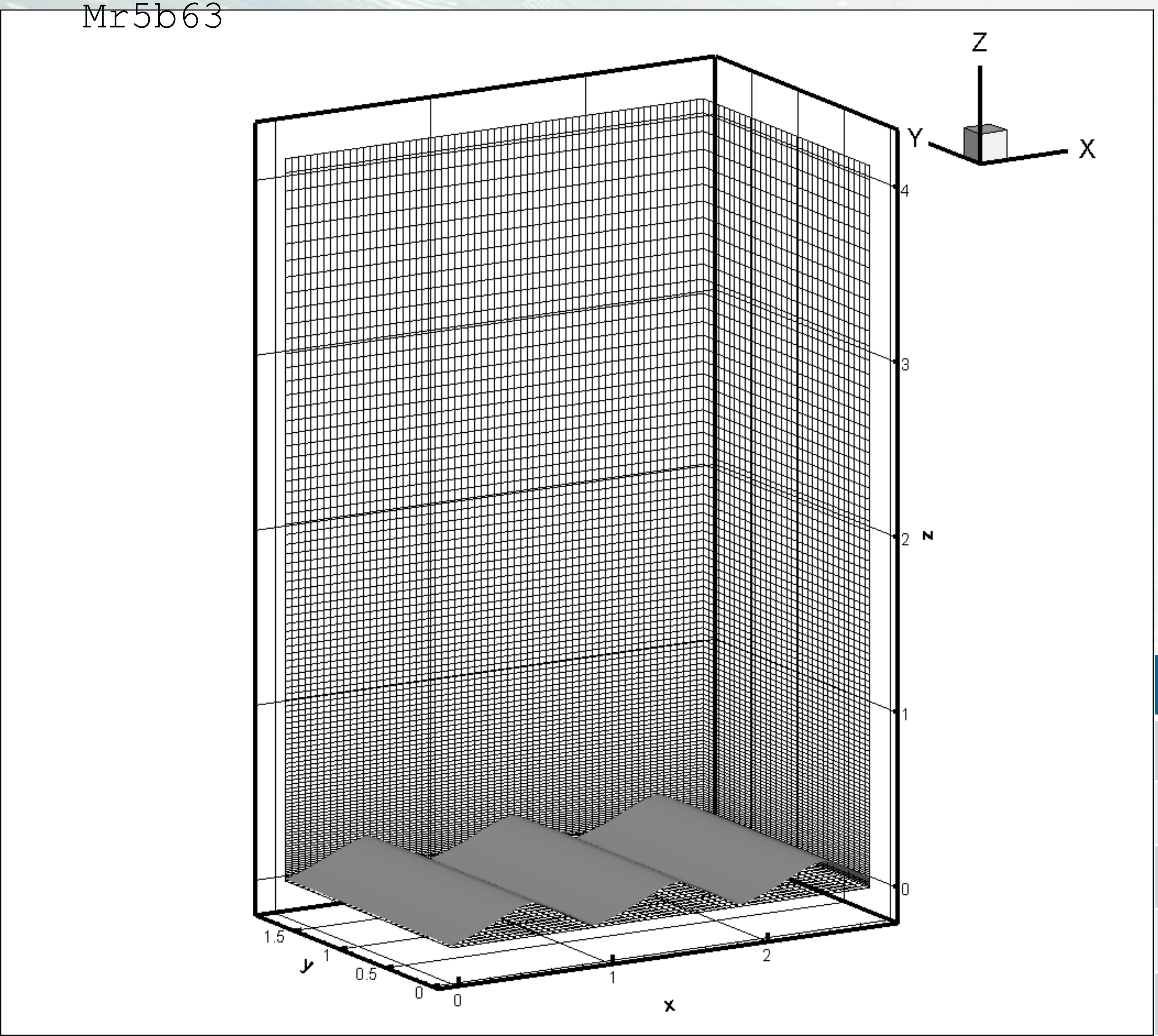

Re = 33000

Lr = 0.94
h_r = 0.17
Δx = 0.01055 m
Δy = 0.01406 m
Δz = 0.0025 -> 0.02719 m
Grid = 257x129x400 = 13261200 cells

D_g (m)	Ψ	a_0/D_g
0.00025	104.4	2100
0.00035	74.5	1500
0.00044	59.3	1193
0.00053	49.2	990
0.00066	39.5	795

Bed Load, Spanwise & Phase(max positive/negative) averaged for every diameter fraction

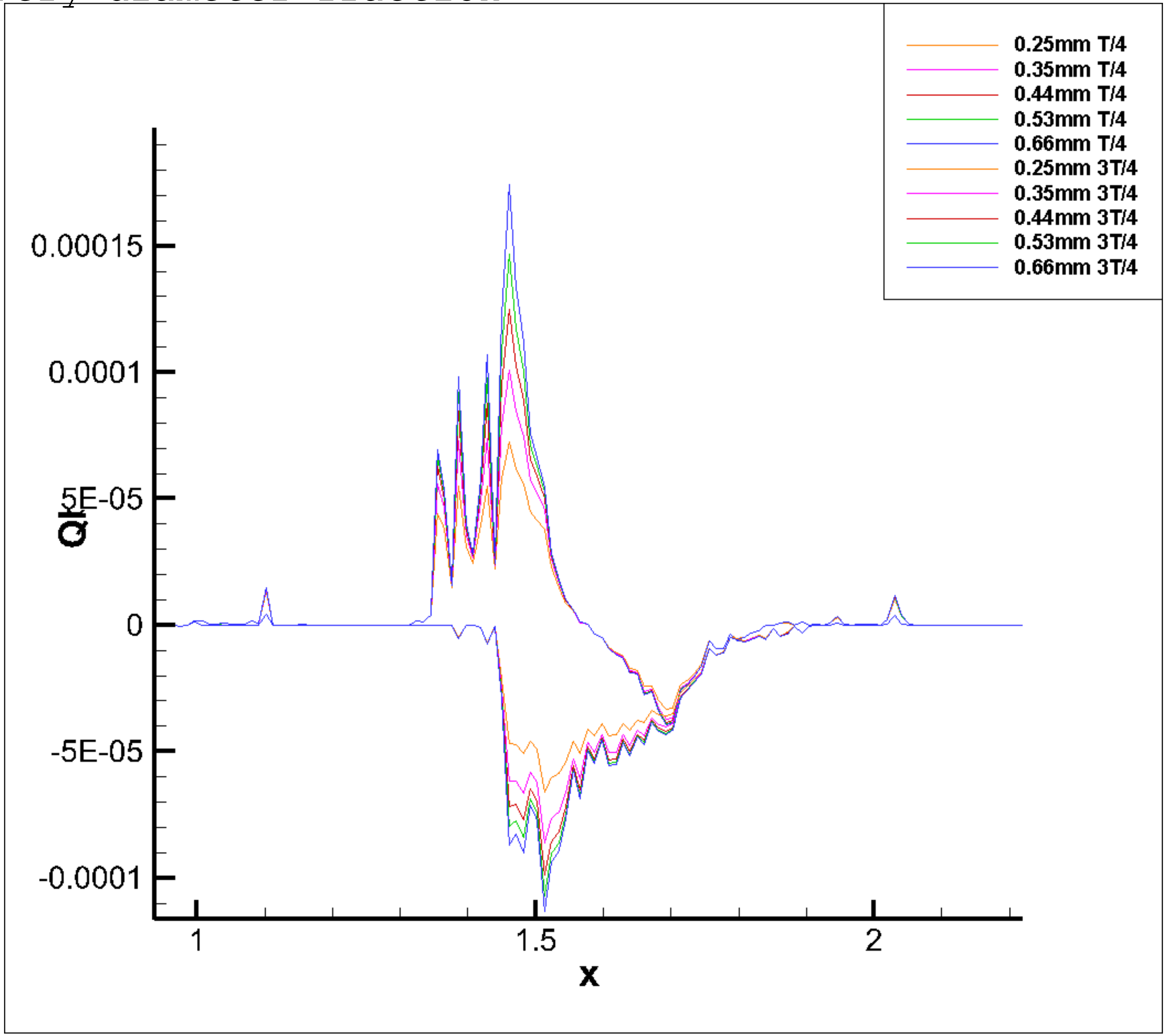

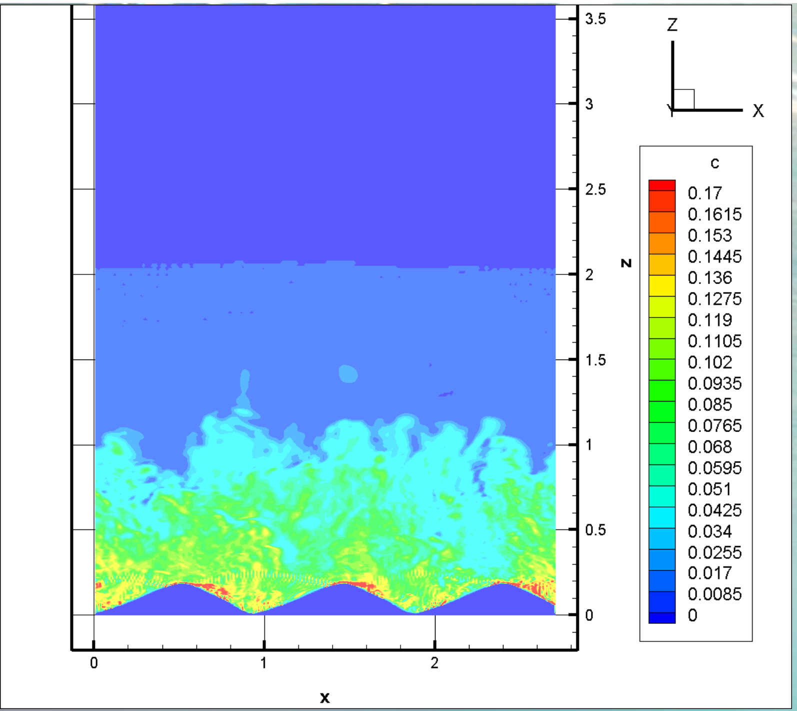

D10 at T/4

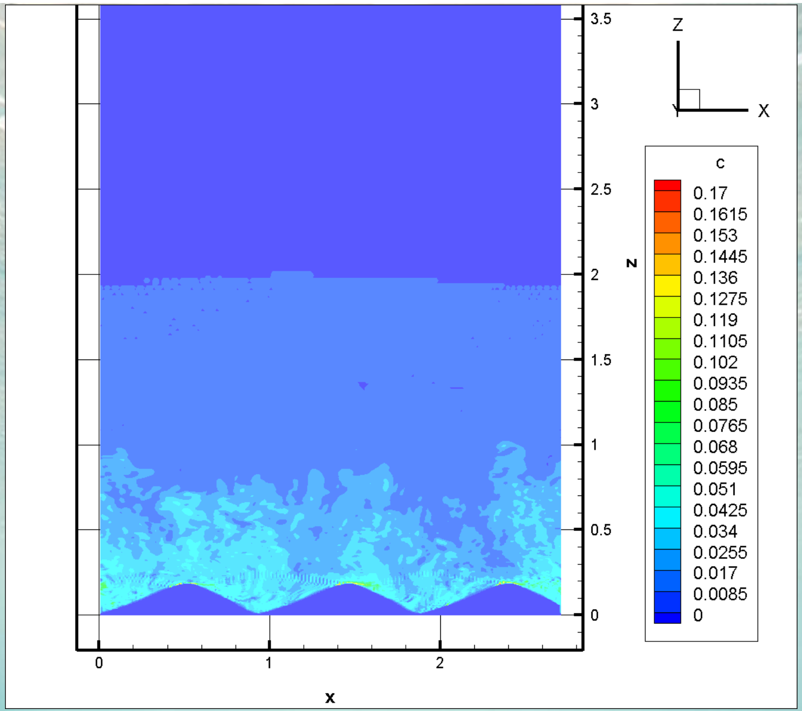

D50 at T/4

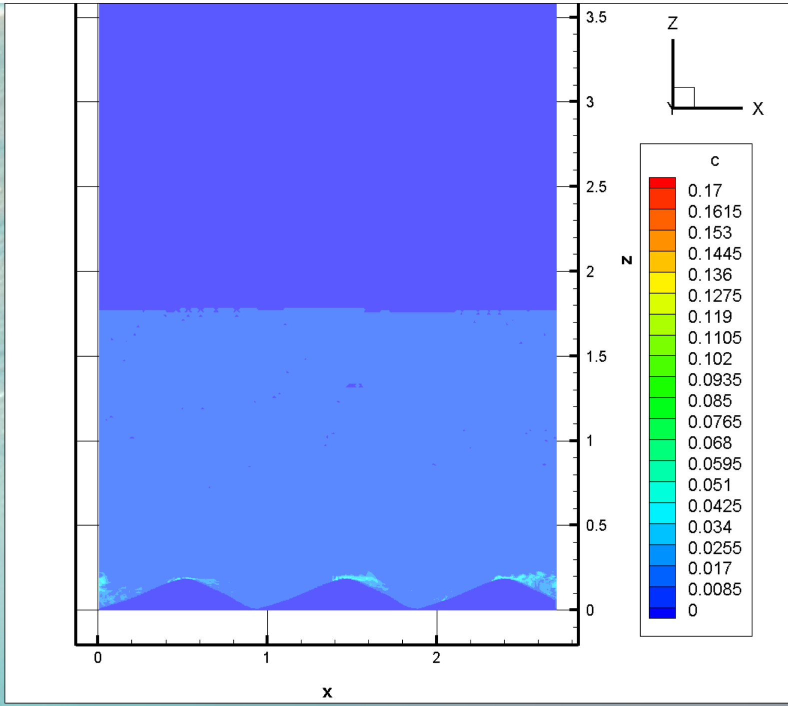

D90 at T/4

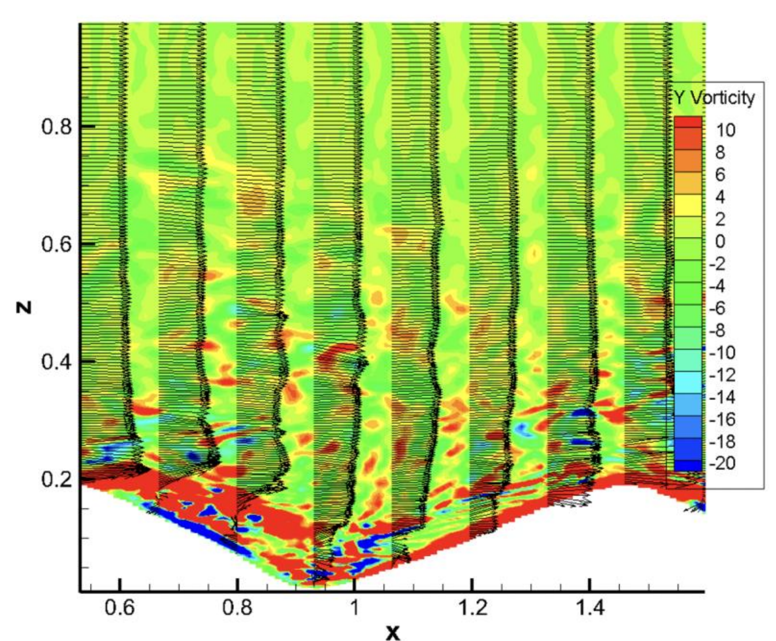

Vorticity Field T/4

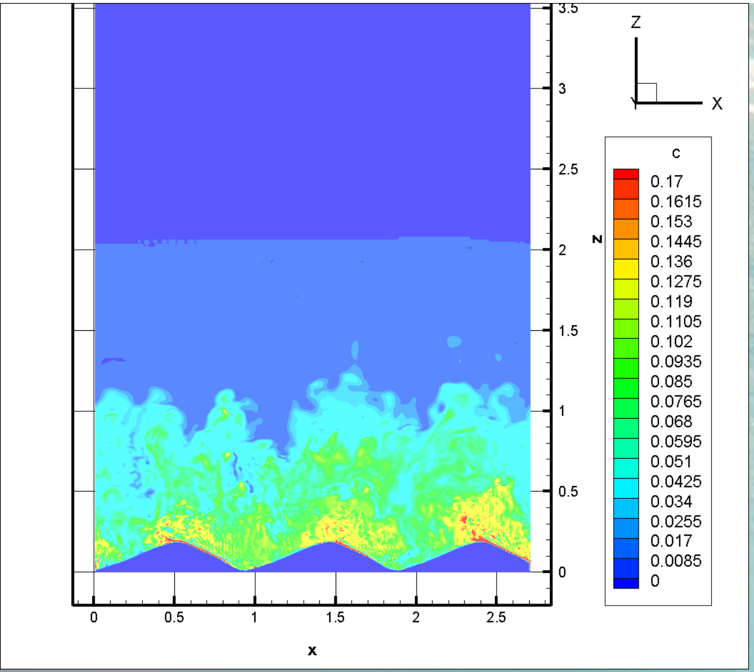

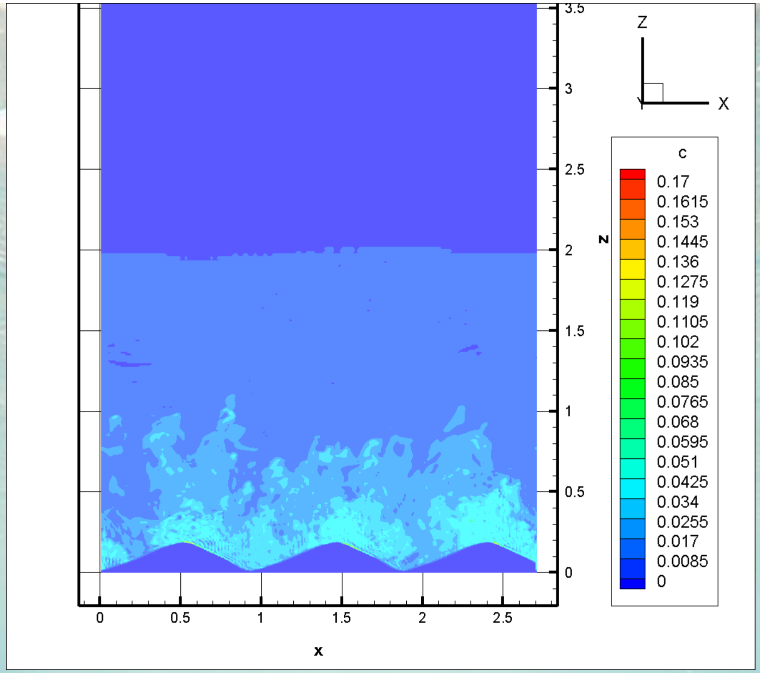

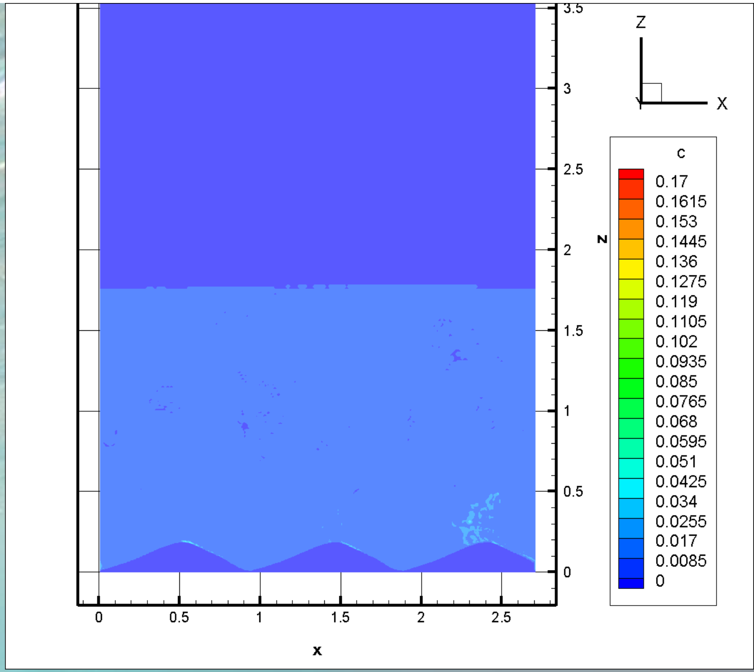

D10 at T/2

D50 at T/2

D90 at T/2

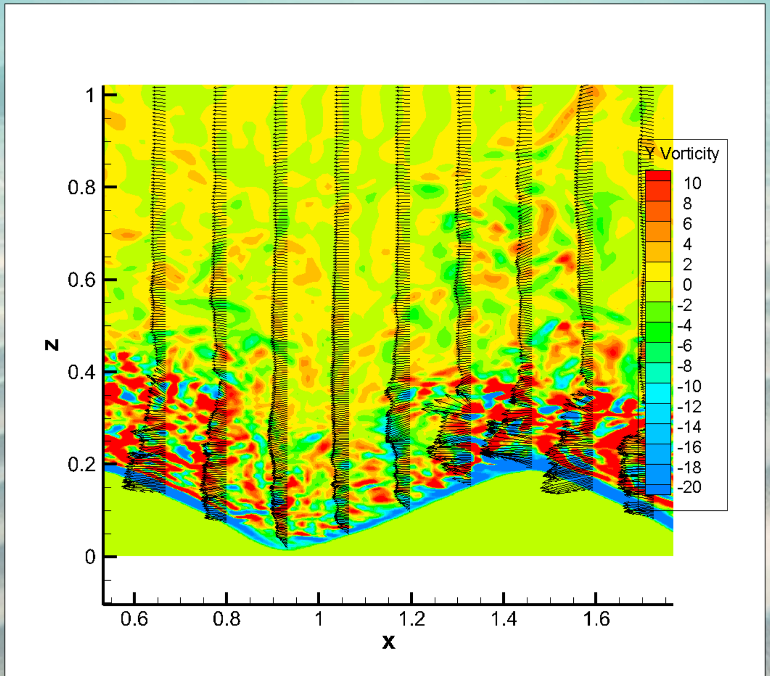

Vorticity Field T/2

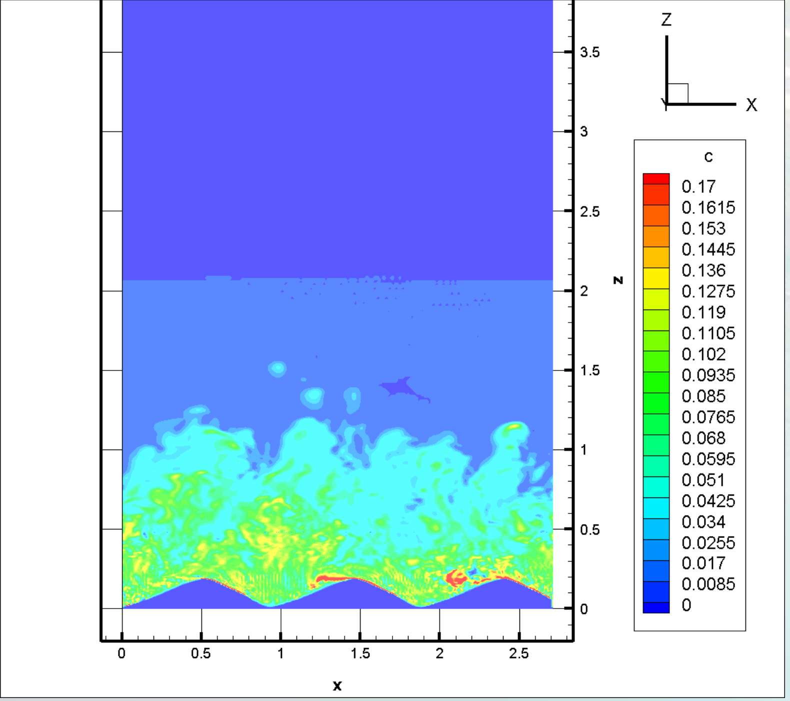

D10 at 3T/4

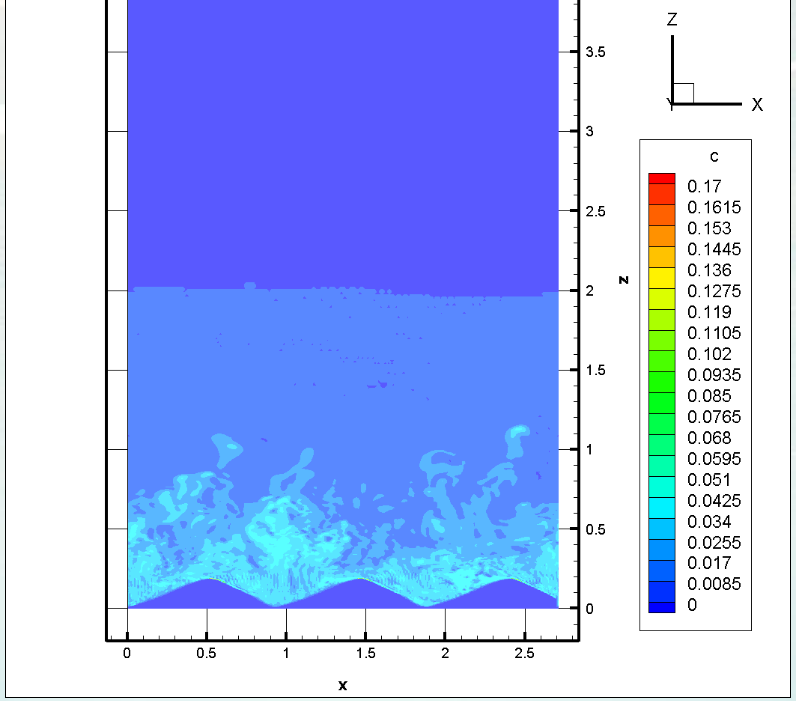

D50 at 3T/4

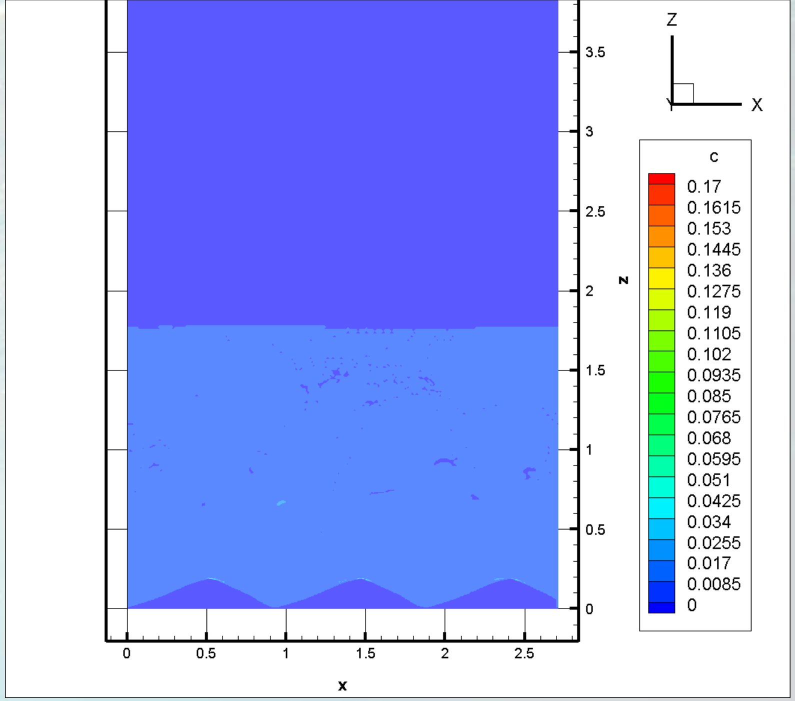

D90 at 3T/4

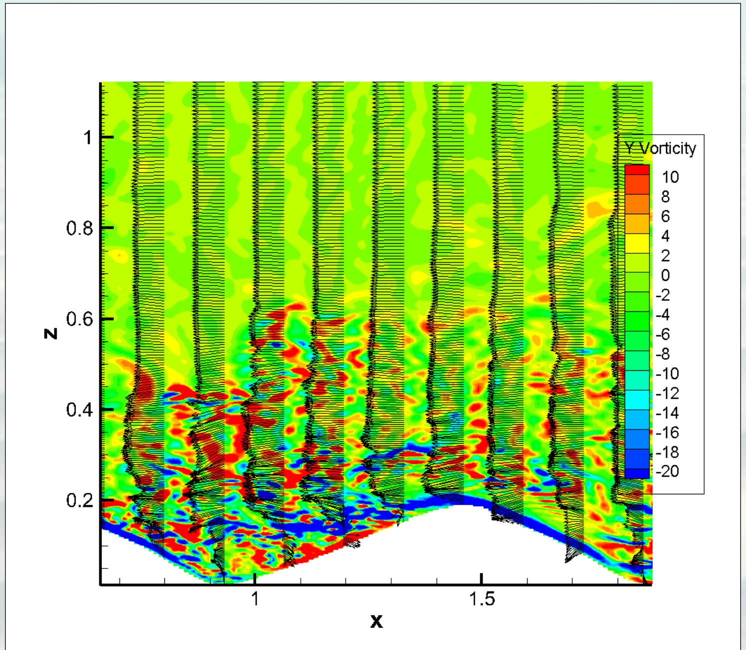

Vorticity
Field 3T/4

Concentration profile for each diameter fraction and the

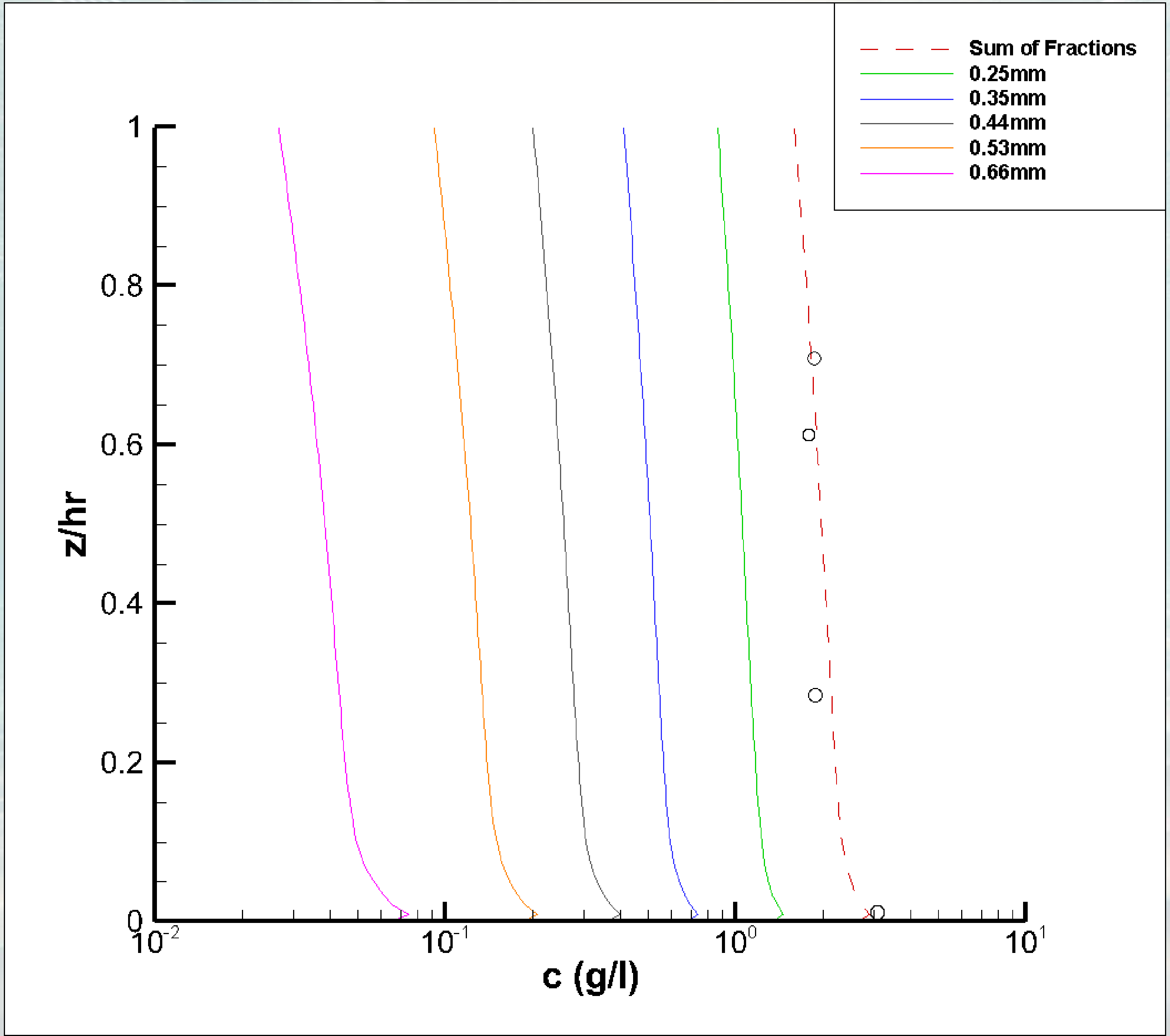

Suspended Load, Spanwise & Phase(max positive/negative) averaged for every diameter fraction

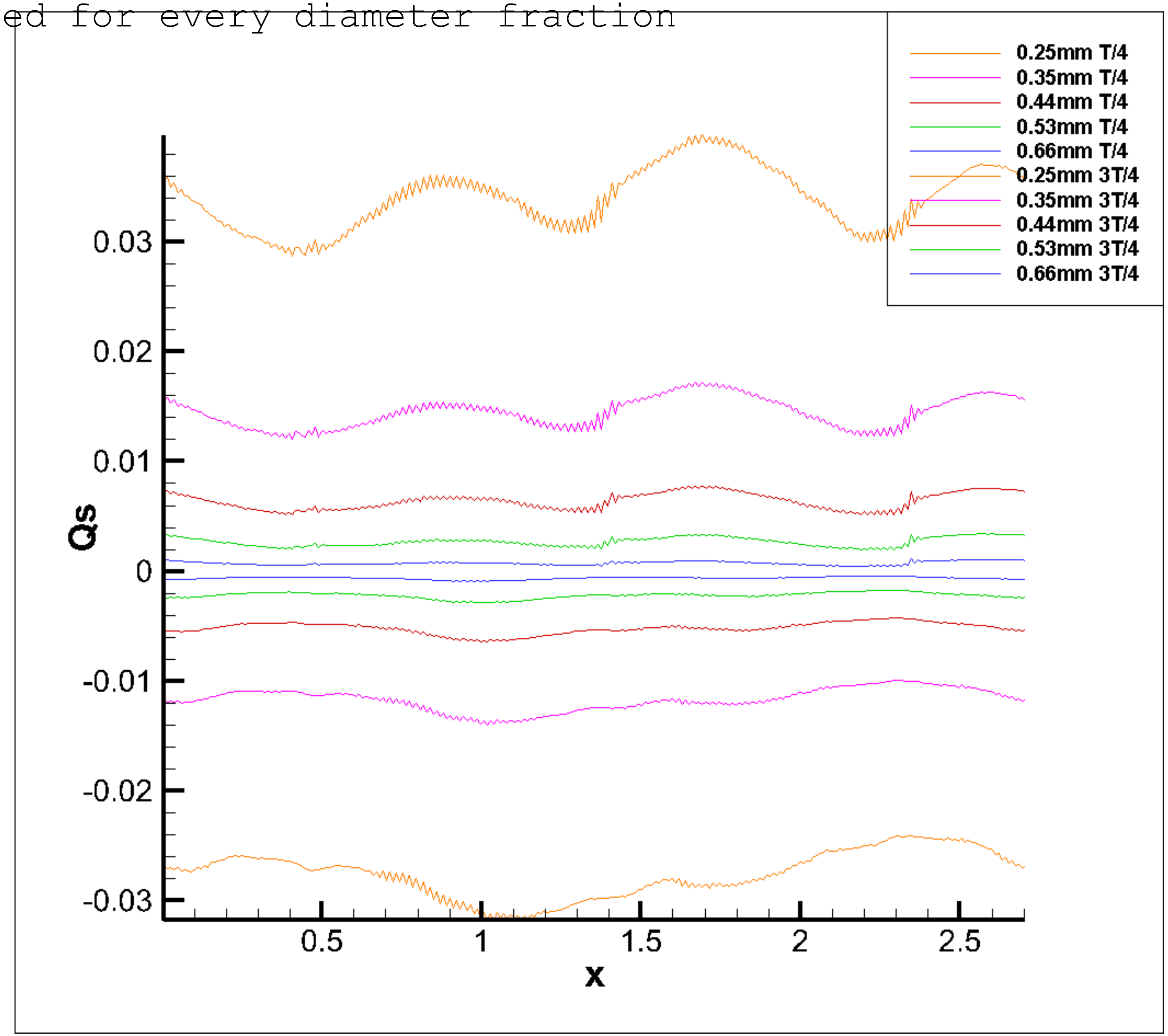

Conclusions

- Bed Load : Diameter Size increasing -> Bed Load Increases
- Suspended Load : Diameter Size Decreases -> Suspended Load Increases
- Concentration : Diameter Size Decreases -> Concentration Increases

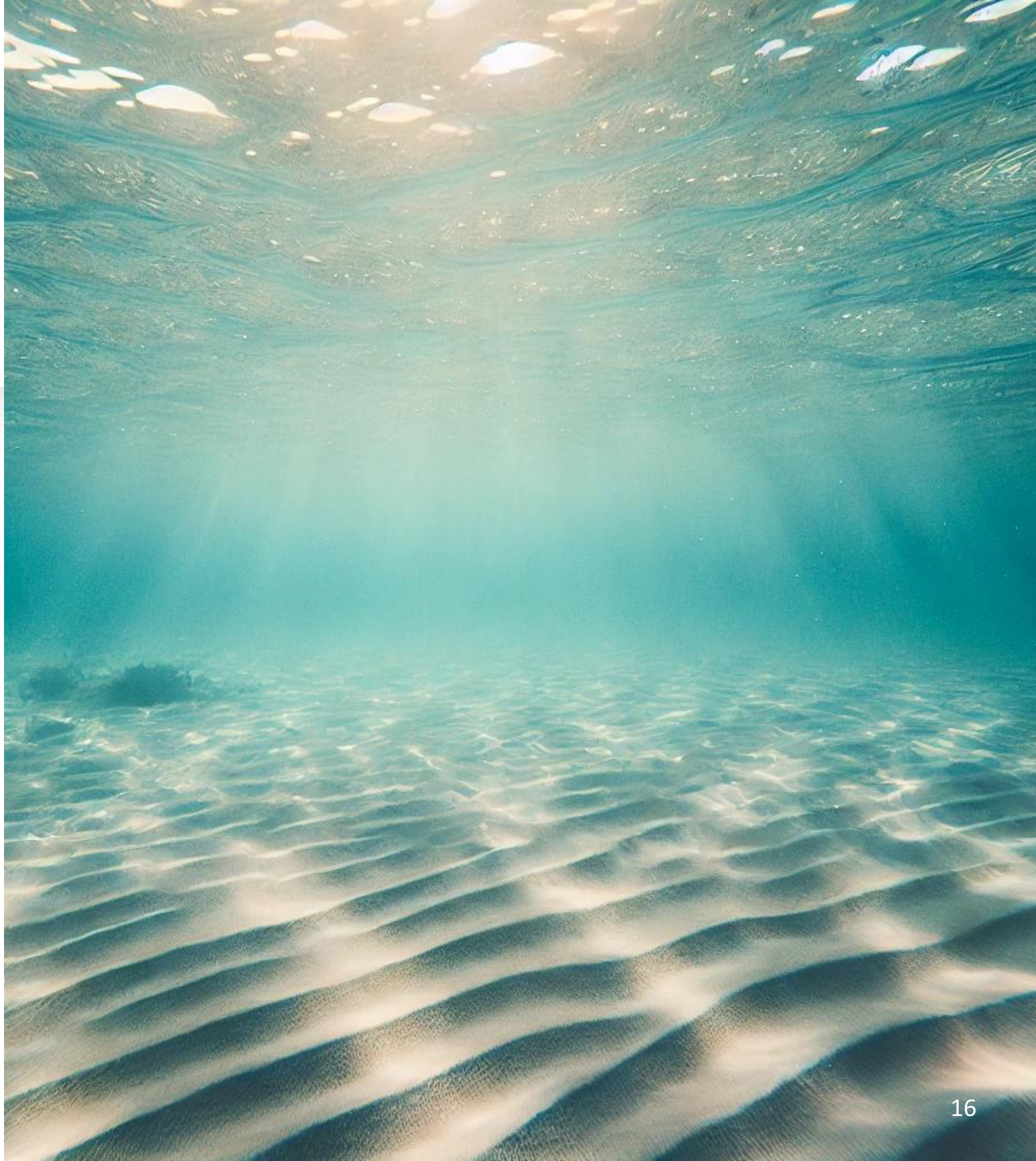

University of Nottingham
UK | CHINA | MALAYSIA

Marie Skłodowska-Curie Actions

HORIZON EUROPE

SEDIMARE 2023-2027
Sediment Transport and Morphodynamics in Marine and Coastal Waters with Engineering Solutions

2nd Network Training School: Experimental and Practical Modelling of Sediment Transport and Coastal Morphology

Deltares, The Netherlands

7 – 8 Nov 2024

Morphodynamic swash zone modelling

Doctoral Candidate: Quan NGUYEN

Supervising Scientists: Nicholas DODD and Riccardo BRIGANTI

Content

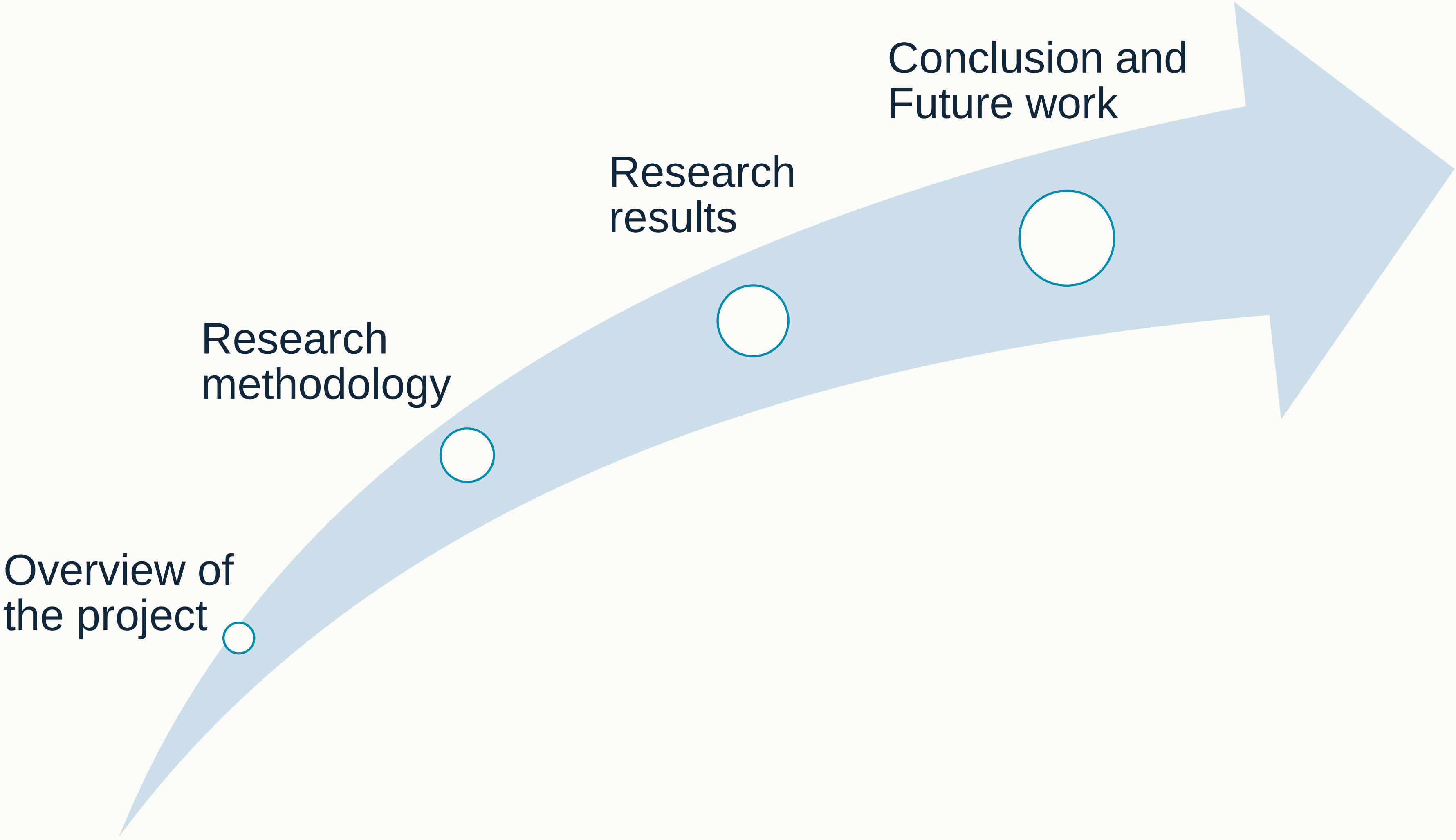
Conclusion and Future work
Research results
Research methodology
Overview of the project

Overview of the project

Overview of the project

The swash zone

- A dynamic region separating land from the inner surf zone
- Wave run-up/run-down impacts the nearshore morphology and sediment transport.
- Unsteady flow, high turbulence, rapid boundary layer growth and decay, large sediment transport rates, and rapid bed level changes

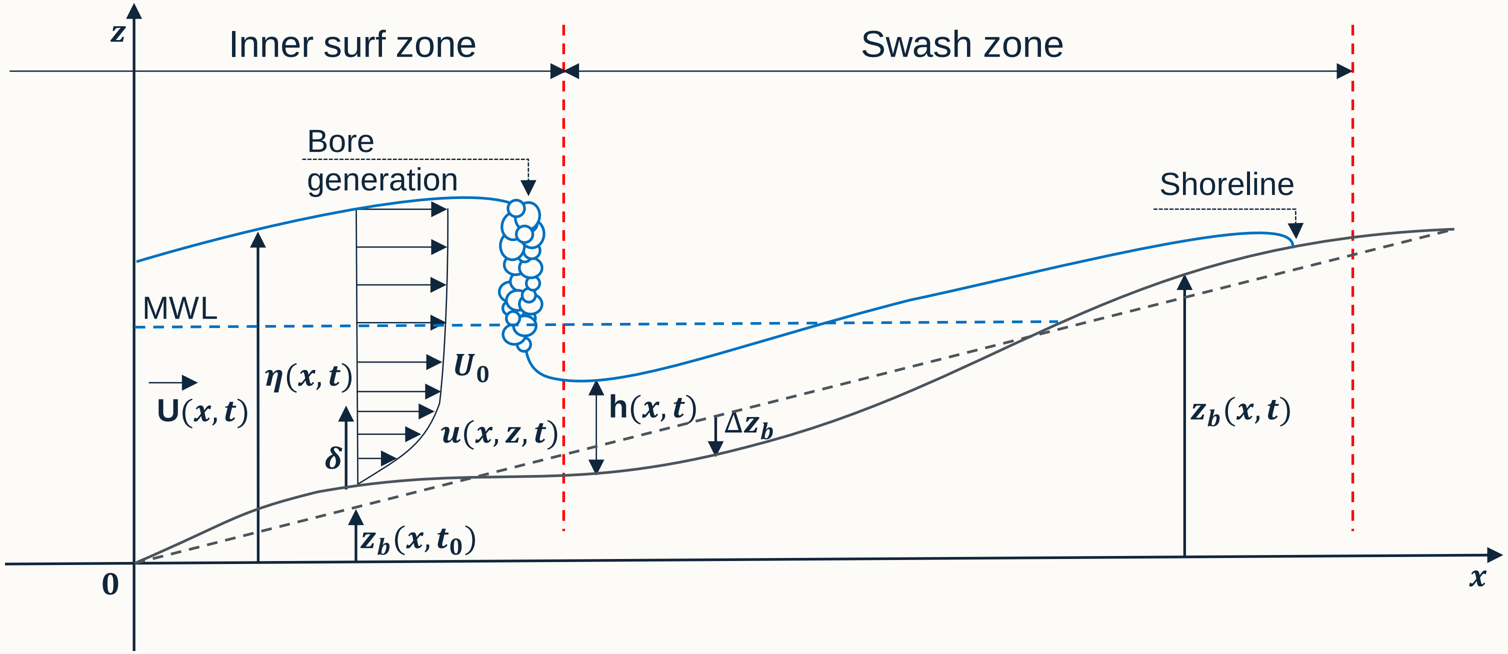

Figure 1. Schematic of general swash geometry.

➢ Important to coastal management and conservation strategies.

Overview of the project

Motivation

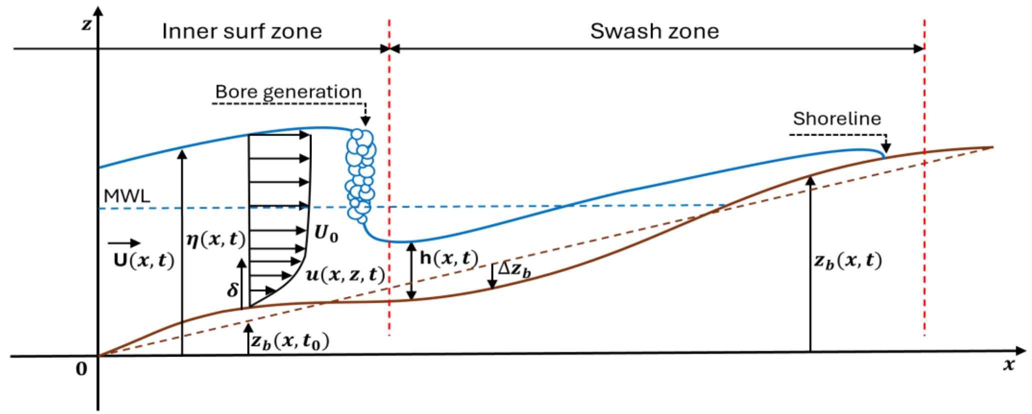

- Difficulty in adequately represent the wave boundary layer in the swash zones.
- Difficulty in directly measure the bed shear stress within the bottom boundary layer (BBL)
- An existing BBL sub-model for a **fixed bed** in the swash zone

➢ Further developed on **mobile bed** beaches, to improve our capacity to accurately described the bed shear stress within the BBL

Overview of the project

Objectives

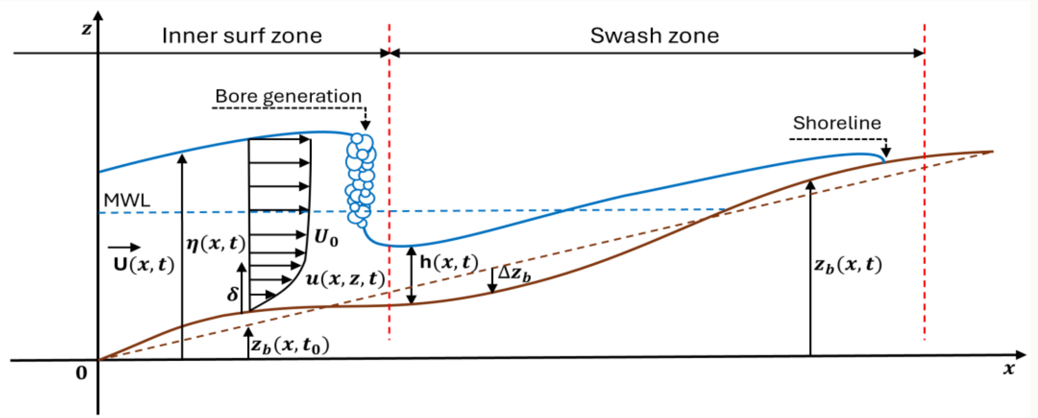

- ➢ To develop an **<u>improved</u>** boundary layer description (sub-model) for a **<u>mobile bed</u>** that is suitable for incorporation into a Nonlinear Shallow Water Wave Equation (NLSWE) morphodynamic solver.
- ➢ To validate the resulting morphodynamic solver against laboratory and existing field data.

Research methodology

Research methodology

Numerical model

❖ Depth-averaged, phase-resolving, fully-coupled model

Hydrodynamics	⓾**1D nonlinear shallow water equations (NLSWEs)**
Morphodynamics	• Coupled with **Exner equation**
Sediment transport	• Coupled with **Meyer-Peter and Müller equation**
Bottom boundary layer model	• **Momentum integral method**

Research methodology

Model validation

❑ Single dam-break-driven swash event on the fixed bed (Kikkert et al., 2012)

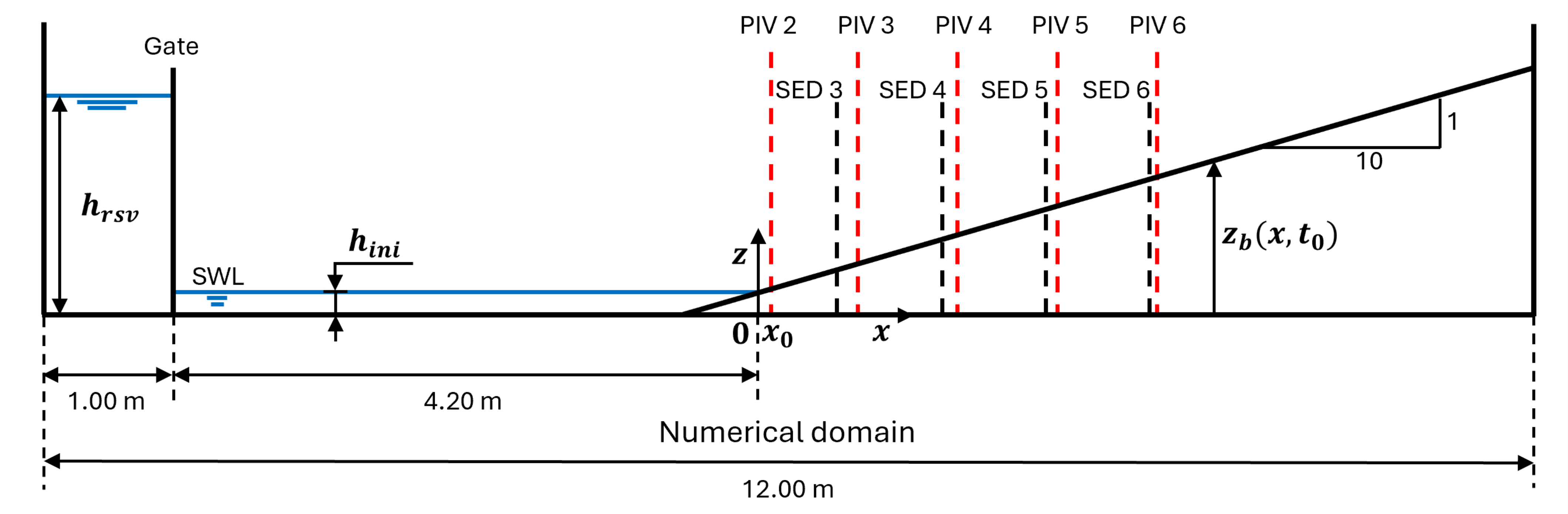

Figure 2. Schematic of the numerical setup based on the Aberdeen Swash facility.

Research results

Model validation: Single swash on impermeable fixed beds

Water depth - Depth-averaged velocity – Bed shear stress

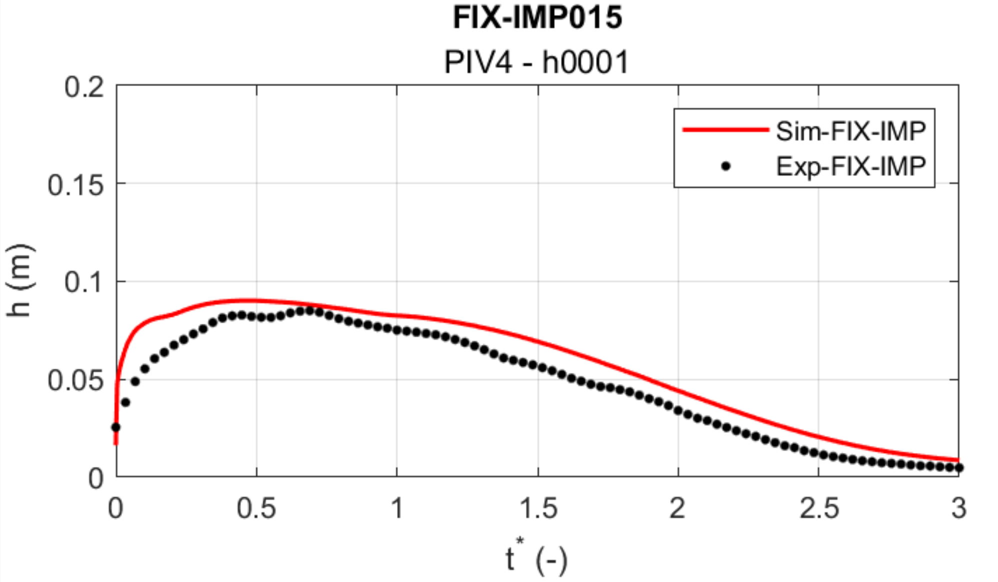

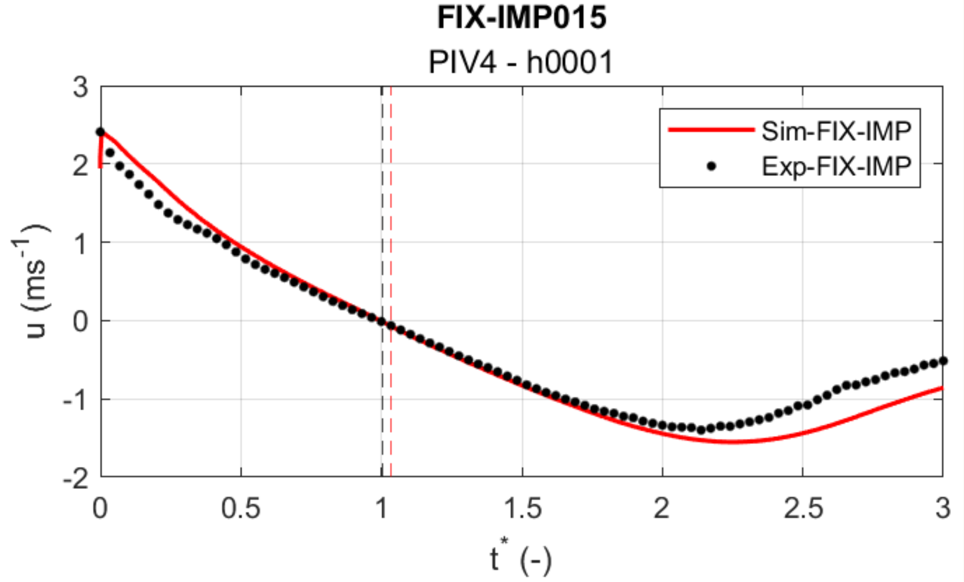

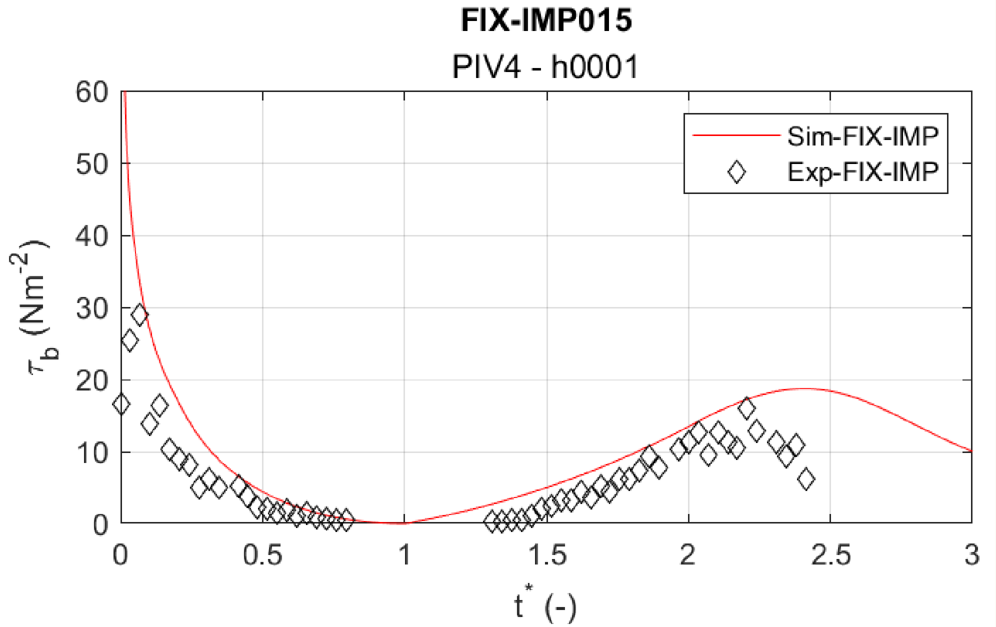

$$t^* = \frac{t - t_{bore\ arrival}}{t_{flow\ reversal} - t_{bore\ arrival}}$$

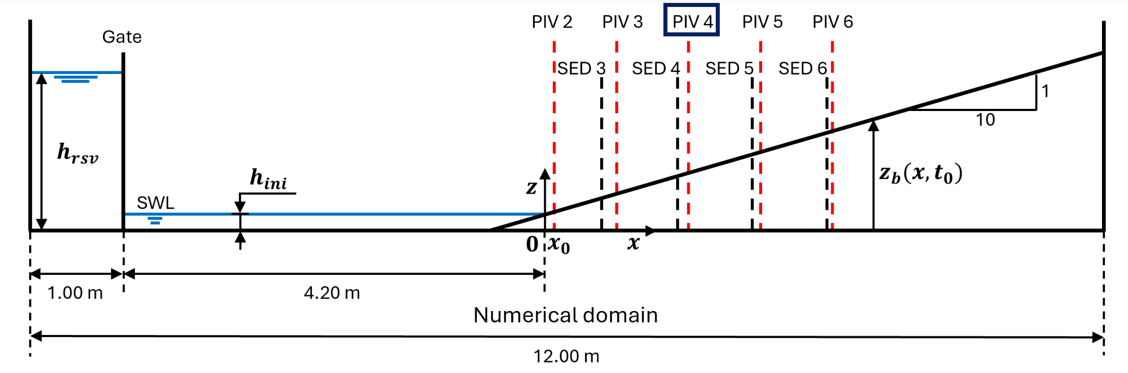

Swash lens

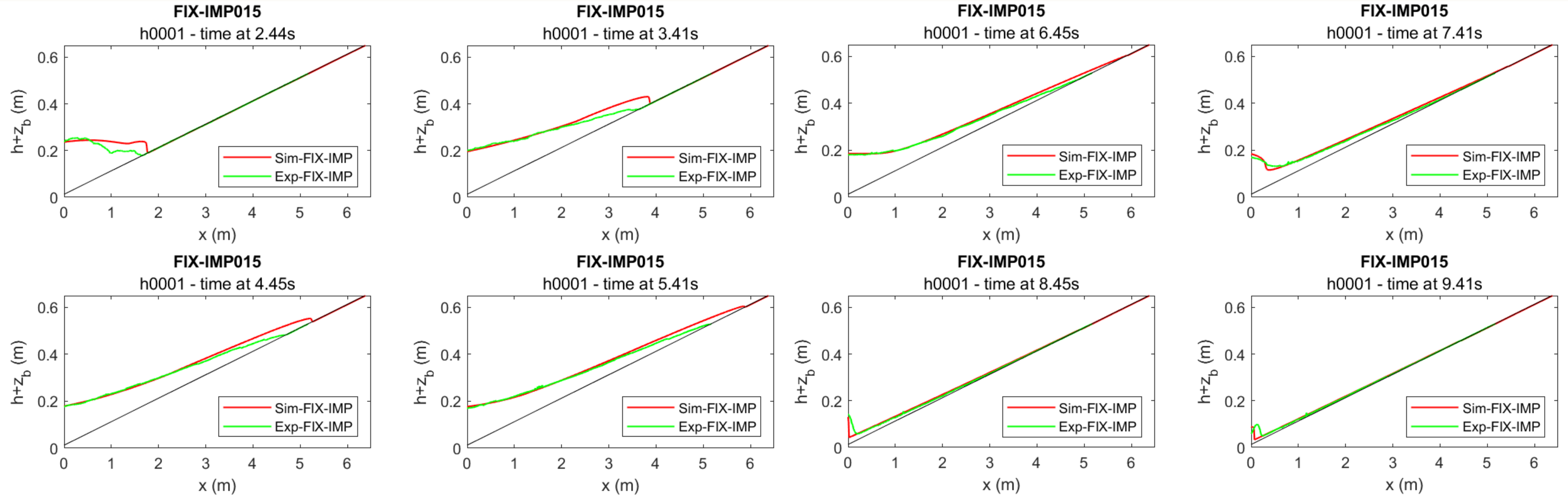

FIX-IMP015
h0001 - time at 2.44s
FIX-IMP015
h0001 - time at 3.41s
FIX-IMP015
h0001 - time at 6.45s
FIX-IMP015
h0001 - time at 7.41s
FIX-IMP015
h0001 - time at 4.45s
FIX-IMP015
h0001 - time at 5.41s
FIX-IMP015
h0001 - time at 8.45s
FIX-IMP015
h0001 - time at 9.41s
$h+z_b$ (m)
x (m)
Sim-FIX-IMP
Exp-FIX-IMP

Vertical profile of horizontal velocity

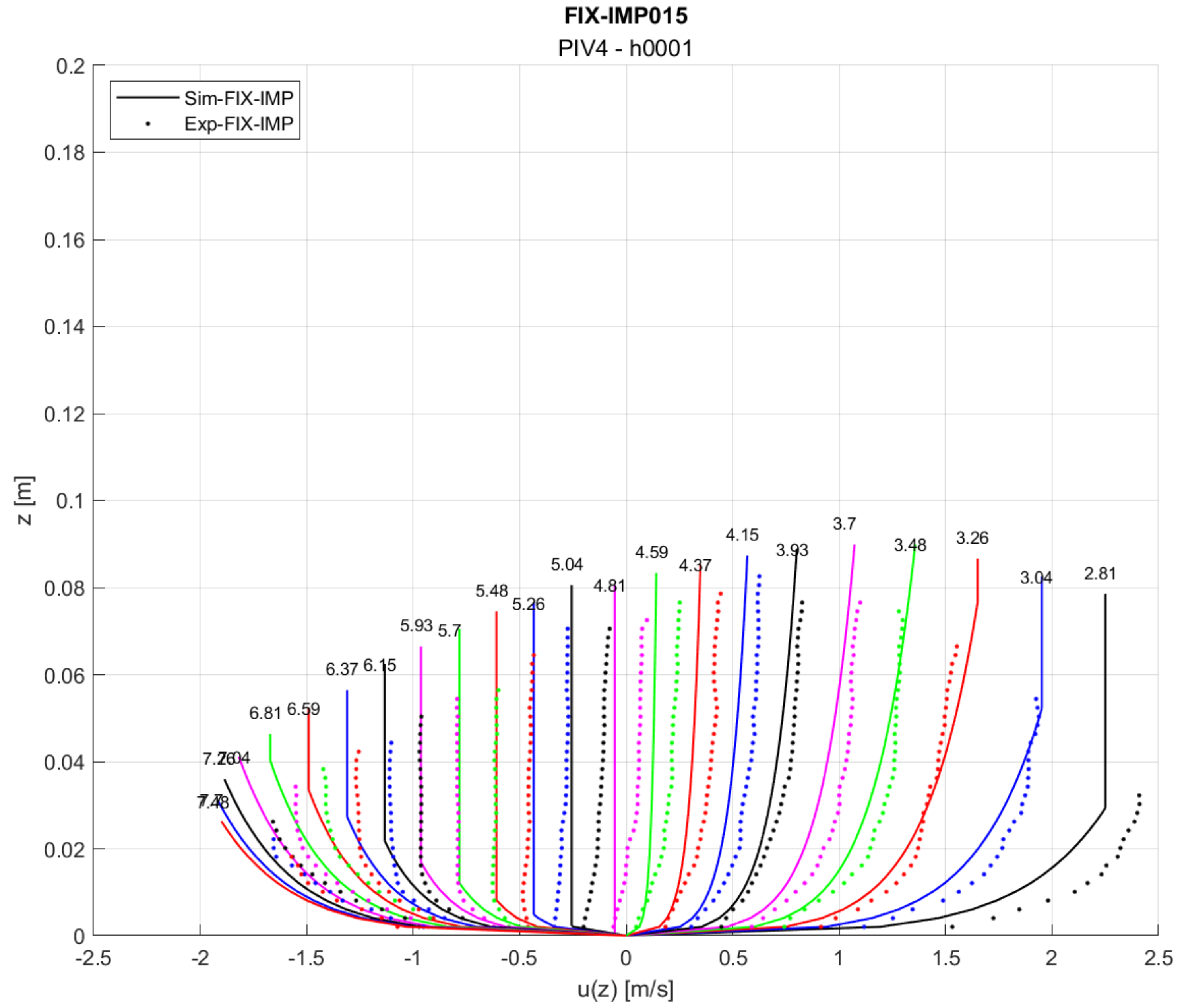

Research results

The impact of mobility on model performance

Water depth - Depth-averaged velocity – Maximum run-up

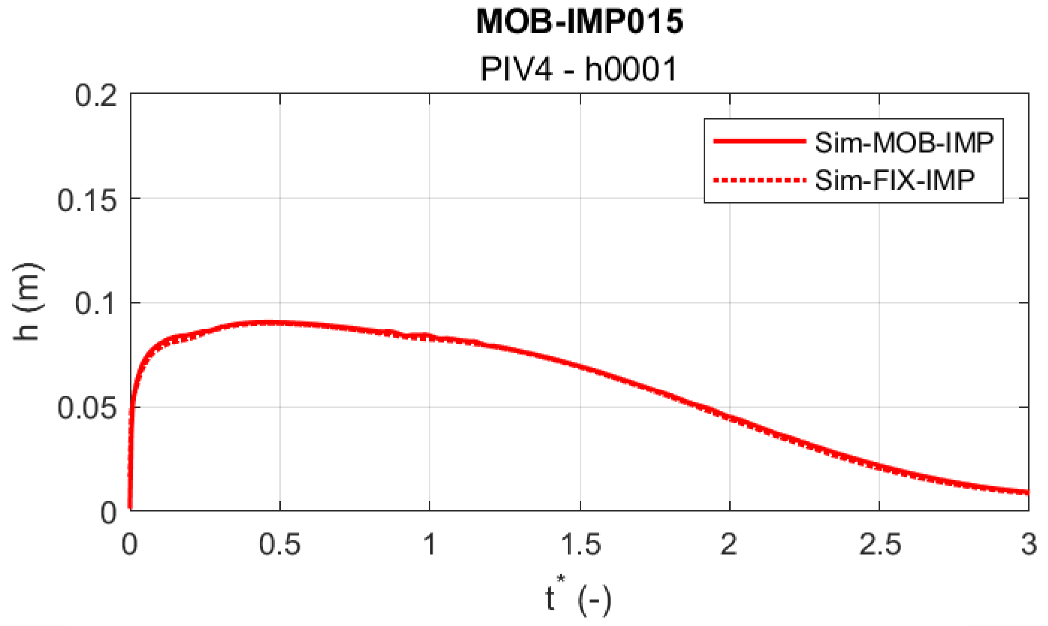

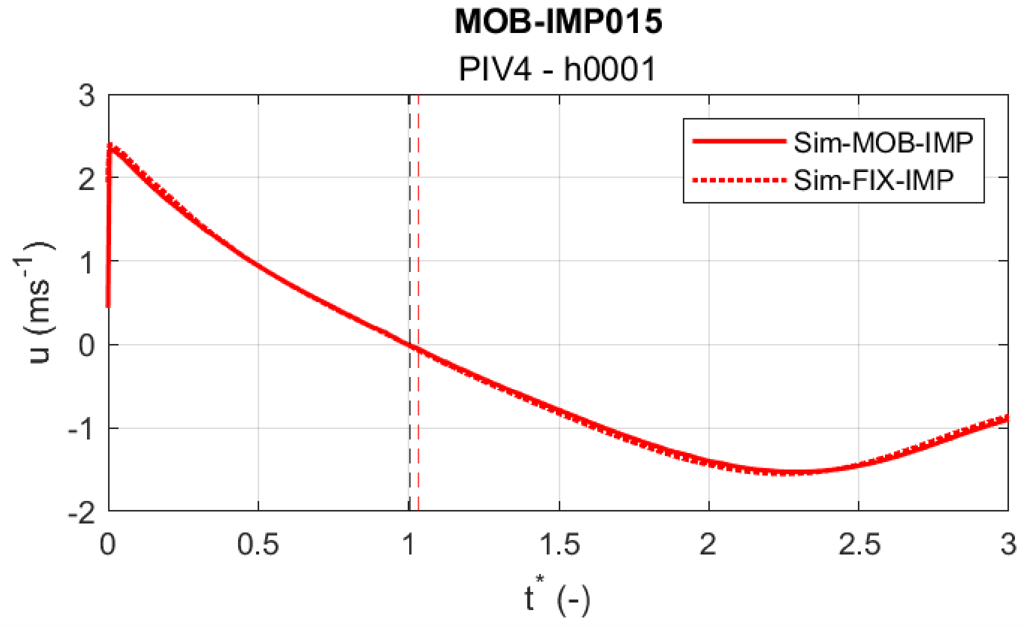

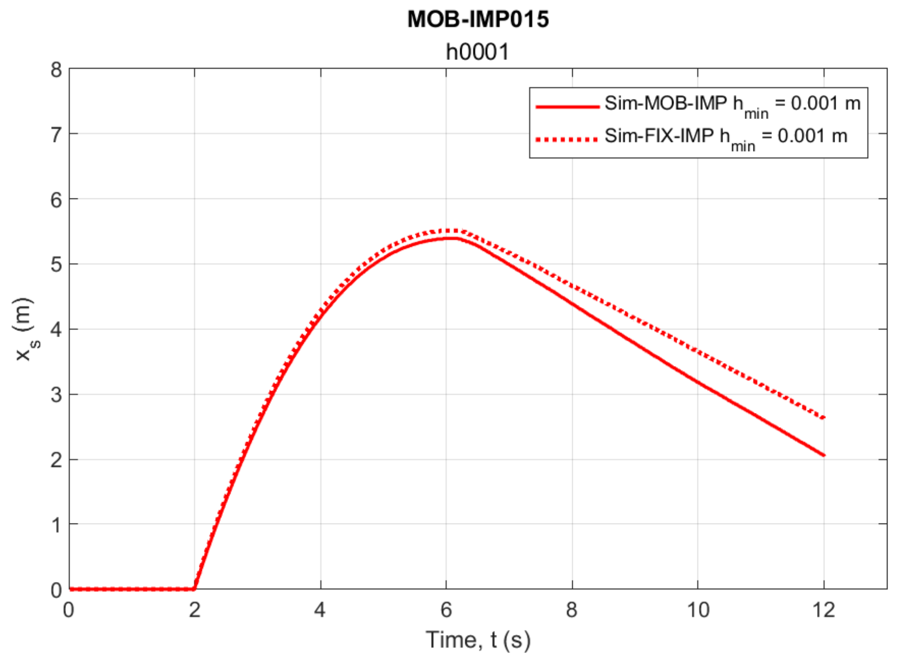

$$t^* = \frac{t - t_{bore\ arrival}}{t_{flow\ reversal} - t_{bore\ arrival}}$$

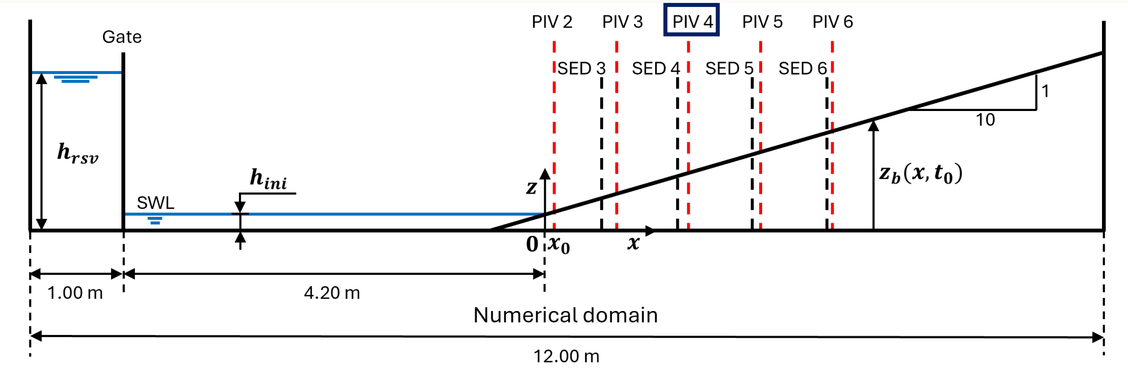

Swash lens

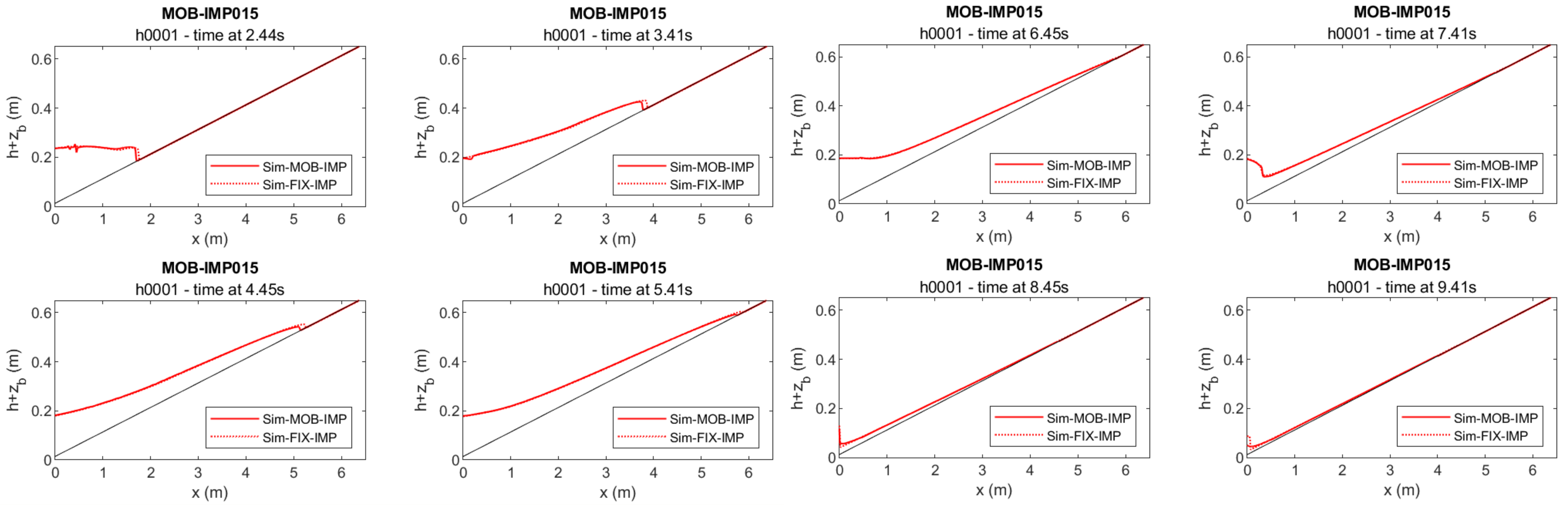
MOB-IMP015
h0001 - time at 2.44s
MOB-IMP015
h0001 - time at 3.41s
MOB-IMP015
h0001 - time at 6.45s
MOB-IMP015
h0001 - time at 7.41s
MOB-IMP015
h0001 - time at 4.45s
MOB-IMP015
h0001 - time at 5.41s
MOB-IMP015
h0001 - time at 8.45s
MOB-IMP015
h0001 - time at 9.41s
h+z_b (m)
x (m)
Sim-MOB-IMP
Sim-FIX-IMP

Vertical profile of horizontal velocity

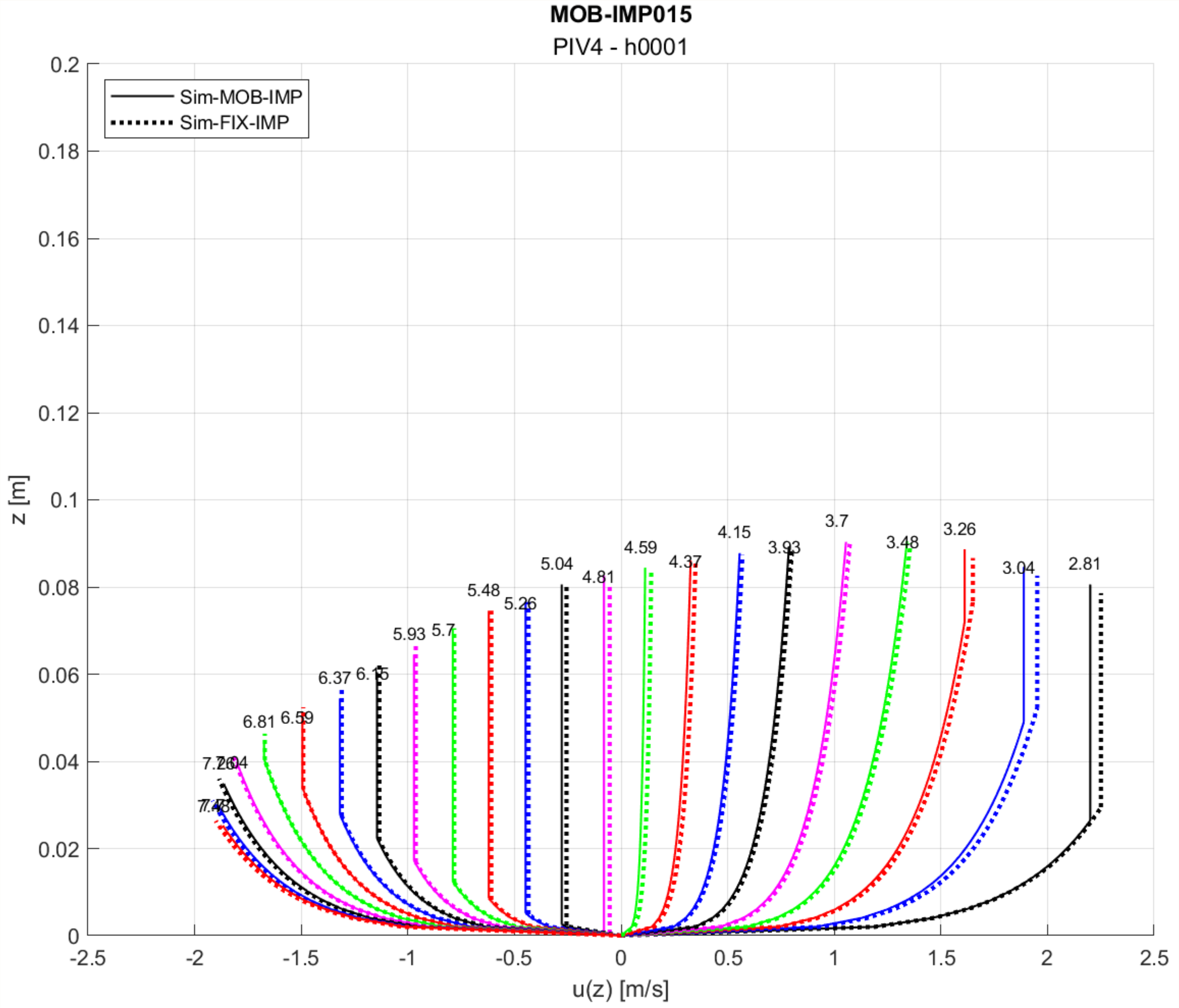

Bed shear stress

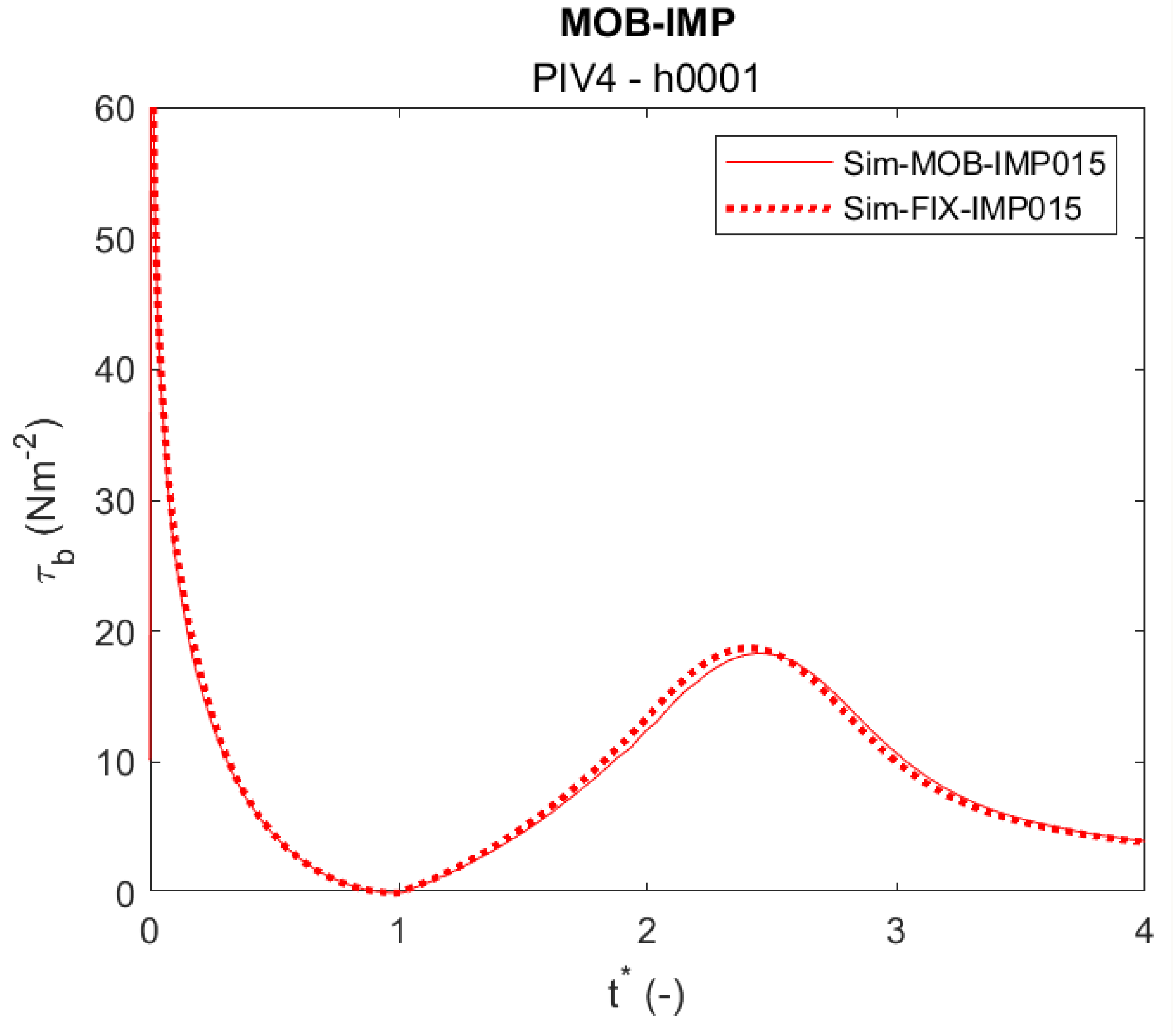

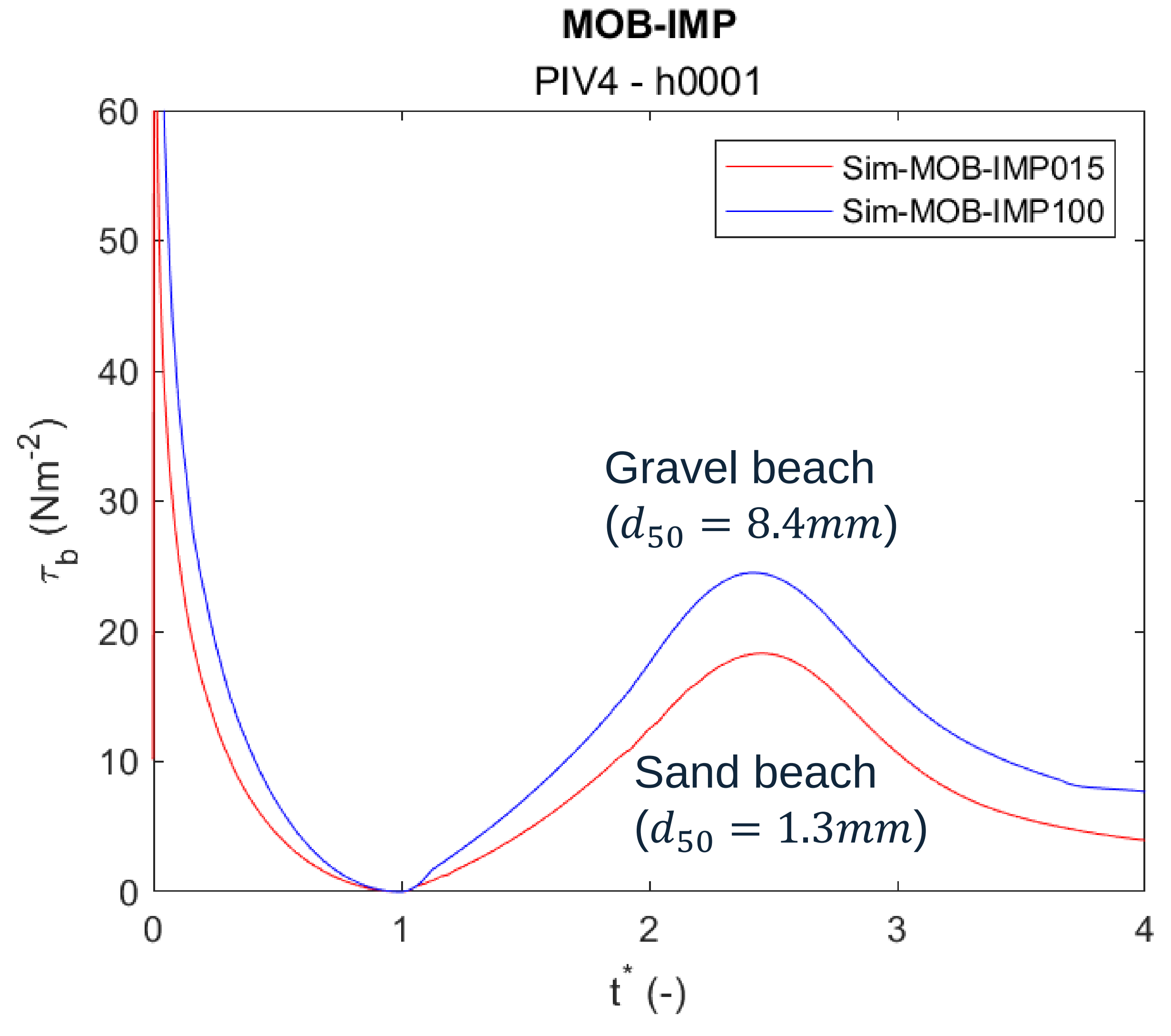

Conclusion

Model advancements

- Numerical results of the flow variables for the test with fixed bed are close to the experimental results
- The model accurately predicts the depth-averaged horizontal velocity in the run-up phase
- The modelled bore arrival time almost coincides with the experimental one
- The modelled bed shear stress is well predicted when compared with the log-law-derived shear stress

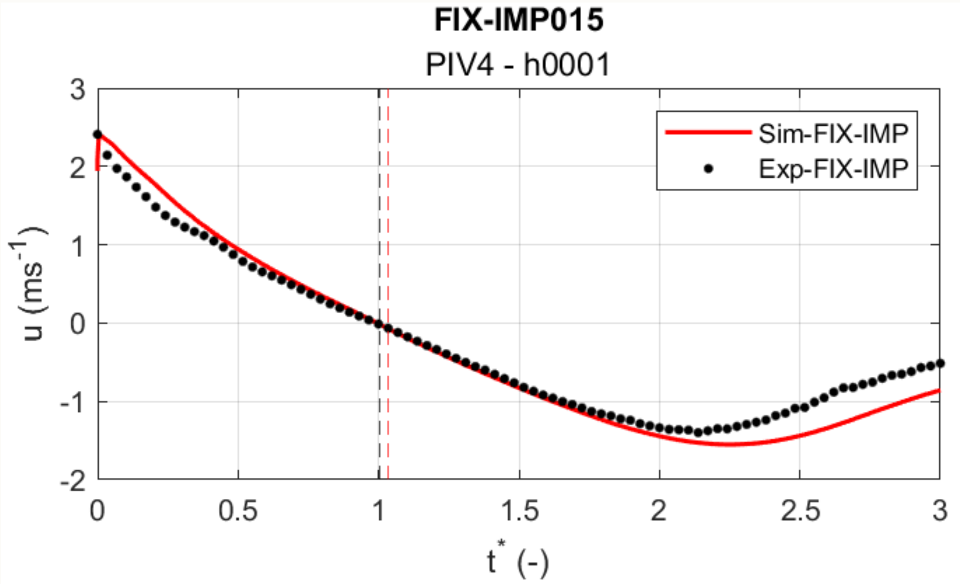

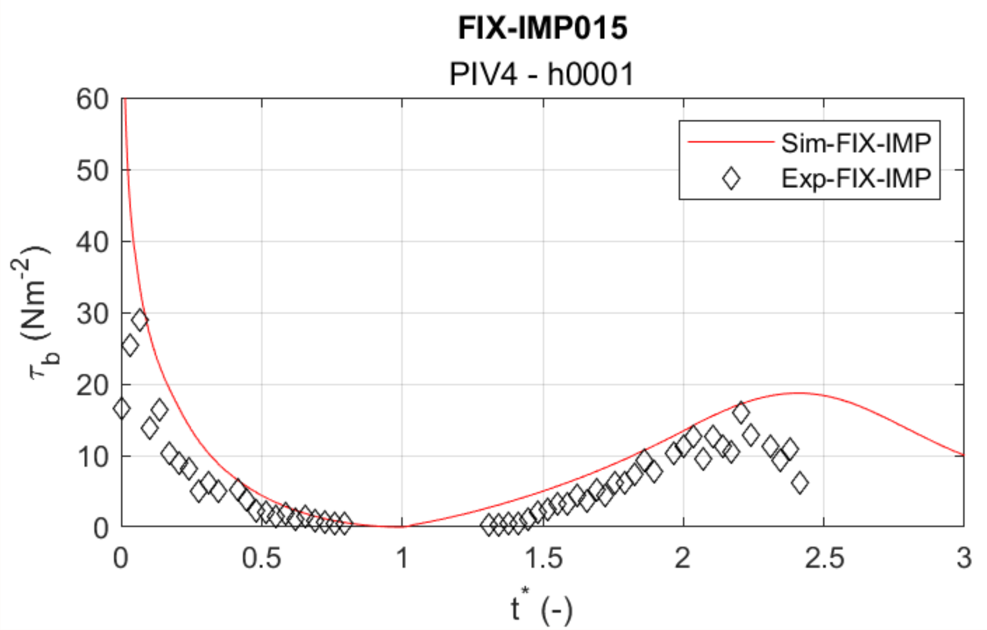

Model limitations

- **Overestimation of boundary layer thickness and underestimation of velocity profile**

➢ Affecting the model's ability to accurately simulate the interactions between the flow and the seabed, which are crucial for understanding the sediment transport processes.

- **Uncertainties in bed shear stress modelling**

➢ Affecting the accuracy in modelling of bed shear stress at critical moments such as the arrival of the bore and during flow reversal

- **Overestimation of Flow Variables**

➢ Affecting the reliability of the model in practical applications.

Future works

- Improving the simulation of the vertical profile of horizontal velocity inside the bottom boundary layer, with a focus on the velocity profile at the flow reversal and the swash tip.

- Parameterising the physical parameters and model configuration on the simulation of the dam-break-driven swash event on an impermeable mobile bed.

Deliverables

01

D2.2. Technical report on evaluation of morphodynamic swash zone model with existing boundary layer sub-model.

02

D2.8. Technical report on evaluation of new boundary layer sub-model.

03

D3.11. Technical report on application of morphodynamic swash zone model.

University of Nottingham
UK | CHINA | MALAYSIA

HORIZON EUROPE

Marie Skłodowska-Curie Actions

SEDIMARE 2023-2027

Sediment Transport and Morphodynamics in Marine and Coastal Waters with Engineering Solutions

2nd Network Training School

University of Twente/Deltares, The Netherlands

Nov 5th – 8th, 2024

Morphodynamic swash zone modelling

Doctoral Candidate (#11): Quan NGUYEN

Supervising Scientists: Nicholas DODD and Riccardo BRIGANTI

Structural stability of the Brinkman–Forchheimer equations for flow in porous media with variable porosity

Evangelos Petridis

UCLouvain
Institute of Mechanics, Materials and Civil Engineering

Funded by the European Union

This project has received funding from the European Union's Horizon Europe research and innovation programme under the Marie Skłodowska-Curie grant agreement No 101072443.

European Commission

Introduction

Payne and Straughan (1999) established continuous dependence in the Brinkman-Forchheimer equations with constant porosity . When the porosity is space dependent :

• Velocity is not divergence free.

• The term describing viscous shear stresses is not the Laplacian .

• We have normal viscous stresses (bulk viscosity ζ) .

• The shear viscosity μ enters the expression for the interfacial drag (Darcy coefficient a) .

• We are working in the weighted L^2 space with the porosity $\phi(\mathbf{x})$ being the weight .

$$\|\mathbf{u}\| = \left(\int_\Omega \phi |\mathbf{u}|^2 d\mathbf{x} \right)^{1/2}$$

Inequalities

Arithmetic-geometric mean inequality

$$ab \leq \frac{1}{2c}a^2 + \frac{c}{2}b^2$$

Hölder's inequality

$$\int_\Omega |\mathbf{f}||\mathbf{g}|d\mathbf{x} \leq \left(\int_\Omega |\mathbf{f}|^p d\mathbf{x}\right)^{1/p} \left(\int_\Omega |\mathbf{g}|^q d\mathbf{x}\right)^{1/q}, \; \frac{1}{p} + \frac{1}{q} = 1$$

Sobolev inequality

$$\int_\Omega |\mathbf{G}|^4 d\mathbf{x} \leq C \left(\int_\Omega |\mathbf{G}|^2 d\mathbf{x}\right)^{1/2} \left(\int_\Omega \nabla\mathbf{G} : \nabla\mathbf{G} d\mathbf{x}\right)^{3/2}$$

Poincare's inequality

$$\lambda_1 \int_\Omega |\mathbf{w}|^2 d\mathbf{x} \leq \int_\Omega \nabla\mathbf{w} : \nabla\mathbf{w} d\mathbf{x}$$

Model

The Brinkman–Forchheimer equations for flow in porous media with variable porosity are

$$\phi\frac{\partial \mathbf{u}}{\partial t} + \phi\nabla p$$
$$= \nabla\cdot(\phi\zeta(\nabla\cdot\mathbf{u})I) + \nabla\cdot\left(\phi\mu\mathbf{V}^d\right) - a^\star(\phi)\mathbf{u} - b^\star(\phi)|\mathbf{u}|\mathbf{u} + \phi\mathbf{f} \quad , \quad \zeta,\mu > 0$$

$$\nabla\cdot(\phi\mathbf{u}) = 0$$

$$\mathbf{V}^d(\mathbf{u}) = \frac{1}{2}(\nabla\mathbf{u} + (\nabla\mathbf{u})^T) - \frac{1}{3}\nabla\cdot\mathbf{u}\ I$$

$$b^\star(\phi) = b(1-\phi) + d(1-\phi)^2 \ \ , \ a^\star(\phi) = a\mu(1-\phi)\ , \ a, b, d > 0$$

$$0 < \phi_{\min} \leq \phi \leq \phi_{\max} < 1$$

where $\mathbf{u}$ is the average fluid velocity in the porous medium, a is the Darcy coefficient, b is the Forchheimer coefficient, ζ is the bulk viscosity , μ is the shear viscosity, p is the pressure , $\mathbf{f}$ is the gravity and ϕ is the varible porosity.

Forchheimer coefficient b

To study continuous dependence on b, we let u and v solve the following boundary initial-value problems for different Forchheimer coefficients b_1 and b_2 :

$$\phi\frac{\partial \mathbf{u}}{\partial t} + \phi\boldsymbol{\nabla} p = \boldsymbol{\nabla}\cdot(\phi\zeta(\boldsymbol{\nabla}\cdot\mathbf{u})I) + \boldsymbol{\nabla}\cdot\left(\phi\mu\mathbf{V}^d\right) - a^\star(\phi)\mathbf{u} - b_1^\star(\phi)|\mathbf{u}|\mathbf{u} + \phi\mathbf{f}\ ,$$

$$\phi\frac{\partial \mathbf{v}}{\partial t} + \phi\boldsymbol{\nabla} q = \boldsymbol{\nabla}\cdot(\phi\zeta(\boldsymbol{\nabla}\cdot\mathbf{v})I) + \boldsymbol{\nabla}\cdot\left(\phi\mu\mathbf{V}^d\right) - a^\star(\phi)\mathbf{v} - b_2^\star(\phi)|\mathbf{v}|\mathbf{v} + \phi\mathbf{f}\ ,$$

$$\boldsymbol{\nabla}\cdot(\phi\mathbf{u}) = \boldsymbol{\nabla}\cdot(\phi\mathbf{v}) = 0\ ,\ \Omega\times\{t>0\}\ ,$$

$$\mathbf{u} = \mathbf{v} = \mathbf{0}\ \ ,\ \partial\Omega\times\{t>0\}\ ,$$

$$\mathbf{u}(\mathbf{x},0) = \mathbf{v}(\mathbf{x},0) = \mathbf{g}(\mathbf{x})\ ,\ \mathbf{x}\in\Omega$$

Ω in these problems is a bounded domain in $\mathbb{R}^3$ whose boundary is $\partial\Omega$ and g is the given initial data.

Forchheimer coefficient b

We define the difference variables $\mathbf{w}$, p and b by

$$\mathbf{w} = \mathbf{u} - \mathbf{v}\ ,\ \pi = p - q\ ,\ b^\star = \ b_1^\star - b_2^\star = b(1-\phi)\ ,\quad b = b_1 - b_2$$

and then $\mathbf{w}$ satisfies the boundary initial-value problem

$$\begin{aligned}&\phi\frac{\partial \mathbf{w}}{\partial t} - \boldsymbol{\nabla}\cdot(\phi\zeta(\boldsymbol{\nabla}\cdot\mathbf{w})I) - \boldsymbol{\nabla}\cdot\left(\phi\mu\mathbf{V}^d\right)\\ &= -a^\star(\phi)\mathbf{w} - (b_1^\star(\phi)|\mathbf{u}|\mathbf{u} - b_2^\star(\phi)|\mathbf{v}|\mathbf{v}) - \phi\boldsymbol{\nabla}\pi\ ,\end{aligned}$$

$$\boldsymbol{\nabla}\cdot(\phi\mathbf{w}) = 0\ ,\ \Omega\times\{t>0\}\ ,$$

$$\mathbf{w} = \mathbf{0}\ ,\ \partial\Omega\times\{t>0\}\ ,$$

$$\mathbf{w}(\mathbf{x},0) = \mathbf{0}\ ,\ \mathbf{x}\in\Omega$$

Forchheimer coefficient b

Using the relations

$$\mathbf{V}^d : \mathbf{V}^d = \mathbf{V^d} : \nabla \mathbf{w}$$

$$\|\mathbf{V}^d\|^2 \geq \frac{\phi_{\text{min}}}{2\phi_{\text{max}}} \|\nabla \mathbf{w}\|^2$$

and calculations we can conclude

$$\|\mathbf{w}\|^2 \leq \frac{c}{\lambda_1^{1/2}\mu^2}(\frac{1}{\phi_{\text{min}}} - 1)^2 \frac{(\phi_{\text{max}})^{7/2}}{(\phi_{min})^{9/2}} \|\mathbf{g}\|^4 e^{-2a\mu(\frac{1}{\phi_{\text{max}}}-1)t} \; b^2$$

This specific estimate establishes continuous dependence on the Forchheimer coefficient b in the weighted L^2 norm.

Results

Also through calculations we can establish continuous dependence on

- the Darcy coefficient

$$\|\mathbf{w}\|^2 \leq \left(\frac{1}{\phi_{\min}} - 1\right)^2 \frac{1}{a_1\left(\frac{1}{\phi_{\max}} - 1\right)^2 (a_1 - 2a_2)} \|\mathbf{g}\|^2 \left(e^{-2a_2\mu\left(\frac{1}{\phi_{\max}}-1\right)t} - e^{-a_1\mu\left(\frac{1}{\phi_{\max}}-1\right)t}\right) a^2$$

- the shear viscosity

$$\|\mathbf{w}\|^2 \leq \Big[\left(\frac{1}{\phi_{\min}} - 1\right)^2 \frac{\|\mathbf{g}\|^2}{\mu_1\left(\frac{1}{\phi_{\max}} - 1\right)^2 (\mu_1 - 2\mu_2)} \left(e^{-2a\mu_2\left(\frac{1}{\phi_{\max}}-1\right)t} - e^{-a\mu_1\left(\frac{1}{\phi_{\max}}-1\right)t}\right)$$
$$+ \frac{\phi_{\max}}{2\mu_1\mu_2\phi_{\min}} \|\mathbf{g}\|^2 \; e^{-a\mu_2\left(\frac{1}{\phi_{\max}}-1\right)t}\Big] \mu^2$$

Energy bounds

Now, let **u** be a solution to the boundary initial-value problem for the Brinkman-Forchheimer equations with variable porosity.

$$\frac{1}{2}\frac{d}{dt}\int_\Omega \phi|\mathbf{u}|^2 d\mathbf{x} + \int_\Omega a^\star(\phi)|\mathbf{u}|^2 d\mathbf{x} + \int_\Omega b^\star(\phi)|\mathbf{u}|^3 d\mathbf{x} + \int_\Omega \phi\mu\mathbf{V}^{\ d} : \nabla\mathbf{u} d\mathbf{x}$$
$$= -\int_\Omega \phi\zeta(\nabla\cdot\mathbf{u})^2 d\mathbf{x}$$

Through basic calculations and Poincare's inequality we can easily establish an upper bound

$$\|\mathbf{u}\|^2 \leq \|\mathbf{g}\|^2 e^{-(2a\mu(\frac{1}{\phi_{\text{max}}}-1)+\frac{\lambda_1\mu\phi_{\text{min}}^2}{\phi_{\text{max}}^2})t}$$

Energy bounds

Next, we derive a lower bound for $\|\mathbf{u}\|$. To do this, let the kinetic energy be

$$\Phi = \|\mathbf{u}\|^2$$

and then by calculation,

$$\frac{d\Phi}{dt} = \\ -2\int_\Omega \phi\zeta(\boldsymbol{\nabla}\cdot\mathbf{u})^2 d\mathbf{x} - 2\int_\Omega \phi\mu\mathbf{V}^d : \mathbf{V}^d d\mathbf{x} - 2\int_\Omega a^*(\phi)|\mathbf{u}|^2 d\mathbf{x} - 2\int_\Omega b^*(\phi)|\mathbf{u}|^3 d\mathbf{x} \\ \leq \chi$$

where we have set

$$\chi(t) = -2\int_\Omega \phi\mu\mathbf{V}^d : \mathbf{V}^d d\mathbf{x} - 2\int_\Omega \phi\zeta(\boldsymbol{\nabla}\cdot\mathbf{u})^2 d\mathbf{x} - 2\int_\Omega a^*(\phi)|\mathbf{u}|^2 d\mathbf{x} - \frac{4}{3}\int_\Omega b^*(\phi)|\mathbf{u}|^3 d\mathbf{x}$$

Energy bounds

By further computation, we find that

$$\frac{d\chi}{dt} = 4\int_{\Omega} \phi |\frac{\partial \mathbf{u}}{\partial t}|^2 d\mathbf{x} = 4\|\frac{\partial \mathbf{u}}{\partial t}\|^2$$

and so with the aid of the Cauchy-Schwarz inequality and some basic calculations we can see that

$$\Phi(t) \geq \Phi(0) e^{\frac{3\chi(0)}{2\|\mathbf{g}\|^2} t}$$

so we have established a lower and an upper bound for $\|\mathbf{u}\|$

$$\|\mathbf{g}\|^2 e^{\frac{3\chi(0)}{2\|\mathbf{g}\|^2} t} \leq \|\mathbf{u}\|^2 \leq \|\mathbf{g}\|^2 e^{-(2a\mu(\frac{1}{\phi_{\max}} - 1) + \frac{\lambda_1 \mu \phi_{\min}^2}{\phi_{\max}^2}) t}$$

This, of course, shows that $\mathbf{u}$ cannot vanish identically in a finite time

Energy bounds

Now that we know $\|\mathbf{u}\|$ is strictly positive, we can improve the upper bound. If we use Holder's inequality and with the aid of Poincare's inequality, we may derive

$$\frac{d}{dt}\|\mathbf{u}\|^2 + (2a\mu(\frac{1}{\phi_{\max}} - 1) + \frac{\lambda_1 \mu \phi_{\min}^2}{\phi_{\max}^2})\|\mathbf{u}\|^2 + \frac{2b}{m^{1/2}(\phi_{\max})^{1/2}}(\frac{1}{\phi_{\max}} - 1)\|\mathbf{u}\|^3 \leq 0$$

where $m = m(\Omega)$ is the measure of Ω. This inequality may be rearranged and integrated into

$$\|\mathbf{u}\| \leq \frac{\|\mathbf{g}\|(2a\phi_{\max}(1-\phi_{\max}) + \lambda_1 \phi_{\min}^2)A(t)}{2a\phi_{\max}(1-\phi_{\max}) + \lambda_1\phi_{\min}^2 + 2\|\mathbf{g}\| b\ m^{-1/2}\mu^{-1}\phi_{\max}^{1/2}(1-\phi_{\max})(1-A(t))}$$

where

$$A(t) = e^{-(a\mu(\frac{1}{\phi_{\max}} - 1) + \frac{\lambda_1 \mu \phi_{\min}^2}{2\phi_{\max}^2})t}$$

Energy bounds

So finally we established a lower and an upper bound for $\|\mathbf{u}\|$

$$\|\mathbf{g}\| e^{\frac{3\chi(0)}{4\|\mathbf{g}\|^2} t}$$

$$\leq \|\mathbf{u}\|$$

$$\leq \frac{\|\mathbf{g}\|(2a\phi_{\max}(1-\phi_{\max}) + \lambda_1 \phi_{\min}^2) A(t)}{2a\phi_{\max}(1-\phi_{\max}) + \lambda_1 \phi_{\min}^2 + 2\|\mathbf{g}\| b\ m^{-1/2} \mu^{-1} \phi_{\max}^{1/2} (1-\phi_{\max})(1-A(t))}$$

Future work

We will work on a problem include the flow of currents over deformable dunes in a channel.
Detailed numerical simulations of shear-driven (Couette) of water-sand mixtures. (Emphasis on sediment mobilization and resuspension)

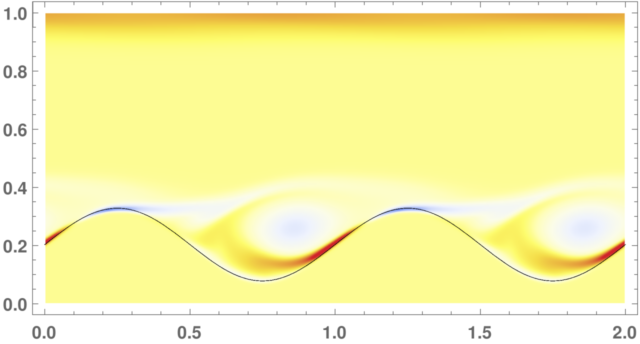

Bibliography

L. E. Payne, B. Straughan *Convergence and Continuous Dependence for the Brinkman–Forchheimer Equations*. Stud. Appl. Math. **102** (1999), 419–439.